

# MINUTES OF THE SEVENTEENTH EXPLOSIVES SAFETY SEMINAR

**VOLUME II** 

AD A O 36 0 1 6





REGENCY INN
DENVER, COLORADO
14-16 SEPTEMBER 1976

COPY AVAILABLE TO DDG DOES NOT PERMIT FULLY LEGIBLE PRODUCTION

SPONSORED BY

DEPARTMENT OF DEFENSE EXPLOSIVES SAFETY BOARD WASHINGTON, D.C. 20314



# CORRECTION

# Minutes, 17th DDESB Seminar, 1976

In place of the last column of Table XII of the paper by C. N. Kingery, page 1808, substitute the following:

2.28

1.91

1.46

1.04

.715

.502

1.01

.782

.735

.580

.590

.474

.348

.223

.135

.521

.512

.474

.415

.338

MINUTES OF THE

SEVENTERINE EXPLOSIVES SAFETY SEMINAR (17 Ch)

Volume II

Held at

Regency Inn

Denver, Colorado 7

14-13-16 September 1976 . Volume II.

Sponsored by

Department of Defense Explosives Safety Board

Washington, D. C. 20314

12/950p.

Approved for public release; distribution unlimited

034 850

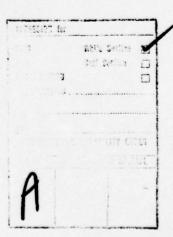


# TABLE OF CONTENTS

# VOLUME II

0

THE PREDICTION OF THE REACTION OF AN EXPLOSIVE SYSTEM IN A FIRE ENVIRONMENT. COATED RDX SYSTEMS FOR PRESSED EXPLOSIVES	
Messrs. C.M. Anderson & J.M. Pakulak, Jr., NWC China Lake, CA	973
MISSILE SYSTEMS PROPULSION COOK-OFF Mr. R. F. Vetter, NWC China Lake, CA	1011
QUANTITY DISTANCES FOR UNDERGROUND STORAGE OF AMMUNITION AND EXPLOSIVES IN DEPOTS: THE GERMAN TWO CHAMBER STORAGE SITE WITH A BLOCK CLOSING DEVICE	1015
G. Gürke, Ernst-Mach-Institut der Fraunhofer Gesellschaft, FRG	1015
MODEL STUDY OF TUNNEL DESTRUCTION BY EXPLOSIVES Mr. C. E. Joachim, USA Engr Waterways Exp Stn, Vicksburg, MS	1025
GROUND SHOCK EFFECTS ON PERSONNEL AND FACILITIES FROM	
ACCIDENTAL EXPLOSIONS  Mr. R. J. Odello, Civil Engineering Lab, Port Hueneme, CA	1045
CORRELATION OF QUANTITY-DISTANCE AND WEAPONS-EFFECTS DEBRIS HAZARDS FOR UNDERGROUND EXPLOSIONS	
Mr. A. D. Rooke, Jr., USA Engr Waterways Exp Stn, Vicksburg, MS	1063
ROCKY MOUNTAIN ARSENAL M34 CLUSTER DISASSEMBLY OPERATIONS Mr. I. M. Glassman, Rocky Mountain Arsenal, Denver, CO	1089
ROCKY MOUNTAIN ARSENAL ENVIRONMENTAL EMISSION CONTROL SYSTEM Dr. R. E. Boyle, Rocky Mountain Arsenal, Denver, CO	1107
GB NERVE AGENT DISPOSAL PROCEDURES	
Mr. R. A. Jacobs, Jr., Rocky Mountain Arsenal, Denver, CO	1145
THE DDESB'S CHEMICAL HAZARDS SLIDE RULE Mr. L. C. Dixon, NSWC Silver Spring, MD	1163
WORKBOOK FOR PREDICTING PRESSURE WAVE AND FRAGMENT EFFECTS OF EXPLODING PROPELLANT TANKS AND GAS STORAGE VESSELS	
Dr. W. E. Baker, Southwest Research Institute, San Antonio, TX	1171
BLAST AND FRAGMENTS FROM PNEUMATIC PRESSURE VESSEL RUPTURE TO 345 MPa	
Mr. J. F. Pittman, NSWC Silver Spring, MD	1203

SECONDARY FRAGMENT SPEED WITH UNCONFINED EXPLOSIVES: MODEL AND VALIDATION	
Mr. J. H. Kineke, Jr., Ballistic Research Laboratory, Aberdeen PG	1225
DESIGN OF LIGHTWEIGHT SHIELDS AGAINST BLAST AND FRAGMENTS Mr. F. B. Porzel, NSWC Silver Spring, MD	1247
FRAGMENT PENETRATION INTO SINGLE AND SPACED TARGETS Messrs. Tony Ricchiazzi & Jim Barb, Ballistic Research Lab	1275
SHIP SURVIVABILITY VERSUS EXPLOSIVE HAZARDS Dr. June T. Amlie, David Taylor Naval Ship R&D Ctr, Carderock, MD	1299
DANGERS OF SECONDARY MISSILES Mr. Kenneth Kaplan, Scientific Service, Inc, Redwood City, CA	1319
SURVIVABILITY IN A NUCLEAR WEAPON ENVIRONMENT  A. Longinow, A.H. Wiedermann, E.E. Hahn, IIT Research Institute and L.E. Bertram, Sandia Laboratories	1349
M55 ROCKET DISPOSAL PROGRAM AT DUGWAY PROVING GROUND, UTAH Mr. Curtis Jones, Dugway Proving Ground, UT	1377
AUTOMATED EXPLOSIVE PELLET MANUFACTURING USING A PDP-14 PROGRAMMABLE CONTROLLER Mr. D. O. Page, Monsanto Research Corp, Miamisburg, OH	1391
EVALUATION OF PYROTECHNIC OUTPUT BEHAVIOR BY HIGH SPEED CINEPHOTOGRAPHY M.D. Kelly, J.H. Mohler and L.D. Haws, Monsanto Research Corp	1403
AUTOMATIC PELLETIZING SYSTEM FOR PYROTECHNIC MATERIALS	1403
Mr. E.J. McCloskey, Monsanto Research Corp	1405
DESIGN, DEVELOPMENT AND APPLICATION OF A VERSATILE ELECTROSTATIC SENSITIVITY TESTER	1100
L.D. Haws, R.C. D'Amico and A. Gibson, Monsanto Research Corp	1423
FORMATION, FUNCTIONS, AND METHODS OF OPERATION OF THE AUSTRALIAN ORDNANCE COUNCIL Air Commodore K. Therkelsen, President, Australian Ordnance Council	1435
SOME PRINCIPLES FOR A QUANTITATIVE APPROACH TO SAFETY PROBLEMS IN EXPLOSIVE STORAGE AND MANUFACTURING IN SWITZERLAND	1445
Th. Schneider, Basler & Hofmann, Zurich, Switzerland	1445
PYROTECHNIC HAZARDS EVALUATION PROGRAM  Mr. Gary L. McKown, Edgewood Arsenal Resident Lab, Bay St Louis, MS	1473

A REVIEW OF HAZARD CLASSIFICATION TEST METHODS FOR PROPELLANTS Dr. W. E. Baker, Southwest Research Institute	1487
HAZARD CLASSIFICATION TESTING OF GAU-8/A 30MM AMMUNITION Mr. F. L. West, ADTC, Eglin AFB, FL	1509
THE UNITED NATIONS SYSTEM OF CLASSIFICATION OF EXPLOSIVES WHERE ARE WE TODAY? Mr. A. E. Adams, AFLC, Wright-Patterson AFB, OH	1567
EXPERIMENTAL DETERMINATION OF EXPLOSIVE SENSITIVITY TO FRAGMENT IMPACT	
R.M. Rindner, Picatinny Arsenal; G. Petino, Jr., Hazards Research Corp.; H. Napadensky, IIT Research Institute	1587
IMPACT INITIATION OF SLURRY (GSX) AND OTHER SMALL DIAMETER HIGH EXPLOSIVES	
Messrs. L.L. Udy and G.L. Hansen, IRECO Chemicals, SLC, UT	1611
CONTRIBUTION TO THE KNOWLEDGE OF FORCE-TIME-DEPENDENCE ON TESTING THE IMPACT SENSITIVITY  R. Wild, Bundesinstitut für chemisch-technische Untersuchungen, WG	1631
EN MASSE DETONATION OF EXPLOSIVE STORES Mr. P.M. Howe, Ballistic Research Laboratories, Aberdeen PG, MD	1641
SAFE SEPARATION DISTANCE FOR 168 POUNDS OF COMPOSITION A-7 EXPLOSIVE IN TOTE BINS A.B. Wenzel, SW Research Inst. & R. Rindner, Picatinny Arsenal	1665
SAFE SEPARATION AND CRITICAL DEPTH TESTS FOR LONE STAR AMMUNITION PLANT	
R.S. Kukuvka & R.M. Rindner, Picatinny Arsenal	1689
NON-IDEAL EXPLOSIONS THE BLAST WAVE FROM LOW ENERGY DENSITY EXPLOSION SOURCES	
Mr. R.A. Strehlow, Univ. of Illinois	1721
AIR-TO-WATER BLAST WAVE TRANSFER Mr. P.J. Peckham, NSWC Silver Spring, MD	1743
BLAST PARAMETERS FROM EXPLOSIONS IN MODEL EARTH COVERED MAGAZINES Messrs. C.N. Kingery & G.A. Coulter, Ballistic Research Lab.	1763
ANALYSIS OF AN EXPLOSION Mr. G.S. Biasutti, Dr.Ing. Mario BIAZZI Soc. An., Vevey, Switzerland	1821
APPLICATION OF SUPPRESSIVE SHIELDING IN LAP PLANTS Mr. D.J. Katsanis, Edgewood Arsenal, Aberdeen PG, MD	1829

SUPPRESSIVE SHIELDING TECHNOLOGY PROGRAM Mr. Bruce Jezek, Edgewood Arsenal, MD	1865
LIST OF ATTENDEES	1907

THE PREDICTION OF THE REACTION OF AN EXPLOSIVE SYSTEM IN A FIRE ENVIRONMENT.

COATED RDX SYSTEMS FOR PRESSED EXPLOSIVES.

Carl M. Anderson and Jack M. Pakulak, Jr. Naval Weapons Center China Lake, California

# ABSTRACT

A means has been found to predict the behavior of an explosive in response to rapid heating as in a fire. The prediction is empirical and is limited at this time to coated RDX systems used for pressed explosives. The prediction is based upon the quality of the coating present on the RDX crystals. A complete, adherent coating is correlated with a mild reaction to rapid heating while a poor to non-existant coating is correlated with violent explosions and detonations.

Assessment of the quality of the coating is made by a scanning electron microscopic (SEM) examination of the interior surfaces of the molding powder. It is suggested that the SEM can be used to guide an explosive development program and as a quality control for explosives production.

The behavior of propellants and explosives in response to rapid heating as would be seen by munitions in a fire, is of major importance for the safety of personnel and equipment. The serious aircraft carrier accidents that produced a loss of hundreds of lives and extensive ship damage were the result of bombs detonating in aircraft fuel fires. These aircraft carrier events have lead to an extensive program of investigation to minimize the damage in future accidents by developing systems to reduce the severity of the response of propellants and explosives to rapid heating. Any useful prediction of this response would have an obvious application in the development and employment of these systems.

Previously, all of the predictions of munitions response to fire have been based on experience with a particular explosive system and on computer modeling of the heat transferred through the munition case into the explosive. There are a number of one and two dimensional computation procedures that have been worked out to describe the heat fluxes and to predict the temperatures produced in the explosive in a fire. In all of the computations, the exothermic decomposition of the explosive or propellant is treated as an additional heat source that leads to a run-away reaction when the chemical reaction kinetics are included. The time to reach the run-away reaction is predicted, but in no case is the violence of the reaction described. Most of the computations do agree with the experimental time-temperature data produced in a shell, bomb, or warhead in a fire. The run-away reaction of the explosive/propellant in the real world ranges from a mild burning or deflagration through explosions of varying violence to a true detonation. Detonations and explosions are to be avoided by whatever means can be found.

<sup>1</sup>Report of "Panel to Review Safety in Carrier Operations", presented to CNO by Admiral James S. Russell (Ret.) 16 Oct. 1967.

<sup>&</sup>lt;sup>2</sup>Lawrence Livermore Laboratory. Trump: A Computer Program for Transient and Steady-State Temperature Distributions in Multidimensional Systems, by Arthur L. Edwards, University of California/Livermore, California/94550, Sept. 1, 1972. (UCRL-14754, Rev. 3)

974

Detonations and explosions can be minimized for main-charge explosives by
the judicious use of external insulation and interior liners, especially liners
with an out-gassing system to pressurize and open the weapon case. Certain PBX
systems, such as PBXC-116/117 (I), using neither liner nor exterior coating, respond
to a fuel fire by opening the case and burning or deflagrating even under heavy
confinement. With main-charge reaction minization systems in place and functioning,
there have been occasions with all-up weapons in which a detonation occurred late
the main-charge burn-out. This effect was traced to the booster explosive's
having finally got warm enough to react violently. Upon investigation, it was
found that all of our currently available booster explosives react to heat by
detonating. The effort to find a cause and a remedy for this booster behavior,
the subject of this report, has lead to a means of predicting the response of
certain explosives to rapid heating.

Current booster explosives are either tetryl or RDX/wax systems. With the cessation of production of tetryl and the non-availability of Class A waxes, new, pressable explosive compositions are needed. Among the properties of any explosive system to be considered is safety, i.e., behavior in a fire environment, and sensitivity to inadvertent impact. In the search for a wax substitute, a co-polymer of ethylene and vinylacetate (EVA) was found to have properties approximating those of a Class A wax. At a concentration equivalent to Composition A-3, EVA/RDX did not explode when heated as in a fire, this in

<sup>3</sup>Naval Weapons Center. Techniques for use in Weapons to Reduce Hazards of Cook-Off. Part 1. Outgassing and Inhibiting Chemicals for Warhead Case Rupture, by Jack M. Pakulak, Jr., NWC, Chian Lake, CA, (in process), NWC TP 5243.

<sup>4</sup>Naval Weapons Center. Cook-Off Studies on the General Purpose Cast Explosives PBXC-116 and PBXC-117, by Carl M. Anderson and Jack M. Pakulak, Jr., NWC China Lake, CA, May 1976, NWC TP 5629.

<sup>5</sup>Pacific Missile Test Center. Fast Cook-Off Characteristics of Air Launched Inservice Weapons, by R. W. Slyker and P. McQuaide, Point Mugu, CA, 29 Dec. 1975, TP-75-22 (Rev. 1).

contrast to Composition A-3 which does explode. An examination of the surfaces of the explosive in the molding powders in the scanning electron microscope (SEM) showed that the EVA had formed a uniform, adherent coating on the RDX while the wax/RDX A-3 showed a coating of flakes of wax. Following this lead, other booster explosives were examined. All showed poor to non-existent coatings. With further experience, a correlation was observed between the quality of the coating and the behavior on rapid heating. This empirical correlation was then extended to the successful prediction of the kind of reaction produced in a fire environment.

This prediction of thermal response is the first successful prediction of DDT that has been accomplished. The prediction is empirical and is limited to RDX/coating systems at this time, but does represent a major break-through in explosives technology. SEM pictures of the molding powder can be used for a quality control procedure and for guidance in the development of new, safe, explosive systems for pressed main charges and booster explosives. The extension of this prediction technique to castable systems appears feasable and will be further investigated.

## PROGRAM GOAL

One goal of this and other programs in the area of explosives development is defined by Mil. Std. 1648<sup>6</sup> which describes the reactions that occur in munitions in a fire. The standard requires that all Navy munitions shall not react at all before five minutes in a fire and that the reaction, at no time, will be more than a deflagration. A mild explosion, throwing pieces no more than fifteen meters (50 ft.), is acceptable. Booster and main charge explosives are included in this requirement. It is considered possible that a violent explosion in a booster assembly with a small shock-wave, but with many hot, high velocity fragments, could initiate the main charge.

EXPERIMENTAL

The scanning electron microscope, SEM, was used to obtain pictures of

<sup>6</sup>Military Standard 1648 (AS), 28 March 1974.

the interior surfaces of the coated explosive molding powder. The SEM was used because its unusual depth of focus allows an investigation of irregular surfaces oriented at various angles and depths. Eight to sixteen photographs were made at various magnifications of two or more areas on the interior surfaces of broken molding powder pellets of each sample. All of the SEM pictures used in this report were produced by Rowland McNeil, NWC, Code 5515, on the various instruments in this region. The techniques of sample preparation, instrument operation, and selection of areas to photograph are given in TP-5897 by R. A. McNeil.

The assessment of the quality of the coating was made on a purely empirical basis looking for such things as bare, uncoated crystals of explosive, sharp edges, non-adherent, crumbly or even crystalline coating material, etc. The choice of areas to photograph in the SEM was made on these same criteria. A scale of four was used to assign a value to the assessment ranging from 1 for a poor to non-existent coating to 4 for a complete, adherent coating.

The small-scale cook-off bomb (SCB) test was used to determine the response of the explosives to a fire environment. The test was devised as a small-scale test to reproduce the heating effects seen by an explosive or propellant in bombs, munitions, and missiles in an aircraft fuel fire. Heating rates can be reproduced in the SCB as high as three degrees Centigrade per second that can be seen by a thermally unprotected bomb to as low as 0.2°C/second as seen by a booster explosive deep inside the main charge in a large warhead. Ten years of experience and hundreds of tests run in the SCB have amply confirmed the direct correlation of the SCB results with the response of explosives and propellants in munitions.

The SCB fixture, Figures 1 and 2, consists of a stainless steel vessel,
6.35 cm inside diameter and 12.7 cm long, with 3 mm walls. The container is
fitted with a 10 ohm Nichrome ribbon heater wound on a mica insulator and covered

<sup>7</sup> Naval Weapons Center. Fast Cook-Off Studies on Explosives, by Jack M. Pakulak, Jr., NWC, China Lake, CA. Memo. Reg. 4532-30, of 26 March 1968.

with thermal insulation. A plate-type thermocouple, Figure 3, is spot-welded to the center of the inside wall. The mild steel cover contains a Neoprene or Teflon gasket seal, feed-throughs for the interior thermocouples, and a pressure take-off. The 10 cm square, 1,27 cm thick steel plates at top and bottom, the top plate has two 2 cm holes to accommodate the cover attachments, serve both as a clamp to hold the vessel together and as witness plates to help define the reaction that occurs.

### SCB PROCEDURE

The prepared SCB unit, heater wound and insulated and wall thermocouple installed, is loaded with about 1 kilogram of explosive by direct casting or by insertion of a pressed and machined billet as appropriate. If a liner is required, the liner is formed in place using a mandrel of the proper size for the thickness needed: a second plate-type thermocouple is placed in the explosive-liner interface. After carefully attaching, and isolating, the interior thermocouple leads to the feed-throughs, the unit is assembled. The cap is firmly screwed down onto the gasket, the thermocouple leads checked for continuity and short circuits, the unit clamped between the top and bottom plates, and the pressure tubing installed. The firing bay at NWC for this size of charge, about 1 kilogram, is a 1.5 meter diameter armour steel cylinder 3 meters long with 9 cm walls. The cylinder, lying horizontal, is closed at one end with a concrete and earth backed, sheet piling wall. During a test, the open end is blocked with sandbags. (A detonation reaction inside will move the sandbags as much as 5 meters.) Thermocouple and pressure transducer outputs are recorded on fast pen-drag recorders. The heating rate is controlled with a Honeywell recorder-controller to produce the desired rate. After a final check, the heater circuit is opened and the test started. Heating is continued until a reaction occurs.

After a reaction has occurred, the fragments of the SCB are collected, examined, and photographed to assess and record the kind of reaction that had

taken place. The milivolt-time records are reduced to time-temperature and timepressure and plotted. A typical plot of the reduced data is shown in Figure 4.

RESULTS

Four levels of reaction intensity are definable by the number and condition of the SCB fragments collected after the reaction. The first level is a detonation resulting in many stressed fragments, often discolored by heat and deformed by collisions with the firing bay walls, and a dented, often punctured, base plate. A violent explosion at the next identifiable level of reaction results in a number of stressed fragments distorted by high velocity collisions with the walls of the firing bay as in a detonation but with little or no deformation of the base plate. The next level, a mild explosion, results in a few large fragments ejected and no deformation of the base plate. The mildest reaction, a deflagration, results in the SCB split open with no fragments thrown out. The noise, the dust cloud, and the conditions in the firing bay produced by the reaction are useful indicators of the reaction violence, but the size and shape of the fragments and the condition of the witness plates are the defining elements in the description of the reaction that occurred.

All of the experiments run for this study are listed in Table I. In the table, the various runs on a single explosive are listed as a group while the SCB number gives the actual sequence in which the tests were run. As indicated in Table I, predictions were made, for all runs after SCB 148, for the violence of the reaction that would occur. The predictions were made from an assessment of the coating on the explosive from the SEM pictures of the molding powder. It is of interest to note the SEM photographs of the broken surfaces of pressed explosive pellets lack any real character and do not provide enough information for a useful assessment or prediction. In fact, there is surprisingly little migration of the coating material even in hot pressing.

The photographs of explosive surfaces and the corresponding SCB fragments included in this report are representative of the many that were made in the

TABLE I
CORRELATION OF SURFACE COATING WITH REACTION
VIOLENCE ON RAPID HEATING IN THE SCB

SCB No.	Figure No.	Sample	Coating Quality1	Heating Rate OC/Sec3	Time to Reaction Min/Sec	Reaction <sup>2</sup>
107	5	A-3, RDX/Wax,	3		1/33	Explosion I
107	and distance	A-3	3	0.22	6/44	Explosion I
143		A-3	3	0.52	6/45	Detonation
148		A-3	3	0.10	31/19	Explosion II
147		A-5, RDX/Wax,	1	0.10	1/19	Detonation
144	6	A-5, KDA/WAX,	î	0.23	14/1	Detonation
145			î	0.23	1/26	Detonation
108	7	CH-6	i	0.21	12/56	Detonation
146	•	CH-6. RDX/EVA, A-3 (C6H6)	Ã	0.21	1/33	Deflagration
106	8		3		1/37	Explosion I
151	9	RDX/EVA, A-3 (THF) PBXC-13, (THF), HS-51353		0.5	8/32	*Detonation
178				0.2	31/32	*Explosion II
179		PBXC-13, (THF), HS-51353	2	0.2	1/29	Explosion I
123	10	RDX/EVA, 95/5 (C6H6)	2	0.2	15/15	Explosion I
128		RDX/EVÀ, 95/5 (C6H6)		0.2	1/28	Explosion II
134		RDX/EVA, 95/5 (THF)	2 2		1/28	Detonation
135		RDX/EVA, 95/5 (THF)				
149	146.00	RDX/EVA, 95/5 (THF)	3		1/37	*Explosion II
150	11	RDX/EVA, 95/5 (THF)	2		1/38	Explosion II
122	12	RDX/EVA, $A-5$ (C6H6)	3		1/31	Explosion II
162		RDX/EHA-VP, A-3	3		1/24	*Explosion I
137		RDX/EHA-VP, 95/5	2		1/19	Detonation
136		RDX/EHA-VP, 95/5	2		1/26	Explosion II
163		RDX/EHA-VP, 95/5	2		1/37	Detonation
138		HMX/EHA-VP, 95/5	1		2/00	Explosion II
139		HMX/EHA-VP, 95/5	1		1/26	Explosion I
140		HMX/EHA-VP, 95/5	1	0.21	16/47	Detonation
164	14	RDX/Estane, 95/5	3		1/37	Explosion I
165		RDX/Estane, 95/5	3	0.2	14/38	*Detonation
182	13	Comp A/PE, NSWC	2		1/54	Explosion II
183		Comp A/PE, NSWC	2	0.2	18/38	*Detonation

\*Predicted from quality of surface coating.

NOTES: 1. Coating quality on a 4-point scale, 1, poor to 4, excellent.

 SCB Cook-off reaction on a 4-point scale, of Detonation, Explosion II, Explosion I, and Deflagration.

 Unless a figure is entered, the heating rate was between 2.5 - 3.0 °C per second. course of this study. With eight to sixteen or more scanning electron photomicrographs made for each sample at various locations and magnifications, the quality of the coating is relatively easy to assess but the selection of examples for this report was difficult.

Composition A-3 is a current G. P. bomb main charge booster explosive that is also used in certain shells. Figure 5a, one of the early SEM scans, shows the wax to be present on the surfaces of the molding powder as flakes. The internal surfaces were not examined. This fairly good wax coating correlates with a mild explosion as shown in Figure 5b.

Composition A-5 is a current fuze-booster explosive used principally for Army applications. At this low additive level, any continuous coating would be difficult to obtain so that Figure 6a shows many bare crystals with occasional flakes of wax. The detonation of SCB 144, Figure 6b, was the result obtained on rapid heating.

Explosive CH-6 is a current Navy fuze-booster used in many warheads, and bombs. Again, at a low additive level, any complete coating of the RDX crystals would be difficult. Figure 7a, shows a fair external coating but the interior shows the additive mixture as discrete flakes and crystals. The result obtained in the SCB fast cook-off was a detonation, Figure 7b.

The preparation of RDX/EVA, as a Comp. A-3 substitute was the initiation point of this study. The very mild deflagration, Figure 8b, of this material relative to Comp. A-3, and its other properties of a reasonable sensitivity with a good abrasion resistance, lead to the investigation of why or how. The SEM, Figure 8a, pictures showed a good coating all over the molding powder particles. This was the first indication that surfaces might be involved in the reaction in response to rapid heating.

Figure 9a, is a scanning electron Licrograph of an RDX/EVA Comp A-3 analogue prepared using a different solvent system. As can be seen in the figure, when

tetrahydrofuran (THF) was substituted for the benzene of the previous preparation, the coating material was not attached to the crystal surfaces. The bare crystals in, and unattached to, a matrix of EVA, a grade 3 or less coating, led to the prediction of a fairly strong explosion, Figure 9b.

Figures 10 and 11 are a pair of RDX/EVA preparations using the same two solvent systems at the 95/5 level. A complete coating at this level is difficult but the difference in adherence of the EVA to the RDX between the two is apparent. This difference shows in the SCB fragments produced, in that Figure 11b from the THF preparation, shows the more violent reaction. Another THF preparation of 95/5 RDX/EVA detonated, SCB 135, Table I.

RDX/EVA, prepared as a substitute for Composition A-5 from a benzene solution of EVA, showed a reaction of the same order of violence as Comp. A-5. A comparison of Figure 12, RDX/EVA, A-5 and Figure 6, Comp. A-5 RDX/Wax, shows that the EVA holds the RDX together in pellets while the wax flakes do not. This difference may account for the lesser violence of the explosion of the RDX/EVA relative to the detonation of A-5.

The electron photo micrographs and SCB results with Comp. A/PE, are given in Figure 13. Comp. A/PE was prepared by NSWC, White Oak, as a replacement for Comp. A-3, using polyethylene to coat the RDX crystals. Figure 13a shows the coating to be porous and discontinuous which led to the prediction of the explosion of considerable violence obtained, Figure 13b. The discontinuous nature of the coating is evident in the many exceedingly bright areas in the photomicrographs that are the result of the rapid changing of the surfaces in the scanning electron beam.

Figure 14 of RDX/Estane 5703, 95/5, is to be compared with Figure 10, a comparable RDX/EVA. Estane 5703 has been identified simply as a urethane crosslinked binder for explosive use. The coating appears to be fairly good but not particularly adherent to itself or to the larger RDX crystals. The SCB result was a medium violent explosion considerably stronger than the comparable RDX/EVA, Figure 10b.

In all of the above systems, extending the time to reaction with a lower heating rate produced an SCB result one or two orders more violent than the fast heating rate. Thus a system that simply exploded on fast heating, 70 to 100 seconds, usually detonated when 6 to 20 minutes were used to reach the runaway reaction temperature.

### DISCUSSION

The four-point assignment of coating quality cannot be too discriminatory since the entire range of a poor or no coating (1) to a complete, adherent coating (4) is so broad. The assessment of the coating quality depends upon the skill of the SEM operator in choosing the areas to photograph and the judgement of the project chemist in making the quality assignment. Also, the definition of the SCB reaction is somewhat subjective in the middle, explosion regions. The least and most violent reactions, deflagration and detonation, are easily defined as the one or two piece remainder of the deflagration and the dented or punched base plate of the detonation. Explosions cover the entire range of fragmentation between these extremes and are arbitrarily divided into two classes, Explosion I, mild, and Explosion II, violent, depending primarily on the number (size) and condition of the fragments with no clear dividing line between them. Correlation of the quality of the coating and the SCB reaction is well illustrated in Table I and the figures chosen to illustrate typical effects. The twenty examples, SCB numbers less than 149, with 10 materials, established a correlation which was then used to predict correctly the reactions obtained in all of the eleven subsequent tests.

The validity of the small-scale bomb test has been thoroughly demonstrated by correlation with fuel fire tests on warheads, bombs, etc., dating from the conception of the test in 1967 and the establishment of the SCB in its current form as a routine test in 1971. The SCB numbers date from the inception of a test register in September of 1971. The correlation of the SCB, at about 1 kilogram of explosive, with the subsequent behavior of larger munitions such as

bombs, warheads, shells and mines, has been excellent. Thus single, or two-sample, tests can be used with considerable confidence. A detonation in the SCB indicates an unsafe material and a pratical certainty of a disastrous reaction in a weapon. A deflagration in the SCB does not preclude the chance of a detonation in a heavily cased weapon, but does indicate a good probability of a reasonably mild reaction.

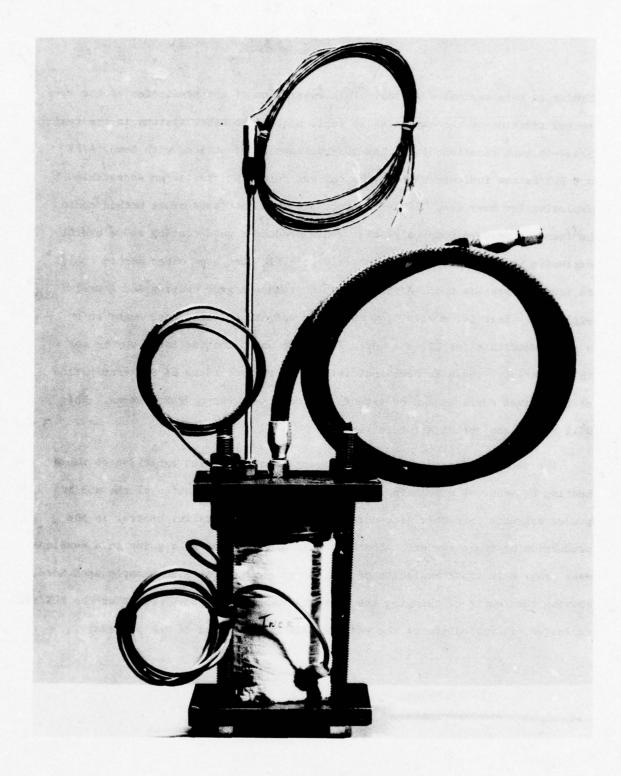
The predictions were made on a purely empirical basis of the appearance of the coating on the surface of the RDX crystals. From this and other studies, there is some indication that a partial solubility, or at least a softening of the RDX surface, promotes the formation of an adherent coating. Figures 8 and 9 are SEM photomicrographs of two RDX/EVA preparations. One, Figure 8, was prepared by adding a benzene-ethyl acetate solution of the EVA polymer to slurry of RDX in water containing some ethyl acetate. The other, Figure 9, was prepared by adding a solution of EVA in tetrahydrofuran (THF) to a water slurry of RDX.

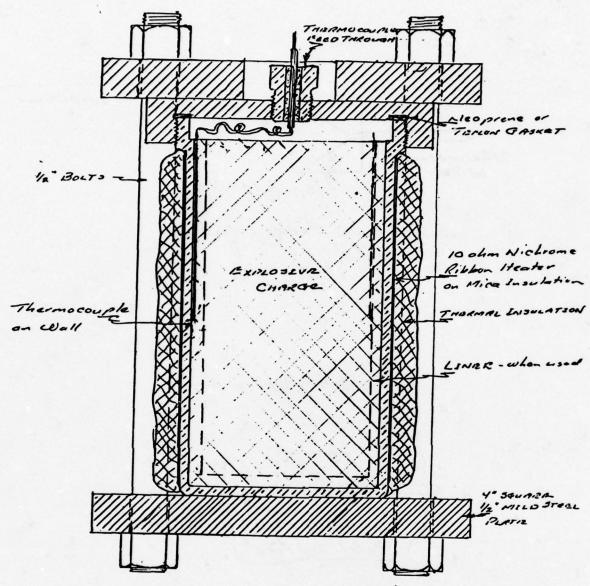
The principal difference between these preparations is the fact that THF is very soluble in water while benzene is but slightly soluble. This difference in solubility could control the rate at which the EVA is precipitated such that with THF, the EVA is rapidly thrown out into the suspension and eventually collects on the RDX producing the non-adherent coating shown in Figure 9a. The corresponding SCB test results, Figures 8b and 9b clearly show the difference produced by this change in technique of preparation.

Included in this series of SEM surface evaluations and SCB tests are two other coating systems that were submitted for SCB tests during the RDX/EVA study. Figures 13a and 13b show the coating and the SCB results with Comp A/PE, a proposed substitute for Comp. A-3 prepared by NSWS, White Oak. Comp A/PE is a polyethylene coated RDX. The coating appears to be granular, porous, and non-adherent and a violent SCB reaction was obtained as predicted. The other system, RDX/Estane 5703, 95/5 shows a fair coating, Figure 14a, and the predicted explosion in the SCB test, Figure 14b. Estane 5703 was listed simply as a crosslinked rubber

binder in this explosive system. This externsion of the prediction of the expected reaction of the explosive to rapid heating to other systems is the real break-through reported here. The observations and reactions with Comp. A/PE and RDX/Estane indicate that in the current forms, neither is an acceptable explosive for Navy use. It is entirely possible that some other method could be found to prepare Comp. A/PE that would produce a good coating and a useful explosive for Navy use. It is entirely possible that some other method could be found to prepare Comp. A/PE that would produce a good coating and a useful explosive. That is, a waxy, low molecular weight, polyethylene, ought to be a good substitute for Class A wax. It may be worth looking for a way to use this material. There is some indication that the procedure of SEM examination of explosives surfaces can be extended to cast main charge PBX systems. This will be the subject of a future report.

The successful prediction of the reaction of a pressed explosive to rapid heating by means of a scanning electron microscopic examination of the molding powder suggests that this procedure could be used for quality control in the production of these systems. The SEM could also be used as a guide in a development program in the formulation of new, safer explosives. The example used here, showing the result of changing the solvent system in the development of the RDX/EVA explosive, is indicative of the guidance and QC potential of the procedure.





CROSS- SACTION SHETCH on SCB Scale . Full size

Figure 2

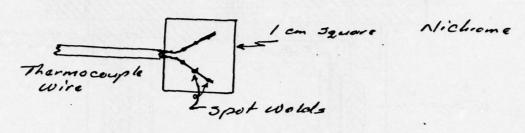


PLATE-TYPIL THERMIOCOUPLIE

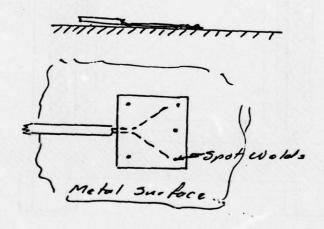
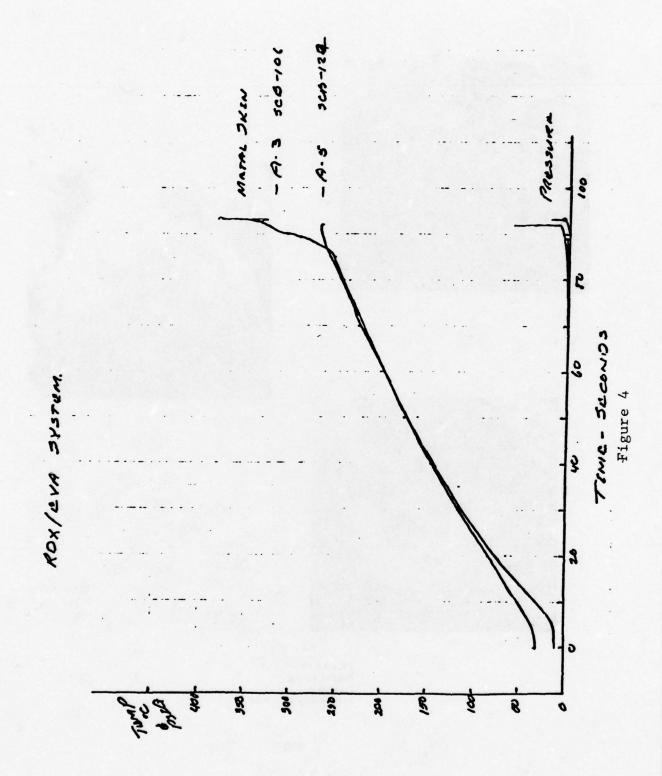
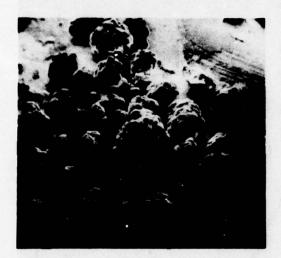


PLATE-TYPE THERMOCOUPLE

Figure 3





18X



72X

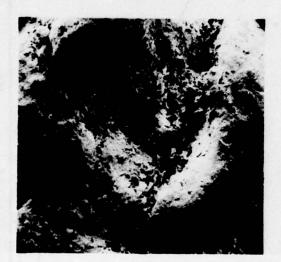


FIGURE 5A Molding Powder Comp A-3 Note: Originals 9 × 9 cm.



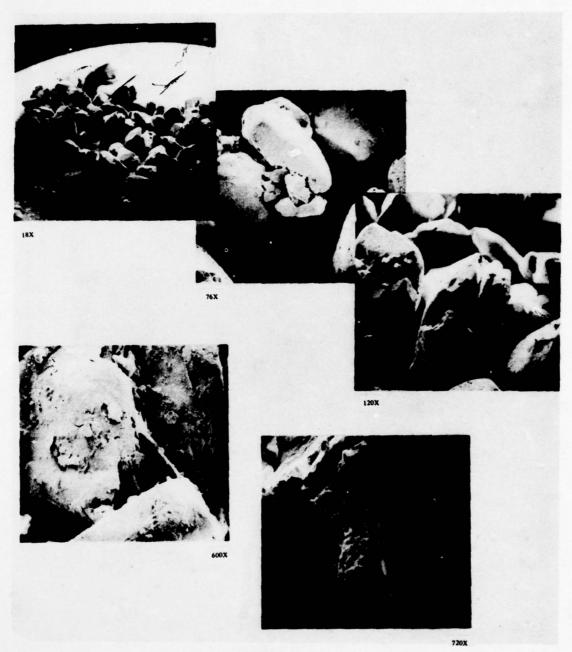


FIGURE 6A Molding Powder Comp A-5 Note: Originals 9 × 9 cm.

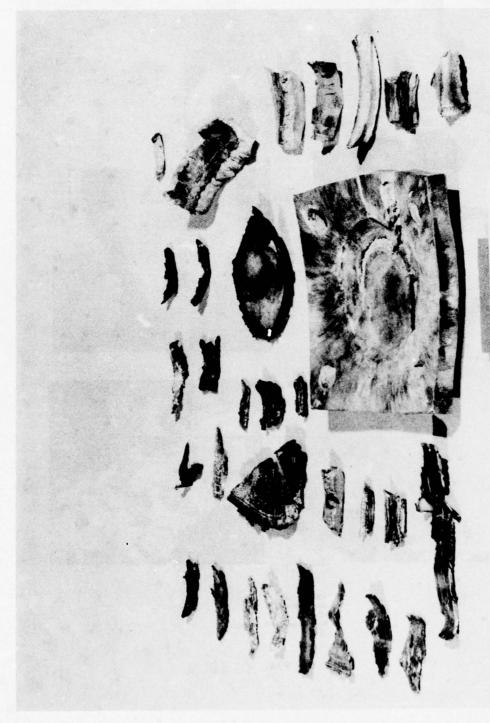


FIG. 6b. Result of Fast Cook-off of SCB Containing Comp A-5 Explosive. SCB-144 (LHL 188344)

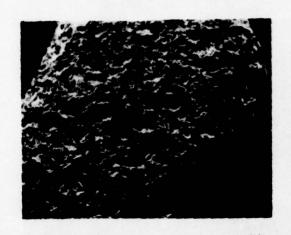


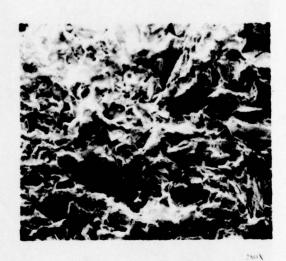
ıĸx

FIGURE 7A Molding Powder CH-6 Note: Originals 9 x 10 cm.

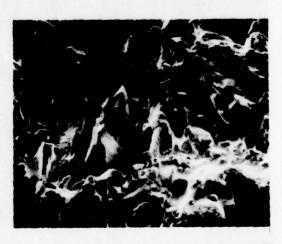


FIG. 7b. Result of Fast Cook-off of SCB Containing CH-6 Explosive. SCB-108 (LHL 184537)









HGCRI 8A Molding Powder Section RDX IVA, A-3 (C<sub>6</sub>H<sub>6</sub>) Note Originals 8 × 9 cm.

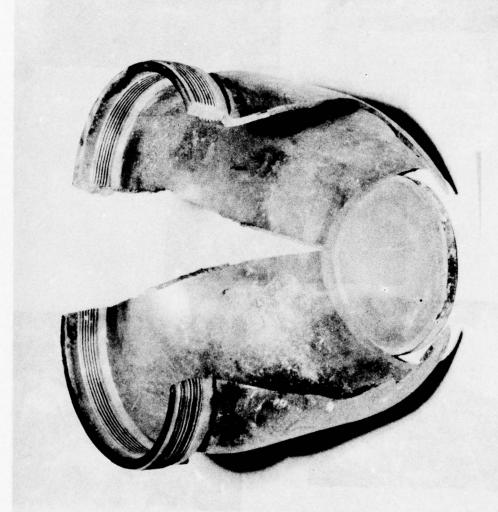


FIG. 8b. Result of Fast Cook-off of SCB Containing RDX/EVA, A-3 (C<sub>6</sub>H<sub>6</sub>) Explosive. SCB-106 (LHL 184533)



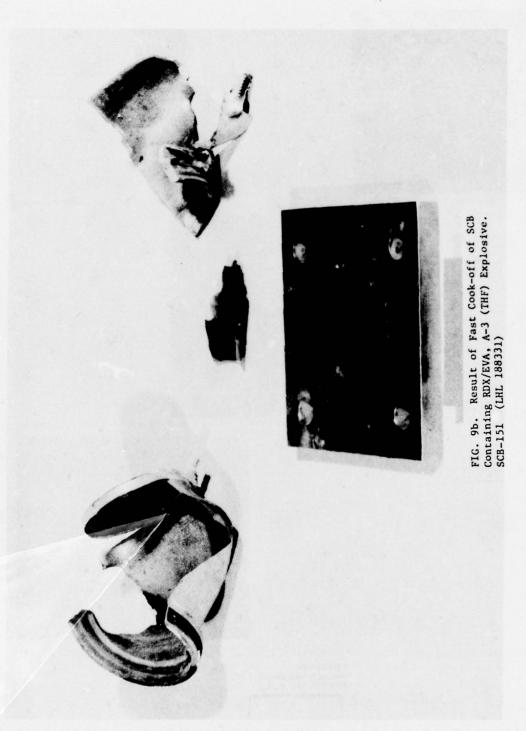








FIGURE 9A Molding Powder Section RDX/EVA, A-3 (THE) Note: Originals 9 × 10 cm.





Sox

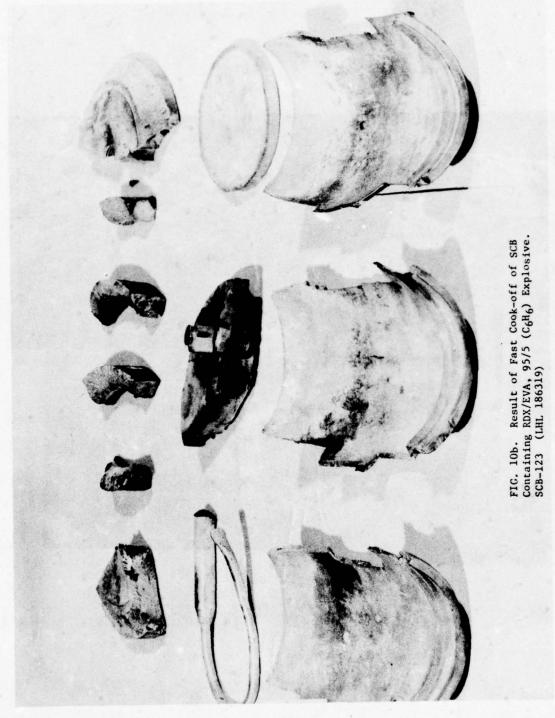


200X



5003

FIGURE 10A
Molding Powder Section
RDX/EVA 95/5 (C<sub>6</sub>H<sub>6</sub>)
Note: Originals 9 × 10 cm.



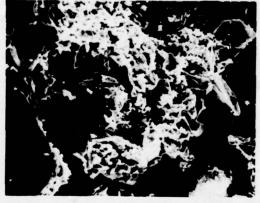


Molding Powder Section RDX LVA (48.8 (HH ) Note: Originals 9 × 10 cm.

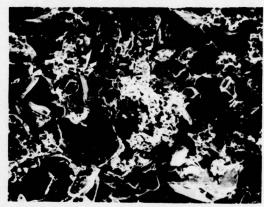








500X



2003

FIGURE 12A Molding Powder Section RDX/EVA A-5 Note: Originals 8 × 9 cm.

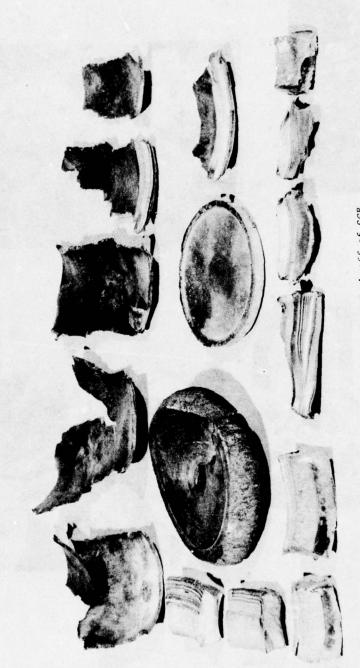


FIG. 12.b. Result of Fast Cook-off of SCB Containing RDX/EVA, A-5 ( $G_6H_6$ ) Explosive. SCB-122 (LHL 186320)



20X



1003



200¥



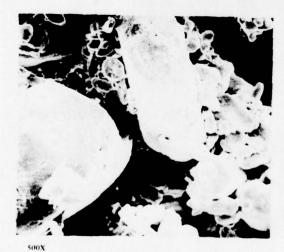
200X

FIGURE 13A Molding Powder Section Comp A/PE. Note: Originals 9 × 10 cm.



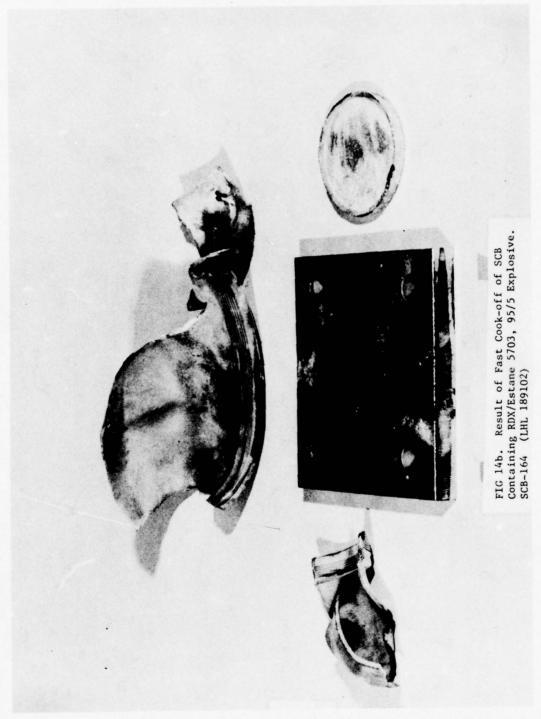


200X



200X

FIGURE 14A Molding Powder Section RDX/ESTANE 5703 95/5 Note: Originals 9 × 10 cm.



#### MISSILE SYSTEMS PROPULSION COOK-OFF

R. F. Vetter Naval Weapons Center China Lake, CA

Aircraft carrier ordnance and missiles (both on and off aircraft) are subject to fuel fire at a significant level of occurrence. The hazard level to life and property is high and should be reduced. Some effort at the Naval Weapons Center in this direction has been funded by NAVAIRSYSCOM exploratory development dollars.

The testing immediately following the Forrestal incident gave a baseline time to "reaction" of about one minute for rocket motors tested individually with pressure vessel rupture being the typical result. Externally insulated Phoenix did withstand heating for a longer time but was perhaps more violent at reaction. The Mk 78 Mod 0 boost-sustain Shrike deflagrated mildly in the tests at Dahlgren and later tests at NWC. A large part of our effort has been to elucidate the mechanisms of failure and especially to understand why mild-burning-reaction occurred with one configuration.

The failure "map" depicted in Figure 1 was deduced. A wide variety of laboratory scale liner/case samples were tested over a flame to observe gross characteristics. Initial attempts with propellant in the "sandwich" showed a great deal of liner and bond failure before the propellant was warmed much. The rather low temperature unbonding and clean release of polyether-based polyurethane liners compared to sticky foaming with most other tactical missile case bonding formulations was postulated to be the cause of mild deflagration observed. Figure 2 became a failure mode goal which was to be proven and improved such that least violence occurred in cook-off. Numerous missile system propulsion sections were approximated except for different liner and insulation materials, configurations, etc.

Four candidate configurations of Agile propulsion were prepared using our suggestions and many thermocouples were installed which provided excellent data. Figure 3 is a post-test view of the least violent steel case tactical rocket motor cook-off test. No pop or case rupture noise was heard and the propellant burned without generating significant pressure even when the bore ignited. The steel case softened while the liner "bladder" and gas layer insulated the propellant. Essentially no pressure was contained when ignition occurred. Thus, the grain was not deformed as occurs when the pressure vessel remains (partially, at least) intact at the moment of propellant ignition.

Pressure rise rate is important and is determined by a number of factors including:

- whether the bore is ignited (this is worst situation and must be avoided)
- quantity of material reaching (auto)ignition temperature
- temperature gradient in propellant contiguous to the initially igniting propellant
- volume of gas "pocket"
- pressure of gas "pocket"

This latter is a function of gas flow dynamics as failure of the pressure vessel is approached and occurs. Gas generation by the pressure sensitive burning of the propellant is also a major factor.

The intrinsic burning rate of the propellant is most favorable if low in magnitude. A low pressure exponent will mean lower pressure rise rate and improved potential that the pressure vessel failure will be of low violence.

Model motors were devised and tested over an array of propane/air burners during the past year since visible results were nearly negligible in the JP-5 fuel fires and it was also recognized that the capability of extinguishing the fire at will might provide much more valuable post-test evidence. A movie shows a portion of these test results quite well.

To summarize: the use of external insulation is not recommended for aerodynamics, weight, and cost reasons but primarily because it leaves the pressure vessel at near full strength when reaction occurs; the use of normal construction with inclusion of a polyether polyurethane liner and a bladder above this with special concern that fore and aft sealing of the bladder is accomplished will often yield mild burning in a cook-off fire; best practice is to include a segment or an entire case wall of plastic bonded filament, tape, or laminate which disintegrates in fire.

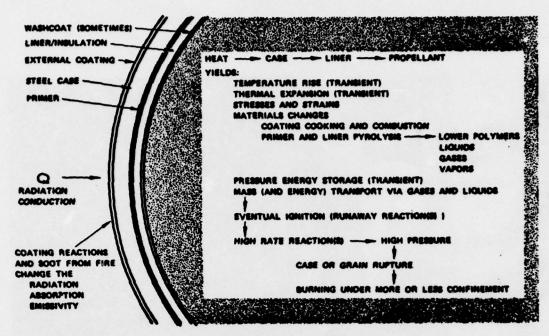


Fig. 1. Sequence of Cookoff Process.

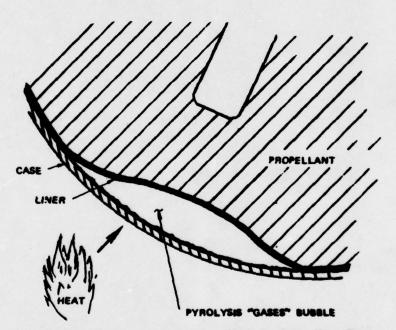
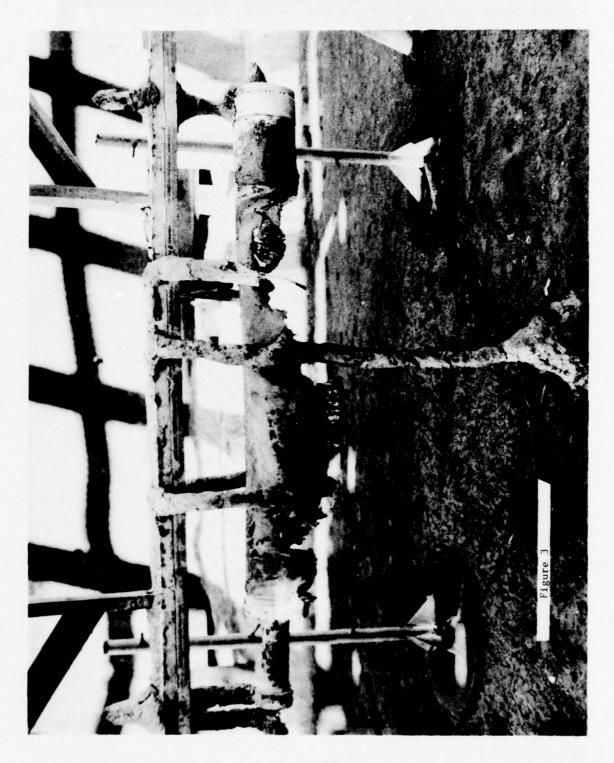


Fig. 2. Cross Section of Case After Pyrolysis Gases Have Been Generated From the Case Primer and a Part of the Liner. Note that the pyrolysis gases bubble forms on the bottom part of the case in a fire and that clean separation is typical of liner which does not form an adhesive char. The hotter surface of the liner will be liquidus (melting) and a boiling heat transfer exists for a time on the inner wall of the case into the bubble.



G. Gürke

Ernst-Mach-Institut der Fraunhofer Gesellschaft Freiburg - FRG

Quantity Distances for Underground Storage of Ammunition and Explosives in Depots: The German Two Chamber Storage Site with a Block Closing Device

The construction of underground storage sites for ammunition and explosives is projected in the Federal Republic of Germany, as shown in Fig. 1. Two storage chambers are planned, each of which having a volume of max. 4 000 m<sup>3</sup> and quantity of explosives of max. 750 000 kg and consequently the whole storage site 300 000 kg. In the main passage-way there should at least be two constrictions to reduce the intensity of blast. A blast door may be used to protect the contents of the site from a blast-wave originated outside. It is supposed that the depots are built into hills with sufficient cover of solid rock to contain the effects of a detonation inside the storage site, as shown in Fig. 2. Then the surroundings are endangered in the case of an accidental explosion by a ground shock that extends circularly around the storage chambers and by blast and debris ejecting through the exit.

It is not possible to establish safety standards for quantity distance tables concerning each underground storage of ammunition and explosives in depots due to the great number of variables involved. Among these are the terrain features (type of rock, thickness of cover), the layout of sites (cavern, single- or connected storage site) and additional protective measures (blast doors, blast traps, block devices). Also the type of ammunition as well as the loading density require individual analysis of the hazards involved.

For more than ten years in Europe large scale tests and model tests are done in order to find out principles for safety standards. The blast wave escaping from the entrance frequently causes the farthest reaching hazards. It was found out that by model tests the blast wave propagation can be well simulated except airblast attenuation in rough-walled tunnel systems.

The blast wave propagation in the two-chamber storage site and in the surroundings in front of the tunnel entrance is investigated by the Ernst-Mach-Institut at model scale 1: 47. Fig. 3 shows the model made from steel tube on the test site.

For the example of 100 000 kg net explosive quantity, Fig. 4 shows as a plan view the distance of the 50 mbar isobars in the surrounding for a detonation inside the two-chamber storage site in comparison with a surface burst. The 50 mbar isobar is ordered by safety standards in the FRG as inhabited building distance. At surfacebursts the blast wave spreads out hemispherically and consequently circularly above the plain surface. The quantity distance is measured from the center point of the source, it amounts to 1040 m for 100 000 kg NEQ. If the same quantity of explosives detonates in the underground storage site, the blast wave escapes from the tunnel entrance and spreads out very asymmetrically with main direction to the extended tunnel center line, colled 00-direction. The blast distance is not measured from the source but from the tunnel entrance. In large scale and model tests it was found out that the isobars are not situated circularly around the tunnel entrance but their distance depends strongly on the angle to the extended tunnel center line. As a result of the tests the protective area is devided into 5 zones with decreasing distance against the 0°-direction. To determine the distances, fixed factors are used. The distance in  $0^{\circ}$ -direction is D1 = 800 m at the example of 100 000 kg NEQ.

At underground storage also a ground shock must be considered. By German Safety Standards (draft ZDv 34/250) the ground shock

distance for buildings on rock amounts to a radius of 300 meters for the explosive quantity of 100 000 kg in a chamber. It is measured circularly from the center of the storage chamber.

As shown in Fig. 4 the required blast distance is much greater than the ground shock distance.

Fig. 5 shows the 50 mbar isobar distance as a function of the quantity of explosives as it was measured at model tests for the two-chamber storage site. At  $P = 150\ 000\ kg$ , the maximum explosive quantity in a chamber, the blast-distance of 1 000 meters is reached.

A quantity distance of 1 000 meters outside the tunnel entrance is too wide considering the dense population of the Federal Republic of Germany with its numerous traffic routes; it considerably restricts the possibilities to build underground storage sites because of floor space and cost requirements. Therefore efforts are made to diminish the blast and debris hazards by protective measures in such a way, that the ground shock distance is not exceeded.

The blast distance can be diminished by installation of a movable concrete block used as a closing device. In Fig. 6 a facility is shown with a closing device in the main passage way of the two-chamber storage site. The reinforced concrete block shuts the main passage way, the whole traffic has to drive through the bypass. In case of an accidental explosion the high chamber pressure of about 125 bar pushes the block 6 meters ahead, whereby the bypass is also closed. When the block is collected in the support, the underground storage is completely closed within about 0.15 seconds at 150 000 kg NEQ in a storage chamber.

The effectiveness of this device is shown in Fig. 7 in which the distance of the 50 mbar isobar is again demonstrated as a function of the quantity of explosives. At small quantities up to about

 $P=40.000~{\rm kg}$  in a storage chamber, the block closes the bypass relatively slow, it works as a blast trap and part of the overpressure can escape. The quantity distance is diminished by the factor  $0.6~{\rm compared}$  with the storage site without block closing device. At higher loading densities the block closes faster, the device gets more effective so that at  $P=150.000~{\rm kg}$  NEQ practically no blast wave gets outside. The block has closed now before the shock front has passed the bypass.

Moreover Fig. 7 shows that for a fixed quantity of explosives the 50 mbar isobar is at a surface burst always in a greater circular distance than in front of the two-chamber storage site. By the block closing device in the main passage way the blast wave is attenuated in such a way, that at large quantities the ground shock distance outside the tunnel entrance is no more exceeded.

This result for the explosive quantity of P = 100.000 kg is demonstrated in Fig. 8. Like in Fig. 4 the blast distance of the surface detonation and the ground shock distance are drawn as circles. The distance of the 50 mbar isobar for the underground storage site with block closing device fits to the ground shock distance in direction of the extended tunnel axis.

As result of the model tests at the two-chamber storage site we can describe the peak overpressure in front of the tunnel in  $0^{\circ}$ -direction D1 in relation to a scaled distance K as it is usually done for surface bursts. Fig. 9 shows that the scaling should not occur with  $P^{-1/3}$  like at the surface bursts, but with  $P^{-0.61}$ . The pressure-distance relation in Fig. 9 is drawn for the far field, where peak overpressure is smaller than 300 mbars. This graph enables to set up quantity distance tables for the two-chamber storage site. Net explosive quantity is used to calculate distance by means of formulae of the type D1 =  $K \cdot P^{0.61}$ , where D1 is the distance in meters and P is the net explosive quantity

in kilograms. Similar to the surface burst K is a factor depending on the risk assumed or permitted. For example we have to calculate the distance of the 50 mbar-isobar with D1 =  $0.72 \cdot p^{0.61}$ .

Model tests with TNT and Comp.B as explosives are made. Although Comp.B produces considerably higher peak overpressures in the tunnel system the effect in the surroundings was found to be the same with both explosives. It does not seem to be necessary to use a loading equivalent for fixing the quantity distance.

For the hazards in the quantity distance not only the peak overpressure of the blast wave is important but also the blast impulse as long as it does not exceed a certain amount. Fig. 10 shows that the blast impulse at the 50 mbar-isobar in front of the underground storage is exceptionally reduced and is much smaller compared with a surface detonation. The damage of buildings in the 50 mbar blast distance is consequently lower than at a surface detonation.

Especially by former investigations of the Norwegian Defence Construction Service and the Ernst-Mach-Institut it could be shown that the model tests give reliable results about the expansion of blast in the surroundings. In May 73 a prototype test with a block closing device called "Operation Block" was made in Sweden. It gave the result that a block and a support can be built from reinforced concrete, being able to resist the effect of a detonation in an underground depot. Consequently it can be stated that by a block closing device it is possible to reduce the quantity area around an underground ammunition storage (with sufficient cover) to the ground shock distance.

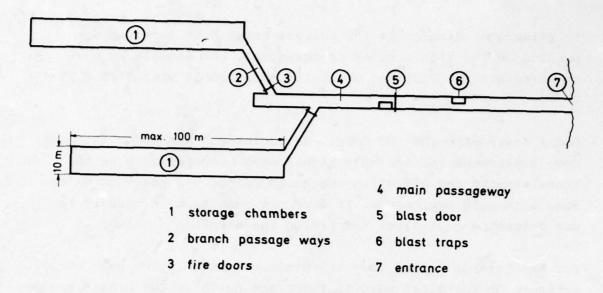


Figure 1 Two chamber storage site

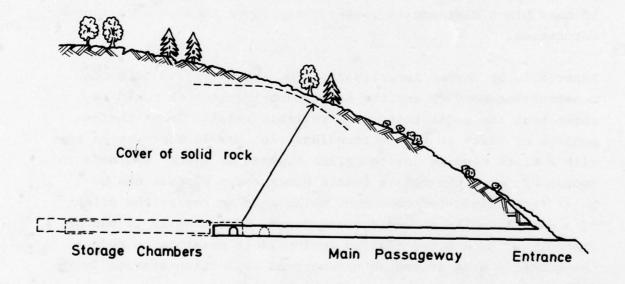


Figure 2 Cover for facilities built into hills

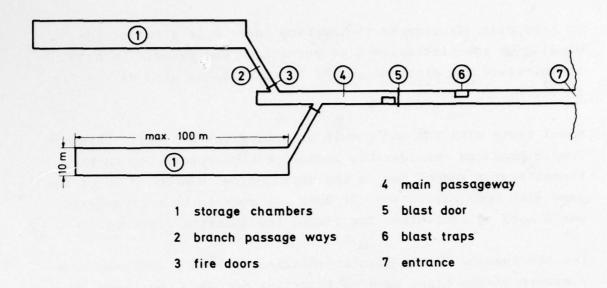


Figure 1 Two chamber storage site

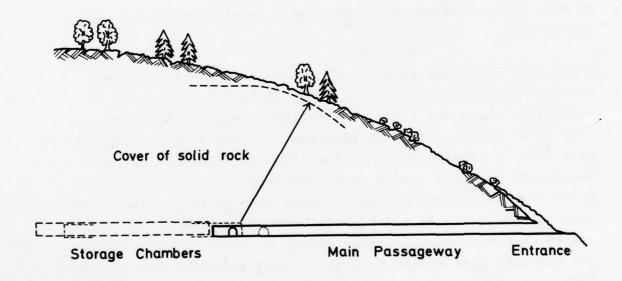


Figure 2 Cover for facilities built into hills

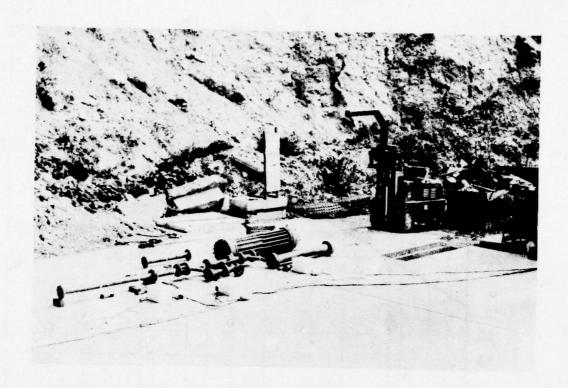


Figure 3 Ernst-Mach-Institut model test

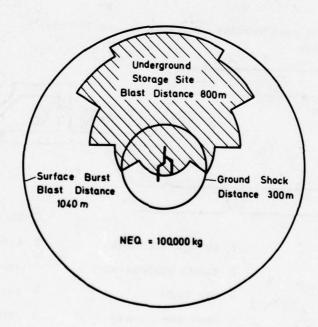


Figure 4 Planview. Blast and ground shock distances

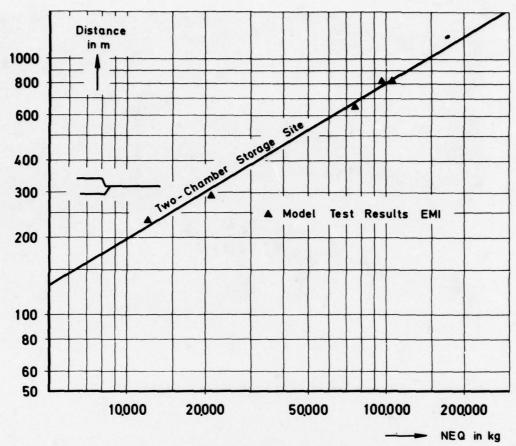


Figure 5 Model test results. Distance of the 50 mbarisobar

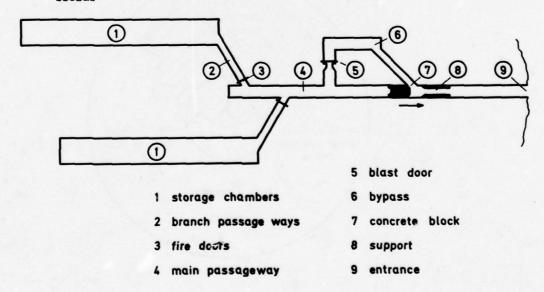


Figure 6 Two chamber storage site with block closing device

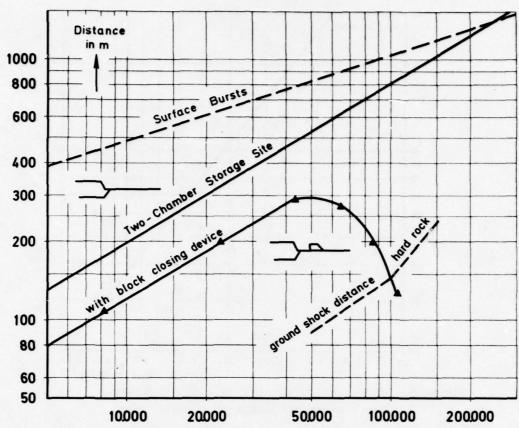


Figure 7 Model test results. Distance of the 50 mbarisobar. Storage site with block closing device

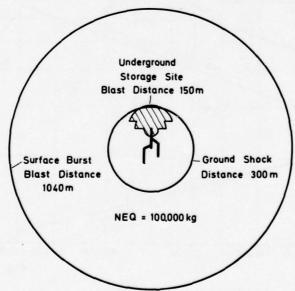


Figure 8 Planview. Blast and ground shock distances.
Storage site with block closing device

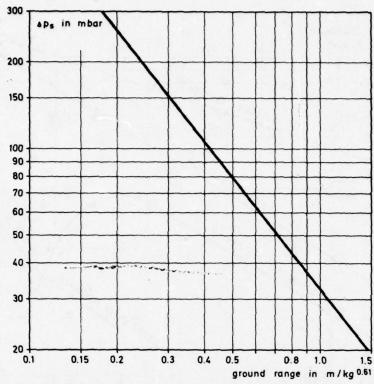


Figure 9 Peak overpressure vs scaled distance. Two chamber storage site  $0^{\circ}$ -direction

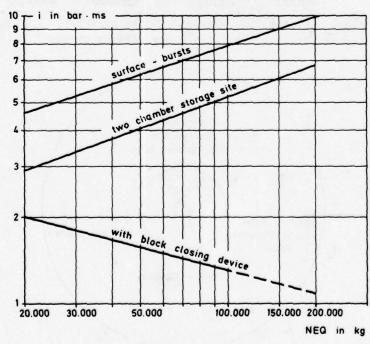


Figure 10 Impulse at the 50 mbar-isobar

#### MODEL STUDY OF TUNNEL DESTRUCTION BY EXPLOSIVES

by

#### C. E. Joachim

U. S. Army Engineer Waterways Experiment Station Vicksburg, Mississippi

#### Background

Current tunnel destruction criteria as provided in Army Manual FM 5-26 (Employment of Atomic Demolition Munitions (ADM)) are based on limited nuclear-explosive (NE) and high-explosive (HE) test data. In these tests, nuclear yields were relatively large and tunnel diameters small compared to typical underground openings and localized stress fields of low yield weapons. The NE data are augmented by HE results from the Underground Explosion Test (UET) Program, a series of model and prototype experiments conducted several years ago in granite and sandstone. Charges were detonated at or near the maximum standoff distance (charge to tunnel distance) for major damage, thus, these experiments established an upper bound for major damage.

This paper describes a series of small-scale tunnel destruction experiments conducted at the Weapons Effects Laboratory of the U. S. Army Engineer Waterways Experiment Station (WES). These experiments were sponsored jointly by the Office, Chief of Engineers (OCE) and the Defense Nuclear Agency (DNA).

## Objective

The objective of these tests was to study the effects of tunnel diameter, charge to tunnel distance, charge confinement, material strength, tunnel spacing and, to a limited extent, liner strength variations on tunnel damage. Results will be used to revise Army weapon and demolition employment procedures.

# Test Block

Since the model was to approximate an infinite half space, it was necessary to configure the experiment to preclude the influence of reflected shocks in the region of interest. Therefore, a trapezoidal-shaped test block was designed which could be inserted into a similar shaped opening in a reusable reaction structure for testing. Block size was a compromise between charge weight and required tunnel diameters which could be contained with a minimum volume for ease of handling and material economy. Test block dimensions were nominally 4 by 3 by 3 feet with the sides and ends tapered on a slope of 9 vertical to 1 horizontal.

Test blocks were constructed by pouring cement grout mixtures into trapezoidal-shaped forms in which the model tunnel and charge hole forms had been placed. Grout unconfined compressive strengths were nominally 10,000, 4,000, and 500 psi. Initial test blocks modeled the UET tunnel tests using horseshoe-shaped tunnel cross-sections 4 and 8 inches in diameter. Other parameters varied during block construction were charge hole and tunnel depths. These parameter variations provided for various degrees of damage and charge coupling.

The 200-gram spherical C-4 charges were placed approximately two weeks after casting. The charges were grouted into the charge holes using property matching grouts with accelerated cure times. Unstemmed charges were not placed until just prior to testing. All stemmed charges included an electric bridge wire (ebw) detonator to initiate the explosive. These were used as a safety precaution because the blocks were left unattended from the time the charges were grouted until tested.

## Tunnel Damage Data

During this test series two tunnel damage parameters were measured. These were the distance from the portal, to the limit of closure, and to the limit of continuous breakage. Damage limits and model parameters are shown in Figure 1. The term "limit of closure" is defined as the point of

intersection of the debris pile and the original tunnel surface at the crown. Damage limits for one of the models tested are shown in Figure 2.

Various techniques for measuring model tunnel damage were tried. Initially, model tunnels were grouted post shot with expansive chemical grout, effectively freezing the debris in place. The grouted model was then sawed to obtain thin sections (1 to 2 inches thick) through the original charge center of gravity, along and perpendicular to the tunnel axis. Damage distance measurements were made directly from the thin sections and from X-ray radiographs of this section. An X-ray radiograph of the typical high strength model is shown in Figure 3. Additional damage definition anticipated from thin sections and radiographic techniques did not materialize; therefore, these methods were abandoned and tunnel damage measurements were made by direct measurement with a carpenter's rule.

Pre- and post-shot model test parameters are given in Table 1. These include the TNT equivalent charge weight, material properties, Hopkinson scaled geometric and damage data. Material property data are averages of several laboratory tests performed on 3-inch diameter samples taken at the time the test blocks were cast. Geometric parameters were measured pre-shot on each block. Damage radii are the distances from center of gravity of the charge to the outer limit of the respective damage.

In addition to physical damage measurements four attempts were made to obtain the spall velocity directly beneath the charge using 10,000- and 50,000-g accelerometers. The acceleration time history and integrations to obtain velocity and displacement are shown in Figure 4. The charge was partially contained at a depth of 1.25 inches in a grouted hole. The charge to tunnel wall distance was 8.26 inches and the tunnel diameter was 4 inches. The accelerometer was mounted on a flat surface of a piece of alluminum 1/4-inch thick, machined on a 2-inch radius. The flat surface was the cord of the circle and approximately 2 inches long. These measurements show that a peak acceleration of 93,000 g's was experienced by the gage as it spalled from the tunnel surface. The gage and mount then travelled across

the model tunnel at a relatively constant velocity of 51 m/sec until it impacted the opposite wall after travelling 9.4 cm.

# Analysis

Tunnel closure data from medium strength models and one scaled tunnel diameter  $(0.47 \text{ ft/lb}^{1/3})$  are plotted versus scaled standoff distance in Figure 5. Symbols denote groups of models tested together under similar conditions. The range of scaled charge depths for each group is shown beside each symbol. The correlation between the shallow (scaled charge depth of 0.13 to 0.15 ft/lb $^{1/3}$ ) and deep (scaled charge depth of 1.5 to 1.6 ft/lb<sup>1/3</sup>) charges indicates that there was no appreciable effect of charge coupling for stemmed charges one radius or greater below the surface. The smaller tunnel closure lengths for the intermediate charge depths (scaled charge depth of 0.4 to 1.1 ft/lb<sup>1/3</sup>) are attributed to variations of test conditions. The reaction structure was cast around these models; therefore, they were in intimate contact with the structure and experienced a high degree of confinement. The other models were tested much later in the program in the same reaction structure. The lower degree of confinement resulted in greater cracking of the exterior surfaces which were in contact with the reaction structure during testing. It is theorized that the small displacements associated with this cracking are responsible for the heavier tunnel damage experienced in these models. It should also be noted that closure did not occur with charges tangent to (and above) the model surface.

Figure 5 also shows that for the medium strength material, very little damage occurred at standoff distances greater than  $1.2\text{W}^{1/3}$  and that the optimum standoff distance for producing tunnel closure is approximately  $0.5\text{W}^{1/3}$ . At closer standoff distances, there is not enough material blown into the tunnel to produce an appreciable obstacle.

A similar plot for continuous breakage is presented in Figure 6. Additional data from charges one radius above the model surface are included in this figure. Here again, smaller damage lengths for the intermediate charge depths are attributed to variations in test conditions. Note that there is significant reduction in damage between charges one radius above and stemmed charges one radius below the surface.

Scaled length of tunnel closure from medium strength models are plotted versus scaled standoff distance in Figure 7. Data for three scaled tunnel diameters, 1.01, 0.47 and 0.063 ft/lb $^{1/3}$ , are shown in this figure. The maximum scaled standoff distance at which closure occurs was essentially independent of scaled tunnel diameter. Note that, as standoff distance decreases, a minimum was reached for the larger tunnels where the debris volume was insufficient to fill the tunnel. Although there is considerable data scatter, the tunnel closure remained relatively constant over the scaled standoff distance ranging from approximately 0.14 to 0.75W $^{1/3}$ . There was a distinct increase in damage, as indicated by closure length, as tunnel size decreased.

Tunnel closure from low, medium and high strength models for scaled tunnel diameters of 0.44 to 0.47  $\rm ft/lb^{1/3}$  are plotted versus scaled standoff distance in Figure 8. Also included for comparison are the UET granite and sandstone data. These data are in agreement with the low strength model results.

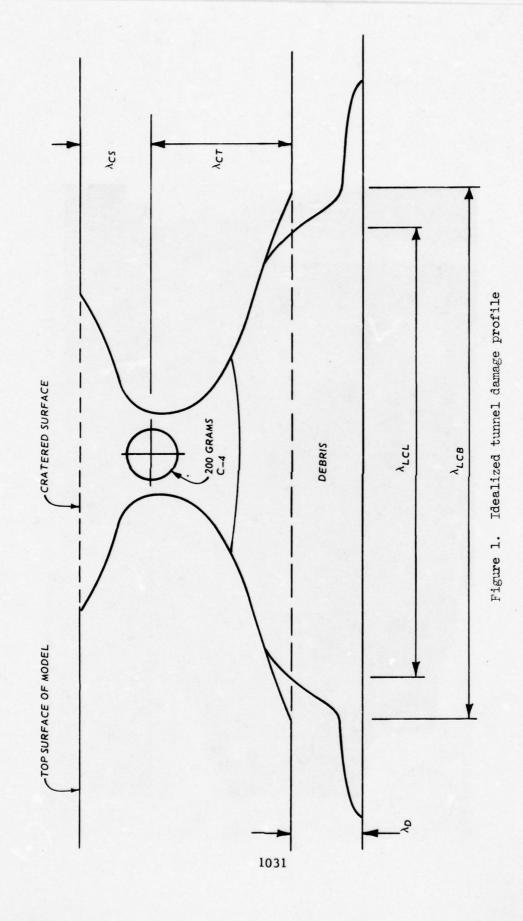
The maximum standoff distance at which closure occurs increases with descreasing model strength. The scaled length of tunnel closed also increases with decreasing strength. As shown in Figure 8, six times the length of the tunnel is closed in the low strength as in the high strength material for similar geometric relations.

The spall velocity data point is shown in Figure 9 where comparison is made to the UET sandstone results. The UET sandstone curve is extended (dashed line) into the region of the model. The model spall velocity is the peak value of the integrated acceleration from Figure 4. Good correlation is shown between the model and UET spall velocity data.

## Conclusions

Tunnel damage, as indicated by closure, is highly strength dependent; more damage is created in weaker materials (Figure 8). Within the bounds of the test conditions, the smaller tunnels suffered the greatest damage for a given charge standoff (Figure 7). For a scaled tunnel diameter of

 $0.47\text{W}^{1/3}$ , the optimum standoff distance for tunnel closure is in the region 0.4 to  $0.8\text{W}^{1/3}$  feet for medium and low strength materials (Figure 8). Virtually no closure occurs at standoff distances exceeding  $2.0\text{W}^{1/3}$  feet. At the optimum standoff distance of  $0.5\text{W}^{1/3}$ , tunnel closure in the low strength grout was approximately 50 percent greater than for the medium strength material; tunnels in the high strength grout were virtually undamaged. A comparison of the model tests with data in real geologic materials (Figure 8) showed that the low strength materials did the best job of modeling tunnel damage. This indicates that the strength properties of the intact rock do not control the model relation and that joints existing in nature play an important role in tunnel response. The UET sandstone spall velocity data corresponds well to the medium strength model results.



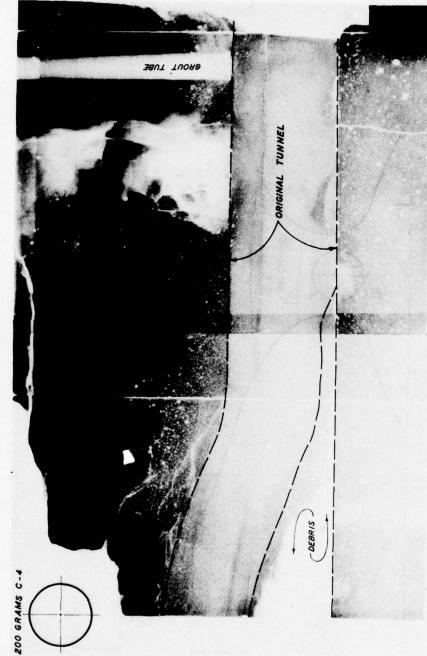


Figure 3. Radiograph of typical damaged high strength model tunnel

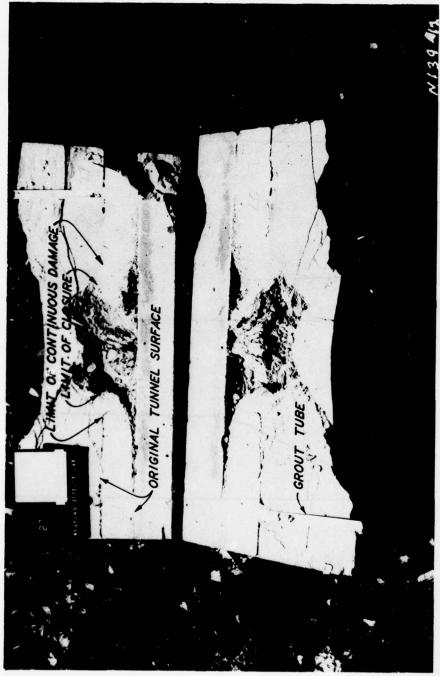


Figure 2. Damage limits

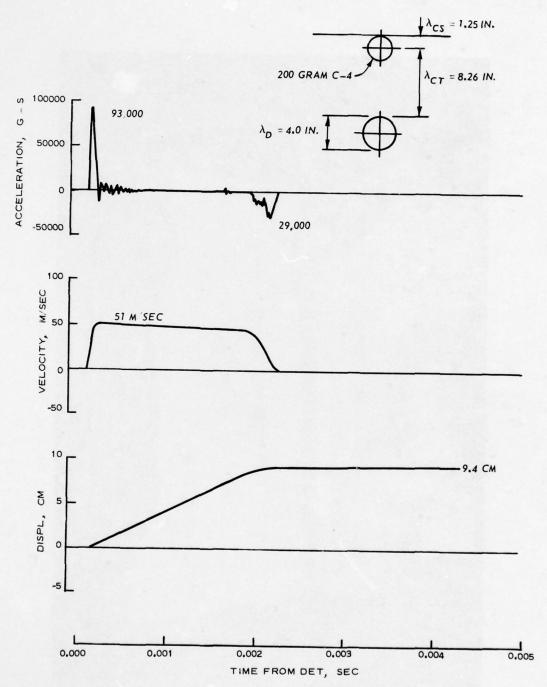


Figure 4. Spall time histories

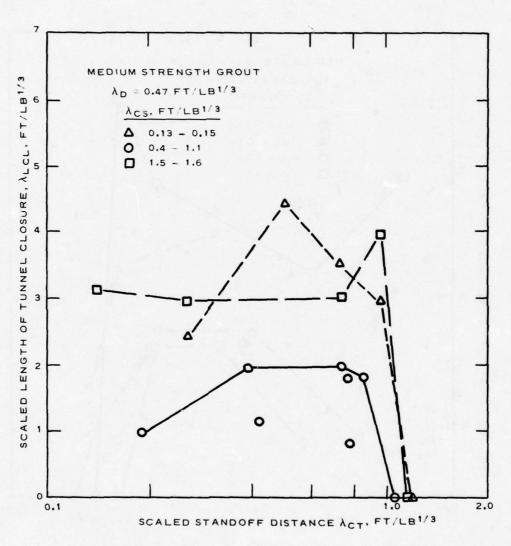


Figure 5. Scaled length of tunnel closure versus standoff distance

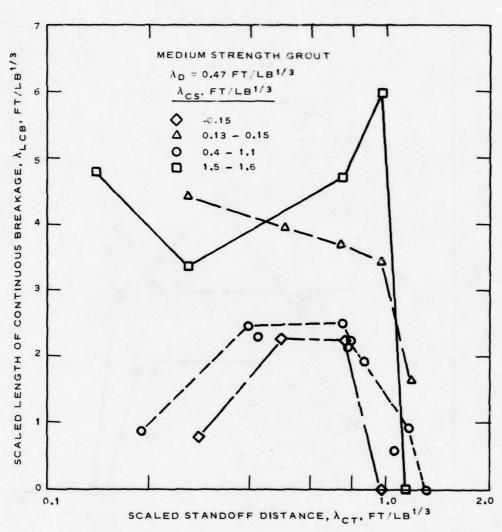


Figure 6. Scaled length of continuous breakage versus standoff distance

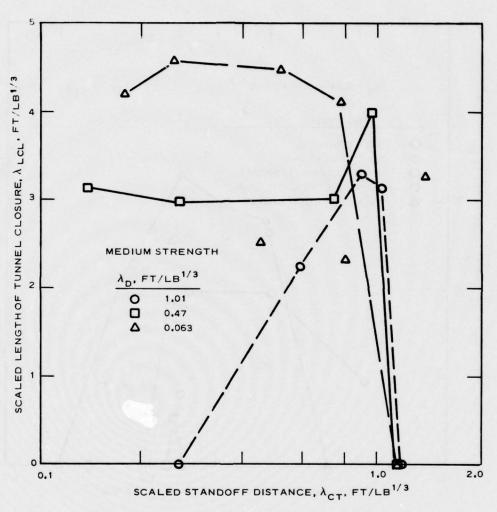


Figure 7. Scaled length of tunnel closure versus standoff distance

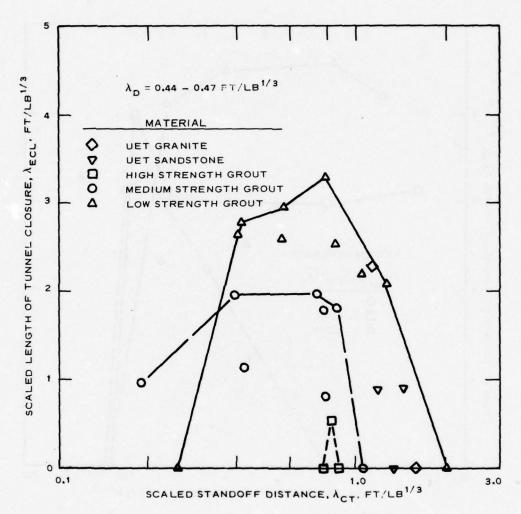


Figure 8. Scaled length of tunnel closure versus standoff distance

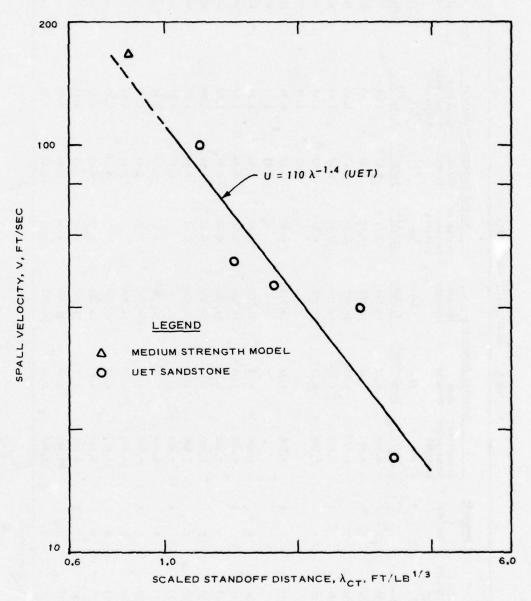


Figure 9. Spall velocity versus standoff distance

Shot TNT Equiv.  Number Charge Weight  (w)  1b.  1 0.37  2 0.37  4 0.37  5 0.37	Weight Weight 7 7 7 7 7 7 7 7 7 7 7 7 7 7 7 7 7 7 7	Yes	Unconfined	Mass	Setante					
(E) 0.3	2 2 2 2 2 2 2 2 2 2 2 2 2 2 2 2 2 2 2 2		Strength		Velocity	Charge to Surface Distance	Tunnel	Charge to Tunnel Wall Distance	Limit of Closure	Limit of Continuous Breakage
0.3 0.3 0.3			(5)	(ø)	(9)	, e	P	ct	λc1	y <sub>cb</sub>
			pst	1b-sec 2/ft	ft/sec	ft/1b1/3	ft/1b1/3	ft/1b1/3	ft/1b1/3	ft/1b1/3
6.00		*	8,300	4.31	14,500	0.41	0.47	1.41	æ	Ð
0.3		*	8,300	4.31	14,500	0.41	0.47	1.43	Ø.	QN.
0.3		×	8,700	4.31	14,500	0.37	0.47	1.43	Ø.	QN
0.3		*	8,700	4.31	14,500	0.34	0.47	1.43	æ	Q.
0.3		×	000.6	4.31	14,500	0.42	0.47	1.16	Q.	QN
0.3							0.47	1.77	QN.	QN
		×	009'6	4.31	14,500	0.39	0.47	1.24	ē	Ø
							0.47	1.77	ē.	ě
0.37	11	×	009.6	4.31	14,500	07.0	0.94	1.24	Ø.	ğ
0.37	11	*	009'6	4.31	14,500	07.0	0.94	1.27	ē	GN.
0.37	1	×	9,300	4.31	14,500	07.0	0.94	1.02	1	1.06
10 0.37	1	×	9,300	4.31	14,500	0.40	96.0	1.90	æ	QN.
0.37		×	9,800	4.31	14,500	0.43	0.94	1.08	Ø	ě
12 0.73	3	×	9,800	4.31	14,500		0.47	0.87	1	1.08
1 0.37	11	×	8,900	4.31	14,500	0.37	0.47	0.82	0.86	1.23
0.37	11	×	8,900	4.31	14,500	0.41	0.47	0.77	1	1.25
69.0	6	*	10,500	4.31	14,500		97.0	98.0	1	1
69.0	6	*	12,600	4.31	14,500		97.0	0.95	1	***
17 0.37	11	×	9,100	4.31	14,500	0.39	0.47	0.53	1	*
18 0.37	1	×	9,100	4.31	14,500	0.37	0.47	0.55	1	1.18
19 0.37	0	×	10,200	4.31	14,500	0.40	0.47	0.43	1	1.19
20 0.37	4	×	10,200	4.31	14,500	0.62	0.47	0.99	1	1.23

TABLE 1, MODEL TUNNEL DAMAGE DATA (continued)

Scaled Damage Radii to Outer	Limit of Continuous Breakage	Ceb	•	1	1.23	0.95	1.08	0.88	0.67	1.30	1.30	96.0	1.23	1.29	1.46	1.37	1.09	1.25	:	1	1	1.80	1.84	1.75	1.80	Page 2 of 5
Scaled Damag	Limit of Closure	Acı	ft/1b1/3	*	1	1	1	!	1	1.18	1.25	0.52	0.71	1.05	1.23	0.88	1	1	1	1	1.45	1.58	1.82	1.51	1.63	
Parameters	Charge to Tunnel Wall Distance		ft/1b1/3	0.86	69.0	0.37	0.67	0.28	0.14	0.77	0.86	0.19	0.42	0.39	0.74	0.78	1.05	1.16	1.30	0.25	0.41	0.57	0.78	1.04	1.25	
Scaled Geometric Parameters	Tunnel Diameter	P	ft/1b1/3	97.0	0.47	0.47	0.47	0.47	0.47	0.47	0.47	0.47	0.47	0.47	0.47	0.47	0.47	0.47	0.47	0.47	0.47	0.47	0.47	0.47	0.47	
Scaled	Charge to Surface Distance	ce	ft/1b1/3		1.41	1.46	1.97	0.62	0.75	0.41	0.41	1.11	0.95	1.12	0.71	0.88	0.54	69.0	0.73	0.42	0.43	0.47	0.43	0.45	0.43	
ties	Seismic	(c)	ft/sec	14,500	14,500	14,500	14,500	14,500	14,500	9,300	9,300	9,300	9,300	9,300	9,300	9,300	9,300	9,300	9,300	2,600	2,600	5,700	009'9	009'9	6,300	
Material Properties	Mass Density	(d)	1b-sec 2/ft	4.31	4.31	4.31	4.31	4.31	4.31	3.54	3.54	3.54	3.54	3.54	3.54	3.54	3.54	3.54	3.54	3.74	3.74	3.80	3.78	3.84	3.74	
W W	Unconfined Compressive Strength	(α)	ps1	10,500	11,000	006'6	006'6	12,700	11,300	3,800	3,700	3,600	4,200	3,900	4,000	4,100	3,900	4,200	4,000	380	380	445	280	650	067	
Stemming	Yes No			×	×	×	×	*	×	*	×	×	×	×	×	*	×	×	×	*	×	*	×	×	×	ent
	TNT Equiv. Charge Weight	(M)	1b.	69.0	0.37	0.37	0.37	0.37	0.37	0.37	0.37	0.37	0.37	0.37	0.37	0.37	0.37	0.37	0.37	0.37	0.37	0.37	0.37	0.37	0.37	*No Measurement
	Shot Number			21	22	23	24	25	56	27	28	53	30	31	32	33	34	35	36	37	38	39	07	41	42	

Page 3 of 5

0

Scaled Damage Radii to Outer Limit of Continuous Breakage ft/1b1/3 2.11 1.50 2.13 2.86 cb 1.57 2.76 2.30 2.05 2.38 1.71 1.91 2,47 Limit of Closure λ<sub>c1</sub> ft/1b<sup>1/3</sup> 1.38 8.45 1.52 2.30 1.38 1.91 2.14 1.96 1.52 1.71 1.38 2.27 1.97 1.94 1.51 Charge to Tunnel Wall Distance ft/1b1/3 Scaled Geometric Parameters 2.00 0.40 0.56 0.84 0.25 0.56 0.80 0.80 1.19 0.32 1.39 1.38 0.62 96.0 0.61 0.88 0.14 1.14 0.23 ct λ<sub>d</sub> ft/1b<sup>1/3</sup> Tunnel Diameter 0.063 0.063 0.063 0.063 0.063 0.47 0.47 97.0 0.47 0.12 0.12 0.12 0.12 0.12 0.22 0.22 0.22 0.22 0.22 0.47 0.47 Charge to Surface Distance λ<sub>ce</sub> ft/1b<sup>1/3</sup> 0.43 0.45 97.0 0.41 1.50 1.52 1.50 1.50 1.56 1.55 1.52 1.50 1.50 1.45 1.49 1.46 1.62 1.50 1.51 1.51 1.51 1,61 Seismic Velocity 6,300 5,900 5,800 000,9 9,800 ft/sec 10,000 10,000 10,000 006'6 10,000 10,000 10,000 10,000 9,900 006'6 9,800 009'6 10,000 3,700 ં Material Properties 1b-sec2/ft4 3.76 3.70 3.70 3.76 3.99 3.91 4.03 3.97 Density 4.01 3.97 3.93 3.99 4.07 4.05 3.91 3.90 3.86 3.95 3 Compressive Strength Unconfined 4,300 4,000 4,500 4,300 4,100 4,100 620 4,200 4,200 3,700 000,4 3,400 3,500 3,300 3,800 3,200 2,600 3,800 3,000 (2) psi Stemming Yes No INT Equiv. Charge Weight 0.37 0.37 0.37 0.37 0.37 0.37 0.37 0.37 0.37 0.37 0.37 0.37 0.37 0.37 0.37 0.37 0.37 0.37 0.37 (3) 15. Shot 59 09 50 51 52 53 53 54 55 55 58 61 62 63 79 77

TABLE 1. MODEL TUNNEL DAMAGE DATA (continued)

Page 4 of 5

TABLE 1, MODEL TUNNEL DAMAGE DATA (continued)

		Stemming	Me	Material Properties	les	Scaled	Scaled Geometric rarameters	arameters	Scaled Damage Madil to Outer	Madil to Out
Shot Number	INT Equiv. Charge Weight	Yes	Unconfined Compressive Strength	Mass Density	Seismic Velocity	Charge to Surface Distance	Tunnel Diameter	Charge to Tunnel Wall Distance	Limit of Closure	Limit of Continuous Breakage
	(%)		(δ)	(0)	(9)	λ <sub>ce</sub>	P	, ct	λ <sub>c1</sub>	y cp
	1b.		psi	1b-sec /ft	ft/sec	ft/1b1/3	ft/1b1/3	ft/1b1/3	ft/1b1/3	ft/1b1/3
65	0.37	×	4,800	3.86	009.6	1.49	0.47	96.0	2.21	3.14
99	0.37	×	3.700	3.97	9,700	1.52	0.47	1.14	1	1
29	0.37	×	4,300	4.05	006.6	0.71	1.01	0.45	1	2.32
89	0.37	×	4,300	4.01	006'6	0.71	1,01	0.59	1.27	2.75
69	0,37	×	4,400	3.95	008'6	0.73	1,01	0.89	1.87	2.88
70	0.37	×	4,200	3.97	9,700	0.73	1,01	1.02	1.87	2.74
11	0.37	×	4,400	3.99	10,000	0.71	1.01	1.16	!	2.75
72	0.37	×	4,100	4.03	9,700	67.0	0.065	0.18	2.11	2.18
73	0.37	×	4,400	4.24	9,700	67.0	0.063	0.52	2.30	†
74	0.37	×	3,800	4.01	9,500	0.47	0.063	0.78	2.17	2.32
75	0.37	×	4,200	3.93	9,700	0.47	0,063	1.14	1	1
92	0.37	×	4,300	3.95	9,700	67.0	0.063	1.35	1	1.75
11	0.37	×	3,900	3.88	9,800	6.34	0.12	0.32		3.01
78	0.37	×	4,300	4.09	008'6	0.48	0.12	0.54		2.40
62	0.37	×	4,400	4.07	006'6	0.47	0.12	0.78		1.21
80	0.37	×	4,500	4.07	10,000	0.47	0.12	1.14	1	2.31
81	0.37	×	4,000	4.09	9,800	97.0	0.12	1.37	1	1.98
82	0.37	×	3,800	4.05	9,900	97.0	0.22	0.22		2.80
83	0.37	×	3,600	4.05	9,800	0.46	0.22	0.59		*
84	0.37	×	4,100	4.05	9,700	97.0	0.22	0.77		1.63
85	0.37	×	3,900	60.4	9,700	97.0	0.22	0.91		1.49
98	0.37	>	7 100	4.07	0 600	37.0	000			

TABLE 1. MODEL TUNNEL DAMAGE DATA (concluded)

INT Equiv.		Unconfined	Mass	Seismic	Charge to	Tunnel	Charge to	Limit of	Limit of Limit of
ght	Yes No	Compressive Strength	Density	Velocity	Surface Distance	Diameter	Tunnel Wall Distance	Closure	Continuous Breakage
		(α)	(d)	ં	ν ce	₽ ~	λet (	$^{\lambda}_{c1}$	λ <sub>cb</sub>
1		pst	1b-sec2/ft4	ft/sec	ft/1b1/3	ft/1b1/3	ft/1b <sup>1/3</sup>	ft/1b1/3	ft/1b <sup>1/3</sup>
	×	10,000	4.30	14,000	1.52	0.063	0.22	1.11	*
0.37	×	10,000	4.28	14,000	1.52	0.063	0.55	2.04	1
	×	11,000	4.40	14,000	1.52	0.063	0.80	1.97	*
	×	12,000	4.34	14,000	1.52	0.063	1.17	1.58	1
	×	10,000	4.40	14,000	1.46	0.063	1.44	*	1
	×	510	3.74	009'9	1.56	0.063	0.21	2.66	1
	×	009	3.68	6,300	1.52	0.063	0.57	2.82	1
	×	610	3.82	5,700	1.56	0.063	0.77	2.13	*
	×	630	3.80	6,400	1.55	0.063	1.16	2.46	1
	×	200	3.84	6,000	1.55	0.063	1.38	2.00	1
	×	3,600	3.84	000,6	-0.15	0.47	1.18	1	1
	×	3,400	3.82	9,100	-0.15	0.47	0.97	1	1
	×	3,500	3.80	8,700	-0.15	0.47	0.75	1	1.34
0.37	×	3,200	3.86	000,6	-0.15	0.47	67.0	1	1.24
	×	3,400	3.82	8,800	-0.15	0.47	0.28	1	0.48
	×	3,500	3.86	8,900	0.15	0.47	1.18	1	1.44
	×	3,300	3.86	8,900	0.15	0.47	96.0	1.76	1.97
	×	3,300	3.84	8,800	0.13	0.47	0.73	1.90	2.09
	×	3,300	3.66	8,700	0.13	0.47	0.50	2.27	2.04
	×	3,200	3.82	8,200	0.15	0.47	0.26	1.24	2.18

Page 5 of 5

# GROUND SHOCK EFFECTS ON PERSONNEL AND FACILITIES FROM ACCIDENTAL EXPLOSIONS

Robert J. Odello Civil Engineering Laboratory Naval Construction Battalion Center Port Hueneme, CA

INTRODUCTION

Objectives

This study was initiated to provide a better understanding of the significance of ground shock in the design of structures to resist the effects of accidental explosions. The results of the effort are intended to supplement existing design criteria. Specific objectives of this effort are to:

- 1. Establish semi-empirical methods and design aids for ground shock prediction.
- 2. Determine the effect of ground shock on personnel, structures and equipment.
- 3. Determine requirements for additional study of ground shock and its effects.

Design Criteria

The criteria of Reference 1 provide extensive data on air blast and fragmentation phenomenology. Extensive treatments of various burst conditions, charge confinement configurations, reflection conditions and fragmentation characteristics are justified by the fact that nearly all designs are controlled by these criteria. Elastic and inelastic response of structures to side-on and reflected pressures and the design of barriers to stop high speed fragments are critical areas of concern, because overpressure loads and fragment impact are usually the critical survivability parameters.

Little effort has been devoted to the description of ground shock phenomenology or to the design of structures to resist ground shock effects. A quantitative description of ground shock would be valuable in evaluating its significance in specific cases. With this knowledge, a designer could determine the significance of these effects. The intent of this study is to provide the designer with the necessary tools to make that decision.

Ground Shock Phenomenology

Ground shock results from energy imparted to the ground by an explosion. Some of the energy is transmitted through the air in the form of air-blast-induced ground shock, and some is transmitted through the ground as direct-induced ground shock. Excellent detailed descriptions of ground shock phenomenology are contained in References 2 and 3.

Air-blast-induced ground shock results when the air blast shock wave compresses the ground surface and sends a stress pulse into the underlying media. The magnitude and duration of the stress pulse in

the ground depends on the character of the air-blast pulse and the ground media. Generally the air-induced ground motions are downward. They are maximum at the ground surface and attenuate with depth.

Direct-induced ground shock results from the explosive energy transmitted directly through the ground. The term as it is used in this report includes both true direct-induced motions and cratering-induced motions. The latter are generally of longer duration and are generated by the crater formation process in cratering explosions. Both of these phenomena tend to be of longer duration than air-blast-induced ground shock and the wave forms tend to be sinusoidal.

The net ground shock experienced by a point on the ground surface is a combination of air-blast- and direct-induced shock. Relative magnitudes and sequencing of the motions are functions of media and absolute distance from the point of detonation. In the super-seismic region, the air blast arrives before the direct-induced ground shock. As the air-blast shock front moves farther from the blast point, it slows and the direct-induced ground shock catches and "outruns" the air-blast. This latter region is called the outrunning region. Waveforms in the outrunning region are generally a complex combination of both wave forms. Relative phasing of each portion of the motion can be estimated by calculating arrival times of each wave. Examples of net ground motions in both regions are illustrated in Figure 1.

#### PREDICTION METHODS

## Approach

4 .

The primary concern of the present study was to evaluate the ground shock effects of accidental explosions. Thus, the data used in this study were entirely from surface bursts. Ground shock data were obtained for detonations from one-half to one-half million kilograms (one pound to one million pounds) of TNT, and for scaled ranges from 0.2 to 24  $^{\rm M}/{\rm kg}^{1/3}$  (0.5 to 60 ft/lb<sup>1/3</sup>). The predominate charge configuration was a sphere which was tangent to and above the ground surface. Results from several half-buried spherical charges and a few hemispherical charges are also included in the data.

Initial data gathering efforts consisted of listing the charge configuration, yield, and ground media properties that were available. At each range for which data existed, ground shock data, air-blast overpressure and air-blast impulse were recorded. Ground shock was recorded only for gages within one metre (three-feet) of the ground surface.

The data reduction process included converting data to consistent units and calculating scaled distances and other parameters used in developing the empirical equations. A review of several previous studies indicated that approximate analytical expressions adequately predicted peak air-blast-induced ground shock; consequently, the predominate effort in developing prediction methods was directed toward obtaining empirical equations for direct-induced ground shock. Constants for the empirical equations were developed using a standard least squares curve fitting technique.

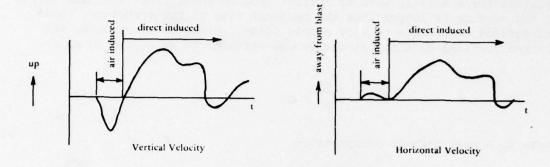


Fig 1a. Superseismic ground shock

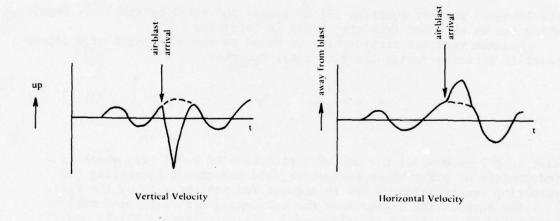


Fig 1b. Outrunning ground shock

In general, the best estimates of air-blast-induced ground shock can be determined through one dimensional wave propagation theory. For surface structures located on ground media in which the travel time required for a seismic wave to reflect from an underlying layer and return to the surface is longer than the response time of the structure, these expressions degenerate to very simple forms. Using this approach, the maximum vertical velocity at the ground surface can be expressed as

$$V_{v} = \frac{P_{o}}{\rho c_{p}} \tag{1}$$

where  $p_0$  = peak side-on overpressure

 $\rho$  = mass density of the ground media

 $c_p$  = compression wave seismic velocity

The maximum displacement is derived by integrating the above expression with respect to time, thus

$$d_{v} = \frac{1}{\rho c_{p}} \int_{0}^{\tau} p(t)dt$$
 (2)

The integral part of equation (2) is simply the total overpressure impulse, which can be obtained from the graphs in Reference 1.

Maximum vertical acceleration is based on the assumption of a linear velocity increase during the rise time,  $t_r$ ; thus

$$a_{v} = \frac{v_{v}}{t_{r}} \tag{3}$$

Reference 2 recommends the use of a rise time of 0.001 sec, which is independent of other blast parameters, and recommends increasing the resulting acceleration by 20% to account for nonlinearity of the rise.

The form of the expressions for estimating direct-induced motions were based on equations of Reference 2. In some cases a slight modification of the expressions was required to put the expressions into formats that were consistent with Reference 1. The primary concern was to express ground shock parameters in terms of the scaled range.

Reference 2 gives the following expression for estimating directinduced vertical displacements

$$d_v = K_D w^{5/6} R^{2/3}$$
 (4)

where dy = vertical displacement

K<sub>D</sub> = constant

W = yield

R = range

Dividing both sides by  $W^{1/3}R^{1/3}$  gives

$$\frac{d_{v}}{w^{1/3}R^{1/3}} = K_{D} w^{3/6}R^{-1}$$

if  $W^{1/3}$  is used in place of  $W^{3/6}$  on the right side, the expression becomes

$$\frac{d_{V}}{W^{1/3}R^{1/3}} = K_{D} \left(\frac{R}{W^{1/3}}\right)^{-1}$$

This expression can be generalized if the exponent of the scaled range is allowed to be an arbitrary constant. Thus, the form of the empirical equation for direct-induced displacement is

$$\frac{d_{V}}{W^{1/3}R^{1/3}} = K_{D} \left(\frac{R}{W^{1/3}}\right)^{n} a$$
 (5)

The generalized expression for velocity is

$$v_{v} = K_{v} \left(\frac{R}{W^{1/3}}\right)^{n_{v}}$$
 (6)

The generalized expression for acceleration is

$$W^{1/3} a_{v} = K_{a} \left(\frac{R}{W^{1/3}}\right)^{n_{v}}$$

The values of the constants can be determined by using least squares curve fitting techniques for plots of scaled range versus the quantities on the left sides of the equations.

Direct-induced ground shock data were separated into three qualitative catagories: dry soil, saturated soil, and rock. Attempts at further divisions or quantitative paramatization did not appear to provide better accuracy or precision in the prediction equations. In some cases, even

the above distinctions were unnecessary. In cases where significant differences existed between empirical equations for different material categories, separate equations were recommended. Conversely, when insufficent data were available to justify a separate equation, the data were combined into a single equation.

# Prediction Equations

Recommended equations for predicting air-blast-induced ground shock are presented in Table 1. These equations are intended to provide reasonable estimates of the air-blast-induced ground shock at the ground surface. They are based on the assumption that the ground medium properties are uniform for a significiant distance below the surface. For design purposes, the gross motions of structures with shallow foundations can be assumed to be equal to these motions. Although this latter assumption is not strictly correct, it should provide estimates of structural ground shock environment which are at least as accurate as the prediction equations.

Figure 2 shows comparisons of the calculated and measured peak vertical air-blast-induced velocities from high explosive field tests. This graph is similar to those for other ground motions. Except in the case of accelerations, the data tends to cluster around the equivalency lines. The scatter band for accelerations is almost on order of magnitude wide. In general, the prediction equation underestimates the accelerations in rock and saturated soil and overestimates accelerations for dry soil. The reasons for these differences are not clear; however, insufficient data are available to justify separate empirical equations. A conservative approach to design might be to use the recommended equation for air-blast-induced accelerations in dry soil and to double those values in other media.

Recommended equations for predicting direct-induced ground motions are presented in Table 2. These empirical equations were based on data from TNT detonations in spherical and hemispherical charge configurations near the ground surface. All of the experiments were conducted with unconfined charges on the bare ground surface. These equations represent the best fit to the available data. Figure 3 shows the direct-induced horizontal velocity equation plotted on a graph of ground motion data from a 91,000 kg (100 ton) burst on soil. This comparison was presented to indicate the general trend of the data with respect to the prediction method; individual data points could differ from predicted values by as much as a factor of 10. In general, however, the data fell into narrow bands.

#### DESIGN IMPLICATIONS

The ground shock phenomenology which has been discussed to this point must be viewed in the context of safety and design requirements. The impact on inhabited building distances and interline magazine distances will be discussed, and recommendations are made for identifying situations where ground shock effects may lead to safety problems.

Vertical

$$D_{v} = \frac{i}{\rho c_{p}}$$

$$V_{v} = \frac{P_{o}}{\rho c_{p}}$$

$$A_{v} = \frac{1,200 P_{o}}{\rho c_{p} g}$$

Horizontal

$$D_{h} = D_{v} \tan \left[ \sin^{-1} (c_{p}/U) \right]$$

$$V_{h} = V_{v} \tan \left[ \sin^{-1} (c_{p}/U) \right]$$

$$A_{h} = A_{v} \tan \left[ \sin^{-1} (c_{p}/U) \right]$$

For  $tan \left[ sin^{-1} (c_p/U) \right] > 1$ , horizontal and vertical motions are approximately equal.

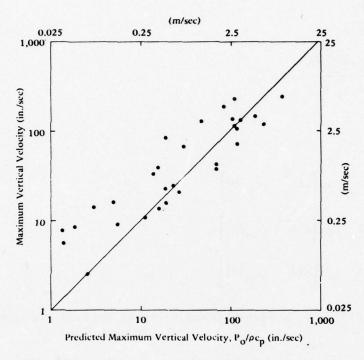


Fig 2. Predicted and measured peak air-blast-induced velocities

Table 2. Recommended Prediction Equations\* for Direct-Induced Ground Motion

		Vertical	1	Horizontal
Parameter	Media	SI Units	English Units	SI or English Units
Displacement	Rock	$\frac{D_{v}}{R_{G}^{1/3}w^{1/3}} = 3.7 \times 10^{-4} Z_{G}^{-1.3}$	$\frac{D_{v}}{R_{G}^{1/3}w^{1/3}} = 0.025 Z_{G}^{-1.3}$	$D_{h} = 0.5 D_{v}$
	Soil	$\frac{D_{v}}{R_{G}^{1/3}W^{1/3}} = 1 \times 10^{-3} Z_{G}^{-2.3}$	$\frac{D_{v}}{R_{G}^{1/3}w^{1/3}} = 0.17 Z_{G}^{-2.3}$	$D_h = D_v$
Velocity	All	$V_{v} = 0.95 Z_{G}^{-1.5}$	$V_v = 150 Z_G^{-1.5}$	v <sub>h</sub> = v <sub>v</sub>
Acceleration	All	$A_v w^{1/3} = 1,200 Z_g^{-2}$	$A_{\rm V} W^{1/3} = 10,000 Z_{\rm G}^{-2}$	
	Dry Soil			$A_h = 0.5 A_v$
	Wet soil & rock			A <sub>h</sub> = A <sub>v</sub>

\*The units used in each set of equations are as follows:

Quantity

SI Units

English Units

In.

V, Vh

V, Vh

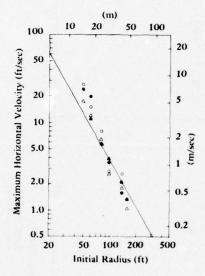
R, M

RG

W

Kg

Ib



0.46-m (1.5-ft) depth

▲ Proj 3.02a

• Proj 3.08

1.5-m (5.0-ft) depth

△ Proj 3.02a

o Proj 3.08

Fig 3a. Maximum direct-induced horizontal particle velocity; Distant Plain Event 6 (Ref 9)

# Inhabited Buildings

A review of the literature revealed that the ground shock vulnerability of residential structures, and by inference, unhardened inhabited buildings in general can be defined in terms of peak ground shock velocity. Reference 4 gives the following criteria for damage prediction in inhabited buildings:

Damage	Peak Velocity (any direction)
None	51 mm/sec (2.0 in/sec)
Minor	137 mm/sec (5.4 in/sec)
Major	193 mm/sec (7.6 in/sec)

Using the equations in Tables 1 and 2, these velocities would be exceeded as a result of ground shock environment at the following scaled distances expressed as  $m/kg^{1/3}(ft/1b^{1/3})$ :

Damage		Soi1	Saturated Soil	Rock
None	6.9 (17.3)	5.7 (14.3)	2.7 (6.8)	1.5 (3.9)
Minor	3.6 (9.2)	3.4 (8.6)	1.7 (4.3)	1.0 (2.5)
Major	2.9 (7.3)	2.9 (7.3)	1.5 (3.7)	0.8 (2.1)

All of these distances are significantly less than the permissible inhabited building distances of 16 to 20 m/kg $^{1/3}$ (40 to 50 ft/1b $^{1/3}$ ), and all are at scaled distances at which air blast and fragment vulnerability levels would be exceeded.

#### Magazines

A second critical area in which ground shock effects might be significant is the design of structures at the various permissible intermagazine distances. The relative severity of ground shock becomes greater at small scaled ranges, and structures located at those ranges are strong and massive enough to resist blast and fragment effects. In general, structures designed to survive these severe environments are not likely to be damaged by the associated ground shock. Reasons for the proceeding generalization will be given by the following discussion, but until adequate data are available, ground shock effects should be checked in all designs.

Air-blast-induced ground shock occurs at the same time as the air-blast loading on aboveground structures. Since the ground tends to move downward and outward at the same time as the air-blast is pushing the structure in the same direction, air-induced ground shock slightly decreases the loading on a structure. This effect is generally negligible, and the effects of air-blast-induced ground shock can be neglected in the design of a close-in structure.

Structural damage to aboveground facilities from direct-induced ground shock is not probable. Although very high accelerations are indicated for small explosive weights at intermagazine distances, these motions are of such high frequency and low energy content that little damage to practical size structures is expected.

For relatively large charge weights, direct-induced ground shock does not present a structural threat because the accelerations are relatively low. The relatively large ground displacements which occur for large charge weights could, however, cause failure of external connections to structures. These displacements may cause relative motions at stiff utility connections to structures. If flexible or ductile connections are not provided, critical utilities such as electrical power or water supply could be severed. Although there are few analytical or experimental data points for quantifying these relative motions, they should be considered in selecting connection details.

### Personnel

Ground shock from accidental explosions could cause injury to personnel working near magazines or other areas of explosive hazards even if the persons are protected from air blast effects. A generally accepted shock tolerance level for a person standing with knees locked is 3 m/sec (10 ft/sec) maximum vertical velocity when accompanying accelerations are greater than 20 g's. These criteria are shown graphically in Figure 4 and apply to upward motion of the floor and would therefore be the motions resulting from direct-induced ground shock. For downward displacements (air-blast-induced ground shock) the floor moves out from under the person, and the injury threshold is reached if the relative velocity between the person and the floor exceeds 3 m/sec (10 ft/sec).

Injury criteria for horizontal motions are more difficult to define because the proximity of persons to solid objects is not known. In general, horizontal accelerations of about 0.5 g are sufficient to knock a person off balance, and cause injury as a result of the person striking a wall, a fixed object or a sharp convex corner. The maximum horizontal acceleration that can be transmitted to a standing person through the floor of a structure is limited by the amount of force that can be transmitted through friction between a person's feet and the floor. Even in the most extreme cases the coefficient of friction is less than 1.0. Thus, horizontal accelerations are limited to 1.0 g, and the critical injury mechanism is impact when the person strikes the floor or other objects in a structure. Injury will generally occur when the impact velocity exceeds 10 ft/sec.

The overturning of heavy objects must also be considered in evaluating the vulnerability of persons to horizontal gound shock. Dynamic overturning moments for critical objects in a structure should be estimated or measured, and, if necessary, tie-down systems should be designed to prevent these objects from overturning.

Ground shock is not a critical injury producing mechanism for personnel who are exposed to air blast. Peak ground motions were estimated for the overpressure levels at which threshold and 50 percent eardrum rupture occur - 34.5 and 103 kPa (5 and 15 psi) respectively. Peak

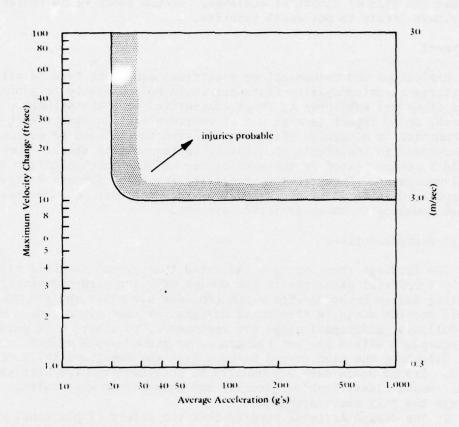


Fig 4. Tolerance of stiff-legged standing persons to short-duration vertical shock motions

velocities at both ranges are much less than 1 ft/sec. Although air-blast-induced vertical accelerations are between 4 and 13 g's, peak displacements are less than 25 mm (1 inch), so free fall velocities greater than 3 m/sec (10 ft/sec) cannot be achieved. Ground shock would therefore contribute little to personnel injuries.

# Equipment

Explosives and mechanical or electrical equipment located within structures at intermagazine distances could be vulnerable to ground shock. These items are subjected to shock transmitted from the structure or mounting or to impact as a result of overturning. Equipment that is hard mounted or otherwise attached to a structure should be evaluated with respect to the item's sensitivity to transmitted shock. These items should be shock tested in the same manner as other mechanical or electrical equipment. Specifically, fragility levels of sensitive items should be expressed in terms of shock spectra, so a designer could properly select mounting or shock isolation systems.

# Design Recommendations

The findings thus far have indicated that ground shock is not generally a critical parameter in the design of blast hardened structures. Existing design methodologies which consider air blast and fragment effects should provide adequate structural designs for most situations. However, the following additional steps are recommended to assure that personnel and equipment within are not vulnerable to ground shock effects.

Calculate the peak ground motions from the equations in Tables 1 and 2. Ground media data may usually be obtained from the site survey data. Media classification, density and compression wave seismic veloc-

ity are the only necessary data.

If the design criteria specify that the safety of personnel within a structure is to be considered, peak velocities and accelerations should be compared with the injury criteria described previously. In cases where the impact limit is exceeded, cushioning material may be used. Where overturning equipment is a potential injury mechanism, the equipment must be tied-down to the floor or restraining devices must be provided.

Equipment vulnerability can be estimated by a relatively simple response spectra approach. The response spectrum is a plot of the response of a single degree of freedom oscillator versus the undamped natural frequency of the oscillator for a given base excitation. If the excitation wave form is precisely known, the response spectrum can be calculated. However, ground shock is characterized by a complex wave form about which little is known for any specific design case. The magnitude of the spectrum envelope can be estimated if the peak values of acceleration, velocity and displacement are known.

Figure 5 shows an example of one method of plotting shock spectra. In this example, all scales are logarithmic. The natural frequency is plotted on the horizontal scale, and the psuedo-velocity is plotted

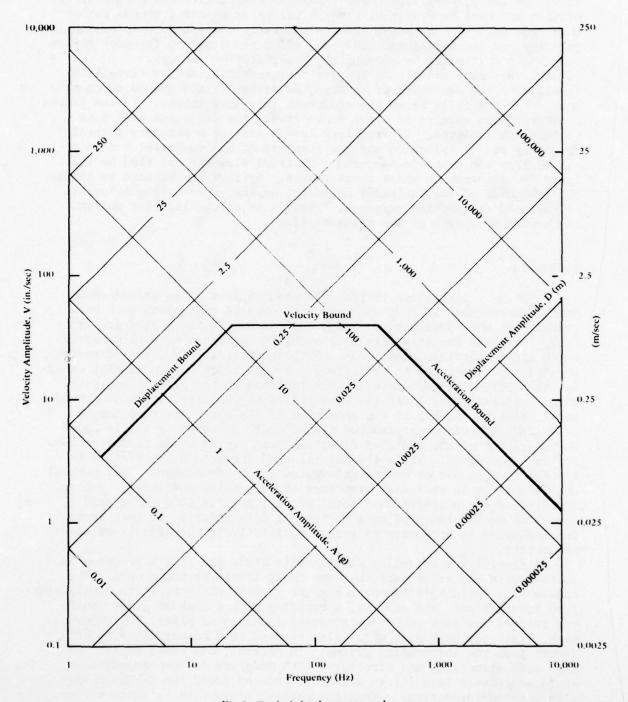


Fig 5. Typical shock spectrum plot

on the vertical scale. Displacement and pseudo-acceleration axes are at 45° to the primary axes. The terms pseudo-velocity and pseudo-acceleration are used to distinguish these values as spectral bounds rather than true motions. Response spectra generally consist of displacement, velocity and acceleration boundaries, which are equal to the peak motion components multiplied by appropriate amplification factors.

If data is available on the critical response spectra (fragility levels) for the equipment of concern, determine if the ground shock response spectra falls below the equipment fragility levels. If the ground shock response spectra is above those levels the equipment will have to be shock isolated. If fragility levels are not known, the natural frequency can be estimated and the response of the equipment can be obtained from the response spectrum. Critical elements can then be analyzed for response to these shock values. Springs may be used to change the frequency of the equipment mounting, or energy absorbing materials may be used to damp the response. Details of shock isolation design are beyond the scope of the present effort.

### DISCUSSION

A primary limitation in the data used in developing ground shock prediction methods is that all were from uncased explosions over bare ground. In many design situations, such as explosives plants and armories, incidents are most likely to occur in buildings or working areas which are on massive foundations. Although the effects of cased versus uncased explosions can be estimated, the effects of a structurally coherent slab below the explosive are not included in the present analysis. This limitation will limit the credibility of the direct-induced ground shock predictions, but if the character of the air-blast wave can be described, the air-blast-induced ground shock expressions should apply. The character of the modified direct-induced ground shock is not obivous for such incidents. While the magnitude of the ground shock could be reduced as a result of energy dissipated in the foundation slab, partial confinement by an enclosing structure could provide sufficient tamping to increase the proportion of total energy, coupled into the ground. Since the author knows of no experimental data relative to this problem, further study is necessary to assess qualitatively the effects of these parameters.

A simplifying assumtion made in this study was that structures tend to move with and experience the same shock levels as the ground. The nature of a building's foundation might significantly alter the soil-structure interaction. For example, a building with a slab on grade would not respond the same as one with spread footings or piles. Structures with relatively high mass might also respond in a manner which is different from the surrounding ground. In general, one would expect that high mass structures and structures with moderate to deep foundations would experience less severe air-blast-induced gound shock than those with shallow foundations. Thus the present assumption is conservative.

The use of the response spectrum to estimate shock effects on structure contents is an approximate and highly simplified approach. More sophisticated levels of utilizing shock spectra are described in

Reference 2 and elsewhere, but these methods generally require more detailed knowledge of the ground motion wave form. The approach presented in the current effort represents at least the same level of rigor as

the equations for estimating peak ground motions.

The relatively large data scatter with respect to the best fit equations for direct-induced ground shock is partially due to errors in measurement and interpretation of data, but the most significant source of variation is the variability of ground shock phenomenology. A factor of two variations between measured quantities at the same range but different directions from the same event is not uncommon. Differences between peak velocity obtained from integrated accelerometer data and from a velocity gage located in the same canister often differ by 50% or more. The overall range of data scatter is approximately a factor of five for accelerations, two for velocities, and three for displacements. A further reason for the large scatter bands is that the ground media properties were not quantified. The broadly defined ground media categories tended to include media with wave variations in properties within single categories. Thus some judgment must be exercised in selecting a particular equation.

Despite the foregoing deficiencies, the discussion and information presented here should provide a rational basis on which the evaluation of ground shock effects can be based. The acquisition of additional data or more sophisticated analyses may improve the precision and accuracy of the prediction methods, but the need for a quantitive approach to the consideration of ground shock effects has been established.

## CONCLUSIONS

The purpose of this study was to determine the effects of ground shock from accidental explosions on structures and their contents. A major portion of the effort was the development of semi-empirical equations for predicting ground shock phemonology. Equations for predicting ground shock as a function of explosive weight, distance from the explosion and ground media properties have been presented. These equations were used to evaluate the design implications of ground shock effects. The study indicated that although ground shock per se is not a critical parameter for structural survivability, it could affect the survivability of a structure's contents such as personnel, equipment or munitions. A design approach by which the effects of ground shock can be determined is presented in the report.

## ACKNOWLEDGMENT

This study was sponsored by Picatinny Arsenal; the technical monitor was Mr. Paul Price. Mr. J. E. Tancreto, formerly of the Civil Engineering Laboratory (CEL) contributed to the initial portions of this study and Dr. H. A. Gaberson of CEL provided guidance in the areas of shock and vibration analysis. Dr. D. R. Richmond of Lovelace Foundation provided data on human shock tolerances.

### REFERENCES

- 1. Department of the Army Technical Manual TM-5-1300: Structures to resist the effects of accidental explosions. Washington, D.C., June 1969. (Also NAVFAC P-397, AFM 88-22).
- 2. Air Force Weapons Laboratory Technical Report AFWL-TR-74-102: The Air Force Manual for Design and Analysis of Hardened Structures, by R. E. Crawford, C. J. Higgins and E. H. Bultman. Kirtland Air Force Base, NM, October 1975.
- 3. Defense Atomic Support Agency. Report DASA-1283(IV): Nuclear Geoplosics, A sourcebook of underground motion and cratering, by F. M. Sauer, G. B. Clark, and D. C. Anderson. Washington, D.C., May 1964.
- 4. Department of the Interior, Bureau of Mines Bulletin 656: Blasting vibrations and their effects on structures, by H. R. Nicholls, C. F. Johnson and W. I. Duvall. Washington, D.C. 1971.
- 5. Atomic Energy Commission Report CEX-65.4: Biological tolerance to air blast and related biomedical criteria, by C. S. White, I. G. Bowen, D. R. Richmond. Washington, D.C., 18 October 1965.

# CORRELATION OF QUANTITY-DISTANCE AND WEAPONS-EFFECTS DEBRIS HAZARDS FOR UNDERGROUND EXPLOSIONS

by

A. D. Rooke, Jr.

U. S. Army Engineer Waterways Experiment Station Vicksburg, Mississippi

#### ABSTRACT

Disagreement in predictions of distances considered safe from explosion debris (ejecta) reveals differences in procedures used by the Department of Defense Explosives Safety Board (DDESB) and other agencies/organizations concerned with weapons-effects explosion research. DDESB predictions for "tolerable risks" given by quantity-distance standards show significantly smaller distances than those generally accepted as maxima for high-explosive tests. Although correlation is limited to storage chambers where debris ejection is essentially upward (i.e., tunnel entrances excluded) and where the loading density approximates the specific weight of TNT, the wide differences in prediction results suggest the need for reexamination of assumptions and procedures. This paper reviews explosion-debris origins and distributions for rocks and soils, highlighting differences in the DDESB and explosion-research problems. Ejecta hazards are discussed, to include impact (strike) probabilities and damage. Applications to the DDESB problem are suggested.

# CORRELATION OF QUANTITY-DISTANCE AND WEAPONS-EFFECTS DEBRIS HAZARDS FOR UNDERGROUND EXPLOSIONS

#### **OBJECTIVE**

1. A recent review of "safe" distances for protection from explosion debris (as prescribed in Department of Defense Explosives Safety Board (DDESB) quantity-distance tables for underground storage and similar criteria used in weapons-effects research) has brought to light some rather significant differences. The objectives of this paper are to define these differences, comparing the underlying problems and procedures for solving these problems, and to suggest a means of bringing the two standards into closer agreement.

## QUANTITY-DISTANCE VERSUS WEAPONS-EFFECTS EXPLOSIVE CASES

2. The DDESB quantity-distance criteria envision an underground storage chamber with some scaled overburden depth, as shown in Figure 1, taken from Reference 1. This concept generally agrees with weapons-effects depth-of-burial (DOB) for an explosive charge.\* However, the quantity-distance criteria are concerned mostly with chambers not completely full of explosive. The chamber is also an elongated, tunnel-like structure, considerably different from the weapons-effects case, which is usually a compact (often spherical) explosive charge completely filling the cavity within which it is contained. The standard explosive for weapons-effects work is TNT, other explosives being converted to "TNT equivalent." Thus,

<sup>\*</sup> Strickly speaking, DOB is measured from the surface to the charge center of gravity. For a spherical TNT charge, the scaled length of a charge radius is approximately 0.14 ft/lb<sup>1/3</sup>. The difference between the two methods of expressing overburden depth is important only in the case of shallow burial.

a comparison of the quantity-distance and weapons-effects cases is restricted to that portion of the quantity-distance table (Table  $7^2$ ) in which loading density equates to TNT specific weights, say, 95 to 100 lb/ft<sup>3</sup>. By looking at the chamber in cross-section, we can temporarily forget that it is elongated, although this must be taken into consideration before our comparison is complete.

3. With the above in mind, the quantity-distance formula for safe distance from debris shown in the memorandum on "Proposed Underground Storage Standards" becomes for our purposes

$$D_{id} = f_c(1.36)W^{0.41}$$

where  $f_c$  is a function of overburden depth scaled by cube-root scaling and the value (1.36) is an interpolation from Table 7, using a loading density of 96 lb/ft<sup>3</sup> for TNT.

4. The weapons-effects problem insofar as debris ejection is concerned is thus seen as a special case of the DDESB problem. Where the two overlap, agreement in "safe" distances would be expected; however as can be seen in Figures 2 and 3, this is not the case. Figure 2 is a graphical comparison of quantity-distance and weapons-effects safe distances versus scaled depth for explosive quantities of 1,000, 10,000, 100,000, and 1,000,000 pounds. Intermediate values approximate a logarithmic dependency, e.g., the curve for 30,000 pounds falls about 0.5 of the distance between the 10,000- and 100,000-pound curves, the curve for 50,000 pounds lies about 0.7 of the distance between the two, etc. Figure 2a shows the quantity-distance data and 2b the weapons-effects data. Figure 3 is a

similar comparison for hard rock. The differences are rather striking, especially for the smaller explosive weights. Not only do "safe" distances differ by factors of ten or more, but the maxima of the curves do not correspond. This latter difference is partly explained by the fact that depth in quantity-distance terms is measured to the top of the underground storage chamber, while in weapons-effects work it is taken to the charge center of gravity. The decreasing disparity between the two families of curves with increasing explosive weight W is attributable to differences in scaling exponents. While W<sup>0.41</sup> scaling is used for DDESB debris distance, W1/6 is used in weapons-effects research to define an envelope which includes maximum ejecta distances recorded for various DOB's, as shown in Figure 4. The latter is an empirically derived exponent. At this point it is important to consider the terms "safe distance" and "maximum ejecta range." As stated above, the latter is a documented maximum, frequently used in weapons-effects tests to insure the safety of exposed personnel. Paragraph 34b of Reference I states that quantitydistance tables are based upon "...distances at which the debris risk is considered to be tolerable for inhabited buildings..." This tends to explain part of the difference in the two procedures; some risk appears acceptable in the DDESB case. The following paragraphs discuss this risk.

## CRATER EJECTA

6. Since a discussion of debris hazards must rely on data from cratering studies of weapons-effects tests, it is necessary to define some of the terms associated with these studies. Figure 5 shows the half-profile

and nomenclature of a crater resulting from a buried detonation. Of the material dissociated from the parent medium, a portion falls back into the crater void, forming the apparent crater, and the remainder is ejected. Of the latter (ejecta), more than half is usually deposited immediately adjacent to the crater, forming the crater lip. That which remains forms the discontinuous portion of the ejecta field and in rock or cohesive soil is deposited as discrete particles ranging in size from a few ounces to many tons, out to distances approximately 100 times or more greater than the apparent crater radius,\* or well into the fractional-psi overpressure range. Figure 6 shows the origins of crater ejecta and general deposition bands; note that the longer-range material originates near the surface and close to ground zero. There is little doubt that crater ejecta presents an injury/damage threat; the question is: how great is the threat? 7. An example may serve to illustrate the debris risk. Consider 50 tons of TNT-equivalent explosive detonated in a completely full chamber in soft rock at depth 0.8 ft/lb 1/3. From a graph such as Figure 7, the apparent crater radius for one ton can be read as 22 feet; by W<sup>0.3</sup> scaling,\*\* the apparent radius of the crater for a 50-ton charge is 22 x  $(50)^{0.3}$  = 71 feet. From Figure 8, we can estimate that a total of 15,000 tons of material will be ejected. The quantity-distance graph for this medium and depth shows a safe distance ~1,800 feet, or slightly more than 25 apparent crater radii. Figure 9 indicates that approximately 1 percent (150 tons) of ejecta will still be aloft at this distance. Figure 10 gives the

<sup>\*</sup> To avoid troublesome problems with scaling "laws," linear measurements in cratering research are often expressed in terms of crater radii.

<sup>\*\*</sup> An empirically derived scaling procedure which produces good results in this range of explosive yields.

expected size (i.e., a straight-line fit of maximum-size data points) of the largest particle at this range. For tuff, this falls just below the abscissa, representing a particle size of slightly less than 10 pounds; for shale, this is approximately 100 pounds. A recent study has proposed a means of estimating probabilities of strikes by ejecta particles of various sizes under varying conditions of explosion geometry, cratered medium, and distance from ground zero. While the development of the procedure is beyond the scope of this paper, Figure 11 shows, in a highly preliminary form, the strike probabilities which might be expected on a single dwelling (say, 4,000 ft<sup>2</sup>) for the conditions of the example problem. It shows a strike probability of 1 or 2 percent for a 10-pound particle, and an insignificant risk for a 100-pound particle. Boundaries of the curve envelope are determined by assumptions concerning secondary (impact) particle breakage, i.e., how closely does the "as found" ejecta field resemble the in-flight field just prior to impact?

8. What sort of damage threat is posed by debris of these sizes? A rough idea can be obtained from the following illustrations. Figure 12 shows one result of a recent study done by McDonnell-Douglas for the Waterways Experiment Station, 4 in which penetration parameters for rock projectiles were determined. (The figure shows penetration by a hard rock projectile, more severe than our example.) Figure 13 shows the result of an accidental impact of a clay/siltstone particle weighing slightly over 100 pounds on a model (3-1/4-inch-thick) runway in a recent test series. By coincidence, the impact occurred 25 crater radii from ground zero. The destructive potential is obvious in both cases.

Figure 14 is a graph from the McDonnell-Douglas study which shows penetration of steel plate as functions of particle size and velocity. Data are also available to link destruction to particle momentum and kinetic energy.

## APPLICATIONS TO QUANTITY-DISTANCE STANDARDS

9. Returning to the problem of the elongated shape of an underground storage chamber, perhaps the best comparison that we can draw with explosion research is from row- and linear-charge experiments. They show that ground shock and ejecta are enhanced in either direction perpendicular to the line of explosives and reduced in either direction parallel to the line of explosives. There are no numbers available to quantify the effect on ejecta, but ground shock may be enhanced as much as 50 percent. Considering this and the figures we have just seen, it appears that one of the worst things that can happen regarding debris from an underground storage explosion is to have competent material, natural or manmade, near the surface and just off the longitudinal axis of the chamber so as to create hard, long-range missiles.

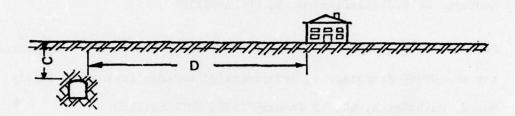
## SUMMARY AND RECOMMENDATIONS

10. In this paper we have examined the differences in hazard criteria between DDESB and weapons-effects research, as well as differences in explosive geometry. While the area of direct correlation is small, it would seem that the two should be in closer agreement, all things considered. The DDESB graphs differ from their weapons-effects counterparts in the implicit assumption of some risk. A rough estimate of this risk is possible where the two problems can be compared; no such estimate can be made for explosion geometries which are unique to the DDESB case.

11. Techniques of evaluating ejecta distribution from weapons employment are fast approaching the point where hazards can be expressed in terms of strike probabilities and associated damage levels for various size particles. It is suggested that DDESB might place a probability on the term "tolerable risk." In view of the rather specialized geometry of the DDESB problem, this would entail experimental testing, either full-scale or model. If the risk should turn out to be less tolerable than supposed, there may be steps that one might take to prevent the formation of large, long-range particles and thus alleviate the problem. Hopefully, a new look at this aspect of storage hazards would result in a better definition of acceptable risk and greater confidence that it will not be exceeded.

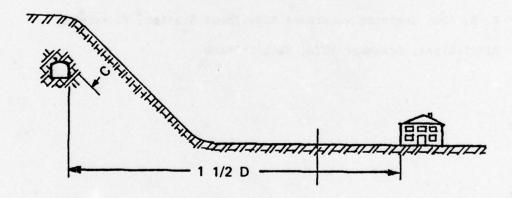
#### REFERENCES

- Quantity-Distances for Military Explosives, Part 3 Underground Storage, ESTC/22/Leaflet No. 5, UNCLASSIFIED.
- Perkins, R. G., "Proposed Underground Storage Standards," Memorandum for the DDESB Secretariat, Department of Defense Explosives Safety Board, Washington, DC, 12 January 1976, UNCLASSIFIED.
- Rooke, Allen D., Jr., "Graphic Portrayal of Discrete Explosion-Produced Crater-Ejecta Characteristics," Miscellaneous Paper N-76-7,
   U. S. Army Engineer Waterways Experiment Station, Vicksburg,
   Mississippi, June 1976, UNCLASSIFIED.
- "Research Study of Ejecta Impact Parameters, Contract Report N-73-2,
   U. S. Army Engineer Waterways Experiment Station, Vicksburg,
   Mississippi, December 1973, UNCLASSIFIED.



Case 1: House is sited at distance D in accordance with tables contained in ESTC/220/LEAFLET No. 5.

The risk from debris at this point is deemed to be tolerable in the context of an accidental underground explosion.



Although the minimum cover is the same as in Case 1, the slope of the terrain will aggravate the debris in the direction of the house. Therefore the house is sited at distance 1½ D.

Figure 1. The debris hazard problem, from ESTC/220/Leaflet No. 5 (Part 3--Underground Storage)

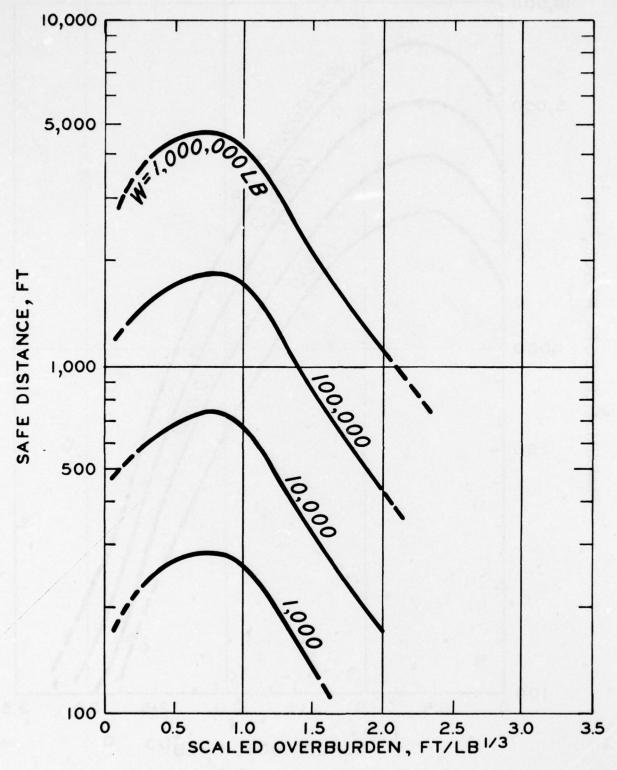


Figure 2a. Quantity-distance safety standards for underground storage in soft rock

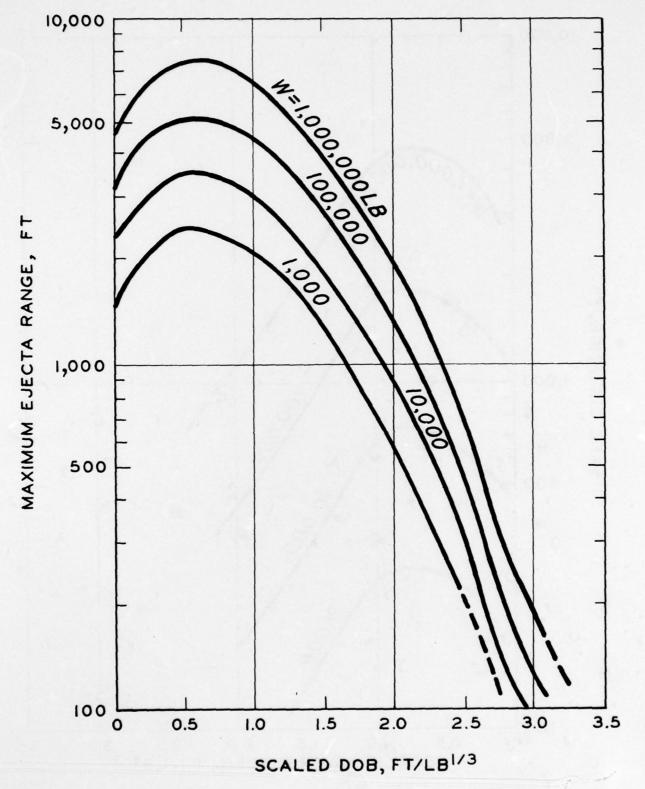


Figure 2b. Weapons-effects maximum ejecta ranges for buried explosions in soft rock

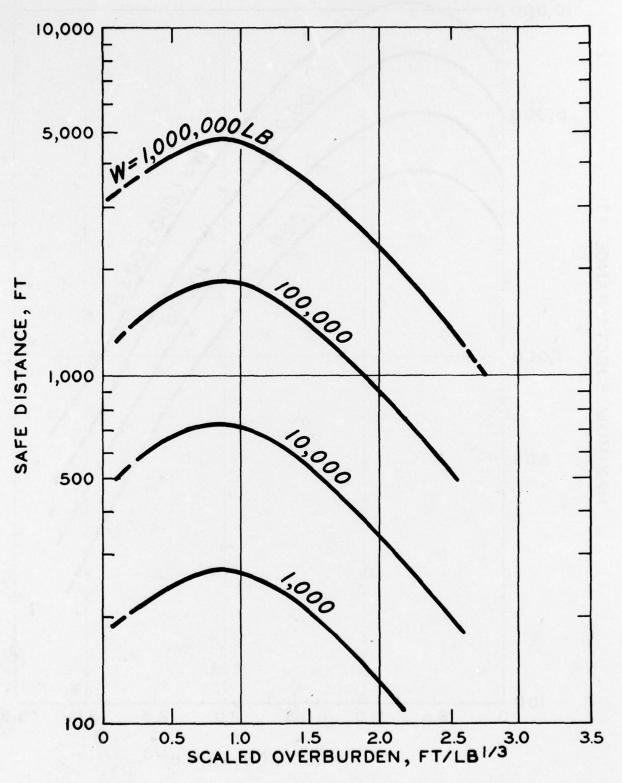


Figure 3a. Quantity-distance safety standards for underground storage in hard rock

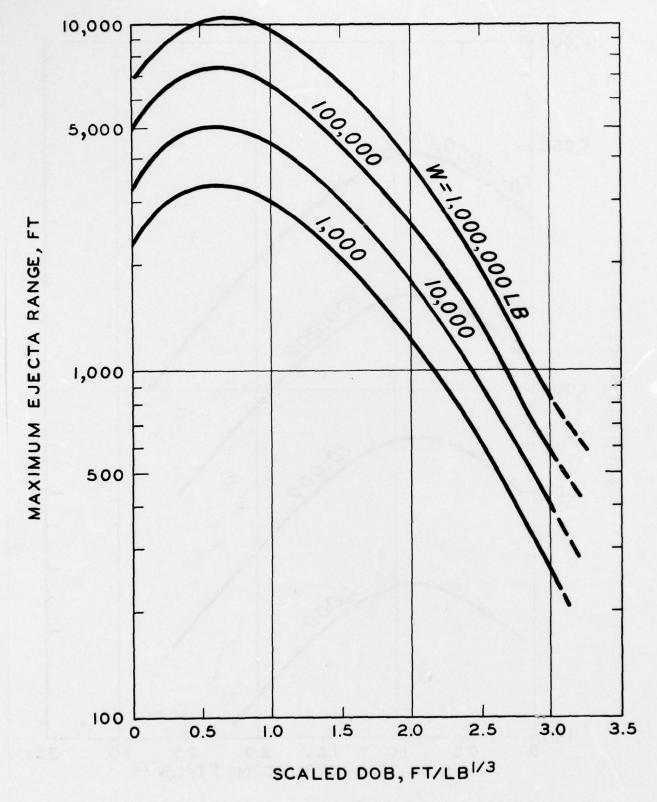


Figure 3b. Weapons-effects maximum ejecta ranges for buried explosions in hard rock

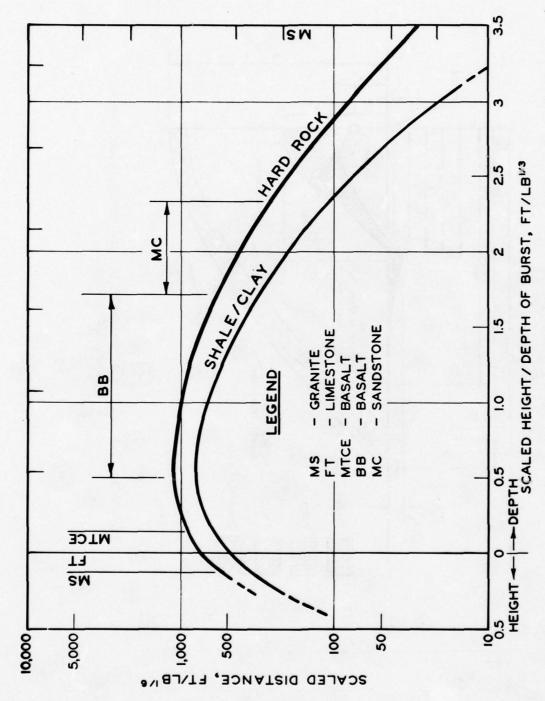


Figure 4. Envelopes of maximum ejecta ranges from weapons effects tests (reference 3)

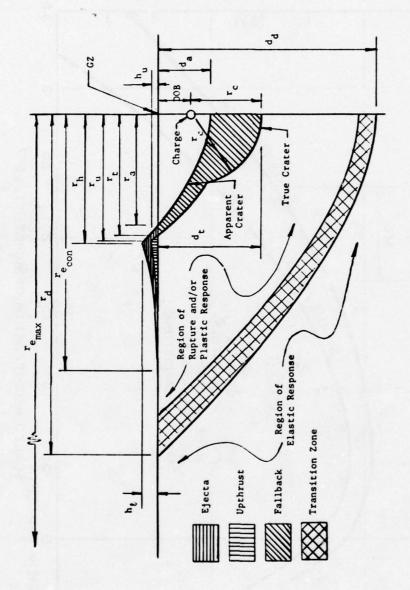
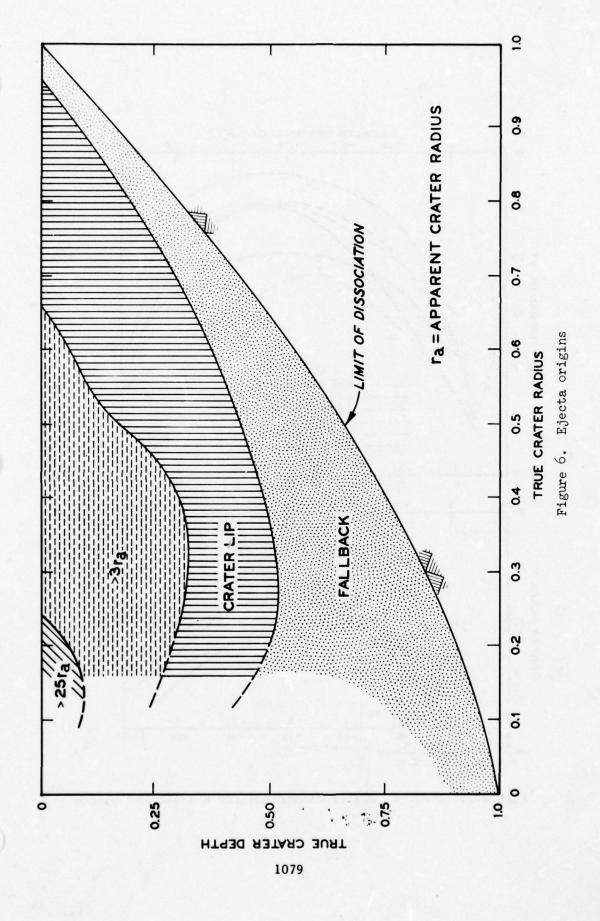


Figure 5. Typical crater half-profile and nomenclature for a buried detonation



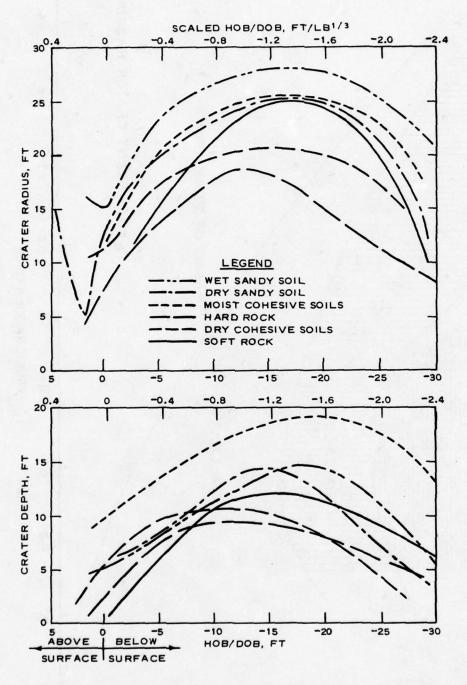


Figure 7. Apparent crater dimensions for a 1-ton TNT charge

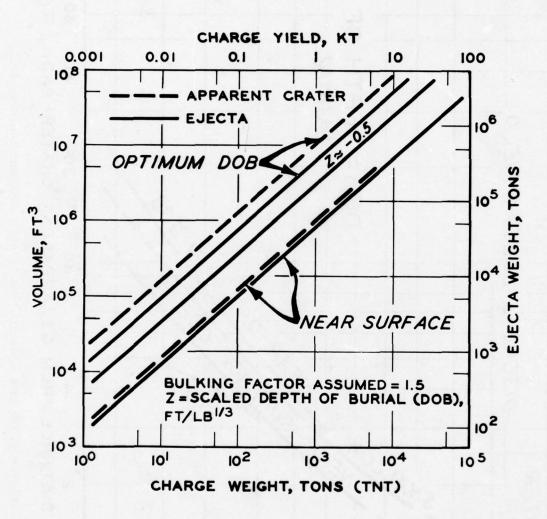


Figure 8. Apparent crater volume and ejecta weight for explosions in soft rock and cohesive soil

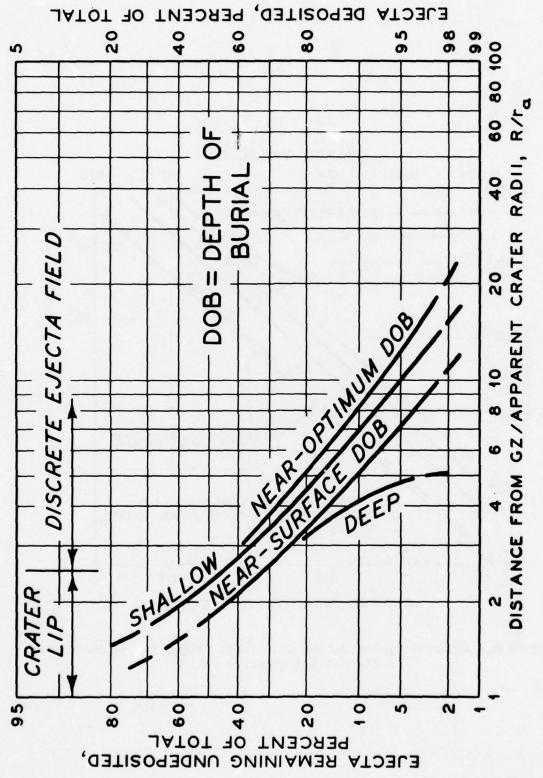


Figure 9. Ejecta distribution in soft rock and cohesive soil

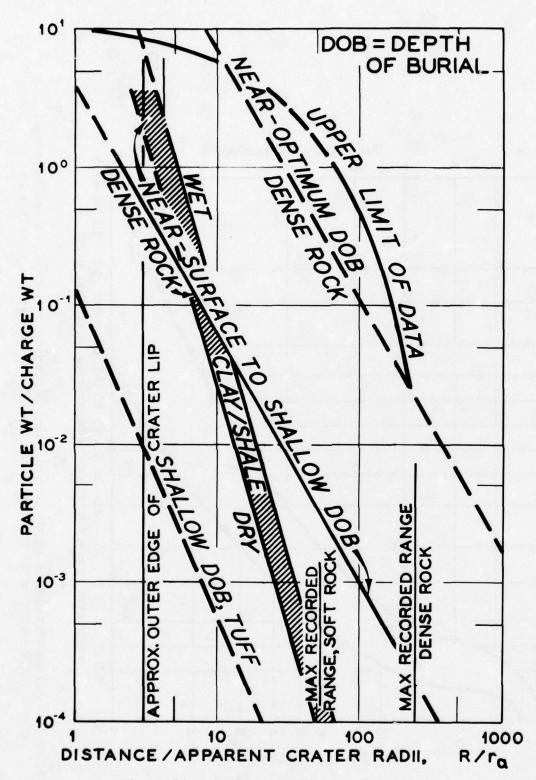


Figure 10. Maximum ejecta size vs range

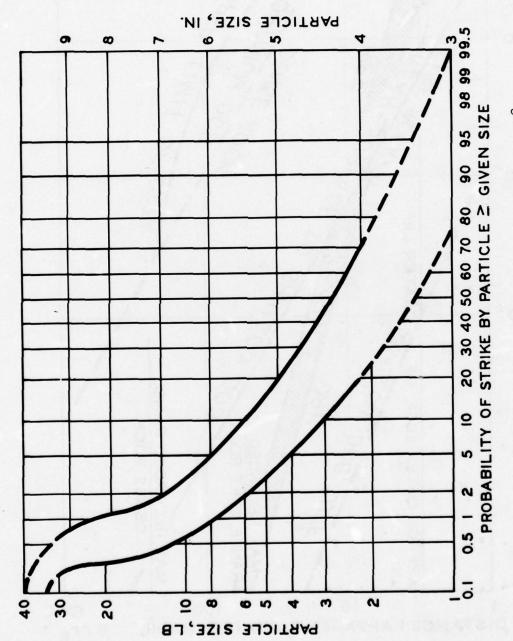


Figure 11. Estimated range of ejecta strike probabilities for a 4,000-ft<sup>2</sup> area 25 apparent crater radii away from ground zero of a 50-ton TNT charge buried in soft rock

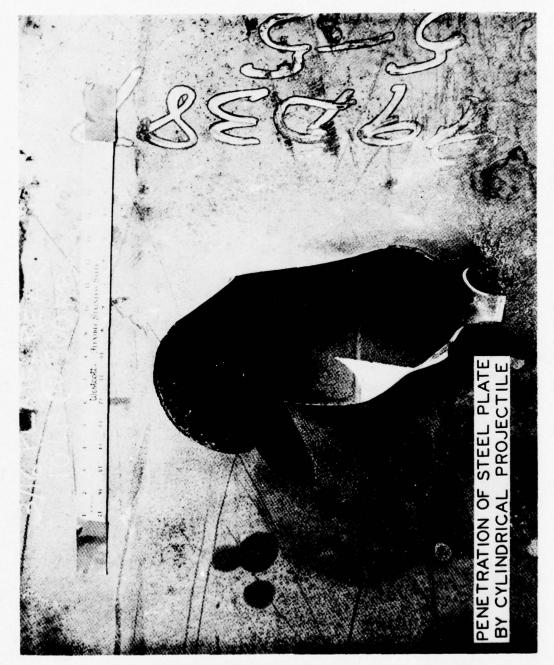


Figure 12. McDonnell-Douglas penetration study

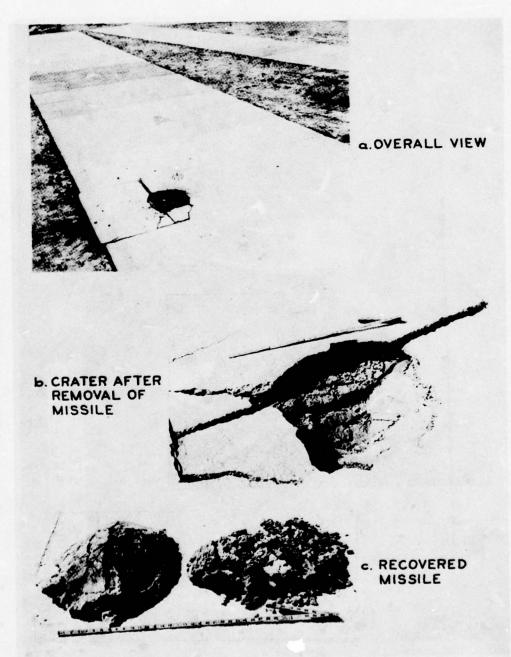


Figure 13. Clay/siltstone missile impact on a model runway

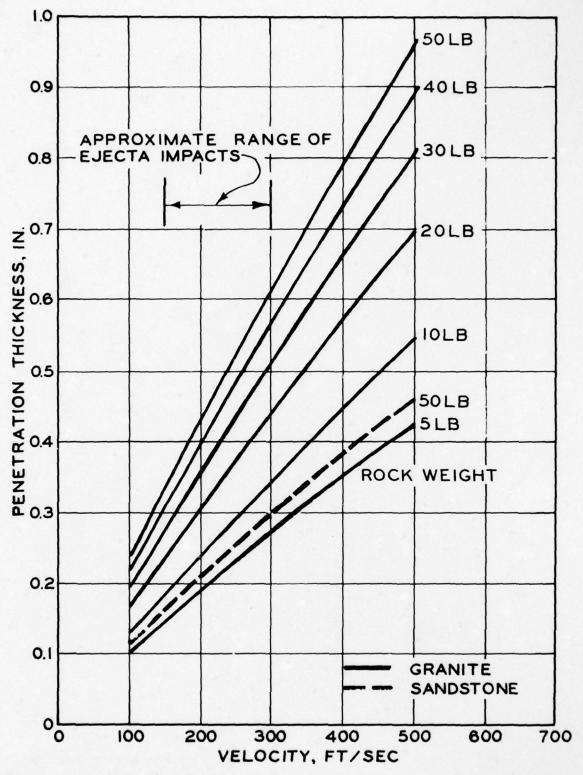


Figure 14. Penetration of mild steel plate by rock projectiles

#### ROCKY MOUNTAIN ARSENAL M34 CLUSTER DISASSEMBLY OPERATIONS

Irwin M. Glassman Rocky Mountain Arsenal Denver, Colorado

#### I. INTRODUCTION

In the fall of 1968, the Department of the Army decided to dispose of certain chemical munitions which were obsolete and excess to the national deterrent stockpile. The proposed disposal plan (Operation CHASE) called for these munitions to be loaded on hulks and taken under U. S. Coast Guard escort to a previously designated explosives dumping site beyond the continental shelf and sunk in the ocean. Included in the planned operation was the disposal of U. S. Air Force M34 GB nerve gas cluster bombs stored at Rocky Mountain Arsenal (RMA), Denver, Colorado.

On 14 May 69, the National Academy of Sciences was requested on behalf of the Department of the Army to make an independent study of the Operation CHASE disposal plan. In response to this request, a panel of 12 distinguished experts drawn primarily from this country's leading industrial, educational, and research institutions, assembled in Washington to consider carefully the proposed chemical disposal plan.

With respect to the M34 Clusters, the panel made the following recommendations: "We recommend, therefore, that the M34 Clusters be disassembled and the withdrawn GB be destroyed chemically either by acid or alkaline hydrolysis. This procedure would result in waste materials without 'nerve gas' properties and not more hazardous than larger volumes of industrial waste that are routinely discharged

elsewhere. On balance, weighing various hazards, we recommend that this disassembly be undertaken at RMA because (1) The hazards arising from transportation by rail will be eliminated; (2) RMA has an experienced staff that has already disassembled M34 Clusters; (3) RMA has facilities that can be fairly rapidly expanded for the recommended operation ..."

Small quantities of M34 Clusters have been demilitarized in the past under field conditions at RMA. Review of the procedures and safety for such outdoor demilitarization indicated their inadequacy to meet the current emphasis and guidance on maximum safety, particularly where many thousands of clusters are involved. Accordingly, Task Force Eagle was established to plan and conduct a program for indoor demilitarization in an explosion-proof, enclosed facility, using remote control and automated equipment to the maximum extent. The objective was to reduce or eliminate the use of personnel in direct proximity to the declustering operation and to provide complete safety to the surrounding environment and population during normal operations or in event of accidental munition functioning.

As an outgrowth of the National Academy of Sciences recommendations and in light of field condition demilitarization experience, the Department of the Army formulated policy guidance which governed planning and implementation of the M34 Demilitarization Program. The guidance provided required the following:

# IEWGRAPH 1

- Absolute safety and security, rather than cost or time.
- Maximum protection for operating personnel.
- . Absolute assurance of total containment of agent.
- Incontrovertible data to justify personnel safety, security,
   and community safeguard aspects.

#### EWGRAPH 2 14 CLUSTER BOMB

CLUSTER CONSTRUCTION - The M34 Cluster consists of a M29 Cluster Adapter filled with 76 M125 Bombs. Omitted is the tail fin assembly, which was not installed in the item stored at RMA and had been disposed of previously. The M34 Cluster is approximately 57 inches long, 19 inches in diameter, and weighs approximately 1,100 pounds. The 76 M125 Bombs are arranged in four groups of 19 each. The bombs are placed so that the arming bar on each parachute opening delay is held in place by an adjacent bomb. Six cluster bars, equally spaced around the bomb groups, are retained by four cluster bands. The cluster bars retain the nose assembly and rear end plate at either end of the M125 Bomb groups. Cardboard spacers are placed between the rear end plate and the bomb groups, to limit movement within the assembly. This assembly is placed within the casing to form the M34 Cluster. A stud through either end of the split nut holds the cluster together. The pressure plate retains the split nut to the rear end plate stud. A rubber gasket, installed between the casing and the nose assembly, provides a

gastight seal. A lead foil seal is installed under the closure cap to prevent any possible leakage through the cluster ejection cartridge holes. This seal is not removed prior to the declustering operation.

III. CLUSTER OPERATION - When the M34 Cluster is air dropped, a wire is withdrawn from the arming fuzes permitting the vanes on the fuzes to rotate in the airstream. After a predetermined number of rotations, the arming fuzes detonate a burster charge, which in turn detonates the cluster ejection cartridges. Expanding gases from the cartridges force the pressure plate toward the nose of the cluster, releasing the rear end plate stud from the split nut. Continued expansion of the gases forces the framework out of the casing. As each cluster band clears the casing, a buckle opens and releases the band. After all four cluster bands are released, the cluster bars, the nose assembly, and the pressure plate drop away, allowing the M125 Bombs to disperse and fall separately. As the bombs separate from the cluster, the arming bar on the MI Parachute Opening Delay springs free; and the firing mechanism strikes the primer, which ignites the delay charge. After three to seven seconds, the delay charge ignites the separation cartridge which separates the steel cable and frees the parachute cap and the fuze arming ring. When the parachute deploys, the bomb slows abruptly, causing the arming ring to fall away from

the fuze. The steel balls then release the firing pin assembly, and the firing pin spring forces the pin toward the nose of the fuze. As the firing pin moves forward, the rotor is released; and a spring forces the rotor toward the other side of the fuze. The rotor revolves 90 degrees as it moves so that the detonator charge is in line with the firing pin and tetryl charge. A spring-driven pin locks the rotor in armed position. When the head of the firing pin strikes a solid object, the detonator tetryl lead charge, and finally, the burster explode. The burster explosion fractures the bomb body and disperses the liquid GB.

'IEWGRAPH 3 10DELS OF :LUSTER & 1125 BOMBLET

#### IV. GENERAL DESCRIPTION OF PROCESS

The M34 Cluster is disassembled and the GB removed in an explosion-proof facility with reinforced concrete walls two feet thick. This facility is capable of withstanding the accidental explosion of an entire M34 Cluster. Explosion-proof and leak-proof entrance and exit doors for personnel and equipment have been installed. The explosion-proof sealed doors allow entrance of the clusters and exit of the inert parts from the explosion-proof cubicle area of the facility. The doors are interlocked to operate one at a time to prevent escape of vapors during declustering operations. Although explosion-proof electrical equipment is not mandatory in the demil program (e.g., GB

vapors do not flash or support combustion), nevertheless in the interest of additional safety and reliability, Class 1 explosion-proof electrical equipment, fittings, and conduit were installed throughout the cubicle area wherever possible. The programmed manipulators were not made explosion-proof because their complexity would require a major redesign that would incur time and cost penalties in excess of the planned program. Also, the auxiliary TV lighting was not available in explosion-proof configuration; but fully enclosed, weatherproof housings with tempered heatresistant lenses were installed. The TV cameras are housed in explosion-proof, see-through cases; and the ordinary cubicle lighting is also explosion-proof.

During normal operations, the cubicle area is continuously ventilated and maintained under negative pressure with respect to ambient. Any GB which may evporate during normal demilitarization operations is carried through a duct to underground scrubbers. The holding area, change room, and the GB pump room are also maintained at negative pressures and exhausted to the scrubbers to prevent the possibility of any leakage to the atmosphere from these locations.

The demilitarization process for M34 Clusters instituted in Oct 73 involved a declustering system wherein the M125 Bombs were

removed from the cluster by a programmed manipulator and placed in a fuze staking machine. The manipulator's robot arm, which contains a vacuum pickup device, removed the bombs one at a time in a predetermined sequence. When a bomb was removed from the cluster, the parachute delay arming bar released, initiating a three to seven second delay train. The bomb was placed in the fuze staker machine where the delay wire was separated from the bomb when the delay charge functioned. The delay wire fell into a disposal chute at the bottom of the fuze staker. The staker cycle includes engagement of a blade that cut any delay wire which had not been separated from the bomb. Any loose delay wire remaining on a bomb was stripped off as it was pushed out of the staker through a gage plate opening. The disposal chute then transferred the delay wires to the inert parts conveyor cart for disposal.

During this initial production operation, many problems were encountered due to the functioning of the delay wire. The principal problems involved were as follows:

Delays functioned prematurely as bombs were transferred from the cluster to the staker. This allowed delay wires to fall into the cluster bundle and adjacent equipment, causing equipment malfunctions and production down time while the delay wires were removed.

Delays frequently functioned prematurely as the cluster bundle became loose during down loading. Delay parts then had to be removed.

As a result of these difficulties, frequent entries of cubicles by personnel were required to clear equipment or repair damage, thereby increasing the danger of exposure to toxic material. In addition, a bomb with no delay wire dropped by the robot arm could become armed.

Engineering studies to prevent this problem led to a determination that premature functioning of the delay could be prevented by inerting its explosion train. Several methods were investigated to accomplish this. Included were freezing, epoxysealant bonding, mechanical clamps, spot welds, and water soaking. The water-soaking technique proved to be the most promising. Delay inerting is now accomplished by wetting the pyrotechnic delay charge. The MIAI delay is defeated by water entry through the threaded brass plug or wax seal. A conveyor takes the M34 Cluster into the Inerting Drill and Tap Booth, which contains a work cabinet into which the cluster is placed while holes are drilled with a one-fourth inch positive stop drill and tapped at either end of the case and double shut-off quick disconnect fittings are inserted. The cluster moves into an air lock for leak checking and from there by a bridge crane to one of two five-cluster capacity soak tanks.

In the soak tank, the cluster receives inlet and outlet hoses which circulate the sodium carbonate inerting solution through the cluster case at approximately 135°F while the cluster is also immersed in a water bath maintained at 135°F. From the soak tanks, the cluster is placed in a tracked leak booth cart which enters the leak booth. The quick disconnects are removed from the cluster case and replaced with plug fittings. The cluster is then checked for leaks and returned to the Inerting Room, where it is placed on one of two ready racks and held until transportation to the demilitarization cubicles. The work cabinet, under negative pressure, is independently ventilated through its own scrubber.

IEWGRAPH 4 HART M34 PROCESS

- V. <u>CLUSTER DISASSEMBLY</u> Essentially, the demilitarization process today consists of the major functions listed below.

  This paper will speak in detail to the declustering actions cited in 2, 3, 4, 6, and 7 below:
- Movement of the cluster from the storage area in the field, through the holding area, through delay inerting, and into one of the declustering cubicles.
- Declustering, consisting of removal of the cluster case and transfer of the individual M125 Bombs to the staker.
- Safing the M125 Bomb fuze by staking the arming ring in place.

- Punching the M125 Bomb body and draining the GB into the GB pipeline from transfer to the detoxification facility.
- Chemical detoxificiation of the GB with a sodium hydroxide solution and subsequent spray drying of the resulting salt solution.
- 6. Shearing the explosive burster charge from the fuze and subsequent burning of the explosive and the fuze in the bomb in a deactivation furnace.
- Decontamination of the inert metal parts in decontamination furnaces and subsequent disposal.

IEWGRAPH 5 )BOT ARM EVICE TO EMOVE BOMBS VI. <u>BOMB PROCESSING</u> - Cluster processing consists of transporting clusters from the storage area to the demilitarization facility where they are placed in the Holding Area in preparation for delay inerting and then entry into the cubicles after delay inerting. Each cluster is moved to the cubicle by cart and placed in front of the cubicle entrance doors. The cluster is lifted from the support by an air-operated, monorail tractor stored in the blast lock and conveyed through the blast lock into a cluster crdale in the cubicle. The case, bands, and bars are removed, leaving the 76 bombs exposed.

LM CLIP

Declustering - The bombs are removed from the cluster by a programmed manipulator called a Versatran and placed in a staking machine. The Versatran's robot arm, which contains a vacuum gripper

pickup head, removes the bombs one at a time in a predetermined sequence. The pickup head contains clamps which prevent the parachute cap and fuze arming ring from being displaced while the bomb is being transferred to the staker. Three air-operated holddowns, one in back and one on either side of the pickup head, hold the adjacent bombs in place while the pickup head is removing a bomb from the cluster.

### Staking

The staker stakes the arming ring in the fuze body. The staker consists of a hydraulically-operated head with three hardened steel points. As the head moves forward, the steel points penetrate the fuze body, displacing metal against the arming ring. The displaced metal secures the arming ring in the body, preventing the fuze from arming. The parachute cap is also staked to the bomb body by two diametrically opposed staking cylinders. When the staking functions are completed, the bomb is pushed out of the staker bed through the gage plate, which strips away the delay wire, then travels down a chute to the punch and weigh conveyor. The delay wire falls into a vibrating chute and is carried to the IP feed conveyor. The delay wire falls into a vibrating chute and is carried to the IP feed conveyor for disposal with the other inert parts.

The staking operations are actuated in a programmed sequence with interlocks to ensure proper completion. Proximty switches

in the staker bed detect a misaligned bomb and automatically stop operation until corrective action is taken. A pressure switch in the hydraulic fluid supply line to the staker cylinder also disables the staking sequence if the pressure is too low to assure satisfactory staking of the fuze. The entire staking sequence is observed continuously by operators using television monitors on the control console. Automatic sequencing can be stopped at any time and the Versatran stepped through a manually-controlled sequence to correct malfunctions, misalignment, etc. The manual manipulators are used to remove delay wires, to reposition bombs, and to correct any minor difficulties arising during the declustering and staking operations.

After the bomb leaves the staker, it is carried on the punch and weigh conveyor to the punch station.

Punching - The punch station uses a hydraulic cylinder to operate a punch head containing two punches. The punches are spaced so that they pierce both top and bottom arcs on the bomb circumference and avoid disturbing the tetryl charge in the burster well in the center of the bomb. After the punches are retracted, the bomb is allowed to remain in the punch station for several seconds until the CB drains from the lower holes into a drain line under the punch station. The punch station is provided with interlocks that stop the conveyor if the full punch and retract strokes are not completed. The punch cycle can be repeated by using manually-operated controls on the control console.

Weighing - The bomb next moves down the punch and weigh conveyor to the weigh station to receive the weight of the bomb. This system is calibrated so that an excessive amount of GB remaining in the bomb will stop the conveyor. If an overweight condition occurs, the bomb remains at the weigh station for a timed interval to allow further drainage if necessary. The weighing operation is then recycled using manual controls on the control console. The punch and weigh conveyor cannot be operated, either automatically or manually, as long as an overweight bomb is on the weigh station.

Caustic Spray and Dipping - After the bomb weight is within acceptable limits, the punch and weigh conveyor is indexed toward the pickup station. When the bomb reaches the end of the punch and weigh conveyor, it is picked up by a zig-zag conveyor. The zig-zag conveyor is an endless conveyor that employs a series of suspended swiveling J-hooks to pick up the bombs and transfer them to the burster shear. A dip tank containing caustic solution is installed in the path of both zig-zag conveyors. The conveyor traverses the tanks so that the bombs travel 15 feet immersed in the caustic solution to detoxify residual GB on the inside of the bomb. The bombs are then conveyed from the dip tank to the burster shead conveyor.

<u>Burster Shearing</u> - The burster shear positions and clamps the bombs to ensure successful shearing of the burster well by

the shear blade. The hydraulically-driven shear blade then penetrates the outside of the bomb and shears the burster well at the fuze end. Thus, when the bomb is ejected into the deactivation furnace retort, the possibility of the burster exploding instead of burning is greatly reduced. An explosive collector in Cubicle 8 with vacuum receivers under the burster shears removes any tetryl particles caused by the shearing action of the blade. The collector mixes the tetryl particles with water, then stores the mixture. Periodically, the mixture is drained into cylindrical containers and placed on the zig-zag conveyor where it is processed through the deactivation furnace and destroyed. The burster shear conveyor is interlocked to shut off if a bomb is in the shear, if a bomb is present in the blast lock tube, if the bomb is not properly clamped, or if the shear blade does not travel its full stroke. The shear sequence can be controlled manually from the control console in event of a malfunction. After shearing, the bomb is ejected into a chute going to the deactivation furnace. The chute extends through the Cubicle 8 wall, slopes 40° to the entrance of the deactivation furnace, and has blast-resistant ball valves installed on one end. In addition, two flappers are installed in the chute to withstand the pressure generated by detonation of burster charges either in the chute or deactivation furnace. The ball valves maintain the integrity of the cubicle area closure in the event of a full cluster detonation.

Deactivating - The deactivation furnace is located in a blast-resistant concrete structure. The furnace consists of a rotating retort built to withstand simultaneous detonation of seven bombs. The bombs are in the retort for approximately 10 to 12 minutes. This ensures that the burster charges ignite near the center of the retort and are completely burned before leaving the furnace. The retort has stationary enclosures at both ends. The enclosure at the feed end of the furnace contains a feed chute for receiving bombs from the ball valves. The enclosure at the discharge end contains the burner assembly and the exit chute for dropping burned bombs into the discharge conveyor. The furnace is gas fired and operates at approximately 1,200°F. Flame propagation and airflow are opposite to bomb travel, so that the bomb travels into the higher temperature. Combustion gases exit from the feed end of the furnace, then flow into an expansion plenum on the roof of the furnace room, through four blast attenuator ducts and into the feed end of the bomb decontamination furnace. The discharge conveyor carries the bombs to the decontamination furnace. The melted aluminum from the bomb fuzes drops through the screen at the discharge end of the retort onto an aluminum recovery conveyor, which deposits the solidified lumps of aluminum into a disposal container outside the building. A TV camera, capable of scanning the deactivation furnace room, is provided for monitoring the discharge end of the deactivation furnace.

Decontaminating - The bomb decontamination furnace is an enclosed steel structure lined with refractory brick and has an endless woven steel conveyor belt that carries the bombs through the furnace. The bombs are in the furnace for approximately 25 minutes. A discharge conveyor at the end of the furnace conveys the burned bombs into a disposal truck. The furnace operates on natural gas and is thermostatically controlled to heat the bombs to 1,5000F to ensure complete destruction of any residual contamination. Combustion gases from the furnace are processed through the furnace scrubber system before they are released to the atmosphere.

Safety interlocks have been designed into the process wherever a possibility of operator error could cause difficulty. The interlocks ensure that equipment is operating at design parameters and each programmed event is completed before the next is allowed to start.

Operators in all work areas are in constant communication with each other through headsets. A public address system, from which the shift supervisor can make announcements, is located in the control room. Telephones and headset jacks are located at every operator's station and throughout the cubicle area to assist in directing maintenance personnel during the maintenance shift. In addition, radio walkie-talkies are utilized.

The control console contains the controls and indicators for operating and monitoring the cluster disassembly and GB removal. The console is divided into eight panel sections.

Each section contains two closed circuit TV monitors for observing the operations controlled from that panel. There are seven cameras in each cubicle (5 and 7), two in Corridor 4, and one in the deactivation furnace room. The cameras have zoom capabilities for observing critical operations and can be positioned to scan wide areas. Every critical and noncritical function in the process is constantly monitored and can be instantly shut down.

In conjunction with the control console, an annunciator panel, located at the far end of the console, monitors all support equipment functions such as hydraulic pressures and temperatures, caustic spray pressures, GB storage tank level, deactivation furnace temperature and retort rotation, decontamination furnace temperatures, conveyor operations, and personnel door status. The indicators on the annunciator flash red and an audible alarm sounds if any of the system do not maintain their design parameters. The console also contains continuously operating strip chart recorders which record all furnace and scrubber air temperatures, cubicle and deactivation furnace room air pressures, the furnace scrubber sump pH index, and air velocities in critical ventilation and furnace combustion gas ducts.

The M34 Cluster Demilitarization Program has been designed to provide complete safety to the surrounding environment and population during normal operations and in the event of accidental munition functioning.

# ROCKY MOUNTAIN ARSENAL ENVIRONMENTAL EMISSION CONTROL SYSTEM

Robert E. Boyle, PhD, FAIC Rocky Mountain Arsenal Denver, Colorado

#### ABSTRACT

THE ROCKY MOUNTAIN ARSENAL ENVIRONMENTAL EMISSION CONTROL

SYSTEM IS A UNIQUE SYSTEM OF SAMPLING STATIONS, STARTING

AT THE PERIMETER OF THE ARSENAL AND CLOSING TO THE POTENTIAL

MAJOR SOURCE OF THE POLLUTANT. THE SYSTEM OPERATES TWENTY
FOUR (24) HOURS A DAY, SEVEN (7) DAYS A WEEK, AND FIFTY-TWO

(52) WEEKS A YEAR. IT EMPLOYS A CONCEPT OF ACTION LIMITS

TO WHICH ANALYSES ARE ACCOMPLISHED SO AS TO DETERMINE WELL

BEFORE EMISSION LIMITS ARE REACHED THAT AN UPSET CONDITION

IS IN THE MAKING OR HAS OCCURRED. THIS CONCEPT THEN ALLOWS

FOR PERSONNEL WARNINGS, AS WELL AS DENOTING TO PLANT ENGINEER
ING PERSONNEL THAT A THOROUGH REVIEW OF THE OPERATING SYSTEM

IS REQUIRED, AND IN MOST CASES, PINPOINTING THE AREA OF

CONCERN. THE SYSTEM EMPLOYS STANDARD ARMY AGENT ALARMS AND

A QUANTITATIVE ANALYTICAL SCHEME SENSITIVE TO CONCENTRATIONS

AS LOW AS 0.2 ng/m1 OF SOLUTION.

### ENVIRONMENTAL EMISSION CONTROL

## I. INTRODUCTION.

Nerve agent GB is one of the most toxic synthetic substances known to man. In the 25 years or so that GB has been studied, manufactured and now demilitarized, thousands of workers have been involved. Accompanying occupational health and safety programs, considered to be among the best in the nation, have exerted a continuous effort to prevent exposure. The few people who were accidently exposed to large enough amounts to require treatment recovered without known disability to date. The hundreds of people who received minor accidental exposures required little or no treatment. No serious consequences developed, only mild shortlasting symptoms.

The possibility that some GB would escape into the environment during demilitarization operations, a unique and venturesome undertaking, made it essential to determine air concentrations to which the working force, general population, flora and fauna could be exposed, even on a continuous, indefinite basis without showing any effects that could be attributed to GB. It is with this in mind that industrial and environmental "no effect" levels were developed.

## II. WHAT ARE THE EMISSION STANDARDS?

<u>VUGRAPH 1</u> shows the specified emission limits as promulgated by the Surgeon General of the United States Public Health Service and are a part of the record in the Environmental Impact Statement for the Demilitarization Operation. Also shown is the Emission Standard generated by the State of Colorado in its Air Pollution Control Regulation No. 8.

## III. HOW WERE THESE STANDARDS ARRIVED AT?

The philosophy employed by the US Army in generating these standards was similar to that of the American Conference of Governmental Industrial Hygienists in their development of Threshold Limit Values. The control limits or standards were based on existing human and annual toxicity data and were calculated from a mathematical model. The objective was to obtain the best controlled and most acceptable levels humanly possible with existing data.

The following parameters served as the basis for study:

- a. Effects of Acute Exposure in Man
- b. Effects of Chronic Exposure in Dogs
- c. Delayed or long-term Effects
- d. Effects on Blood Chemistry and Liver and Kidney Function

  Effects of Acute Exposure in Man

It was determined experimently that the LD50 for GB for several animal species was 15 ug/kg by the intravenous (IV) route, and assuming that the LD50 for inhalation approaches the IV LD50, it was estimated that the LCt50 for an average man, breathing at 10 liters per minute (lpm), approximated 100 mg-min/cu m; ECt50 for collapse, paralysis, and convulsions was 70 mg-min/cu m; the ECt50

for miosis, tightness of the chest, rhinorrhea and headache was 15 mg-min/cu m. The "no death" dose was established at 10 mg-min/cu m, and the "no neuromuscular effect" was determined to be 4.0 mg-min/cu m.

The validity and appropriateness of the relationships is obviously open to question, but were retained because they gave the "most conservative" estimates, with what data was available.

## Effects of Chronic Exposure in Dogs

Extensive studies on dogs were performed to determine chronic effects. Variable dosages, times of exposure and length of exposure with comensurate parameter measurements were employed in accordance with standard practices using ct's from 2-38 mg-min/cu m.

The experiments indicated that repeated exposures to concentrations as low as 0.5 mg/cu m for 20 minutes (daily Ct of 10 mg-min/cu m) produced no more than mild "mucuous surface" signs of salivation, rhinorrhea, and miosis with some cholinesterase inhibition. The effects produced by daily repetition do not become more severe with continued exposure, and though persisting for the exposure time, were not permanently harmful to the animals.

## Delayed or Long Term Effects

There is no definite evidence suggesting that GB is mutagenic, teratogenic or carcinogenic, or that GB adversely influences fertility or reproduction.

A study was completed at Edgewood Arsenal, in January 1975, entitled, "Long-term Vapor Exposures in Animals as A Basis for Controlling Emission of GB Into the Environment." In this study various

species of animals (dogs, rats, mice) were exposed to GB vapors in concentrations of 0.0001 mg/cu m and 0.001 mg/cu m, 5 days per week, 6 hours per day, for periods up to 52 weeks - one year.

Effects on Blood Chemistry and Liver and Kidney Functions.

In these experiments, GB was administered orally in repeated doses of 0.088-0.102 mg/kg, at intervals of several hours over 3-3-1/2 days to dogs and rats. These doses produced GB symptoms, sweating, salivation, respiratory difficulty, subjective weakness, central nervous system symptoms and slight cholinesterase depression. There was no alteration in temperature or body weight, nor were there any changes in hematocrit, hemoglobin, red blood cell count, white blood cell count, eosinophils cell count, sedimentation rate, clot retraction time, nonprotein nitrogen, fasting blood sugar, serum chloride, carbon dioxide combining power, calcium, phosphorous, cholesterol, uric acid, alkaline phosphatase, bilirubin, albumin or globulin content. Hepatic and renal functions were normal by standard tests. The electroencephalgram and basalmetabolism rate remained unchanged. No occult blood was detected.

Based on the data, other than cholinesterase depression, it was concluded that there were no effects evident from the doses administered.

# Development of Air Concentration Control Values

The "no effect" dose concentration times time (Ct) of 0.5 mg-min/cu m indicated that with a daily exposure of 0.05 mg-min/cu m, the

"no effect" dose could be accumulated. Based on this indicator, Maximum Safe Concentration for one (1) hour was set at 0.001 mg/cu m. Worker Threshold Limit Values may be averaged for a maximum of ten (10) work periods per worker, as long as he does not work more than seven (7) shifts a week, and is not exposed to more than 0.05 mg-min/cu m in any one shift. Since a cholinesterase depression of 10% occurs with 1 ug GB/kg, and since 0.5 mg-min/cu m is equivalent to 0.075 ug/kg, the level of 0.0001 mg/cu m for an eight (8) hour exposure was set, which would result in less than an average of 1% cholinesterase depression for approximately 50% of the population.

Maximum influence of age and sex has been established as a factor of 2. Considering all factors and unknowns and considering conservatism of the estimated safe level for occupational exposure, an additional factor of 0.1 was added for safety.

As a result of all this, the standards, as shown previously, were then made mandatory and are considered quite conservative and safe.

# IV. Action Limits.

If we were to use these standards per se and exceeded them, we would, of course, be in trouble, However, in order to be aware that an upset condition is in being, working limits were established.

These standards are more stringent than the emission standards, and we have divided them into areas of concern.

VUGRAPH 2 depicts these action limits. What this means if that during

our normal course of operations, we are continuously (24 hours a day, 7 days a week) analyzing samples, and when the emissions approach these action limits, we take action necessary to avoid exceeding the limiting standards. The laboratory opens communication channels with the responsible Plant Engineer and advises him as to which station is doing what. It is from this information that a rapid assessment is made and the cause investigated, and the necessary action carried out in the plant.

# V. Philosophy of Monitoring.

The Philosophy of Monitoring Emissions at RMA is unique, and it is attributable to our awareness of the material we are dealing with on a regular basis.

## VUGRAPH 3

This viewgraph depicts our Triple Concept. We monitor on the perimeter of the arsenal, the plant stacks, and within the plant. At each successive level we have shorter sampling times and less sensitive action limits as previously described.

The Air Monitoring Network at the Perimeter of the Arsenal consists of nine (9) monitoring stations, dispersed at approximately 40° intervals, as a function of terrain features. The positioning represents an optimization for detection of pollutants in relation to population centers.

## VUGRAPH 4

The stations consist of modified camping trailers and are environmentally controlled. Note the transmitting antenna.

## VUGRAPH 5

Each station is equipped for monitoring the following parameters:

Agent GB, (Agent HD-By-Products during demil operations), sulfur dioxide, nitrogen oxides, acid mist/chlorides, ozone (oxidants), particulates, wind speed and wind direction.

## VUGRAPH 6

The wind direction and nitrogen oxide data are telemetered to a central panel in the laboratory on a continuous basis, and the information is monitored. This panel has both visual and audio alarms to indicate upset conditions. This system operates 24 hours per day, seven days per week. In addition, the data is correlated and sent to the National Bureau of Standards where it becomes a part of the International Weather/pollutant monitoring system. The computerized feedback data is sent to the State of Colorado and EPA Region 8. As an example of the type of information generated from these data: VUGRAPH 7 depicts a computed Wind Rose Pattern for the arsenal. There is in this computation one year's worth of data. What this tells us is that the predominate wind direction on the arsenal is South to North. The data points indicate percentage of time the wind is from the given direction indicated by the compass points. If we add up the South  $60^{\circ}$  arc, we have that some 46% of the time the wind direction is from the South to the North.

Very quickly, I'll show some viewgraphs of the equipment in the trailers.

<u>VUGRAPH 8</u> - Bubbler Sampling System for Agent GB (enzymatic).

VUGRAPH 9 - Technicon Automatic Analyzer for NO2(SO2) (colorimetric).

VUGRAPH 10 - Mast Ozone Meter (Oxidants) (Redox w/KI).

VUGRAPH 1! - Wind Speed/Wind Direction (Geotic Corp. WS-101 Wind Set).

VUGRAPH 12 - Depicts the Standards for the various pollutants.

VUGRAPH 13 - is a summary of the data from the perimeter stations for the year 1975.

Should the analysis of perimeter bubblers exceed 0.000003 mg/GB/cu m, operations are discontinued, if the wind direction is from the plant. It is to be noted that we have an occasion seen values exceeding this limit, which were caused by material of some nature coming from off the arsenal. This has also happened with the other detectors. In addition to this outer ring, we have also established some stations at various places on the arsenal where people are, but no operations; the Officer's Quarters Area, the Administrative Building (111), the Fire Stations, the Toxic Yard and Safety Office building. All of these stations monitor for anticholinesterase activity only, and we have negative results.

Supplementing all of these stations, we have our Ringelman Rambler, which is a portable truck will full monitoring capabilities, which we exercise periodically under/with the auspices of the Army Environmental Hygiene Agency.

I will now move into the plant area and discuss the monitoring as related to the stacks, scrubbers, and the plant proper.

VUGRAPH 14 - 1606 Bubbler Stations

VUGRAPH 15 - Other area Bubbler Stations

VUGRAPH 16 - ACHE Bubbler with Bath and Sequencer

VUGRAPH 17 - HJ Area Bubbler Stations

In the M34 area we have some 30 sampling stations and in the Honest John area we have some 15 stations composed of this equipment (Bubbler) located predominatly where people are positioned, and of course, on the stacks and the scrubbers. These stations are sampled over time intervals running from one hour to eight hours. When indications are noted of values approaching action limits or slightly exceeding them, we go to 0.5 hour sampling times in order to help diagnose the area of upset conditions. The samples are collected and returned to the laboratory for analysis in Automated Technicon Enzymatic Instruments. The enzymatic technique is based on the inhibition of Bovine cholinesterase by GB and the generation of a color with the dye DTNB (5, 5' - Dithio-Bis-2-Nitrobenzoic acid) and the color is read at 665 nm.

When the data from the analysis exceeds the action limit, 0.0003 mg GB/m<sup>3</sup> for a stack,  $0.0001 \text{ mg/m}^3$  in work areas, the plant shift engineer is notified, as noted before, by telephone and corrective action is initiated.

Monitoring in non or sparsely populated areas within the plant is accomplished with the standard alarms designated M5 and M8. We have some 15 of these alarms. In addition, we are currently utilizing a modified M8 as the M8 concentrator.

Before I describe these instruments, I would like to interject here an on-going R&D project, which we call the Real Time Monitor. This is an extremely active R&D project at Edgewood Arsenal to come up with devices which respond in real time, which is defined as less than 10-15 minutes and detect agent concentrations less than 0.0001 mg/cu m. One such device, now undergoing evaluation, is called the Eel Esterase Detector, for lack of a better name. In this device the enzyme is maintained on a solid support, such as GC column material and responds to 0.0001 mg/cu m in 5 minutes or less. This device is currently being evaluated.

## VUGRAPH 18

The M5 is a self-contained, fixed chemical agent alarm and responds to a GB concentration equal to or exceeding 0.2 mg/cu m, with a response time of 3-15 seconds. It samples at a flow rate of 5 lpm, and its principle of operation is based on fluorescence utilizing indole dye. It also has a recording capability for back tracking and analysis. VUGRAPH 19

The M8 is portable alarm which responds to the presence of GB when the concentration equals or exceeds 0.2 mg/cu m in approximately the same time frame as the M5. It samples at a flow rate of 2 liters per minute.

# VUGRAPH 20

This is the M10 configuration of the M8 which employs a power supply unit rather than the battery pack.

The principle of operation is electrochemical in nature.

VUGRAPH 21

The M8 concentrator utilizes the basic M8 Detector, but is augmented by a concentrator device. This concentration takes place in a separate module attached to the M8. The sampled air is drawn through a small column packed with 300 mg Porpak P, standard gas chromatographic column GC packing material. Constituents in the air sample are trapped on the column, and then purged by rapid heating of the column to 350° F every 33 minutes with the effluent introduced to the M8 detector. A dual sampling system enables the M8 alarm to sample and monitor in a normal mode while collecting material on the column maintaining its capability at 0.2 mg/cu m level and with concentrator, we are able to see levels at 0.001 mg/cu m. The concentrator cycle can be shortened, but at a loss in sensitivity, eg, 10 minutes at 0.0005 mg/cu m.

The total agent dosage collected on the column and purged is the key to the alarm's effectiveness. On both cycles, a dosage of 0.03-0.05 mg min/cu m is required for an alarm level. These levels are related to the Worker Threshold Limit Value previously mentioned.

In addition to these alarms and samples we also have available the M18A2 Chemical Agent Detector Kit. The blue band tube is used and detects approximately 0.5 mg/cu m of GB.

Another chemical which we have stored here at RMA, and is tentatively scheduled for transfer and sale is phosgene - carbonyl chloride. During the transfer operations, the process will be monitored by a new instrument called the UEI Detector. In addition, utilization will also be made of the standard M8 Detector previously described, which has about the same or greater sensitivity to phosgene. An Air sampling bubbler system is also available.

## VUGRAPH 22

The characteristics of the UEI Detector are:

Alarm Range 0.05 - 0.4 ppm and 0.10-50.0 ppm

Response Time to 0.1 ppm = 4 minutes

Sample Rate = 400 ml/min

The monitor operates on the principle of the chemical reaction caused by the gas on a moving, impregnated paper tape. A stain is produced on the tape as a result of the reaction with a dye, the density of which is related to the concentration of toxic gas (Phosgene) present in the sample.

The paper tape is continuously moving past a sensing head at 100 mm/hr (168 hr running time per cassette), and a metered sample of atmosphere is drawn into the detector and passed through the tape by means of an internal pump. A colored stain is produced on half of the tape, the intensity of which is related to the concentration of the particular gas present in the atmosphere. The same part of the tape is then illuminated via a fibre optic light guide, from a controlled light source, and the reflection monitored by a photocell. The output finis photocell is amplified and displayed on the meter on the front panel as a ppm gas concentration.

The other half of the tape, which has not been exposed to the sample, is also monitored by a photocell, using the same light source through a separate fibre optic light guide. The signal from this photocell is taken as a reference level and used to balance out changes caused by variations in tape color, so that the signal presented to the meter and alarm circuits is entirely due to the "gas stain."

# VI. Mustard Demil SO2

During the Mustard Demilitarization Program, which has been successfully completed ahead of schedule, monitoring for  $\mathrm{SO}_2$  emissions was performed at the nine perimeter monitoring stations, as well as in the plant proper. The air quality standards for  $\mathrm{SO}_2$ , applicable during the demilitarization at RMA, were:

Annual Arithmetic Mean of 0.02 ppm; 24 hr maximum value of 0.1 ppm, not to be exceeded more than once in any 12-month period.

Three hour maximum value of 0.5 ppm, not to be exceeded once per year, and one hour maximum value of 0.28 ppm, not to be exceeded more than once in any one-month period.

The monitoring at the perimeter was continuous on a Technicon Auto-analyzer, using the colorimetric technique with a minimum detectable limit of 13.1  $\text{ug/m}^3$  (0.005 ppm). This system automatically alarmed if the SO<sub>2</sub> level equaled or exceeded 0.05 ppm for ten minutes and the prevailing wind direction was coming from the plant to the

respective station. The alarm was transmitted to the Product & Environmental Assurance Laboratory by dual channel FM telemetry system.

Reports covering all the data generated at the ambient air perimeter stations during the Mustard Demilitarization Program were forwarded to Colorado Dept of Health, Air Pollution Control Division, and to the USAEHA for review and analysis.

Background data was taken by USAEHA January 1970 to February 1971 at RMA to determine a base from which to evaluate the net change in air quality, during the actual plant operations.

The average RMA SO<sub>2</sub> concentration prior to plant operations, Jan 70 to Jun 71, was 0.9050 ppm; average SO<sub>2</sub> during operations, Jul 71 to Feb 74, was 0.0044.

The trend lines for RMA data were consistently lower than the Colorado data for  $SO_2$  during comparable periods.

The ambient air quality at RMA was compared to the ambient air quality in the Denver Metropolitan area during the demil program with the conclusion that no significant impact in ambient air quality occurred.

# VII. Conclusion.

It can be concluded that Environmental Emission Control System, as employed at Rocky Mountain Arsenal, has been effective not only as a monitoring system for emission, but as equally effective as a diagnostic tool to plant engineering personnel.

# SELECTIVE BIBLIOGRAPHY

- McNamara, B. P. et al, Toxicological Basis for Controlling Emission of GB Into The Environment, EASP 100-98, March 1971.
- Demilitarization and Disposal of The M34 Cluster at Rocky Mountain Arsenal, Final Environmental Impact Statement, February 1973.
- McNamara, B. P. et al, Long Term Vapor Exposures in Animals as a Basis for Controlling Emission of GB Into the Environment, EASP (to be published), January 1975.

# SPECIFIED LIMITS

# SURGEOIL GELIERAL

- THE CONCENTRATION IN ANY AREA TO WHICH THE GENERAL POPULATION HAS ACCESS WILL EXCEED NEITHER. GENERAL POPULATION:
- (1) 0.0001 mg/cu m AVERAGED OVER ANY ONE-HOUR PERIOD; WOR
- (2) 0.000003 mg/cu m AVERAGED OVER AHY 72-HOUR PERIOD.
- THE CONCENTRATION IN ANY AREA TO WHICH UNIMASKED WORKERS HAVE ACCESS WILL EXCEED MEITHER. U.V. MASKED WORKERS: 8
- (1) 0.001 mg/cu m AVERAGED OVER ANY ONE-HOUR PERIOD; NOR
- 2) 0.0003 mg/cu m AVERAGED OVER ANY 8-HOUR PERIOD; NOR
- 9.0001 mg/cu m (8 HR/DAY) FOR AN INDEFINITE PERIOD, AVERAGED OVER ANY 10 CONSECUTIVE WORK PERIODS. 3
- THE MAXIAUM EMISSION LITO THE ATMOSPHERE OF AGENT GB FROM ANY SOURCE SHALL BE LESS THAN 7.0793 mg/cu m. ن
- THE MAXIMUM GROUND LEVEL CONCENTRATION OF AGENT GB OUTSIDE THE PHYSICAL PLANT WILL NOT EXCEED 0.000003 mg/cu m. 3

# STATE OF COLORADO

MAXIMUM EMISSION LITO THE ATMOSPHERE FROM ANY SOURCE 0.003 mg/m3 (TWO HOUR AVERAGE).

# BUBBLER DECISION POLNTS

# STACK

0.0003 mg/m3 - TAKE CORRECTIVE ACTION - REPORT TO PROJECT MANAGER 0.003 mg/m³ - DISCUNTINUE OPERATIONS, COLLECT PERIMETER BUBBLER

WURK AREAS

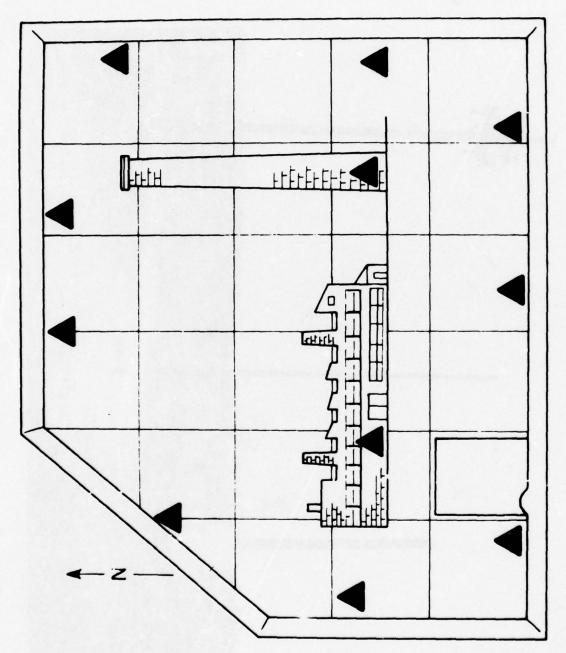
0.02 mg/m3 - MASK, DISCONTINUE OPERATIONS, EVACUATE

0.001 mg/m3 - MASK, POST SIG.1S

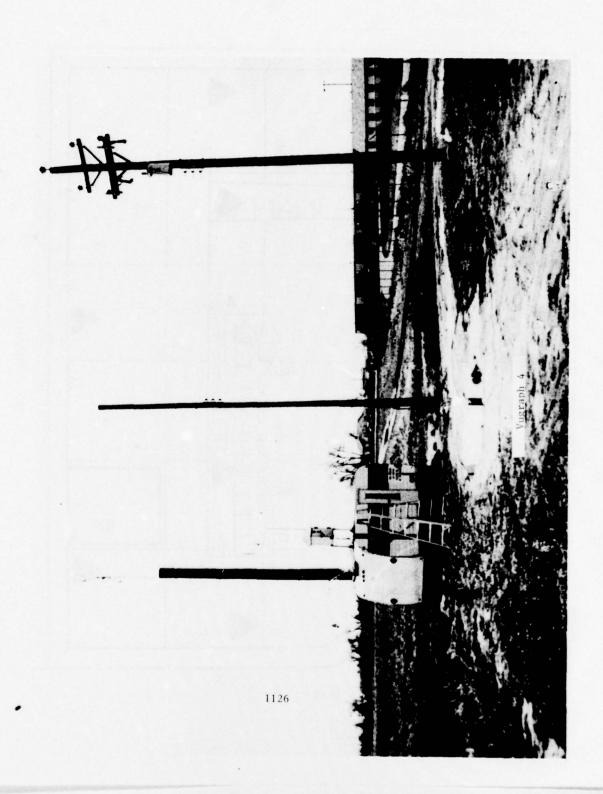
0.0001 mg/m<sup>3</sup> - TAKE CORRECTIVE ACTION, REPORT TO PROJECT ARMAGER

# PERI.1ETER

0.003 mg/m3 - DISCOLITILUE OPERATIONS, NOTIFY CAICP EMERGENCY CALL LIST 0.000003 mg/m3 - DISCO.ITI: UE OPERATIO: IS IF WIND IS FROM PLANT.



Vueraph 3



# AIR MONITORING PERIMETER

S 0.

O N 7

1127

3 3

0 xidants

4

S

Particulates

Direction જ Wind Speed

9

(Technicon [A)

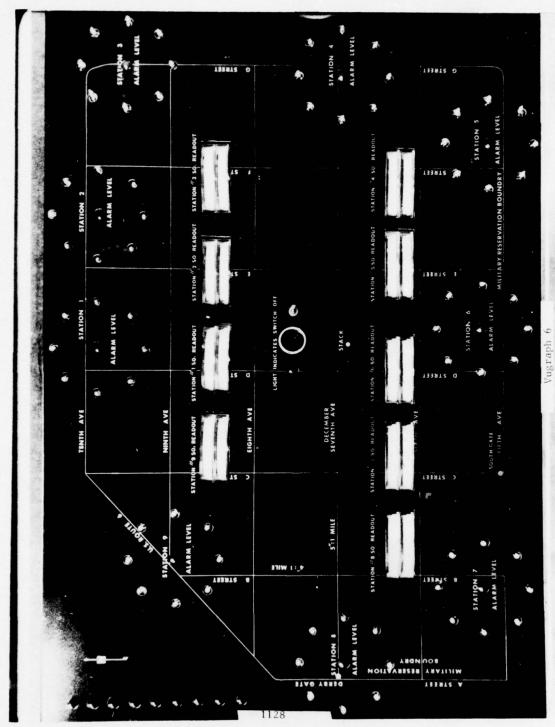
(Technicon []A)

(Laboratory)

(Laboratory

Meter)

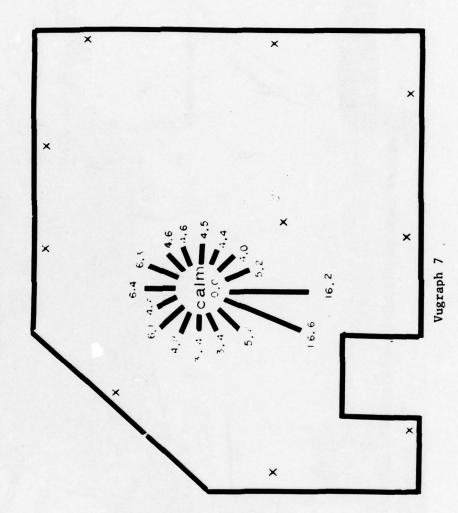
(Mast Ozone

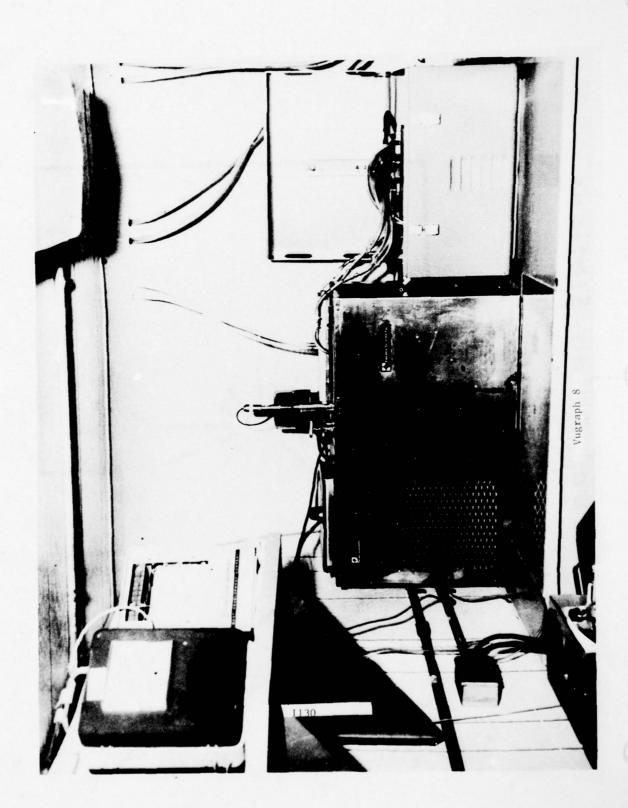


# Air Monitoring Stations

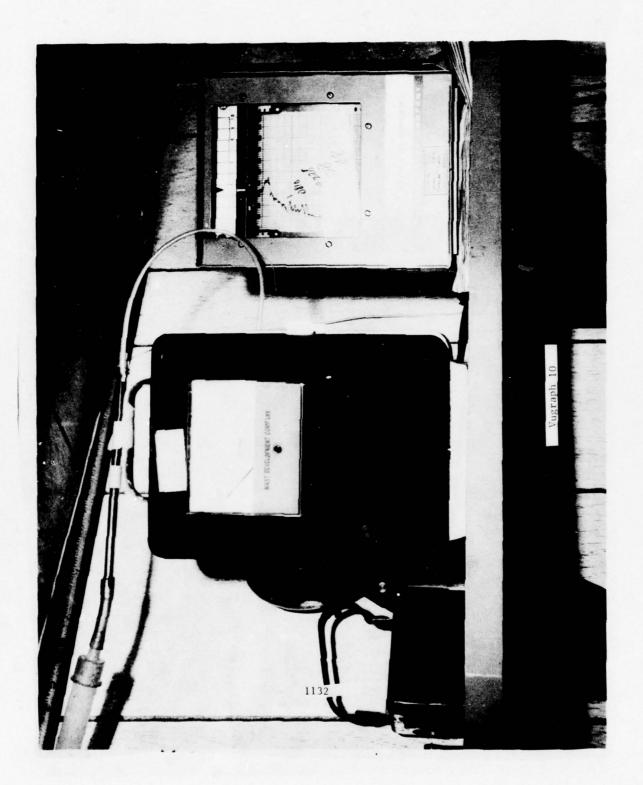
And

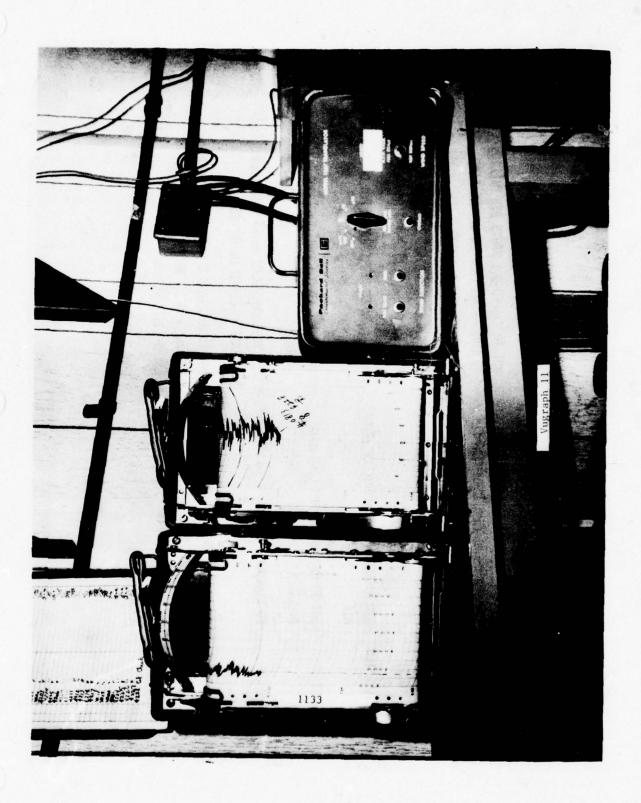
Wind Rose











# AIR POLLUTION STANDARDS

RMA	NOT TO EXCEED 0.1 PARTS PER MILLION (VOLUME) MORE THAN 1% OF THE TIME	IN ANY 12-MONTH PERIOD	NEVER TO EXCEED 0.015 PARTS PER MILLION (VOLUME) AT ANY TIME	80 MICROGRAMS PER CUBIC METER OF AIR	NOT TO EXCEED 0.1 PPM (ONE HOUR AVERAGE)	NOT TO EXCEED 0.03 mg/m³ (ONE HOUR AVERAGE MEASURED IN THE STACK)	NOT TO EXCEED 0.1 PPM FOR ONE HOUR AVERAGE FOR 1% OF THE TIME DURING ANY 3-MONTH PERIOD	CONTINUOUS
COLORADO	NOT TO EXCEED 0.1 PARTS PER MILLION (VOLUME) MORE THAN 1% OF THE TIME	IN ANY 3-MONTH PERIOD	NO STANDARD	120 MICROGRAMS PER CUBIC METER OF AIR	NOT TO EXCEED 0.1 PPM (ONE HOUR AVERAGE)	NO STANDARD	NOT TO EXCEED 0.1 PPM FOR ONE HOUR AVERAGE FOR 1% OF THE TIME DURING ANY 3-MONTH PERIOD	EVERY 3 DAYS
	1. SULPHUR DIOXIDE	(205)	2. HYDROCHLORIC ACID (HC1)	3. PARTICULATES	4. OXIDANT (0 <sub>5</sub> )	5. H & HD	6. NO <sub>X</sub>	7. SAMPLING FREQUENCY

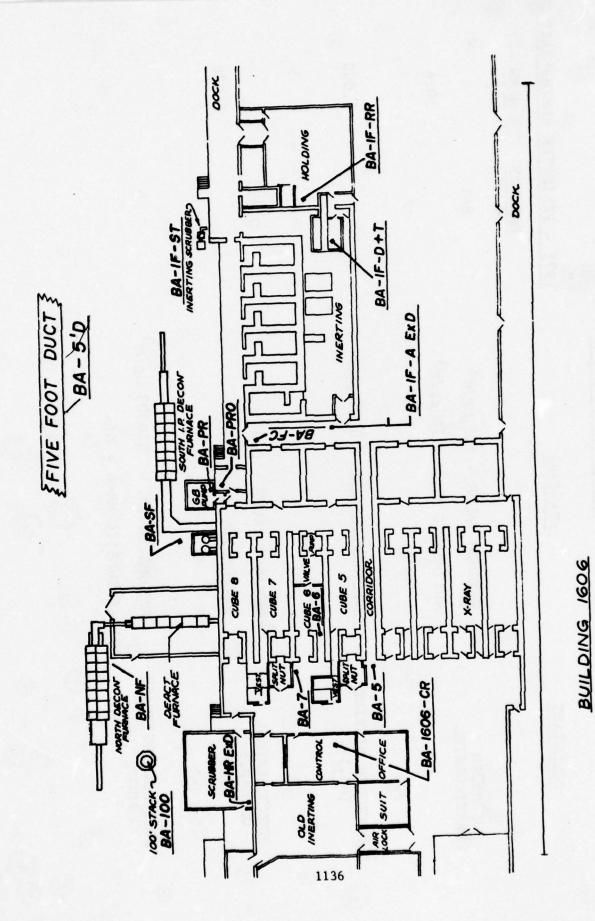
# PERIMETER EMISSIONS

STANDARD

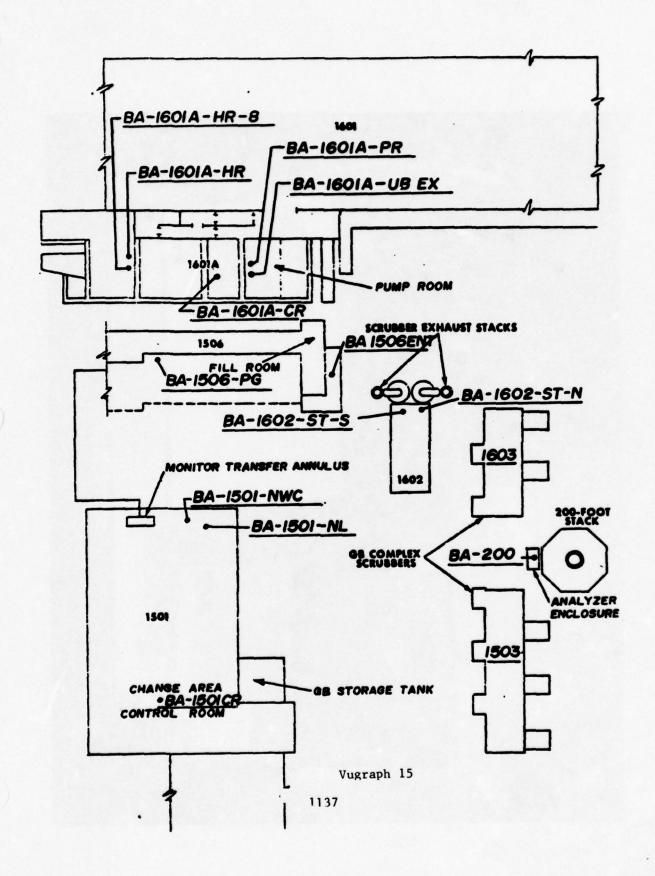
POLLUTANT

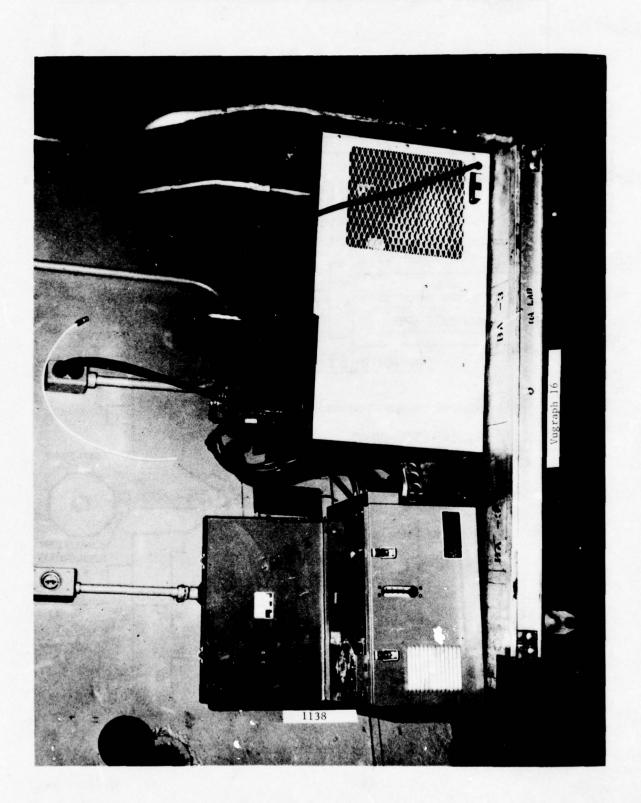
1975 - PERIMETER PERFORMANCE

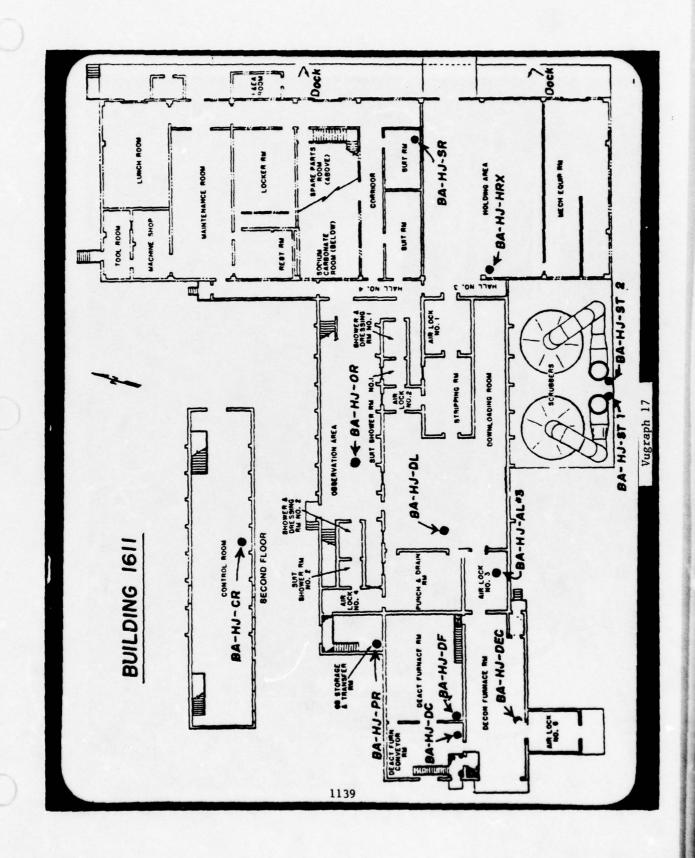
MEAN	50.4	0.005	0.026	0
MAXIMUM	841		0,629	0
	MAXIMUM VALUE - 200 µg/m <sup>3</sup> ARITHMETIC MEAN - 70 µg/m <sup>3</sup>	ARITHMETIC MEAN - 0.05 ppm	MAXIMUM VALUE - 0.08 ppm ARITHMETIC MEAN - N/A	MAXIMUM VALUE000003 mg/m <sup>3</sup> AR THMETIC MEAN - N/A
	SUSPENDED PARTICULATES	NITROGEN DIOXIDE (NO <sub>2</sub> )	PHOTOCHEMICAL OXIDANTS	ANTICHOLINESTERASE AGENT (GB)

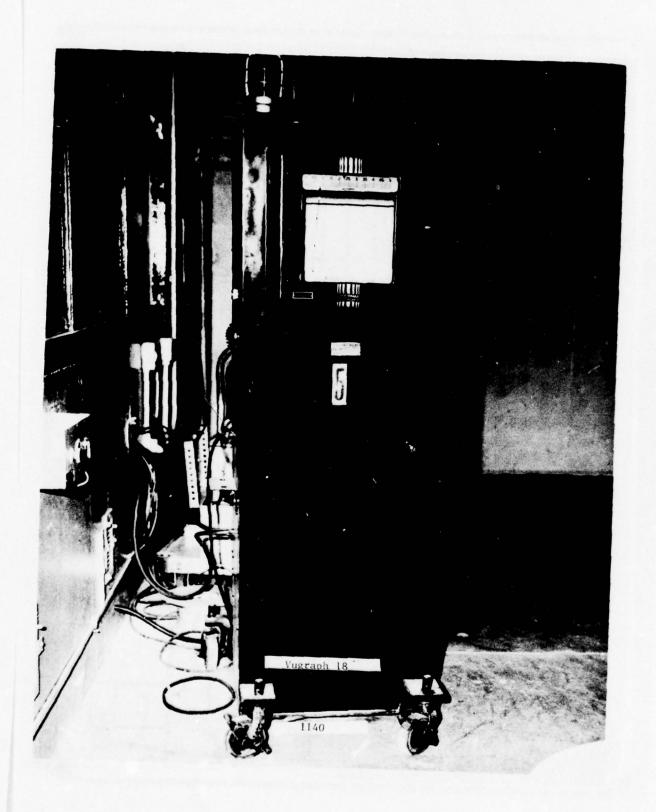


Vugraph 14

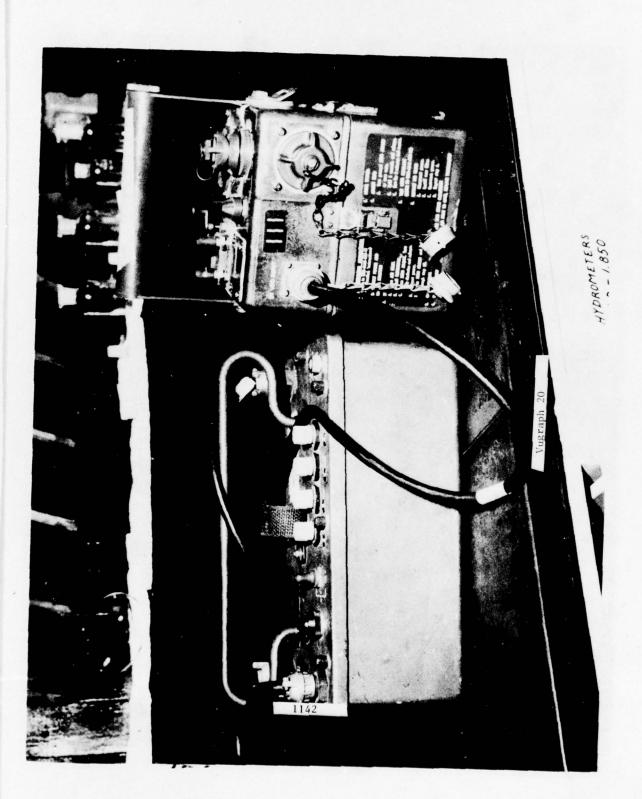


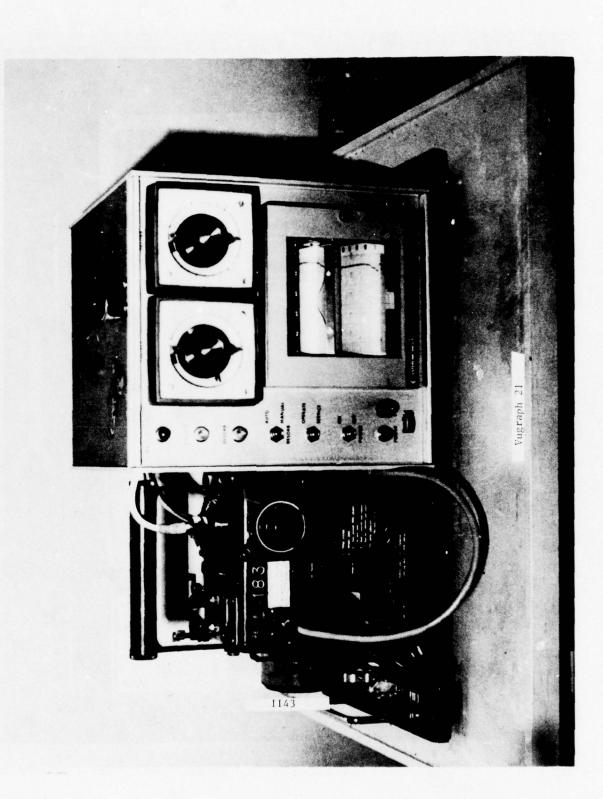


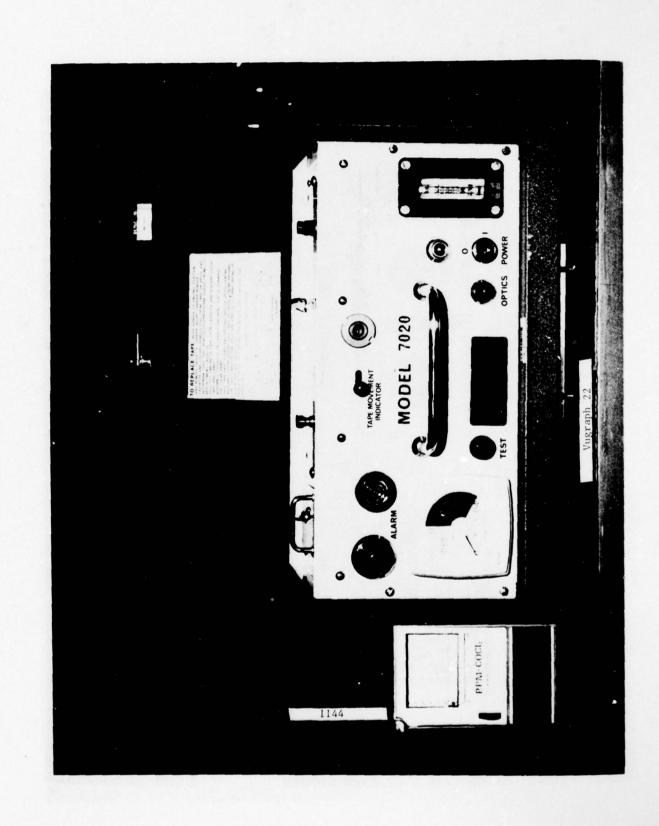












## GB NERVE AGENT DISPOSAL PROCEDURES

Richard A. Jacobs, Jr. Rocky Mountain Arsenal Denver, Colorado

BACKGROUND

In May 1969, after the Department of the Army had decided to dispose of certain obsolete chemical munition stocks, the National Academy of Sciences was requested to make an independent study of disposal methods. In response to this request, a panel of twelve distinguished experts drawn primarily from the country's leading industrial, educational, and research institutions assembled in Washington to consider the disposal problem. Among the processing methods considered were incineration, acid hydrolysis and alkaline hydrolysis. Incineration was rejected because, although it provided the greatest degree of molecular destruction of nerve agent, it also produced phosphorous-pentoxide as a finely divided particulate in the exhaust air streams, creating a substantial air pollution hazard. Both acid and alkaline hydrolysis effectively "neutralized" the nerve agent by cleaving the phosphorous-fluoride bond. Acid hydrolysis, however produced hydrogen fluoride, which in aqueous solution is extremely reactive and presents significant corrosion problems with normal chemical process equipment. Alkaline hydrolysis, on the other hand, produces sodium fluoride and the sodium phosphonate salt which are chemically inert. Thus, alkaline hydrolysis was selected as the preferred detoxification method because it would result in relatively non-hazardous waste materials not significantly different from larger volumes of industrial waste that are discharged elsewhere. With the selection of a neutralization reaction, several additional elements of the detoxification process had to be considered. These are shown in the following viewgraph. (VG I).

Once the nerve agent has been neutralized, the resulting aqueous salt solution must be processed to remove the liquid prior to storage because the salts are relatively corrosive when wet. Some thought was initially given to separation of the solution into fluoride and phosphonate rich fractions either through centrifugation or filtration prior to final drying, but this idea was rejected because complete separation could not be achieved and because of the additional energy required to conduct such a separation. It was finally decided that spray drying the brine by atomization and direct contact with a fuel-heated air stream was the most economic and energy conservative approach which could insure control of exhaust emissions to environmental standards. A centrifugal atomizing spray dryer equipped with cyclone separation and liquid scrubbing capability was selected as the equipment to process neutralized brine and other liquid effluents from the disposal plants.

The remaining elements in the disposal operation consist of the equipment used to contain toxic emissions from the process equipment to the ambient air in the plant and to the atmosphere through exhaust stacks. It was initially recognized that some toxic vapor would be released during normal disposal operations and that this emission had to be contained and

removed prior to exhausting the ambient air from the contaminated environment to the atmosphere. To accomplish this, process facilities were constructed so that the potentially contaminated and non-contaminated areas were separately ventilated by enclosed, forced-air systems, and these systems were operated so the non-contaminated environment always remained at a higher pressure than the potentially contaminated area. This combination of physical separation from the active process and pressure barrier between contaminated and non-contaminated areas resulted in the ability to conduct toxic operations without application of extensive personal protective measures for workers in the immediate vicinity such as a continual requirement for protective clothing. This approach has resulted in marked improvement in employee morale and productivity.

This method of in-plant containment, however, also necessitated the development of air treatment facilities which could process large volumes of air containing extremely low concentration of nerve agent (E.G., less than 100 PPM) and remove almost 100 percent of the nerve agent present. A variety of wet scrubbing equipment was reviewed, and finally an array of venturi, cross-flow and packed tower scrubbers was selected as the optimum mix of new and existing facilities required to process the air. This array was modified as each new disposal program was developed to provide the special processing capability required. The total air processing capacity that now exists at Rocky Mountain Arsenal is approximately 260,000 CFM of air with nerve agent scrubbing efficiencies in excess of 99.99 percent.

The facilities performing these four elements compose a unique toxic handling capability which has been tested in extensive pilot and production operations and has provided a mechanism for the examination and resolution of several technical problems of general interest when processing toxic chemicals.

NEUTRALIZATION PROCESS (VG II)

Nerve Agent detoxification is accomplished by mixing with aqueous sodium hydroxide solution at controlled flow and temperature conditions. The reaction is essentially instantaneous and highly exothermic; therefore, the ability to monitor and control flows and temperatures is of paramount importance. The bulk nerve agent is stored in a 1500 gallon intermediate holding tank which is independently ventilated and isolated from the ambient atmosphere. From this tank, it is pumped through a flow control valve to an eductor tee where the mixing with sodium hydroxide occurs. The sodium hydroxide flows by gravity from three 10,000 gallon holding tanks located on the roof of the building to a refrigeration machine where its temperature is lowered to approximately 40°F. From here it flows through a flow control valve to the eductor tee.

At the eductor, the nerve agent and sodium hydroxide react producing

sodium fluoride, sodium isopropyl methyl phosphonate and several other minor components, and releasing heat of over 45 kcal/gm-mole of nerve agent. This heat raises the temperature of the reaction mixture to approximately 200°F, but it is reduced to approximately 160°F by the reaction cooler immediately downstream of the eductor. Temperature control is maintained by three independent mechanisms: (VG III)

- a. Within certain limitations, the temperature of the sodium hydroxide solution can be varied by adjusting the operation of the refrigeration machine. This compensates for fluctuations in the ambient atmospheric temperature and the strength of the sodium hydroxide solution being used, both of which affect the final reaction temperature.
- b. A second method is modulation of the cooling water flow to the reaction cooler. This flow is automatically adjusted to maintain the  $160^{\circ}$ F temperature at the cooler discharge.
- c. Finally, the nerve agent flow control valve is linked to the exit temperature sensor and will be automatically modulated to reduce flow if the temperature exceeds 160°F. This provides protection in the event of a primary flow sensor failure in either the nerve agent or the sodium hydroxide lines.

Once the reaction mixture exits the reaction cooler it flows by gravity into one of two 3500 gallon reactor vessels which simply stir and recirculate the solution allowing the reaction to proceed fully to completion. During the reactor filling cycle, several samples of the reaction mixture are collected and analyzed for sodium hydroxide in solution. These analyses are used to adjust reactant flows to the eductor to produce a final neutralized brine solution with sodium hydroxide content of 8 percent by weight + one half percent. Originally, it was envisioned that the neutralized brine would be analyzed for nerve agent content to insure complete destruction prior to spray drying, but attempts to analyze the highly alkaline salt solution for minute traces of nerve agent proved to be inconclusive because of extensive analytical interferences with the enzymatic technique being used. Attempts were also made to extract the solution and separate the GB fraction of the extract using gas chromatography, but serious questions were raised concerning extraction efficiencies and the viability of nerve agent in solution during the extraction process. After extensive efforts in both these areas, it was decided that since no nerve agent could be detected in the immediate atmosphere surrounding the neutralized solution, and since emission difficulties within the spray drying process were minimized when the solution contained sodium hydroxide content of 8 percent or greater, the percentage sodium hydroxide in the neutralized solution could be used as a control point indicating completeness of the reaction. Once the reactor is filled and this percent achieved, the neutralized brine solution is ready to be spray dried.

SPARY DRYING PROCESS (VG IV)

The neutralized salt solution from the detoxification reaction is pumped from the reactors to three 7,000 gallon holding tanks in another building. At this point the solution contains 10-15 percent undissolved solids, mostly sodium fluoride, and must be continuously agitated to insure these remain suspended. The spray dryer itself consists of a 24 foot diameter stainless steel chamber into which hot gases from natural gas combustion are supplied. The salt solution enters the chamber through an annular space in a high speed rotating disc and is centrifugally atomized and mixed with the hot gases. As this mixture passes through the chamber, the water in each atomized droplet evaporates leaving a dry particle of salt. These particles are separated from the main air stream in four high efficiency cyclone separators, and pass through a compacting operation where they are briqueted and stored in drums.

Because the cyclone separators are approximately 95 percent efficient in removing the salt particles, additional particulate removal equipment is necessary to reduce mass emissions to allowable levels. Extensive testing revealed that the particulate escaping the cyclones had mean particle diameter of less than 0.5 microns which presented a particularly difficult removal problem. Since the air stream was saturated and at a temperature of 275°F filtration equipment was relatively infeasible, and it was decided to use a high energy venturi-type scrubber to capture the particulate through a combination of inertial impaction and brownian motion. To obtain the additional pressure drop required by the venturi design, the main fan power had to be increased from 200 to 500 hp and the fan itself had to be completely redesigned. This redesign essentially changed the spray drying equipment from low energy to high energy operation and greatly increased the need for control and sensing equipment. The modified system was retested several months after initial testing and, this time, particulate emissions were within acceptable limits.

When the particulate emission problem was finally resolved, the spray dryer was formally tested for production demonstrating purposes by the Army Environmental Hygiene Agency. It was during this testing that the problem of nerve agent emissions from the spray dryer was discovered. As mentioned earlier, analytical difficulties encountered when trying to detect nerve agent in the neutralized solution necessitated the utilization of percent sodium hydroxide in solution as the control parameter indicating completion of the neutralization reaction. Thus, when minute quantities of nerve agent were detected in the spray dryer exhaust stact, it was not readily apparent where they were coming from. In fact, because of previously experienced analytical interferences, there was some question as to whether the detected nerve agent might be an analytical artifact.

In order to obtain a positive identification of nerve agent in the

stack, exhaust, a special analytical technique was developed. First a sample of the exhaust gas was collected in a buffered solution using an impinger type collector. This solution was then extracted with chloroform, concentrated, and injected into a gas chromatograph column. At the retention time measured for pure nerve agent, the effluent from the GC was diverted through a fractionating mass spectrometer and the mass spectra of the fractions were compared against spectra observed for nerve agent fractions. Identical matching of the spectra provided positive identification of nerve agent in the stack exhaust in quantities exceeding the emission standard. Now the problem was reduced to identify the source of the emission and to develope measures to eliminate it.

Two theories were proposed to explain the presence of nerve agent in the exhaust stream from a supposedly uncontaminated operation. The first assumed that the neutralization reaction was not 100 percent complete and that trace quantities of nerve agent remained in the neutralized solution either mechanically occluded within the salt particles or unreacted because of chemical equilibrium conditions. Proponents of this theory concentrated their research efforts on methods of detecting nerve agent in the highly alkaline neutralized brine solution. The second theory proposed that nerve agent was reformed by a reversal of the neutralization reaction in the presence of the hot gases and acid conditions within the spray drying chamber. It was postulated that the large amounts of carbon dioxide present in the burner exhaust gases used to dry the brine produced an acid catalysis of salt hydrolysis reaction and that the reformed acids of the phosphonate and fluoride salts reacted in the presence of the heat of the drying chamber to reform nerve agent. Proponents of this theory concentrated their efforts on the pilot spray drying tests where various operating parameters could be manipulated and the resulting nerve agent emissions measured.

Analytical proof of the first theory was never obtained, and even though most researchers suspect that the nerve agent reaction is 100% complete, it cannot be stated with absolute certainty. There is also no direct proof of the second theory, however experimental data developed during extensive pilot and full scale spray dryer testing plus resulting successful measures to control the emission problem provided strong evidence to indicate that reformation was the most likely source of the nerve agent emission. Evidences of this fact are shown on the following viewgraph. (VG V)

- 1. Firing the burner with fuel oil (with subsequent increase in sulfur dioxide content of the spray dryer air stream) resulted in increasing emissions from the spray dryer.
- 2. Increasing the amount of sodium hydroxide in the neutralized brine resulted in decreased emissions from the spray dryer.

- 3. Keeping the walls of the spray drying chamber free of salt build up resulted in decreasing emissions from the spray dryer.
- 4. Decreasing the operating temperature resulted in decreasing emissions from the spray dryer.

Items 1 and 2 reinforce the idea that acid catalysis reforms nerve agent and that by increasing the alkalinity of the spray drying operation, nerve agent emissions can be reduced. Item 3 substantiates the postulation that the presence of large quantities of dried, heated slats enhance the reformation reaction and finally, the proportionality of nerve agent emissions and operating temperature observed as item 4 lend credence to an Arrehenius type behavior and indicate a formation reaction.

The nerve agent emissions were finally reduced to acceptable levels by instituting the following operational measures. (VG VI)

- 1. Eliminating all oil-fired spray dryer operations.
- 2. Increasing the amount of sodium hydroxide in the neutralized brine from 2% to 8% by weight.
  - 3. Cleaning the spray dryer chamber more frequently.
  - 4. Reducing the operating temperature from 1150°F to 725°F.
- 5. Adding sodium hydroxide to the venturi scrubber to obtain some final scrubbing of any nerve agent which might be reformed.

These measures were implemented in the summer and fall of 1975 and since that time, the spray dryer has performed in a satisfactory fashion, although at somewhat less than one half of design feed rates. An additional effect of increasing the sodium hydroxide in the neutralized brine is the production of larger quantities of sodium carbonate in the drying chamber from the reaction with carbon dioxide. This extra carbonate formation has increased the total salt production from the neutralization operations by approximately 30 percent resulting in a much larger solid waste generation than originally envisioned.

## VENTILATION AND SCRUBBING TECHNOLOGY TO CONTROL ENVIRONMENTAL EMISSIONS (VG VII)

Although neutralization and spray drying represent the major process steps for disposal of nerve agent, they are only a portion of the total technology required to conduct the operation in a safe and environmentally protective manner. In order to handle and process nerve agent without undue exposure to working personnel a method of remote control and operation had to be devised. This was accomplished by placing all processing equipment in sealed and isolated areas with control and sensing instrumentation remotely located in a central control area. To further enhance the separation of the processing area from the personnel working area, a ventilation system was constructed to supply air into the personnel

area and exhaust it through control dampers into the process equipment area and finally through sealed ducts to air scrubbers for final processing. By carefully adjusting the control dampers a pressure differential can be maintained between the personnel and process areas so that any nerve agent leakage from the process will tend to remain localized in the process area rather than diffusing into the personnel area as well. Visual contact with the process is maintained through large observation windows and remote television monitors. Visual observation plus process instrumentation readout provide adequate means of process control without direct personal contact. As a final protective measure to minimize vapor leakage from process equipment, all key contaminated items were independently ventilated and maintained under negative pressure during operation. Thus, any minute leakage which did occur would be into the process rather than out into the process area. This ventilation control scheme has functioned exceptionally well throughout the nerve agent disposal operation maintaining the non-contaminated status of the personnel working areas of the facility on a continuous basis even during emergency situations when equipment leakage has severely contaminated the process area.

Operation of this ventilation system to obtain plant area nerve agent emission control, however, poses significant technical problems for protecting the general atmosphere from exhaust emissions. In order to insure the proper functioning of the in-plant ventilation system, extremely large quantities of air must be moved through the system and exhausted to the atmosphere. Thus, even a massive process leak will only present mimimal nerve agent-concentrations in the exhaust air stream by industrial air scrubbing standards. (E.G. Calculations for the one process area indicate the emission from a nerve agent spill 120 square feet in area would only yield a concentration in the exhaust air stream of approximately 40 PPM). Compounding the scrubbing difficulty is an atmospheric standard for nerve agent emissions which is extremely low (I.E. approximately 0.3 PPB) and represents a level of contaminant removal not normally achieved in standard industrial applications.

Because each scrubber had to be capable of processing the ventilation air during a maximum crediable accident condition without exceeding emission standards, required scrubbing efficiencies were abnormally high (i.e., in excess of 99.99 percent) and the equipment necessary to produce these efficiencies would necessarily be very large or consist of several smaller systems connected in series. For the initial disposal program a series of three venturi-type scrubbers which already existed as part of previous manufacturing operations was selected. When charged and operating with a dilute sodium hydroxide solution, these scrubbers provided a theoretical nerve agent removal efficiency of 98% each providing an overall scrubbing efficiency of 99.9992 percent. Actual scrubbing efficiencies of 96 percent per scrubber were measured by challenging the scrubbing system with nerve agent and measuring the inlet and outlet.

(VG VIII)

concentration of each scrubber.

Initial operations of the venturi scrubbing system surfaced several problem areas which had not been anticipated during the design phases of the ventilation system. First of all, because these scrubbers had necessarily been selected because of their high removal efficiencies, they also effected significant removal of the carbon dioxide present in the air stream. The carbon dioxide was present at approximately ten times the normal atmospheric concentration because several process furnaces exhausted into the ventilation air and the sodium carbonate buildup in the scrubbers resulting from the carbon dioxide removal continually plugged the venturi nozzles and associated piping necessitating frequent cleaning. Besides being costly, this cleaning generated large amounts of industrial waste liquid which had not originally been planned. A related problem arose in controlling the amount of free sodium hydroxide in the scrubbing solution. Because the carbon dioxide was present in the ventilation stream at concentrations approximately seven orders of magnitude larger than the inlet nerve agent concentrations, it became the chief cause of sodium hydroxide depletion in the scrubber sumps. Additionally, the resulting carbonate-bicarbonate solution tended to act as a buffer and effectively eliminated pH as a measurable control variable. Attempts to lessen the amount of free sodium hydroxide in the scrubbing solution to reduce carbon dioxide removal only resulted in excessive nerve agent emissions from the scrubbers. It was finally observed that a pH of 10 or greater was necessary to effect good nerve agent scrubbing, and it was decided not to control the pH, but the actual free sodium hydroxide in solution. Even though this resulted in greater carbon dioxide removal, it insured continued nerve agent scrubbing at the required efficiencies.

When the second nerve agent disposal operation was considered, a review of the ventilation scrubbing performance during the first operation was conducted to determine whether a more effective method was available. After considerable review of available scrubbing technology, a packed tower was selected because it offered the optimum mass transfer rates, and because of its simplicity of design with the limited mass transfer data available from laboratory experiments. The tower diameter and internal configuration were designed to accomodate the projected ventilation air flow from the proposed disposal operation. The height and type of packing were selected on the basis of the maximum credible emission and the predicted mass transfer coefficient.

Two identical towers were constructed and packed with 1.5 inch diameter polypropylene pall rings to a depth of 25 feet. Design process

parameters and experimentally established characteristics of the pall ring were combined to predict a design height of a transfer unit necessary to scrub the potential nerve agent input from the disposal facilities. A series of tests consisted of spraying nerve agent into the tower inlet air stream and measuring the inlet and outlet nerve agent concentrations. The measured concentrations were then used to compute the height of a transfer unit. The data showed the actual height of a transfer unit to be 1.91 feet which was in excellent agreement with the design value.

Even though the testing was completely successful from the stand-point of proving the ability of the packed tower to scrub nerve agent, a problem arose during the course of the test which had not been anticipated. Excessive solids began to build up in the scrubbing solution and create plugging problems within the tower packing. After approximately 40 hours of operation, the pressure drop became prohibitive and the tower had to be shut down for clean up operations. A sample of solid material was removed from the sump and analyzed as sodium carbonate.

When the towers were originally designed, no thought had been given to the potential for reaction between the small amount of carbon dioxide in the ventilation air streams (approximately 0.03 percent by weight) and the sodium hydroxide present in the scrubbing solution. But test operations showed that operating the packed tower with a scrubbing solution containing five percent by weight sodium hydroxide effected removal of all the carbon dioxide entering the tower with the air stream, and produced the accompanying buildup of solid sodium carbonate in the solution.

A solids buildup rate of the magnitude experienced during testing would have necessitated either operating with a large bleed rate from the scrubber sump to the chemical sewer, or a shut down of the scrubber system every 40 hours for cleanup. Since neither of these alternatives was acceptable, it was decided to alter the mode of tower operation to prevent the solids buildup problem.

Reducing the amount of sodium hydroxide in the scrubbing solution to approximately 0.25 percent would allow most of the carbon dioxide in the incoming air stream to pass through the solution, but would still scrub the nerve agent. Even though the chemical reaction time of nerve agent in such a solution would be greatly increased (i.e., to several minutes), it was expected that the tower scrubbing efficiency would be unaffected by such a change. (Indeed, such a change should not have altered the mass transfer characteristics of the tower greatly). Thus the scrubbing solution was reconstituted so that it contained approximately 0.3 percent sodium hydroxide and 3.3 percent sodium carbonate. It had a pH of 11.0

which theoretically increased the half-life of nerve agent in the solution substantially.

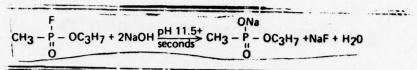
The scrubber was now tested in the same manner as previously tested to assess the operability and ability to scrub nerve agent with the altered scrubbing solution. While the scrubber performance from an operational standpoint remained unchanged from previous operations, ability to scrub nerve agent was greatly affected. The amount of nerve agent emitted from the tower increased more than two orders of magnitude over emissions during the first testing. This apparent decrease in scrubbing efficiency was not readily explainable by application of mass transfer theory, because essentially nothing had been done to alter the mass transfer parameters of the tower. Liquid and gas flows remained constant, the packing configuration was unaltered from previous tests, and all process parameters were duplicated for both sets of tests.

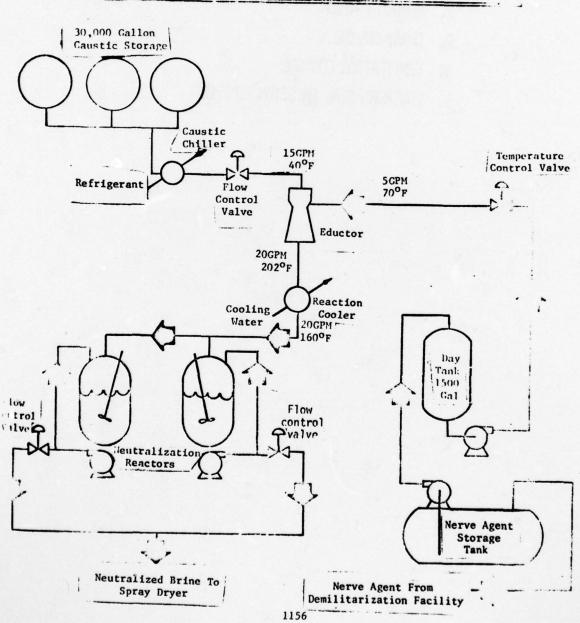
Since there was no reason to suspect that the conditions of mass transfer had been altered from one series of tests to the other, it was proposed that the lower pH of the scrubber solution during the second test series altered the reaction kinetics of the entrapped nerve agent, establishing a chemical equilbrium and causing an offgassing of nerve agent from the scrubbing solution at the top of the tower. A mathematical model of the chemical reaction characteristics of the packed tower was developed and applied to the data from the second test series. The predicted result was excellent agreement with the measured emission, confirming the theory that the altered reaction kinetics of the scrubbing solution and the nerve agent were responsible for the excessive emission. Thus, when the packed towers were placed in operation, the amount of sodium hydroxide in the scrubbing solution was closely controlled as the most important parameter affecting scrubbing efficiency. Since that time, the packed towers have operated essentially as designed and additional towers have been constructed and successfully operated based on the initial design.

### MAIN ELEMENTS OF NERVE AGENT DETOXIFICATION

- 1. NEUTRALIZATION
- 2. SPRAY DRYING
- 3. VENTILATION CONTROL
- 4. ENVIRONMENTAL EMISSION CONTROL

Nerve Agent Neutralization Facility





# MECHANISMS FOR CONTROLLING THE NERVE AGENT 'NEUTRALIZATION REACTION TEMPERATURE

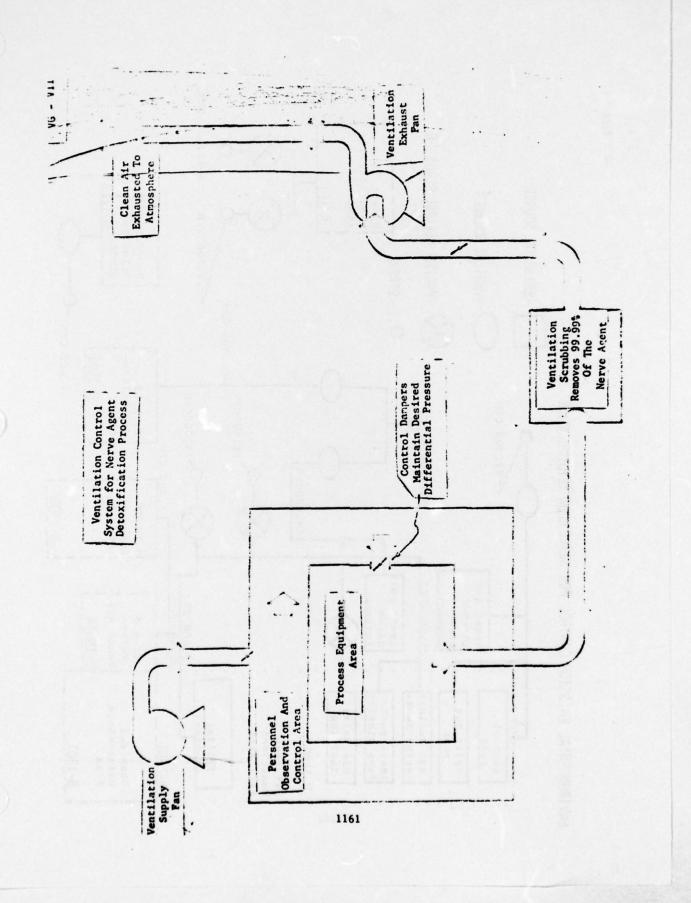
- $1.\,$  Controlling the temperature of the sodium hydroxide solution from the refrigeration machine.
- 2. Modulating the cooling water flow to the reaction cooler.
- 3. REDUCING THE NERVE AGENT FLOW TO THE EDUCTOR.

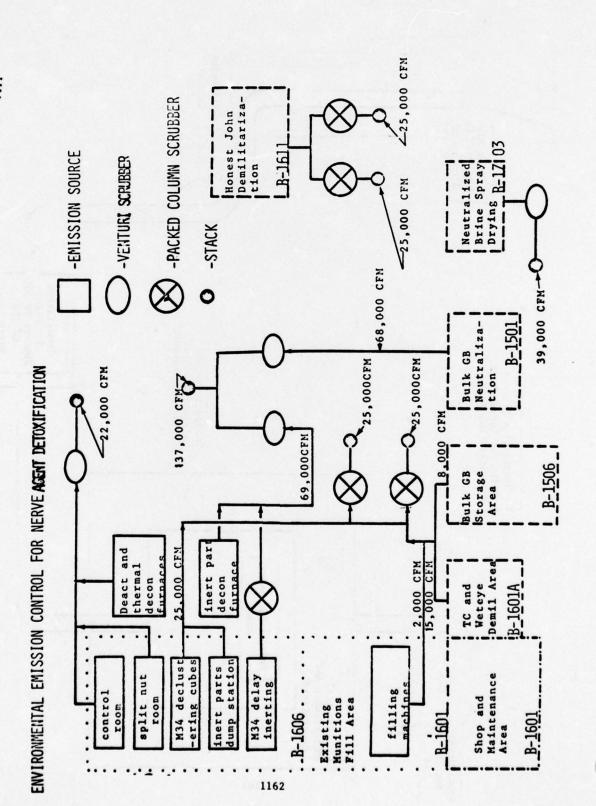
# EVIDENCES OF NERVE AGENT REFORMATION DURING THE SPRAY DRYING OPERATION

- 1. FIRING THE BURNER WITH FUEL OIL (WITH SUBSEQUENT INCREASE IN SULFUR DIOXIDE CONTENT OF THE SPRAY DRYER AIR STREAM)
  RESULTED IN INCREASING EMISSIONS FROM THE SPRAY DRYER.
- INCREASING THE AMOUNT OF SODIUM HYDROXIDE IN THE NEUTRALIZED BRINE RESULTED IN DECREASING EMISSIONS FROM THE SPRAY DRYER.
- 3. KEEPING THE WALLS OF THE SPRAY DRYER CHAMBER FREE OF SALT BUILDUP RESULTED IN DECREASING EMISSIONS FROM THE SPRAY DRYER.
- 4. DECREASING THE OPERATING TEMPERATURE RESULTED IN DECREASING EMISSIONS FROM THE SPRAY DRYER.

### OPERATIONAL MODIFICATIONS TO REDUCE NERVE AGENT EMISSIONS FROM THE SPRAY DRYER

- 1. ELIMINATING ALL OIL-FIRED SPRAY DRYER OPERATION.
- 2. INCREASE THE AMOUNT OF SODIUM HYDROXIDE IN THE NEUTRALIZED BRINE FROM 2% TO 8% BY WEIGHT.
- 3. CLEANING THE SPRAY DRYER CHAMBER MORE FREQUENTLY.
- 4. REDUCING THE OPERATING TEMPERATURE FROM 1150°F TO 725°F.
- 5. ADDING SODIUM HYDROXIDE TO THE VENTURI SCRUBBER TO OBTAIN SOME FINAL SCRUBBING OF ANY NER VE AGENT WHICH MIGHT BE REFORMED.





The Department of Defense Explosive Safety Board's

CHEMICAL HAZARDS SLIDE RULE

Ву

Lewis C. Dixon

NAVAL SURFACE WEAPONS CENTER
White Oak Laboratory
Silver Spring, Maryland 20910

#### I. The Problem

The specific problem is the estimation of hazards to human beings as the result of accidental releases of toxic chemical aerosols and vapors. The problem is not a lack of math models, but in part the complexity of the existing models. The solution to about 50 equations may be required, depending upon the specific situation. Computers and mathematicians are required. The process is slow. It is difficult to communicate an understanding to those who are not skilled in the subject.

The problem is not unusual or unique to the chemical hazards area. A common problem in the analytical world of high-speed high-output computers is the multitudinous stacks of data. The problem is the great quantities of data and the resulting lack of visibility to those who attempt to use the data. It is a problem to one who may be attempting to assess the data. He also finds it difficult to explain the data to others. In the case of the chemical hazards problem, it is also desirable to communicate more effectively at the technician level and to give the technician a tool that he might be able to use with a degree of confidence.

#### II. The Graphical Slide Rule

A Graphical Slide Rule approach to general open-ened solutions of complicated problems is proposed whenever it is applicable, and it is not always applicable. The Graphical Slide Rule is an analogue technique in which the results from more sophisticated simulations are reproduced in graphical form on transparent acetate slides. The slides may contain more than one curve or set of data. In use the slide has a reference base such as that found in Figure 1.

The base is mounted in a special fixture and a "slide" of a type such as that found in Figure 2 is superimposed over the base. The clear acetate slide will permit the base to be viewed through the slide. The curves and scales printed on the slide are by this technique permited to have their position relative to the base changed as input parameters would direct the shifting of the curve.

A composite of the base and the slide is shown in Figure 3. The vertical line headed by the letter "A" on the slide is aligned with the vertical line on the base headed by the letter "B." This specific orientation fixes the curves on the slide relative to the base in a situation in which  $10^7$  milligrams of a chemical has been effectively aerosolized in a meteorological regime that will transport it to downwind points. Levels of source strength other than  $10^7$  may be used by aligning the appropriate value on the slide along the "Source strength" scale with the "B" line on the base.

The breathing rate of human beings downwind from a cloud is important. The effect upon a population that would be sleeping and, therefore, breathing slowly ("Resting") would be much less severe than it would be for a population that would be moderately active ("Moderate") or under some physical strain ("Brisk"). The second scale on the slide, Figure 2, provides for variations in breathing rates to be used precisely.

The slide, Figure 2, has six different curves on it, one for each of six different standard meteorological regimes called "Pasquill Categories." The definition of each of the Pasquill Categories may be found in Figure 4. As may be seen, the specific meteorological category is dependent upon the wind speed, the level of solar radiation and the level of cloud coverage.

In operation, the level of source strength and breathing rate is fed into the slide rule. The appropriate Pasquill Category is selected and from the corresponding curve, combinations of dosages are read from the abscissa as the downwind distances increase along the ordinate.

The slide rule at this point is not agent specific. It becomes specific simply by adding another transparent overlay, this time one similar to that illustrated in Figure 5 for VX Vapor. The influence upon the human population is shown on the overlay, and thus, the degradation of effects expected as the cloud moves may be followed directly.

In situations involving classified defense information, the Graphical Slide Rule need not be classified until the "human effects" (or other effects) overlay is added. The security classification would be associated with the overlay only.

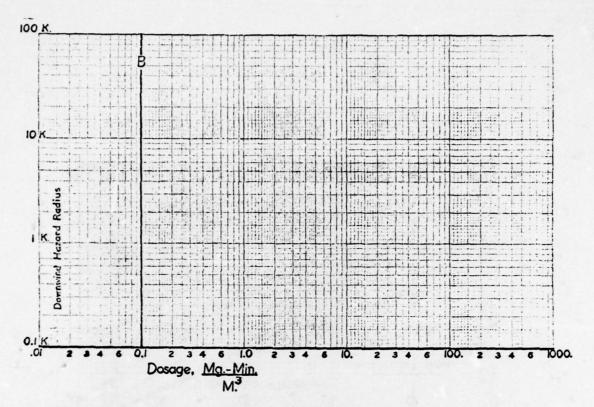


Figure 1, Reference Base

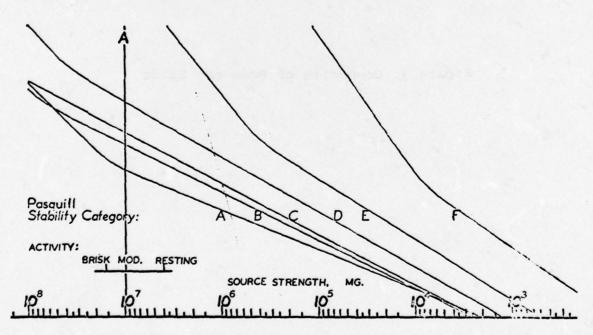


Figure 2, Slide

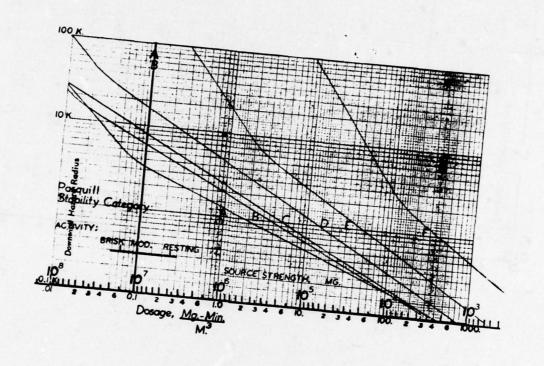


Figure 3, Composite of Base and Slide

Su	rface Wind Speed	Incomir	ng Solar Ra	diation	Thinly Overcast or	< 3/8
	t 10m), m sec-1		Moderate		≥ 4/8 Low Cloud	Cloud
	<2	A	A-B	В		
	2-3	A-B	В	С	E	F
	3-5	В	в-с	С	D	E
	5-6	c	C-D	v	D	D
	>6	С	D	D	D	D
					Reference (a)	

Figure 4, Definitions, Pasquill Categories

NO DISCERNIBLE EFF	H	INMING	INESS ISION MITING		VX	Vapor
ond or Swift was straightful to the	Г	D EYES				
ob' es layal o		E ACHE				
el scott let est el ette attica le	10 100	1000	į			
as the first of	į	ORS	LITIES	ALLIES		
no do Veligi No Sept	MIOSIS	NO TREMORS	NO LETHALITIES	I & LETHALITIES		
	3	ž	2	٦		

Figure 5, Overlay, Human Effects Due To VX Vapor

#### III. Discussion

The simulation used for the DDESB Chemical Hazards Slide Rule is found in two documents, reference (a), and reference (b).

The basic equation for computing the axial dosages at ground level from an instantaneous point as employed by the slide rule is:

- D(x) = 0 (mathematical treatment of MET Parameters)
  - D = the axial dosage in mg-min/cu m at a point, x, downwind
  - Q = the source strength in milligrams.

The meteorological parameters associated with each of the Pasquill Stability Categories may be found in Figure 6. These values used as a part of another program could involve nearly 50 other equations and complicated procedures that will not be reported here. The point to be made is: The Chemical Hazards Slide Rule does not solve equations; rather through plots of the results of sophisticated simulations it can re-establish thousands of sets of such solutions with an adequate degree of precision.

The simplified basic equation above is presented in this form to emphasize a point: Dosage is directly proportional to the source strength (Q). The treatment of Q in the slide rule on a log-plot is as precise as its construction and the ability of a person to read a graph. The Wind Speed ( $U_X$ ) and Breathing Rate are also directly proportional; however, the magnitude of the wind is considered to a degree when the appropriate Pasquill Category is selected. Since the Pasquill Category uses a range of wind velocities, some thought has been given to the use of a wind scale on the slide. Given the probable error in selecting the proper Meteorological Category, it is not believed that the additional complications would give a net advantage.

Dosage, "D" in mg-min/cu m, is also directly related to "dose" in milligrams by the breathing rate in liters per minute. Dosage and its use as a scale on the slide to vary this important function is also a precise mathematical treatment.

The relative positions of the curves for each of the Pasquill Categories is fixed and, therefore, their combined display on one slide is justified. Thus one slide such as that found in Figure 2 will permit hazard estimates from the total spectrum of meteorological regimes, source strengths and breathing rates for an instantaneous release of a toxic chemical at ground level. Continuous type releases may be added to the slide with the instantaneous releases but with some complications and a loss of precision. The elevation of the release point in ground-oriented (non-airborne) situations has the effect of changing the dosage levels in the vicinity of the source, but not at downwind positions beyond about 100 meters.

## PARAMETRIC VALUES FOR USE WITH PASQUILL STABILITY CATEGORIES

Pasquill Stability Category	oyr(10 min) meters	σ <sub>yr</sub> (2.5 sec) meters	g.	δ <sub>zr</sub> meters	В	H <sub>m</sub>	Ux meters/ min
A	27.0	9.0	1,0	14	2.0	2750	62
В	19.0	6.33	1.0	11	1.4	2250	124
c	12.5	4.2	1.0	7.5	1.0	1750	216
D	8.0	2.7	0.9	4.5	0.9	875	216
E	6.0	2.0	0.8	3.5	0.85	125	154
F	4.0	1.33	0.7	2.5	0.7	30	62
					Refe	rence	(a)

Figure 6, Meteorological Parameters for Pasquill Categories

A utility slide will be added to the DDESB Chemical Hazards Slide Rule that will permit the estimation of the time a given cloud will reach some position downwind, using estimated wind speeds, or those associated with the specific Pasquill Category.

Another important attribute of the Chemical Hazards Slide Rule is an inherent ability to move with ease from one Pasquill Category to another. The procedure is a little tricky, but with the use of the time scale, the meteorology situation may be treated as the dynamic everchanging situation that it really is. Procedures of this type will be presented in subsequent publications.

#### IV. The Task for DDESB

In the next few months, the DDESB will be supplied with a number of copies of the Chemical Hazards Slide Rule as presented, along with a treatment for Continuous Sources, a Standard Operating Procedure, a Technical Report, sets of overlays giving human response information for specific agents of interest, suggested source strengths for specific situations, a set of utility slides including one that will assist in the estimation of the source strength from the evaporation of accidental spills, and some suggestions as to training aids.

#### V. Future Potentialities

The one treatment of the Chemical Hazards Slide Rule as presented herein used only about 100 data points to plot a set of curves that may be used to reproduce many thousands of combinations. It is designed for the person facing real problems and the limited data that he has available to him. Slides may be generated that would include appropriate scales to estimate more precisely the exact meteorological regime using routine meteorological data. Another approach would be the use of programmable desk calculators to estimate hazard levels treating the inputs in the same manner as the Graphical Slide Rule, but obviously without the visibility of the Graphical Slide Rule.

#### VI. References

- a. DDESB Technical Paper No. 10, "Methodology for Chemical Prediction," Mar 1975
- b. ORG Report 40, (C) "Methods of Estimating Hazard Distances for Accidents Involving Chemical Agents (U)," US Army, Edgewood Arsenal, Feb 1970.

#### WORKBOOK FOR PREDICTING PRESSURE WAVE AND FRAGMENT EFFECTS OF EXPLODING PROPELLANT TANKS AND GAS STORAGE VESSELS

W. E. Baker Southwest Research Institute San Antonio, Texas

#### ABSTRACT

Damaging accidental explosions in launch vehicles or spacecraft usually involve exploding liquid propellants or bursting gas storage vessels. These explosions can generate blast waves and can also accelerate fragments of bursting vessels and nearby objects or appurtenances. This paper discusses a recently published workbook which is intended to provide the designer and the safety engineer with methods for prediction of damage and hazards from such explosion sources, over a wide range of distances. The information in the workbook is presented in the form of tables, graphs, and nomographs to allow easy calculation without recourse to difficult mathematical manipulation or the use of extensive computer programs. When complex methods have been used to develop simple prediction aids, they are fully described in appendices.

Topics covered in the workbook, which will be summarized in the paper, are:

- (1) Estimation of explosive yield
- (2) Characteristics of pressure waves
- (3) Effects of pressure waves
- (4) Characteristics of fragments
- (5) Effects of fragments
- (6) Risk assessment and integrated effects

#### INTRODUCTION

The likelihood of accidental explosions, in the various activities that involve liquid propellants for space vehicles, can best be decreased by improvements in design practices and operating procedures. Over the years, the frequency of occurrence of accidental explosions in the space programs has decreased with advances in technology. Nevertheless, the possibility of space vehicle fuel/oxidizer explosions or pressure bursts

will always exist, especially with reusable propulsion systems that must be more reliable than those in the "one-shot" space vehicle. Excessive cyclic stresses, wear of moving parts, and the accumulation of contaminants are some of the factors that could contribute to component malfunctions or material failures during the lifetime use of such systems. These malfunctions or failures could, in turn, contribute to accidental explosions with risk of damage to facilities and hazards to people. Thus, it becomes important to predict the explosive yield and the effects of pressure wave and fragments in a quantitative manner.

The intent of a recently published workbook [1] is to provide the designer and the safety engineer with the best available technology that they need to predict damage and hazards from explosions of propellant tanks and bursts of pressure vessels in the near and far fields of interest.

In a launch configuration within tankage in a rocket motor, liquid propellants and nonreacting gases are initially contained within vessels of various sizes, geometries, and strengths. Various modes of failure of these vessels are possible, from either internal or external stimuli. If the vessel is pressurized with static internal pressure, one possible mode of failure is simply fracture, instituted at a critical size flaw and propagated throughout the vessel. A similar kind of failure can occur if the vessel is accidentally immersed in a fire and pressure increases internally because of vaporization of the internal propellant. Some launch vehicles have the liquid fuel and oxidizer separated by a common bulkhead. Accidental over-pressurization of one of these chambers can cause rupture of this bulkhead and subsequent mixing, and explosion of the propellant. External stimuli that can cause vessel failure include high-speed impact by foreign objects, accidental detonation of the warhead of a missile, dropping of a tank to the ground (as in toppling of a missile on the launch pad), as well as many other external sources. Vessel failure can result in an immediate release of energy, or it can cause subsequent energy release because of mixing of propellant and oxidizer and subsequent ignition. Other modes of failure which have resulted or could result in violent explosions are fall-back immediately after launch due to loss of thrust, or low-level failure of the guidance system after launch, resulting in impact into the ground at several hundred feet per second.

Failure of a vessel containing liquid propellants or compressed gas can result in various levels of energy release, ranging from negligible to the full heat value of the combined propellant and oxidizer, or full value of stored energy in the compressed gas. Toward the lower end of the scale of energy release might be the failure of a pressurized vessel due to ductile crack propagation. Here, the stored pressure energy within the compressed propellant or gas in an ullage volume above the propellant could split the vessel or generate a weak blast wave. In the intermediate range of energy releases could lie vessel failure by

external stimulus and ignition, either very rapidly or at very late times, so that only small proportions of mixed propellant and oxidizer contribute to the energy release. In this intermediate range could also lie the rapid fracture of gas storage vessels after heating or very rapid crack propagation. At the upper end of the scale could be the explosion in a vessel wherein a premixed propellant and oxidizer detonate in much the same fashion as a high explosive and explosions resulting after violent impact with the ground. In past studies of possible blast and fragmentation effects from vessel rupture, a critical problem has been to accurately assess the energy release as a result of the accident or incident. A common method of assessment of possible energy release or correlation of the results of experiments has been to assess the energy release on the basis of equivalent pounds of TNT. This method is used because a large body of experimental data and theoretical analyses exist for blast waves generated by TNT or other solid explosives (Refs. 2 and 3). Although the comparison with TNT is convenient, the correlation is far from exact. Specific energies which can be released, i.e., energy per unit volume or mass of material. differ quite widely between TNT, various liquid propellants or mixtures of liquid propellants and oxidizers, and gases stored in pressure vessels. The characteristics of damaging blast waves from explosions which can occur in flight vehicle accidents can therefore be quite different from blast waves from TNT explosions. The accidental explosions usually generate waves with lower amplitudes (peak overpressures) and longer durations than equivalent energy TNT explosions, at least close to the explosion source. Reference 4 discusses in some detail the blast waves from accidental explosions of the classes covered in Reference 1.

Dependent on the total energy release and the rate of this energy release, the sizes and shapes of fragments generated by bursting liquid propellant vessels and their appurtenances, and bursting gas vessels, cover a very wide spectrum. At one extreme is the case of a vessel bursting because of seam failure or crack propagation from a flaw wherein only one "fragment" is generated, the vessel itself. This fragment, from a very slow reaction, can be propelled by releasing the contents of the vessel. At the other extreme is the conversion of the vessel and parts near it into a cloud of small fragments by an explosion of the contents of a vessel at a very rapid rate, similar to a TNT explosion (Refs. 5 and 6). For most accidental vessel failures, the distribution of fragment masses and shapes undoubtedly lies between these two extremes. The modes of failure of the vessel may be dependent upon details of construction and the metallurgy of the vessel material. Some of the masses and shapes are dictated by the masses and shapes of attached or nearby appurtenances. In any event, assessment and prediction of these parameters are much more difficult than is true for the better understood phenomenon of shell casing fragmentation.

Once the masses, shapes, and initial velocities of fragments from liquid propellant vessels or bursting gas vessels have been determined

in some manner, then the trajectories of these fragments and their losses in velocity due to air drag or perforation or penetration of various materials must be computed. This problem is primarily one of exterior ballistics. It differs from conventional exterior ballistic studies of trajectories of projectiles, bombs, or missiles in that the body in flight is invariably very irregular in shape and can be tumbling violently. Exact trajectories cannot be determined then in the same sense that they can be for well-designed projectiles. Only approximate trajectories can be estimated, usually by assuming relatively simple geometric shapes, such as spheres, discs or cylinders, for which exterior ballistics data and techniques exist. But, in some fashion, one can predict the ranges and impact velocities for fragments which were initially projected in specified directions from the bursting vessel with specified initial velocities.

This problem is not complete until one can assess the effects of blast waves and fragments from the accidents on various "targets." For a proper assessment of hazards, one should consider a wide variety of targets, including human beings, various classes of buildings, vehicles, and perhaps even aircraft. Problems of fragment damage are exceedingly complex, not only because of the inherent statistical nature of the characteristics of the impacting fragments, but also because the terminal ballistic effects for large irregular objects impacting any of the targets described are not very well known. In most past studies of fragment damage from accidents, the investigators have been content to simply locate and approximate the size and mass of the fragments in impact areas and have ignored the important problem of the terminal ballistic effect of these fragments. Prediction of blast damage is also not simple, but much more work has been done, and reasonable estimates can be made for most structures and for humans, provided the characteristics of the blast waves can be defined (Refs. 7 and 8).

#### Means for Assessment of Risk

Reference 1 is directed toward estimation of blast and fragmentation effects of accidental explosions in flight vehicles. It is not intended to encompass the entire problem of risk assessment for launch and operation of these vehicles. This more comprehensive task includes the estimation of the probability of occurrence of various types of failures or accidents, and must employ methods such as failure mode analysis or fault-tree analysis to obtain such probabilities. In the handbook, it is assumed that a specific explosive accident has occurred, and the hazardous effects of that accident are predicted.

#### Scope of Material Presented

The material presented in the handbook is based on a previous study of fragmentation from bursting propellant vessels (Ref. 9) and

on the literature on characteristics and effects of blast waves and fragment impact. Methods are given for predicting the damage to facilities and hazards to people from exploding liquid propellant tanks or bursting gas storage bottles. Various chapters present material which allows estimation of explosive yield or energy for a variety of propellant explosions and gas vessel bursts, give predictions of characteristics of pressure waves from these explosions, and present techniques for making damage estimates for structures and facilities, and mortality or injury to people subjected to the blast waves. Other chapters include shape, terminal velocities and impact conditions, and effects of such impact on facilities, structures, and people. Throughout the workbook, presentations are made in the form of scaled graphs, equations, nomographs, or tables which allow easy calculation without recourse to difficult mathematical manipulation or use of extensive computer programs. When such methods have been used to develop simple prediction aids, they are fully described in appendices.

It is believed that this workbook is the first to provide safety engineers with relatively simple yet comprehensive methods for estimating blast and fragment hazards for accidental explosions in liquid-propellant fueled flight vehicles. Some methods for estimating blast yield for classes of liquid propellant accidents are given in Reference 10, and Reference 11 discusses blast and fragmentation from such explosions. But, neither of these references allows estimation of fragment characteristics and effects for liquid propellant explosions, nor do they treat gas vessel bursts. Special features not seen elsewhere are the prediction of blast wave characteristics for gas vessel bursts, effects of fragment impact on structures and facilities, and extensive application of the pressure-impulse (P-I) damage concept to a wide variety of structures and to humans.

#### ESTIMATION OF EXPLOSIVE YIELD

We noted in the introduction that the classes of accidental explosion covered in the workbook can differ in their characteristics from TNT explosions. The first step in predicting blast effects is therefore the estimation of the yield, or total energy which drives the blast wave and/or accelerates fragments, for a number of particular propellant combinations or gas vessel burst conditions.

For liquid propellant explosions, the concept of "TNT equivalency" is retained in a modified sense because the blast waves at large distances from such explosions were found to be similar to those for some equivalent quantity of TNT. This so-called "terminal yield" is used as a basis for the test results reported in Reference 12. Chapter 1 in the workbook has a number of graphs which allow one to predict this terminal

yield  $\gamma$  as a percent of TNT equivalence for different liquid propellant combinations and accident conditions, as a function of ignition time after occurrence of the accident. Figure 1 is typical of these graphs. The solid curve gives the most probable value for Y, while the upper and lower dashed curves give the ranges of experimental data. The propellant combination is liquid oxygen and RP-1 fuel, and the type of accident is Confined By Missile (CBM), i.e., a mixing following rupture of an internal bulkhead. Other propellant combinations considered are liquid oxygen and liquid hydrogen, and hypergolic propellants. Other types of accidents considered are spill on the ground and subsequent ignition (CBGS) and high velocity impact after liftoff (HVI).

As the quantities of liquid propellant involved in an explosive accident are increased, the chances of early ignition before significant mixing can occur are greatly enhanced. Consequently, the fraction of propellant which can actually contribute to the explosion decreases with total mass of propellant and oxidizer. Reference 13 gives methods of estimating this limit as shown in Figure 2. Here, y is the limiting fraction of the total propellant mass which contributes to blast yield. To obtain maximum TNT equivalent, the multipliers given in the figure must be used. If values calculated from this figure are less than values obtained from Figure 1 or similar ones, they are used to predict blast yield.

In bursts of gas vessels, one can easily estimate the energy E driving the blast wave from the simple equation

$$E = \left(\frac{p_1 - p_a}{\gamma_1 - 1}\right) v_1 \tag{1}$$

In this equation,

E = blast source energy (FL)

 $p_1$  = initial absolute pressure in bursting vessel (F/L<sup>2</sup>)

 $p_a$  = absolute atmospheric pressure  $(F/L^2)$ 

 $V_1 = \text{volume of vessel } (L^3)$ 

 $\gamma_1$  = ratio of specific heats of gas in vessel (-)

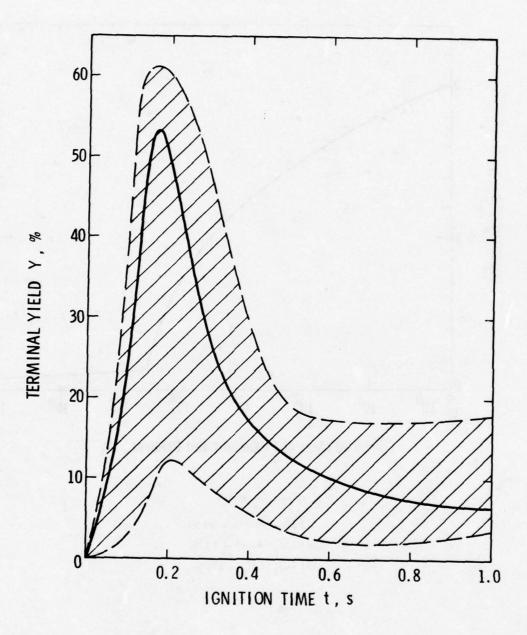
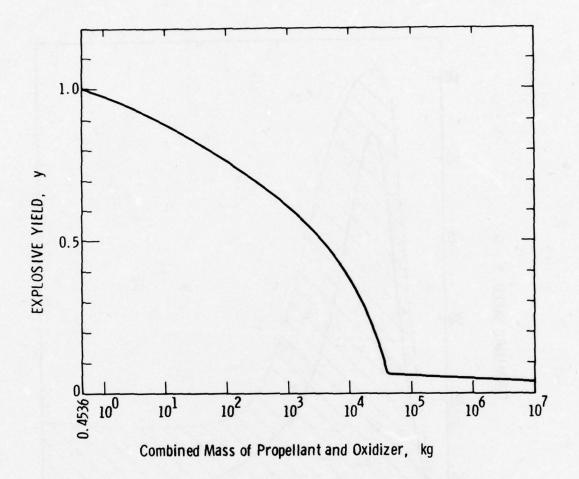


FIGURE 1. TERMINAL YIELD VS IGNITION TIME FOR  $LO_2/RP-1$  CBM.



#### Multiplier Factors:

- (1) Hypergolic 240%
- (2) LO<sub>2</sub>/RP-1 125% (3) LO<sub>2</sub>/LH<sub>2</sub> 370%

FIGURE 2. ESTIMATED TERMINAL YIELD AS A FUNCTION OF COMBINED PROPELLANT AND OXIDIZER MASS (REF. 13).

#### CHARACTERISTICS OF PRESSURE WAVES

Blast waves from propellant explosions and gas vessel burst differ enough from those from TNT explosions, particularly close to the source, that one cannot use compiled TNT data or calculations to predict their characteristics. Instead, the workbook offers in Chapter 2 alternate methods for predicting blast overpressure P and impulse I as functions of distance R, for specific blast yield and type of blast source.

Typical of the data for exploding propellants are Figures 3 and 4. The propellant combination and type of accident are the same as for Figure 1. In these figures, W is a mass of propellant for blast calculated from

$$W = W_T \times \frac{Y}{100} \tag{2}$$

where  $W_T$  is total mass of propellant and oxidizer. As in Figure 1, the solid curves give the most probable values for P and I, and the dashed curves indicate limits of experimental data from Reference 12.

Curves for predicting blast pressures and impulses for gas vessel bursts are based primarily on calculations in References 1 and 14 because very little experimental data exist for such explosions. The results of the calculations are shown in Figures 5 and 6. Dimensionless side-on overpressure  $\overline{P}_{\rm S}$  and side-on impulse  $\overline{I}_{\rm S}$  are given in these figures as functions of dimensionless scaled distance  $\overline{\rm R}.$  These terms are defined by

$$\overline{P}_{S} = \frac{P_{S} - P_{a}}{P_{a}} \tag{3}$$

$$\bar{I}_{s} = \frac{I_{s} a_{a}}{p_{a}^{2/3} E^{1/3}}$$
 (5)

$$\overline{R} = \frac{R p_0^{1/3}}{E^{1/3}}$$
 (6)

where  $p_s$  is absolute peak pressure, and  $a_a$  is sound speed in ambient air. The separate curves in Figure 5 each relate to a different set of bursting sphere initial conditions. Differences in impulse are small enough

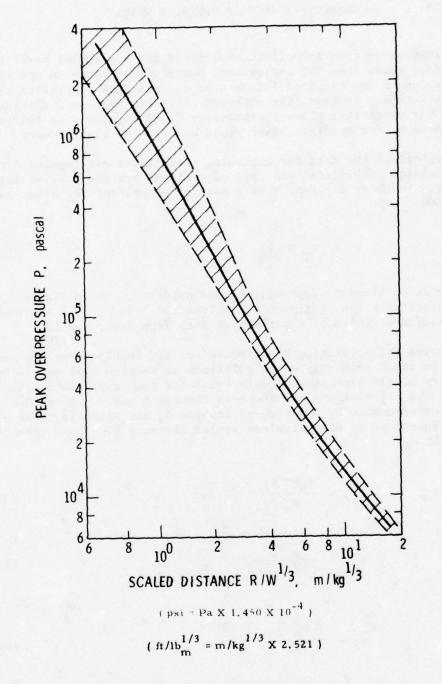


FIGURE 3. PRESSURE VS SCALED DISTANCE. LO<sub>2</sub>/RP-1 PROPELLANT; CBM FAILURE MODE.

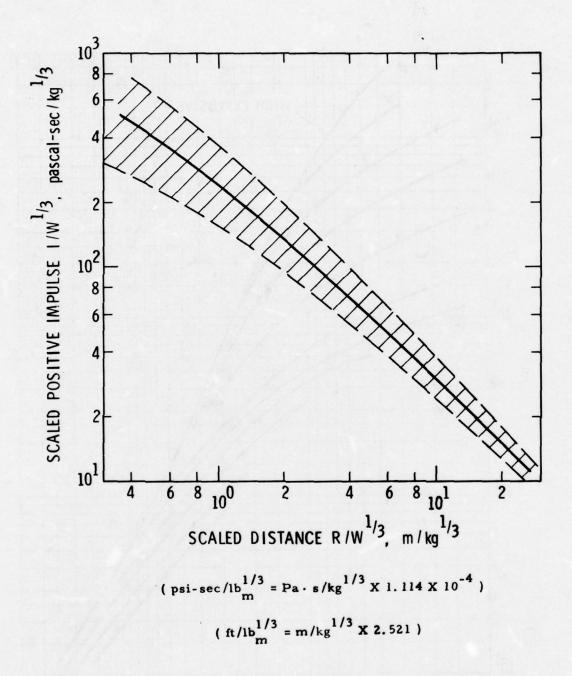


FIGURE 4. SCALED POSITIVE IMPULSE VS SCALED DISTANCE.  ${\rm LO_2/RP\text{--}1}$  PROPELLANT; CBM FAILURE MODE.

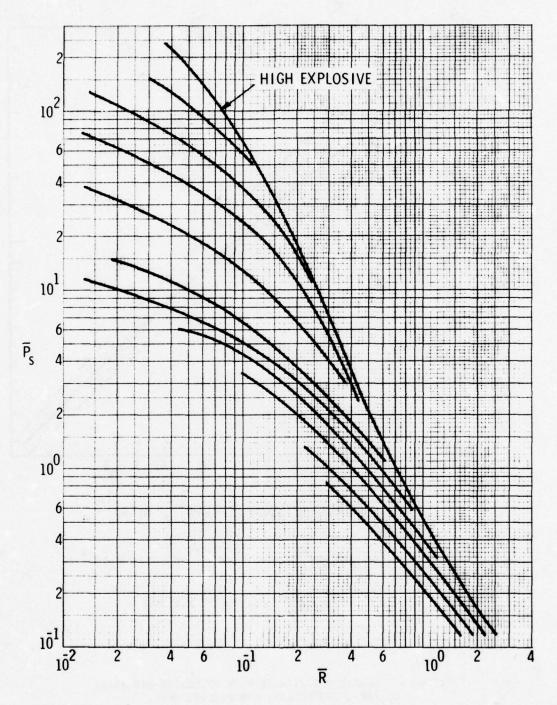


FIGURE 5.  $\overline{P}_s$  VS  $\overline{R}$  FOR OVERPRESSURE CALCULATIONS.

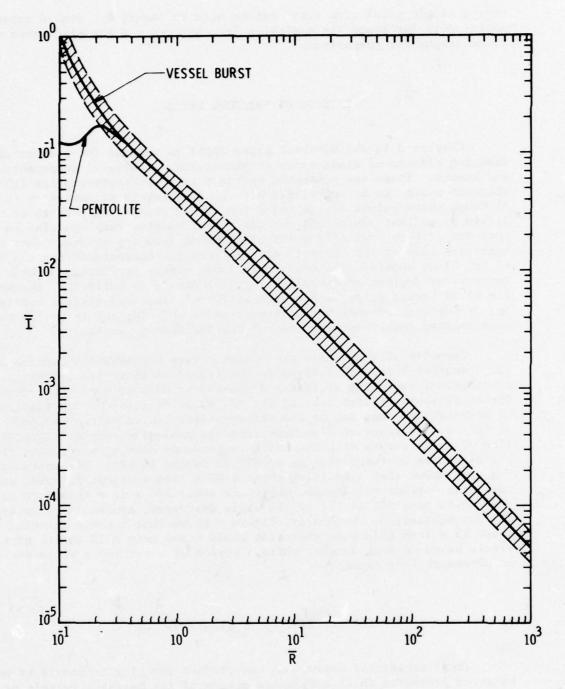


FIGURE 6.  $\overline{I}$  VS  $\overline{R}$  FOR PENTOLITE AND GAS VESSEL BURSTS.

that a single prediction curve can be used in Figure 6. Scaled experimental data for Pentolite explosive from Reference 2 are also shown on these graphs for comparison.

#### EFFECTS OF PRESSURE WAVES

Chapter 3 in the workbook gives detailed methods for predicting damaging effects of blast waves on structures, structural components, and humans. These are presented in the form of pressure-impulse (PI) diagrams which can be correlated with various levels of damage or injury. Although these curves are intended for use in predicting effects of liquid propellant explosions and gas vessel bursts, they can also be used for effects predictions for blast waves from any source. They are functions only of the "target" dynamic response characteristics and not of the blast source. The chapter includes damage prediction methods for various degrees of overall structural damage to buildings, threshold for glass breakage, permanent deformation of beams and plates, overturning or toppling of unanchored structures or objects, and injury to humans ranging from temporary loss of hearing through mortality.

Examples of the damage prediction curves are shown in Figures 7-9. The scenarios 1 through 4 noted in the figure captions are different hypothetical explosive accidents discussed in Chapter 6 of the workbook. Curves in these figures labeled #1, #2, #3 or #4 give the combinations of pressure and impulse, or the corresponding scaled values, which would be felt over a range of distances from the explosive source. Intersection of these curves with the basic response or damage curves then gives the distances corresponding to specified damage levels. For instance, Figure 7 shows that a building about 1100 m from accident #1 would sustain minor structural damage, while one about 250 m from this same accident would have 50% to 75% of the walls destroyed, and would be unsafe for any habitation. Similarly, Figure 9 shows that a human standing about 55 m from this same explosion would stand only a 1% chance of survival, based on lung damage, while a person at about 200 m would sustain no permanent lung damage.

### CHARACTERISTICS OF FRAGMENTS

These accidental explosions can produce damaging fragments by unbalanced pressures which accelerate pieces of the bursting vessels or propellant containers, and by the blast waves engulfing nearby objects or appurtenances and accelerating them by drag forces. Chapter 4 presents methods for predicting initial velocities of these two classes of

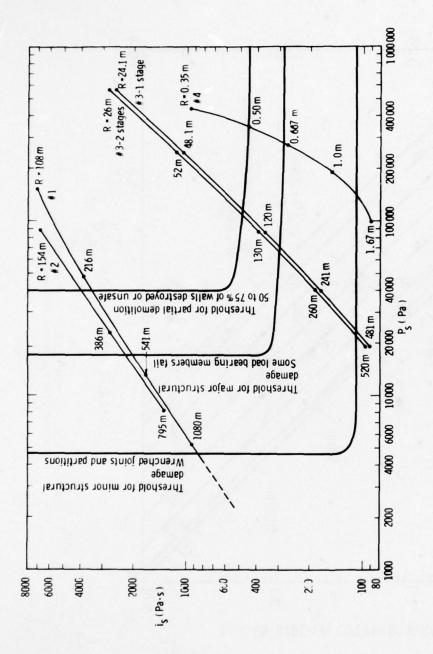


FIGURE 7. PRESSURE VS IMPULSE DIAGRAM FOR BUILDING DAMAGE WITH BLAST CURVES FOR SCENARIOS 1 THROUGH 4.

( psi-sec = Pa. s X 1.450 X 10-4)

( psi = Pa X 1.450 X 10-4 )

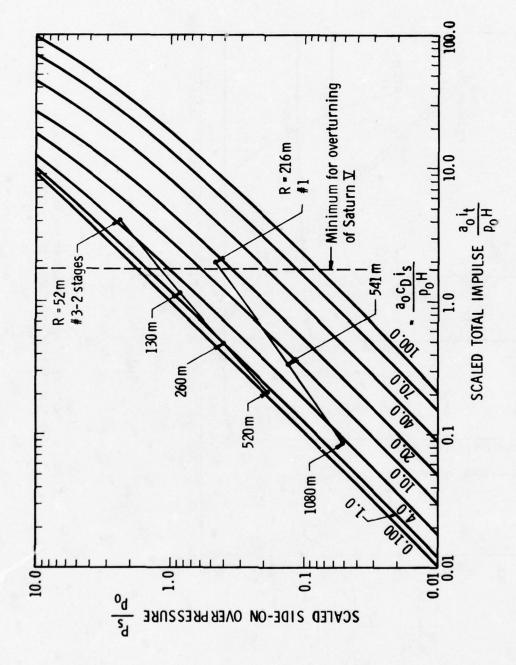


FIGURE 8. SPECIFIC IMPULSE IMPARTED TO A TARGET WHICH MIGHT OVERTURN WITH CURVES FOR SCENARIOS 1 and 3.

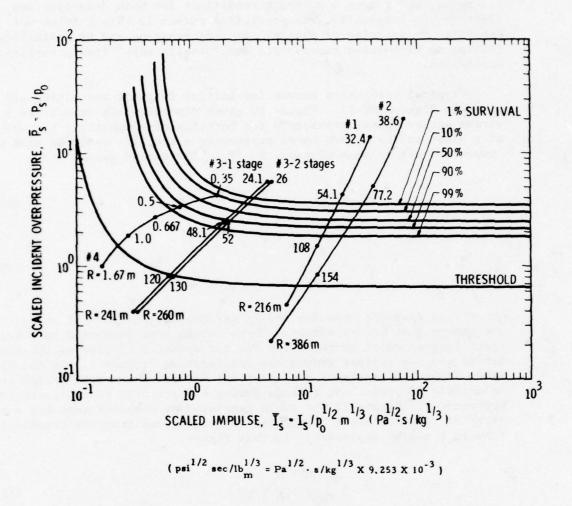


FIGURE 9. SURVIVAL CURVES FOR LUNG DAMAGE WITH CURVES FOR SCENARIOS 1 THROUGH 4.

fragments, and ranges and impact conditions for both drag-type and lifting-type fragments. The prediction curves in this chapter were generated by exercise of special computer programs and by statistical fitting to high-speed camera data and "missile maps" from propellant explosions.

Typical prediction curves for initial fragment velocities are given in Figures 10-12. Figure 10 gives dimensionless velocities  $\bar{v}$  versus scaled vessel pressure  $\bar{p}$  for bursting of a spherical air tank of a given radius. Each curve represents a specific ratio of mass of compressed air to mass of tank,  $\frac{M}{os}$ . The scaled values are

$$\frac{\overline{v}}{v} = \frac{v}{a_a} \tag{6}$$

$$\overline{p} = \frac{p_0}{p_a} \tag{7}$$

where v is fragment velocity and  $P_O$  is absolute pressure of the air in the sphere just before bursts. These curves were generated by a computer program which accounts for the gas dynamics of flow as the vessel bursts and gas escapes around the accelerating fragments. On the other hand, Figure 11 is simply a statistical fit to camera data on measured velocities of propellant tankage during Project PYRO tests, reported in Reference 9. Figure 12 was again generated by computer runs for a variety of "appurtenances" subjected to drag forces from the transient flow in a nearby explosion. In this figure,

$$\overline{V} = \frac{M V a_a}{P_a A (KH + X)}$$
 (8)

$$\overline{P}_{S} = \frac{P_{S}}{P_{a}} \tag{9}$$

$$\overline{I}_{s} = \frac{C_{D} I_{s} a_{a}}{P_{s} (KH + X)}$$
 (10)

where

M = total mass of the appurtenance (M)

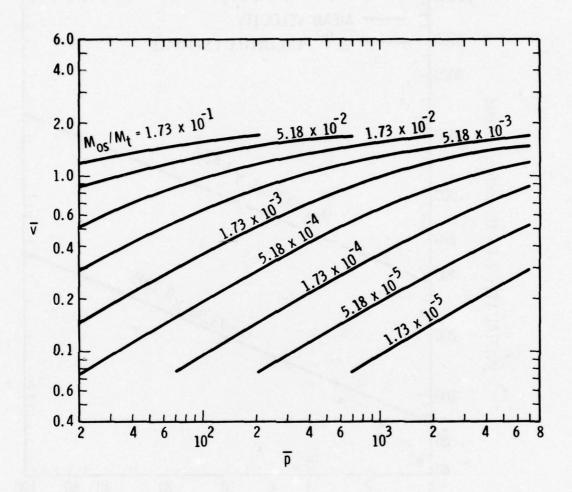


FIGURE 10. FRAGMENT VELOCITIES FOR CONTAINED AIR IN A SPHERE OF RADIUS 0.254 m.

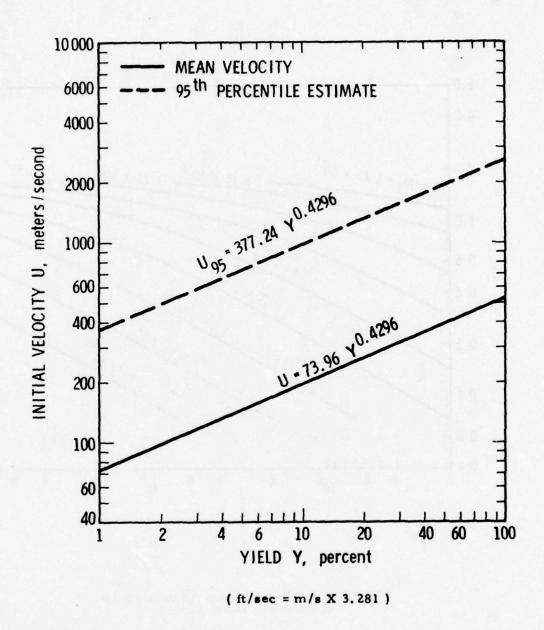


FIGURE 11. INITIAL VELOCITY VS YIELD, CBM,  $\rm Lo_2/LH_2$ .

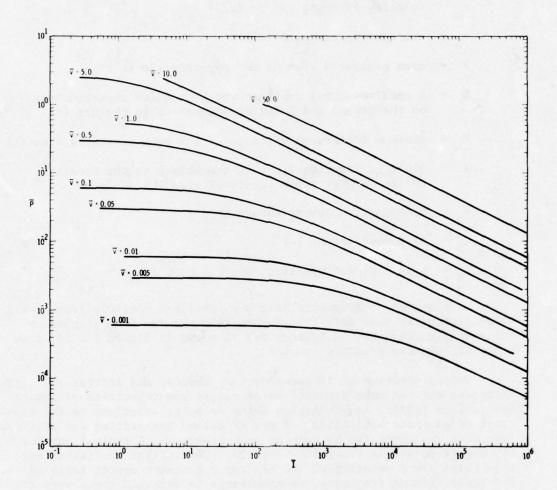


FIGURE 12. NONDIMENSIONAL APPURTENANCE VELOCITY  $\overline{V}$  AS A FUNCTION OF NONDIMENSIONAL PRESSURE  $\overline{P}$  AND NONDIMENSIONAL IMPULSE  $\overline{T}$ .

V = velocity of the appurtenance (L/T)

 $a_a = \text{velocity of sound in air } (L/T)$ 

 $p_{a} = atmospheric pressure (F/L)^{2}$ 

A = mean presented area of the appurtenance (L<sup>2</sup>)

K = a nondimensional constant which is 4 for appurtenances on the ground and 2 for appurtenances in the air (-)

H = minimum transverse distance of the mean presented area (L)

X = distance from the front of the object to the location of its largest cross-sectional area (L)

 $P_s = peak incident overpressure (F/L<sup>2</sup>)$ 

C<sub>D</sub> = drag coefficient (-)

 $I_s = peak incident specific impulse (FT/L<sup>2</sup>).$ 

Mean masses of fragments have been obtained entirely from statistical fitting to mass data from fragments recovered from planned or accidental explosions. A typical fit is shown in Figure 13, for four tests of bursting pressure spheres.

Once a spectrum of fragment masses, shapes, and initial velocities is known, one can make predictions of ranges and velocities of impact for various initial launch angles using computer solutions to the equations of exterior ballistics. A set of curves for lifting and drag type fragments was generated by running such programs. A typical one for lifting fragments is shown in Figure 14. The initial conditions for this curve are a velocity of 100 m/s and a fragment aspect ratio of 10. For these lifting fragments, maximum range is obtained for a very flat launch angle of 10°. Each curve represents a different mass per unit area of a fragment. Supplementing fragment range calculations by computer program are empirical fits to "missile map" data for propellant explosions, such as Figure 15. Unlike the computer program results, which give impact conditions as well as range, the latter plots give only the maximum and mean ranges for fragments versus explosion yield.

#### EFFECTS OF FRAGMENTS

Effects of impact of the relatively large, slow fragments generated in this class of explosion are poorly known, but some methods for

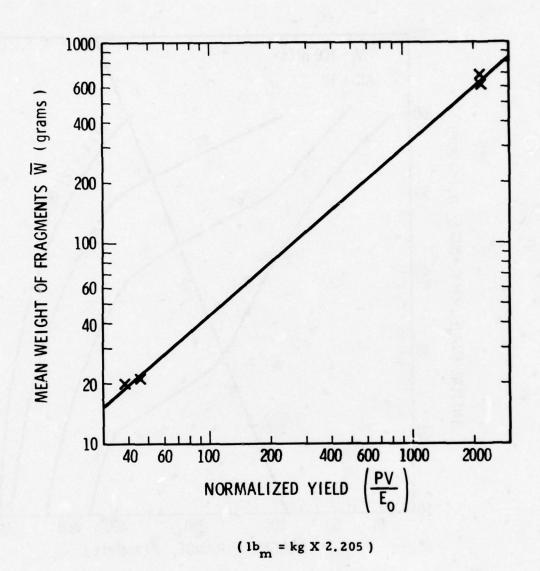


FIGURE 13. NORMALIZED YIELD VS MEAN FRAGMENT MASS FOR BURSTING TANKS.

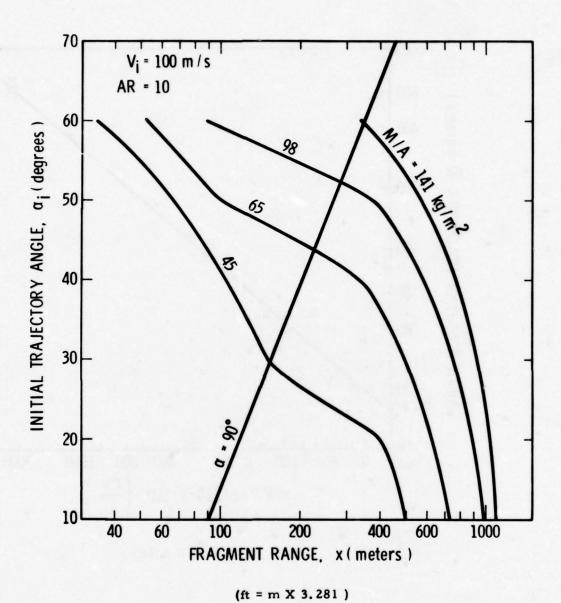


FIGURE 14. DISC FRAGMENT RANGE FOR  $V_i$  = 100 m/s, AR = 10.

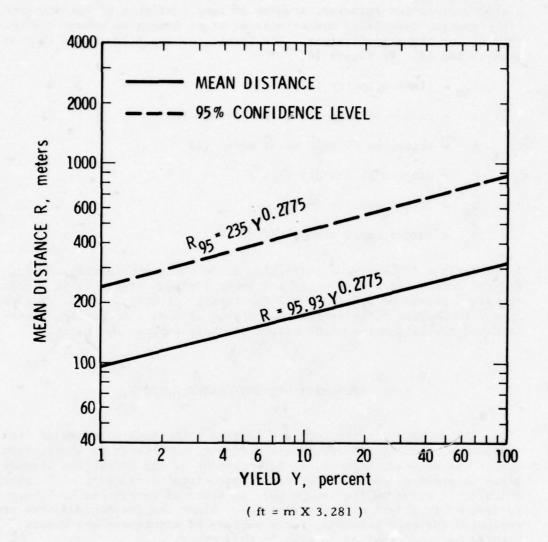


FIGURE 15. FRAGMENT RANGE VS YIELD, PROPELLANT EXPLOSIONS.

predicting these effects are given in Chapter 5 of the workbook. Ballistic perforation formulas, studies of impact effects of hailstones on light roofing materials, and effects of blunt trauma on humans are the sources for these predictions. The former two are illustrated in Figures 16 and 17. In Figure 16,

 $V_{50} = limit velocity (L/T)$ 

a = radius of a spherical projectile (L)

h = thickness of thin sheet metal (L)

 $\rho_{\rm D}$  = projectile density (M/L<sup>3</sup>)

 $\rho_{t} = \text{target density } (M/L^{3})$ 

 $\sigma_{t}$  = target yield stress (F/L<sup>2</sup>)

As in earlier figures, the solid line gives the most probable answer, and the dashed lines give upper and lower limits. Figure 17 is similar, but gives permanent deformation  $\delta$  for impact velocity V < V $_{50}$ . Tables appear in Chapter 5 for estimating effects of impact on roofing materials and for estimating blunt trauma for head impacts on humans.

### RISK ASSESSMENT AND INTEGRATED EFFECTS

The workbook is not intended to give a thorough coverage of risk assessment, but its essentials are discussed in Chapter 6. Most of this chapter is devoted, however, to illustration of the prediction methods given in previous chapters for five hypothetical accidents, or "scenarios" which could occur on the launch pad, in tests of subsystems in laboratories, or in flight of space vehicles. Blast and fragment effects are estimated for each scenario, for a variety of structures and humans. Details are too involved to give in this paper.

#### CONCLUSIONS

It is possible using methods given in the workbook to make reasonable estimates of blast wave characteristics over a wide range of distances from the source of the accident. These characteristics can then be used to predict damage to structures, for a number of types of structures and damage modes, and can also be used to predict various levels

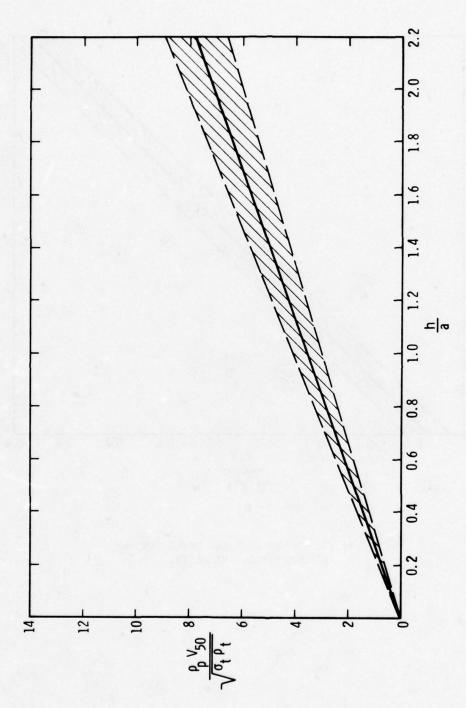


FIGURE 16. NONDIMENSIONAL LIMIT VELOCITY VS NONDIMENSIONAL THICKNESS.

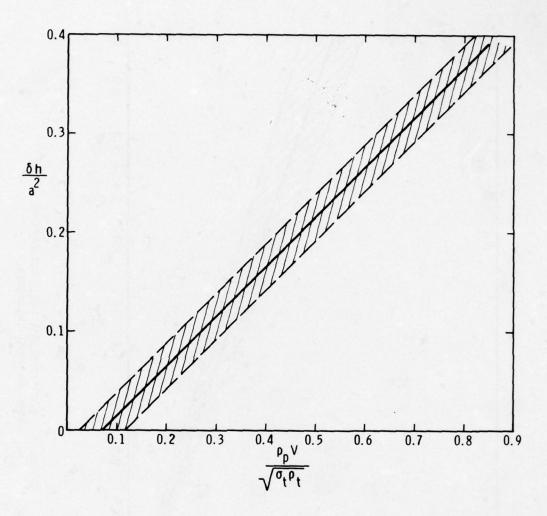


FIGURE 17. NONDIMENSIONAL DEFLECTION VS NONDIMENSIONAL VELOCITY.

of injury to and probability of mortality of humans. Confidence in blast damage and injury prediction is good, given knowledge of the blast wave properties, because of extensive past testing and analysis. The blast damage prediction methods are cast in a format which allows their use for other types of explosions.

Prediction methods are given for estimating initial velocities, ranges, masses, and impact conditions for fragments generated by propellant explosions and gas vessel bursts. The methods for predicting initial velocities are reasonably well founded on theoretical analyses and experimental data, and apply over a wide range of simulated burst conditions. Methods for predicting fragment ranges and impact conditions have a good theoretical basis and can be used for other predictions involving flight through the air of high-velocity objects. Such predictions can be made for objects launched over a very wide range of initial Mach numbers. Methods for predicting fragment mass and shape distributions are entirely based on statistical fits to quite limited data, and therefore involve considerable uncertainty, as well as being impossible to accurately extrapolate.

Some predictions can be made of fragment impact effects on structures and structural elements from graphs and equations given in the workbook. These effects are much less well known than are blast effects, so only limited predictions are possible. Some effects of fragment impact on humans can also be predicted, but these predictions are limited by security restrictions on wounding potential of fragments. Throughout the workbook, limitations such as this are noted when they are known.

This workbook is hopefully presented in a manner which allows easy use by typical safety engineers. For readers who are interested in the detail behind the relatively simple equations or graphs used to make predictions, a number of detailed appendices are included in appropriate chapters. We believe that the workbook is the first to provide safety engineers with relatively simple estimates of blast and fragment hazards for accidental explosions in liquid-propellant fueled flight vehicles.

As noted before, some parts of the workbook have wider potential applications than explosive hazard prediction for liquid-fueled rockets. The sections on fragment trajectory prediction, or the associated computer programs, can be used to predict ranges and impact conditions for many types of fragments or objects thrown into the air. The sections on blast effects apply for blast loads from any source. The methods for estimating fragment impact damage, though limited, are independent of the sources of these fragments or impacting objects.

#### REFERENCES

- Baker, W. E., J. J. Kulesz, R. E. Ricker, R. L. Bessey, P. S. Westine, V. B. Parr, and G. A. Oldham, "Workbook for Predicting Pressure Wave and Fragment Effects of Exploding Propellant Tanks and Gas Storage Vessels," NASA CR-134906, NASA Lewis Research Center, Cleveland, Ohio, November 1975.
- Baker, Wilfred E., <u>Explosions in Air</u>, University of Texas Press, Austin, Texas, May 1973.
- Kingery, C. N., and B. F. Pannill, "Peak Overpressure vs Scaled Distance for TNT Surface Burst (Hemispherical Charges)," BRL Memo Report No. 1518, Aberdeen Proving Ground, Maryland, April 1964. AD 443-102.
- 4. Strehlow, Roger A., and Wilfred E. Baker, "The Characterization and Evaluation of Accidental Explosions," NASA-CR 134779, NASA Grant NSG3008, June 1975.
- Gurney, R. W., "The Initial Velocities of Fragments from Bombs, Shells, and Grenades," BRL Report 405, Aberdeen Proving Ground, Maryland, 1943.
- Henry, I. G., "The Gurney Formula and Related Approximations for the High-Explosive Deployment of Fragments," Hughes Aircraft Company, Report No. PUB-189, Culver City, California, April 1967.
- 7. Custard, G. H., and G. R. Thayer, "Evaluation of Explosive Storage Safety Criteria," Falcon Research and Development Company, Contract DAHC04-69-C-0095, March 1970.
- 8. White, Clayton S., Robert V. Jones, Edward G. Damon, E. Royce Fletcher, and Donald R. Richmond, "The Biodynamics of Airblast," Technical Report to Defense Nuclear Agency, DNA 2738T, Lovelace Foundation for Medical Education and Research, July 1971. AD 734-208.
- Baker, W. E., V. B. Parr, R. L. Bessey, and P. A. Cox, "Assembly and Analysis of Fragmentation Data for Liquid Propellant Vessels," NASA CR-134538, NASA Lewis Research Center, Cleveland, Ohio, January 1974.
- 10. Willoughby, A. B., C. Wilton, and J. Mansfield, "Liquid Propellant Explosion Hazards. Final Report Dec. 1968. Vol. III Prediction Methods," AFRPL-TR-68-92, URS 652-35, URS Research Company, Burlingame, California.

- Jensen, Andreas V. (ed.), "Chemical Rocket/Propellant Hazards, Vol. I, General Safety Engineering Design Criteria," Chemical Propulsion Information Agency, CPIA Publication No. 194, Vol. 1, October 1971.
- 12. Willoughby, A. B., C. Wilton, and J. Mansfield, "Liquid Propellant Explosive Hazards, Final Report Dec. 1968. Vol. I Technical Documentary Report," AFRPL-TR-68-92, URS-652-35, URS Research Company, Burlingame, California.
- 13. Farber, E. A., F. W. Klement, and C. F. Bonzon, "Prediction of Explosive Yield and Other Characteristics of Liquid Propellant Rocket Explosions," Final Report, Contract No. NAS 10-1255, University of Florida, Gainesville, Florida, October 31, 1968.
- 14. Ricker, Randall Edward, "Blast Waves from Bursting Pressurized Spheres," Department of Aeronautical and Astronautical Engineering, Master of Science Thesis, University of Illinois at Urbana-Champaign, May 1975.

# Blast and Fragments from Pneumatic Pressure Vessel Rupture to 345 MPa

by

## J. F. Pittman

Naval Surface Weapons Center White Oak, Silver Spring, Maryland 20910

# 1. Introduction

Vessels containing gases at high pressure are commonplace in industrial and research areas. Hazards resulting from accidental rupture must be considered for their safe deployment. The expansion energy from pneumatic pressure vessel rupture may be calculated from formulae based on the isentropic expansion of the fill gas from the pressure at rupture to ambient pressure. Ideal gas behavior is usually assumed. This approach is adequate for most low pressure situations. However, the ideal gas assumption for higher pressure ruptures gives expansion energies that are unrealistically high. Accurate estimates of blast and fragment parameters from high pressure bursts require calculations based on real gas equations of state supported by empirical data. This paper presents the results of an investigation to supply such information.

# The Investigation

Seven spherical steel vessels, each with a volume of 1 ft<sup>3</sup> were pressurized with argon until they burst. The vessels were designed to burst at nominal pressures of 15,000, 30,000, or 50,000 psi. They were made of two hemispheres joined with an equatorial weld. The 50,000 psi vessel is shown in Figure (1). The vessels were machined to final tolerance. The undercut area in Figure (1) was peculiar to that size vessel. Information pertinent to the pressure vessels is shown in Table 1.

The test vessels were placed on a stand with their center 19.2 inches above the ground and burst. Airblast and fragment parameters were measured. Airblast gages were set up along two lines separated by 90°. In addition, a single gage was placed at 135° to either gage line as shown in Figure (2). Breakwire screens were set up around the vessel to record fragment velocities.

For planning purposes, a one-dimensional hydrocode WUNDY (reference (1)) was modified to compute the airblast overpressures about the vessel. A two dimensional hydrocode, TUTTI, (reference (2)) was developed to generalize and expand the data.

## Results

Generally the test vessels burst into two roughly hemispherical sections. In doing so, they opened somewhat like a clam shell. The argon fill gas jetted strongly along a line defined by the vessel's center and the point on the vessel equator where first opening occurred.

In reaction to the argon motion, the two hemispheres of the vessel rocketed off. The bottom half slammed down against the firing block as shown in Figure (3). The top half went upward at an estimated angle of elevation greater than 50°.

The airblast overpressures showed no increase in magnitude that could be attributed to an increase in burst pressure. However, they were strongly influenced by the proximity of the airblast gage line and the direction of argon jetting.

Figure (4) shows the measured airblast overpressure data as a function of ground range from the 30,000 psi bursts. Also shown in the upper right hand corner of Figure (4) is the geometry of the gage lines/argon jets. Note that the highest airblast overpressures were measured on shot 3, gage line 2. (The data are represented by the closed circles.) Note that the lowest airblast overpressures were measured on shot 7 along gage line 1. (These data are represented by the open squares.) In the upper right hand corner of Figure (4), we see that the high airblast overpressures on shot 3, gage line 2, come about because the argon jet and gage line 3 are in close proximity. The shot-7 jet and gage line are widely separated, resulting in very low airblast overpressures along this gage line for shot 7.

Curves were fitted to the data from the other tests (such as in Figure (4)) and replotted in Figures (5), (6), and (7); this time the curves are grouped according to their angular relationship to the argon jet. Thus, the curves in Figure (5) were for conditions where the gage lines were within 33° of the argon jets. Similarly, the data in Figure (6) are for conditions where the jet/gage line angle fell within the range

<sup>(1)</sup> Lehto, D., and Lutsky, M., "One-Dimensional Hydrocode for Nuclear Explosion Calculations," Naval Ordnance Laboratory Report (NOLTR) 62-168, AD 615801, March 1965.

<sup>(2)</sup> Pittman, J., "Blast and Fragments from Superpressure Vessel Rupture," Naval Surface Weapons Center Report (NSWC/WOL/TR), 75-87, 9 February 1976.

of 47° to 71°. Figure (7) shows the curves fitted to the remainder of the data.

Figures (5), (6), and (7) show then, that increasing burst pressure beyond 15,000 psi did not measurably increase the airblast overpressures. The variations in airblast overpressures closer in to the point directly beneath the vessel (ground ranges less than 3 feet) in Figures (5), (6), and (7) were due to vessel breakup geometry. These differences are discussed in reference (2).

The reason that burst pressure increases do not greatly increase expansion energy may be seen in Figure (8). Here the isothermal compression curve and expansion isentropes for real argon have been plotted. These data (references (3) and (4)) are for argon at temperatures around 290°K. Note that the isothermal compression curve becomes quite steep above about 15,000 psi indicating that little work is done in further compression to 50,000 psi.

The expansion energy available from argon equated to TNT energy is shown in Figure (9). Note that for argon at 15,000 psi and 290°K the expansion energy in 1 ft<sup>3</sup> is equal to about 0.82 pounds of TNT. At a 50,000 psi burst pressure, 290°K, the equivalency has increased to about 1.0 pound of TNT.

If the temperature of the compressed gas is elevated, then increasing burst pressure does increase the expansion energy. This increase in energy approaches a maximum when the gas approaches ideal behavior. This occurs for argon at a pressure of 15,000 psi as the temperature approaches 1350°K. Higher gas pressures require increasingly higher temperatures to approach ideal behavior.

The effect of temperature and burst pressure on calculated shockwave overpressures is shown in Figure (10). These results are strictly for a free air explosion with radial flow. In our case, the vessels were placed some 19 inches above the ground so that the flow is no longer one-dimensional. The two-dimensional flow Eulerian hydrocode, TUTTI, was written for

<sup>(3)</sup> Din, F., "Thermodynamic Functions of Gases, Volume 2: Air, Acetylene, Ethylene, Propane, and Argon," Butterworth, London, 1956.

<sup>(4)</sup> Bralinsky, H., and Neel, C., "Tables of Equilibrium Thermodynamic Properties of Argon. Volume III, Constant Entropy," Arnold Engineering Development Center, AEDC 69-19, AD 684532, March 1969.

this case. It is based on the FLIC (Fluid-in-Cell) method of reference (5). FLIC as described in reference (5) is for only one material. TUTTI was written as a two material hydrocode in which the argon and air do not mix. This avoids computational diffusion of the materials into each other at the contact surface.

Figure (11) sums up the airblast overpressure measurements and caluclations. The shaded area represents the measured data. The upper band of the shaded area is an average of the data in Figure (5). The lower band is an average of the data from gage lines displaced furthest from the argon jet as shown in Figure (7).

Also shown in Figure (11) are data from 1-pound TNT spheres fired at the same Height of Burst as were the pressure vessels. (Actually, the data are from 1-pound pentolite spheres scaled to TNT by equating 1-pound of TNT to 1.3 pounds of pentolite.) Note that at distances greater than about 10 feet, the TNT data follows the upper band of the pressure vessel data.

Also shown are the calculated airblast overpressures. Strictly speaking, the one-dimensional hydrocode, WUNDY, is not applicable to our case where the pressure vessel was near the ground surface. To account for the presence of the ground, the WUNDY calculations were treated as follows. For pressures along the ground in the regions of regular reflection (airblast pressures above 40 psi) the airblast pressures were obtained by applying the reflection factors from reference (6) to the free air overpressures. To account for the presence of the ground at airblast pressures below 40 psi, the expansion energy was doubled.

Also shown in Figure (11) are the airblast overpressures calculated from the two-dimensional hydrocode TUTTI. Both hydrocodes yield airblast pressures in the higher range of the measured values since neither account for the kinetic energy of the vessel fragments

<sup>(5)</sup> Gentry, R., et al., "An Eulerian Differencing Method for Unsteady Compressible Flow Problems," Journal of Computer Physics, 1: 87-118, 1960.

<sup>(6)</sup> Porzel, F., "Height of Burst for Atomic Bombs, 1954. Part II. Theory of Surface Effects," Los Alamos Scientific Laboratory Report LA-1665, May 1954.

In the reference (7) workbook, a technique is given for obtaining airblast overpressures from pneumatic pressure vessel rupture. This method was applied for the conditions of the 15,000 psi vessel rupture. The results are compared with the empirical data from Figure (11) in Figure (12). Note that pressures based on this technique compare with the highest values from the measured data.

# 4. Fragments

The vessels designed to burst at 15,000 and 30,000 psi burst into halves at the equatorial weld, Figure (1). The vessel designed to burst at 50,00 psi also burst into two pieces. However, this vessel burst in a plane normal to the weld and slightly off center. Therefore, the two pieces from each of these vessels were of unequal weights. The weights of the recovered vessel fragments are given in Table 2.

Unfortunately, the velocity screens set up to measure fragment velocities did not operate properly. In only one case was a fragment velocity obtained by this technique. However, when the vessels burst, one of the sections usually slammed down against the concrete firing pad. The resulting disturbance in the form of an "N" wave, was picked up by pressure gages mounted in the pad. This gave us the transit time of the vessel segment over the distance between its test position and the point of contact on the pad.

All the fragment velocities are shown in Table 2. The reliability of these measurements is not known. However, they are expected to be maximum velocities.

Calculated values for fragment velocities tend to agree with measured values at lower burst pressures. However, at higher burst pressures calculations tend to over estimate fragment velocities. Table 3 has been prepared to illustrate this point. The measured data from the 15,000 psi burst are from this paper. The other measured data are from reference (8) as are the calculated velocities by Lorenz. The Baker data

- (7) Baker, W., et al., "Work book for Predicting Pressure Wave and Fragment Effects of Exploding Propellant Tanks and Gas Storage Vessels," National Aeronautics and Space Administration Report CR-134906, Prepared by Southwest Research Institute, San Antonio, Texas, November 1975.
- (8) Pittman, J., "Blast and Fragment Hazards from Bursting High Pressure Tanks," Naval Ordnance Laboratory Report (NOLTR) 72-102, 17 May 1972.

are from reference (7). Both the Lorenz and Baker technique calculate about the same fragment velocities for all burst pressures in Table 3. Even the values from the WUNDY calculations by Lehto in reference (2) are not very different. For the 600 - and the 8,000 psi bursts, the calculated and measured values are in reasonable agreement. However, the measured values for the 15,000 psi burst are 50% lower than any of the calculated values. We might attribute this difference to the ideal gas assumptions made in the computational efforts. However, the Lehto calculation used a real gas equation of state.

# 5. Summary

The expansion energy from pneumatic pressure vessel rupture depends on fill gas temperature, ratio of specific heats, pressure, and volume, For a monotomic fill gas and a temperature below about 350°K, increasing burst pressure above about 15,000 psi results in only slight increases in expansion energy. At elevated temperatures, increasing burst pressure does increase expansion energy. For a given pressure and temperature, the limit is reached when the gas approaches ideal behavior. The way in which this temperature and pressure increases airblast overpressures is nonlinear. The airblast overpressure-distance relationship must be computed for each burst pressure/temperature regime.

The blast field from from pressure vessel rupture is strongly influenced by burst geometry. The vessels used in this investigation burst into two pieces creating strong argon motion along a line defined by the vessel's center and the point on the vessel where first rupture occurred. Airblast overpressures measured along the line of this jet were more than a factor of 4 greater than those measured in the opposite direction.

The two-dimensional hydrocode, TUTTI, was developed to give airblast parameters near the vessel and in non-ideal situations, i.e., when the burst occurs near a boundary. In uncomplicated situations at distances greater than 5 or 6 vessel radii, the one-dimensional hydrocode, WUNDY, may be used to arrive at airblast parameters.

The vessel wall fragments observed in this investigation weighed from 50 to 271 pounds. These attained velocities up to 350 feet/second. For many situations, the fragment hazard dominates in safe siting procedures.

## References

- Lehto, D., and Lutzsky, M., "One-Dimensional Hydrocode for Nuclear Explosion Calculations," Naval Ordnance Laboratory Report (NOLTR) 62-168, AD 615801, March 1965.
- Pittman, J., "Blast and Fragments from Superpressure Vessel Rupture," Naval Surface Weapons Center Report (NSWC/WOL/TR) 75-87, 9 February 1976.
- Din, F., "Thermodynamic Functions of Gases, Volume 2: Air, Acetylene, Ethylene, Propane, and Argon," Butterworth, London, 1956.
- Bralinsky, H., and Neel, C., "Tables of Equilibrium Thermodynamic Properties of Argon, Volume III. Constant Entropy," Arnold Engineering Development Center, AEDC 69-19, AD 684532, March 1969.
- Gentry, R., et al., "An Eulerian Differencing Method for Unsteady Compressible Flow Problems," <u>Journal of Computer</u> Physics, 1: 87-118, 1960.
- Porzel, F., "Height of Burst for Atomic Bombs, 1954.
   Part II. Theory of Surface Effects," Los Alamos Scientific Laboratory Report LA 1665, May 1954.
- 7. Baker, W., et al., "Workbook for Predicting Pressure Wave and Fragment Effects of Exploding Propellant Tanks and Gas Storage Vessels," National Aeronautics and Space Administration Report CR-134906, Prepared by Southwest Research Institute, San Antonio, Texas, November 1975.
- 8. Pittman, J., "Blast and Fragment Hazards from Bursting High Pressure Tanks," Naval Ordnance Laboratory Report (NOLTR) 72-102, 17 May 1972.

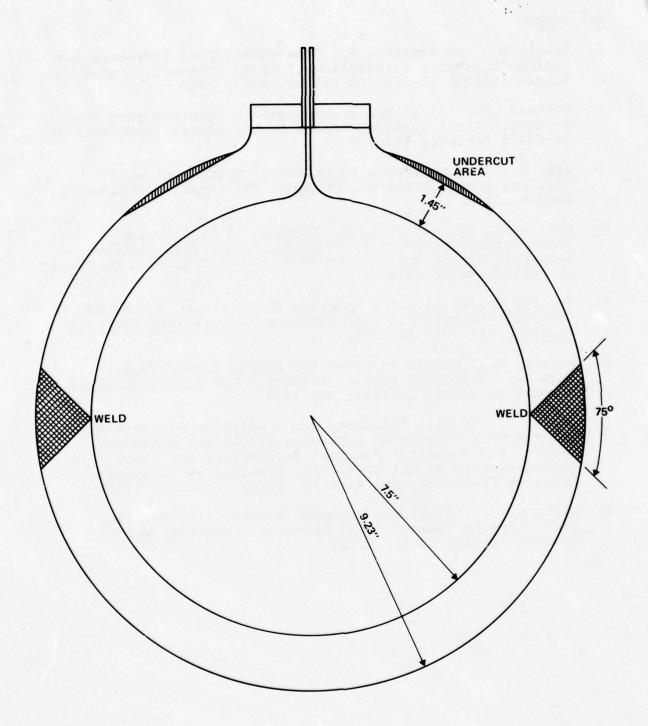


FIG. 1 50,000-PSI TEST VESSEL

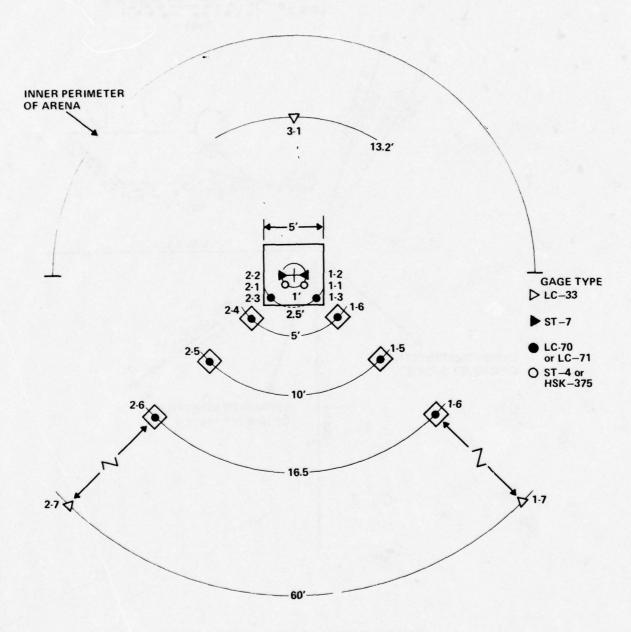


FIG. 2 FIELD LAYOUT FOR UNCONFINED TESTS

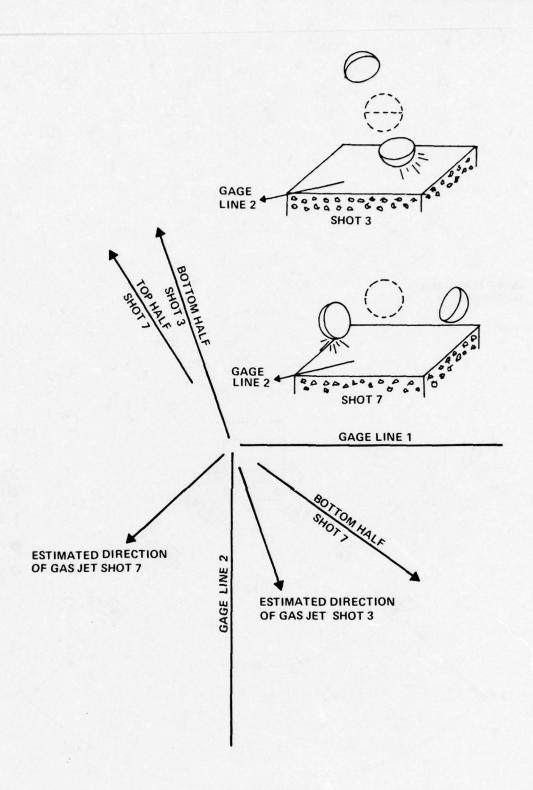


FIG. 3 VESSEL RUPTURE GEOMETRY OF SHOT 3 AND SHOT 7; 30,000-PSI. 1212

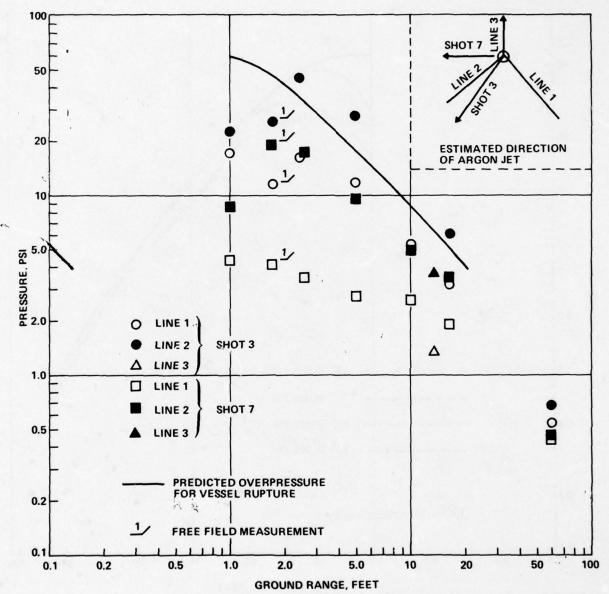


FIG. 4 AIRBLAST OVERPRESSURE FROM 30,000 - PSI VESSEL RUPTURE

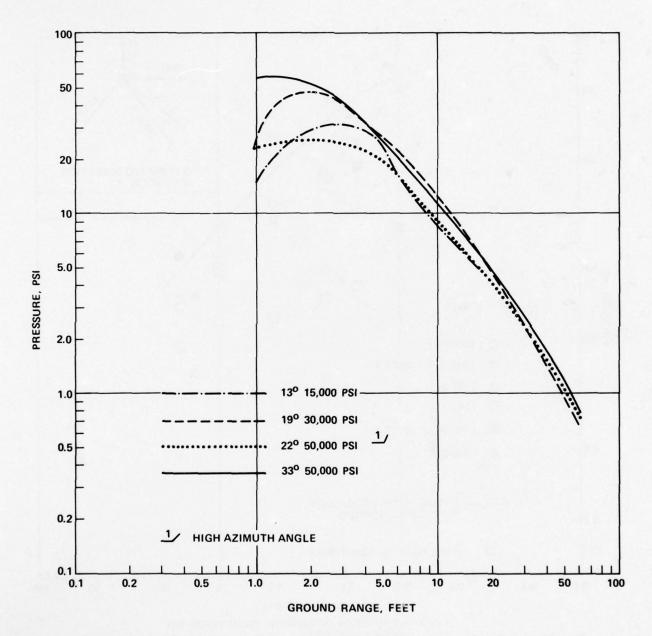


FIG. 5 OVERPRESSURE ALONG GAGE LINES ORIENTED WITHIN 33° OF THE ARGON JET

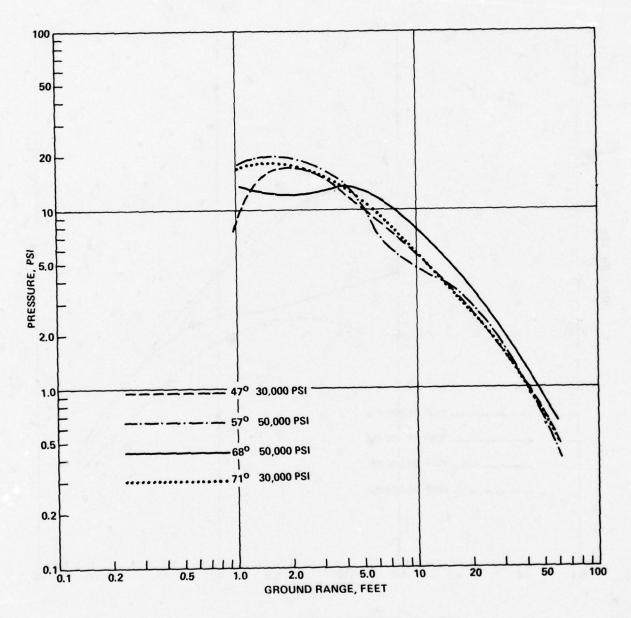


FIG. 6 OVERPRESSURE ALONG GAGE LINES ORIENTED WITHIN 470 to 710 OF THE ARGON JET.

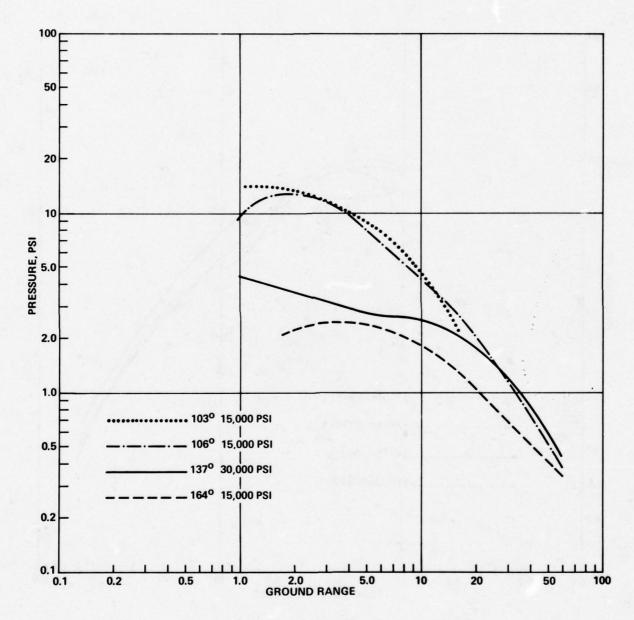


FIG. 7 OVERPRESSURE ALONG GAGE LINES ORIENTED WITHIN 103° TO 164° OF THE ARGON JET.

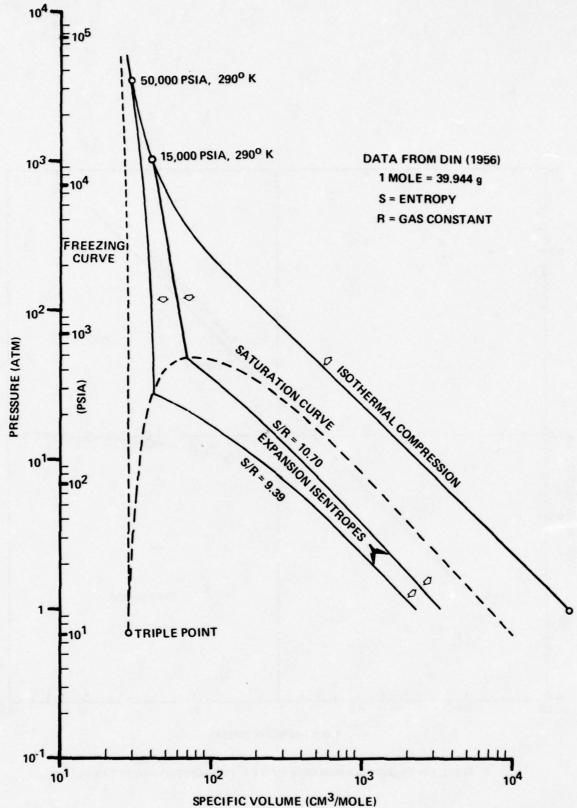


FIG.  $\epsilon$  ARGON P - V COMPRESSION AND EXPANSION PATHS FOR COLD TANKS 1217

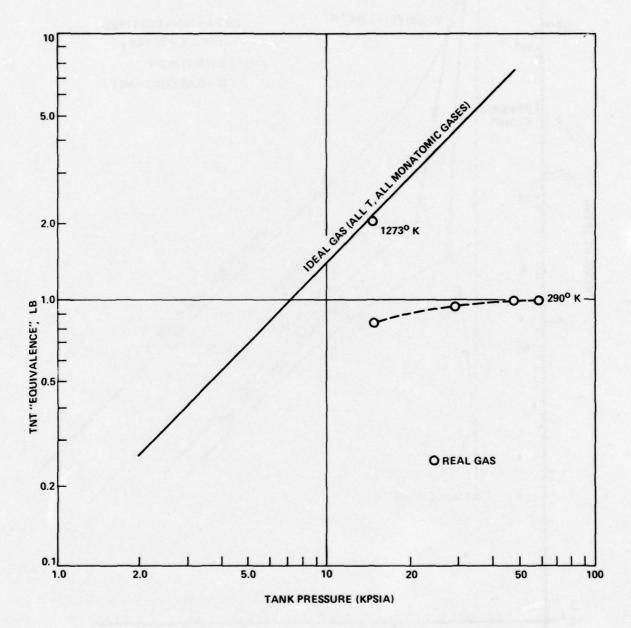


FIG. 9 THT ENERGY EQUIVALENCE OF 1 FT<sup>3</sup> PRESSURIZED ARGON TANKS.

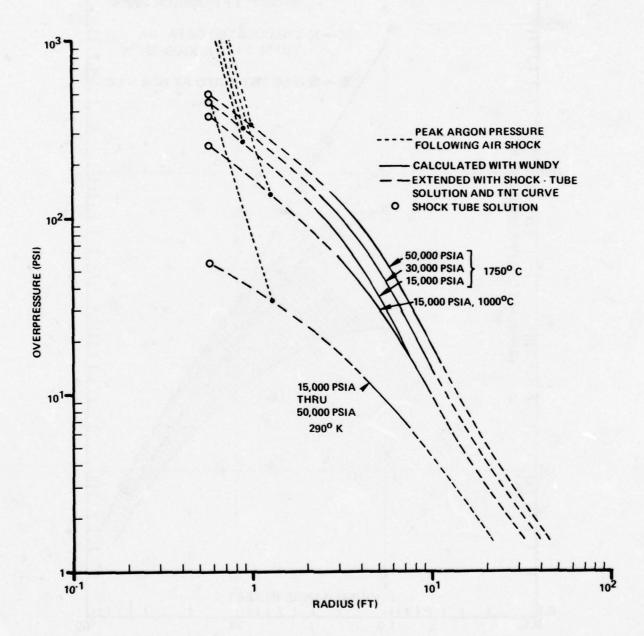


FIG. 10 PEAK FREE - AIR SHOCK OVERPRESSURE VS DISTANCE FOR 1 FT<sup>3</sup> ARGON TANKS

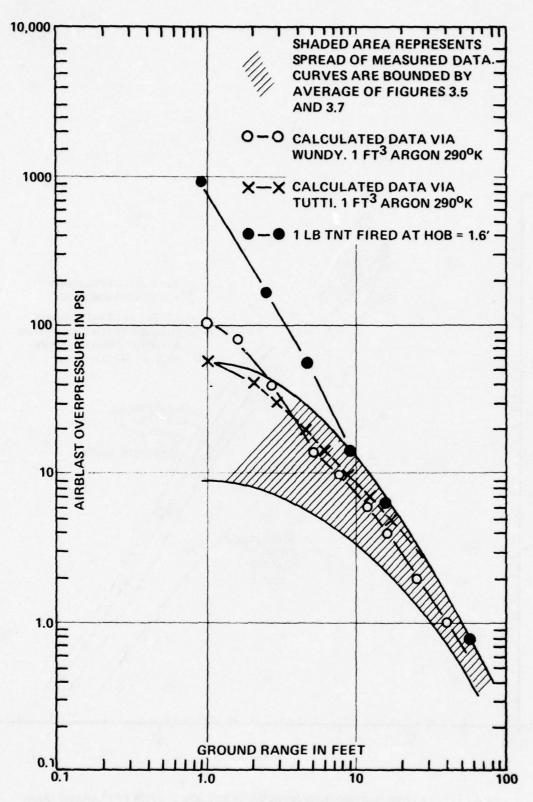


FIG. 11 COMPARISON OF DATA

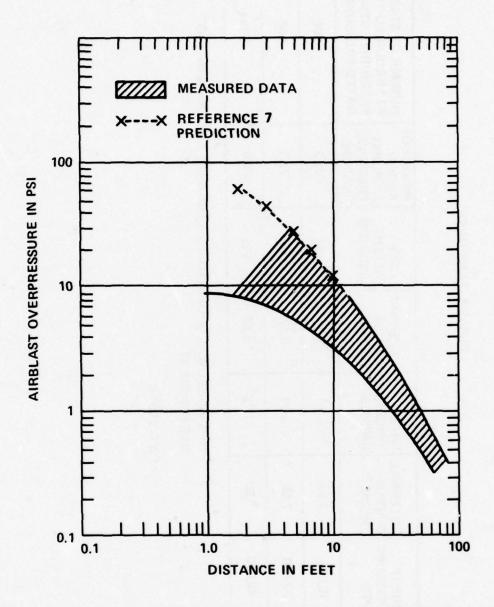


FIG. 12 COMPARISON OF HANDBOOK PREDICTIONS AND MEASURED DATA

TABLE 1 TANK DATA

	T		
NUMBER OF STANDARD FT <sup>3</sup> REQUIRED TO PRESSURIZE VESSEL TO RATED PRESSURE**	260	700	780
WEIGHT OF ARGON AT BURST PRESSURE (POUNDS)	62.2	77.5	86.6
TANK WEIGHT (POUNDS)	102	~240	413
EXTERNAL TANK RADIUS WEIGH (POUN	7.98	8.49	9.23
SHELL EXTERN THICKNESS RADIUS (INCHES)	0.48	0.99	1.73*
INTERNAL SHELL RADIUS THICKN (INCHES)	7.50	7.50	7.50
BURST PRESSURE (PSI)	15,000	30,000	20,000

\*THIS VESSEL WAS UNDERCUT TO A MINIMUM THICKNESS OF 1.45" (SEE FIGURE 1)

\*\* AT 290° K

**TABLE 2 FRAGMENT DATA** 

DESIGN BURST PRESSURE	VESSEL PORTION	FRAGMENT WEIGHT	FRAGMENT VELOCITY
15,000 PSI	воттом	52.4 POUNDS	315 FT/SEC
15,000 PSI	воттом	52.7 POUNDS	323 FT/SEC
30,000 PSI	воттом	147.5 POUNDS	353 FT/SEC
30,000 PSI	воттом	108.0 POUNDS	270 FT/SEC
50,000 PSI LARGE PORTION		258.0 POUNDS	215 FT/SEC
50,000 PSI LARGE PORTION		271.0 POUNDS	270 FT/SEC <sup>(1)</sup>

<sup>(1)</sup> VELOCITY MEASURED WITH BREAKWIRE

# TABLE 3 INITIAL VESSEL WALL VELOCITY

BURST PRESSURE	WALL THICKNESS	MEASURED (PITTMAN)	VELOCITY CALCULATED (LORENZ)	CALCULATED (BAKER)	
600 PSI	0.020 INCHES	1200 FT/SEC	1000 FT/SEC	1100 FT/SEC	
8,000 PSI	0.375 INCHES	1400 FT/SEC	1100 FT/SEC	1056 FT/SEC	
15,000 PSI	0.500 INCHES	320 FT/SEC	600 FT/SEC (675) <sup>(1)</sup>	725 FT/SEC	

(1) VALUE FROM LEHTO'S WUNDY CALCULATION

## Secondary Fragment Speed With Unconfined Explosives:

## Model and Validation

John H. Kineke, Jr. Ballistic Research Laboratory Aberdeen Proving Ground, MD 21005

#### INTRODUCTION

The accidental detonation of masses of explosive can produce serious fragment hazards, in addition to the blast and air shock environment. In order to contain fragments it is necessary to know their penetrating capability, and hence their speed. While the speed of fragments from most munitions is usually well characterized, that of potential secondary fragments common to munitions plants is not. To fill this gap the Army, thru the Suppressive Shielding Applied Technology Program, has been supporting an effort to provide a predictive capability for secondary fragment speed.

Fragments which are launched as a result of detonations can be classed as either primary or secondary. Primary fragments have as their source, material, usually metal, which is in intimate contact with the explosive. Such material might be the casing of an explosive-filled artillery, the body of a press used for compaction of powdered explosive, or the walls of a kettle used for melting explosive.

Secondary fragments are other objects, again usually metal, which while not in contact with the explosive, are sufficiently proximate to it so that they could experience substantial acceleration given an accidental detonation. A secondary fragment scenario is shown in Figure 1. An M-1 105 mm artillery shell is cradled on a pallet for the purpose of fuze insertion. The shell, already loaded with several kilograms of Composition B, is rotated by means of neoprene rubber wheels, as the fuze is inserted from the left. Various steel shafts, representing potential secondary fragments are labeled. The drive roller shaft (C) can be used to illustrate three principal features of secondary fragment problems. The shaft can experience acceleration from explosive products impinging upon it. An additional acceleration is also felt because of the impact of the expanding metal case, or fragments therefrom, on the shaft. (Of course, the presence of the case can also mitigate the acceleration due to blast). Finally, the shaft is a member of a structural complex, which can consume some or all of the delivered impulse. For instance, the drive roller shaft, to become a potentially hazardous secondary fragment.

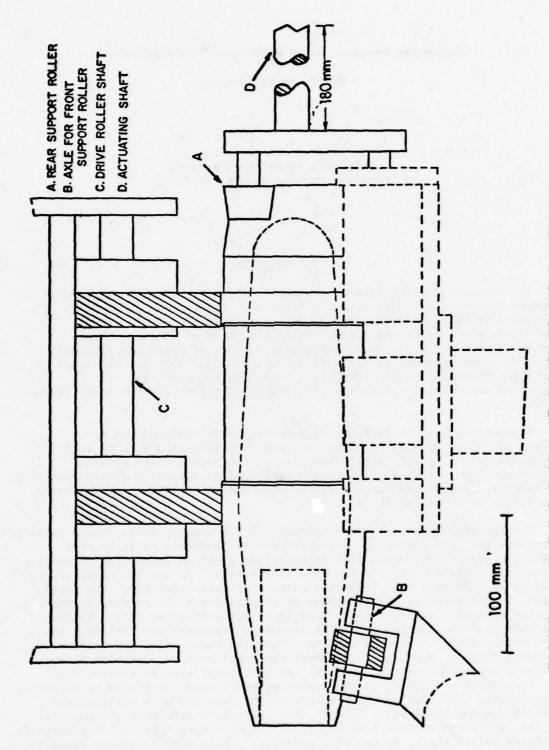


FIGURE 1. AN EXAMPLE OF A SECONDARY FRAGMENT SCENARIO

must fracture at or near the two natural stress concentrators represented by the roller housings. Thus, energy will be consumed in deformation and fracture of the fragment, in addition to remote deformation of other parts of the structure.

From whatever source, primary or secondary, fragments represent potential penetration threats and thus their characteristics must be defined. This paper describes the investigation of the first listed influence on secondary fragment speed: the acceleration derived from explosive products or blast. On-going programs, soon to be reported are concerned with modeling the influences of metal cases and constraints on secondary fragment acceleration.

### THEORETICAL CONSIDERATIONS

This paper is concerned with satisfying the need for a predictive tool for calculating secondary fragment speed in the environment of an explosive detonation. The fragment is located relatively closely to the explosive charge, typically at distances of 1.25 to ten times the charge radius from the geometric center or axis of the charge. Thus it experiences the influence of the explosive products, which impinge upon it and are diffracted around it, in addition to an envelope of shocked air. Only at locations outside the fireball would impetus to the fragment be provided solely by shocked air. Thus the physical processes in the region of concern are complicated and rapidly changing, having not been subjected to the leavening of distance.

In order to calculate secondary fragment speed from first principles it is necessary to know in detail the pressure history experienced by the secondary fragment as it undergoes acceleration. In that case Newton's second law could be integrated to calculate fragment speed and trajectory. the pressure history to which a secondary fragment is subjected depends on its original position with respect to the explosive charge, certainly; however, it also depends on the histroy of the motion of the fragment itself, since the acceleration process is not instantaneous. Thus a mapping of the free field pressure in position and time is required, in addition to a modeling of the diffraction of the field around the secondary fragment. Obviously, a calculational tool based on the first principle approach would require numerical solution on a large computer, even if the requisite pressure field information were available.

A key facet of the program is the requirement that the predictive tool developed be tractable. Thus the treatment of the physics of the processes occurring should not be so detailed that simple analytic expressions cannot be written. The implications of this requirement, then, is that a model of the process be constructed. Modeling frequently implies simplification of processes such that they might be treated with gross statements, perhaps balances, of some physical parameters, such as mass, force, momentum or energy. Implicit in this approach, then, is the existence of empirical parameters which must be determined in order to put the model to use. The same empiricism is actually also present, when describing a process such as secondary fragment acceleration from first principles. In that situation, the empiricism is contained in the free field pressure data, which must itself be measured, or be derived from an experimental equation of state for the explosive products.

In the present circumstances, the variety of potential models which might be considered devolve to two: energy and momentum. In either case, a unique dependence of secondary fragment speed on its original distance from the explosive charge is sort. Adopting Hopkinson scaling for the quantity of explosive, a momentum model can be stated as:

$$\frac{M_{sa}V_{s}}{R_{e}} = f(R/R_{e})$$
 (1)

and an energy model as:

$$\frac{M_{sa}V_{s}^{2}}{2R_{e}} = g (R/R_{e})$$
 (2)

where  $M_{sa}$  = mass per unit presented area of a plane surface secondary fragment, measured in  $kg/m^2$ 

vs = secondary fragment speed after acceleration is complete, in m/s

R<sub>e</sub> = radius of a spherical explosive charge, measured in m, and proportional to the cube root of charge weight

R = distance of the secondary fragment from the geometric center
 of the charge, measured in m

Thus, from a momentum point of view, the secondary fragment speed should be a unique function of scaled distance and inversely proportional to the fragment specific mass. On the other hand, from a specific energy point of view, the secondary fragment speed should be a unique function of scaled distance and inversely proportional to the square root of the fragment specific mass.

The experiments and results presented in this paper serve to delineate between these models and provide a predictive tool relating secondary fragment speed to its mass per unit area  $\rm M_{sa}$ , its standoff distance R, and a measure of the explosive mass, specifically the charge radius  $\rm R_e$ . It will be evident that these three are the principal determining factors for secondary fragment speed.

Several other factors, while anticipated to have lesser significance, might be considered to be influential, in an unconstrained secondary fragment scenario, in determining fragment speed. These include the type of explosive charge and its shape, the area of the fragment itself and the fragment geometry.

Experimental results are presented relating to the influence of charge type, and shape for cylindrical charges. Cylindrical charges exhibit two distinguishing features from spherical charges in accelerating secondary fragments. The divergence of the expanding detonation products in a radial direction is two dimensional, while for a sphere it is three dimensional. In addition, for progressively greater length to diameter ratio ( $F_e$ ) charges, explosive more remote from the fragment can participate to a lesser extent in the acceleration. An analytic treatment of charge shape has been suggested by Westine of Southwest Research Institute (1) and will be compared to experimental results subsequent to this paper.

Deviations of fragment geometry from a plane surface exhibited toward the explosive product field have been treated with an approximate geometric analysis. Consider a fragment presenting a cylindrical surface to the flow, which will be supposed to be approximately plane in the vicinity of the fragment. Only the component of the flow normal to the fragment surface will be operative on the fragment. In turn, only the component of the fragment acceleration parallel to the flow will be non-cancelling. Integrating over the hemicylinder presented by the fragment to the flow yields an expression for effective presented fragment area A<sub>s</sub> (eff):

$$A_{s} (eff) = g_{s} A_{s}$$
 (3)

 $^{1}\mathrm{P.}$  S. Westine, Southwest Research Institute, private communication.

where A = secondary fragment presented area to the explosive product field

g = secondary fragment shape factor

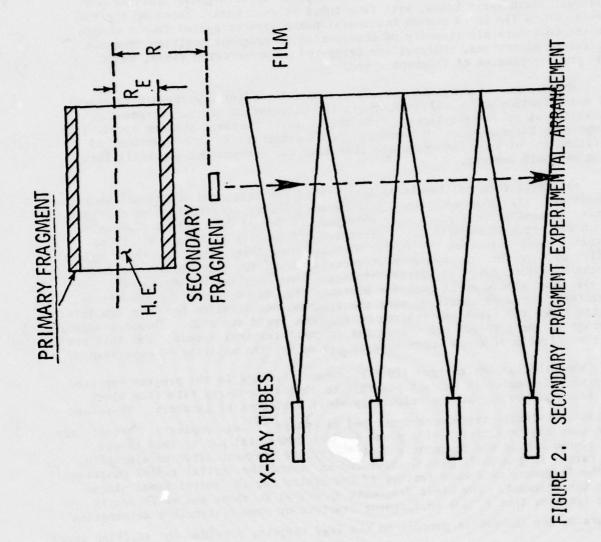
- = 1 for an exhibited plane surface with the axis of a cylindrical cross-section fragment parallel to the flow and denoted as ||\_r
- =  $\pi/4$  for an exhibited cylindrical surface with the axis of the fragment perpendicular to the flow and denoted as  $L_r$ .
- = 2/3 for a spherical fragment.

Obviously such an analysis is simplistic, neglecting the finite lateral extent of the fragment in a diverging flow and ignoring the details of the flow diffraction around the fragment. Nevertheless it will be shown in the subsequent section to be reasonably adequate.

#### EXPERIMENTAL CONSIDERATIONS

Experimental observations of secondary fragment speed were accomplished, with either of two techniques: flash radiography and a passive velocity transducer. Alternative techniques, such as high speed cine-photography or electronic timing with either make or break screens, are not useful for various reasons. Since it was desired to measure fragment maximum speed after acceleration is complete it was necessary to make observations fairly close to the explosive charge, usually within one to two meters. At these distances the necessity for an inverse drag calculation is obviated; however, at these distances the fragment is enveloped in the cloud of opaque detonation products. Thus the use of optical wavelengths is precluded. Again, at these short distances the functioning of electronic screens is generally unreliable, since the fragment is preceded in its trajectory by detonation products.

The sequential flash radiographic arrangement is illustrated in Figure 2. The explosive charge is emplaced directly above an aperture in a 180 mm thick armor blast shield (not shown). The fragment to be accelerated is placed at a distance R, measured from the geometric center or axis of the explosive charge. The fragment is supported by a thin sheet of expanded polystyrene generally one to three mm thick, just sufficiently thick to support the fragment's weight. Auxiliary tests have indicated no influence of the supporting sheet on the fragment terminal speed.



Subsequent to detonation the fragment is accelerated in a downward direction, passing thru the aperture in the blast shield and in front of, and approximately parallel to, a pair of orthogonal vertical arrays of shielded flash X-ray film. The film is exposed by orthogonal banks of 300 kilovolt flash X-ray tubes, with four tubes in each bank. Tubes at a given level, which lie in a common horizontal plane, are triggered from a common pulser to assure simultaneity of observation of fragment position from two different directions. Pulsers are triggered at preselected times, based on prior estimates of fragment speed.

Measurement of fragment shadows on the film, after appropriate treatment of magnification and parallax, permits the calculation of true fragment positions at successive times. From these, level to level average speeds are computed. Uncertainties in measured speeds attributable to measurement of position and of time intervals are less than one percent and generally less than one half percent.

When more than two levels of X-ray tubes are triggered additional average speeds are calculable and thus a measure of fragment acceleration or deceleration during the measurement process is obtained. A set of data from a quadruple flash radiographic experiment is presented graphically in Figure 3. In no instance where more than two levels of tubes were triggered did average speeds differ by more than the measurement uncertainty of the particular experiment. At the same time drag calculations indicate that no discernible fragment deceleration should occur over the distances traversed during the experiment. Therefore it can be concluded that the fragment acceleration had been completed by the times the first observation of fragment speed was made. Thus the measured average fragment speeds are indeed the fragment terminal speeds. For this reason only two levels of X-ray tubes were triggered for the majority of experiments.

When the largest charges (20.8 kilograms) treated in the program reported here were detonated it was not possible to shield the X-ray film from blast and shock adequately at the relatively short distances of interest. Therefore a passive velocity transducer described elsewhere  $\ensuremath{^{(2)}}$  was employed. Briefly the technique consists simply of a plane surface commercial purity lead target positioned behind the fragment and struck by the fragment after acceleration. The target is generally placed about 200 mm beyond the initial radial position of the fragment. A second feature of the system are the restrictions placed upon the fragment. For steel fragments spherical in shape and sufficiently hard (greater than R  $_{\rm C}$  30) no fragment fracture or even discernible deformation occurs during the impact process on the lead targets, provided the striking speed

<sup>&</sup>lt;sup>2</sup>J. H. Kineke, Jr., "A Passive Speed Transducer for Measurement of Fragment Speed," BRL Memorandum Report (in preparation).

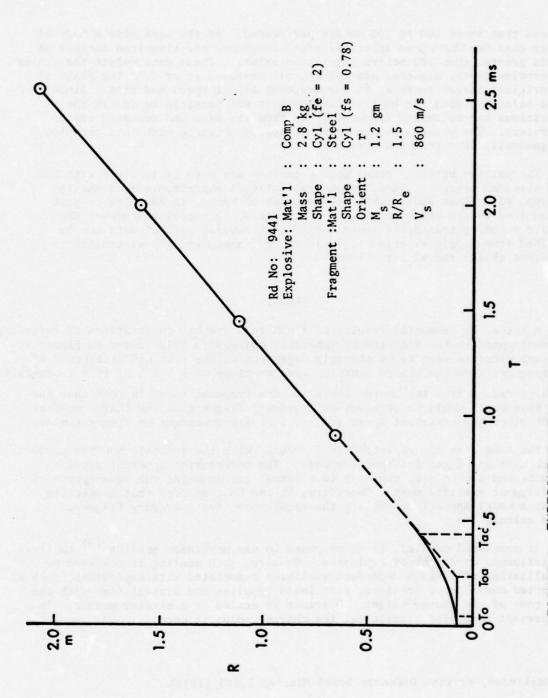


FIGURE 3 EXPERIMENT MEASUREMENTS OF SECONDARY FRAGMENT TRAJECTORY

is less than about 600 to 700 meters per second. At the same time a body of crater data for these same spherical ster' fragments striking lead targets at speeds greater than 100 meters per second exists. These data relate the crater penetration depth, diameter and volume, all measured at or from the plane of the original target surface, to the fragment impact speed and mass. Since these selective data are highly correlated it was possible to invert the regressions and calculate fragment speed from its mass and measured crater parameters. The uncertainty in fragment speeds obtained with this technique are generally less than ten percent.

The passive velocity transducer technique was used exclusively with the 20.8 kilogram charges. In addition, validational experiments with smaller charges, with flash radiographic observation of speed, in addition to post mortem lead target measurements, were conducted. A useful feature of the passive velocity transducer technique is that several sets of data can be obtained from single experiment, by locating fragment-target assemblies in different charge radial directions.

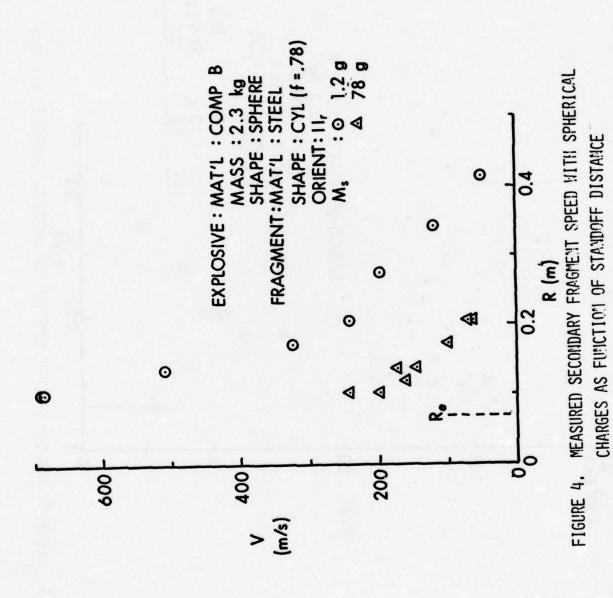
#### RESULTS

A set of experimental results of flash radiographic observations of secondary fragment speed in the vicinity of spherical charges is illustrated in Figure 4. Fragment speed is seen to be strongly dependent on the standoff distance R of the fragment from the charge center. Even as close as R = 1.5 R $_{\rm e}$  (i.e., one-half a charge radius from the charge surface), the fragment speed is less than one-half that which would be acquired by a primary fragment on the charge surface. On the other hand fragment speed is less strongly dependent on fragment mass.

The same data are replotted in Figure 5, with the ordinate now the product of fragment speed and its specific mass. The correlation apparent appears adequate and is, indeed, superior to a normalization using the square, root of the fragment specific mass. Therefore, it can be concluded that a specific momentum model appears to satisfy the requirement for secondary fragment speed calculation.

As mentioned earlier, it is proposed to use Hopkinson scaling (3) to treat the influence of weight of explosive. Usually, such scaling is achieved by normalization of various dependent variables associated with explosions, such as reflected and side-on pressure, associated impulses and arrival time with the cube root of the charge weight. Distance is scaled in a similar manner. In the present case, for simplicity, the charge radius is used.

<sup>&</sup>lt;sup>3</sup>B. Hopkinson, British Ordnance Board Minutes 13565 (1915).



SECONDARY FRAGMENT SPECIFIC MOMENTUM FOR SPHERICAL CHARGES VS DISTANCE FIGURE 5.

The experimental results of Figure 5 are shown normalized by charge radius in Figure 6. In addition, data acquired from the detonation of 20.8 kilogram spheres are also plotted. Since data acquired with both cylindrical and spherical fragments are included, the fragment specific masses are also normalized by the shape factor  $\mathbf{g}_{\mathbf{s}}$ . The correlation between data from charges differing in mass by almost an order of magnitude is apparent. Therefore it can be concluded that Hopkinson scaling meets the requirement for charge scaling.

It will be noted that the product  $M_{sa}$   $V_{s}$ , the specific acquired momentum of a secondary fragment, is dimensionally identical to a specific impulse. Since specific reflected impulse  $I_{r}$  is available in the literature, <sup>(4)</sup> a comparison of it with the experimental data is shown. Note that fragment speeds predicted from  $I_{r}$  would be as much as 100% greater than the experimental data. Thus, while  $I_{r}$  could be used to calculate conservative upper bounds for secondary fragment speed, an undue penalty would be imposed on any proposed fragment-containing structure.

The dichotomy between specific reflected impulse and specific acquired fragment momentum can be attributed to the different character of the experiments involved. In the former case impulse is obtained from integration of pressure histories recorded by Eulerian guages, i.e., guages which remain fixed during the measurement process. In the latter case the fragments can be thought of as impulse guages, but mixed, Eulerian-Lagrangean guages, in that they are free to move, but do so at continually changing rates with respect to the flow. In addition, diffraction of the flow around unconstrained fragments is unimpeded by lateral confinement. Finally, the fragment data are illustrated for distances quite close to the explosive charge. For Composition B, a scaled distance

 $R/R_e = 2$  for instance, is equivalent to  $Z(=R/W^{1/3})$  of 0.26 ft/lbs. <sup>1/3</sup>. Thus reported reflected impulses at these distances are undoubtedly extrapolations.

<sup>&</sup>lt;sup>4</sup>Structures to Resist the Effects of Accidental Explosions, TM 5-1300, June 1969.

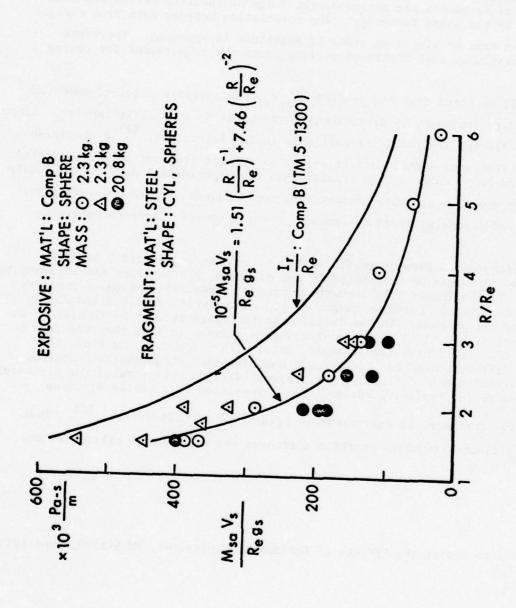


FIGURE 6. SECONDARY FRAGMENT MOMENTUM SCALED WITH SPHERICAL CHARGE RADIUS AS FUNCTION OF SCALED DISTANCE.

A tentative regression on the spherical charge data is shown in Figure 6. While it is of the form of a power series in the reciprocal of scaled distance, it differs from that suggested by Baker (5) for reflected impulse. He showed that reflected impulse should be the sum of two terms in the reciprocal of scaled distance: the square and the square root, with the latter insignificant close to the charge where the mass of engulfed air is negligible. The specific acquired momentum, on the other hand, appears to require, in addition to the square term, a first power term.

The three parameters discussed thus far, scaled distance  $R/R_{\rm e}$ , secondary fragment specific mass  $M_{\rm Sa}$ , and charge radius  $R_{\rm e}$ , are the dominant features in determining secondary fragment speed. The lesser influences on secondary fragment speed have been examined experimentally by limited excursions. Such a set of data illustrating the influence of type of explosive is shown in Table I. At two selected scaled distances, three explosives, Composition B, 50/50 Pentolite, and an aluminized explosive H-6, were used. For each case the explosive was a 2.8 kg cylinder. The data indicate that at least over the range of distances examined, differences between the three explosives are within the limits of experimental replicability.

The effect of shape of cylindrical charges on secondary fragment speed is shown in Table II. All charges were identical in mass, but with length to diameter ratios of 2 and 4.67. When compared, not at equal distances, but at equal scaled distances in charge radii, individual values of specific acquired momentum consistently are within 15% of mean values. Thus data for one fineness ratio cylinder can be used to predict secondary fragment speed for other cylinders.

In Table III, the result of varying both the mass and fineness of cylinders simultaneously is examined. The charges were identical in radius  $\mathbf{R}_{\mathbf{e}}$ , but their lengths varied by a factor of two. A modicum of agreement is achieved by scaling the specific acquired momentum with the radius of an equivalent sphere, but obviously additional analysis will be required on this issue, as on the issue of relating cylindrical charges to spherical charges.

It might be expected that secondary fragment area would play a dominant role. Table IV shows results for fragments whose areas varied by a factor of 64. Reasonable agreement in  $_{sa}^{N}$  v is observed for these fragments, which both subtend relatively small fractions of the explosive. This issue is not closed and data for larger fragment areas is being incorporated in the final report on this program (6).

<sup>5</sup>W. E. Baker, "Prediction and Scaling of Reflected Impulse from Strong Blast Waves," Int. J. Mech. Sci., Vol. 9, pp 45-51, 1967.

<sup>6</sup>J. H. Kineke, Jr., "Secondary Fragment Speed with Unconfined Explosives: Model and Validation," BRL Report (in preparation).

R/R <sub>E</sub>	EXPLOSIVE	MsA	٧s	MsaVs
7 E.		KG/M <sup>2</sup>	M/S	PA-s
1.5	COMP B	38.1	1134	$45.2 \times 10^3$
1.5	COMP B	49.3	92.7	45.7
1.5	PENTOLITE	49.1	789	38.7
1.5	H-6	9.84	938	45.6
9	COMP B	38.3	253	9.7
9	COMP B	49.3	207	10.2
9	PENTOLITE	49.1	201	6.6
9	H-6	49.5	205	10.1

TABLE I EFFECT OF TYPE OF EXPLOSIVE

M <sub>SA</sub> V <sub>S</sub> PA-S	35.4 × 10 <sup>3</sup>	39.1	31.7	16.7	15.3	14.8	8,5	6.5
V <sub>S</sub> M/s	924	252	814	龙巾	86	388	223	170
M <sub>SA</sub> KG/M <sup>2</sup>	88.3	155.0	39.0	38.4	155.8	38.2	38.3	38.0
r <sub>n</sub>	2 5	2	4.67	2	2	4.67	2	4.67
S, E	.051	.051	.038	.051	,051	.038	.051	.038
R/R <sub>E</sub>	1.5	1.5	1.5	3	2	3	9	9

EXPLOSIVE: 2.77 kg COMPOSITION B FRAGMENT ORIENTATION: LR

TABLE II EFFECT OF SHAPE OF CYLINDRICAL CHARGES

M <sub>SA</sub> V <sub>S</sub> /R <sub>E</sub> (EFF) PA-S/M	649 x 10 <sup>3</sup>	589	623	335	393	81	132	139
V <sub>S</sub>	1000	1134	92.7	126	186	123	253	207
MsA KG/M <sup>2</sup>	37.7	38.1	49.3	155.1	154.9	38.3	38.3	49.3
T.	ι	2	2	1	2	1	2	7
R <sub>E</sub> (EFF)	.058	.073	.073	850	.073	850'	.073	.073
M <sub>E</sub> KG	1.38	2.77	2.77	1.38	2.77	1.38	2.77	2.77
R/RE	1.5	1.5	1.5	3	3	9	9	9

R<sub>E</sub> = .051M

TABLE III EFFECT OF SHAPE AND MASS OF CYLINDRICAL CHARGES

	As mm <sup>2</sup>	M <sub>SA</sub> KG/M <sup>2</sup>	V <sub>S</sub> M/S	M <sub>SA</sub> V <sub>S</sub> PA-S
1.5	507	49.3	92.7	45.7 × 10 <sup>3</sup>
1.5	ᅜ	38.1	1134	43.2
9	507	49.3	207	10.2
9	쩐	38.3	253	9.7

TABLE IV. EFFECT OF SECONDARY FRAGMENT AREA

The influence of secondary fragment shape and orientation is shown in Table V. The validity of the proposed shape factor  $\mathbf{g}_{\mathbf{S}}$  for treating spherical and cylindrical fragments (in two orientations) is substantiated by the agreement of normalized specific acquired momentum.

A body of data for cylindrical charges is summarized in Figure 7. Data for different masses and shapes of Com, sition B cylinders, with various specific masses and orientations of fragments, are plotted. As yet, no regression analysis has been performed with the entire range of experimental conditions, which extend out to scaled distances of ten charge radii.

#### SUMMARY

It might have been desireable to conclude this paper by pointing out a single equation which would permit the calculation of secondary fragment speed for all of the variety of situations and conditions described. This is not possible until additional analysis is completed.

The status of the original list of influences on secondary fragment speed can be summarized. A specific momentum model has been shown to be appropriate for predicting speed. The specific acquired momentum varies as a two term power series in scaled distance, and should be scaled with the effective radius of the charge. Essentially no relevance of fragment presented area, per se, nor of type of explosive, has been indicated. Finally a potential treatment of charge shape is being developed.

	2			
M <sub>SA</sub> V <sub>S</sub> /G <sub>S</sub> PA-S	28.7 × 10 <sup>3</sup> 30.7	19.7 21.2 19.4	9.1	9.7
M <sub>SA</sub> V <sub>S</sub> PA-S	19.1 × 10 <sup>3</sup> 24.1	13.1 16.7 15.3	6.1 6.5	9.7
V <sub>S</sub> M/s	5 <i>7</i> 3 62 <i>7</i>	39.2 4.34 9.8	182	253
MsA KG/M <sup>2</sup>	33.4 38.5	33.4 38.4 155.8	33.5 38.3	38.3 49.3
s <sub>9</sub>	2/3 <sup>-7</sup> 4	2/3 "A "A	2/3 <sup></sup> /4	7
ORIENT	L.	_ L R L R	' T	== R R
SHAPE	SPHERE CYL	SPHERE CYL C'YL	SPHERE	נגר
R/R <sub>E</sub>	2 2	w w w	9	9 9

TABLE V EFFECT OF SECONDARY FRAGMENT SHAPE AND ORIENTATION EXPLOSIVE = 2.77 kg COMPOSITION B

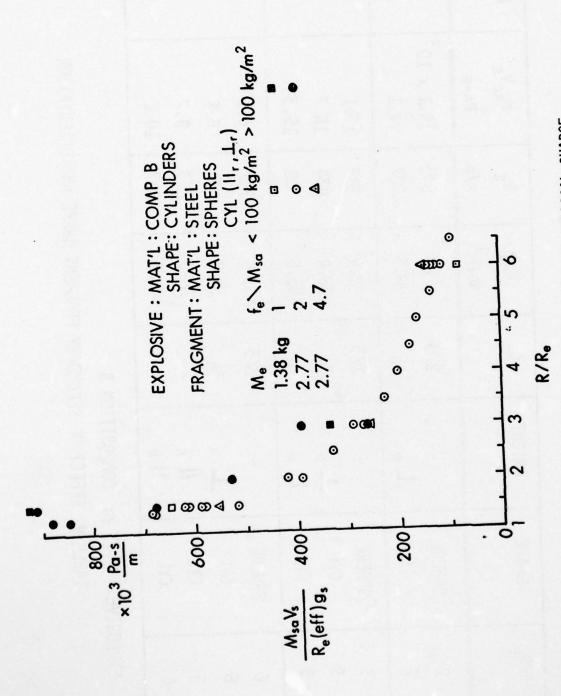


FIGURE 7 SECONDARY FRAGMENT MOMENTUM SCALED NITH CYLINDRICAL CHARGE RADIUS AS FUNCTION OF SCALED DISTANCE

# DESIGN OF LIGHTWEIGHT SHIELDS AGAINST BLAST AND FRAGMENTS Francis B. Porzel Naval Surface Weapons Center White Oak, Silver Spring, Maryland

#### INTRODUCTION

History. Much of the work on shields reported here was done for a current NAVY program concerning safety criteria in handling explosive warheads. These shielding ideas and techniques originated in extensive work done two decades ago for the Atomic Energy Commission on the containment of nuclear reactors against internal explosion (UNP 434)\*. About ten of the early full-scale power reactors built in the United States (UNP 1892 for example), and the nuclear-powered merchant ship SAVANNAH (UNP 1023) all contain porous material "blast shields" which are ancestors to the "porous-friable" shield I will describe today.

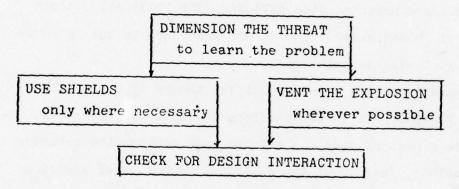
The software is mostly from the unified theory of explosions (UTE) (NOLTR 72-209). This theory offers a simple comprehensive way to include a host of physical effects that control the behavior of real explosions, instead of the classical technique of ignoring them by idealization. The use of UTE as a tool for predicting damage was discussed at the 1974 DDESB Explosive Safety Seminar (DDESB 74).

What is lightweight? To contain any explosion is itself straightforward design: just pile on enough steel, concrete or sandbags to smother it by brute strength and brawn. Do that, and a bomb calorimeter weighs about a thousand times the weight of explosive — and they occasionally fail. A suppressive shield, we found, can weigh up to fifty times the explosive, which is OK for fixed installations. But for explosives handling operations, one wants something light enough to be carried by some vehicle, such as a truck, and yet does not become an abundant source of secondary

<sup>\*</sup>References are cited by corporate document number and listed at at the end of the paper. 1247

fragments if it should fail. A nominal 2 1/2 ton truck can carry 10,000 pounds (on good roads), and a typical truck load of warheads has about 1000 pounds net explosive weight. So by "lightweight" we mean, in round numbers, a shield that weighs less than ten times the explosive.

Minimal shield concept. It is emphasized that we do not seek complete containment (but shun it in fact). Instead, we seek only to reduce the threat to some reasonable, acceptable hazard specified in terms of overpressure, fragment energy and numbers. Here are the main ideas:



The body of this paper follows the same format.

Typical shield. Figure 1 shows what we have in mind. We can think of it as a wall of sand or water placed between the warhead and whatever we wish to protect. For some warheads, a steel plate may do as well as the sand wall, but could be a disastrous source of secondary fragments if inadequately designed.

## BLAST AND FRAGMENT CALCULATIONS

To dimension the threat, or even to design a meaningful test, a sequence of simple and comprehensive methods for predicting hazards is required:

- 1. Blast -- far field and as input loading UTEDAM to warhead case and shield
- 2. Fragment Size Distribution -- as case N=N<sub>o</sub>e<sup>-L/L</sup>1
  and shield breakup
- 3. Fragment Trajectories -- with variable NEXTRJ air drag
- 4. Fragment Energy and Numbers -- on the target, FEN506 from warhead, shield and truck FET506

The methods we used are simple enough for hand calculation or pocket computers, but the codes shown take the drudgery and mistakes out of it. I will not try to discuss the theory. But it is of general interest to note briefly why these particular methods were developed or used.

Blast. For far-out effects, around 1 psi, all blast theories predict about the same pressure-distance curve. But for so close-in effects as loading on the warhead case and the shield, only the unified theory of explosions (UTE) (NOLTR 72-209) appears to predict total head and reflected pressures at all, or which are in reasonable agreement with measurements (see Figure 5 and DDESB 74).

There are large differences for close-in effects between UTE and other theories and here is why I think UTE is more realistic. UTE is the only theory I know which treats the explosive debris as smoke and other solid particles which jet through and mix in the surrounding air. All hydrocodes inherently model the shock and debris as laminar zones, concentric shells, which cannot mix. Moreover, they describe the shocked air and explosive debris almost entirely as transparent gasses: N2, O2, CO, CO2, H2O (as steam). Their boundary is a "contact discontinuity", a spherical shell, which ought not appear in a photograph. Figure 2

shows what a real TNT explosion looks like. Here we see mountains of particulate debris, evidently hundreds of times more dense than air. This is the kind of stuff that breaks up the warhead and shield. I think the photograph speaks eloquently in favor of the UTE model over all other models for chemical explosions.

<u>Fragment Size Distribution</u>. From first principles and with a few easy, general assumptions, one can derive a friendly old analytic expression for fragment size distribution:\*

$$N(>L) = N_O e^{-L/Ll}$$

where

N(>L) = number of fragments larger than L

No = total number of fragments (L = 0)

L<sub>1</sub> = a characteristic fragment size, expected to be about 1/2 the case thickness

L = fragment size (mean) = (mass/density)<sup>1/3</sup>

As is well known, if log N is plotted versus L, the points should fall on a straight line, whose slope and intercept give the parameters  $L_1$  and  $N_0$ . This relation was tried and found successful on aerial bombs. Figure 3 is another example, shows how the equation correlates torpedo fragments collected on the ground 500 to 1000 feet from the explosion. Figure 4 is even more interesting as it shows the distribution of fragments from the truck the

<sup>\*</sup>Note that this expression is similar to, but is more specific than the Mott distribution or other published equations (NASA CR 134538, APGBRL R468, APGBRL R522, NOLTR 73-83).

torpedoes were on. As H. Bethe once remarked, "If this is not the correct theory, it is still an excellent way to correlate the data".

Fragment Trajectories. This is almost a do-it-yourself problem nowadays. You don't even need a machine -- a pocket calculator will do. Table 1 gives the recipe for calculating the trajectory path length as a closed analytic function of the angle of flight.

A main advantage is the large number of cases one can thereby afford to calculate. Figure 6 shows the range as a function of initial angle of elevation for almost any combination of drag coefficient, initial velocity, and fragment size. One finding: while the maximum range does occur at angles less than 45°, the curve is flat, so the range for high speed or small particles is nearly independent of initial angle; they all go the same distance. It greatly simplifies the subsequent analysis.

Of course many trajectory calculations exist. But for various reasons, none of the available solutions were adequate for our needs -- too complex, too much machine time, errors in formulation, incomplete description, etc.

Fragment Energy and Numbers (FEN charts). All the previous calculations are summarized in Table 2 and "FEN chart". Figure 7 shows a case of typical fragments assuming two warheads totalling 1500 pounds of explosive and 1000 pounds case, .36 cm thick. The x-axis gives the fragment energy E in foot-pounds. The y-axis gives the number of fragments/1000 ft<sup>2</sup> whose energy is E or greater. In the upper right is a box; the left edge is an example using

58 foot-pounds as an energy criterion. Every point to the left of the box would be an acceptable hazard because its energy is less than the criterion. The bottom line of the box is an example using 1.67 frags/1000 ft<sup>2</sup> areal density criterion. Every point below the box would be an acceptable hazard because the fragments are fewer than the areal density criterion. Every point within the box would be unacceptable, exceeding both criteria.

One family of curves, running downhill to the right, give loci for fragments at fixed distances from the explosion. Reading the curve R = 600, we find that 600 feet is almost "safe" because the curve just misses the corner of the box; 630 feet would be acceptable. The other family of curves, running uphill to the right, give loci for fixed fragment sizes and masses. The most critical fragment size is seen to lie closest to the corner, is between .9 cm and 1 cm, with a mass between 6.5 and 8.9 grams. Interpolation gives the critical mass as 7 grams. Smaller fragments would be more numerous (reading up and to the left) but are likely to be too weak to exceed the assumed energy criterion. Larger fragments are more energetic (reading down and to the right) but are likely to be too few to exceed the areal density criterion.

Figure 8 is a similar FEN chart for hypothetical truck fragments. We cannot calculate the truck fragments a priori but can construct the chart by assuming an initial fragment velocity, (400 f/s) and an areal density N = 4, at 500 feet for 1 cm fragments. A similar interpolation shows that 630 feet would be a "safe"

distance and the critical size truck fragment be about 56 grams, or about 860 grains.

#### VENTING AND DECOUPLING

Venting and decoupling are both blast phenomena and are powerful means to reduce fragment energy because it is blast pressure that initially drives the fragments. By far the fastest and best way to reduce blast pressure is to dump the energy into large volumes of air. For both phenomena, their significane lies, not in the mechanism as such, but the enormous quantitative difference they make. They change the loading by factors of a thousand.

Venting or "channeling" (UNP434) refers to an overwhelming tendency for shocks to propagate into rarified and compressible media like air instead of dense, incompressible media like most solids. The energy partition at an interface may be estimated by recalling that the rate of work W of a shock per unit area and time is the product of its pressure P and material velocity u; like a piston at pressure P advancing with velocity u.

## $\dot{W} = P u$

As shown in UNP434 and elsewhere, a rate of work in air usually is a thousand times greater than in most solids. That is why nearly all the blast energy can be reflected from a dense shield or from the ground in a 2W theory. That is why a few percent venting area can quickly carry off most of the blast energy in a suppressive shield. Furthermore for a minimum shield most of the area seen by the shock is air, only a small fraction seen is the shield; all the more reason why energy will be deflected upward -- vented -- into air.

Decoupling is closely related to venting, and a means of lowering fragment energy. It is illustrated in Figure 9. If a shock is passing through the wall, the rate of change of the momentum of the material can be shown to be simply the difference between P(0), the pressure on the left side of the wall and  $P_0$ , the ambient pressure on the right side of the wall. The rate of change is independent of the shape of the pressure pulse within the wall. No matter what pulse shape, the momentum acquired by the wall is given by the integral

$$M = \int [P(0) - P_0] dt$$

This is why we shun complete containment like the plague. If the explosion were confined within a box, then the wall is everywhere impelled by a high internal blast pressure P(0). Whereas, if the shield is open to ambient air, the internal blast is quickly reduced to ambient pressure  $P_0$  and the wall is no longer accelerated outward.

#### SHIELD DESIGN

Waste Heat Concept. Where you cannot vent, the next most powerful way to reduce blast energy is to convert it to heat and dump it into a large reservoir of inert mass -- like sand. Figure 10 is a conventional thermodynamic pressure-volume diagram for solids and liquids and shows how the trick can be done using porous absorbers. When any material is shocked from ambient pressure  $P_o$  to some shock pressure  $P_s$ , it compresses effectively along the straight line shown. The internal energy delivered to the material is exactly represented by the area under the line. When the

material expands behind the shock adiabatically, it does so along the lower curved path. Following UTE (NOLTR 72-209, UNP434) the energy it gives back is the area under the curve, even if the material expands back to its initial volume. The lens-shaped area between the expansion curve and the straight compression line is the waste heat Q; it appears as wasted heat in the finally expanded debris. An elastic material is compressed and expands nearly along the same straight line, nearly all the energy acquired is given back, and Q is small. In a porous material like sand, virtually all the internal energy of the shock is wasted as the shock traverses it. That is the trick in using porous, crushable materials. We note that in both cases, the kinetic energy is the triangle above the straight line; it is the same for both materials and is available to drive the shock ahead.

Drag, In Shield and In Air. Drag forces play analagous roles in two places: 1) in slowing the warhead fragments within the sand shield and 2) in slowing the sand fragments in the surrounding air. The warhead fragments could travel hundreds and thousands of feet in air, but are slowed in sand a thousand times more rapidly than in air because sand is a thousand times more dense. After travelling ten times or so their own length, they will have transferred most of their energy to the sand. When the sand grains are ejected in air, they require ten thousand times or so their own length to effectively transfer their energy to air. But how much is that? For large grains, say .1 inch, 10,000 x .1 = 1000 inches = 83 feet. Actually, the sand travels most of the way thereafter by a free ride on the blast wave, which is about 200 feet for 1000 lbs explosive.

The same drag equation applies to both cases, well enough:

$$\mathbf{v} = \mathbf{v_i} \exp \left[ -\frac{\mathbf{c_d} \mathbf{D_o} \mathbf{X}}{2 \mathbf{D_1} \mathbf{L}} \right]$$

where

V = terminal velocity of the fragment

 $V_4$  = initial velocity of the fragment

Cd = drag coefficient (always of the order 1)

D = density of the traversed medium

D = density of the fragment

X = distance traversed

L = fragment length in the direction of travel

Shield Mass and Stand-Off. As just noted, the warhead fragments are quickly slowed in the shield and soon brought into velocity equilibrium with it. Beyond that, the addition of mass to the shield will further decrease fragment velocity, because it dilutes, so to speak, the incoming momentum or energy. Assume the mass of debris and fragments within a given angular sector is "m" before the shield, and the mass of shield in the sector is M. Then, aside from details -- confined or vented explosion, whether conserving momentum or energy -- the incoming energy or momentum will always be reduced, by a factor involving

$$\frac{m}{m+M} = \frac{1}{1+M/m} < 1$$

Stand-off refers to the distance between the center of the explosion and the shield. Figure 11 is perhaps sufficient to show that increasing the stand-off is equivalent to increasing the

the shield thickness, for the same area shield. At first glance we are inclined to feel we have swindled ourselves into believing in something for nothing. But we see from the figure that the more distant shield really subtends a smaller solid angle and correspondingly less momentum. Hence the equivalent thickness goes as the square of the stand-off. That is a powerful argument for stand-off and a good time to recall that this bonus from stand-off applies only to vented explosions.

Minimum Shield Thickness and Stand-Off. The end result of most of the previous analyses for hazards and shield design appears in Figure 12. Using the same example as the FEN chart, Figure 7, (1500 lbs HE, 1000 lbs case) it shows the acceptable hazard distance as a function of shield thickness and stand-off. The FEN chart showed that 650 feet is an acceptable distance with no shield at all; that is shown for T = 0. We read here, for a 20 inch shield and 30 inch stand-off, that 480 feet would be acceptable. However, by increasing the stand-off to 48 inches, the shield could be reduced to 12 inches and prove "safe" at 480 feet.

Loose sand weighing 100 lbs/ft<sup>3</sup> was assumed for these calculations. For packed sand, the shield could be thinner but the weight remains the same. If a 4' x 6' shield were used, say to prevent a vehicle cab, motor and hood from becoming secondary fragments, it would weigh about 200 pounds per inch thickness of shield. The thickest shields shown, about 20", weigh about 4000 pounds, plus a few hundred pounds for the wooden structure to contain it. This is portable, well within the criteria set for a "lightweight shield" at the outset of the paper -- less than ten times the NEW or 10,000 lbs.

#### SUMMARY

This report offers:

- 1. A simple, comprehensive methodology for calculating blast and fragment hazards from explosive munitions of all kinds and at all distances. Because it starts from first principles, it will be especially useful where no data or conflicting data exist, for safety test planning, and as a reassurance for evaluating safety problems that is independent of test measurements.
- 2. A concept and methods of minimal, balanced and selective shielding whereby the shielding effort can be placed where it does the most good.
- 3. A practical design for a portable shield that can easily be constructed from readily available and literally "dirt-cheap" materials.

#### REFERENCES

APG BRL R468 "Computing Effect of Distance on Damage by Fragments" L. H. Thomas, Aberdeen Proving Ground, Ballistics Research Laboratory Report No. 468, May 1944

APG BRL R522 "On Determining Parameters for a Theoretical Formula To best Fit an Observed Fragment Distribution by the The Method of Maximum Likelihood", L. H. Thomas, Ballistics Research Laboratory Report No. 552, June 1945

DDESB 74 "Damage Potential from Real Explosives: Total Head and Prompt Energy", F. B. Porzel, 16th DDESB Safety Seminar. September 1976

MASA CR 134538 "Assembly and Analysis of Fragmentation Data for Liquid Propellant Vehicles", W. D. Baker, R. L. Bussey, V. B. Paar, P. A. Cox, Southwest Research Institute, January 1971 for National Aeronautic and Space Administration.

NOLTR 72-209, "Introduction to a Unified Theory of Explosions", F. B. Porzel, Naval Ordnance Laboratory, September 1972

NJLTR 73-83 "Fragment Weight Distribution from Naturally Fragmenting Cylinders Loaded with Various Explosives", H. M. Sternberg, Naval Ordnance Laboratory, October 1973

UNP434 Porzel, F. B. "Some Hydrodynamic Problems of Reactor Containment", Volume 11, Second UN Conference on Peaceful Uses of Atomic Energy, Geneva, 1958, UN Paper 434

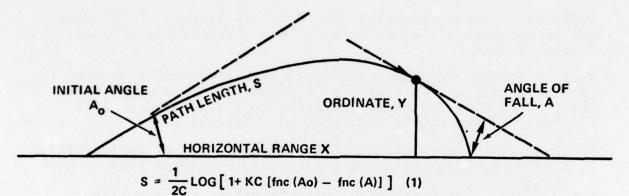
UNP1023 Godwin, Worf "Safety of Nuclear Merchant Ships", Volume 11, Second UN Conference on Peaceful Uses of Atomic Energy, Geneva, 1958, UN Paper 1023

UNP1892 Monson, Sluyter "Containment fo EBR-II", Volume 11, Second UN Conference on Peaceful Uses of Atomic Energy, Geneva 1958, UN Paper 1892



#### TABLE 1

# NOMENCLATURE AND DERIVED EQUATIONS FOR V2 DRAG



WHERE

C = DRAG DECAY CONSTANT

= 1/2·DRAG COEFFICIENT · AIR DENSITY 1
FRAG DENSITY FRAG LENGTH

K = "TRAJECTORY LENGTH" = 1/2 MAXIMUM RANGE IN VACUUM

 $= \frac{\text{Vo}^2 \text{ COS}^2 \text{ Ao}}{\text{g}} = \frac{[\text{INITIAL VELOCITY} \cdot \text{COS} (\text{INIT. ANGLE})]^2}{\text{GRAVITY}}$ 

fnc (
$$\triangle$$
) =  $\frac{\text{TAN A}}{\text{COS A}}$  + LOG TAN  $\left[45^{\circ} + \frac{\text{A}}{2}\right]$ 

THEN

VELOCITY V = Vo [ COS Ao COS A ] e-CS

dx = dS-COS A

dy = dS-SIN A

dt = dS/V

Do S IN INCREMENTS S2-S1 FOR VARIABLE DRAG COEFFICIENT Cd (v)

# FRAGMENT AREAL DENSITY AND TERMINAL ENERGY NOMENCLATURE AND EQUATIONS

Cd = DRAG COEFFICIENT

Do = AIR DENSITY

D1 = FRAGMENT DENSITY

K; = INITIAL KINETIC ENERGY OF FRAG

K = TERMINAL KINETIC ENERGY OF FRAG

L = FRAGMENT DIMENSION

L<sub>1</sub> = TYPICAL FRAGMENT DIMENSION

M = FRAGMENTING CASE MASS

N(>L) = CUMULATIVE FRAGS LARGER THAN L

No = TOTAL NUMBER OF FRAGS

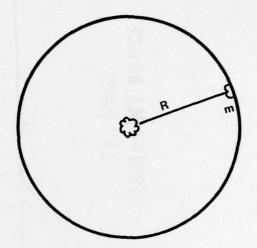
Q = WASTE HEAT OF FRAGMENTATION

V: = INITIAL FRAGMENT VELOCITY

V = TERMINAL FRAGMENT VELOCITY

W = WEIGHT OF EXPLOSIVE

Yo = AVAILABLE ENERGY OF EXPLOSIVE



m = FRAGMENT MASS R = TARGET RANGE

FRAGMENT SIZE AND MASS

$$L = \left(\frac{m}{D1}\right)^{1/3} \qquad m = D_1 L^3$$

**TOTAL NUMBER OF FRAGMENTS** 

$$No = \frac{M}{6D_1 L^3} = \frac{M}{6m}$$

SIZE DISTRIBUTION FUNCTION

AREAL DENSITY OF FRAGMENTS

$$\frac{N(>L)}{AREA} = -\frac{N(>L)}{4\Pi R^2}$$

INITIAL KINETIC ENERGY OF FRAGS

$$Ki = 1/2 \quad \frac{m \quad Yo}{W+M} \quad \left(1 - \frac{Q}{Yo}\right)$$

TERMINAL KINETIC ENERGY OF FRAGS

$$K = K_i e^{-C_D} \frac{D_0 R}{D_1 L}$$

TERMINAL VELOCITY

$$V = Vie - \frac{C_D}{2} - \frac{D_0}{D_1} \frac{R}{L}$$

$$K = 1/2 \text{ mV}^2$$
,  $V = \sqrt{\frac{2K}{m}}$ 

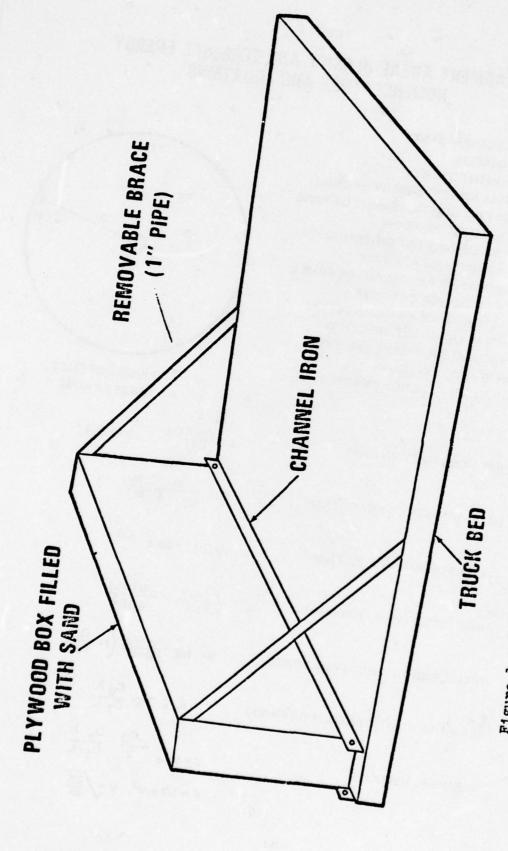


Figure 1. TYPICAL MINIMUM SHIELD

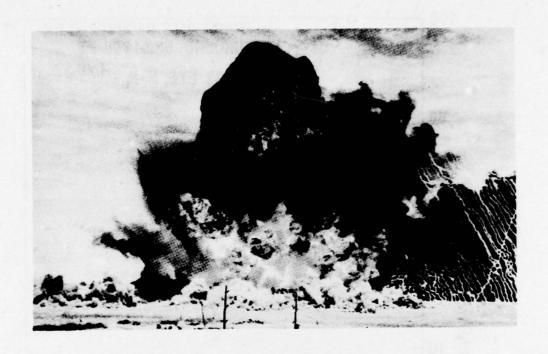


Figure 2. 500 TONS OF THT DETONATED AT THE EARTH'S SURFACE

The unified theory of explosions (UTE) (NOLTR 72-209) describes the explosive debris as particulate matter -- smoke and fragments -- which jets through the surrounding air until stopped in it by drag forcess.

Two basic fallacies inherent in all hydrocodes are seen here:

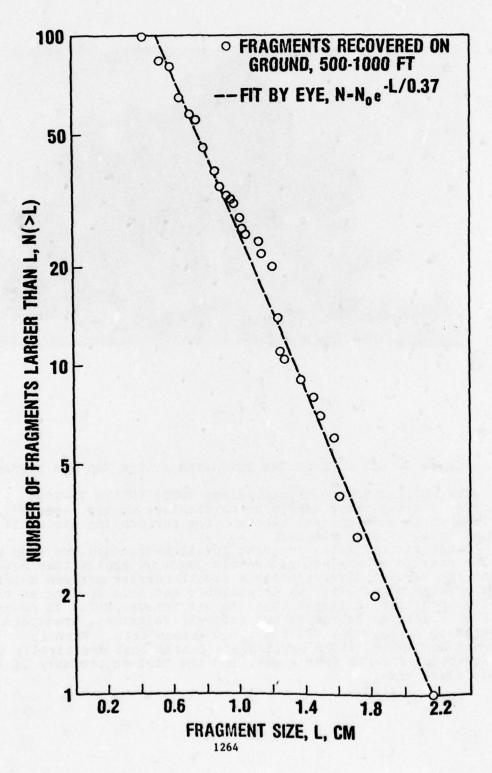
1) The mass zones are not concentric laminar shells that never mix. Nor is the contact discontinuity a smooth barrier between debris and the surrounding air; it is unstable and jets so long as the density of debris is larger than the air through which it moves.

2) The explosives debris is not entirely colorless, transparent gasses such as  $N_2$ ,  $O_2$ ,  $CO_2$ ,  $H_2O$  (steam) etc. Much is unburned carbon and other particulate debris that drastically alters the equation of state from a gas, and the head-on pressure of the (sand) blast wave.

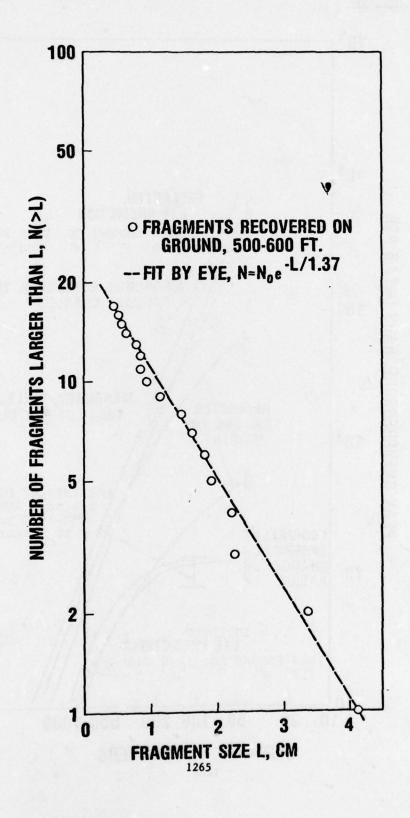


## FIGURE 3

# MK 16 TORPEDO FRAGMENT SIZE DISTRIBUTION



# TRUCK FRAGMENT SIZE DISTRIBUTION





PRESSURE-DISTANCE CURVES

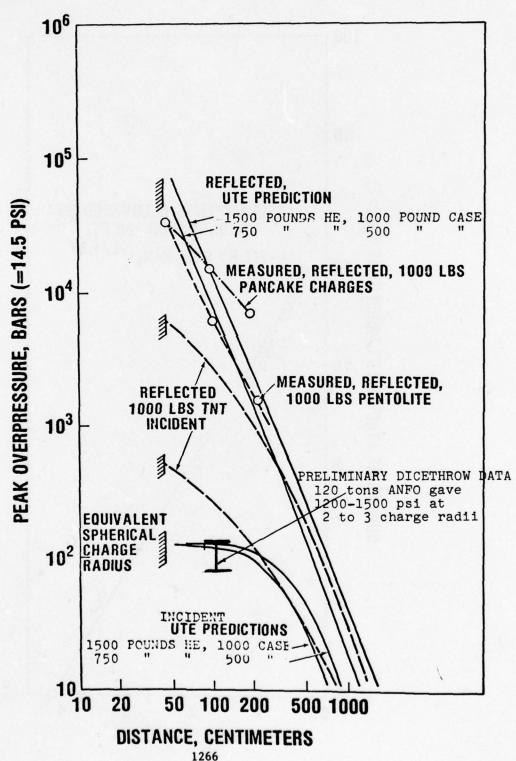
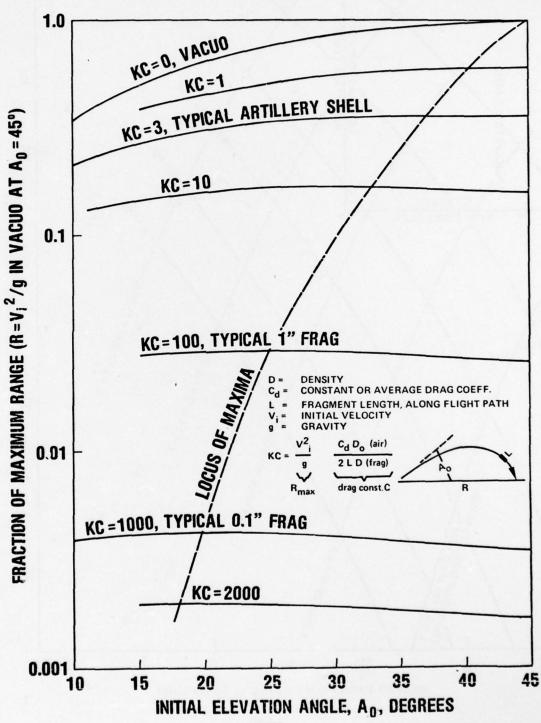
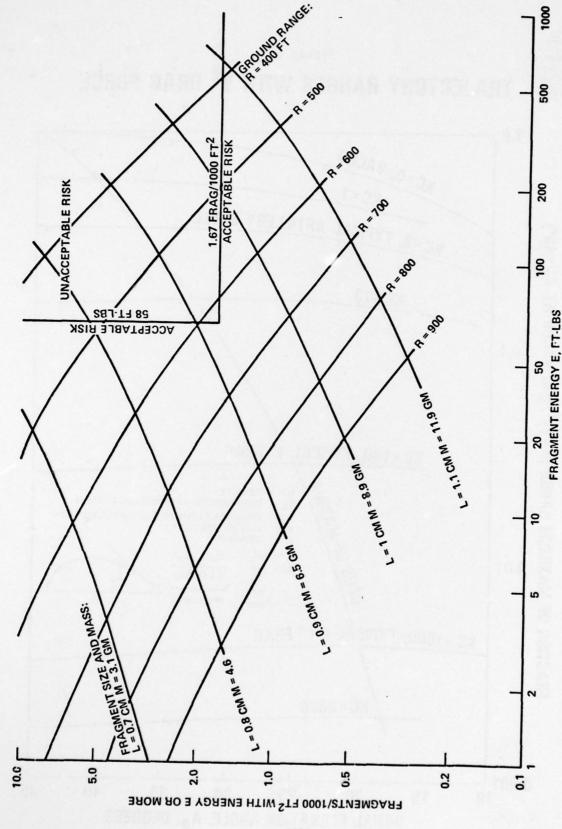




FIGURE 6

# TRAJECTORY RANGES WITH V<sup>2</sup> DRAG FORCE





FRAGMENT ENERGY AND NUMBERS (FEN CHART) TYPICAL FRAGMENTS, TWO WARHEADS TOTALLING 1500 LBS HE. 1000 LBS CASE. .36 CM THICK FIGURE 7

FRAGMENT ENERGY AND NUMBERS (FEW CHART) SLOW TRUCK FRAGRENTS FIGURE

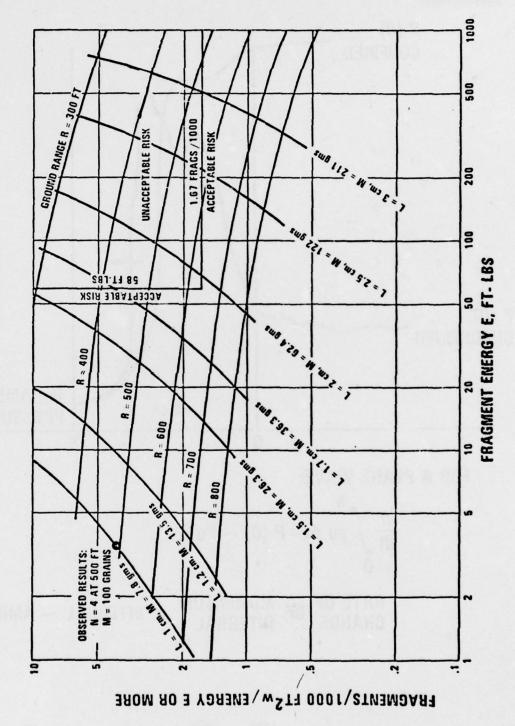
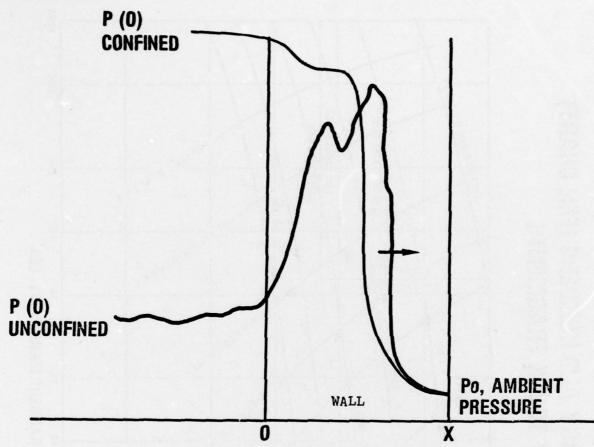




FIGURE 9

## **DECOUPLING**



FOR A PLANE WAVE:

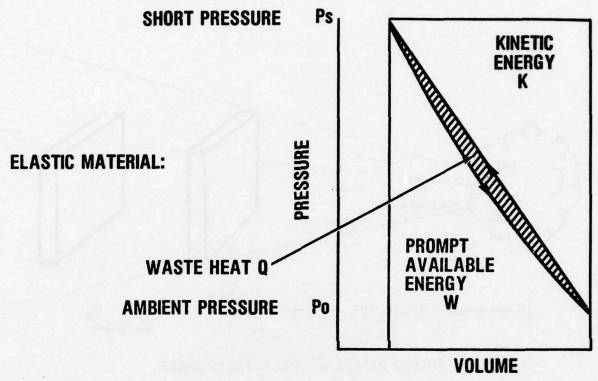
$$\frac{d}{dt} \int_{0}^{X} pu \ dx = P (0) - Po$$

RATE OF OF MOMENTUM = INTERNAL — AMBIENT

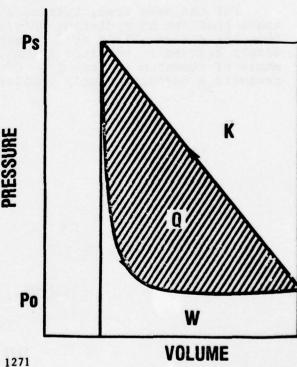


FIGURE 10

## **WASTE HEAT CONCEPT**



**ABSORBER: POROUS COMPRESSIBLE** CRUSHABLE ETC.



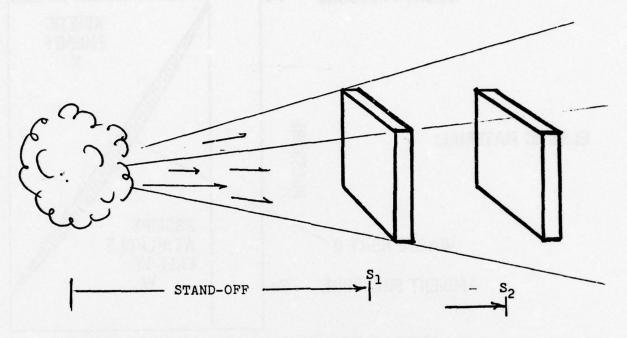


Figure 11. SHIELD STAND-OFF AND EFFECTIVENESS

For the same area, thickness and weight of shield, the geometry shows that the more distant shield at  $S_2$  will will be more effective than the cloaer shield at  $S_1$ , apparently by the facor  $(S_2/S_1)^2$ . Simply because it subtends a smaller mass of debris and solid angle of momentum and energy. Of course, the more distant shield protects a correspondingly smaller solid angle behind it.

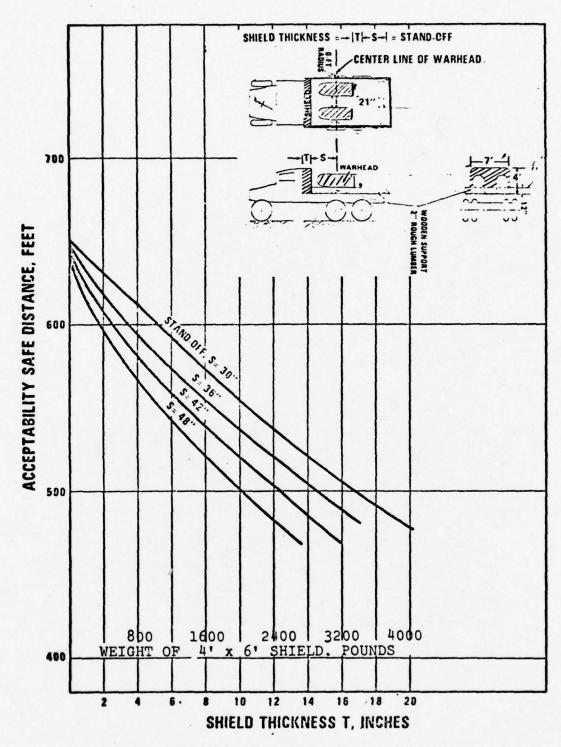


Figure 12. ACCEPTABLE DISTANCE.VS. SHIELD THICKNESS

#### FRAGMENT PENETRATION INTO SINGLE AND SPACED TARGETS

Tony Ricchiazzi Jim Barb

US Army Ballistic Research Laboratory Aberdeen Proving Ground, MD

#### **ABSTRACT**

An experimental program was conducted to determine the terminal ballistic performance of mild steel single and spaced double targets of equivalent thickness when attacked by 6.5 gram, 13 gram, and 26 gram blunt steel fragments. Results from a limited number of tests are presented for stainless steel cubes and pipes weighing 608 grams. Also, results are presented for a multiple target array having very small distances between the elements. The data shows that, in general, appropriately spaced double targets are better protective devices, but that crossovers do exist.

The program was funded by the Picatinny Arsenal for the Advanced Technology for Suppressive Shielding of Hazardous Production and Supply Operations for Production Modernization and Expansion Program.

#### INTRODUCTION

The Penetration Mechanics Branch, Terminal Effects Division of the Ballistics Research Laboratory was funded by Picatinny Arsenal to provide a fragment penetration model for the Advanced Technology for Suppressive Shielding of Hazardous Production and Supply Operations for Production Base Modernization and Expansion Program.

A fragment penetration model has been submitted and will not be discussed in this paper. Primarily this paper presents results from a recent experimental study of light and heavy fragment terminal ballistic performance against single and double spaced targets of equivalent thickness.

Results of fragment attack against multiple target arrays are also presented.

#### FRAGMENT DESCRIPTION

Table I gives the description of the fragments used in the tests. The 6.5 gram steel fragment was considered to be a fragment simulant from an 81mm mortar shell. The 13 gram and 26 gram weights were chosen to determine the mass and geometry scaling effects for light fragments.

An additional series of tests were conducted using simulants of stainless steel heavy fragments (608 grams) indicative of "worst case" fragment threats from an explosive melt-pour operation.

Table I. Fragment Description

	Mass (gm)	Material	Hardness BHN	Length (cm)	Width (cm)
Cube	6.5	AISI 1043	290	0.94	0.94
Cube	13.0	AISI 1043	290	1.18	1.18
RPP	26.0	AISI 1043	290	3.76	0.94
RPP	26.0	AISI 1043	290	2.37	1.18
Cube	608	Stainless Steel, 304	130	4.27	4.27
Pipe	608	Stainless Steel, 304	130	11.07	5.24 I.D., 6.03 O.D.

#### TARGET DESCRIPTION

Table II and Table III give the target material descriptions and double target configurations respectively. The target material was as received mild steel. Figure 1 shows a schematic of the 81mm suppressive shield. The target obliquity for all test conditions was set at 0 degrees to the line of fire.

Table II. Target Material Description.

Plate Thickness (cm)	Plate Hardness (BHN)	
0.476	110	
0.635	148	
0.953	137	
1.27	175	
1.63	90	
1.91	80	

Table III. Target Array Description

Fragment Mass(es) Tested (gm)	Number of Elements in Target	Thickness of Each Element (cm)	Total Line- of-Sight Thickness (cm)	Spacing(s) (cm)
6.5	1	0.953	0.953	
6.5	2	0.476	0.953	10.16
13, 26	1	1.27	1.27	-
13, 26	2	0.635	1.27	10.16 (varied to 20.32)
13, 26	1	1.91	1.91	-
13, 26	2	0.953	1.91	10.16
6.5	81mm Panel	(Shown in Figu	re 1)	
6.5	1	1.63	1.63	-
608	1	5.08	5.08	-
608	2	2.54	5.08	46

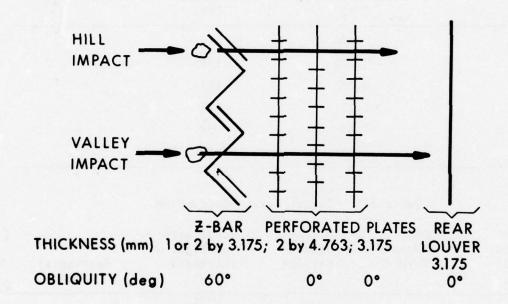


Figure 1. 81mm Panel Impacts

Table IV shows the resulting test matrix for the fragment/target configurations of the double targets.

Table IV. Test Matrix for Fragment Containment Comparison Between Single and Double Targets of Equivalent Thickness

Fragment			Target Single Element	
Mass gm	Presented Area cm <sup>2</sup>	Length cm	Thickness cm	L/T*
608 cube	18.20	4.27	2.54	1.68
608 pipe	<del>-</del>	11.07	2.54	4.36
6.5	0.88	0.94	.476**	1.97**
13	1.40	1.18	.635	1.87
13	1.40	1.18	.953	1.24
26	1.40	2.37	.635	3.73
26	1.40	2.37	.953	2.49
26	0.88	3.76	.635	5.92

\*Fragment length to target thickness ratio.

\*\*This is the maximum value also for the individual elements of the 81mm suppressive structure.

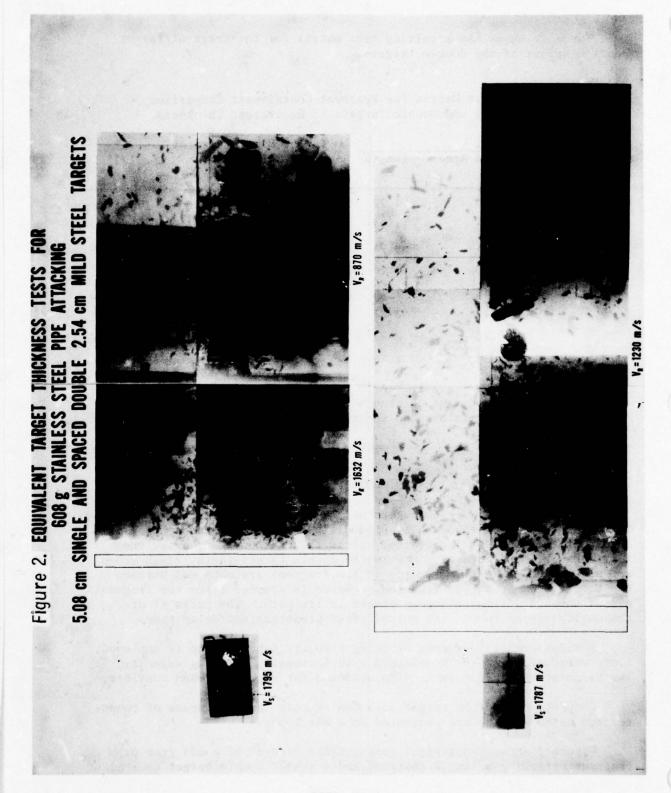
#### EXPERIMENTAL SET-UP

The experiments were conducted at the Ballistic Research Laboratory, BRL using multiple, orthogonally placed flash radiography? so that a film record of the fragment is obtained before target impact and after the target has been perforated. For spaced double target tests, flash tubes are placed such that film records of the fragment are obtained between the target elements. The flashing sequence is started after the fragment passes through a trigger screen placed in its path. The pairs of orthogonally placed tubes are pulsed after predetermined delay times.

Residual velocity versus striking velocity type testing is employed, i.e., residual velocity is obtained with increasing striking velocity. The fragment residual mass is also obtained for each test when possible.

Complete behind the target data can be calculated by means of computerized methods which are presented in a BRL report<sup>3</sup>.

Figure 2 shows two typical radiographic records of a 608 gram pipe fragment attacking a single (bottom) and a spaced double target equivalent



thickness (top). The figures show only one portion, the side view of the event before target impact and after target perforation.

### EXPERIMENTAL TECHNIQUE

The experimental technique employed is as follows. The striking velocity  $\mathbf{V}_S$ , is increased by varying the propellant weight. At each striking velocity the residual velocity,  $\mathbf{V}_R$  is calculated from measurements obtained from the x-ray records. A curve is fitted to the data. From this curve fitting technique the ballistic limit velocity  $\mathbf{V}_L$ , is determined at the point where the  $\mathbf{V}_R$ -  $\mathbf{V}_S$  curves intercepts the abscissa. For multiple targets the  $\mathbf{V}_R$ -  $\mathbf{V}_S$  curves can conceivably intercept the abscissa more than once, due to mass loss effects.

For some of the heavy fragment tests a complete  $\rm V_R$  -  $\rm V_S$  curve could not be obtained because of erratic free flight characteristics.

For the light fragment tests the post perforation fragments were recovered from stacked celotex and weighed. This was not accomplished in the heavy fragment tests due to limited funding.

#### EXPERIMENTAL RESULTS

### A. 608 Gram Fragments

Figures 3 and 4 show the results of limited  $V_R$  -  $V_S$  tests for 608 gram pipe and cube fragments against single 5.08 cm thick mild steel targets and spaced (46 cm) double 2.54 cm mild targets.

For single targets the pipe fragment has a higher ballistic limit velocity by approximately 24%, however at high striking velocities the pipe has higher residual velocities. This is due to the poor stability in flight of the pipe. For example, at a  $\rm V_S$  of 1800 m/sec the residual velocity of the pipe was about 90% higher than the residual velocity of the cube. At striking velocities below about 1450 m/sec the striking yaw of the pipe was greater than 10° and apparently (judging from the impact craters on the target surface) buckled and/or turned side-on during the impact, presenting a large area and therefore decreasing its ability to penetrate. Impacts of this type defeated the projectile. At the higher velocities (> 1450 m/sec), the pipe became more stable in flight, greatly increasing its efficiency to perforate the target.

On Figure 4 the dotted line represents the results of the predictive technique developed at the BRL. The constants for the relationships were derived from light fragment data. The predictions of the  $\rm V_L$ , and  $\rm V_R$  show that the relationship scales well for cubic fragments. Figures 3 and 4 also show that spaced double targets of equivalent thickness provide more protection against the fragments than single targets. For example, in

608 g PIPE FRAGMENT ATTACKING 5.08 cm MILD STEEL TARGETS; SINGLE AND SPACED DOUBLE OF TOTAL EQUIVALENT THICKNESS Figure 3.

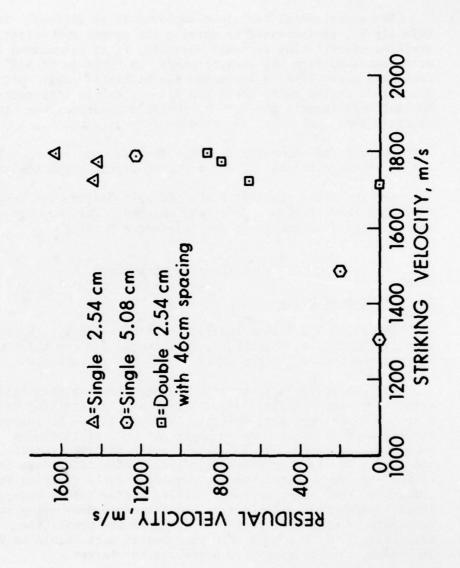


Figure 4. 608 g CUBE FRAGMENT ATTACKING 5.08 cm

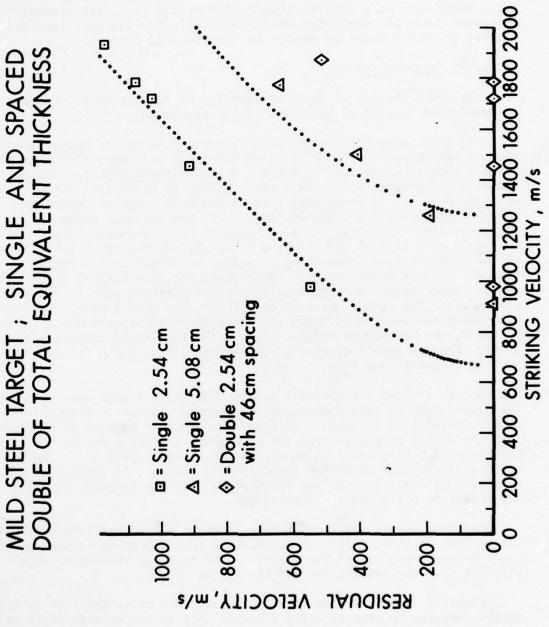


Figure 3 the increase in the ballistic limit velocity is about 14% for pipe fragments and about 50% for cube fragments. Predictions were not made for spaced double targets since this requires a more accurate description for the residual mass of the fragment than is available now. The residual mass model works fairly well for fragments that do not break up entirely but that deform and erode. The impact condition of these tests were such that the fragment dimension to target element thickness ratio was small and the striking velocity was well into the shatter or severe break up regime for the fragment material.

### B. Light Fragment Results

Figures 5 through 11 shows the results of testing single targets and spaced double targets of equivalent total thickness.

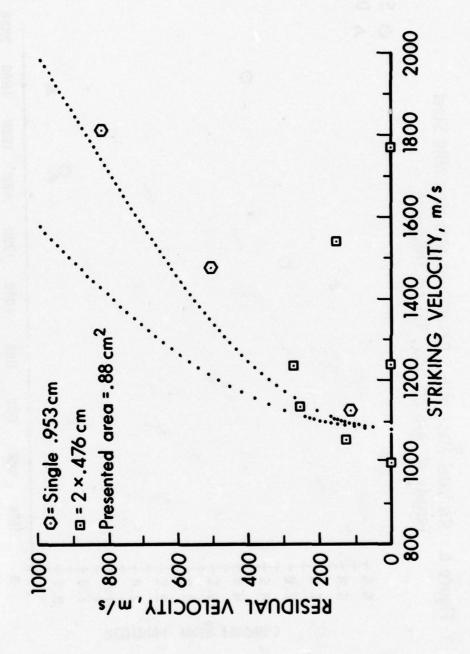
Figure 5 shows the results of a 6.5 gram cube tested against two .476 cm targets separated by 10.16 cm air space and results from tests using a single target .953 cm thick. The data shows that the single target has a greater ballistic limit velocity by about 15%. At a striking velocity of about 1230 m/sec a residual velocity cross over occurs between the two types of targets and the residual velocity decreases with increasing striking velocity for the double target due to increased mass loss of the fragment after perforating the first element of the double target. The residual velocity increases with striking velocity for the single target. Therefore, for this test condition the double target offers more protection above a striking velocity of about 1230 m/sec. The impact orientations of the cube were random. The dotted line shows the results of using the fragment penetration model to predict  $V_{L}$  and  $V_{R}$  for the single target. Prediction for double targets requires a more accurate relationship for residual mass especially for the shatter made of fragment mass loss.

Figure 6 shows the residual masses from the 6.5 gram cube attacking the single .953 cm target (hexagons). Some data acquired from a .476 cm single target is also shown. Although this data is sparse, it is clear that the double target is superior at higher velocities due to the large mass loss (due to shatter in this case) above about 1400 m/s. These results are typical of all of the fragments tested. At initial velocities of 1200 - 1300 m/s or less the residual mass of the fragment is still sufficient to perforate a second target.

Residual masses for the 6.5 gram fragment behind the .476 cm double target are not shown, since no substantial (> 0.5 gram or larger) piece could be recovered behind the target. (The residual velocities were obtained from the leading edge of the ejecta cloud).

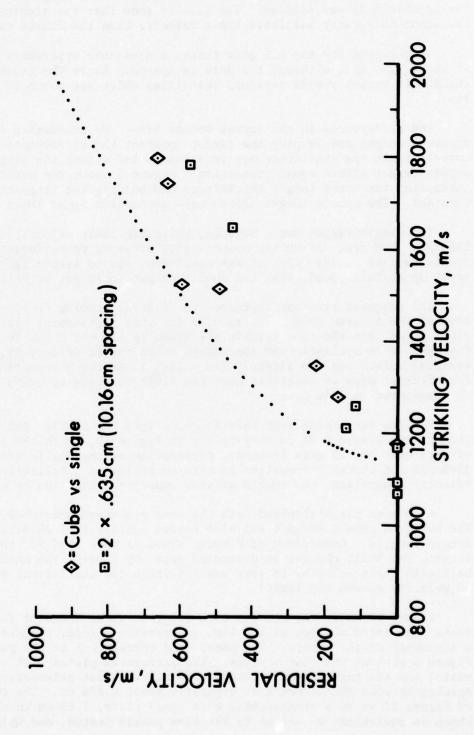
Figure 7 shows the results of a 13 gram cube attacking 1.27 cm steel target compared to results using a double .635 cm target with 10.16 cm spacing. It was decided to use heavier elements for the heavier fragment because with the number of tests planned the velocity range would cover both deformation mass loss mode and shatter mass loss mode determined by

Figure 5. 6.5 g FRAGMENT ATTACKING.953 cm MILD STEEL TARGET; SINGLE AND SPACED DOUBLE OF TOTAL EQUIVALENT THICKNESS



SingleDouble Residual Mass of 6.5 Gram Cube Attacking Mild Steel Targets of . 476 cm and . 953 cm Thickness 1288 1488 STRIKING VELDCITY (N/S) Figure 6. RESIDURE NESS (ERRNS)

Figure 7. 13 g FRAGMENT ATTACKING 1.27cm MILD STEEL TARGETS; SINGLE AND SPACED DOUBLE OF TOTAL EQUIVALENT THICKNESS



previous tests with the 6.5 gram steel fragment. The fragment length to target thickness was similar. The results show that the single target has about 8% greater ballistic limit velocity than the double target.

As observed for the 6.5 gram tests, a crossover apparently occurs at about 1290 m/s, although the data is sparse. Above the crossover, the double target yields residual velocities which are about 12 - 25% less.

The differences in the curves become less. By increasing the fragment weight and keeping the target constant the differences in the curves within the statistics are very small, and either the single or double target afford equal protection. Figure 8 shows the effect of increasing the total target thicknesses and holding the fragment weight constant. The double target offers more protection by at least 18%.

The single target has a measured ballistic limit velocity of between 1550 and 1600 m/s. After two unsuccessful attempts to perforate the double targets at 1800 m/s, it was concluded, due to severe fragment break up at this speed, that the double target could not be perforated.

The fragment mass was increased to 26 grams keeping the presented area of the 13 gram cube. The results for this rectangular parallelepiped fired into the same targets are shown in Figures 9 and 10. Only a few shots were available for the double 0.635 target (Figure 9). The residual velocities are slightly (10 - 15%) lower for the double target. Insufficient data is available near the limit velocity to demonstrate any crossover in this case.

The few tests made with this fragment into the double .953 cm targets and single 1.91 cm targets are in Figure 10. With the increase of mass over the 13 gram fragment, perforation of the double was possible. Although not enough information is here to arrive at a ballistic limit velocity comparison, the double affords superior protection by about 50%.

A 26 gram parallelepiped with the same geometric presented area as the 6.5 gram cube (.88 cm $^2$ ) was also tested against 1.27 cm single and double targets. Comparison of Figures 9 and 11 show that for the single target, for small changes in presented area by itself, the change in ballistic limit velocity is very small (within the statistical variations in velocity around the limit).

Figure 12 shows the results of a 6.5 gram steel fragment (cube) tested against a portion of the 81mm suppressive shield. Figure 1 shows a schematic of the shield. The panel used corresponds to the panel on Figure 1 without the rear louvers. The perforated plates (10% vent area ratio) and the bar elements provide venting for blast attenuation. The spacing between the elements is typically about 0.476 cm. The comparison of Figure 12 is to a single solid mild steel plate, 1.63 cm in thickness, which is equivalent by weight to the 81mm panels tested, and which accounts

Figure 8. 13.9 FRAGMENT ATTACKING 1.91cm MILD STEEL TARGET; SINGLE AND SPACED DOUBLE OF TOTAL EQUIVALENT THICKNESS

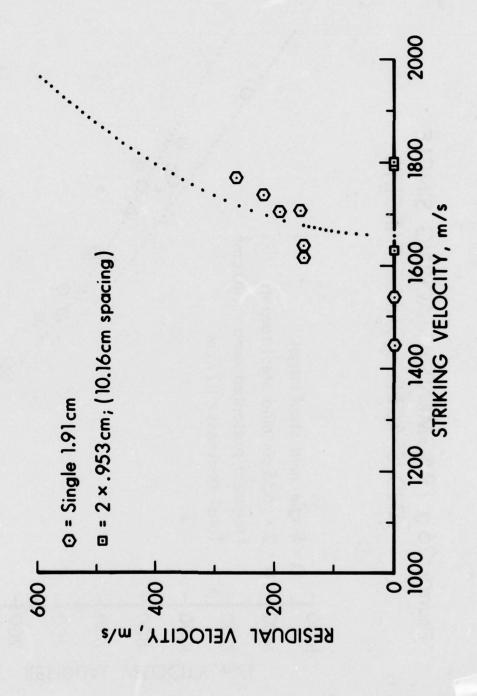


Figure 9. 26 g FRAGMENT ATTACKING SINGLE AND SPACED DOUBLE TARGETS

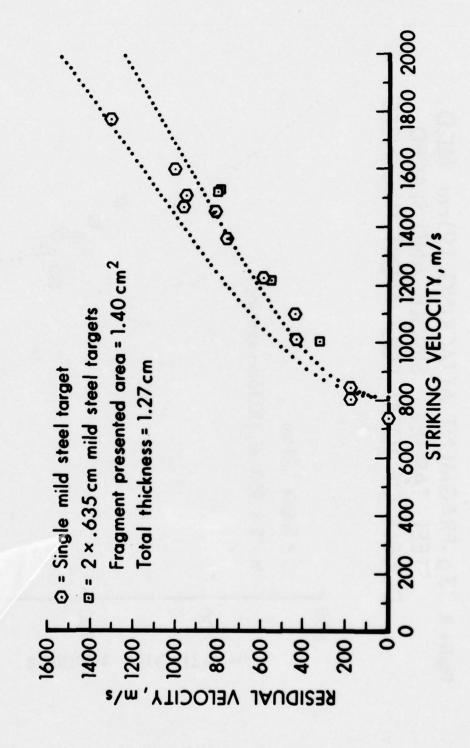


Figure 10. 26g FRAGMENT ATTACKING 1.91cm MILD STEEL TARGET; SINGLE AND SPACED DOUBLE OF TOTAL EQUIVALENT THICKNESS

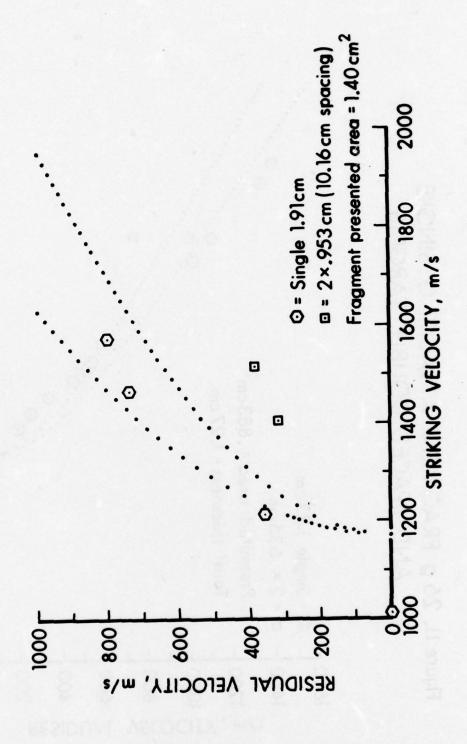


Figure 11. 26 g FRAGMENT ATTACKING SINGLE AND SPACED DOUBLE TARGETS

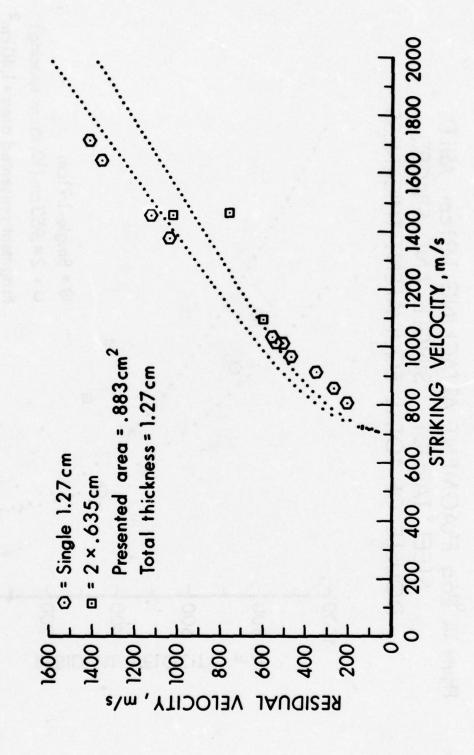
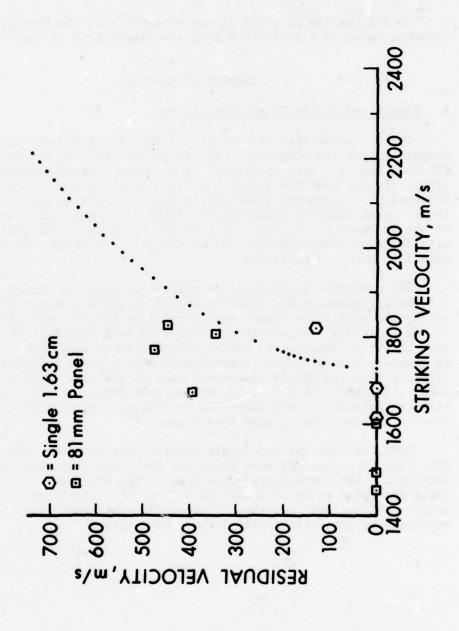


Figure 12. 6.5 g CUBE ATTACKING 81 mm PANEL AND TARGET OF EQUIVALENT THICKNESS



for the perforated plates. In this case, the single target provides

In this series of shots it was observed that the three perforated elements acted as a laminate during the penetration of the fragment.

# SUMMARY OF RESULTS

# A. Single and Double Target Comparison

Table V summarizes the results of the single and double target comparison for the fragments. As can be seen, only in two instances do the data show a clear superiority of a single over a multiple or double array. In one case the individual elements are either two weak (perforations) or the spacing (.476 cm) is poor. In the second case, shown by the 6.5 gram fragment attacking the light (.476 cm) double array, a crossover results. A crossover probably exists also for the last 26 gram fragment (Length/Width = 4) on the list. Limited data above the

The crossover in residual velocities as shown in Figure 5 for the 6.5 gram fragment is a characteristic of single and double targets borne out by the predictive equations for multiple targets and will occur only if the individual target elements are each weak enough that the fragment can survive an impact with little deformation or mass loss. That means, in general, that a double target should have a lower ballistic limit velocity than its single equivalent only if the mass loss in the first target is slight. For 6.5, 13, and 26 gram fragments this requires striking velocities less than 1000 to 1200 m/s, since above these velocities considerable mass loss occurs.

Model results for the double targets have not been shown since, at this time, the residual mass equations for these fragments are not fully developed. The current predictions as in the BRL report on the subject! yield predicted residual masses in between the targets which are too large by 50 to 100% for these lighter fragments, and thus yield very conservative predictions behind the second target.

Table V. Equivalent Thickness Studies Double and Single Targets

Fragment	Total Target Thickness	Velocity Range	
Mass (grams)		Advantage for Single (m/s)	Advantage for Double (m/s)
6.5, (cube)	1.63 Single (81mm panel)*	Complete V <sub>I.</sub> = 1800 m/s	81mm (none)
6.5, (cube)	0.953 (2 by .476)	1000 - 1200	> 1200
13, (cube)	1.27 (2 by .635)	< 1290	> 1290
13, (cube)	1.91 (2 by .953)	None	No perforation up to 1800 m/s
26, L/W = 2	1.27 (2 by .635)	None	
26, L/W = 2	1.91 (2 by .953)	None	
26, $L/W = 4$	1.27 (2 by .635)	None above 1000 m/s	

\*Thickest single element is a .476 cm perforated plate

### B. Spacing Effect Observations

The results listed above for the double targets may be largely a result of the choice of spacing. The 10.16 cm spacing value initially chosen for the light fragment tests was chosen after observing the behind the target ejecta spread from the single target data. It was seen that the target ejecta and projectile residues had become separated from one another at least by this distance, so that there was little chance of projectile and target "plug" or ejecta attacking the second target synergistically, and also there would be adequate distance for the individual fragment pieces to separate when fragment shatter occurred. This distance worked well for the 13 and 6.5 gram fragments. For the 26 gram fragments, this space was extended to 20.3 cm with no difference. Due to the heavier striking mass, the residual fragment remains, by itself, heavy enough to perforate the second target.

These results are summarized in Table VI. Included are the results of another short firing program including the 608 gram cube and an equivalent weight 304L stainless steel rod (Length to diameter ratio of

ten). The targets used in this program are the Category I Suppressive Shield Candidate designs. The complete results have been published<sup>5</sup>. The observations are limited, since between the target data was not possible. The thicknesses of the target elements were the same (2.54 cm).

For the long rod, and the two 26 gram fragments it is apparent that no improvements in multiple or double target effectiveness occurs due to increasing the spacing, (at least for these element thicknesses) since after a single impact, the projectiles have retained enough integrity to perforate the next element. However, larger spacing than those tested would allow more time for the unstable longer fragments to tumble and impact the next element with high yaw which would improve the effectiveness of the target.

Table VI. Spacing Effects Observed for Multiple Panel Targets

	Description	Length Target Thickne	Length ss Spacing	Results	
I.	304L Stainless Steel Fragments				
	Rod, L/D - 10, 608 grams	8.5	9 and < 1.0	Limited data, apparently no change	
	Cube 608 grams	1.7	1.7	Not effective Limited data, possibly effective Effective	
ττ	1340 Steel Fragments		••	Directive	
11.					
	Cube 6.5 grams	≥ 1.97	2	Multiple targets act as laminated targets	
			.09	Effective distance for shedding target material	
			< .09	No change	
	Cube, 13 grams	1.87 1.24	< .4	Adequate spacing Adequate spacing	
	Rectangular parallelepipe 26 grams (L/W = 4)	ed 5.92	.4 to < .2	No change	
	Rectangular parallelepipe 26 grams (L/W = 2)	ed 3.74	.2 to .1	No change .2 is adequate	
	The second of th	2.48	.2 to .1	No change .2 is adequate	

For the compact (cubic) fragment data, however, it appears that some target advantage can be obtained by chosing a sufficient spacing (small fragment length to spacing ratio as listed in Table VI.). Values of this ratio of about .1 is sufficient for the 6.5 gram and heavy 608 gram cubes. The targets for the 13 gram tube however, had as sufficient spacing the same absolute value as for the 6.5 gram cubes suggesting that an absolute spacing requirement, independent of the fragment dimensions may be necessary as well.

#### REFERENCES

- BRL Memorandum Report No. 2578, "A Tentative Model for Predicting the Terminal Effects of Blunt Fragments Against Single and Spaced Targets. A Comparison of Predicted and Experimental Results", A. Ricchiazzi and J. Barb, January 1976.
- 2. BRL Technical Note 1634, "X-Ray Multi-Flash System for Measurement of Projectile Performance at the Target", C. Grabarek and E. L. Herr, September 1966, AD#807619.
- 3. BRL Memorandum Report 2264, "A Computerized Method for Obtaining Behind-the-Target Data from Orthogonal Flash Radiographs", A. Arbuckle, L. Herr, and A. Ricchiazzi, January 1973, AD#908362L.
- 4. BRL Report 1852, "Towards Standardization in Terminal Ballistics Velocity Representation", J. P. Lambert and G. H. Jonas, January 1976, AD TBL 20376.
- BRL Memorandum Report 2592, "Test Results for 608 Gram Fragments Against Category I Suppressive Structures", A. Ricchiazzi and J. Barb, February 1976.

#### SHIP SURVIVABILITY VERSUS EXPLOSIVE HAZARDS

Dr. June T. Amlie David Taylor Naval Ship R&D Center Carderock, MD

The effects of detonations of explosives on steel ships will be demonstrated by a collection of experimental data from the exploratory tests done in support of the development and characterization of an anti-ship warhead; documentation from the explosives accident aboard the USS SOLAR will be presented for comparison. The potential for damage from the detonation of explosives in various locations on steel ships will be examined: for explosions within the hull, externally in contact with the hull above the waterline, and in locations above the main deck. The effects of both blast and fragments will be considered as they apply in ships. For internal detonations, blast effects are most important because the primary fragments are quickly soaked up by surrounding structure. The secondary fragments generated from the ship structure are of importance to the Navy because of the Quantity-Distance relationships established by the Explosives Safety Board. Test film clips at several film speeds will document the type of ship fragments generated and typical distributions. Diligent search has produced applicable data from two ship disasters - one the accidental explosion aboard the USS SOLAR, and the other the loss of the USS LISCOME BAY in World War II. The LISCOME BAY was lost at sea, but structural damage contours were reconstructed from survivors' accounts. The USS SOLAR was at pierside when the accident occurred, and pictures are available for comparison of similitude of damage contours and an indication of secondary fragment distribution.

To the person who tests warhead effects, the ship is essentially a series of built-in witness plates. The fate of primary fragments from a cased

detonation within a ship can be illustrated by the photographic record of a detonation of an explosive charge in a fragmenting case in the forward end of a destroyer escort. Figures 1 and 2 show the condition of the transverse bulkheads that formed the forward and aft boundaries of the damage envelope on the same platform. As one can see, there are no fragment holes. As a qualification, there is a threshold below which the fragments are important as has been demonstrated in tests.

The question of the potential for damage by explosive detonations in various locations in the ship is illustrated with selected views of an exploratory warhead test series. The maximum internal damage occurs when the detonation is confined within ship structure when there is no venting. The damage caused by the same weight of explosive in various locations in, on, and over ships is shown in Figures 3 through 13. Figures 4 and 5 represent the special case of two charges detonated sequentially at locations 16 feet apart.

The distribution of secondary fragements, debris from the ship, can only be shown in film clips from the test series. This documentary evidence was not collected for this purpose, but is the only data of its kind known to the author. Several statements can be made about secondary fragments from the ship after examination of this film.

- Detonations above or alongside the ship create little debris in addition to that from the original detonation source, which is entirely consistent with the limited structural damage.
- For detonations within the hull of the ship, secondary fragmentation outside the ship envelope increases with the degree of venting from the ship.

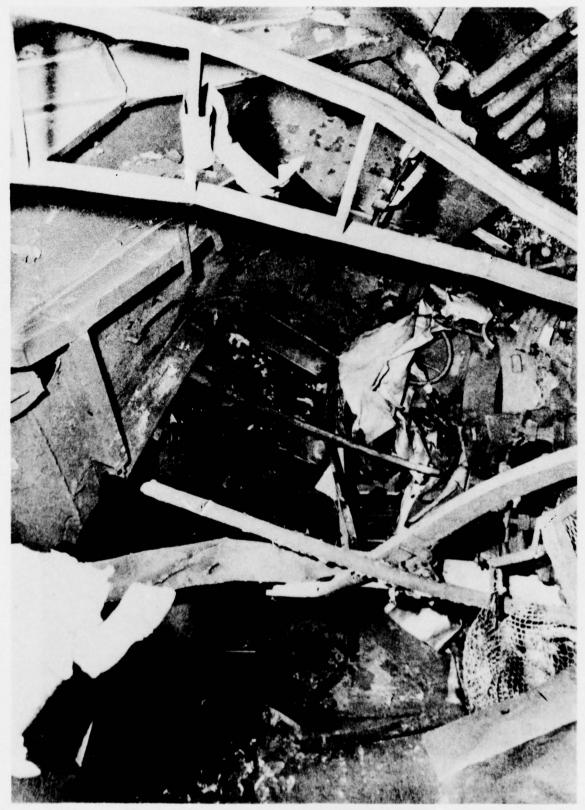
- a. Smaller detonations or those deeper in the ship that are contained by the main deck or superstructure may result in only the hull opening with fragment spray restricted to the lateral direction. Fragments fell within an estimated radius of 100 to 150 feet in these tests.
- b. When the explosion is large enough to open up the ship, the deck is laid back on itself fore and aft of the detonation site, and debris travels vertically as well as laterally. Most of the debris travels up and falls back in an area relatively close, to the ship estimated from the film data to lie within a radius of from 100 to 150 feet. A much different trajectory will be imparted to a few larger fragments, typically of very irregular shape (for instance, a gun barrel, equipment, or piece of steel plate). Distances from the detonation site of from 200 to 500 feet have been estimated for a few fragments.

Personnel of the USS SOLAR were unloading 288 Torpex-loaded HEDGEHOGS from the forward magazine when an accidental detonation occurred, probably in the forward gun tub on the main deck. The Board of Inquiry concluded that the second and third detonations (of the forward magazine) occurred soon thereafter as a result of cookoff. Note the damage in Figure 14, certainly of greater severity in a localized sense, but little greater structural loss than that produced by a much smaller amount of explosive. Figure 15 shows the amount of debris on the after end of the ship, and Figure 16, the debris on the pier after the explosion. The ship moved about 300 feet aft as a result of the explosion in the forward end, so the farthest area shown of the pier is less than 500 feet from the detonation site.

This paper has presented data related to the question of debris from detonation of explosives aboard ship. There has been an attempt to relate the damage to the ship and the debris produced to the location of the detonation of a given threshold of explosive. General patterns of debris from detonations aboard ship are apparent for each case. When the ship opens up topside, most debris travels up and falls down nearby. However, some few

larger fragments develop trajectories that carry them farther away. Documentary evidence of the scene after accidental detonation of as much as 10,000 pounds of Torpex in the forward magazines of the USS SOLAR is consistent with the test data.

These and other similar data are being examined in detail in support of miltestone E-2 of the ongoing Navy Explosive Safety Improvement Program approved by the Chief of Naval Operations on 23 January 1975.



IG. 1. Damage Forward of Detonation Site

FIG. 2. Aft Boundary of Damage

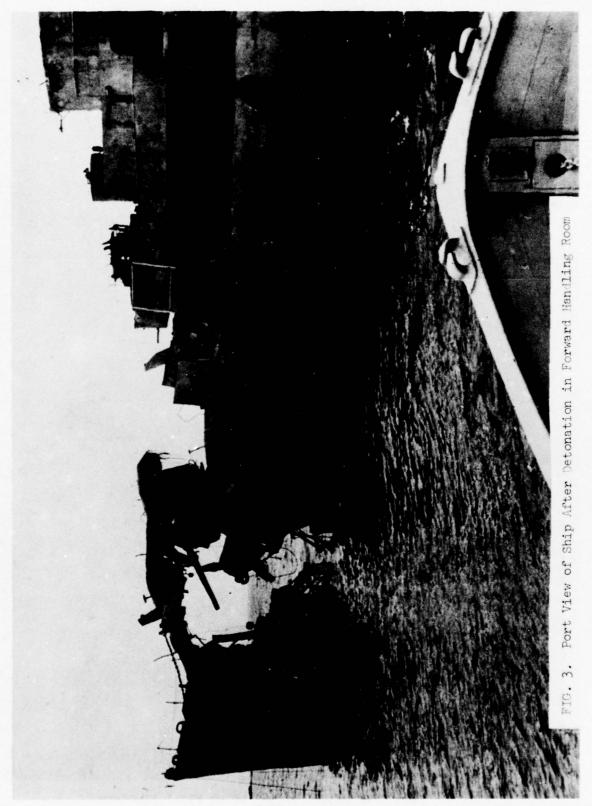




FIG. 4. Port View After Detonation on First Platform 1306



FIG. 5. Starboard View After Second Detonation in Stern 1307

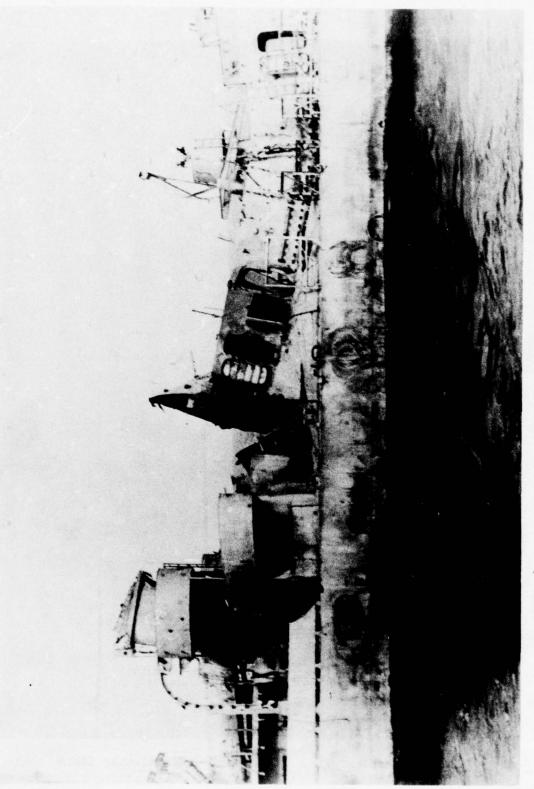


FIG. 6. Topside Damage After Detonation on First Platform



IG. 7. Starboard View After Detonation on Third Deck

1309

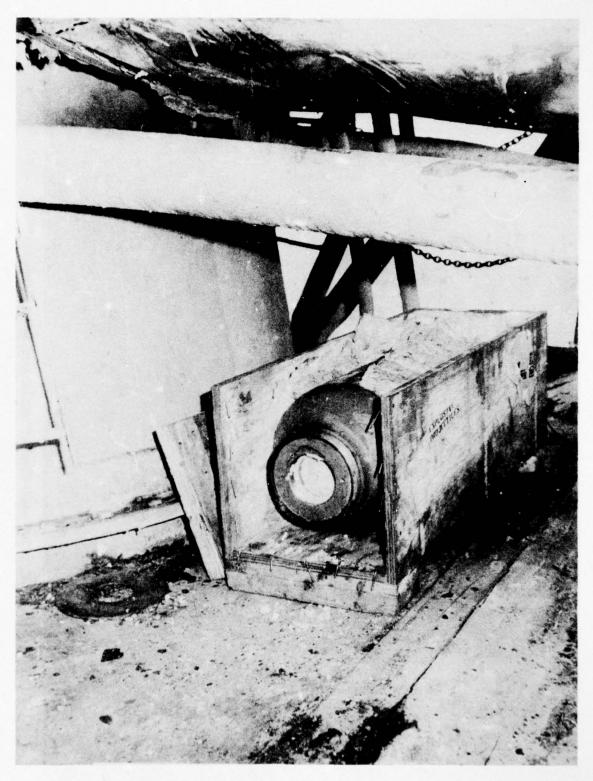


FIG. 8. Warhead in Place on Deckhouse 1310



FIG. 9. Port View From Main Deck of Major Damage From Detonation of Warhead at Location in Figure 8

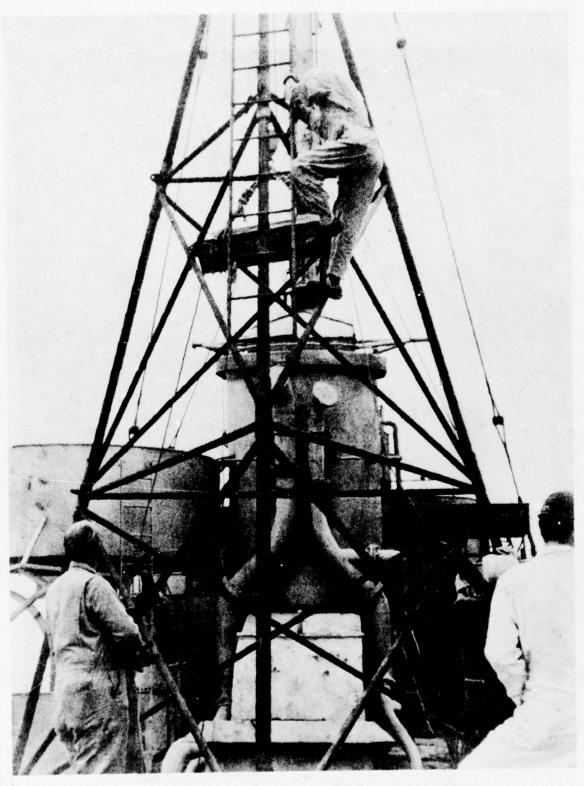


FIG. 10. Warhead Being Placed Twenty-Five Feet Above the Deckhouse

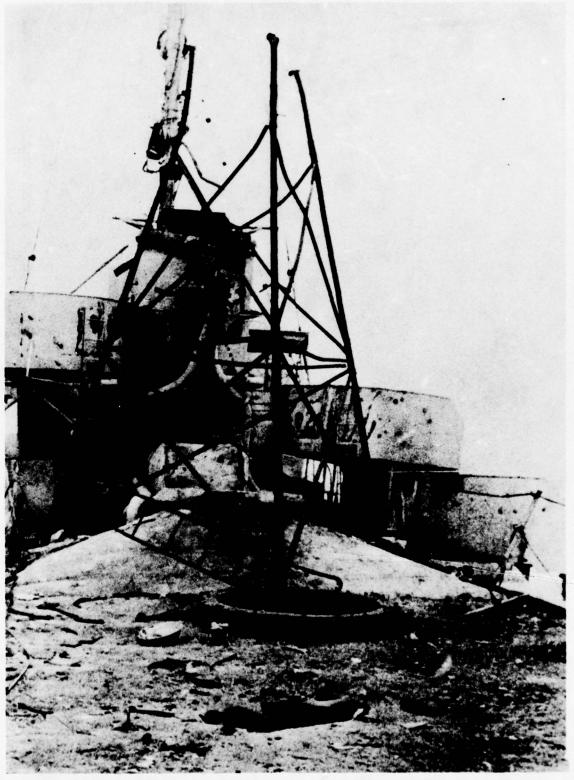
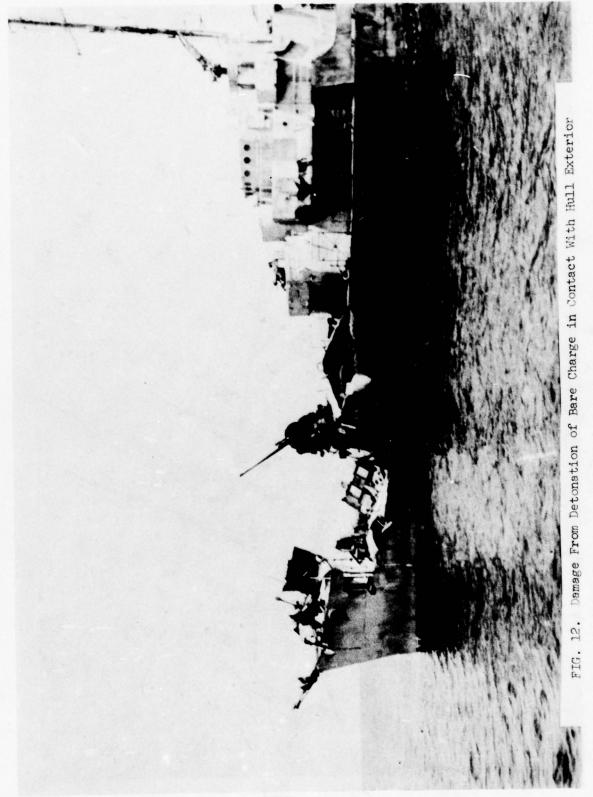


FIG. 11. Damage From Detonation of Warhead Shown in Figure 10 1313



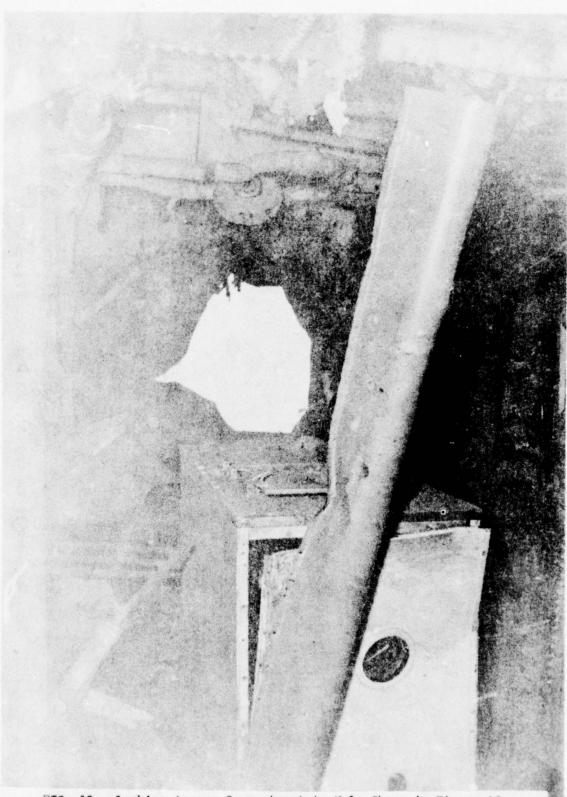


FIG. 13. Looking Across Compartment to Hole Shown in Figure 12

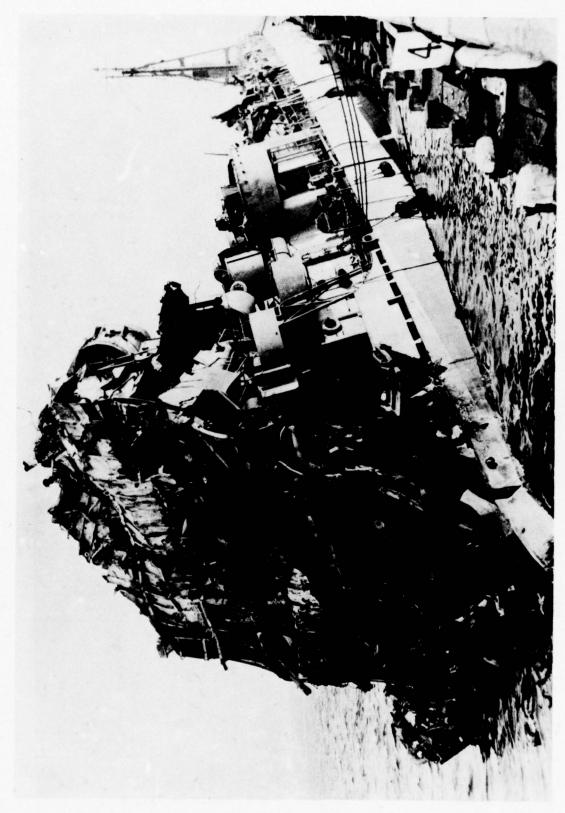


Fig. 14. Forward End of USS SOLAR After Third Detonation

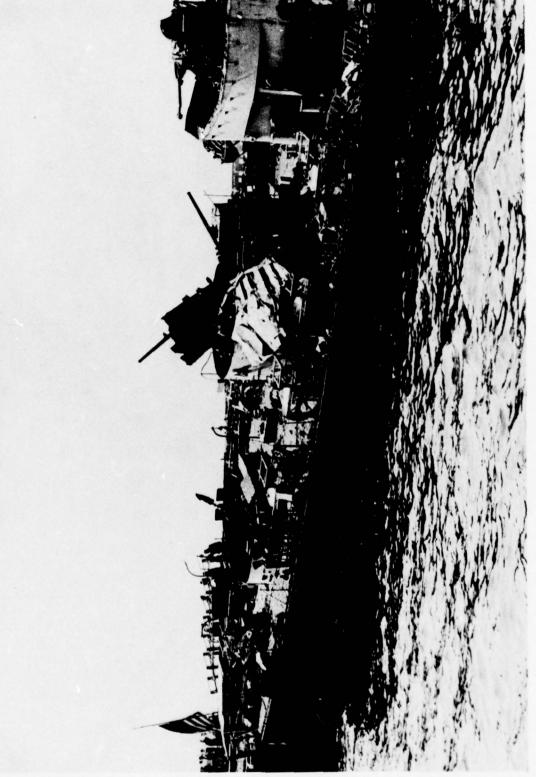
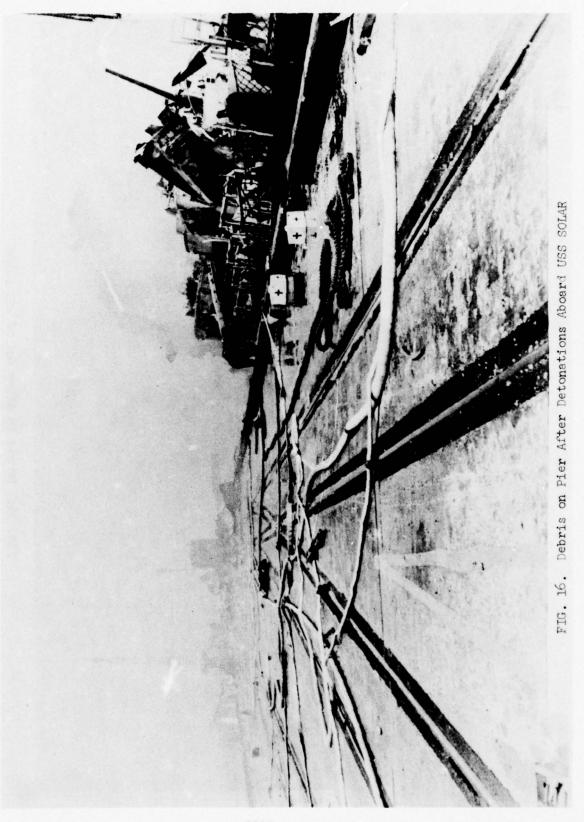


FIG. 15. Debris in After End of USS SOLAR



#### DANGERS OF SECONDARY MISSILES

Kenneth Kaplan Scientific Service, Inc. Redwood City, California

Ordinarily, discussions of secondary missile hazards revolve around missiles (and objects) originally located in the immediate vicinity of an explosion. These can attain very high velocities, can be thrown great distances, and certainly can be hazardous. The principle focus of this paper, however, is on missiles from structures located relatively far from an explosion, in particular, at inhabited building, unbarricaded intraline, and barricaded intraline distances given in Ref. 1. In addition, the paper will concentrate on missiles from structures, or structural elements, built with relatively low blast resistance.

As part of a long-term analytical and experimental program dealing with the response of walls to blast, some walls typical of such structures have been studied. These include interior walls of sheetrock over studs and of reinforced masonry (concrete block, and clay tile), and exterior walls of unreinforced masonry (brick and concrete block).

Most recently, an effort was made to develop simplified, reasonably correct methods for predicting velocities that could be achieved by debris from these walls after their failure. The study was largely supported by the Defense Civil Preparedness Agency, and thus emphasis was on blast waves of long duration, that is, on blast from very large explosions. Approximations for smaller explosive sources can be derived, however.

## EXPERIMENTAL CONDITIONS

The experimental portion of the program was carried out in the large shock tunnel installed in a former coastal defense facility, cutaway views

of which are sketched in Fig. 1 (the shock tunnel is in the foreground) and Fig. 2. The compression chamber was an 8-ft diameter steel cylinder, 63 ft long, and closed at one end, in which 60-ft long strands of Primacord (detonating fuse) were strung. The hot, high pressure gas created by exploding the Primacord generated a shock wave which propagated down the length of the  $8\frac{1}{2}$ -ft high, 12-ft wide expansion chamber, near the end of which walls of various kinds were installed.

As shown in the plan view of Fig. 3, walls could be installed in three places. They could also be equipped with window or doorway openings so that the equivalent of a room could be investigated, with the loading on an "interior" wall at Location B, for example, being caused by a blast wave that had to pass through the window of the "exterior" wall at Location A.

The type of pulses generated in the shock tunnel and experienced by an interior solid wall is shown in Fig. 4. The solid line shows a shock pulse experienced by the solid wall at the back of a room whose front (exterior) wall had a window opening that occupied 20% of the wall area. The trace shown is actually the average pulse from a number of gauges on the wall. The dashed line shows the approximation of that shape used for calculation purposes. Its initial value is approximately 1.5 times the incident, or unreflected, blast pressure in the tunnel, the shape of which was very similar to that shown by the dashed line, i.e., initially flat-topped. A solid wall in the tunnel also experienced a flat-topped pulse, whose initial pressure was somewhat more than twice incident pressure.

The net loading experienced by an exterior wall with a 28-in. wide doorway such as that sketched in Fig. 5, is shown by the solid line of Fig. 6, along with the approximation of that pulse (the dashed line) used for calculation. The measured pulse represents an averaging of pressures on the upstream and downstream faces of the wall. The initial value of the approximation pulse is about 1.5 times incident pressure. For interior walls with a doorway, or interior walls that extend to a light-weight ceiling.

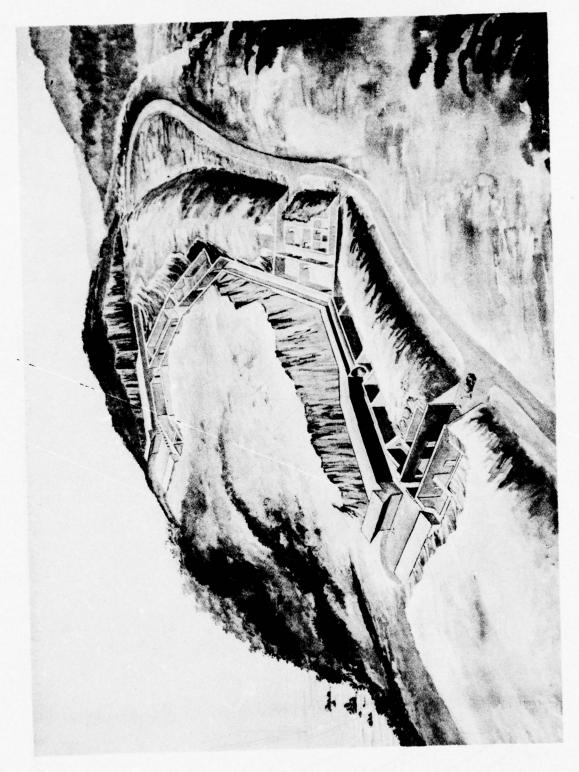


Fig. 1. Cutaway View of the Shock Tunnel Test Facility.

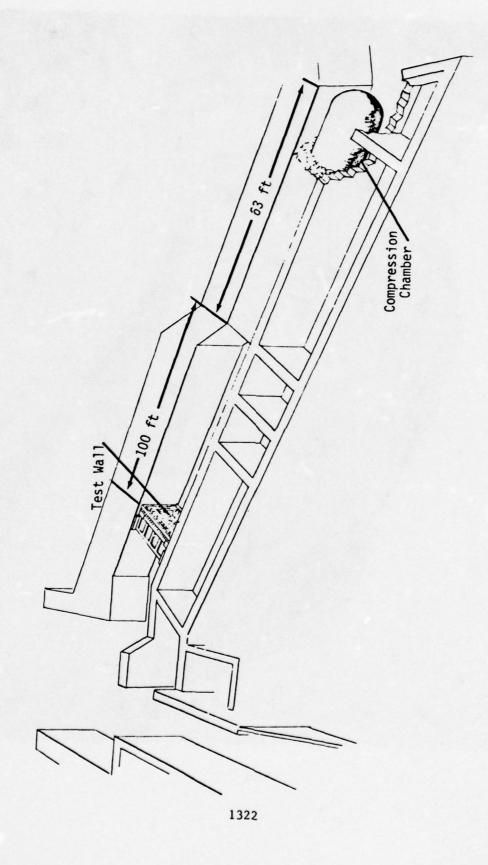


Fig. 2. Cutaway View of Shock Tunnel Showing Wall in Place.

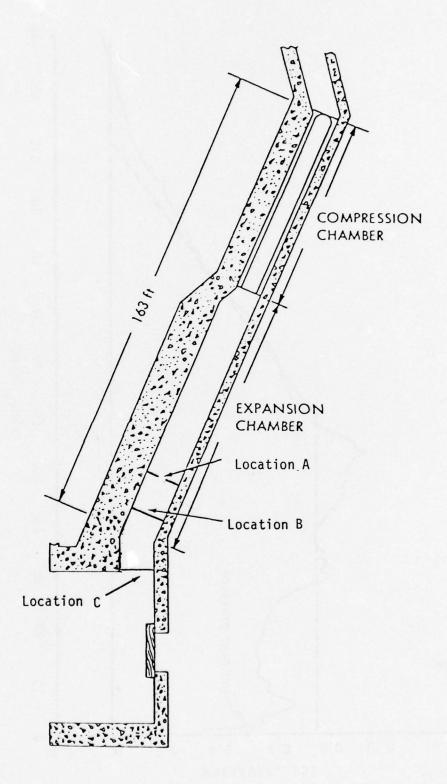
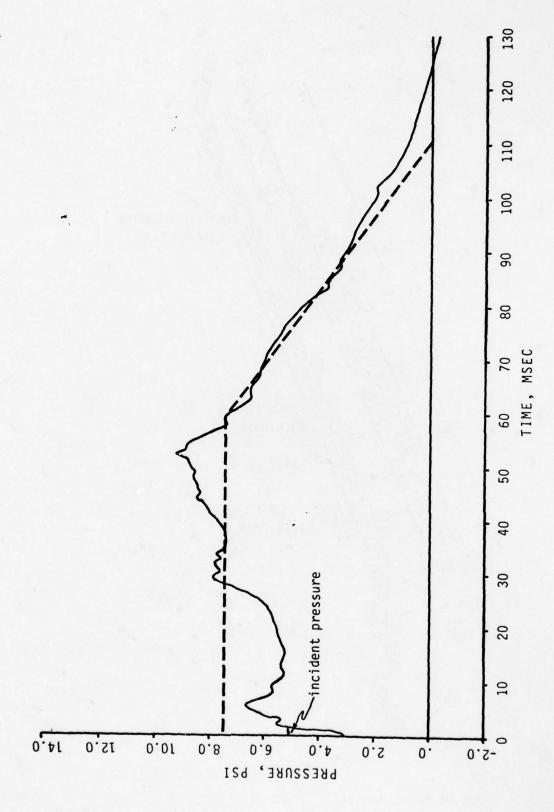


Fig. 3. Plan of Shock Tunnel.



Average Peak Overpressure as a Function of Time on the Back Wall of a Room with a 20 Percent Open Window. Incident Pressure on the Window Wall ~5 psi. Fig. 4.

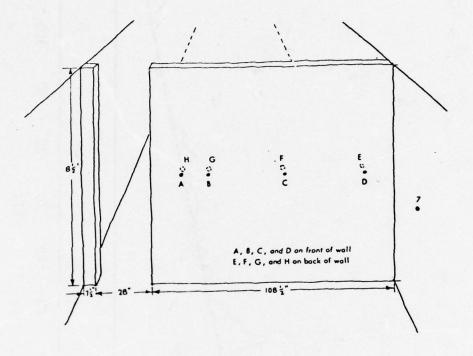
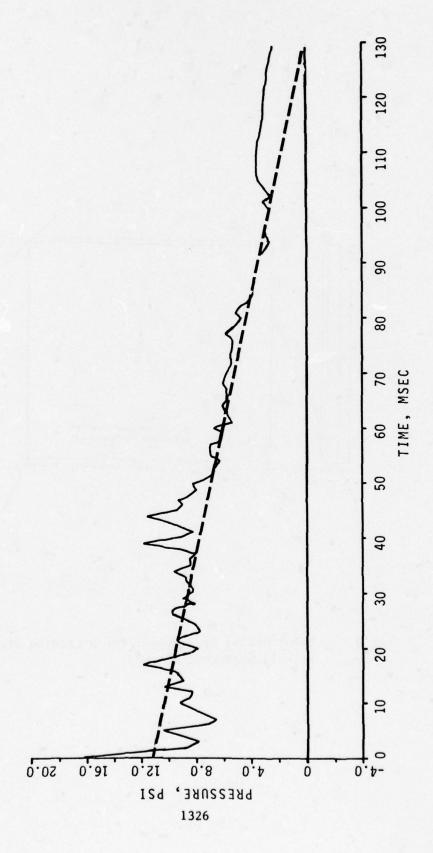


Fig. 5. Experimental Arrangement for a Loading Study Test with 17.5 Percent Doorway.



Average Net Pressure as a Function of Time on a Wall With a Doorway. Fig. 6.

with space above the ceiling for utilities, etc, a similar triangular pulse has been used, the initial value of which is equal to incident pressure.

Four different types of wall mountings are discussed here: cantilevered walls fixed to the tunnel floor; simple beam walls with pin type supports, top and bottom; rigid arching walls that were fixed, or attached, to the tunnel floor and ceiling; and walls attached to the tunnel on all four edges. The first three of these were of unreinforced masonry and are shown in Fig. 7. The last was of sheetrock, with either wood or metal studs.

#### DEBRIS VELOCITY RELATIONSHIPS

# Sheetrock and Cantilevered Masonry Walls

The simplified debris velocity relationships, derived in Ref. 2 for sheetrock and cantilevered masonry walls accelerated by long duration blast pulses are:

for solid walls,

$$v = pt/m; \quad v_f \simeq 7.2p/m \tag{1}$$

for walls with a doorway or false ceiling,

$$v = p[t - (t^2/0.22)]/(1.5m); v_F \approx 3.84p/m$$
 (2)

where:

v = wall debris velocity (ft/sec)

 $v_F \approx$  "final" wall debris velocity at a time  $t_F$  when blast wave acceleration becomes negligible (ft/sec)

p = loading pressure (psi). For interior walls, p = 1.5p;
for exterior walls, p = 2p;

p<sub>i</sub> = peak overpressure in the incident (unreflected) blast wave (psi)

t = time (sec)

m = mass of wall per unit area (1b-sec<sup>2</sup>/ft<sup>3</sup>)

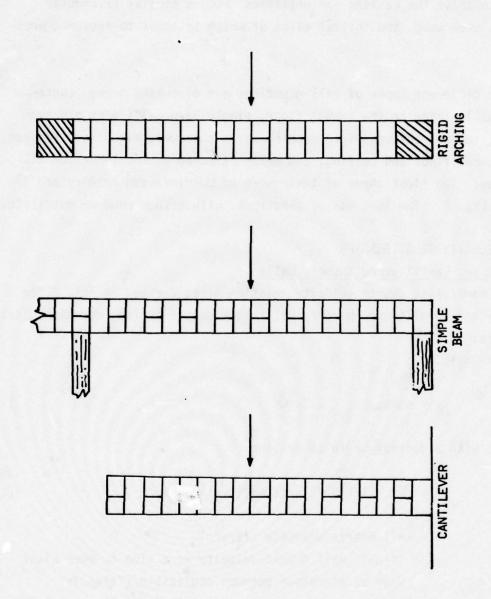


Fig. 7. Types of Walls

While of simple form, predicted values of displacement derived from these expressions correlate quite well with experimental results, as can be seen in Fig. 8 for solid walls, and Fig. 9 for walls with doorways. The experimental values shown in these figures are reduced from high-speed motion picture records. Wall motions were followed from the time of shock arrival until wall elements came to rest on the floor of the tunnel.

## Solid Masonry Walls Mounted as Simple Beams

Analysis of these walls was extended to include the most general case, where a wall is "preloaded", that is, loaded before blast wave arrival with a vertical force equivalent to the weight of bearing walls on top of the wall of interest, in the manner shown in Fig. 10.

Such walls should crack in flexure at their centers, midway between floors, and at each floor level. Then the top and bottom parts of each wall should rotate about their pin supports until "failure" occurs (when the centerline of the wall displaces one wall thickness). After that, the two parts would be free to be accelerated downstream by the blast wave. Because of the initial rotation, the top of the wall acquires an upward velocity immediately after failure, and thus travels further than the bottom of the wall.

The simplified relationships from Ref. 2 for horizontal velocity of debris from solid, masonry, beam-mounted walls, accelerated by long duration blast waves are:

for  $0 < t \le t_f$ : (that is, up to the point of wall failure)

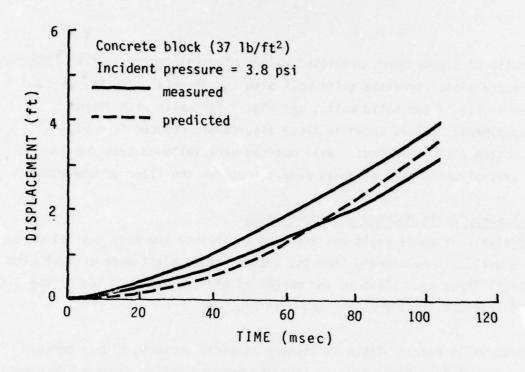
$$v = 108pt/m \tag{3}$$

where:

$$t_f = time to wall failure (sec) = 0.028[m\tau/p]^{\frac{1}{2}}$$
  
 $\tau = wall thickness (in.)$ 

for  $t_f \le t \le t_F$ :

$$v = 3.0 [p_T/m]^{\frac{1}{2}} + p(t - t_f)/m; v_f = 5.0[p_T/m]^{\frac{1}{2}}$$
 (4)



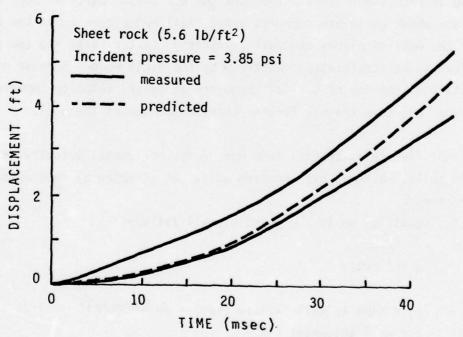
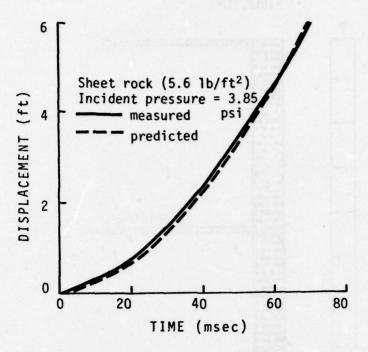


Fig. 8. Debris Displacement vs Time for Interior Concrete Block and Sheet-rock-stud, Solid Walls.



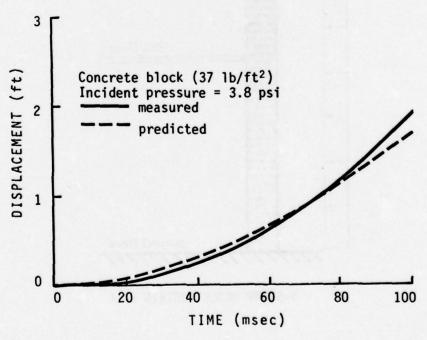
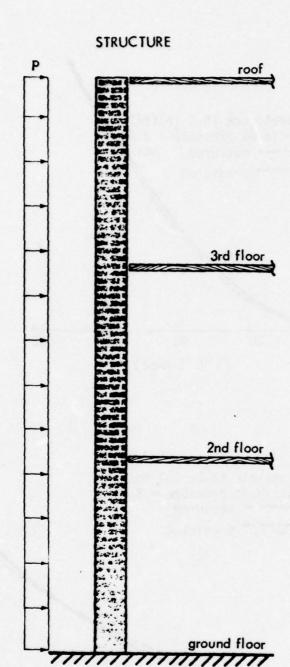


Fig. 9. Debris Displacement vs Time for Interior Sheetrock-stud and Concrete Block Walls with Doorways.



3-STORY BRICK CURTAIN WALL

Fig. 10. Preloading in Bearing Wall Construction

Shock tunnel measurements were made on these walls up to the time of their failure. Thus, to compare measured and predicted displacements, the displacement relationship derived from Eq. 3 applies. Fig. 11 compares measurements made on an 8-in. thick brick wall subjected to a pressure loading of 4 psi, with three predicted values. The two "preload" lines bound the range of in-plane vertical load to which the shock tunnel wall was exposed; the line labelled "simplified" is from the wall displacement vs time relationship derived from Eq. 3.

#### SOLID MASONRY WALLS FIXED IN RIGID MOUNTINGS

A wall confined between rigid supports that prevent in-plane motion and rotation about the supports can display very high resistance to out-of-plane loads through the phenomenon known as arching. Theories of arching were developed more than 20 years ago (Ref. 3, 4), and new theories have more recently been developed to take into account behavior of arching walls observed in shock tunnel dynamic tests, and material properties observed on specially devised static tests (Ref 2, 5).

The wall cracks in flexure at the supports and in the center, and forms a three-hinged arch in the manner shown in exaggerated fashion on the left in Fig. 12. For the wall to fail, wall material at the hinges must fail through crushing or spalling caused by the forces at the hinges which, as shown in the free body diagram on the right in Fig. 12, are directed into the wall or parallel to its face.

As an example of the very large strengths attainable by such walls, an 8-in. thick brick wall (which, mounted as a simple beam, would fail at an overpressure loading of less than 2 psi) withstood overpressure loadings of 13 psi and 15 psi on successive tests, and finally failed at a loading of 20 psi. (See Fig. 13.) The theory based on crushing at the hinge points predicts all observed aspects of arching behavior, including failure at a loading pressure of 17 psi and above for an 8-in. thick brick wall, and the oscillations that occur when a wall does not fail. Fig. 14 compares measured and predicted wall behavior for a second (15 psi) test of the series shown in Fig. 13.

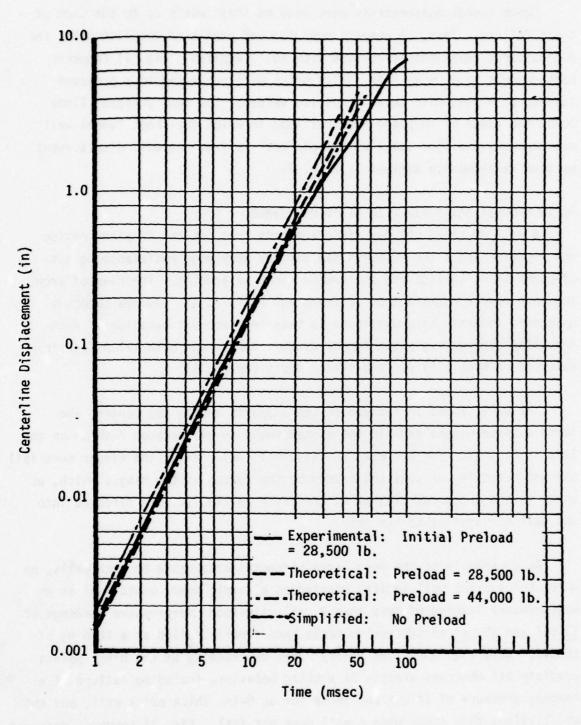


Fig. 11. Experimental and Theoretical Centerline Displacement vs. Time for a Preloaded, 8-in. Thick, Beam-Mounted, Brick Wall Responding to a 4 psi Blast Wave in the Shock Tunnel.

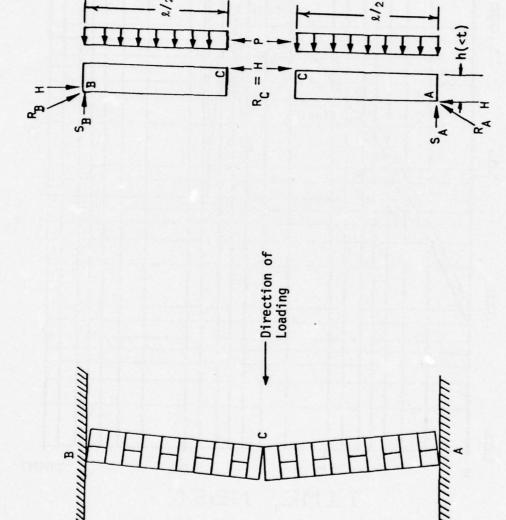


Fig. 12. Rigid Arching Behavior (exaggerated) and Free Body Loading Diagram.

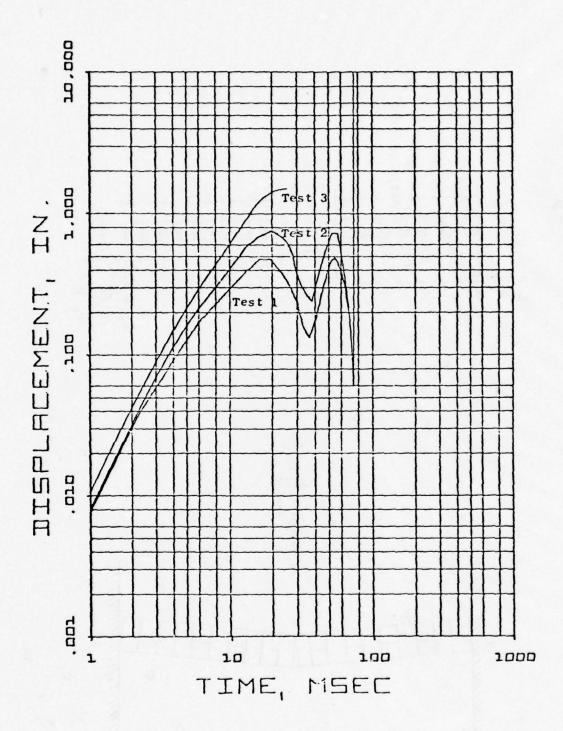


Fig. 13. Displacement as a Function of Time, Wall No. 87, Test 1, 13 psi; Test 2, 15 psi; Test 3, 20 psi.

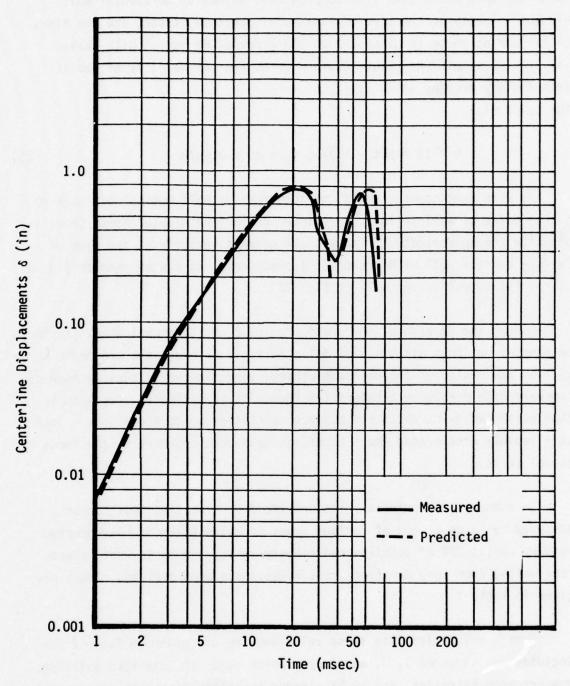


Fig. 14. Predicted and Measured Wall Centerline Displacements for a Rigidly Arching Wall vs Time from Initial Blast Loading.

Wall No. 87, Second Test

Loading Pressure = 15 psi

Loading pressures between 18 and 20 psi (the highest for which calculations were made) give rise to predicted values of horizontal wall element velocity at the time of failure of about 15 ft/sec, and the times to failure at these loadings are on the order of 50 msec. With these values, the simplified relationships for horizontal velocity of debris from rigidly arching walls is:

for  $t_f \le t \le t_F$ .

$$v = 15 + p(t - t_f)/m; v_F = 15 + 3.6p/m$$
 (5)

As with beam mounted walls, measurements of wall motion were made up to the point of wall failure. Predicted centerline displacements compatible with the approximate 15 ft/sec wall element velocity at the time of failure compare well with measured displacements, as can be seen in Fig. 15, of the third test on the wall of Fig. 12.

Though the hazards of the phenomenon have not been evaluated, it should be pointed out that after a wall fails in rigid arching, the crushed material from the center of the wall can achieve very high velocities because of the very high pressures accelerating them. It is estimated, for example, that particles ½-in. thick can achieve velocities up to 400 ft/sec. Such very rapidly accelerated small particles have been observed in the shock tunnel tests.

In summary, approximate relationships for velocities that can be achieved by large pieces of various types of walls (half of beam-mounted masonry walls; 2/3 of cantilevered masonry walls; and up to whole sheet-rock walls) from long duration blast waves, have been derived. These are given in Table 1.

Debris velocities from these relationships are given in Table 2 for incident pressures of 1, 3, and 7 psi, which occur at inhabited building, unbarricaded intraline, and at barricaded intraline distances respectively.

The relationships in Table 1 (and the associated velocities given in

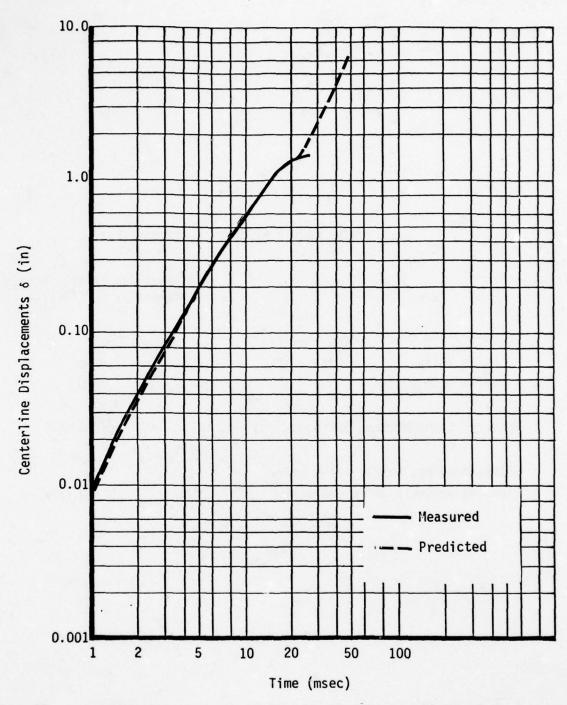


Fig. 15. Predicted and Measured Wall Centerline Displacements for a Rigidly Arching Wall vs Time from Initial Blast Loading.

Wall No. 87, Third Test

Loading Pressure = 20 psi

Table 1

# WALL DEBRIS VELOCITY RELATIONSHIPS\*

Wall Type	Approximate "Final" Debris Velocity, v <sub>F</sub> (ft/sec)
Sheetrock and Cantilevered Masonry	
Solid Walls	7.2p/m
Walls With Doorways	3.8p/m
Masonry, Beam-Mounted, Solid	5.0[pτ/m] <sup>12</sup>
Brick, Arching, Solid, $\tau = 8$ in.	
(loading pressure 18 < p < 20 psi)	15 + 3.6p/m

<sup>\*</sup>  $p = 1.5p_i$  for interior walls; =  $2.0p_i$  for exterior walls  $p_i$  = incident blast wave pressure (psi) m = wall mass per unit area (lb-sec<sup>2</sup>/ft<sup>3</sup>)  $\tau = wall$  thickness (in.)

Table 2

WALL DEBRIS VELOCITIES FOR VERY LARGE QUANTITIES OF EXPLOSIVES\*

ft/sec ure p <sub>i</sub> = 7 psi	445 66 63	235	89 192
Debris Velocity in ft/sec for <u>Incident</u> Pressure p <sub>i</sub> = 1 psi 3 psi 7 psi	191 28 27	101 15	82 88
Debris V for Inci	64 9	34	13
Weight per Unit Area (1b/ft)	5.6 37.0 40.0	5.6 37.0	80.0 37.0
ъ	Interior, Solid 4-in. sheetrock-stud 8-in. concrete block, cantilevered 6-in. clay tile, cantilevered	Interior, Doorway (or false ceiling) 4-in. sheetrock 8-in. concrete block, cantilevered	Exterior, Solid 8-in. brick, beam-mounted 8-in. concrete block, beam mounted
Wall Type	Interior, Some 4-in. slan. con 6-in. con 6-in.	Interior, Do 4-in. sl 8-in. co	Exterior, S. 8-in. bl

\* As a rough approximation, velocities for explosives weighing 1000 lb can be taken as 1/10 the values shown here.

7.5 (18) 8.2 (20)

44

41

80.0

Incident (and Loading) Pressures in psi for Arching Walls

8-in. brick, rigid arching

Table 2) were derived for blast waves with very long durations (on the order of seconds) which were associated with very large quantities of explosives. It was shown in Ref. 2, however, that most of the blast induced forces from these very large explosions are actually imparted to the walls in a relatively short time,  $t_0$  on the order of a tenth of a second or less. This suggests that the blast forces are essentially impulsive, in which case, debris velocity would be related to blast impulse. If  $t_0$  is small enough, the loading pulse from a long duration wave can be considered to be flat-topped, that is, the plot of pressure vs time to to is essentially a rectangle. As the pulse duration decreases, the departure from this rectangular shape can be calculated, until, at a duration of to, the pressure vs time plot would be roughly triangular. (It would actually have a modified exponential shape which is almost triangular for low overpressures.) For durations less than  $t_0$ , impulse imparted to a wall is the same as the reflected blast wave impulse which, for a given peak pressure in the blast wave, scales as the cube root of the explosive weight.

With these considerations, the fraction of the maximum blast impulse imparted to a wall by various weights of explosives can be calculated. Fig. 16 shows three such relationships for the three wall types discussed, using values of  $t_{\rm o}$  from Ref. 2.

Figs. 17 and 18 show debris velocities calculated from the velocities in Table 2, and the reduction factors from Fig. 16, for two incident overpressure levels: 7 psi (barricaded intraline distances); and 1 psi (inhabited building distances). Of course, with very small quantities of explosives, the wall break-up mechanisms on which the relationships in Table 1 are based would no longer occur, and the relationships would no longer hold. At what charge sizes this occurs has not been investigated, but as a caution, the curves for lower explosive weights in Figs. 17 and 18 are shown as dashed lines.

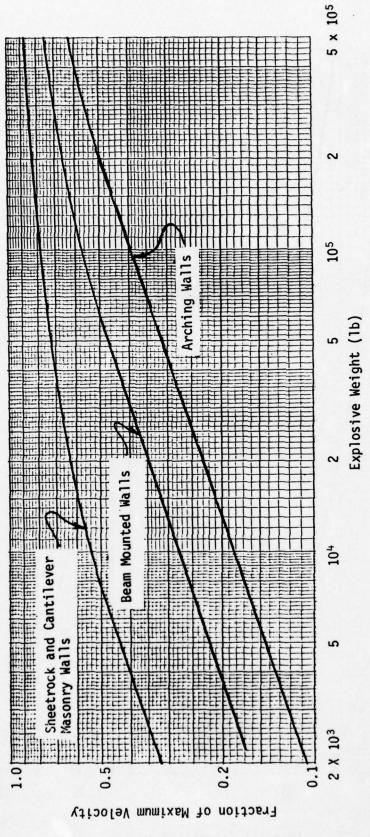
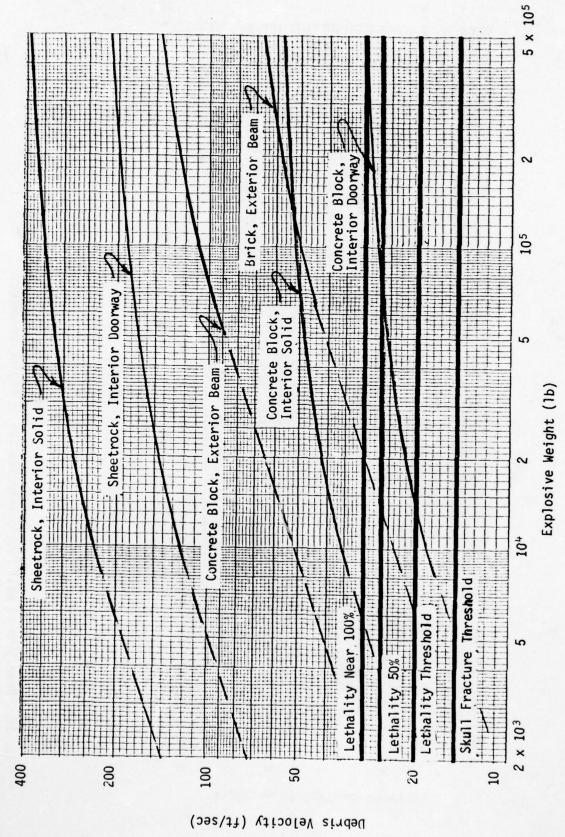
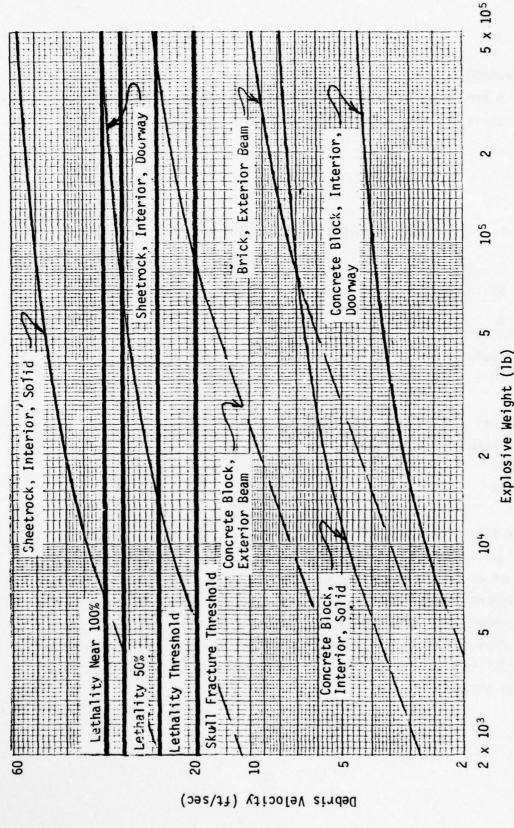


Fig. 16. Reduction of Wall Debris Velocity Due to Explosive Weight.



Barricaded Intraline Distance (7 psi) Debris Velocity vs Explosive Weight; Lethality and Injury Criteria. Fig. 17.



Inhabited Building Distance (1 psi): Debris Velocity vs Explosive Weight; Lethality and Injury Criteria. Fig. 18.

#### MISSILE HAZARDS

Ref. 6 provides, in tabular form, criteria for head injuries from non-penetrating missiles weighing 10 lb or more. These are given in Table 3.

Table 3

HEAD INJURIES FROM SEONDARY MISSILES

Type of Injury	Impact Velocity (ft/sec)
Cerebral Concussion	
Mostly "Safe"	10
Threshold	15
Skull Fracture	
Mostly "Safe"	10
Threshold .	15
Near 100%	23

It is clear from the previous discussion that some (or all) of the "missiles" we have been considering weigh considerably more than 10 lb. (One half of an 8-in. thick brick wall, for example, weighed some two tons.) Probably a more appropriate measure, therefore, of injury (or death) potential from these large missiles is that known as tertiary blast effects, in which a person is thrown against an unyielding surface. According to Ref. 7 (the material is also given in Ref. 6) lethality criteria for total body impact are as given in Table 4.

Table 4

#### TOTAL BODY IMPACT LETHALITY CRITERIA

Lethality Measure	Impact Velocity (ft/sec)
Mostly "Safe"	10
Lethality Threshold	20
Lethality 50%	26
Lethality Near 100%	30

(Tertiary blast effects related to head injuries are as given in Table 3.) Some of these lethality and head injury criteria are plotted on Figs. 17 and 18.

Putting aside for the moment, the effects of sheetrock walls on people, it is clear from Fig. 17 that at barricaded intraline distances, missiles from both interior and exterior masonry walls could be lethal even with relatively small quantities of explosives. Fig. 18 indicates that exterior concrete block walls can cause severe injuries even at inhabited building distances, if explosive quantities are large enough.

Injury and/or lethality criteria that apply to sheetrock walls were not found at the time this paper was prepared, but the <u>very</u> large velocities they can achieve, even at low blast overpressures, are impressive indeed. While their weight per unit area is about 1/7 that of concrete block walls, the velocities they achieve are about 7 times as great. (This tends to confirm that debris velocities are impulse dependent.)

If, however, injury is proportional to the energy of a missile, which seems to be the case, (in Ref. 1, for example, a hazardous missile is defined in terms of its energy) then a light weight sheetrock missile should be far more likely to cause injury than a concrete block missile, since (for the same size missiles) its energy would be about 7 times greater.

#### REFERENCE LIST

- --"DOD Ammunition and Explosives Safety Standards", DOD Standard 5145.4S, Department of Defense, Office of the Assistant Secretary of Defense (Installations and Logistics), Washington, D.C., March 1976.
- Wilton, C., K. Kaplan, B. Gabrielsen, J. Zaccor, "Blast/Fire Interaction, Blast Translation, and Toxic Gases", SSI 742-8, Scientific Service, Inc., Redwood City, California, 1976 (in publication).
- 3. McDowell, E.L., K.E. McKee, E. Sevin, "Arching Action Theory of Masonry Walls", ASCE Journal of the Structural Division, Proceedings Paper 915, March 1958.
- McKee, K.E., E. Sevin, "Design of Masonry Walls for Blast Loading", ASCE Transactions, Paper No. 2988, Volume 124, 1959.
- Gabrielsen, B.L., C. Wilton, "Shock Tunnel Tests of Arched Wall Panels", URS 7030-19, URS Research Company, San Mateo, California, December, 1974.
- 6. C.S. White, "The Scope of Blast and Shock Biology and Problem Areas in Relating Physical and Biological Parameters", Annals of the New York Academy of Sciences, Volume 152, Art. 1, October 28, 1968.
- White, C.S., I.G. Bowen, D.R. Richmond, "Biological Tolerance to Air Blast and Related Biomedical Criteria", <u>USAEC Report CEX-65.4</u>, 1965.

#### SURVIVABILITY IN A NUCLEAR WEAPON ENVIRONMENT

A. Longinow, A. H. Wiedermann, E. E. Hahn IIT Research Institute, Chicago, Illinois

L. E. Bertram Sandia Laboratories, Albuquerque, New Mexico

### INTRODUCTION

This narrative describes a computer simulation model which was developed for predicting the survivability of people located in conventional buildings when subjected to the prompt effects of nuclear weapons. Prompt effects considered include thermal radiation, prompt nuclear radiation, primary and secondary blast. The formulation of the model, its physical basis and usage are discussed, and representative results are described by means of an example problem.

This simulation model was developed for civil defense purposes and specifically for the rating of existing buildings in terms of inherent protection afforded. Therefore the usage of this simulation model is discussed herein in civil defense terms. However, the overall methodology produced can also be used for the assessment of primary and collateral damage resulting from a nuclear weapon attack.

The empahsis here is on casualty mechanisms produced by secondary blast effects, i.e., diffraction loadings and blast winds. Only the models used in predicting and quantifying these casualty mechanisms are described in detail. Simulation models used for predicting casualties due to thermal radiation, prompt nuclear radiation and primary blast are described in general terms. For a more detailed description of these models, the reader is referred to Refs. 25 and 15. The following paragraphs provide a brief discussion of the relationship of this work to previous studies in this area.

## BACKGROUND

Casualty/survivability studies are performed for the purpose of damage assessment and for designing or evaluating alternative shelter systems. Initial efforts in this area relative to a nuclear weapon environment were performed following the detonation of the first nuclear device. Shortly after World War II, the U. S. Strategic Bombing Survey teams examined casualties

and destruction at Hiroshima and Nagasaki with the object of determining the effects of nuclear weapons on these two cities. A large quantity of information was collected and included data on casualties and structural damage. These data were analyzed with the object of establishing damage-distance relationships. As a result a median lethal radius corresponding to an overpressure of 7.0 psi for the 13 KT airburst was established. Fatalities in general were taken to be the result of initial nuclear radiation, blast, thermal radiation, and fires. In subsequent time periods attempts to establish how these effects broke down were made by numerous individuals (e.g., Ref. 12). The results, however, were in general sketchy and not entirely conclusive. Further, relationships for extrapolating effects from low-yield airbursts to high-yield near-surface bursts are not as yet established nor necessarily capable of being established.

In the 1950's a series of nuclear weapon field tests were conducted (Ref. 3). Subjects of these tests were full-scale structures, scaled structures, structural components, and animals. This was followed by high explosive (HE) tests on similar subjects. Since then a great deal of effort was devoted to the simulation of weapon effects mostly in the laboratory. Concurrently with experimental studies, analysis methods aimed at predicting casualties based on weapon effects and associated casualty mechanisms were initiated. In the civil Defense sector of this subject area the work of Smith (Ref. 34), Childers (Ref. 6) and Heugel and Feinstein (Ref. 20) was included. The method described herein is a revision/update of that originally formulated in Ref. 20.

### EMPHASIS OF THIS SIMULATION MODEL

The civil defense planner must have knowledge of the best available shelter space in his community. Conventional buildings constitute the only significant, current sheltering resource. Each building has some level of inherent ability to provide protection from the effects of nuclear weapons, and also natural disasters such as earthquakes, tornados and hurricanes. It is important to have reliable and readily usable knowledge on their protective capabilities and on the possible types of evasive action that can be taken by personnel to gain full advantage of these capabilities in any emergency situation.

Buidlings of primary interest to the civil defense planner are those which contain substantial numbers of people for significant portions of the day. Representative types include large, multistory, reinforced concrete or steel framed buildings, combination reinforced concrete shear wall and framed buildings, load-bearing buildings, and combination load-bearing and framed buildings.

Framed buildings with weak walls are for the most part diffraction sensitive, i.e., when interacting with the blast wave the walls are expected to fail and be removed early in the loading history with the frame remaining essentially intact. In the upper stories, hazards to occupants in a nuclear blast environment are due to thermal radiation, prompt nuclear radiation, blast diffraction, high velocity winds and debris from the breakup of walls, partitions and furniture. People located in unprotected areas are expected to be translated by the blast winds and experience impacts with the floor, walls, debris and/or the ground surface. In deep basements the hazards are primarily due to nuclear radiation and debris from the breakup of the overhead slabs.

The simulation model described is capable of considering low- and highrise framed and partially framed buildings and determining the extent of survivability afforded with a fairly high degree of confidence. It is not capable
of treating load-bearing buildings with the same level of confidence. Loadbearing buildings are expected to collapse catastrophically once the structural (load-bearing) walls fail. Although in load-bearing buildings with
large or moderate window sizes, blast translation of personnel will pose a
serious hazard prior to the failure of walls, debris casualties produced by
the breakup and collapse of the structure are expected to be at least as significant.

In evaluating the survivability potential in buildings, this simulation model considers only the prompt effects which occur in the Mach region of a nuclear weapon. These effects, corresponding casualty mechanisms, and types of casualties considered in this analysis process, are listed in Table 1 in the order of event.

- 4. Secondary Blast (Diffraction and Dynamic Pressure)
  - Translation -----> Impact Casualty ------> Head, Whole Body

  - Acceleration ———> Whole Body Acceleration Casualty

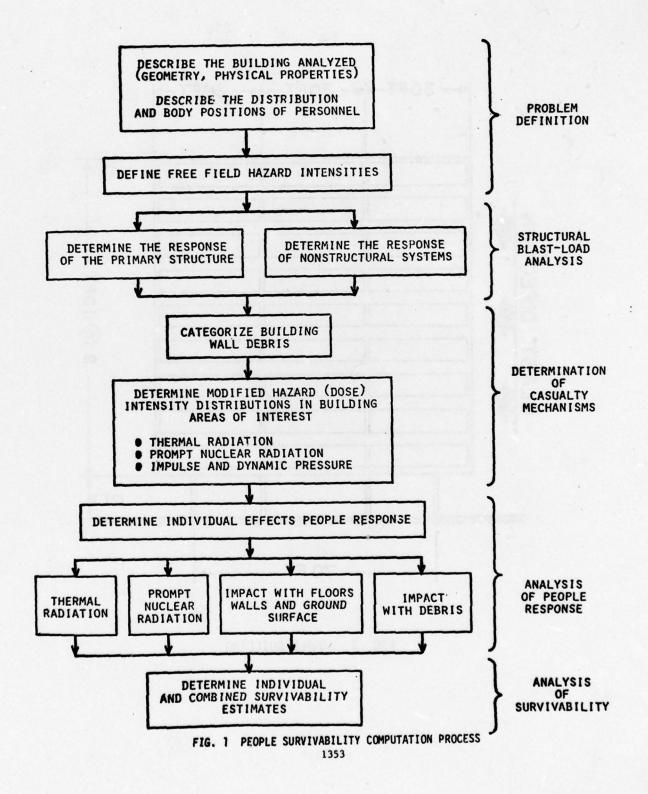
This simulation model does not make a distinction between injured and uninjured personnel in its predictions. Numbers of survivors based on several general, major categories of trauma are predicted (see Table 1). Survivors include those persons who are expected to live (survive) at least one week after the event provided that basic rescue operations are carried out and injured survivors are removed to areas conducive to recovery. Influence of fires which may occur subsequent to the prompt effects is not considered.

The ultimate usage of results obtained from this analysis is to provide for reliable on-site assistance at the local civil defense level. The results would take the form of a concise building classification scheme which would be used for the rating of buildings in terms of their inherent protective capabilities and thus provide for the optimum distribution of the local population within them in the event of an emergency.

The simulation model is specifically oriented for predicting people survivability in a direct effects nuclear weapon environment. As such, in addition to being able to provide shelter information for the civil defense planner, this methodology can also be used by the damage assessor to assess primary and collateral damage resulting from a nuclear weapon attack.

#### PEOPLE SURVIVABILITY SIMULATION MODEL

The computational process used in this simulation model is described in Fig. 1, and a typical application is illustrated in Fig. 2. This is an elevation view of a ten-story, reinforced concrete framed building.



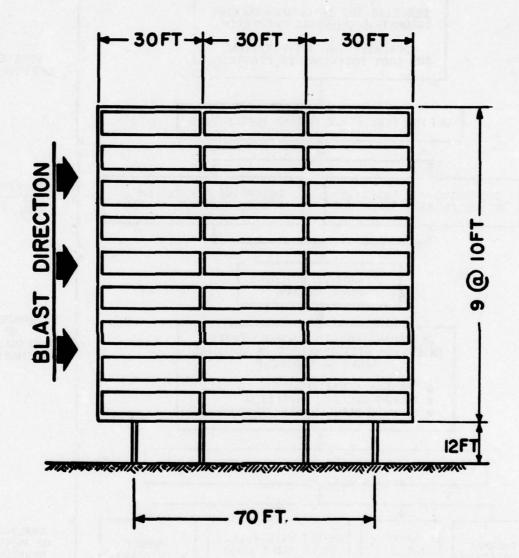


FIG. 2 SAMPLE BUILDING

<u>Problem Definition</u>.— The building to be analyzed is described in the terms of overall and room geometries, type of structural system, relevant nonstructural systems (exterior curtain walls, interior partitions) and the distribution of building mass. Data also include information on window sizes, sill heights and types of interior window covering.

Information on people located within the building is provided in terms of their distribution in various building areas and their initial body positions, i.e., standing or prone.

The hazard environment is specified in terms of a single weapon, its size, height of burst, and range to ground zero. This information is used to determine the time-dependent free field intensities of thermal radiation, prompt nuclear radiation, overpressure and dynamic pressure at the building location.

Structural, Blast-Load Analysis.— The structural analysis portion of the process is a separate computation. Its purpose is to determine the onset of debris effects should this be important at the given overpressure level. Debris is defined as any structural or nonstructural component that separates from the building as a result of blast wave passage. For most framed buildings of interest, in the relevant range of overpressures, this includes exterior walls, interior walls and partitions, and slabs over basements. Glass fragments and furniture items are not considered in the present model.

The structural analysis uses procedures such as described in Ref. 40. It determines incipient collapse overpressures, times to collapse and average velocities at collapse for exterior walls, interior walls and partitions, and slabs over basements. A check is made to see if the particular failure mode is the lowest for the particular structural system considered.

Masonry (brick, concrete block, clay tile) walls break up into a series of fragments when their incipient collapse overpressures are exceeded. In the analysis process, probable crack patterns, number of pieces, sizes and their location prior to separation that are expected to be produced by a given masonry wall are estimated based on full-scale experimental results (Ref. 14). Available experimental results indicate that initial crack patterns for masonry walls generally follow classic yield lines. Reinforced concrete components (walls, floor slabs) are also assumed to separate along major yield lines.

Determination of Casualty Mechanisms and Analysis of People Response.—
A set of routines is provided to determine the intensities of individual effects and casualty mechanisms that are experienced by personnel in the building analyzed.

- Thermal Radiation: Thermal energy incident in each room facing the direction of blast is determined by modifying the intensity of the free field thermal energy by the presence of window glass, curtains, window sills, and neighboring buildings. Resulting intensities are applied uniformly to occupants in affected portions of respective rooms.
- Prompt Nuclear Radiation: The intensity of prompt nuclear radiation incident in a given building area (upper stories or basements) is determined by modifying the free field intensity by the use of building mass and geometry. Resulting intensity is then applied uniformly to the occupants in the given building area.
- Interior Blast Winds: By making use of free field blast wave characteristics, building geometry, window sizes, sill heights, room geometries, incipient collapse overpressures for walls and interior partitions, diffraction impulses and dynamic pressure-time histories are computed at specified locations in the room(s) analyzed.
- Debris: Using previously determined wall fracture patterns, times to incipient collapse and average velocities at collapse, this routine determines trajectories for each debris piece comprising a given wall. Use is made of a two-dimensional (vertical plane) trajectory model which includes both the translational and rotational motions of a given piece of debris which are induced by the aerodynamic forces generated by the blast winds. Once separated from the wall, debris pieces are assumed not to break up while in flight. Also, possible interaction between debris pieces while in flight is ignored in the present procedure. Information computed includes displacements, velocities and accelerations of each debris piece.
- Blast Translation and Impact of Personnel: This routine determines the types and magnitudes of impact velocity experienced by personnel located within the building when subjected to blast winds and debris from the breakup of walls.

Blast loadings (diffraction impulses and dynamic pressure-time histories) determined previously are applied to individual persons. Individuals are

simulated using a two-dimensional (vertical plane) free-flight model. Individual trajectories are computed and impact velocities (head and/or whole body) with walls and/or floor and/or ground surface are determined for comparison with casualty criteria.

Previously computed debris trajectories are compared with corresponding people trajectories for the same time intervals to see if interactions occur. If an interaction occurs, the relative velocity between man and debris at the point of contact is determined for comparison with casualty data. Types of interactions considered include contact with head, thorax, abdomen or limbs. Possible people with people interactions while in motion are not considered.

<u>Analysis of People Survivability</u>.— A routine is provided to relate each of the computed hazard (dose) intensities to corresponding casualty criteria. These criteria are contained within the simulation model and are described:

- Thermal Radiation: The thermal pulse producing second and third degree burns resulting from direct exposure of the skin, reradiation and ignition of clothing and subsequent burning of the skin is considered. The probability of mortality is then related to percent of body area burned (Ref. 1 and 31).
- Prompt Nuclear Radiation: Radiation casualties from initial gamma and neutron radiation are determined in extrapolating animal data based upon Hiroshima and Nagasaki results. The mean lethal dose (50 percent probability of mortality) was estimated at 500 REM (Ref. 8,16,18 and 33).
- ullet Primary Blast: Blast casualties due to fast rising overpressures are based on data collected from animal experiments and extrapolated by weight of species. This resulted in an estimated LD<sub>50</sub> (mean lethal overpressure) of 75 psi for man (Ref. 7,10,21,29 and 39).
- Blast Translation: Translation of people by the blast winds can cause casualties with resulting impacts on hard surfaces. Impact data from animal experiments, related human free fall accident experience, and skull impact experiments resulted in mean lethal velocities for two types of impacts; head and whole body (Refs. 28, 37 and 29). The mean lethal velocities for man are estimated at 18 ft/sec for head impact and 54.4 ft/sec for whole body impact.
- Debris: Blast generated debris from building walls and contents accelerated by the blast winds may cause casualties. Three debris mechanisms were

identified (Ref. 15): impulse loading related to debris momentum (MV); crushing or tearing related to debris energy (MV $^2$ ); and cutting or penetration related to energy times the square of the velocity (MV $^4$ ). Wound data for human cadavers and animals were reviewed (Refs. 4,19,22,26 and 30) and casualty criteria developed as function of mass and velocity of the debris particles.

• Acceleration: Persons in direct line of the blast jet as it enters a building are subject to possibly harmful accelerations without translation. The mean lethal dynamic pressure (q) as related to acceleration casualties is estimated at 8.7 psi (Refs. 6 and 17).

After considering these effects in context of given building parameters, the model arrives at probabilities of mortality for each effect for the building occupants. Combination of the separate effects results in a combined effects survivability estimate for the building as a whole or for various areas of interest.

# BLAST WIND MODEL

Brode's equations for the free field conditions in the Mach region of a nuclear blast (Ref. 5) may be used to estimate winds and pressures in and around an isolated building on which the blast impinges. The coupling between flowfield and failing building elements constitutes a novel feature of this analysis.

Since a point in the free field experiences a pressure-time history consisting of a shock wave which produces an overpressure  $\Delta p$  over ambient pressure  $p_i$ , followed by an exponential decay of p(t) over the "positive phase" duration  $t_{p}^{\dagger}$ , it follows that the pressure-time history in a particular room exposed to this blast will consist of a shock wave increase in pressure due to shock penetration through window or door orifices followed by a short period of "filling" of the room by outside air until the room pressure equalizes with the exterior pressure. After all rooms in a particular story have reached nearly free field pressure, the flow through the story will be retarded only by the viscous dissipation of the subsonically (incompressibly) flowing air. This "flow through" phase will then persist throughout the positive phase t Typically, 1  $\sec \le t_n^+ \le 4$   $\sec$ , and a single room with no outflow at the rear has a filling time  $t_f \simeq V/kA$  where V = volume of room (ft<sup>3</sup>), k = 2 ft/msec, and A =area of orifice (ft<sup>2</sup>), giving a typical order of magnitude of 10 msec. Thus, the most significant wind-delivered impulses will be those occurring during the flow through phase.

With the flow through phase being dominant, the temptation arises to ignore the shock penetration and filling phases altogether, but this cannot be justified since the peak pressure differentials across walls occur during these phases. Wall failures are initiated by the early-time loading, and this analysis must be included to set the cracking times,  $\mathbf{t}_{\mathbf{c}}$ , of the walls. Once a wall is cracked, the model assigns as immediate loss of 15 percent of its area, and the remainder is removed by falling, so that the orifice area  $\mathbf{A}(\mathbf{t})$  of a wall of height H and width W, which originally had an orifice (window or door) of area  $\mathbf{A}_{\mathbf{0}}$ , becomes

$$A(t) = A_0 + \left[0.15 + g(t - t_c)^2 / 2H\right] + W 1(t - t_c)$$
 (1)

where g=32.2 ft/sec<sup>2</sup> and  $1(t-t_c)$  is the Heaviside unit step function. It should be noted that equation (1) represents a lower bound on the rate of removal of failed walls, since it ignores the streamwise separation of wall elements as they are moved downstream. Also, because A(t) has a time scale of  $(H/g)^{\frac{1}{2}}=0.5$  sec, comparable to  $t_p^+$ , while the flow adjustment time is on the order of the room filling time, there is no need to track expansion waves produced at initial wall crackings, which provide only negligible perturbations on the quasi-steady flow impulse.

In addition to the flow through wind impulse, occupants of the room will experience shock-imparted impulses, once from the incoming shock wave, plus, depending on position in the room, possibly from the shock reflected off the rear wall. The many possible secondary diffracted shocks and impulses delivered by the high-speed but short duration jet flows of the filling phases are all crudely lumped with the shock penetration impulses by assigning

$$I = I_F + (x - x_F) I_R/L$$
 (2)

as the total impulse I delivered to an object at distance x from the front of the building. Here  $\mathbf{x}_F$  is the position of the front wall of the chamber, L is the chamber length, and  $\mathbf{I}_F$  and  $\mathbf{I}_R$  are the impulses imparted by the forward propagating and reflected shocks, respectively. Details of this computation are given in Ref. 25.

The flow through phase winds are in the incompressible flow range for any problem in which the building has not been totally destroyed, so they are modeled using conventional orifice plate coefficients (Ref. 36). To determine

the flow through a chain of orifices representing a story, one must know the driving pressure drop front-to-rear on the building. This is specified by assigning a wake pressure  $p_{\omega}(t)$ ;

$$p_{w}(t) = p_{ff}(t) + C_{d}(q_{ff} - q_{w})$$
 (3)

where  $C_d$  = -0.4 is the "drag coefficient" for flow over a solid block (Ref. 18) and  $q_{ff}$  and  $q_w$  are the dynamic pressures of free field and wake, respectively. The form of equation (3) is chosen to obtain appropriate limits for flow through a story with walls gone (where  $q_{ff} = q_w$ , so that  $p_w = p_{ff}$ ) and for a story with no flow through it due to solid walls (where  $q_w = 0$ , so that  $p_w = p_{ff} + C_d q_{ff}$ ). With these assumptions, a quadratic equation results for the volume flowrate Q(t) through the story:

$$\left\{ \sum_{i=1}^{NB1} \left[ r_1^2 (-1 + 1/\alpha_i^2) / C_V^2 + (2r_{i+1}^2 - 2r_i r_{i+1} / \alpha_i) \right] + 2 - C_d \right\} U^2 - 2u + C_d = 0$$
(4)

where i is the wall index = 1,2,...NBl with NBl = number of bays in story + 1;  $r_i = A_{ext}/H_iW_i$ ;  $\alpha_i = A_i(t)/H_iW_i$ ; and  $U = Q(t)/V_{ff}A_{ext}$  with  $V_{ff}$  = free field velocity of flow and  $A_{ext}$  = area of upstream exterior face of story, including frame area. The coefficient of velocity for the orifices is  $C_v$ . Note that the flow is coupled to wall failures through the time dependence of  $\alpha_i(t)$ , computed from equation (1).

Once the flowrate at each station is determined from equation (4), a jet flow geometry can be specified (Ref. 25) and the interior dynamic pressure q(x,y,z,t) is known. Aerodynamic loading on objects and occupants can be computed, and the impulse from equation (2) gives initial velocities.

When the very open construction of the sample building in Fig. 2 is considered, the interior winds can be obtained as a special case analytical solution. Specifically, the absence of the rear walls removes the reflected shock impulse, and there is no filling phase duration. The large constant area orifices imply a constant solution to equation (4), so that the interior wind is simply a constant factor times the free field wind.

Extensions of the interior wind analysis would be desirable in two directions: effects of nearby structures should be included if urban areas are to be realistically simulated; and the free field winds of natural origin should be considered.

The blast problem for groups of buildings contains several features for which wholly new models will have to be developed. Considering that separation distances will typically be less than building heights, it becomes clear that all shocks to which a building is exposed will be diffracted shocks. Thus, no simple free field exists below roof level. Secondly, a high density of windborne debris can be expected, producing intense, hard-to-analyze loads on upwind surfaces. In short, a statistical, highly-parameterized approach would be necessary, perhaps based on Monte Carlo runs of deterministic models of type used here.

### PERSONNEL RESPONSE MODEL

Several simulation models have been used to predict the response of building occupants in a blast wind environment. Two of these are illustrated in Fig. 3.

Originally, a simple rigid block free to translate and rotate in two dimensions (vertical plane) was used to simulate the gross response of a person when subjected to blast loading. Its basic geometry is an indicated in Fig. 3a. The simulated person is defined by four corner points such that points 3 and 4 define the head. The dashed line is used to identify the front and the back of the individual in the plotted output.

Under the action of blast loading a person would be subjected to diffraction, drag, lift and contact forces. Contact forces come into play when impact with the floor, wall or the ground plane occurs. Diffraction loading occurs when the shock front interacts with the individual and lasts approximately for the time required for the wave to clear around him. Drag (D) and lift (L) forces are assumed to as as indicated in Fig. 3a.

$$D = q(t) A_d(\theta)$$
 (5)

$$L = q(t) A_o(\theta)$$
 (6)

Where q(t) is the dynamic pressure of the flow and  $A_d$ ,  $A_\ell$  are the position-dependent drag and lift areas respectively. The particular dynamic pressure-time history used in any one case is the free field dynamic pressure modified by dominant local conditions such as building geometry, aperture (window and door) size and location, and room geometry. Drag and lift areas are computed using the relationships:

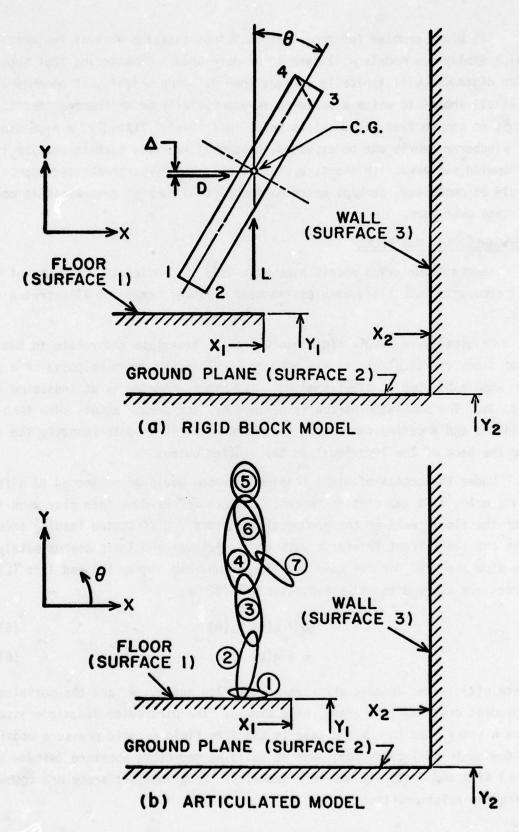


FIG. 3 MATHEMATICAL MODEL OF MAN 1362

$$A_{d} = A_{dmin} + (A_{dmax} - A_{dmin}) \sin^{2}(\theta - \pi/2)$$
 (7)

$$A_{\ell} = A_{\ell max} \sin(2\theta - \pi)$$
 (8)

Rotation is produced because the drag force is assumed to act through the center of pressure, i.e., the center of projected area (Fig. 3a) and thus has an eccentricity, relative to the center of gravity. The lift force is assumed to act through the center of gravity and therefore has no associated eccentricity.

The final set of forces which may act on the individual are contact forces due to impact with a horizontal or vertical surface. Contact forces are assumed to occur at corner points only. The force generated during contact is taken to be deflection and deflection-rate-dependent. The deflection is defined as the maximum perpendicular distance that the corner of the block extends into the contact surface. This force tends to push the block outward perpendicular to the contact point. A tangential force also may be generated during contact, which is considered to be a frictional force. Its value is proportional to the value of the normal force and its direction depends upon the tangential velocity vector existing between the block and the impacted surface. The approach used in determining contact forces is similar to that described in Ref. 2. The simulated individual can contact three surfaces described by coordinates  $X_1, Y_1, X_2, Y_2$  in the fixed global coordinate system. The two horizontal contact surfaces represent the building floor and the ground plane. The vertical surface represents a wall which has not yielded at the time contact is made.

In the more recent simulation model (Ref. 23) the individual is represented by means of seven elliptical cylinders interconnected at six flexible joints as shown in Fig. 3b. Since only planar motions are allowed, this results in 21 degrees of freedom. As in the case of the rigid block model, forces acting on any element of the simulated man include gravity, joint, contact, aerodynamic and pressure forces. The gravity force is merely the weight of the element directed in the global negative Y direction. Each element has springs resisting motion in the local X(I) and Y(I) directions as well as torsional springs resisting rotation at each joint associated with the element. The total stiffness at a joint consists of a combination of the stiffnesses associated with the two elements joined. Force-deflection characteristics of the springs are general piecewise linear functions.

Normal and frictional contact forces acting between an element and the three possible contact surfaces are modeled as piecewise linear functions of the contact interference volume. They are assumed to act through the centroid of this volume. The contact interference volume is defined as the volume of an element that would extend beyond a contact surface if there were no deformation. Different functions are used for deformation and restoration.

Initial velocities can be applied to all or several components of the model. Aerodynamic forces are determined for each element using equations (5) and (6). The dynamic pressure is obtained for each element using its own velocity and wind parameters. Effective drag and lift areas are computed using equations (7) and (8).

Physical data describing the size, weight and joint positions of the elliptical elements were obtained from Refs. 2,9, and 13. These data correspond closely with the fiftieth percentile American male. Surface contact force and joint torsional spring data are approximately the same as those used in Ref. 2. Since a "hard stop" was used at the ends of the range of normal motions of the joints in this reference, these torsional spring data were altered to approximate the large increase in the stiffness at these positions. Deflections in this range would ordinarily indicate injury, probably fatal in the case of the neck joint.

Figure 4 illustrates typical results using the two models. In this example a standing individual at a large window (not shown), with his back to the direction of blast is subjected to an overpressure at the range of 10 psi. Partial trajectories are given at increments of 0.1 sec. For the particular problem and physical data used, the gross response of the individual is essentially the same for both models. The articulated model provides more information on the probable casualty state of the individual.

Parametric studies utilizing the rigid block model have been conducted to examine the sensitivity of the first impact conditions on the statistical variation of parameters such as weight, height, width, moment of inertia, areas, and location of center of gravity. Generally impact conditions are not very sensitive to expected parameter variations. The validity of multiple impact conditions is indefinite due to the uncertainty of the response detail during the initial contact, and the somewhat unrealistic assumption of a rigid body.

Development of the articulated man model represents an attempt to overcome such limitations and uncertainties. However it is not clear that any real gain in the quality of the transport information or the details of the impact conditions is obtained. A more realistic motion appears to exist and a better geometric appearance is evident. Nonetheless the substantial increase in the number of degrees of freedom used to describe the motion requires the introduction of a rather large number of connection parameters, the character and values of which are not well defined. The magnitudes of the aerodynamic forces acting on each element of the model are complex functions of the collective orientation of all the elements. These shielding and interaction effects have not yet been adequately described. Under some conditions, voluntary internal forces may exist and thus influence certain aspects of the motion. For example, instead of the man falling over he may literally run with the wind or just squat down on the floor.

## ILLUSTRATION OF THE PEOPLE SURVIVABILITY ANALYSIS PROCESS

The use of the analysis process is illustrated by applying it to the analysis of people survivability for the building shown in Fig. 2 when subjected to the prompt effects of a single, IMT surface burst. Results are obtained for a range of distances from the building to the point of detonation.

Figure 2 shows an elevation view of a ten-story steel frame building which is assumed to be located in the open and "sufficiently" removed from other structures in the area so as not to be affected by them during the passage of the blast. Stories from the second through the tenth are identical. The typical floor plan is shown in Fig. 5. The first story floor plan is essentially the same except for its smaller size as indicated in Fig. 2.

Data required by a people survivability analysis include building data and people data. Required building data include; building geometry, materials, type of structural system, strength of the primary structure and of the critical building components when subjected to the postulated blast environment and amount of shielding provided by window covering. People data required for analysis include; number of people, their distribution and initial body positions. Building data for the subject building are given in Table 2.

Building strength data required for the analysis include failure (incipient collapse) strength of the building frame, exterior walls and interior partitions. Failure strength in each case is arbitrarily expressed in terms of

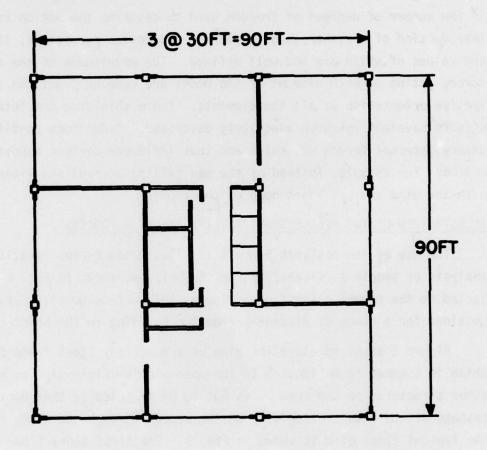


FIG. 5 TYPICAL UPPER STORY FLOOR PLAN

## 1. Building Description

Number of stories

10

• Floor area per story - 8100 sq ft total

7200 sq ft usable

• Building height

- 102 ft

• Type of construction - Steel frame, steel deck, masonry walls and

interior partitions

## 2. Exterior Walls

Story	Description	Strength*
1	Glass	0.5 psi
2 to 10	4-in. and 8-in. brick non-load-bearing walls inset in the frame	9.1 psi

## 3. Interior Partitions

Story	Description	Strength*
1 to 10	8-in. nonreinforced concrete masonry	4.0 psi

## 4. Windows

Story	Window Size	Sill Height
1	12-ft by 30-ft	0-ft
2 to 10	7-ft by 30-ft	3-ft

<sup>\*</sup>Incipient collapse overpressure based on normal to the plane of the wall blast loading.

the corresponding peak free field overpressure at the site of the building referenced to the given weapon yield. Correspondence between peak overpressure, peak dynamic pressure and range to ground zero for a 1MT surface burst is provided in Table 3.

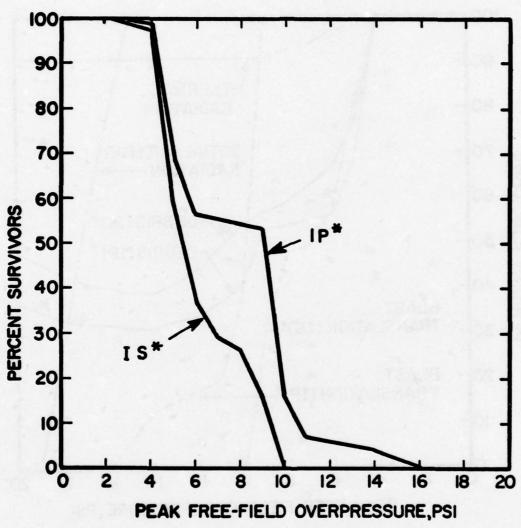
Table 3.—IMT Surface Burst Blast Characteristics

Peak Free Field Overpressure, psi	Peak Free Field Dynamic Pressure, psi	Range to Ground Zero, Miles
4	0.37	3.14
8	1.44	2.08
12	3.13	1.67
16	5.38	1.44
20	8.14	1.29

As indicated in Table 2, upper story building walls facing the direction of blast (Fig. 2) are estimated to be at the point of incipient collapse at 9.1 psi. Corresponding overpressure for the interior partitions is 4 psi. This is a framed building with moderately strong walls, though large window areas and is therefore considered to be primarily diffraction sensitive. For the range of overpressures relevant to this problem (up to about 16 psi) the building will lose its windows, exterior walls and interior partitions. However the building frame is not expected to collapse.

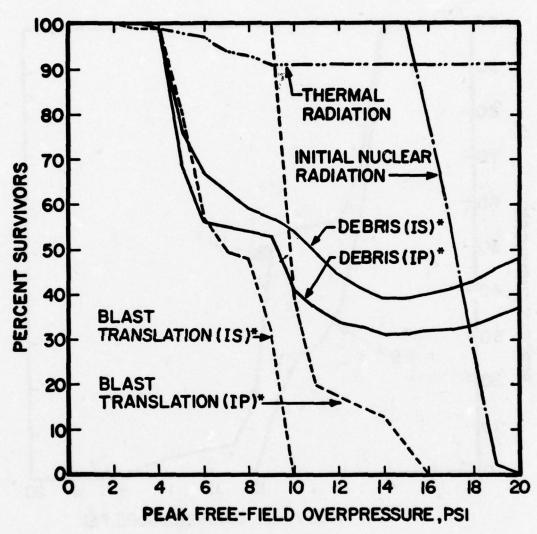
People are assumed to be uniformly distributed in all usable building areas at approximately 10 sq ft per person and both the "initially prone" and the "initially standing" cases are examined. In the context of this analysis the initially standing case is considered to represent the condition when no warning is given. The initially prone case then represents limited evasive action ocrresponding to limited warning time. In this example problem people are simulated using the "rigid block" model shown in Fig. 3a.

Results are given in Fig. 6. They represent total (combined) survivors taking into account all relevant prompt effects. They were obtained by selecting discrete overpressure levels, computing percent survivors for the individual effects, combining individual results and connecting the points with straight lines. Conceivably smoother curves would be produced with a larger number of discrete points. The individual effects results on which the results of Fig. 6 are based are given in Fig. 7. These results are briefly discussed.



\*IS - Initially Standing Occupants
\*IP - Initially Prone Occupants

FIG. 6 PEOPLE SURVIVABILITY ESTIMATE - COMBINED EFFECTS



•IS - Initially Standing Occupants •IP - Initially Prone Occupants

FIG. 7 PEOPLE SURVIVABILITY ESTIMATE-INDIVIDUAL EFFECTS

The number of casualties produced by thermal radiation and prompt nuclear radiation depends on the quantity of energy delivered and therefore is independent of the initial body positions of the occupants. Major variations in the thermal radiation curve (see Fig. 7) occur at 4 psi and 9.1 psi. These are overpressures at which respectively the interior partitions and exterior walls fail and are removed. This provides for a larger opening and therefore for more energy to be delivered.

The number of blast translation and debris impact casualties is fairly strongly dependent on which initial body position is used by the occupants. Consider the blast translation of the initially standing occupants (Fig. 7). Due to shielding provided by the sill, sidewalls and the interior partitions, essentially no fatal casualties occur prior to 4 psi. At 4 psi the interior partitions fail exposing all occupants to blast translation. At 9.1 psi exterior walls fail exposing all occupants to being swept out of the building. It will be noted that at 10 psi no initially standing survivors remain. However, about 40 percent remain for the initially prone case. The difference in survivors for these two body positions is due to the following reasons. First, more shielding is provided by the sill and sidewalls for the initially prone people and therefore less casualties. Second, the drag area is smaller and the floor contact area is larger for the initially prone people resulting in slower initial motion when compared to the initially standing case.

The second difference works in the opposite direction as far as debris impact is concerned. Initially standing people are translated by the blast faster than the initially prone people, resulting in less interaction with debris. One reason for the upswing in the debris curves (see Fig. 7) at higher overpressures is that debris tend to be translated further before impacting the floor. This reduces interaction with building occupants.

Results produced allow for the rating of individual building areas and the relative effectiveness of evasive action. Such results can also be used for rating individual buildings relative to protection afforded.

#### SUMMARY AND CONCLUSIONS

Conventional buildings constitute the only viable, current sheltering resource. In providing for population safety in the event of an emergency, the civil defense planner is faced with several difficult problems. One is

to identify the best available shelter space in various buildings in his particular locality. Another is to identify modes of evasive action that can effectively be used by building occupants so as to enhance the inherent protective capabilities of these buildings. The goal is to save lives and provide for continuity of the community in complex, multieffect situations, i.e., prompt and indirect effects of nuclear weapons, and natural disasters such as earthquakes, hurricanes and tornados.

A simple reliable building classification and rating system is needed, that can be quickly and effectively used at the local level by nonengineers for the purpose of classifying individual buildings in accordance with their overall protective capabilities and for the rating of the various spaces within them using an easy to apply ranking procedure. The task of developing effective, easy to apply tools is a difficult one. Numerous building types vary according to the socioeconomic function, geographic location, local building codes, year of construction, whim of the architect, etc. On the commercial or the professional plane a building classification system that identifies and categorizes the salient features of buildings in desirable detail, and one that can be used as a starting point for developing the classification and rating system described does not exist at this time.

Some believe that integrity of the building primary structural system is a good indicator of its inherent protective capabilities. This is not generally true. This is amply demonstrated in several recent natural disasters (Ref. 24) where the primary structure survived and numerous persons were killed or injured by so-called nonstructural items such as failed masonry partitions and fallen ceilings. A classification system which uses the strength of the primary structure as a rating base can lead to serious errors if applied by inexperienced personnel.

The simulation model bypasses many of these difficulties. Assuming that representative buildings can be surveyed as described in Ref. 35, this simulation model can be used to develop a reliable classification system after analyzing a sufficiently large and representative sample. It can also be used for the judging of the relative merits of various modes of evasive action. These are two of the purposes for which it was developed.

The problem is one of establishing relative safety in a complex, multihazard environment. For stated purposes the model is considered to be sufficiently valid, and adequate.

## **ACKNOWLEDGEMENT**

Work reported herein was supported by the Defense Civil Preparedness Agency (DCPA) under Contract DAHC20-68-C-0126 and Contract DAHC20-73-C-0196. It appeared previously in cleared for publication DCPA reports given herein as references 23 and 25. Work was performed at IIT Research Institute, Chicago, Illinois and was monitored by Mr. D. A. Bettge of DCPA, Washington, D.C.

#### REFERENCES

- 1. Alden, "Annals of Surgery," Vol. 140, 1954.
- Bartz, J. A., "A Three-Dimensional Computer Simulation of a Motor Vehicle Crash Victim - Phase 1 - Development of the Computer Program," CAL Report VJ-2978-V-1, July 1971.
- 3. Beck, C., ed., "Nuclear Weapons Effects Tests of Blast Type Shelters,"
  A Documentary Compendium of Test Reports, Civil Effects Branch, Division
  of Biology and Medicine, U. S. Atomic Energy Commission, Washington, D.C.,
  June 1969.
- 4. Bowen, G. I., et al, "Biological Effects of Blasts from Bombs," AECU-3350, June 18, 1956.
- 5. Brode, H. L., "Review of Nuclear Weapons Effects," Annual Review of Nuclear Science, Vol. 18, 1968, pp 152-202.
- 6. Childers, H. M., et al, <u>Protective Capability of the National Fallout Shelter System</u>, Vertex Corporation for Office of Civil Defense, Nov. 1968.
- 7. Clare, V. R., et al, "The Effects of Shock Tube Generated Step-Rising Overpressures on Guinea Pigs Located in Shallow Chambers Oriented Side-on and End-on to the Incident Shock," Technical Progress Report, DASA 1312, Department of Defense, Washington, D.C., May 1962.
- Cronkite, E. P., et al, "12 Month Post Exposure of the Marshallese Exposed to Fallout Radiation," Brookhaven National Lab., BNC-384(T-71), 1955.
- Damon, A., Stoudt, H. W. and McFarland, R. A., <u>The Human Body in Equipment Design</u>, Harvard University Press, 1966.
- 10. Damon, E. G., "The Effects of Ambient Pressure on the Tolerance of Mice to Airblast," Technical Progress Report DASA 1483, 1963.
- 11. Davenport, A. G., "Gust Loading Factors," <a href="Proc. ASCE Journal Structural Division">Proc. ASCE Journal Structural Division</a>, ST3, 1967, pp 11-34.
- 12. Davis, W. J., "Analysis of Japanese Nuclear Casualty Data," Contract OCD-PS-64-196, Work Unit 3411A for Office of Civil Defense, Dikewood Corp., April 1966.
- Dempster, W. T., "Space Requirements of the Seated Operator," WADC Technical Report 55-159, Aeromedical Laboratory, Wright Air Development Center, 1955.
- 14. Edmunds, J. E., "Experiments to Determine Debris Formation for Corrugated Steel and Brick Walls," Contract <u>DAHC20-60-C-0129</u>, Work Unit <u>3313</u> for office of Civil Defense, URS Research Company, January 1970.

## REFERENCE (Contd)

- Feinstein, D. I., et al, "Personnel Casualty Study," Contract OCD-PS-64-201, Subcontract B-10923 (4949A-24)-US for Office of Civil Defense, IIT Research Institute, July 1968.
- 16. Gerstner, H. B., "Acute Radiation Syndrome in Man," <u>U.S. Armed Forces Medical Journal</u>, Vol. 9, 1958, pp 313-354.
- Gillies, J. A., ed., <u>A Textbook of Aviation Physiology</u>, Pergamon Press, 1965.
- 18. Glasstone, S., ed., Effects of Nuclear Weapons, U. S. Government Printing Office, 1964.
- 19. Gurdjian, E. S., American Journal of Surgery, Vol. 78, 1949, pp 736-742.
- 20. Heugel, W. F. and Feinstein, D. I., "Shelter Evaluation Program," for Office of Civil Defense, Contract OCD-PS-64-50, Work Unit 1614-A, IIT Research Institute, February 1967.
- 21. Journal of Aviation Medicine, Vol. 28, p 454.
- 22. Journee Rev. D'Artillerie, May 1907.
- 23. Longinow, A., "Casualties Produced by Impact and Related Topics of People Survivability in a Direct Effects Environment," Contract DAHC20-73-C-0196, Work Unit 1614D for Defense Civil Preparedness Agency, IIT Research Institute, Chicago, III., August 1974.
- 24. Longinow, A. and Bertram, L. A., "Casualty Mechanisms Associated with Building Failures," <u>Conference</u>, <u>Designing to Survive Disaster</u>, IIT Research Institute, Chicago, Ill., November 1973.
- 25. Longinow, A., et al, "People Survivability in a Direct Effects Environment and Related Topics," Contract <u>DAHC20-68-C-0126</u>, DCPA Work Unit 1614D, for Defense Civil Preparedness Agency, IIT Research Institute, May 1973.
- 26. McMillen, J. H. and Gregg, J. R., "Missile Casualties," Report 12, National Reserach Council, Office of Scientific Research and Development, November 6, 1945.
- Minor, J. E., Mehta, K. C., and McDonald, J. R., "Designing Critical Facilities for Extreme Wind Conditions," <u>Proc. of Conference, Designing</u> to Survive Disaster, IIT Research Institute, Chicago, Ill., November 1973, pp 97-114.
- Richmond, D. R., Bowen, G. I. and White, C. S., "Tertiary Blast Effects: The Effects of Impact on Mice, etc.," <u>Aerospace Medicine</u>, Vol. <u>32</u>, 1961, p 789.

## REFERENCES (Conc1)

- Richmond, D. R. and White, C. S., "A Tentative Estimation of Man's tolerance to Overpressures from Airblast," Technical Progress Report DASA 1335, 1962.
- Richmond, D. R. and White, C. S., "Biological Effects of Blast and Shock," Technical Progress Report, Contract <u>DA-49-146-XZ-055</u>, Lovelace Foundation, Albuquerque, N.M., April 1966.
- 31. Rittenbury, M. S., et al, "Burn Mortality Study of 1831 Patients," DASA 1687, November 1965.
- 32. Simiu, E., "Logarithmic Profiles and Design Wind Speeds," Proc. ASCE, Journal Engineering Mechanics Division, EM5, October 1973.
- Smith, E. H. and Company, Final Report, Contract AF 33(657)-9712, August 1963.
- 34. Smith, E. H., et al, "Development of Analytical Relationships and Criteria for Blast and Fire Vulnerability of Fallout Shelter Occupants," for Office of Civil Defense, Contract <u>DAHC 20-67-C-0147</u>, System Sciences Inc., October 1, 1968.
- 35. Tolman, D. F., Lyday, R. O. and Hill, E. L., "Statistical Classification Report, Estimated Characteristics of NFSS Inventory," Contract <u>DAHC20-72-C-0277</u>, Research Triangle Institute, December 1973.
- 36. Vennard, J. K., Elementary Fluid Mechanics, 4th Edition, Wiley, 1961.
- 37. White, C. S., "The Nature of Problems Involved in Estimating the Immediate Casualties from Nuclear Explosions," CEX-71.1, Lovelace Foundation, U. S. Atomic Energy Commission, July 1971.
- 38. White, C. S., Bowen, G. I. and Richmond, D. R., "Biological Tolerance to Airblast and Related Biomedical Criteria," <u>CEX-65.4</u>, Lovelace Foundation, U. S. Atomic Energy Commission, April 1965.
- 39. White, C. A., et al, The Biodynamics of Airblast, Lovelace Foundation.
- 40. Wiehle, C. K. and Bockholt, J. L., "Existing Structures Evaluation, Part 1: Walls," Contract OCD DAHC20-67-C-0136, Work Unit 1126C, for Office of Civil Defense, Stanford Research Institute, November 1968.

#### M55 ROCKET DISPOSAL PROGRAM AT DUGWAY PROVING GROUND, UTAH

Curtis Jones Dugway Proving Ground Utah

I WILL BRIEFLY DISCUSS THE BACKGROUND ON THE M55 ROCKET DISPOSAL PROGRAM.

IN THE MID 60's THE ARMY WAS FACED WITH THE TASKS OF DISPOSING OF APPROXIMATELY 36,000 UNSERVICEABLE M55 GB ROCKETS. THESE ITEMS WERE LOCATED AT SEVERAL SITES WITHIN THE CONTINENTAL UNITED STATES AND OVERSEAS. THE PROBLEMS OF HOW AND WHERE TO DISPOSE OF THESE ITEMS RECEIVED A GREAT DEAL OF ATTENTION. AT THE ONSET OF THE M55 DISPOSAL PROGRAM, THERE WAS NO APPROVED PROCEDURE FOR DEMILITARIZATION OF CRATES OF FULLY ASSEMBLED AGENT-FILLED M55 ROCKETS. SEVERAL MONTHS WERE SPENT STUDYING ALTERNATE METHODOLOGIES. DEMILITARIZATION BY BURNING WAS FIRST SELECTED BECAUSE THIS METHOD PROVIDED AN EFFECTIVE BALANCE BETWEEN SAFETY REQUIREMENTS, OPERATIONAL EFFICIENCIES AND AVAILABLE DOLLAR RESOURCES. THE REMOTENESS AND ISOLATION OF THE SITE, TOGETHER WITH THE EXTENSIVE METEOROLOGICAL CAPABILITIES OF DUGWAY PROVING GROUND, WERE KEY CONSIDERATIONS. THE PREPARATION AND COORDINATION OF THE FINAL DISPOSAL PROCEDURE WERE A JOINT EFFORT OF THE U.S. ARMY TEST AND EVALUATION COMMAND: U.S. ARMY MATERIEL COMMAND, EDGEWOOD ARSENAL AND DUGWAY PROVING GROUND. THE PROGRAM WAS INFORMALLY COORDINATED WITH BOTH LOCAL AND NATIONAL HEALTH AND AIR POLLUTION AUTHORITIES. BECAUSE OF ITS LOCATION AND ISOLATION, DUGWAY WAS SELECTED AS THE SITE FOR DEMILITARIZATION OF THE ROCKETS VIA OPEN AIR INCINERATION.

THE ORIGINAL PLAN WAS DESIGNED TO PROVIDE THERMAL

DECOMPOSITION OF TOXIC AGENT, TO BURN OFF THE AGENT, PROPELLANT

IN EACH ROCKET MOTOR AND TO DETONATE AND RENDER HARMLESS ALL

EXPLOSIVE COMPONENTS. PRIOR TO PROGRAM INITIATION, THE PLAN

WAS COORDINATED AND APPROVAL BY THE DEPARTMENT OF DEFENSE,

THE UTAH BOARD OF HEALTH, STATE AND FEDERAL AIR POLLUTION

AUTHORITIES.

IN APRIL OF 1967, TECHNOLOGY TRIALS WERE CONDUCTED TO REFINE AND VALIDATE PROCEDURES. VARYING QUANTITIES OF ROCKETS WERE PLACED IN PITS, DUNNAGE, DIESEL FUEL ADDED AND IGNITED. THE PYRE WAS INSTRUMENTED TO ACQUIRE DATA ON TEMPERATURE AND THE EFFLUENT WAS CHEMICALLY SAMPLED. WHEN A WARHEAD IS EXPOSED TO THE HEAT OF AN INTENSE FIRE, TWO EVENTS OCCUR. FIRST THE WARHEAD RUPTURES RELEASING THE CONTENTS INTO THE FIRE. THE SECOND EFFECT OCCURS SOME MINUTES LATER WHEN THE BURSTER DETONATES. IN JUNE OF 1967, THE ACTUAL DISPOSAL OF THE 36,000 M55 ROCKETS WAS BEGUN. INITIAL PREPARATION CONSISTED OF PREPAR-ING SIXTY-ONE TRENCHES, SEVEN FEET DEEP, SEVEN FEET WIDE AND UP TO 100 FEET LONG. THESE PITS WERE EXCAVATED IN THE DISPOSAL AREA LOCATED ON THE BORDER OF THE GREAT SALT LAKE DESERT. WOODEN CRATES, CONTAINING 15 ROCKETS EACH, WERE THEN PLACED WITH THEIR WARHEADS FACING DOWN IN 61 OF THE TRENCHES (IN THE EVENT OF MOTOR FUNCTION, THE WARHEADS WOULD BE FORCED INTO THE GROUND AND THE AGENT CONFINED WITHIN THE TRENCH). DUNNAGE, CONSISTING OF SCRAP LUMBER AND OTHER FLAMMABLE WASTE, WAS USED

TO FILL THE VOID BETWEEN THE TRENCH WALLS AND THE ROCKET CRATES. ON DAYS WHEN THE METEOROLOGICAL CONDITIONS THROUGHOUT WESTERN UTAH MET THE SPECIFIED REQUIREMENTS, THE ROCKETS WERE BURNED. PRIOR TO COMPLETION, THE M55 BURN DISPOSAL PROGRAM WAS STOPPED IN CONFORMANCE WITH A DEPARTMENT OF THE ARMY DIRECTIVE, DATED 30 JULY 1969. THIS DIRECTIVE ORDERED A MORATORIUM ON ALL OPEN AIR BURNING OF TOXIC MATERIALS. ON 19 NOVEMBER 1969 AND 7 OCTOBER 1970, RESPECTIVELY, ENACTMENT OF UNITED STATES PUBLIC LAWS 91-121 AND 91-441 PLACED ADDITIONAL RESTRICTIONS ON THE DISPOSAL OF TOXIC MATERIALS. AT THE TIME BURNING WAS SUSPENDED, ALL 61 PITS HAD BEEN BURNED AT LEAST ONCE, 23 HAD BEEN BURNED TWICE, AND TWO HAD BEEN BURNED A THIRD TIME. ALTHOUGH DISPOSAL OPERATIONS WERE CEASED, A ROUTINE MONITORING PROGRAM AND ECOLOGICAL STUDIES WERE INITIATED BY DUGWAY PROVING GROUND TO ASSURE THAT THE REMAINING PIT RESIDUE WAS NOT HAVING AN ADVERSE IMPACT ON THE ENVIRONMENT.

SUBSEQUENT TO THE PASSAGE OF THESE PUBLIC LAWS, THE

DEPARTMENT OF THE ARMY, IN CONJUNCTION WITH THE NATIONAL

ACADEMY OF SCIENCES, RE-EVALUATED THE METHODS OF DISPOSAL

FOR CHEMICAL MUNITIONS. THE NATIONAL ACADEMY OF SCIENCES

RECOMMENDED THAT FUTURE DISPOSAL OPERATIONS EMPLOY "OPTIMAL

METHODS OF DISPOSAL . . . INVOLVING NO HAZARD TO THE GENERAL

POPULATION AND NO POLLUTION OF THE ENVIRONMENT."

IN THE FALL OF 1972, THE ARMY ESTABLISHED THE DEMILITARIZATION OFFICE AND GAVE IT THE TASK OF MANAGING THIS DISPOSAL EFFORT.

INITIALLY, AN ASSESSMENT WAS MADE OF THE PITS AND IT WAS
ESTIMATED THAT 569 WARHEADS WHICH COULD POSSIBLY CONTAIN AGENT
WERE DISTRIBUTED AMONG THE ROCKET DEBRIS. BASED ON THE NEW
ENVIRONMENTAL RESTRICTIONS LIMITING ALL OPEN BURING, ALTERNATIVES
FOR THE CLEANUP OF THIS PIT AREA WERE EVALUATED. THESE ALTERNATIVES RANGED FROM COVERING THE PITS WITH CONCRETE OR EARTH AND
PERMANENTLY CLOSING THE AREA, TO THAT OF FILLING THE PITS WITH
ALTERNATE LAYERS OF CAUSTIC AND EARTH TO STIMULATE CORROSION
OF REMAINING ROCKETS. THE OPTIMUM COURSE OF ACTION, HOWEVER,
APPEARED TO BE CHEMICAL DESTRUCTION BY CAUSTIC NEUTRALIZATION,
A PROCESS BASED ON SODIUM HYDROXIDE REACTION. THIS CONCEPT
INVOLVED EXTRACTING THE ROCKET DEBRIS FROM THE PITS AND PLACING
THOSE MUNITIONS WHICH COULD POSSIBLY CONTAIN AGENT INTO METAL
BASKETS.

## (SEGREGATION CHART)

THIS SEGREGATION CHART SHOWS THOSE STEPS OF THE OPERATION REQUIRING REMOTE HANDLING BY A BLACK SQUARE AND THOSE REQUIRING AGENT PROTECTION BY A DOT. BRIEFLY, THIS CHART SHOWS THE FIVE CATEGORIES OF MATERIAL TO BE REMOVED AND THE DISPOSITION TAKEN WITH EACH. WARHEADS CONTAINING AGENT WILL BE TREATED BY CAUSTIC NEUTRALIZATION AND THE RESIDUE FROM THE REACTION SORTED. INTACT EXPLOSIVE TRAINS ALSO REQUIRE REMOTE HANDLING, AND WILL BE DISPOSED OF BY DETONATION. LOCSE EXPLOSIVES AND PROPELLANT WILL BE BURNED, WHILE CASED EXPLOSIVES, SUCH AS SEPARATE BURSTERS, WILL BE DETONATED.

AFTER INSPECTION HAS ONE OF THREE CHOICES: FIRST AND MOST
OFTEN, DETERMINATION IS MADE OF INNOCUOUS SCRAP AND HE PLACES
IT IN THE DUMP TRUCK: SECOND, IF EXPLOSIVE COMPONENTS ARE
PRESENT HE PLACES IT IN AN EXPLOSIVE TRAILER FOR APPROPRIATE
EOD PROCEDURES: THIRD, IF IT HAS AN INTACT CHEMICAL WARHEAD
WITH AGENT, HE PLACES IT IN AN AREA FOR SUBSEQUENT EOD PERSONNEL
EXAMINATION FOR AGENT VERIFICATION AND LOADING INTO A BASKET
AND TRANSPORTATION TO THE NEUTRALIZATION TANKS.

THE METAL BASKETS ARE THEN LOWERED INTO STEEL TANKS AND COVERED WITH A 15 PERCENT SODIUM HYDROXIDE SOLUTION WHICH HAD BEEN PREHEATED TO 170°F. THIS SOLUTION DIGESTS THE ALUMINUM WARHEAD AND NEUTRALIZE THE CHEMICAL AGENT.

THE CHEMISTRY OF THE GB-SODIUM HYDROXIDE REACTION, WHICH HAS BEEN WELL DOCUMENTED AND SUCCESSFULLY DEMONSTRATED UNDER LABORATORY AND FIELD CONDITIONS, IS:

GB + SODIUM HYDROXIDE = SODIUM ISOPROPYL METHYLPHOPHONATE + SODIUM FLUORIDE + WATER.

DISSOLUTION OF THE ALUMINUM WARHEAD CONTAINING THE AGENT PRODUCES SOLUABLE SALTS AND SUSPENDED SOLIDS PLUS HYDROGEN GAS WHICH IS READILY DISSIPATED INTO THE ATMOSPHERE. THIS REACTION BETWEEN ALUMINUM AND SODIUM HYDROXIDE IS:

ALUMINUM + SODIUM HYDROXIDE = HYDROGEN + SODIUM ALUMINATE

UPON COMPLETION OF THE CHEMICAL NEUTRALIZATION PROCESS,

ONLY THE ROCKET MOTOR CASING AND ROCKET EXPLOSIVES REMAIN.

THIS CHEMICAL REACTION IS GENERALLY COMPLETE IN 24 HOURS. HAVE A FILM THAT WILL SHOW THE RESULTS OF A 24 HOUR REACTION ON ROCKETS WITHOUT SHIPPING AND FIRING TUBES. THE WARHEAD SKIN HAS BEEN EATEN AWAY, EXPOSING THE FUZE AND BURSTER. THE STEEL PROPELLANT CASE IS VIRTUALLY UNAFFECTED. FURTHER TESTING OF THIS CONCEPT CONFIRMED THAT THE AGENT WAS COMPLETELY DESTROYED, THE BRINE CONTAINED NO AGENT, AND THE OPERATION COULD BE CONDUCTED WITH NO ADVERSE IMPACT ON THE ENVIRONMENT. TESTS TO DETERMINE THE EXPLOSIVE SENSITIVITY OF THE RESIDUE DEMONSTRATED THAT THE PROBABILITY OF A DETONATION OCCURRING AS A RESULT OF THE PROPOSED HANDLING OF THE 569 ROCKETS WITH AGENT WAS LESS THAN ONE IN 500,000. WE HAVE NOT HAD A DETONATION TO DATE. BASED ON THE RESULTS OF THESE TESTS, IN JUNE 1974, CAUSTIC NEUTRALIZATION WAS ADOPTED AS THE METHOD OF CHOICE AND ACTION WAS TAKEN TO PREPARE THE DISPOSAL PLAN AND THE ENVIRONMENTAL IMPACT STATEMENT REQUIRED BY PUBLIC LAW. THE OPERATIONS AS OUTLINED IN THESE DOCUMENTS WERE DESIGNED WITH SAFETY FOR PERSONNEL AND THE ENVIRONMENT AS THE PARAMOUNT CONSIDERATIONS. BECAUSE OF THE CONDITION AND CONFIGURATION OF THE ROCKETS IN THE PITS, REMOTE HANDLING PROCEDURES WERE SPECIFIED FOR MANIPULATION OF ANY INTACT EXPLOSIVE MUNITION TO ASSURE MAXIMUM SAFETY TO OPERATING PERSONNEL.

OPERATIONS IN THE PITS ARE DIVIDED INTO THREE PHASES. PHASE
A CONSISTS OF REMOVING NON-HAZARDOUS DEBRIS FROM AROUND THE PITS
THAT OBSTRUCT FREE MOVEMENT OF EQUIPMENT. THIS PHASE HAS BEEN
COMPLETED ON ALL PITS.

PHASE E CONSISTS OF REMOVING VISIBLE ROCKET RESIDUE

FROM THE PITS BY REMOTE MEANS USING TWO ARMORED PERSONNEL

CARRIERS EQUIPPPED WITH ROTATING HYDRAULIC BOOMS. AN

ARTICULATED PICKUP HEAD IS LOCATED AT THE END OF THE BOOM.

THIS HEAD MOVES IN ALL DIRECTIONS, FORWARD AND BACK, SIDE TO

SIDE, AS WELL AS ROTATING AT THE PICKUP FINGERS. THROUGH USE

OF REMOTE TELEVISION CAMERAS, SUCH AS YOU SEE HERE, AND DIRECT

VIEWING THROUGH A CUSTOM-MADE ARMORED WINDOW IN REAR RAMP,

OPERATORS EXAMINE THE EXTRACTED RESIDUE, IDENTIFY IT FOR

DISPOSITION, AND PLACE IT IN AN APPROPRIATE CONTAINER FOR

DISPOSAL. THE TWO APC'S ARE EQUIPPED WITH PROTECTIVE FILTERS

FOR CHEMICAL AGENTS AND OTHER MODIFICATIONS TO ALLOW THE OPERATORS

TO WORK IN RELATIVE COMFORT.

WHEN ALL VISIBLE ROCKET RESIDUE HAS BEEN REMOVED FROM A
PIT, PHASE C COMMENCES. THIS PHASE INCLUDES EXCAVATION OF
PITS TO THEIR ORIGINAL DEPTH OF SEVEN FEET AND SUBSEQUENT
ANALYSIS AND DISPOSITION OF ITEMS UNCOVERED. TWO CRANES,
MODIFIED BY THE ADDITION OF ARMORED OPERATOR CABS FOR PERSONNEL
PROTECTION ARE USED IN THIS PHASE. NORMALLY, ONE APC WORKS WITH
EACH CRANE TO SEGREGATE EXCAVATED MATERIAL. ONCE EACH PIT HAS
BEEN EXCAVATED TO ITS ORIGINAL DEPTH, SOIL SAMPLES ARE TAKEN
AND ANALYLED TO VERIFY THE ABSENCE OF RESIDUAL AGENT PRIOR TO
THE PIT BEING CLOSED BY A BULLDOZER. TO DATE, NO AGENT HAS
BEEN FOUND IN THESE SOIL SAMPLES.

A COMMUNICATION SYSTEM LINKS ALL TEAMS OPERATING IN THE

PIT AREA WITH THE CONTROL CENTER. CONSTANT AUDIBLE AND VISUAL COMMUNICATIONS ARE MAINTAINED WITH ALL EQUIPMENT OPERATORS.

IN ADDITION, THE OPERATIONS CENTER CAN COMMUNICATE WITH ALL FIELD TEST OPERATIONS AND EMERGENCY REACTION AND MEDICAL TEAMS VIA THE DUGWAY COMMAND RADIO SYSTEM.

AN INTEGRATED SYSTEM OF CHEMICAL AGENT ALARMS AND MONITORS
IS USED FOR IMMEDIATE DETECTION OF ANY INADVERTENT AGENT RELEASE
AND TO ASSURE THAT AGENT CONCENTRATIONS IN EXCESS OF THE STANDARDS
ESTABLISHED BY THE DEPARTMENT OF HEALTH, EDUCATION AND WELFARE
ARE NOT VIOLATED DURING OPERATIONS. THIS SYSTEM USES THE M8
ALARM AND BUBBLER MONITORS, AROUND THE NEUTRALIZATION TANKS,
DOWNWIND OF PITS ON WHICH OPERATIONS ARE BEING CONDUCTED, AND
IN AREAS WHERE OPERATING PERSONNEL ARE LOCATED, SUCH AS IN THIS
COMMAND POST TRAILER. THIS MONITORING SYSTEM WAS REVIEWED BY
THE DEPARTMENT OF HEALTH, EDUCATION AND WELFARE AND OTHER
AGENCIES SUCH AS THE ENVIRONMENTAL PROTECTION AGENCY FOR COMMENT
AND RECOMMENDATIONS.

PERSONNEL AND ENVIRONMENTAL SAFETY IS GIVEN PARAMOUNT
ATTENTION. MINIMUM SAFETY DISTANCES HAVE BEEN DEVELOPED FOR
THE VARIOUS ACTIVITIES, AND BARICADES EMPLOYED WHERE APPROPRIATE.
CHOLINESTIRASE BASE LINES HAVE BEEN ESTABLISHED ON ALL PERSONNEL
AND ARE CHECKED AT INTERVALS DEPENDENT ON PROBABILITY OF
EXPOSURE. THE INTERVAL IS TWO WEEKS FOR PEOPLE WORKING IN
THE PIT AREA.

WE HAVE A METEOROLOGICAL TOWER IN THE AREA WHICH CONSTANTLY

SENSES WIND SPEED, WIND DIRECTION AND TEMPERATURE AND DISPLAYS
THEM IN THE CP AND TELEMETERS THE DATA TO DITTO AREA, MET
LABORATORY. METEOROLOGICAL CONSTRAINT PROHIBIT OPERATIONS,
DURING PRECIPITATION OR WITH THUNDERSTORM ACTIVITY IN THE AREA.
A HAZARDS ANALYSES WAS PERFORMED TO DETERMINE THE MOST SERIOUS
CREDIBLE ACCIDENT AND DOWNWIND HAZARD ASSOCIATED WITH SUCH AN
ACCIDENT.

THE ENVIRONMENTAL IMPACT STATEMENT AND THE DEMILITARIZATION
PLAN FOR THIS OPERATION WERE REVIEWED PRIOR TO INITIATION OF
OPERATIONS BY THE DEPARTMENT OF HEALTH, EDUCATION AND WELFARE,
THE DEPARTMENT OF LEFENSE EXPLOSIVES SAFETY BOARD AND OTHER
FEDERAL AGENCIES. THE ENVIRONMENTAL IMPACT STATEMENT WAS
ALSO REVIEWED BY THE REQUIRED UTAH STATE AGENCIES. DUE TO
THE NATURE OF THIS PROGRAM THE POTENTIAL EXISTS FOR THE
INADVERTENT RELEASE OF A SMALL AMOUNT OF CHEMICAL AGENT DURING
DEMILITARIZATION OPERATIONS. ACCORDINGLY, STEPS WERE INCORPORATED
IN OUR PLANS TO INCLUDE RAPID RESPONSE TEAMS IN ORDER TO
MINIMIZE THE EFFECT OF ANY SUCH RELEASE.

TO DATE, THIS OPERATION HAS BEEN CONDUCTED SAFELY AND WITHOUT INCIDENT. ADDITIONALLY, THE RESULTS FROM OUR INTEGRATED MONITORING SYSTEM HAVE SHOWN THAT THE PERMISSIBLE STANDARDS AND SAFETY CONSTRAINTS HAVE NOT BEEN VIOLATED.

## CURRENT STATUS OF THE PROJECT AS OF TODAY FOLLOWS: (15 September 1976)

PITS TO BE CLEARED	61
PITS COMPLETED BY APC TO DATE	61
PITS EXCAVATED BY CRANE	61
NUMBER OF PITS CLOSED	31
AVERAGE NUMBER OF APC HOURS PER PIT	5.43
AVERAGE NUMBER OF CRANE HOURS PER PIT	4.68
CUBIC YDS. OF SCRAP PER PIT	11.5
LEAKERS	86
NONLEAKING WARHEADS	309
TOTAL WARHEADS	395
AVERAGE PER PIT	6.46

I HAVE A FILM COVERING THE OPERATION THAT GIVES AN OVERVIEW OF THE ENTIRE OPERATION.

## FILM (SHORT 12 MINUTES)

## M55 ROCKET DISPOSAL

INITIALLY ROCKETS WERE TO BE DESTROYED VIA OPEN PIT INCINERATION. WE STARTED OFF BY RUNNING METHODOLOGY TRIALS WHEREBY THE NUMBER OF CRATES PLACED INTO A PIT WAS GRADUALLY INCREASED UNTIL THE MAXIMUM OF 40 CRATES PER PIT WAS REACHED. ROCKETS PLACED IN PITS, DUNNAGE ADDED, FUEL OIL AND NAPALM THEN IGNITED. NOTE AS THE PIT BURNS, ROCKETS ARE THROWN OUT OF THE PIT. THE PITS WERE BURNED SEVERAL TIMES.

ALL PITS - AT LEAST ONCE

23 PITS - TWICE

2 PITS - THREE TIMES

OVERHEAD SHOT OF PITS - BEFORE PITS CLEANED UP - YOU CAN SEE SOME OF THE DEBRIS. NOTE THE DESOLATION OF THE AREA.

SCENES OF SITE PREPARATION - PRIOR TO TEST INITIATION THERE
WAS ONLY A TOWER AND A BUNKER LEFT OVER FROM A PREVIOUS TEST
LOCATED IN THE SITE. CONSTRUCTION OF A SUPPORT FACILITY WAS
THE FIRST ORDER OF BUSINESS. SUCH FACILITIES AS THE MAINTENANCE
BUILDING, CHANGEHOUSE, DECON PAD, CP TRAILER SITE, ETC. HAD TO
BE ESTABLISHED. TOWERS WERE SET UP FOR CAMERA EMPLACEMENT.
THESE CAMERAS WERE USED FOR OPERATIONAL CONTROL AND SAFETY.
- 150' TOWER CAMERAS WERE EMPLACED AT THE 125' LEVEL FOR
OPITMUM COVERAGE AND STABILITY. MET INSTRUMENTATION WAS ALSO
LOCATED ON ONE OF THE TOWERS. THIS DATA WAS TELEMETERED BACK

TO DITTO AREA. THIS SCENE SHOWS THE COMPLETED CP AREA
FACILITY AS IT LOOKS TODAY. THIS SCENE SHOWS THE CREW
ENTERING THE APC TO BEGIN DAYS WORK - MOVING TO PIT AREA LOOK AT PIT OPERATION THROUGH EYE OF APC OPERATOR - CLOSE UP
OF RESIDUE. NOTE THE BURIED DEBRIS INSIDE THE PIT AND THE
VERSITILITY OF THE GRAPPLE. THE UNIT CAN PICK UP ROCKET
DEBRIS IN ANY ORIENTATION OF ATTITUDE. OPERATOR USE ON BOARD
CAMERAS OR LOOK OUT REAR WINDOW TO ASSIST IN IDENTIFICATION AND
AND APPROPRIATE SORTING OF THE DEBRIS.

WHAT OPERATOR SEES ON MONITORS INSIDE APC, NOTE THE DETAILS OF THE PICTURE.

SAMPLER PREPARATION - ACIDIFIED WATER - PACKED IN ICE TO KEEP AT 0°C TO PREVENT VOLUME LOSS DURING ASPIRATION - FLOW RATE IS 2 LITERS PER MINUTE.

M8 ALARM PREPARATION - ALARMS MUST ACCOMPANY ANYONE GOVING DOWNRANGE - ALARM PLACED DOWNWIND OF EACH OPERATION.

CAUSTIC NEUTRALIZATION SET UP - NOTE SAMPLING ARRAY OVERHEAD SHOT SHOWING OUTER ARC.

NEUTRALIZATION TANKS - 2 TANKS ARE USED AT A TIME TO DIGEST A TOTAL OF 5 ROCKETS PER TANK.

APC PICKS UP CONTAINMENT BASKET W/5 ROCKETS FOR PLACEMENT IN CAUSTIC NEUTRALIZATION TANK.

APC PLACES ROCKET IN BASKET - CLOSURE OF BASKET. HOOK UP TO APC - NOTE STRONGBACK HAS BEEN ELIMINATED.

EOD WORKING WITH APC IN REMOVING BASKET FROM TANK - REMOVAL

OF EXPLOSIVE AFTER NEUTRALIZATION. PUMPING OF BRINE FROM BRINE NEUTRALIZATION TANK INTO TANKER - TRANSPORT OF BRINE TO THE EVAPORATION SITE - PUMPING OF BRINE INTO EVAPORATION TROUGHS WHERE BRINE IS ALLOWED TO EVAPORATE VIA NORMAL METEOROLOGICAL SITUATION.

AERIAL OF EVAPORATION SITE, NOTE THERE ARE 20 EACH, 5000 GALLON CAPACITY TANKS. THE TOTAL CAPACITY FOR THE SITE IS 1000,000 GALLONS OF BRINE.

CRANE DURING EXCAVATION - NOTE GRATE SIFTING OF EXCAVATED

MATERIAL - THE GRATE SEPARATES THE METAL DEBRIS FROM THE

EXCAVATED DIRT AND FACILITIES CLEAN UP OF THE EXCAVATED MATERIAL.

PIT AFTER EXCAVATION - AT THIS POINT - THE WALLS ARE CHECKED BY

EOD WITH A METAL DETECTOR - SOIL SAMPLES ARE TAKEN FROM THE

BOTTOM OF THE PIT.

APC RAKING OF EXCAVATED MATERIAL TO CLEAR ANY EXCAVATED DEBRIS, EXPOSED WARHEAD OR INTACT EXPLOSIVE TRAIN THAT MAY BE UNCOVERED. EOD CHECKING EXCAVATED MATERIAL.

CLOSING OF PITS BY DOZER - PRIOR TO CLOSURE AN INSPECTION IS

ACCOMPLISHED TO INSURE THAT ALL ROCKET DEBRIS HAS BEEN REMOVED.

AERIAL OF CLOSED PITS.

DECON OF VEHICLE - ALL EQUIPMENT TAKEN INTO THE CONTAMINATED AREA (PIT AREA) MUST PROCESS THROUGH A DECON POINT PRIOR TO BEING CARRIED TO EQUIPMENT PARKING AREA.

# AUTOMATED EXPLOSIVE PELL T MANUFACTURING USING A PDP-14 PROGRAMMABLE CONTROLLER

Duane O. Page
Monsanto Research Corporation
Mound Laboratory
Miamisburg, Ohio
operated for
UNITED STATES ENERGY RESEARCH
AND DEVELOPMENT ADMINISTRATION
U.S. Contract No. E-33-1-GEN-53

#### ABSTRACT

A Digital Equipment Corporation PDP-14 Industrial Programmable Controller was employed to provide automatic, closed-loop control for an explosive pellet manufacturing system at Mound Laboratory. Programmable controllers allow the application of sophisticated and flexible control, through programming. Advantages of the PDP-14 controller are ease of installation and maintenance, capability for modular expansion, and immunity to electrical noise. Safety requirements were met by using new techniques for adapting electrical equipment to a hazardous environment and by locating the PDP-14 remotely outside the explosive area. Another advantage of the new explosion proofing (EP) methods/equipment was that they produced a minimum of clutter on the controlled explosive pellet manufacturing system.

## INTRODUCTION

Originally the system for the manufacture of explosive pellets at Mound Laboratory was automated with electro-mechanical control. The several operations, of which the system consisted, were set in motion at the proper times by switches actuated by cam-wheels as they were rotated with a motor drive. With this setup, operations were initiated, but there was no means for follow-up to ensure that operations were completed. An operation was turned on, a definite time was allowed for it to be completed, then the next operation was turned on, and so on. This method of manufacture wasted time, since the time allotted for each operation was the maximum envisioned; completion of an operation in a shorter time could not provide any advantage. Nevertheless, the system worked well as long as no mechanical difficulties were encountered and each individual operation functioned as it should. But should such an adverse situation occur, consequences could be severe before the system was shut down. In an adverse situation, operations continued to be activated in their scheduled sequence, as controlled by their cams. By the very nature of the process, the system could inflict severe mechanical damage to itself before the situation was noticed by the operator and the system shut down. With the presence of explosives, the possibility always existed that the severity of the incident could be compounded.

An obvious deficiency to be corrected in upgrading the control system for the pellet-pressing operation was the open-loop nature of the original system. This could be overcome by the installation of a closed-loop system, including a controller that would accommodate this type of control. Other features desired in upgrading the existing control system were a control instrument with programming flexibility and modular expandability. Compactness of system components other than the control instrument that would alleviate the clutter of hardware mounted on the press was considered very desirable. A programmable controller was selected for attaining the improved system. Other types of control methods that were considered were air logic and fluidic.

#### DESCRIPTION OF CONTROLLED EQUIPMENT

The process equipment to be controlled consisted basically of a mechanical press to compact pellets from a high explosive powder and an air gauge for measuring the pellet thickness. Both of these units were located in an explosive environment. The process was subsequently controlled by Digital Equipment Corporation's PDP-14 Programmable Controller which was located remotely in a nonhazardous area. A diagram of the PDP-14 based control system is depicted in Figure 1; an additional description

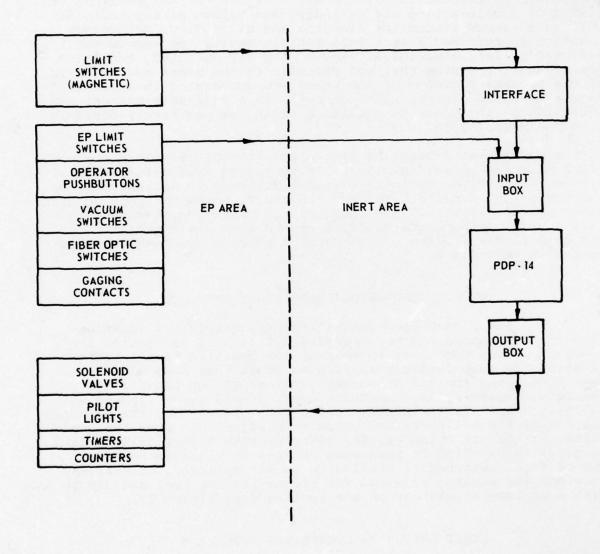


Figure 1 - Control system safety requirements were met by using new techniques for adapting electrical equipment to a hazardous environment, and by locating the PDP-14 remotely outside the explosive area.

of some of the ancillary subsystems and/or components will follow this section. The basic construction of the press included a method for accurately filling the die cavity with a predetermined amount of loose powder from which a pellet was formed. An air-operated, mechanical parts-handling system was retrofit to the press. It consisted of double-acting air cylinders and vacuum pickup heads as well as a vacuum system for cleaning the die cavity. Mechanisms position a preformed insert into the die cavity and remove the finished pellet. A pictorial view of the air-operated, mechanical parts-handling system that was retrofit to the press and a listing of the process sequence of the press are documented in Appendix A. An air-operated clutch, which operates in a fail-safe manner, was installed on the press to provide a means for positively controlling the press cycle.

A second parts-handling system was retrofit to the air gauge which measures pellet thickness. It consisted of double-acting air cylinders and fiber optic sensors for determining pellet presence. The system gated pellets through the gauge, moved the gauging transducer against a pellet, and operated an accept-reject gate. A pictorial view of the parts-handling system that was retrofit to the air gauge and a listing of the gauging process sequence are documented in Appendix B.

#### COMPACT, EXPLOSION-PROOF LIMIT SWITCHES

Since the closed-loop control technique requires verification that a command has been carried out as well as issuing the command, it was necessary to monitor the position of all air cylinders. The comparatively small size of the parts-handling systems prohibited the use of conventional explosion-proof limit switches. An air-cylinder manufacturer offered air-cylinders with built-in "reed" limit switches which were operated by the magnetic pistons of the cylinders and which were adjustable over the entire stroke of the air cylinder. The switches were hermetically sealed in glass tubes which in turn were encased in aluminum housings. Two of these switches, installed on an air cylinder, effectively provided the sensing required for closed-loop control and did so with a minimum of clutter on the tooling (see Figure 2).

#### LIMIT SWITCH TO CONTROLLER INTERFACE

Although the "reed" limit switches were hermetically sealed and further protected with an aluminum housing, they still did not meet the EP (explosion proof) requirements for electrical equipment in hazardous areas. To accomplish this, an exceptionally low control power level of approximately 16 mW was selected for use in all "reed" limit-switch circuits. This low power level was well below the accepted limit for intrinsically safe operation.

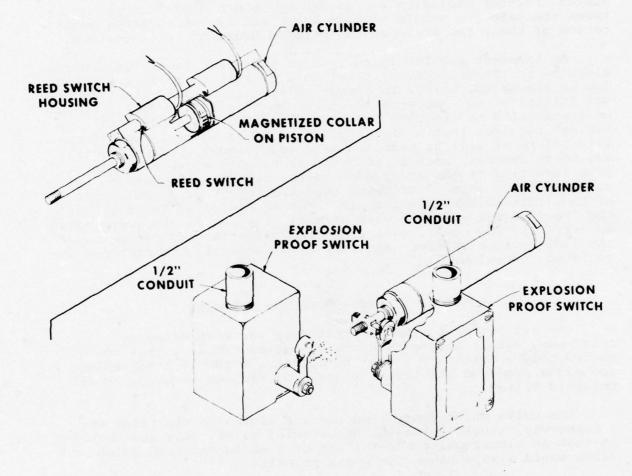


Figure 2 - Because of size comparison, the compact reed switches that mounted onto air cylinders greatly alleviated the clutter of hardware that was mounted on the press and gauge.

To complete this "intrinsically safe" limit-switch circuit, an interface, as shown in Figure 3, was designed to couple the limit switches to the PDP-14 Controller input. The interface converted the limit-switch signal from approximately 4 V d. c. to 110 V a. c., as required by the PDP-14 Controller, while positively preventing any unsafe voltage from appearing in the explosive area. This isolation was accomplished by an Instrument Society of America (ISA) approved circuit called a "Redding Barrier". The "Redding Barrier" used series resistors to limit current, Zener diodes to control the voltage level, and fuses to protect the Zener diodes. Further isolation was gained by "photo diode" coupling between the safe and unsafe voltage areas and by the physical separation of these two areas on the printed board of the interface.

An inherent problem in the use of low power levels in sensing circuits is the susceptibility of that circuit to false triggering due to electrical noise. To combat this, a technique called "digital filtering" was employed to ensure that no false signals would be transmitted to the PDP-14 input. Basically, this "digital filtering" requires that a signal pulse be of at least 20 msec duration before it will be accepted as a true signal. Common electrical noise sources, such as 60 cycle a. c. pulses due to collapsing inductive fields and random noise, all normally have pulse durations less than 20 msec and thus are rejected. A photograph of the limit-switch interface is shown in Figure 4. The fact that the "reed" limit switches were hermetically sealed and operated at an extremely low power level prevented oxidation and corrosion of the limit-switch contacts and thus eliminated all the problems associated therewith.

#### SOLENOID VALVES AND VACUUM SWITCHES

The air supply to the air cylinders was controlled by three-way, double solenoid, detented valves. These valves required only a momentary signal to operate. A PDP-14 programming technique produced electrical signals of minimum duration to all solenoid valves.

The valve which controlled the air clutch on the press was a three-way, single solenoid, nondetented valve. This was selected so that an electrical power failure or a malfunctioning solenoid valve would always cause the press to halt.

Housed in the same cabinet with the valves were two vacuum switches which monitored the vacuum on the pickup heads. If a vacuum head failed to pick up a preformed insert or a pellet, no vacuum would be detected by the vacuum switches, and the proper signal would not be sent to the PDP-14 Controller input. The process would then stop and the operator would correct the malfunction.

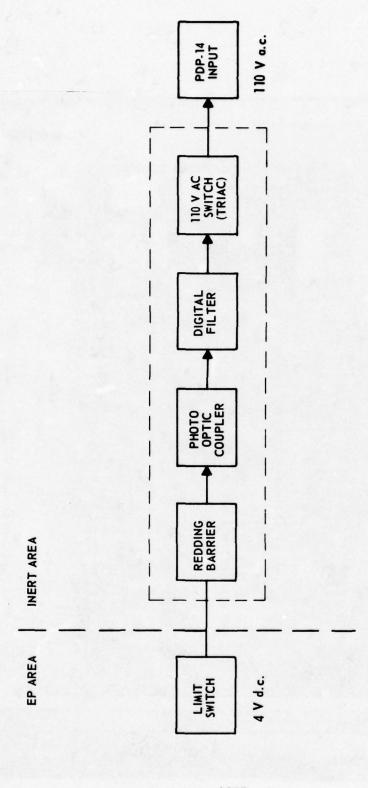


Figure 3 - The limit switch interface converted an intrinsically safe 4-V d.c. at 4 mA switch signal to the required  $110-{\rm V}$  a.c. PDP-14 input signal.

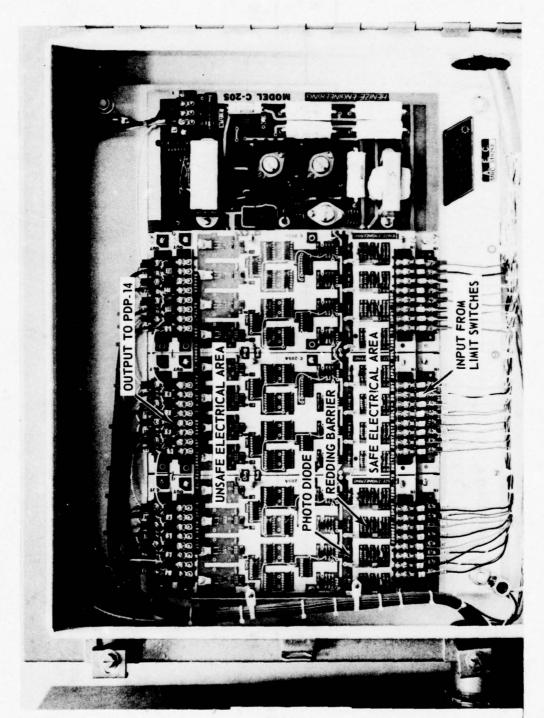


Figure 4 - A unique LIMIT SWITCH INTERFACE isolated all unsafe voltages from the explosive area, and eliminated false signals due to electrical noise.

#### THE PDP-14 CONTROLLER

The PDP-14 Controller operates similarly to a computer in that it executes a program of instructions sequentially. It has a hard-wired, read-only memory in which the program is stored and which cannot be altered electrically. This is a very desirable feature in an electrically noisy, industrial environment. A control program is a collection of control equations which are solved in a period of milliseconds. Every output device, such as solenoid valve, motor, and pilot lamp, has its own individual equation which states under what conditions that output device will be energized. These equations are written in Boolean symbology and can refer to any input and/or output. This type of control has great versatility so therefore a high degree of sophistication can be obtained at no additional cost.

The PDP-14 has complete software support for both control programming and diagnostic trouble shooting. There is a software program which will convert Boolean equations, which were written in symbolic form, into terms of inputs and outputs. Another program will convert that form into actual 12-bit, binary inst uctions which are used to make the ROM (read-only-memory). Other software programs are used for locating trouble in the central processor, the input and output boxes, and the ROM. Another program can be used to simulate the actual controlled process so that many start-up problems can be avoided. All software requires the use of a mini-computer.

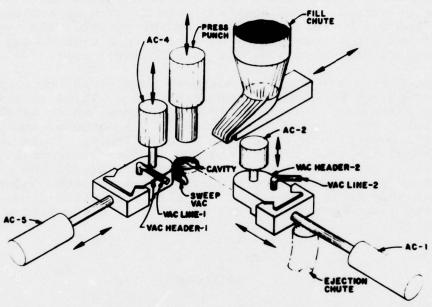
#### **EPILOGUE**

This automatic system for manufacturing explosive pellets has been in operation approximately three years. The production yield greatly improved due to a 25% faster pressing cycle and less system downtime. The improved safety features which closed-loop logic control allows have prevented any equipment damage because of control failure. The quality of the product and the reject rate have both improved because of the consistancy of completely automatic control. Only two or three electronic failures were encountered and they occurred within the first 45 days of operation. The "reed" limit switches, which are an integral part of the air cylinders, have performed extremely well. The only replacement was a lead which was broken by the movement of the tooling mechanism. When the manufacturing system had been in operation approximately 13 years, another identical pellet manufacturing system was fabricated and placed under control of the same PDP-14. The capacity of the PDP-14 Programmable Controller will permit at least five more similar systems to be placed under its control.

Additional information presented in this seminar was published in D. O. Page and C. F. Draut, "An Automatically Controlled Electrical Heating System for Use in an Explosive Environment," MLM-2136 (OP), August 8, 1974, 5 pp.

#### APPENDIX A

METAL INSERT LOADING AND PELLET REMOVAL MECHANISMS AUTOMATED THE PELLET MANUFACTURING PROCESS.



- Step 1. AC-1 extends, placing vacuum head #2 over the cavity.

preformed insert.

Step 4. AC-2 retracts, lifting pellet from cavity.

AC-4 retracts, lifting preformed insert from pickup position.

Step 5. AC-1 retracts, placing pellet over ejection chute.

AC-5 extends, cleaning the cavity with a sweeper vacuum and placing the preformed insert over

the cavity.

- Step 6. AC-2 lowers pellet into ejection chute.
- Step 7. AC-4 lowers preformed insert into cavity.

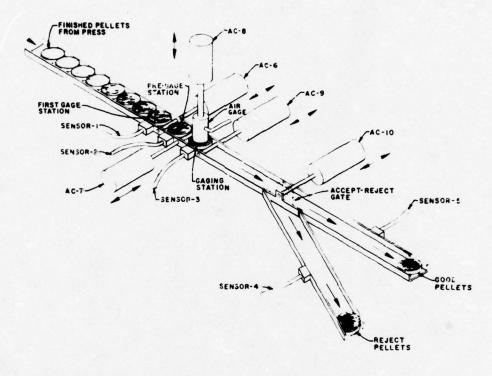
  VAC-2 deactivates, releas-
- Step 8. VAC-1 deactivates, releasing preformed insert. AC-2 retracts

ing pellet in ejection chute.

- Step 9. AC-4 retracts.
- Step 10. AC-5 retracts.
- Step ll. Air clutch is activated starting press cycle. (Press cycle includes filling the cavity with powder and pressing the pellet.)
- Step 12. Repeat 1, starting the next pellet producing cycle.

#### APPENDIX B

AN AIR GAGE WAS AUTOMATED THROUGH THE USE OF PART SENSORS AND GATING LOGIC.



- Step 1. Pellet arrives at first gage station after sliding down ejection chute.
- Step 2. Sensor 1 detects the pellets presence and AC-6 retracts, allowing pellet to slide into pregage station.
- Step 3. Sensor 2 detects the pellet's presence and AC-6 extends, segregating this pellet from any others in line.
- Step 4. AC-7 retracts, allowing pellet to slide into gaging station.
- Step 5. Sensor 3 detects the pellet's
   presence and AC-7 extends.
- Step 6. AC-8 extends, lowering air transducer into contact with pellet, thus gaging its thickness.

- Step 7. AC-8 retracts after preset gaging time.
- Step 8. AC-9 retracts, allowing pellet to slide out of gaging station.
- Step 9. Depending upon results of gaging, AC-10 will either extend or retract, gating pellet into accept or reject channels.
- Step 10. When pellet slides past
   sensor 5 (accept sensor) or
   sensor 4 (reject sensor),
   AC-9 extends.
- Step 11. This completes the sequence for one pellet through the gage parts handling system. It should be noted that all stations can handle pellets simultaneously, permitting minimum delay in processing.

# EVALUATION OF PYROTECHNIC OUTPUT BEHAVIOR BY HIGH SPEED CINEPHOTOGRAPHY

M. D. Kelly, J. H. Mohler and L. D. Haws
Monsanto Research Corporation
Mound Laboratory
Miamisburg, Ohio
operated for
UNITED STATES ENERGY RESEARCH
AND DEVELOPMENT ADMINISTRATION
U.S. Contract No. E-33-1-GEN-53

This 15-minute motion picture film described the output characteristics of selected Ti/KClO4, TiHx/KClO4, and Al/KClO4 pyrotechnic systems at quantity levels of 10 and 25 g. High-speed cinephotography was used to compare the reaction behavior of these pyrotechnic systems. Of particular interest was an assessment of burn times and fireball sizes. Additionally, millisecond-response thermocouples were placed at various locations above the primary reaction zone in order to establish temperature profiles. These two techniques - high speed cinephotography and temperature profiling - are providing information essential for evaluating the hazard potential of selected pyrotechnic formulations at Mound Laboratory.

# AUTOMATIC PELLETIZING SYSTEM FOR PYROTECHNIC MATERIALS

#### ABSTRACT

An automatic system was developed for producing pellets from blends of finely divided pyrotechnic materials and DAP (diallyl phthalate) plastic. Operational restrictions imposed by the hazardous nature of pyrotechnics are met with equipment powered with air and controlled in operational sequence with air-logic circuits. The process consists of moving the blend from a hopper to a cavity where it is pressed into a pellet, which is subsequently ejected. The pellets are used as preforms for a rolding process.

The automatic pelletizing system provides improvement in safety, production rate, and product consistency over the manual system it replaced.

#### INTRODUCTION

A device was desired to mechanize the pelletizing of pyrotechnic material into preforms for loading into a Drabert molding press. The press molds pyrotechnic parts which consist of 70% pyrotechnic material and 30% DAP by weight.

The purpose of pelletizing the pyrotechnic material is to eliminate the handling of loose powder in the loading operation. In a pelletized form the pyrotechnic material is significantly less hazardous than it is in a loose form. On a sensitivity scale of 0 (can safely be carried in one's pocket) to 7 (highly volatile) the raw pyrotechnic material is rated at 7, as illustrated in Figure 1. Blending the pyrotechnic material with DAP lowers the sensitivity to a level of 4 or 5. Pelletizing the pyrotechnic/DAP blend lowers the sensitivity further to 3, so handling the pellet in lieu of the loose powder is one to two levels of sensitivity safer for the press operator. The final molded part has a sensitivity level of 2 and weighs approximately 1.5 g. The amount of material required for pressing is 10 g, which provides an excess of material for the sprue.

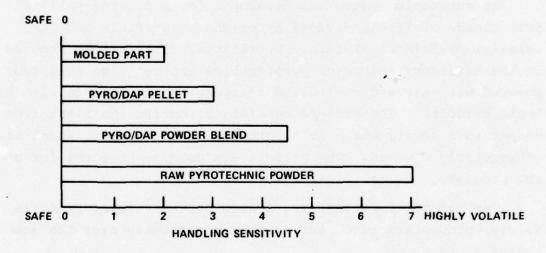


Figure 1 - Pelletizing the Pyro/DAP powder blend reduces the material handling hazard.

At first, pellets were made with an isostatic press. Loose blended powder was poured into 3/8 in. diameter Tygon tubing and the ends were capped. Six or seven filled lengths of tubing were placed in the isostatic (oil medium) press and the press was pumped down manually to the pressure required to compress the powder to a stable density. The tubes were then taken from the press, wiped free of oil, and opened. The compacted powder was extruded and divided, preferably into cylindrical pieces about 3/8 in. long and whatever fragments occurred.

This method of production has various drawbacks. The main one is the hazard of this spark-sensitive material to the technician during the manual filling of the tubes. Although this operation was conducted behind a safety screen and the technician wore protective clothing, the operation was nevertheless hazardous. With pyrotechnics, the concern is not "if it goes off," but rather "when it goes off". To be best prepared for when the event happens, the operator would have a tremendous advantage if he could oversee the pressing from a remote location rather than be beside it.

Another disadvantage of the manual operation is the inconsistent size of the pellets. If the pellets were the same size and density, the 10 g of material required for molding could be measured easily by counting the pellets as they were deposited in the press. Otherwise, the operator must use his own judgment and employ the number of pellets that "looks about right".

The use of oil in the isostatic press is another undesirable feature, since oil has long been known to be detrimental to explosive powders. Various accidents are possible during the isostatic operation, some of which could allow oil to get inside of the Tygon tubing undetected. Contamination by oil leads to varied firing characteristics and could possibly stop ignition of the part.

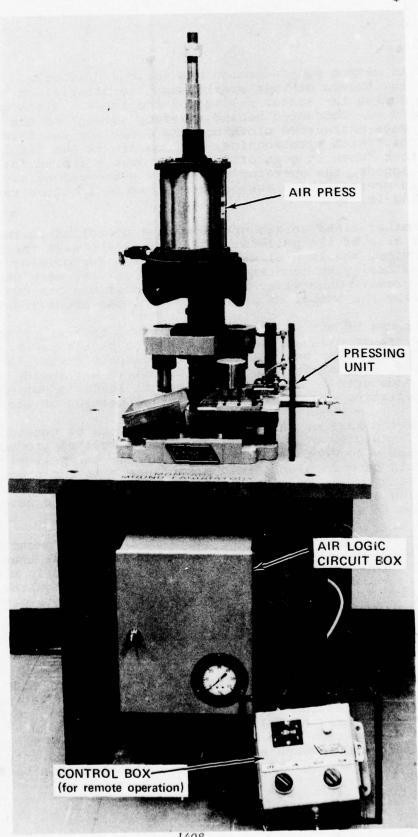
The slowness of the manual operation was of considerable concern. In view of an ever increasing number of products to be processed to meet development schedules, the pelletizing operation could have developed into a bottleneck in the program. Pelletizing by manual operation required a number of weeks for processing a batch of material which feasibly could have been processed in days with automated equipment.

For these reasons, we proceeded in the development of an automatic pyrotechnic pelletizing system (Figure 2) that operates remotely and produces a pellet which is consistent in size and density. Although mechanical interactions were required within the system, safety features were also implemented to provide a safe and dependable operation.

#### AUTOMATED SYSTEM

The pyrotechnic pelletizing system consists of four major parts: (1) the powder shoe and hopper, (2) the pellet pressing unit, (3) the ejection system, and (4) the automatic controls. The system operates as follows: The powder shoe assumes a position over the die cavity. The material to be compressed moves from the hopper, into and through a channel in the shoe, and into the die cavity. After the cavity is filled, the shoe slides back to expose

- Air logic circuitry permitted remote operation of the automatic pelletizing system for pyrotechnic materials. In the insert is the remote control box. Figure 2



the cavity. A punch descends into the cavity and compresses the contents into a pellet. The punch is pulled out of the cavity and a lower punch, which forms the bottom of the cavity, rises to eject the pellet from its mold. The shoe slides forward to push the pellet out of the way and to bring the channel into position for loading material with which to press another pellet. Simultaneously, the lower punch descends and creates a suction in the cavity which facilitates the filling. A detailed description of each part is given below.

Powder Shoe and Hopper

The assembly comprised of the powder shoe, its attached hopper, and the associated parts is shown in Figure 3. The shoe is moved back and forth across the die cavity by an air cylinder. A small vibrator attached to the shoe operates during the filling of the cavity to stimulate the gravity flow of the filling material. A strip of nylon was mounted on the end of the shoe to enable it to glide more easily across the die block. The shearing action on the pyrotechnic/DAP material as it is leveled flush with the die block is less with the nylon than with bare metal. A grounding strap was mounted to the device to bleed any static charge which could build up on the nylon material.

The shoe and hopper were fabricated of stainless steel to avoid contamination of pyrotechnic materials with oxides which might be formed if these items were built of less corrosion-resistant metals. The internal walls of the hopper and of the channel through the shoe were highly polished for best flow of material and assurance that material did not adhere to them. The assembly holds about 65 g of material which is enough for about 130 pellets. This is well below the safety limit of 100 g maximum amount of material allowed in one location.

Pellet Pressing Unit

The pellet pressing unit consists of a die, upper punch, upper punch holder, lower punch, die set, and an air-actuated press. The press drives the upper punch down into the die cavity to form the pellet. The punch is stopped by the compression limit of the pressed material rather than by a dead stop to eliminate variations in pellet density from differences in amounts of material submitted to pressing. Conceptually, a usable pellet will be obtained from any amount of material entering the die cavity, including the final amount in the hopper. A picture of the pellet pressing unit is shown in Figure 4.

The compaction force is furnished by a column press with a 4-in. bore cylinder. The press drives the upper plate of the die set. The upper plate holds the upper punch, which is attached to it by a punch holder. A pivot joint connection between the press

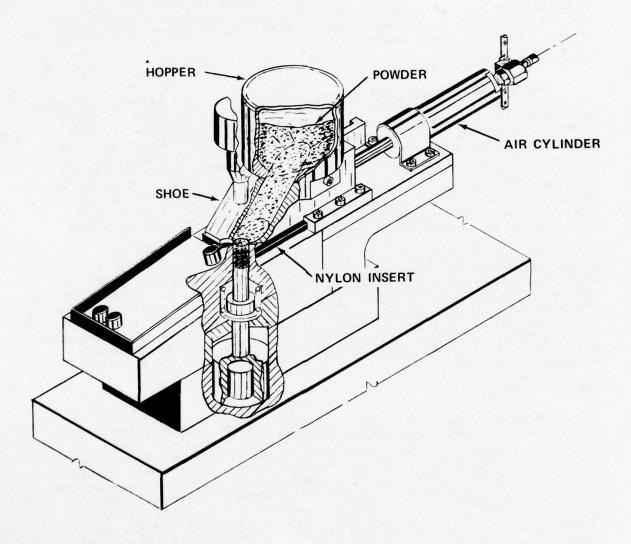


Figure 3 - The powder shoe and hopper assembly is positioned by an air cylinder.

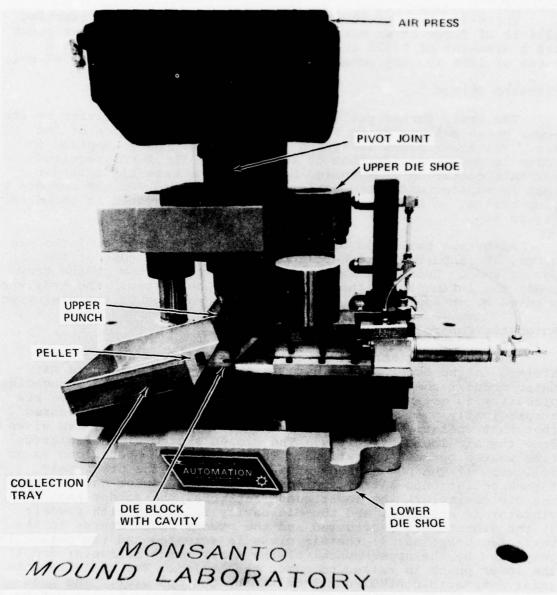


Figure 4 - The pellet pressing unit compacts the powdered material into a pellet.

and the die plate allows pressure to be applied without problems of alignment. The die block, which contains the powder cavity, is mounted on the lower plate of the die set. Alignment between the upper punch and the cavity is obtained with the guide posts on the die set. The bottom of the cavity is formed by the lower punch which in its retracted position is fixed to give a fill depth of 0.625 in. With a compression ratio of roughly 2:1, the upper punch enters the cavity half way to form a pellet about 0.300 in. thick, which weighs approximately 450 mg.

The 4-in. bore of the press cylinder is capable of exerting 1256 lb of force at an air pressure of 100 psig. The upper punch has a diameter of 0.300 in. or an area of 0.0707 in. With a force of 1256 lb, the potential compaction pressure is 17,765 psi.

# Ejection System

The newly formed pellet is ejected from the die cavity by the lower punch raising up to a position flush with the top of the die. The lower punch is spring loaded so the force supplied to raise it must override that of the spring. The force required for this operation is supplied by a 2.50-in. bore air cylinder that is mounted under the table that is the base for the compaction system. A sectional view of the ejection system is shown in Figure 5.

After the pellet is brought up flush with the top of the die block, it is pushed into a collection tray by the nose of the powder shoe. Subsequently, it travels to the bottom of the tray under the influence of the vibrations in the system. The tray was mounted on an appropriate angle to take advantage of the vibrations.

#### Automatic Controls

The automatic control circuitry is housed in an enclosure affixed to the front of the base (see Figure 2). Clippard Minimatic modular components and air valves are used in the sequencing circuitry to establish a closed-loop system. The air valves are strategically positioned to detect each operation to be assured that that operation actually took place once the signal was given from the air logic circuitry. The closed system also eliminates time wasted between operations. The sequence of operations is as follows: 1) The powder shoe advances, pushing the previously formed pellet onto a tray and positioning the powder channel over the die cavity; 2) the lower punch retracts, the powder shoe vibrator is actuated, and the die cavity is filled with powder; 3) the vibrator is deactuated and the powder shoe returns to its retracted position; 4) the air press is actuated and the pellet is compacted by the upper punch; 5) the upper punch retracts; and 6) the lower punch is raised to eject the pellet. The cycle repeats under automatic control until halted by the operator. The pneumatic circuit for this sequence is shown in Figure 6. It can be seen that the air-logic circuit is a series of three- and four-way valves positioned to achieve the proper sequencing.

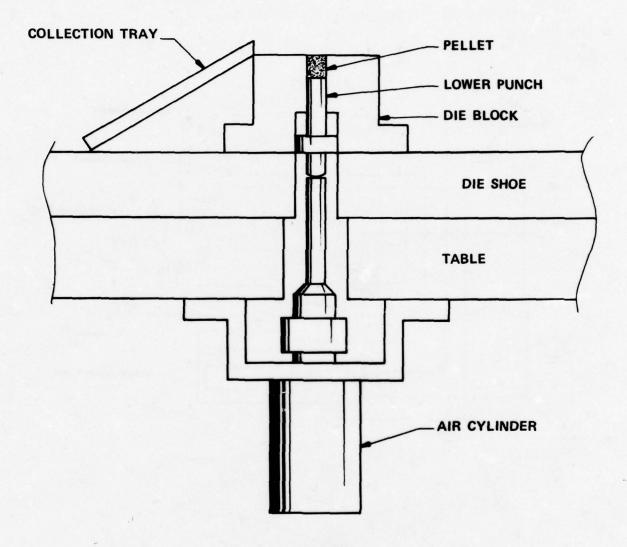


Figure 5 - The ejection system removes the pellet from the die cavity.

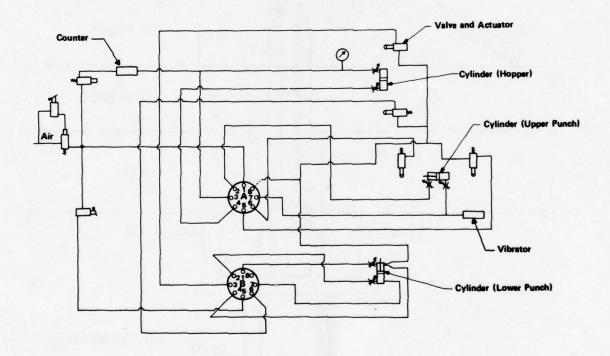


Figure 6 - Pneumatic circuit for pyrotechnic pelletizing system.

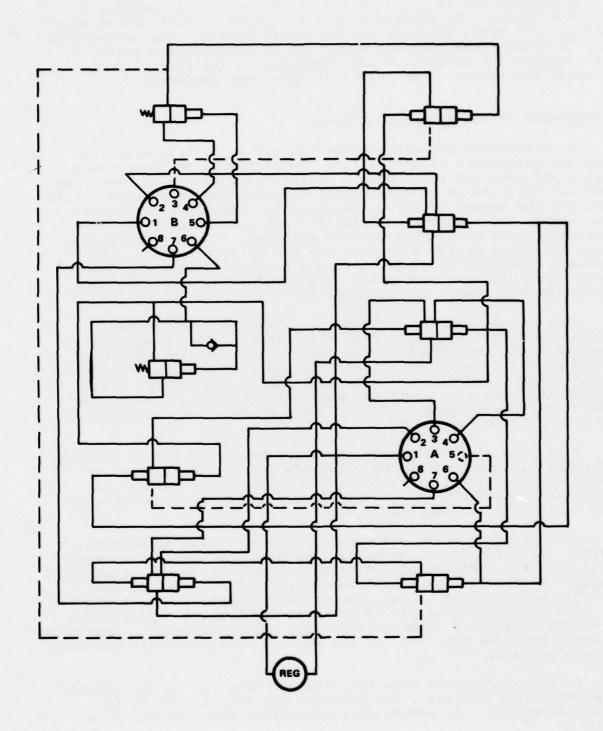


Figure 6 (Continued)

A control box is provided for remote control to start and stop the system. An emergency control button (on-off switch shown in Figure 2) shuts down air to the entire system. The conventional stop lets the cycle continue and cease at a designated point in the sequence. A counter is also included in the control box to count the number of pellets that have been produced.

#### DEVELOPMENT OF THE PELLETIZING SYSTEM

A preliminary pressing device was set up to determine the pressing parameters of the pellet. To arrive at an approximate fill depth required to produce a pellet 0.300 in. thick, the compression ratio of an inert simulant material was calculated. This was also the amount of stroke required for the ejection process. Even though the simulant material did not have exactly the same characteristics as the pyrotechnic material, it was close enough since the final pellet thickness was not critical. Also, the amount of pressure required to form a simulant pellet was determined. Calculations made using this information indicated that a 2-in. bore cylinder was required for the production equipment.

Once the pelletizing system was fabricated, development efforts were continued. In the original concept, the suction created by the retraction of the lower punch plus the vibration caused by the movement of the air cylinders were expected to be enough to move the material into position in the cavity. This was not the case. An auxiliary air vibrator was mounted on the side of the powder shoe to break up the bridging of the material and move it into the cavity.

A bar was also installed across the hopper to aid in breaking the material loose during the vibratory action. Because it was feared that continual vibration would separate the pyrotechnic and plastic materials, the air logic was set to run the vibrator only during the loading operation.

Various pyrotechnic mixtures were tried in the production device. In a few cases, material flow problems were encountered even after the addition of the vibrator, and the amount of material supplied to the cavity was not sufficient for a normal pellet. Although not required at the time of development, a bigger vibrator with frequency controls is proposed for general applications to ensure adequate flow of material for normal pressing. Frequency controls could be adjusted for the particular pyrotechnic material being processed.

In the progression from the simulant material to the actual pyrotechnic/DAP material, the pressure was not sufficient for pellet formation. To remedy this situation, the original 2-in.

cylinder on the pellet press was replaced with a 4-in. cylinder which quadrupled the pressing power. This resulted in well-formed pellets from all the various powder blends. The air line pressure was adjusted to achieve the proper density and size of pellets.

#### SAFETY CONSIDERATIONS

With the design of any new system, new problems in safety are inherent. The combination of mechanical operations and sliding assemblies presents possibilities of sparking, and the application of sudden excessive pressure cannot be tolerated by the powder.

The hazards associated with sparking were eliminated by strategically designing nonsparking materials into the system. The die body (A) and the bottom slide (B), which guides the powder shoe, were fabricated of nonsparking aluminum bronze. These are shown in Figure 7. The upper and lower punches slide in and out of the die body; the powder shoe slides across the die body and the bottom slide. Any mechanical interference in the movement of the punches or the powder shoe could produce sparking if non-sparking material was not employed for fabrication of one of the contacting surfaces. Also, the nylon strip mounted on the powder shoe, which levels the charge to the die cavity and is a sliding surface, is nonsparking.

With an automatic system there is always the danger of damage to the equipment in the case of a control failure or mechanical bind. Such a mechanical incident may be compounded by a pyrotechnic incident caused by the mechanical components striking or punching the pyrotechnic material. To avoid mechanical damage to the press from control-circuit failure, limit switches were introduced into the system to ensure that a cylinder does retract if it is given the signal to do so. An example of the switches used is illustrated in Figure 8. It can be seen that the upper die plate must be at the top position for the limit switch to be activated. Each operation is detected by switches before the next operation can take place. In this way, a failure or mechanical bind would result in the device coming to a stop until the corrective action of an operator.

Precautions were taken that pressing and ejecting forces were not applied to the material too quickly or too hard. To prevent either of these potentially hazardous situations from occurring, control of the respective pressing motions was doubled. Dual flow controls were installed on both directions of the appropriate air cylinders so that if one controller failed the other would function to ensure a steady, regulated application of force.

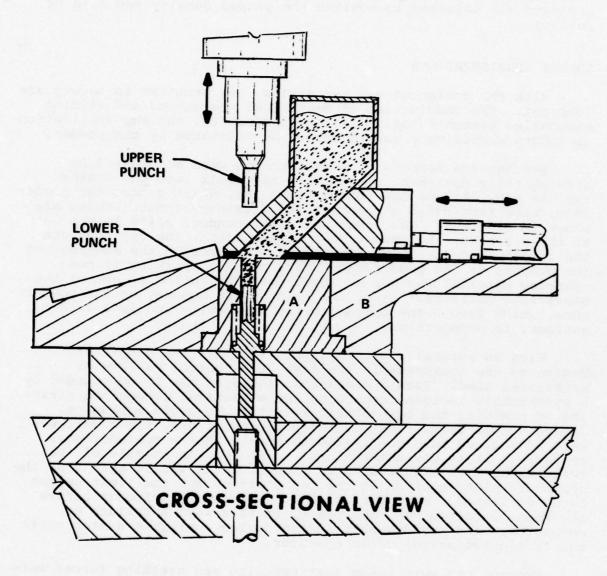


Figure 7 - Nonsparking materials were designed into the system to retard sparking at contacting surfaces of metallic components.

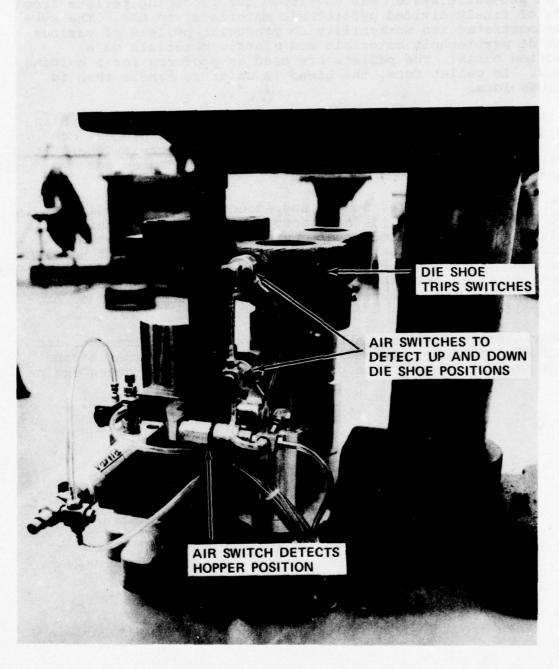


Figure 8 - Air switches detect the positions of mechanical components to ensure proper component sequencing.

# SUMMARY

An automatic system was developed for producing pellets from blends of finely divided pyrotechnic materials and DAP. The system demonstrated its workability in producing pellets of various blends of pyrotechnic materials and plastic materials on a production basis. The pellets are used as preforms for a molding process. In pellet form, the blend is safer to handle than in the loose form.

The process equipment is powered with air and controlled in operational sequence with air logic circuits. The process consists of moving the blend from a hopper to a die cavity where it is pressed into pellets which are subsequently ejected and collected for use.

The process is safe, quick, and economical. It meets the restrictions imposed by the hazardous nature of pyrotechnics. It is safe with respect to means of operating power and control, materials of construction, and features of operation. It permits remote operation which provides safety to personnel and economy in operator time. With a 4-sec cycle time, the automatic process is four to five times faster than the prior manual method of producing pellets.

Savings are realized in both operator time requirements and product availability. In addition, the process provides a consistent product that is free of contamination from process equipment.

#### APPENDIX - COMPONENTS AND MANUFACTURERS

# Pressing System

Air Press

Mead Column Press, Model #CP-7-S, 3-in. stroke, 4-in. bore Mead Fluid Dynamics, Inc. 4114 N. Knox Avenue Chicago, Illinois 60641

Die Set

Danly, Cat #0604-C1 with guide post #5-0834-1
Danly Machine Corp.
Chicago, Illinois

Vibrator
 Model VM-25
 Cleveland Vibrator Co.
 2828 Clinton Avenue
 Cleveland, Ohio 44113

Air Cylinders
 Model BF-041-D, 3/4-in. bore, l-in. stroke
 Bimba Manufacturing Co.
 Monee, Illinois

Model DM-15, 2-1/2-in. bore, 5/8-in. stroke with inter pilots
Mead Fluid Dynamics
4114 N. Knox Ave.
Chicago, Illinois 60641

#### Pneumatic Controls

Pressure regulator - Model BR Bellows - Valvair Akron, Ohio

Pressure gauge #191880 (0-15 PSI) Corning Glass Works Fluid Products Dept. Corning, New York

Counter #HP 15.12 H. Kuhnke Inc. Atlantic Highlands, N. J.

# Logic

Clippard four-way valve, Model #R-401
Clippard four-way valve, Model #R-402
Clippard three-way delay valve, Model #R-331
Clippard three-way valve, Model #R-302
Clippard three-way valve, Model #MAV-3
Clippard three-way valve, Model #MJV-3
Clippard push button, Part #13100-9
Clippard Instrument Lab., Inc.
Cincinnati, Ohio

# DESIGN, DEVELOPMENT AND APPLICATION OF A VERSATILE ELECTROSTATIC SENSITIVITY TESTER

L. D. Haws, R. C. D'Amico and A. Gibson
Monsanto Research Corporation
Mound Laboratory
Miamisburg, Ohio
operated for
UNITED STATES ENERGY RESEARCH
AND DEVELOPMENT ADMINISTRATION
U.S. Contract No. E-33-1-GEN-53

#### **ABSTRACT**

An electrostatic sensitivity tester was developed recently at Mound Laboratory and tested with selected pyrotechnic compositions. Basically, the system permits evaluation of sensitivity under controllable environmental conditions (temperature and humidity) using a variety of electrical parameter combinations.

#### INTRODUCTION

After many years of work in the field of secondary high explosives technology (PETN, RDX, HMX, etc.), Mound Laboratory during the past 2 yr has been involved in the development and production of pyrotechnic materials. In order to establish satisfactory operational safety criteria for working with sensitive, finely divided metal fuels and pyrotechnic composites, we first reviewed much military and commercial literature and talked with a host of people having many years of experience in the pyrotechnic field. Of particular interest to us were sensitivity data and the procedures used to generate the data banks. Being preconditioned by our experience with secondary high explosives, which are generally less sensitive than pyrotechnics to ignition by electrostatic stimuli, and because a review of various accident reports indicated electrostatic problems were major contributors to accidental ignition of pyrotechnics, we directed our first efforts to an evaluation of electrostatic sensitivity of the bulk pyrotechnic materials that we were handling as well as the hotwire ignited units we were producing. Some of the pyrotechnic materials were developmental and no electrostatic sensitivity data were readily available. Furthermore, as reported recently, no really standardized test method exists to evaluate the electrostatic discharge resistance of energetic materials and devices; in fact, test conditions vary from item to item, even with specifications prepared for the same program. 1

One additional concern developed during our initial pyrotechnic project: What are the effects of the operating environment (temperature and humidity) on sensitivity to electrostatic discharges? Practical trade-offs exist. A high working humidity should alleviate the problem of the accumulation of electrostatic charges on the human body; on the other hand, a high humidity may produce other problems associated with finely divided, reactive reductant fuels and hydroscopic oxidizers. Unfortunately, only a limited amount of data has been published relative to testing under a variety of environmental conditions.

Because of the various factors cited above and because Mound Laboratory has an organizational entity experienced in designing and fabricating materials and product testers, we decided to construct our own electrostatic sensitivity tester (designated MT1032). Design considerations for an electrostatic sensitivity tester suitable for a variety of uses included:

- 1. In-house development of a hazards data base to establish the most appropriate materials-handling criteria.
- Correlation of existing data generated elsewhere using a variety of electrical conditions and test procedures.
- 3. Capability to ascertain apparent electrostatic sensitivities under a variety of environmental conditions.

Versatility was the key "ingredient". Provisions were to be made to enable creation of a variety of environmental conditions. In addition, it was considered desirable to have the capability to easily change electrical parameters to match those associated with "standard" electrostatic sensitivity tests run elsewhere.

#### MT1032 TESTER DESCRIPTION

A photograph of the MT1032 Electrostatic Sensitivity Tester is presented in Figure 1. The tester consists of a two-bay console with a Thelco Model 19 Vacuum Oven located in the right-hand bay; a closeup of this environmental test chamber is shown in Figure 2. The test chamber can be evacuated to 30 in. of Hg or pressurized to 2 psig; chamber temperature can be varied from ambient to 200°C. If desired, various gaseous environments can be produced via the vacuum inlet and exit lines.

Power required to operate the tester is 115  $\pm$  10 V a.c., 60 Hz, 15 A. The simplified pulse circuit is shown in Figure 3. Capacitance selections include 250, 500, 600, 1000, or 2000 pF. Series resistance can be selected from 100, 500, 1000, 10,000 or 100,000  $\Omega$ . Test voltage can be varied from 0 to 50 kV.

The upper electrode consists of a steel phonograph needle. For testing bulk powders, the lower electrode consists of a circular steel sample block with a 3/8 in. diameter x 1/32 in. depression in the center. Normal test configuration is illustrated in Figure 4. The sample block rests on top of a movable plunger whose vertical motion is controlled by a stepping motor. In a "fixed gap" testing procedure this stepping motor is used to reliably achieve any gap between 0.025 and 2.5 in. Alternatively, the stepping motor can be used in such a way that the lower electrode approaches the upper (fixed) electrode at a "dialed in" rate; when gap breakdown occurs the current pulse through the test sample switches off the stepping motor. A cutaway sketch of the placement of the stepping motor and electrodes inside the environmental chamber is shown in Figure 5.

## STANDARD TEST CONDITIONS

Under the proper environment the human body is an excellent accumulator and generator of static charge. This charge is of low energy but sometimes of high potential, and stored potentials of 10-20 kV are not uncommon. A person so charged who comes in contact with a pyrotechnic material will, under the proper conditions, discharge the stored energy through the pyrotechnic and thus cause ignition.

The literature contains a great deal of confusion regarding the electrical circuit simulation of the human body. S. Moses has compiled<sup>2</sup> a listing of many of the studies that have been reported

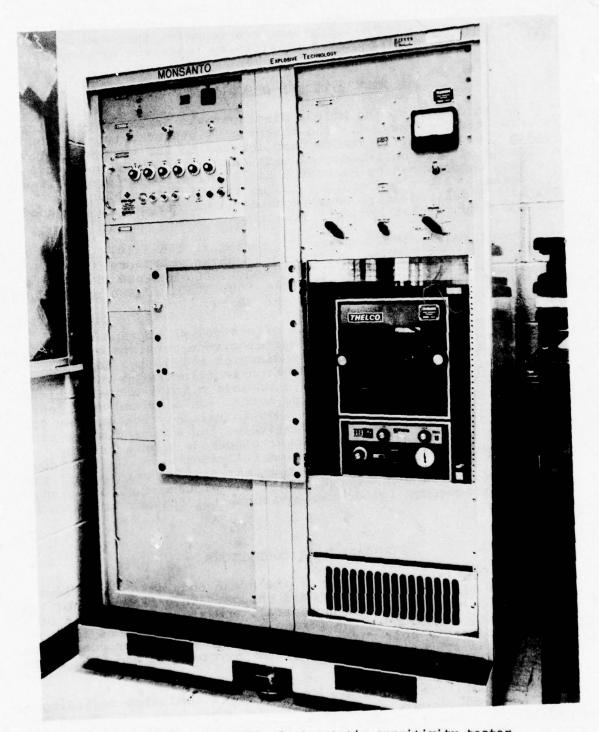


Figure 1 - MT 1032 electrostatic sensitivity tester.

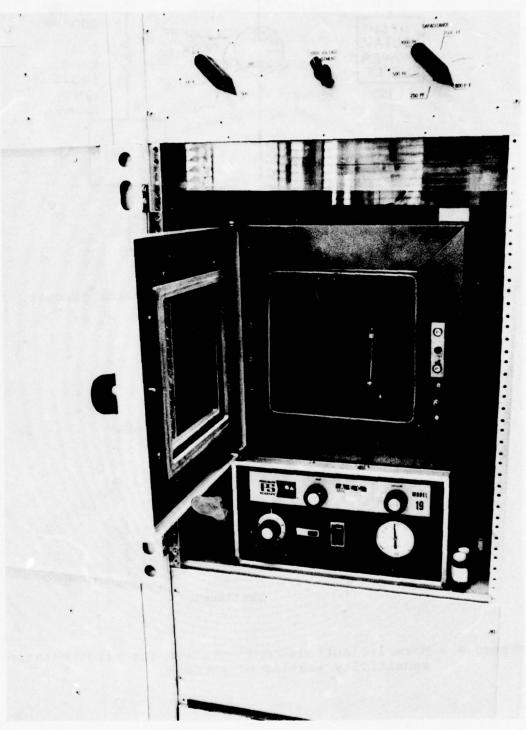


Figure 2 - MT 1032 test chamber. 1427

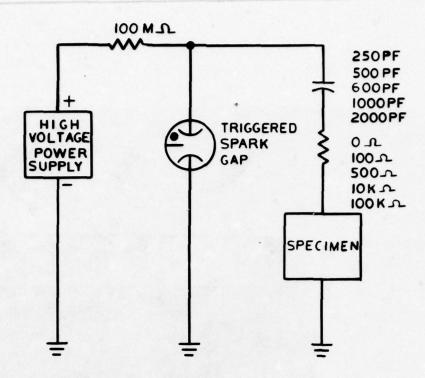


Figure 3 - MT1032 simplified electrostatic pulse circuit.

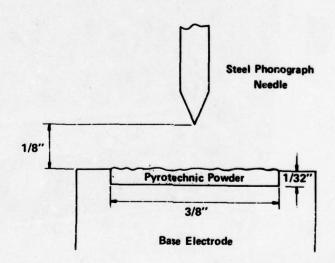


Figure 4 - Normal electrode configuration for electrostatic sensitivity testing of powders.

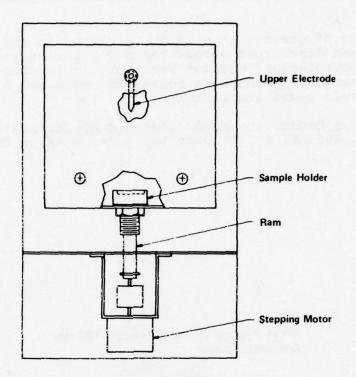


Figure 5 - Stepping motor assembly.

to date. Capacitance values for a 6-ft person range from 100 to 4,000 pF although most investigators agree on a value of 100 to 500 pF. Maximum potential values range from 20 to 40 kV. However, in at least one Sandia study, T. Tucker reported³ that "at the 40-kV level a corona discharge was observed as the subject's hand approached the monitoring electrode." Because the discharge occurred prior to the main spark, body potential at spark time was reduced below the initial level. It is improbable, therefore, that 40 kV would be sustained by the human body in practical situations. Tucker's study suggested that the spark discharge characteristics of the human body could be approximated by a critically damped LRC circuit corresponding to the equation:

i =  $CV_O t\alpha^2 e^{-\alpha t}$ where  $\alpha$  = 2/CR, C is capacitance,  $V_O$  is the initial voltage, R is the series resistance, and i is the instantaneous current at time t. Subsequent Sandia studies determined that appropriate capacitance and resistance values for human body simulation were 600 pF and 500  $\Omega$ , respectively. The MT1032 output waveform of a 600-pF capacitor discharged through a 500- $\Omega$  calibration resistor is shown in Figure 6.

If a voltage of greater than 20 kV is stored in the 600-pF capacitor and then discharged across the  $500-\Omega$  series resistance and through the pyrotechnic without ignition, it is doubtful that electrostatic charges developed on bodies of personnel handling that material could cause its ignition.

This then has become the Mound standard electrostatic test procedure, i.e., 600 pF, 500  $\Omega$ , vary the voltage using the Bruceton technique.

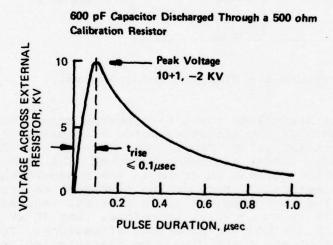


Figure 6 - MT1032 output wave form.

#### APPLICATIONS

During the design development of a pyrotechnic valve actuator for an ERDA application, Sandia Laboratory (Albuquerque, N.M.) selected a Ti/KC104 formulation because it best satisfied the performance features required. Unfortunately, the threshold spark sensitivity of the optimum Ti/KC104 formulation was less than 7.5 mJ. This is a borderline material insofar as a general Sandia philosophy shared by Mound Laboratory is concerned; namely - "If a component contains a sensitive material it must be regarded as inherently hazardous independent of engineering design and procedures." In fact, one of our mutual objectives was to develop metal powders with reduced sensitivity without impairing functional performance in pyrotechnic compositions.

Studies at Sandia suggested that if titanium were replaced with an equivalent particle size titanium hydride ( $TiH_2$ ), the sensitivity to electrostatic stimuli of the pyrotechnic was reduced by approximately two orders of magnitude to >480 mJ. This was an acceptable material insofar as handling safety was concerned. Unfortunately, during device development, some unacceptable performance features developed when  $TiH_2$  was substituted for Ti:

- Tenuous ignition reliability at low temperatures (-65°F)
- 2. Dubious long-term material stability  $H_2O$  and KCl were produced during accelerated aging presumably as a result of the solid state reaction:

 $4\text{TiH}_2 + 3\text{KClO}_4 \rightarrow 3\text{KCl} + 4\text{H}_2\text{O} + \text{TiO}_2$ 

The following unacceptable trade-off prevailed:

	Ti/KC104	TiH2/KC104	
Acceptable	Reliability Stability	Handling Safety	
Unacceptable	Handling Safety	Reliability Stability	

The Hydride Chemistry Group at Mound prepared various partially hydrided titanium fuels for evaluation. The general result of these extensive studies is stylized in Figure 7. Notice that at a stoichiometry of TiH  $_{0.6\,\,5}$  a near optimum condition was achieved, and that titanium hydride stoichiometry when combined with KClO  $_4$  produced satisfactory performance characteristics without compromising handling safety.

Some associated safety studies with  ${\rm TiH_X/KC10_4}$  sys ems included an evaluation of electrostatic sensitivity as a function of surface area as well as hydrogen content of the fuel ( ${\rm TiH_X}$ ). Results

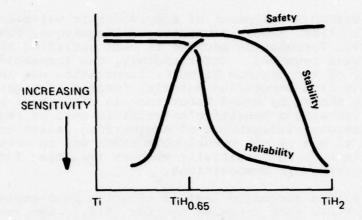


Figure 7 - Partial hydriding of titanium provided an acceptable fuel.

typical of these studies are suggested by the three curves of Figure 8. The results clearly indicate the importance of reducing the surface area (increasing particle size) of the fuel in reducing electrostatic sensitivity. This effect was further demonstrated by fractionating samples of  $\text{TiH}_{\text{X}}$  into narrow particle size ranges using a Bahco Microparticle Classifier. Results of one of these studies with  $\text{TiH}_{1.9\,3}$  are presented in Figure 9. In this case electrostatic threshold sensitivity is shown for  $\text{TiH}_{1.9\,3}$  undiluted with KClO<sub>4</sub> oxidizer. The diluting effect of KClO<sub>4</sub> on the electrostatic sensitivity of  $\text{TiH}_{\text{X}}$  samples is shown in Figure 10.

In addition to hydriding of titanium, we have been experimenting with other means of reducing electrostatic sensitivity without sacrificing functional performance. One of the most successful approaches has been microencapsulation of the finely divided metal fuel. A typical result is illustrated in Figure 11.

Although the nature of the individual constituents of a given pyrotechnic composition contributes to its electrostatic sensitivity, other "external" factors may contribute as well. One of these "external" factors considered was humidity. The design features of the MT1032 tester facilitate production and maintenance of a variety of humidity conditions.

An illustration of the effects of chamber humidity on measured electrostatic sensitivity results of evaluating a  $TiH_{0.83}$  material are shown in the following tabulation:

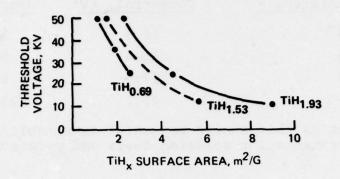


Figure 8 - Electrostatic sensitivity of  ${\rm TiH_{X}/KC10_{4}}$  is a function of fuel surface area and hydrogen content.

FUEL: TiH1.93

	SURFACE	THRESHOLD VOLTAGE KV	OXYGEN
TOTAL POPULATION	4.0	> 50	1.71
FRACTION 1 (COARSE)	0.5	> 50	0.97
FRACTION 2	1.4	1/10@ 50	1.42
FRACTION 3	2.7	29.6	2.53
FRACTION 4 (FINES)	4.3	7.2	3.98

Figure 9 - Fractionated samples of a fuel powder population yield discrete sensitivities.

	TiH <sub>x</sub>	THRESHOLD VOLTAGE	
X IN TIHX	SURFACE, m <sup>2</sup> /G	TIH, ONLY	TiH <sub>x</sub> /KCIO <sub>4</sub>
1.93	2.33	15	> 50
1.47	7.84	6.3	14.8
1.11	1.04	32.9	> 50
0.75	1.86	<1	37
0.58	1.59	< 1	28.5
0.19	8.16	< 1	< 1

Figure 10 - The static sensitivity of the fuel  $\text{TiH}_X$  is reduced on combination with the oxidizer KClO4.

Chambon Hamida	Threshold		
Chamber Humidity, %	Potential, kV	Energy, mJ	
10	11.5	39.6	
45	13.6	55.5	
65	17.0	86.7	
85	27.7	230.1	

Information such as this should be useful in establishing safe operating environments for selected fuels and pyrotechnic compositions.

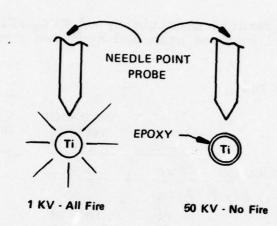


Figure 11 - Microencapsulation reduces electrostatic problems associated with 1-micron titanium.

#### REFERENCES

- S. A. Moses, "Electroexplosive Devices: A Survey of Electrostatic Hazards Testing," MDAC Paper WD2120, McDonnell Douglas Aircraft Co., presented to Picatinny Arsenal, May 23-24, 1973.
- 2. S. A. Moses, op. cit.
- T. J. Tucker, "Spark Initiation Requirements of a Secondary Explosive," <u>Annals of the New York Academy of Sciences</u>, <u>152</u>, 643 (1968).

# FORMATION, FUNCTIONS, AND METHODS OF OPERATION

## OF THE AUSTRALIAN ORDNANCE COUNCIL

prepared by

Air Commodore K. Therkelsen BScApp, MSc(USAFIT), FIE(AUST), RAAF President, AOC

- 1. I am very pleased to have this opportunity to talk with you about the Australian Ordnance Council. The main reason for its existence is to ensure that explosive stores used by the Australian Defence Force are designed to take account of user safety and the need for these stores to continue to be safe for use in the service environment. Safety is the name of the game where the AOC is concerned, and performance is incidental unless there are safety implications. As you are well aware, judgements in respect of safety depend very heavily on past experiences. The wider the range of experiences which can be taken into consideration, the more likely it is that sensible and reasonable judgements will be made. For these reasons I am very happy to meet with so many people who are concerned with explosives safety and are prepared to make their experiences in this field available to others. I hope that in time the Australian Ordnance Council will be able to make some contributions which will be worthy of your attention.
- 2. Turning to the subject of this talk, I will tell you of some of the considerations which led to the formation of the Council, I will discuss its functions and its terms of reference, and will try to explain the way in which we operate. I will also try to give you some idea of our reasons for operating in this fashion.
- 3. The Council has only been in existence since October last year, but the possibility of forming such a Council has been the subject of discussion for many years. I raised the subject myself as long ago as 1954 when I returned from a tour of duty with the UK Ordnance Board. Since then, the matter has been raised many times, by other service weapons engineers, by scientists in our R&D Establishments, and by people concerned with munitions production. As a matter of history, our military services were developed on the lines of the UK military services and for a long time we depended on the UK for the supply of explosive stores for use by our Navy, Army, and Air Force. This meant that we have had ready access to Ordnance Board Proceedings relating to UK equipment, and have tended to rely on this information for our assessments of the design safety of UK explosive stores which have been introduced for service use in Australia. In recent years we have put into service an increasing number of explosive stores from other countries, including USA, and for one reason or another we have not been able to obtain the type of data we had previously obtained from OB Proceedings for UK stores.

This then was one of the stimuli which led to the formation of the Australian Ordnance Council.

- 4. In my opinion, the most important consideration leading to the formation of the AOC was the increasing emphasis for local production of explosive stores to meet the requirements of the Australian Defence Force, and the realisation that even if these stores are produced to an overseas design, they are in fact new stores which need to be fully evaluated before they are taken into service use. They are usually made from different materials, there may be minor changes in design, the explosive fillings and propellants used have somewhat different characteristics, and there can be other changes due to different manufacturing processes. Even in the case of a store produced locally to a UK design which has been fully tested and reported by the Ordnance Board, there is still a need for an Australian produced store to be evaluated to determine its acceptability for service use. The AOC plays its part in the evaluation process by advising Approving Authorities on the safety and suitability for service use of such stores. In this context, suitability for service use relates to the ability of a store to function as designed and for this function not to be unacceptably downgraded by the service environment. Prior to the formation of the Australian Ordnance Council, the safety and suitability for service use aspects of the evaluation of locally produced stores was carried out in a somewhat haphazard fashion by service staff officers who might or might not obtain the expert advice which is available from R&D Establishments.
- 5. The Council also becomes involved when explosive stores are purchased overseas for use by the Australian Defence Force. It is required to review all available data which can be obtained from the supplier and to advise Australian Defence Authorities whether there is a need for any trials or investigations to be carried out in Australia to supplement this information. The need for this activity to be performed in an objective manner was also a factor leading to the formation of the Australian Ordnance Council. It is an activity which highlights the need for the AOC to establish effective lines of communication with overseas workers in the field of explosives safety to ensure that expensive trials carried out in Australia do not duplicate trials which have already been carried out overseas. Conversely, whenever Australian trials are carried out which add something to the total information available on a munitions subject, this information should be made available to overseas workers.
- 6. On the subject of functions and terms of reference I refer you to the terms of reference of the AOC which will be published as an attachment to this paper. I would however like to comment on some of the material included in these terms of reference.
- 7. The Council is an inter-service, independent, advisory body. To meet this requirement, each service is represented on the technical staff of the Council and the positions of President and Secretary are rotational service posts. The next President can be expected to be either a Navy or Army Officer and the next Secretary either an Army or Air Force Officer,

since the present Secretary is a Commander RAN. Independence is achieved by having the Council functionally responsible jointly to the Senior Military Officer of our Department of Defence and to the Head of our Defence Science and Technology Organization. These officers are not likely to place tasks on the Council, but their assistance can be sought in the unlikely event that Council recommendations are ignored to the detriment of the safety of Defence personnel. Administrative support is provided by a Division of the Department of Defence concerned with Service Laboratories and Trials. The Council does not have any executive powers and is purely an advisory body. Its recommendations do not have to be accepted if there are overriding operational considerations and I believe that this is the way that the system should operate. So long as Council recommendations are taken into account, the safety of the users of Defence explosive stores is safeguarded to the extent which is possible in a military environment.

- 8. You will note that the fields of operation of the Council are very wide so that the Council is not restricted in the areas in which it may take an interest. It is not, of course, likely to be active in all of these fields at any one point in time, and it is expected that the majority of Council tasks will be concerned with ammunition, explosives, propellants, and with electrical explosives hazards and other design safety aspects.
- 9. The duties of the Council are largely concerned with establishing the aspects of design safety which should be the subject of investigations or trials to support Council recommendations on the safety and the suitability of a store for service use. The Council is concerned with arranging such investigations and trials and with the analysis of results obtained. The strength of the Council lies in its charter to publish results of trials and investigations, and related recommendations, for all to see. It will also publish other information such as advice received from explosives specialists and designers so that recipients can see the reasoning behind Council recommendations. The Council must establish and maintain its credibility in this manner to be fully effective.
- 10. A further note worthy feature of the Council's Terms of Reference is that they provide wide powers of communication. The Council is able to communicate directly with the sources likely to be able to assist it in carrying out its duties, and can seek assistance from R&D and Trials Establishments on its own authority.
- 11. We come now to the methods of operation of the Council. These are constrained by the structure of the Council since apart from support staff the only full time staff are the President, the Secretary, and four Technical Staff Officers (TSOs). The four Members, who with the President form the Council, have full time appointments elsewhere in the Department of Defence and attend Council meetings once a month to review the progress of Council tasks, and to discuss any draft Proceedings which have been prepared to publish Council recommendations or to promulgate trials or other requirements,

- 12. The concept for Council operations is that the objectives of the Council should be achieved with the minimum number of staff possible, and that this staff should have access to all Defence resources which are able to contribute advice, or carry out investigations or trials which are necessary to provide data in support of Council deliberations. Our methods of operation are, of necessity, devised to ensure that Defence resources outside the Council are used to the maximum possible extent to support Council operations.
- 13. Probably the best way of explaining to you the way in which the Council operates is to take an example such as the general case when the Council is tasked to advise on the safety and suitability for service use of a store which is to be produced in Australia to an overseas design for use by one or more of the Australian Defence Forces. In this case the operations of the Council would be on the following lines:
  - a. the Technical Staff officer to who the task is allocated will communicate with the staff of the appropriate service Approving Authority to assemble all available information in relation to the store in question. This would include drawings, specifications, and any local or overseas reports concerning the store or its overseas equivalent. This action may highlight the need for further information to be obtained either from within Australia or overseas:
  - b. the TSO will then prepare a task description to describe the store and to define the extent to which the Council is to be involved, either directly or in conjunction with service, development, or production authorities. The originator of the task will be asked to confirm that the task description is an accurate statement of his requirements;
  - c. once the task description is approved it will be forwarded to those Establishment and production and other Authorities who are likely to be able to contribute to Council activities. They will be asked to advise the manner in which they are able to assist the Council in this matter;
  - d. a meeting of all interested persons will be convened to determine the type and extent of investigations and trials which will be necessary to provide all the data which should be obtained so that the Council is able to provide the advice which has been requested;
  - e. an Ordnance Council Proceeding will then be drafted which describes the store, and also includes drawings which show all pertinent details, and defines the types of investigations and trials to be carried out in support of the task;

- f. the draft Proceeding will be considered by the Council in session, and after amendment if necessary, the Proceeding will be published and distributed to all concerned. It is hoped that any overseas authorities who receive the Proceeding and feel that they would like to comment, will feel free to do so;
- g. from this point, a TSO will monitor the progress of the various activities taking place, and may draft Proceedings to publish results of individual investigations or trials. When all necessary data has been obtained a final Proceeding will be drafted, which includes Council advice and recommendations concerning the task as defined in the task description.
- 14. One of the part-time Members of the Council will normally be recognised as the Member most concerned with the subject, and will guide the activities of the TSO who has been allocated the task. This Member will be responsible for the presentation of Proceedings on the subject to the other Members of the Council.
- 15. The operations of the Council aim to make maximum use of the total resources available within Department of Defence, and also aim at ensuring that tasks are considered in a more objective manner than is possible for line managers who have a direct responsibility for acceptance of an explosive store into service use.
- 16. Before closing this talk I should refer to two items which have special importance in relation to Council activities. The first is that the terms of reference of the Council make provision for standing committees to be set up under the aegis of the Council. These committees perform a coordinating role to assemble those people who probably should have been communicating a long time ago. The Council attempts to identify those areas where it would wish to have a corporate body of experts to refer to and if such a body does not exist it sponsors the formation of such a body. So far, we have set up two committees, one concerned with Electrical Explosives Hazards and the other concerned with Explosives Storage requirements. We see a need for a similar coordinating committee to be concerned with fuze development in Australia and may be asked to set it up under the aegis of the Council. The major benefit of this arrangement to the committees concerned is the fact that we can provide wide circulation of the results of their deliberations by means of Ordnance Council Proceedings.
- 17. The other item which is worthy of mention is that the AOC is responsible for the development and maintenance of a data bank of information on explosive stores of interest to Australia. We have developed a computerised system which can be added to the Australian Defence Science and Technology Information Service (ADSATIS). I do not believe that this is the best answer in the long term. ADSATIS is a generalised information service which is handled wholly by computers. It requires a large amount of information to be held on computer files and has provision for many different ways of

sorting the information which is held. As a general information service it is very good, but to my mind it has a basic weakness in that the service which can be provided must deteriorate as the amount of information on file is increased and must deteriorate also with increasing demands on the system.

- 18. The type of system which attracts me is one in which all information is held on microfiche in such a way that individual microfiche can be located by a device which reacts quickly to the input of location keys. It would make use of a computer to store codes relating to the information held on microfiche. These data would be available for immediate access through an input/output station so that all codes relating to a particular ordnance safety topic could be easily retrieved for input to the microfiche locating device. Many of you will be aware that such a system is already in use in the USN.
- 19. It would not be impossible for all authorities concerned with ordnance safety to have similar systems. This would allow each authority to pass on to other authorities copies of any microfiche which may be of interest to them. For example, Australia has produced 5" ammunition which is based on a USN design. If we had a suitable microfiche system I would be able to accept microfiche relating to USN 5" ammunition and in return could pass to the USN microfiche relating to Australian 5" ammunition. The availability of compatible microfiche systems would open the way for easy exchange of ordnance safety information between the services in the USA and between them and say the United Kingdom, Canada and Australia. I believe that this approach has enormous possibilities for improvement of ordnance safety for all contributors.
- 20. I will leave you with this thought and will be interested to hear any views you may have on the subject.
- 21. Thank you very much ladies and gentlemen for your attention.

# TERMS OF REFERENCE OF THE AUSTRALIAN ORDNANCE COUNCIL

# Status and Function

- 1. The AOC is an inter-service independent advisory body whose function is to advise responsible Authorities on safety aspects and suitability for service aspects in any one or more of the fields of design, development, test and evaluation, production, and Service use of weapons and weapons systems containing explosive material.
- 2. The term 'suitability for service' when used in the context of the OAC advice means the ability of the explosive and certain other elements of the weapon or weapon system to function as designed and this functioning will not be unacceptably degraded by the Service environment. The AOC assessment may include the ability of the weapon or weapon system to meet certain Staff Requirements but will not necessarily include a quantitative assessment of functional reliability.

# Fields of Operation

- 3. The Council may undertake work in the following fields:
  - a. Guns, small arms, mortars, grenades and associated ammunition.
  - b. Weapon mountings and launchers.
  - c. Torpedoes, anti-submarine weapons and Naval mines.
  - d. Anti-armour and anti-personnel mines and demolition stores.
  - e. Unguided rockets and aircraft bombs.
  - f. Guided weapons.
  - g. Pyrotechnic stores.
  - h. Power cartridges and miscellaneous explosive devices.
  - i. Explosives, pyrotechnics and incendiary compositions in general.
  - j. Electrical explosive hazards to weapons systems, including those from electro-magnetic and electrostatic influences.
  - k. Applied ballistics.
  - 1. Attack of armour.
  - m. Ship magazine safety.
  - n. Laser safety.
  - o. Range safety for conventional and guided weapons.
  - p. Any other matters, not inconsistent with the function of the Council, as may from time to time be referred to the Council.

## Membership

4. The Council is to draw its Members from serving or retired officers of the Services who are qualified in the defined fields of interest and from civilians with similar expertise within and outside the Defence Group.

# Tasking and Administration

- 5. Action by the AOC normally arises from a request for advice by a Service or by a Research and Development, Design, or Production Authority; however, the Council may of itself initiate consideration of any matter in the fields of activity described above. Nothing in the constitution of the AOC abates the responsibility or authority of the appropriate Service Authority to make a decision regarding acceptability to the relevant Service.
- The Council is responsible on technical matters within the terms of reference to CDFS and CDS.

### Duties

- 7. Within the defined fields it is within the ambit of the AOC to carry out any or all of the following:
  - a. Establish general principles for the design of weapons and ammunition with respect to the safety and suitability for service requirement which should be satisfied.
  - b. In association with the relevant Service, establish programs for the testing and evaluation of weapons and ammunition being designed in Australia or, for items of overseas origin, adopted or under consideration for adoption by the Australian Defence Force and define criteria that should be satisfied in respect of safety, effective functioning and suitability for service under the variety of conditions required by the Defence Force. Arrange or be associated with trials, assess the results and when appropriate make recommendations.
  - c. At the request of the appropriate Authority undertake the following:
    - the examination in detail of the designs of all new devices falling within the purview of the Council or of modification or changes to existing devices previously accepted under other authority;
    - (2) the examination in detail of the designs, and of the test and evaluation reports of overseas origin, either for importation or for partial or complete manufacture in Australia;
    - (3) advising the appropriate Authority of the results of the above examination and of the recommendations arising therefrom.
  - d. Establish procedures for determining the safe service and storage life of items in the defined fields with special reference to the climatic conditions likely to be encountered in Australia or areas of Defence interest to Australia.
  - e. Advise, on request, on principles to be applied in the packaging, handling and storage of items in the defined fields.
  - f. At the request of the appropriate Authority assist in the following as they apply to items in the defined fields:
    - investigation and rectification of malfunctions and defects, as thought necessary, and recommend changes of design where appropriate.
    - (2) investigation and rectification of excessive deterioration in storage; and

- (3) timely investigation of the causes of fatalities or major damage arising from suspected malfunctions.
- g. Establish channels of communication with:
  - Official bodies, firms or persons associated with scientific or technical development in Australia;
  - (2) the UK Ordnance Board;
  - (3) appropriate Authorities in allied countries;
  - (4) appropriate Authorities in those countries whose weapons or ammunition may be used in the Australian Defence Force; and
  - (5) appropriate Authorities in those countries using weapons or ammunition of Australian origin.
- h. Disseminate to appropriate Authorities:
  - (1) programs of tests and trials;
  - (2) opinions and recommendations of the Council;
  - (3) other relevant information.

# SOME PRINCIPLES FOR A QUANTITATIVE APPROACH TO SAFETY PROBLEMS IN EXPLOSIVE STORAGE AND MANUFACTURING IN SWITZERLAND

Th. Schneider
Basler & Hofmann
Consulting Engineers
Zürich, Switzerland

# Abstract

The basic ideas for a quantitative and more output-oriented safety assessment model are presented. The problem is divided into two parts, the risk analysis and the risk appraisal.

The objective of the risk analysis is discussed and risk terms are defined which can be quantified. The distinction between the "group risk" and the "individual risk" is established. The problem of risk aversion is introduced.

The main considerations for the risk appraisal are grouped and discussed. Examples for tolerable risk leverls are given. The problem of measureable and not measurable values is presented.

"The main consequence of the scientific revolution beginning with Galileo was not only the development of technology but also the divorce between the system of values and the system of knowledge, which had hitherto been assumed to be inseparable."

Michael Batisse UNESCO

# Introduction

The safety of technical activities and facilities has been considered until now essentially as a problem for engineers and technicians. In the course of the past decades and even centuries, appropriate rules and measures were developed by these specialists, and it was generally assumed that all possible and necessary precautions would be taken. This process which basically followed the principle of "trial and error" cost many victims. Yet, faith in technological progress, and perhaps also the untouchable and bright image of the engineers were evidently always able to make up for it.

In the last years, this situation began to change, and I think in the US probably essentially earlier than in Switzerland. Various factors are responsible for this change. One very decisive event, as far as public awareness is concerned, was surely the emergence of nuclear energy.

But not only in the special field of nuclear energy public opinion began suddenly to be concerned about what is really going on. In a much more general sense, people started to look at technology and civilization more critically: Protection and safety against the hazards of technology increasingly began to become a counterweight to the desire for further technical development.

Voluntarily or unvoluntarily many engineers, technicians and scientists began to deal more intensively, more consistently and consciously with safety questions. Soon the field of explosives became also involved in this process. Just the name of these substances persuades everybody that they must be very dangerous.

As safety problems were studied more intensively, some important facts came up:

Nobody was actually dealing fundamentally and comprehensively with the problem of safety. Especially, there were no accepted models of general validity which could be applied to safety problems. Safety was just regarded as a sub-problem in every single field of technology.

The civil engineer deals with his safety factors of whose physical significance he may be barely aware. In the field of explosives, safety distances define "safe" and "unsafe" zones. The traffic engineers discuss about speed limits, and so forth.

In the late sixties, when we were still at the beginning of our activities in this field and primarily dealing with the problems of explosion effects, we felt already the deficiencies in the traditional safety philosophy. The article by Chauncey Starr in Science Magazine of 1969 finally contributed considerably to our break-through. In this article, we read for the first time the striking formulation of the whole problem in the question: "How safe is safe enough?"

By that time, it became evident to us that we would never solve safety problems satisfactorily as long as we were only concerned with the physical and technical aspects of explosives. We were convinced that a contribution to what one could call a safety philosophy would be at least as important.

When we started to look for such a basis or model, three requirements seemed decisive to us (fig. 1):

- . First of all, "safety" has to become a clear and well-defined notion.
- . Secondly, the basic model must be generally valid so that safety assessments in different fields can follow the same ideas and therefore can be compared.
- . Finally, these ideas must be able to enter our practical work.

  They must not stand as an isolated theory and they must be understandable also to a lay-man.

The purpose of my paper is now to give you a brief idea of how we look at these problems today, and which way we have chosen - and we are trying to follow that way today as consequently as possible in our design and regulations.

# The Basic Idea

The basic idea is actually very simple. We came across it when we heard over and over again people asking the question: "Is this safe?" As a civil engineer building a bridge, you may perhaps answer such a question without hesitation with "yes". Everything seems quite clear in this case, and you assume that if you have followed all the rules and regulations accurately, your bridge will not cause you any trouble.

However, as we started to get involved in the design of ammunition plants, we were not feeling very comfortable when people asked this question, and it was quite difficult to answer it. On the one hand, we felt how the absolute character of the word "safe" does somehow not correspond to the nature of the problem, because it leaves only "yes" or "no" as an answer. But on the other hand, we agreed that people from outside should be entitled to ask such a question.

In trying to think over the dilemma in which we are placed by this kind of question, we realize that we are actually dealing with two questions (fig. 2):

The first question being "What can happen?" and the second "What do we accept?".

When we looked at the problem consequently in this way, many things started to clear up. Above all, it was important to realize that these questions are of a completely different nature. The first question is definitely a technical question. It must be answered by the engineers, technicians and scientists. The second question is of a fundamentally different nature. It is certainly not a primarily technical question. Whom do we ask this question? - this was one of the biggest problems we came across with. For sure it is not correct, if the engineer has to answer this question alone.

Let me go back to our basic idea. The logical conclusion thereof was for us to divide a safety assessment into two parts. We have defined these two parts as "Risk Analysis", and "Risk Appraisal".

I have to make a short comment at this point: An intellectual clarification of a certain domain requires a clear definition of terminology in the first place. This has not yet been done in the field of safety, at least not on an international level. Now, as I do not want to interfere with the English terminology, I would like you to understand the different specific terms which I am using in this paper just as a possible translation of the terms we have defined in German. But even in the German language, these definitions are not at all generally accepted.

In the following two sections of this paper, I would like to speak briefly about these two elements of an assessment of safety.

# The Risk Analysis

Having the question "What can happen?" in our mind, the objective of the risk analysis is basically clear and well-defined. Of course, that does not mean that it cannot be very difficult to find the answer in many cases. Each one of you knows how many technical problems in the field of explosives are still far from being solved today.

Let us go back to our question. To answer it means that we have to describe the possible undesirable events which can be caused by a technical system. But how should we describe this? It seems to me that the most essential requirement is to make this description in a quantitative and output-oriented way (fig. 3). What do I mean by that?

All decisions which we make as engineers are actually quantitative: Walls are x centimeters thick, distances are specified in y meters, z kg of explosives are being stored, and so on; and above all, the costs caused by these decisions are measurable quantities. Is it not logical that "safety" being the result of all these decisions must be a measurable quantity too? And I think there should be no problem to answer the question "What can happen?" quantitatively.

Now, what do we mean by "output-oriented" in this context? Here we should ask ourselves: What do we actually want to prevent with safety measures? I should say, damage to persons and property. Therefore, we should express the answer to our question "What can happen?" in those terms.

The notion which is both quantitative and output-oriented is what we will call "risk". This risk depends basically on two types of dimensions: A probability dimension expressing the frequency of undesirable events, and a dimension measuring the possible consequences of a given event.

I would like to illustrate this by a little example (fig. 4): Three different depots of explosives are shown in this figure. In front of the first one is a one-family house, in front of the second a club-house, and a railroad track passes in front of the third one.

How can we describe these three situations? First of all, we know, for instance, that 4 persons live in the house, that an average of 10 persons take part in the club meetings, and an average of 100 passengers are traveling in the train. We assume that in all the depots the probability of an event is equally great. Should this event take place, we must count with a lethality of 25 % for the house dwellers, 100 % for the persons in the club-house and in the train, because these two depots are loaded with more ammunition.

But there is still another difference. The 4 persons in the house are practically continuously present, the club-house is occupied only 10 % of the time, and a train is only 1 % of the time in the dangerous zone.

A comparison of the risk for these three situations, examined under the aspect of damage to persons only, shows the following facts: An event causing damage to persons is possible in each case; in situation (a) we must count with 1 victim, in situation (b) with 10 victims, and in situation (c) with 100 victims. But the probability varies that this damage will occur: In situation (a) it will always occur in the case of an explosion, in situation (b) only with a probability of 10 %, and in situation (c) with a 1 % probability.

Thus, the three situations are well-described. Yet, there is one thing we can still not tell: Which is the worst situation? This is a very decisive question of course, because only when we can answer this question, "safety" will be measurable.

Now, some will say that this is quite simple; we only have to make the product of probability and consequences and we already get a definite

one-dimensional risk value. If we apply this to our example, it appears that this value is each time 1. The 3 situations would therefore be of equal risk.

But is this really correct? Let us examine the idea of the product of probability and consequences. Anyone who knows something about statistics and decision theory knows that this risk definition corresponds exactly with the expected value of the damage. But is this really a valid definition in this case? An expected value can be an objective value only, if we are dealing with a statistical situation, i. e. with a very big number of events. In case of very rare events, the expected value has no objective significance. The elementary theory of decision shows this very clearly. It would be too time-consuming to enter this problem in detail at this point and I must refer you to the literature on decision theory.

However, I would like to illustrate this point with a little example:

Imagine a lottery ticket with which you have a 1 % chance to win 1 million dollars (fig. 5). It is evident that if you could take part in a lottery with such a ticket very often, your average gain per participation would tend toward 10'000 dollars; in this case, 10'000 dollars per participation would be an objective value for this ticket. Now, think about this: Would you pay 10'000 dollars for this ticket, if you could participate in such a lottery only once?

It is obvious that hardly anybody would do this. Most people would pay far less for such a ticket.

We could now show through many plausible examples that this problem applies exactly the same way for us - only with our tickets we can usually only lose! That means that for rare events the expected value of the damage is not an objective measure for the risk.

In the decision theory, the problem is formally solved in the following way: The product of probability and consequences is complemented by

another factor which depends upon the consequences; this product is no longer called "expected value" in the decision theory, but "expected utility"; the factor or function is called "aversion function". Such an aversion function would cause, for instance, that 100 events with 1 victim are rated differently from 1 event with 100 victims; this latter situation being rated worse than the first one.

As unpleasant as it sounds, there is no objective way to define such an aversion function.

For the application of the risk analysis, we have tried to define such an aversion function (fig. 6) We have done this by appraising many different situations and examples with the responsible committees until there was the impression that the function was reasonable. In the field of explosive manufacturing and storage, for example, we work with the following function today:

R = 
$$p \cdot C \cdot 2^{C/5}$$
 for C = 20 victims  
R =  $p \cdot C \cdot 16$  for C > 20 victims

I am well aware of the fact that it is impossible for you to comment on this function. However, I mainly want to show you that we actually apply this principle in practice.

Thanks to this risk definition, it is now possible to assess various situations against one another, as we have seen them in one little example. Of course, it is possible to apply this to far more complex situations. It is very important that in this way we really assess a situation as a whole and not only various objects in isolation, as it is the case when working with safety distances. And with this risk definition we can describe a whole complex situation with one single value which is a measure for the risk.

Now, the risk of which we have spoken until now is what we call the "group risk". But there is still another aspect beside this "group risk". Again,

I would like to illustrate this with a little example (fig. 7):

This figure shows again two explosive magazines. In front of the one on the left there is a house, in front of the magazine on the right there is a road. Let's assume that we have calculated that in case of an explosion we would have four victims in both situations. From the point of view of the "group risk" these situations are equal. But let us now consider the single endangered individual; he relates differently to such a danger. As far as he is concerned, it is irrelevant to him whether or not others are killed at the same time; he is only interested in how great the danger is for himself. If we look at these two situations from this point of view, they are quite different. In one case, the same risk is carried by 4 persons, in the other probably by many thousands.

We have come to the conclusion that this consideration is just as important as the previous one. This is why we have introduced the so-called "individual risk" beside the "group risk".

For plants as well as for storages either of these two risk criteria may become decisive for the necessary safety measures, depending on the situation.

So far, about the objective of risk analysis and the definition of risk values. For the application of risk analysis, you need of course mainly a lot of technical information. But beside that it is very helpful, if you can make use of standard techniques which help you to tackle the problem. Nowadays, you have many such techniques at your disposal, as e.g. the fault tree analysis, and others. I do not want to enter here this field in detail.

But since every systematic framework for a complex problem such as the risk analysis can be useful in practice, I shall briefly present to you a general scheme that we use today. It has proved useful, by the way, not only for the solution of problems in the field of explosives (fig. 8):

In this scheme, the risk analysis is subdivided into three main parts. In a first part, which we call "event analysis", we determine the type, place, size, and probability of possible events. In this particular case, it deals with the substitution of a quantity of ammunitions by a characteristic equivalent TNT charge.

In a second step, the so-called "effect analysis", the physical effects of the characteristic events are determined and, for instance, described in danger zones or lethality zones.

In a last step, the "exposure analysis", one has to investigate what objects are endangered and to what extent. Beside the geographical location of the objects and their vulnerability, the time factor of the exposure is of great importance.

What is important above all, is that a risk analysis should be well-balanced in regard of its different parts. To ensure this, it is much easier, if one disposes of a scheme of sub-problemes, as e.g. the one proposed here.

# The Risk Appraisal

Here we deal with the question "What do we accept?" That means a risk value must be set which we consider as acceptable or tolerable. From then on, it makes sense to say that something is "safe", as long as this risk value is not exceeded.

The risk appraisal is a complex problem because beside the technical aspects many others are involved. Here we leave by definition the domain

of objectivity. We do not deal anymore with mere facts. On the contrary: Here we have to express our will and set goals.

It cannot be calculated whether it makes sense to set a 50 mbar criterium for an explosion in an underground storage which may occur maybe once in a 100 years in our country. As well as it cannot be calculated whether it makes sense to kill 1200 persons every year on our roads. These are decisions even if we make them unconsciously.

I shall surely not present you a solution to this problem. I can only summarize some of the aspects which are relevant in this context. First of all, I would like to group the various types of considerations about this problem and then make a few remarks to each of these points.

We have the feeling that one could summarize the various considerations about safety criteria in four groups (fig. 10):

- . Comparisons of risk
- . Risk-benefit considerations
- . Risk-cost considerations
- . Psychological, social, political, legal considerations, etc.

Let me make a short comment on each of these points:

Comparisons of risks are important because we can hardly measure up to an absolute "safety". Comparisons of risks are also important, if we think of an optimal distribution of our safety effort. It basically does not make sense, if we want to make safer what is already a hundred times safer than something else.

Chauncey Starr whom I mentioned before was already concerned with the considerations on risk-benefit. Here we are confronted, of course, with a very basic question: If we were not expecting any benefit from technological activities, we would certainly not accept any risk from it. It seems therefore also plausible to assume that the higher we estimate the benefit of an activity, the higher risk we are willing to accept, and vice-versa.

Considerations on costs are maybe the most obvious ones. It is easy to show that practically every system could be made safer with more money. On the other hand, it is clear that we never dispose of unlimited funds. This is true not only for an enterprise or a single plant, but also for a nation as a whole. If we want to spend more money for safety, we have to take it from somewhere; then we must spend less on something else. This sounds truly very simple and logical and yet, until now, we still hear a lot from politicians about where more money should be spent, but seldom where less should be spent.

They distinguish themselves from the others because they often cannot be brought into a direct relation with technical and rational thinking. I would like to suggest this symbolically with the following figure (fig. 11). You will even today easily find individuals who do not feel the least emotion when they have to cross daily a dangerous street; but, to stay at night at a cemetery, which is certainly not very dangerous, will cause weird feelings in the same person. The following figure may be somewhat more common. Roughly simplified, we have a world divided into two parts (fig. 12):

On the left, our technological engineer's world where we try to capture events in mathematical-scientifical patterns; we work with measurable dimensions, strive toward objectivity and rationality. Here we work with weights, pressures, probabilities, number of victims, costs of damage etc.

On the right, another world: Here we have suffering, fear, irritation, feelings of threat, newspaper headlines, political debates. Here we cannot measure anymore, here, we often hardly understand how things

work, here personal feelings and opinions are more important than facts. You may understand what I am trying to say. I think it is sometimes difficult for us as engineers to accept that part of the world. But I think that if one part tries to ignore the other the latter rebels - I would say fortunately.

One big problem is that these four aspects are of course interacting very much in each specific case and it is not easy to see how. This is for instance also the case in the last graph which I would like to show you now (fig. 14):

Here, you see a curve which shows the probability of a fatal occupational accident in Switzerland. 100% of the working people have a probability which is smaller than about  $10^{-2}$  per year, 10% a probability smaller than about  $3 \cdot 10^{-5}$ , etc. On the very right, you find the average probability for all death causes. According to Starr, this corresponds more or less with the risk that a man takes voluntarily. Also, according to Starr, existing unvoluntary risks are about a thousand times smaller. An interesting completion could be the following: We asked ourselves whether or not occupation or traffic participation e.g. are voluntary or unvoluntary. We came to the conclusion that they are either voluntary or unvoluntary; we think we could call it "semi-voluntary". In fact, the corresponding values in Switzerland are found pretty exactly in the middle.

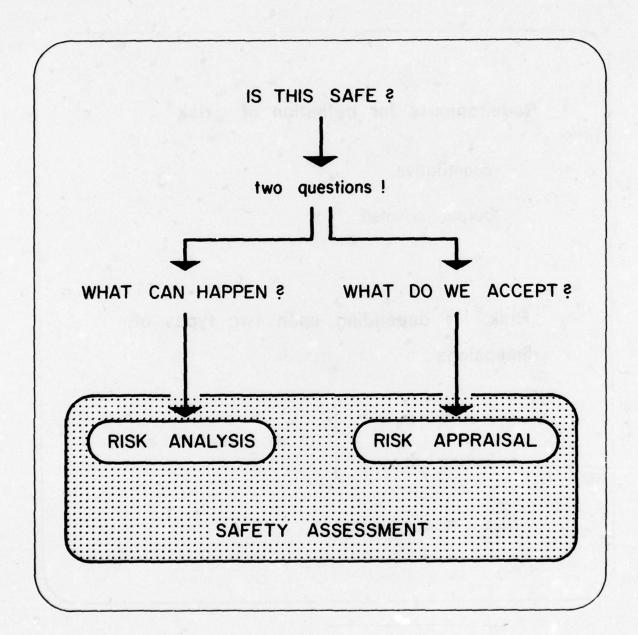
As a practical consequence derived from this graph, we have established a value of 10<sup>-5</sup> per year as a tolerable death probability for non-participating third parties in relation to explosive plants or storages. I mention this criterium just as an example to indicate that we have really tried to establish quantitative values for all the terms we have defined.

Let me come to the end of my paper with the following final remark: We certainly have to deal with a very complex problem when tackling the

question "What do we accept?" or "How safe is safe enough?". But I think we must be aware that this problem is basically inevitable. Whenever we built a facility or what ever we do, we make decisions on safety levels - the question is only how conscious we are about what we are doing.

Requirements for safety assessment model

- · clear definition of "safety"
- generally valid model
- · practically applicable model



Requirements for definition of "risk"

- · quantitative
- · output oriented

"Risk" is depending upon two types of dimensions:

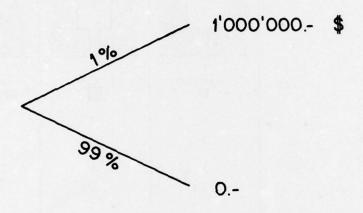
probability p
 consequences C

of an undesirable event

Risk 
$$R = f(p;C)$$

AMMUNITION MAGAZINE	a	b	C
		00	80
	LIVING HOUSE	CLUB HOUSE	RATLWAY
MAXIMUM NUMBER OF PERSONS	4	10	100
LETHALITY IN CASE OF EXPLOSION	25 🕻	100 %	100 \$
MAXIMUM NUMBER OF FATALITIES IN CASE OF EXPLOSION	1	10	100
PROBABILITY OF EXPOSURE	100 \$	10 %	15
PROBABILITY OF C IN CASE OF 100 \$	orma to asom	nud Spatistilinu	
takin matau			
10 £ <b>b</b>	C 100	MAXIMUM NUMBER OF FATALITIES C IN CASE OF EXPLOSION	

# Lottery ticket



- unlimited number of participations:
   expected gain per participation 10'000.-
- one participation:
   no objective value of lottery ticket
   can be spezified

# Example for definition of aversion function

used in the risk analysis for explosive storages and manufactoring plants

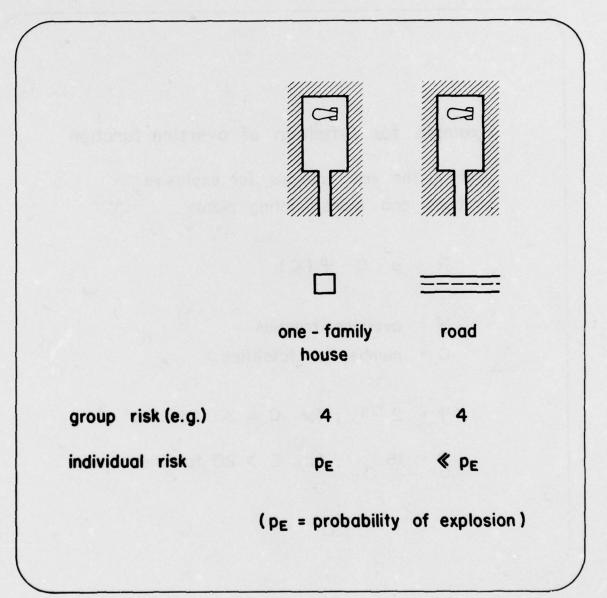
$$R = p \cdot C \cdot \mathcal{G}(C)$$

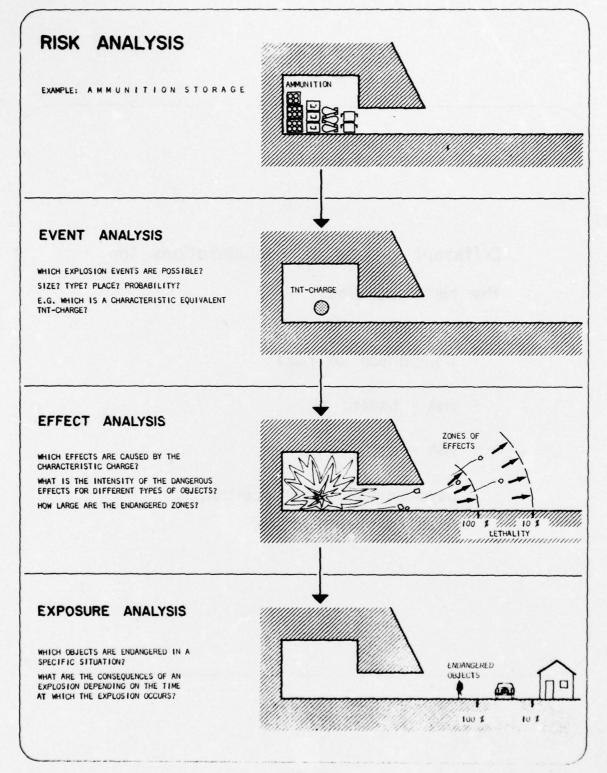
 $\mathcal{G}$  = aversion function

C = number of fatalities

 $\varphi = 2^{C/5}$ ; for  $C \le 20$  fatalities

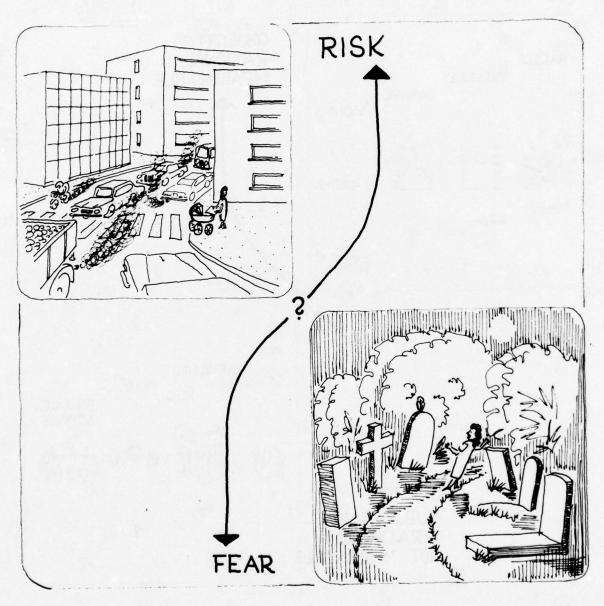
 $\varphi$  = 16 ; for C > 20 fatalities

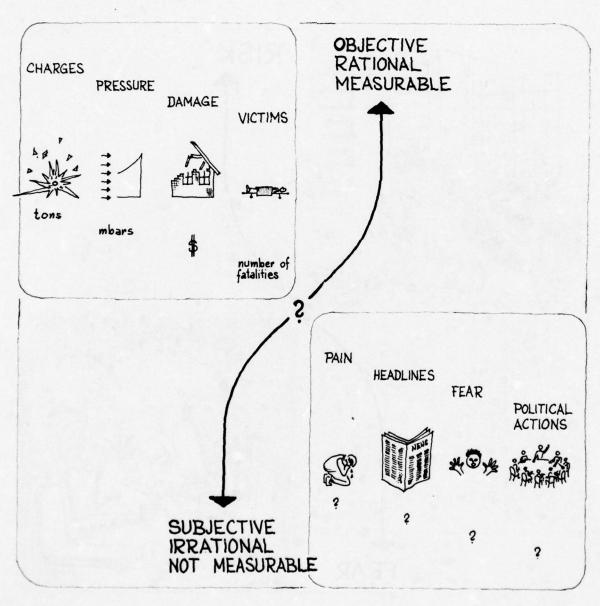


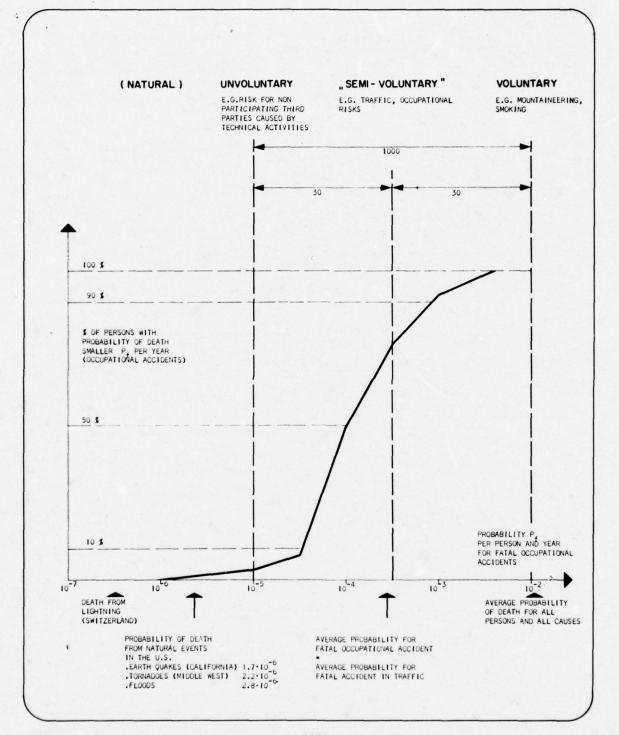


Different groups of considerations for the risk appraisal:

- · Comparison of risks
- · risk benefit
- · risk cost
- psychological, social, political,
   legal considerations, etc







### PYROTECHNIC HAZARDS EVALUATION PROGRAM

Gary L. McKown

Manufacturing Technology Directorate
Edgewood Arsenal
Edgewood Arsenal Resident Laboratory
Bay Saint Louis, Mississippi 39520

#### ABSTRACT

A series of experimental and analytical engineering projects have been conducted under a US Army project entitled Hazard Analysis and Classification of Pyrotechnic Compositions and Operations. Composition sensitivity data has been compiled for thermal, shock, impact, and electrostatic initiation sources, and the output energy of a wide variety of bulk materials has been evaluated by bomb calorimetry, by the Hartmann technique, and by high explosive equivalency methods. Large scale tests performed to evaluate the hazards associated with blending of 1000-2000 pound quantities of pyrotechnic smoke compositions by the Jet Airmix process indicate fire hazards only can be anticipated. A laboratory study of HC White Smoke Mixing showed that sublimation of the hexachloroethane is significant, that adverse ambient temperature and humidity levels do not significantly affect product sensitivity, and that the output energy depends heavily on mix composition. The ability to suppress a propagating flame flont by quenching with pressurized inert fluids has been successfully demonstrated. Electrostatic charge generation by moving solid and suspended materials has been measured by a large scale Faraday cage detector. Significant differences exist in charge generation depending on the pyrotechnic components and the material used on the pneumatic system. Recent tests suggest that significant differences in damage potential may be expected depending upon the ullage during transport of end-item materials. Detonation of and transition phenomena in pyrotechnic materials as functions of mass and geometry are currently under investigation.

# I. INTRODUCTION

The US Army Program, Hazard Analysis and Classification of Pyrotechnic Compositions and Operations, originated as a medium for performance of classification testing according to US Army Technical Bulletin 700-2, and for development of recommended changes to that document. During the course of these studies, it became evident that

problem areas in manufacturing processes had been completely neglected and that assignment of hazard classification indices to in-process and finished products was severely hampered by incomplete information on the fundamental behavior of pyrotechnic materials, compositions and handling methods. Accordingly, the program was extended to include development of basic data and

1473

an analytical understanding of the problems encountered in the manufacture, transportation, storage, and use of those pyrotechnic items for which Edgewood Arsenal is responsible. The investigations are categorized as follows:

- 1. Technology of Materials and Processes
- 2. Scenario Development
- Phenomenology (mechanistics and methodology)
- 4. Engineering Development Studies:
  - Preventive Measures Evaluation
  - Classification Tests
  - Hardware Evaluation
  - Hardware Development

The first category of studies pursue basic knowledge and technology of deflagrating compositions and production processes in order to better understand what is the nature of these materials. Continuous monitoring of current production facilities and plans for modernization or expansion defines the scenario, i.e., where materials are found. In-depth physical and chemical behavioral studies, guided by systems analysis approaches, attempt to explain why a problem exists. Thus the mechanistic studies correlate sensitivity, energy output and kinetics data on materials with simplified physical models of energetic handling processes. Effort is made to utilize appropriate methods and techniques for data reduction and evaluation. Finally, engineering studies of prototype hardware and procedures are conducted to determine how a problem may be solved and/or circumvented. The result of this four-phase probe is a thorough solution to problems that arise, based on sound fundamental knowledge rather than experience or intuition. However, this approach can be both expensive and time-consuming and for these reasons complete solutions have not always been possible. Most of the fundamental work to date has been performed as adjuncts and prerequisites to work on specific engineering problems. In any case, a large volume of data of prime interest to the developing agencies has been collected and analyzed during the investigations described in this report.

# IL HAZARD CLASSIFICATION STUDIES

Extensive explosive classification testing of compositions and end items has been performed in accordance with the original program objective. To date, 38 bulk compositions and 34 end items have been evaluated. The most recent tests were performed on a series of four experimental colored smoke formulations. To improve processing, loading, and filling characteristics, these materials are made from coarse starting materials, are briquetted and then regranulated. The oxidizer/fuel ratios were increased to produce the desired burn characteristics. Compared to standard mixes, the new red, green, yellow and violet smoke compositions yielded essentially identical test results except that greatly enhanced impact sensitivity in the bulk form was exhibited. This behavior is probably due to the increased percentage of KClO3 in the mixes.

The subject of improved hazard classification procedures for pyrotechnic materials has been

widely discussed. It has been pointed out that significant cost savings and reduction in accident occurrence and severity could be realized if adequate classification procedures could be developed. We have proposed a series of test sequences (1) to supplement the information obtained from modified present standard tests. Three of the tests contained in the US Army Technical Bulletin 700-2 are considered to be applicable only to explosive materials and are not recommended. Two tests: Impact Sensitivity modified by the addition of pressure or load cells and optical transducers, and Thermal Stability Tests are considered suitable. In addition, it is proposed to add the following instrumented test procedures:

Differential Thermal Analysis

Parr Bomb Calorimetry

Electrostatic Spark Sensitivity

Propagation Rate

Mass Effects Test

**Friction Sensitivity** 

No completely satisfactory apparatus has been found for the latter determination. A complete evaluation of some 46 test procedures with final recommendations is contained in the referenced Edgewood Arsenal Report. These recommendations are considered to be optimum, given the state of present-day knowledge and cost/facility limitations for conduct of tests.

# III. MATERIALS TECHNOLOGY STUDIES

A significant effort has been directed toward more complete understanding of material characteris-

tics, i.e., the physico-chemical behavior of pyrotechnic compositions; such factors are instrumental in arraying quantitative data for the purpose of classification and evaluation. A compilation of composition sensitivities toward thermal, shock, impact, and electrostatic initiation sources is shown in Table 1. A complete evaluation of results to date has been published (2), which reference also contains the results from determination of the output energy of bulk materials as obtained by bomb calorimetry, by the Hartmann technique and by High Explosive Equivalency methods.

The large scale bomb calorimeter which was described in a previous paper (3, 4) is currently being used to determine the effect of controllable processing parameters on the output energy of colored smoke compositions. Fifty gram samples of red, green, yellow, and violet colored smoke formulations were burned in the calorimeter to evaluate the effects of: (a) sample consolidation density, (b) change in the dye and (c) ambient pressure on the energetics of reaction. Some early results are shown in Figure 1. The reaction output energy, as monitored by the peak gauge pressure in the calorimeter, is observed to be an inverse function of the consolidation density over the limited range of the tests, and rapidly approaches a constant value. Similar behavior was found for the burning rates of these samples. These results correlate with observations that consolidation of smoke compositions into end items ofttimes reduces the hazardous characteristics of the materials.

It is evident that the seriousness of accidental functioning of pyrotechnic material will depend not

							Table 1. Pyrotechnic Sensitivity Test Results	Hechnic	Sensitivit	ty Test Resu	offs							
		The state of the s	1	8	1	-	100		Impact Sensitivin	da	Parr Bomb	D. T. A.	High Explosive	dosive	Elevirostatic	3	Hartmann Chamber Min. Mass	abber .
Compound (Drawing No. 1	Demotity (g/cc)	Reaction & Burned)	Result D	fem.	Result	Result Burn Time	Wr. Loss	Mass (mg)	Loudes	Response	Heat of Comb.	Temp.	Equir. H.	н. Е.	Energy (Joules)	C.B.1.	Wir.	Spark
NC White Smoke (Bi43-1-1)	1.34 = 0.08	.'B'.	x.p.	2.2	x.e.	807 - 972	95 - 54	91	1.56	1/3/76*** 7/23/40 9/24/37 4/37/39 3/20/37	1.27 40	193 667 <u>_</u> 13	۰	TXT	0.12 _ 0.03	>2.0	>2.0	)3. 0 · 56J.
Green Smale IV	0.05 ± 0.05	ж. Б.	х. р.	:	N.B.	30 - 100	X.R. **	20 20	1.96 4.97 1.96 3.49 4.97 7.47	0/0/10 0/0/10 0/0/10 0/3/7 0/7/3	2.91 42	209 _ 15	•	F	0.13 _ 0.05	>2.0	.01	0. 50 (30),
Green Smale (\$145-2-4)	0.00 2 0.00	N. D.	70 'X	3.8	N.D	12 - 31	K.R.	10	1.86	6/1/0	2.96	332	11 - 9	TXT C-4	0.12 _ 0.02		0.008	
014-3-1)	0175470	k p	N. D.	3.5	N.D.	23 - 82	N.R.	2 2	*5125	0/0/10 0/6/4 0/0/10 0/3/5 0/3/4 1/3/4	57.3	709 : 4		¥2	0.15 _ 0.02	>1.0	0.045	)a. o (861)
44-98	****	K. B.	N. D.	4.0	K.D.	16 - 28	N.B.	10	1.06	6/7/0	2.00	197	9	TNT C-4	0.24 _ 0.01			
Teller Banks VI (Bish-4-1)	***	K.B.	K.B.	3	K.D.	38 - 38	K.R.	2 2	353355	0/0/10 0/0/5 0/0/10 1/0/3 1/0/3		3			9'11 F 0.02			6. 45 (ML)
Taller Seate (0145-4-7)	0.012.0.0	N.B.	N.D	3	K.D.	25 - 38	N.R.	10	1,86	01/0/0		111	•	ĘĮ	0.10 = 0.01		3	
The same of	89 <sup>2</sup> 87	W.K.	K.B.	2	K.p.	# · H	N.R.	2 2	353355	\$7.74 \$7.74 \$1.74	2. 35 ± . 36	20° ± 11		FJ	0.160.0E		•	4.15 A.57 4.12 A.57 4.12 A.57 4.13 A
Water Seats (\$142-5-2)	0.75 = 0.00		w.b.	4.3	K.D.	10 - 13	N. R.	91	1.86	01/0/10	1.34	210	n - s	TNT C-4	0.21 ± 0.00			
Starter Min 12 (\$145-7-1) (#/o binder)	1.04 ± 0.04	N. P.	K.D.		K. P.	0.6 - 1.6 17 - 28	N. R.	2	**	6/6/3								
Starter Mir J (B143-7-2)	2.28 ± 0.00	901	N.D.		x.b.	n - n	N.R.	2	1.8	0/0/10	No loution	516 <u>_</u> 6						
Charter Mis VI (Bleb-1-3) (w/o bander)	1.13 2 0.10	8 .	N.D.		N. D.	12 - 28	N.R.	2	**	1,0,4			20	T.S.I				

Electrostatic Energy (Joules) High Explosive
Equivalency
Equiv. H. E. EI 1 3 I 2 32 D. T.A. Temp. 324.56 3 Parr Bomb Heat of Comb. (Kcal/gm) Table 1. Pyrotechnic Sensitivity Test Results (Cont'd) Mass Energy Response (mg) (Joules) 1.86 0/0/10
4.89 0/0/10
4.89 0/0/10
4.89 0/0/10
4.89 0/0/10
4.89 0/0/10
4.89 0/0/10
4.89 0/0/10 9,9/16 9, 1.86 0/0/10 0/0/10 10/0/0 0/0/0 1/1/8 3/0/7 33335 35 35 == 355255 9 10 2 2 2 2 2 9 2 9 2 2 9 Therm. Stab. Wt. Loss N. R. N. N. N. R. N. N. N.R. N. R. X.R. N. P. 21 75 - 110 10 - 13 22 - 39 - 11 3-8 4-1 13 - 22 9 - 14 4-1 5-7 ---3 - 6 N.D. N.D. N.D. N. D. N.D. N.D. N.D. N.D. N.D. N.D. N.D. N.D Card Cap
Result Def. ; N.D. N.D N.D. N.D. 100 90 8 8 8 8 8 8 8 1.14 ± 0.05 1.22 ± 0.06 0.62 - 0.07 1.24 ± 0.00 0.75 ± 0.35 1.33 ± 0.15 1.32 ± 0.12 1.16 \_ 0.06 0.88 ± 0.13 1.30 - 0.12 Density (g/cc) 2.33 1.45 Starter Min XXV (B143-7-4) Starter Min III
(M145-T-4)
Starter Min V
(M145-T-4)
Starter Charge
(M145-E-1)
Starter Min III
(G145-E-1) Starter Mix II (B143-7-5) Piret Pire VII (Bi44-1-1) Piret Pire X (Ci44-1-3) First Pire 31 (B143-9-5) March 19-19-19
March 19-19-19
March 19-19

						Table	Table 1. Pyrotechnic Sensitivity Test Results (Cont'd)	c Sensit	ivity Test	Results (C.	ont'd)							
Compound	į	Detonation	Card Gap	de		ign./Unconf. Burn.	Therm. Stab.	Ē	Impact Sensitivity		Parr Bomb	D. T. A.	High Explosive Equivalency	plosive	Electrostatic	2	Hartmann Chamber Min. Mass (gm)	samber 65
Orawing No. 1	(35/2)	& Burned:	Result	ig is	Result	Burn Time	Wt. Loss	Mass (mg)	Coules	Response	Heat of Comb. (Kcal/gm)	('C')	Equiv.	H.E.	(Jonles)	c. D.1.	C.D.I. Wire	Spark
Delay Mtx V (B143-12-1)		001			. р.	3-4		10	1.86 1.86 3.48 7.47	0/0/10 0/0/10 0/0/10 8/9/16 0/0/10	9.6	<b>19</b> 2	•	7.5				
Thermale (B143-13-1)	•	N. D.	N. D.		N. D.	No Len.	N.R.	o.	4.96	0/0/10				3				
CS Pyro Mirture (C143-14-10)		N. D.	K. D.		N. D.	e .	ä X	9 2	258985	0,0/10 0,0/10 0,0/10 0,1/5 0,1/5	3.28	â	a	1				
Min Min (014-15-1)		м. р.	ų, ž		N. D.	180 - 465	<b>a</b>	20 20	353355	0/0/10 0/0/10 0/0/10 0/0/10 0/0/10		1	•	I				
Sernteher Mix (B143-15-2)	1.06 ± 0.06	N. D.	N. D.		N. D.	E	N.R.											
CS Not Gas T-755	0.98 ± 0.07	N. D.	N.D.	3.0	N.D.	13 - 17	N. R.	9	3.8	0/0/10								
Plantic Bonded Starter Min	1.22 ± 0.07	N.D.	N. D.		N. D.	14 - 25	N. R.	9	1.86	0/3/7	*	172		3				
Ligation Mix R-20C		N. D.	N.D		N.D.	g - g	N.R.	10	1.86	0/0/10	8.16	44		I				
Tracer Composition B-294		N. D.	N.D		N.D.	23 - 27	N. R.	9	1.86	1/0/8	7.37	TIS .	2	ī				
Yellow Star Mix		N. D.	N.D.		N. D.	26 - 59	N.R.	01	4. 98 4. 98	3/0/7	1.68	629	ı	Z				

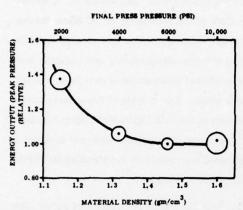


Figure 1. Effect of Material Density on Output Energy from Pressured Violet Smoke Samples

only on energy output but also on whether explosive force is involved. Correlations between mass of materials and tendency toward detonation have been sought. Investigation of mass effects were continued in attempts to define and determine critical mass behavior of deflagrating materials. Until recently, efforts were limited to exercises based on the principle of worst-case behavior; i.e., a quantity of material in the configuration normally found in a given operation is subjected to thermal and/or shock input far in excess of expected levels and the energetics of the resultant reaction are measured.

Case studies were performed relative to blending of pyrotechnic smoke compositions within a 64 cubic foot jet airmixer; this equipment figures prominently in plans for modernization of colored and white smoke production lines, and tests were performed to evaluate the hazards resulting from use of the mixer with quantities of 454 and 907 kg for colored smoke compositions and HC White Smoke Mix, respectively. Some of the tests

performed and results obtained have been described in an earlier paper (4). In addition to those burn tests, the susceptibility of the materials toward shock initiation was investigated. A shock source capable of generating an approximately plane blast overpressure front of 7 x 104 kPa was fabricated from standard detonation cord. as shown in Figure 2. The shock impinges upon a large quantity of the material under the same configuration and consolidation as that found in use of the actual processing equipment. Blast, thermal, and in situ shock velocity measurements signify the reaction rate and form of output energy compared to similar measurements with inert materials. Overall results on HC White Smoke Mix and Violet Smoke Mix are shown in Table 2. Only normal deflagration of the materials with no evidence of detonation was observed although the burn times indicate vigorous reaction.

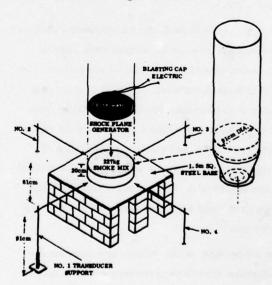


Figure 2. Shock Initiation Test, Jet Airmix Study

Table 2. Summary Test Results, Jet Airmix Studies

Test	Smoke Mix	Contributed Mast or Static Pressure kPs (psi)	Internal Shock Velocity (m/sec)	Burn Time (min)
Shock Initiation	HC White	0	180 ± 23	N/A
(227 kg)	Violet IV	0	128 ± 15	N/A
	Sand (Inert)	8	250 ± 6	N/A
Thermal Initiation	HC White	0		3 min
(227 kg)	Violet IV	34. 5 (5. 0) (Static)		5 ± 1 min.
Full Scale Burn (454 kg)	Violet IV	34. 5 (5.0) (Static)		1.8 min.

These experiments do not determine critical mass or critical diameter thresholds, but rather determine whether such has been exceeded in an actual or simulated situation. Because of the large scale simulation of operating equipment, these experiments are expensive in terms of material quantities; for example, the complete series of tests required 11,000 pounds of HC White Smoke Mix. Obviously, it would be desirable to make measurements on smaller quantities of material and to predict critical masses or whether such asymptotes are approached with quantities involved in normal operations.

Studies have been performed to determine whether reaction kinetics can be deduced from internal measurements of temperature or pressure in a reacting mass of material. The aim of experimentation is to determine whether the reaction front velocity increases within a material as the reaction proceeds, and whether extrapolation of these rate measurements will indicate if a critical mass is expected. Critical mass tests that have been performed were also presented in the previous paper (4).

On a laboratory scale, efforts have been made to determine variations in the behavior of materials under processing conditions and to correlate the resulting chemical characteristics with safe operating procedures. For example, an extensive study of the sensitivity of HC White Smoke Mix under varying process and storage conditions of temperature, composition, and humidity has been conducted to supplement data from the Jet Airmix study. The results of these tests were presented at the last Explosives Safety Seminar (5,6), and are summarized here only in terms of operational requirements for blending HC White Smoke in a Jet Airmixer (7):

- (1) Suitable means for control of sublimation of hexachloroethane must be provided in all phases of the manufacturing operation. For example, interim storage in open containers for more than a short time cannot be tolerated.
- (2) Stringent control of operating parameters such as air pressure, pulse width, duration, and number of repetitions must be instituted to provide a homogeneous blend.
- (3) Rigid quality control of composition is required to minimize variations in output energy of the end item grenades.

#### IV. PROCESSING HAZARDS

In order to accommodate reduced labor requirements and increased throughput, a large number of munition production lines are installing or considering use of pneumatic transfer methods, and several tasks have been completed to address the problems unique to this operation. A study was performed to determine the conditions required for pneumatic transfer and whether such conditions generate peculiar problem areas<sup>(8)</sup>. Components and mixtures of various colored smokes

were propelled through tubes at velocities required for transport and for maintenance of homogeneity. Electrostatic charge generation within the moving mass and upon impingement was measured, and visual observation of the impacts were made. The results show charge generation to be significantly less than measured electrostatic sensitivities for colored smoke mix components, and no observable reactions were noted within the moving cloud or on impact. In a related study, the propagation of flame and detonation fronts is currently being studied within enclosures containing dispersed and suspended material. A modified, extended Hartmann apparatus was utilized to determine initiation and propagation thresholds and for evaluation of transducers and instrumentation. Results are shown in Table 3.

Table 3. Reaction Propagation of Sulfur Dust Suspension in 3-Inch Tube

Distance from Ignition Source	Front Veloc	ity from Detect Ft/Sec.	or Response
(Nominal, Feet)	Pressure	Optical	Thermal
2.5	130 ± 30	230 ± 40	190 ± 90
5		410 ± 70	110 ± 30

A larger dust suspension chamber has also been fabricated, see Figure 3. The gallery is 10.4 m long with a 0.46 m square cross section. In addition to providing data on propagation of reaction fronts, the fixture provides a test bed to evaluate methods for suppressing or quenching of the deflagration. In this connection, a suppression system similar to that previously studies by the Bureau of Mines to prevent propagation within mine shafts is being utilized. This system consists of an ultraviolet detector which triggers

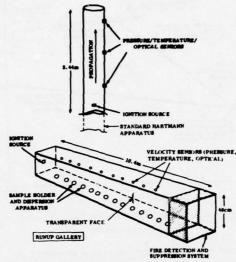


Figure 3. Reaction Propagation Test Fixture

quenching devices that operate on a combination of chemical and back-pressure effects. Halon and water suppressants under pressure have been evaluated. Figure 4 shows the sequence of events that occurred during one series of tests where a sulfur dust suspension was thermally ignited. A pressure wave propagates down the gallery at approximately sound velocity, followed by a slower flame front. The ultraviolet detector triggers an explosive-activated burst disphragm in the suppression system, and the pressurized Halon suppressant is ejected at high velocity to quench the flame front. Propagation of the suppressant was sensed by pressure transducers, and the high velocity (Mach 1.7) indicates that the suppressing action probably is due to shock wave backpressure rather than thermal or oxidation quenching. The optical quench data correlates well with scorching of passive sensors (cotton balls) placed along the gallery, as shown in the figure.

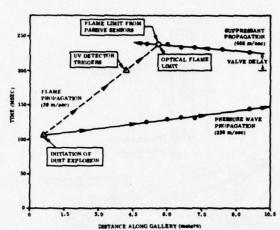


Figure 4. Quenching of Sulfur Dust Fire by Halon Suppressant

The total time delay from detection to quench in these experiments has consistently been on the order of 50 milliseconds when Halon was used, and the largest portion of that time is occupied by delays in the mechanical valve/disphragm arrangement. The use of water as a suppressant is less satisfactory; total delays on the order of 150-200 msec have been found, and detection of the suppressing action challenged the limitations of the fixture.

For several years it has been believed that electrostatic charge generation constitutes a severe hazard in the production of pyrotechnic compounds. Measurement systems have been devised to determine localized and gross charge generation within processing equipment and results have been evaluated in terms of the measured electrostatic sensitivity of the various materials. Means for determination of electrostatic charge generation within pneumatic transfer equipment are currently being developed. Large scale apparatus based on the Faraday cage concept have been fabricated for

this application. These experimental developments will serve for evaluation of electrostatic environments both in simulated experiments and within an actual operating production line. A schematic of one particular Faraday pail concept that has been developed is shown in Figure 5. The apparatus is being used to determine charge generation during transport of Violet Smoke Mix IV components, both separately and in mixtures. A plot of total measured charge versus air pressure is shown in Figure 6, for propulsion through a steel pipe of 3.05 meter length and 7.6 cm inside diameter. The generated charge is observed to be proportional to flow velocity, although a negative slope was obtained for the NaHCO2. The same data was used to determine the charge generated for transport of a given mass of material, see Figure 7. Very little variation in charge/mass ratio is observed with changes in Reynolds number. Thus for pneumatic transport of materials, use of higher flow velocities does not appear to result in much larger generated charge densities.

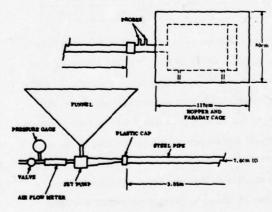


Figure 5. Large Scale Electrostatic Generator-Detector

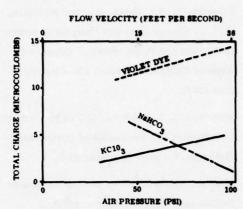


Figure 6. Electrostatic Charge Generation, Violet Smoke Mix Components

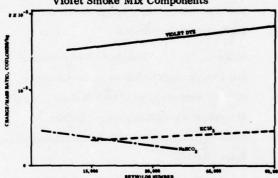


Figure 7. Charge Density in Flowing
Dust Clouds

In a separate experiment, the relative charge generated for flow of materials through various metallic pipes at constant flow velocity was investigated. As shown in Figure 8, the charge was found to depend on the work function of the metal, i.e., the energy required to remove an electron from the metallic surface. This is being studied further to evaluate materials of construction for pneumatic transfer equipment from the standpoint of relative hazards.

### V. TRANSPORTATION HAZARDS

Work has been performed on transport and storage operations within the life cycle of com-

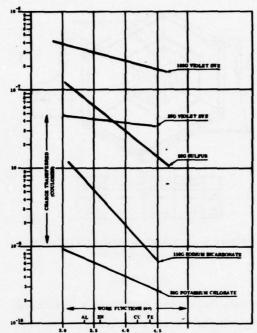


Figure 8. Generated Charge Versus Metal Work Function

modities. A previous report presented the results of tests utilizing end-item munitions within a simulated over-the-road trailer. Recently, a test fixture was designed and fabricated to investigate the behavior of pyrotechnic materials within a simulated railcar transporter (9). A schematic of the scale model that was developed and the results of experiments on M127A1 signal illumination parachute flares are given in Figure 9. Tests were performed using two realistic ullage values, 45 percent and 64 percent void. It is observed that significant differences exist in the damage expected from the two sequences. Such information is of supreme importance in evaluation of material classification appropriate during transport processes and in design of suitable transportainers to minimize accident severity.

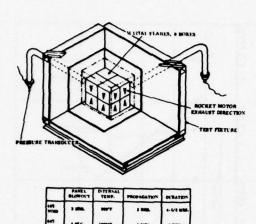


Figure 9. Pyrotechnic Railcar Transport Simulator Tests

#### SUMMARY

The work that has been performed in conjunction with pyrotechnic hazards evaluation may be summarized in a mnemonic verse:

Hazard Analysis of Pyro Equipment
Evaluation for Storage and Shipment.
Analytic Study of Critical Diameters,
Reaction Kinetics and Process Parameters.
Suppression of Fires; Recommended Actions
Effect of Confinement on Pyro Reactions.

Careful attention to the results of these hazard evaluation studies by munition developing agencies and facility designers will contribute to improved safety engineering. If such work is ignored, the implications are cryptic indeed.

#### REFERENCES

 Wilcox, W. R., "Evaluation of Test Methods for Pyrotechnic Hazard Classification," Edgewood Arsenal Contractor Report EM-CR-74051, March 1975.

- Schmidt, R. E., Dabul, A., and McIntyre, F. L., "Compilation and Analysis of Sensitivity Data for Pyrotechnics," Edgewood Arsenal Contractor Report EM-CR-75017, May 1975.
- McKown, G. L., Nimitz, K., et al., "Bomb Calorimetry for Evaluation of Pyrotechnic Materials," report in preparation.
- 4. McKown, G. L., "Effect of Confinement on Pyrotechnic Reaction Rate and Output Energy," Minutes of the 17th Explosives Safety Seminar, Department of Defense Explosives Safety Board.
- 5. McKown, G. L., "Effects of Environmental and Processing Conditions on the Composition and Sensitivity of HC White Smoke Mix," Minutes of the 16th Explosives Safety Seminar, Department of Defense Explosives Safety Board.
- Pankow, J. F., and McKown, G. L.,
   "Effects of Environmental and Processing
   Conditions on Composition and Sensitivity of
   HC White Smoke Mix," Edgewood Arsenal
   Contractor Report EM-CR-74053, March
   1975.
- McIntyre, F. L., "Identification and Evaluation of Hazards Associated with Blending of
  HC White Smoke Mix by Jet Airmix Process,"
  Edgewood Arsenal Contractor Report EM-CR75001, March 1975.
- Nestle, W., "Formulation of Hazard Evaluation Indices for Pyrotechnic Processes,"
   Edgewood Arsenal Contractor Report

EM-CR-74052, March 1975.

 Duhon, J., Lasseigne, A., and McKown, G., "Pyrotechnic Transportation Railcar Simulator Tests," Edgewood Arsenal Contractor Report EM-CR-74056, March 1975.

## A REVIEW OF HAZARD CLASSIFICATION TEST METHODS FOR PROPELLANTS

Wilfred E. Baker Southwest Research Institute San Antonio, Texas

#### **ABSTRACT**

This paper includes a review of current hazards classification and safety regulations for propellants and discusses recent work in sensitivity and hazards classification. Deficiencies which have been noted in existing regulations or the test methods on which these regulations are based are discussed in some detail. A progress report is then given on work of a Joint Army, Navy, NASA, and Air Force (JANNAF) committee on hazards analysis, whose aim is to correlate available test methods with stimuli which can cause accidental initiation of propellants or their ingredients, and with the effects of the resulting reactions and/or explosions.

#### INTRODUCTION

Even a cursory review of the existing regulatory Hazards Classification Bulletin, TB 700-2, reveals that the tests required by that bulletin are only appropriate for bulk explosives, propellants pyrotechnics, and for completed ordnance items. In the manufacture of the energetic materials usually incorporated in munitions, and in the manufacture of the munitions themselves, the materials, the stimuli which can cause accidents, and the effects of the accidents can be quite different from those occurring in storage or transport of bulk hazardous materials or munitions containing such materials. The need for improvement of or addition to the hazards classifications methods in TB 700-2 therefore seems quite apparent.

A number of individuals in the government and in private concerns involved in munitions manufacture and testing have indeed felt that the existing explosives hazard classification procedures are inadequate. They have either developed additional test methods or equipment, or participated in committee activities to try to improve this situation. This paper presents some of the background of hazards classification testing of propellants, and gives a progress report on work of a JANNAF (Joint Army, Navy, NASA, and Air Force) subcommittee which has been reviewing hazards test methods for the past several years.

## CURRENT HAZARDS CLASSIFICATION AND SAFETY REGULATIONS

The twin "bibles" for hazards classification by the ordnance engineer engaged in manufacture, testing, or transport of potentially explosive materials or Army hardware are [1,2]:

- -- TB 700-2, Department of the Army Technical Bulletin, Explosives Hazard Classification Procedures, 19 May 1967.
- -- AMCR 385-100, Safety Manual, Headquarters, U. S. Army Materiel Command, April 1970.

The former publication includes an introductory chapter covering its purpose; materials, hardware, and hazards covered by test procedures; and hazards which are <u>not</u> covered by the bulletin. (In this latter category, it specifically excludes hazards during various stages of manufacture and assembly, and initiation by electrostatic influence.) Next, a general chapter gives administrative procedures, documentation required for tests, and some discussion of instrumentation required for some of the tests. The remaining three chapters give minimum test criteria for (a) bulk explosive and solid propellant compositions, (b) ammunition and explosives items, and (c) quantities of large ordnance containing solid propellants for establishing quantity-distance criteria.

As an example of the requirements of this bulletin, bulk explosives or other potentially hazardous solid materials must be subjected to the following tests:

- (1) Detonation tests of 2-in. cubes using a No. 8 blasting cap.
- (2) Ignition and unconfined burning test.
- (3) Thermal stability test at temperature of 75°C for 48 hours.
- (4) Impact sensitivity test using Bureau of Explosives impact apparatus.
- (5) Card gap test for detonability.

Depending on the results of these tests, the material is assigned to a quantity-distance (QD) military class (1 through 7) which determines its exclusion distance for safety, and to an Interstate Commerce Commission Class (ICC) which determines shipping requirements and restrictions.

We noted earlier that TB 700-2 is limited to tests of bulk materials and end ordnance items. It is also limited to solid materials and hardware containing such materials, and therefore excludes any liquid or gaseous hazardous materials. Finally, effects of stimuli

such as electrostatic discharge and friction are not covered at all. All of these omissions render the bulletin of doubtful use in classifying hazards for in-plant processes in manufacture of munitions.

The AMC Safety Manual, AMCR 385-100, contains the general safety rules of the Army Materiel Command. It is supplemented by national safety codes and standards, where they are applicable. It contains safety information on storage and handling of a number of explosives, propellants, pyrotechnics, and chemicals used in their manufacture. It lists those materials and ordnance items which constitute the seven military classes, and also groups them for storage compatibility. For each military class, it includes quantity-distance (QD) tables for inhabited buildings, public railways, public highways, between operating lines in a munitions plant (intraline), and between storage magazines. Allowable spacings for ammunitions and explosions on conveyor lines are also given. One chapter in this Safety Manual is devoted to QD tables for liquid propellants.

The Safety Manual includes chapters on safety in munitions loading and disassembly operations in which they discuss safety precautions which must be followed in mechanical operations in loading plants. They do not, however, address process operations involved in manufacture of explosives or propellants. The manual relies on tests performed according to TB 700-2 to establish the military class for QD tables. So, this publication is also quite limited in application to stages of manufacture and assembly because of the limitations of TB 700-2 which were previously discussed.

Another manual is available for hazards analysis of solid and liquid rocket propellants. This three-volume handbook is [3]:

-- CPIA/194, <u>Hazards of Chemical Rockets and</u> Propellants Handbook, May 1972.

Because it is limited to rocket propellants, it does not cover many of the materials and munitions considered in References I and 2. However, Volume II of the handbook [3b] includes material on solid rocket propellant processing and handling, and describes hazards analyses and a number of tests related to hazards encountered in manufacture of solid propellants. Some of the tests are similar to those required in TB 700-2, but many are quite different and relate to other stimuli which can cause initiation. The tests described are:

- (1) Basic electrostatic discharge
- (2) Electrostatic discharge human spark
- (3) Impingement test
- (4) Differential thermal analysis (DTA)
- (5) Self-heating test
- (6) Copper block test

- (7) Wenograd test
- (8) Taliani test
- (9) Standard heat test
- (10) Potassium iodide starch test
- (11) Methyl violet test
- (12) Impact test (this is similar to the impact sensitivity test in Reference 1)
- (13) Friction test
- (14) Thin film propagation test
- (15) Dust explosibility test
- (16) Critical height to explosion test
- (17) Critical diameter for propagation test
- (18) Bottle drop test
- (19) Card gap test (this test appears to be identical with the card gap test in TB 700-2)
- (20) Susan test
- (21) Shear water hammer test.

Some of the above tests are specific for certain classes of propellants or propellant ingredients. The descriptions in Reference 3b indicate greater test sophistication than in TB 700-2, as well as a much greater variety of tests. This reference also includes a chapter on propellant manufacturing which gives hazardous properties of many of the chemical ingredients in solid propellants, describes some manufacturing processes, and describes general and specific safety precautions to be taken in manufacture.

# RECENT WORK IN SENSITIVITY AND HAZARDS CLASSIFICATION

Propellant and explosive hazards tests have been conducted by Army ammunition plants, private companies, and other government organizations for many years, and these programs have generated considerable sensitivity and hazard classification data for military propellants and explosives. In this section, we give a review of some general references and sources of data which are available in published reports or papers.

The first paper we will discuss, by Brown [4], is not a source of data, but is instead a critique of TB 700-2 and a plea for its revision. Some of the same limitations noted in the previous section are reiterated by Brown. His primary reasons for recommending revision of the bulletin are:

- Its limited scope should be extended to cover more environments.
- (2) Tests relevant to the environmental stimuli should be added.

(3) The hazard classification resulting from application of the Procedures must be correct for all explosives materials in all life cycle environments. The classification scheme as a practical matter must fit within the U.N. scheme and be modified to fully cover the explosives industry in the U.S. as it relates to military propellants, explosives, and pyrotechnics.

Brown recommends a major revision of procedures described in the bulletin, obtaining comments and suggestions from experts, and demonstration that hazards tests are relevant to the environment and applicable to all military explosive materials. He characterizes the interpretation scheme for bulk materials in TB 700-2 as shown in Figure 1. He feels that the scheme in Figure 1 is flawed because the Bureau of Explosive impact apparatus uses too small a sample, that impact test results are considered separately from other test results, that the No. 8 cap test and the NOL card gap test are redundant, and that no data are obtained on subdetonation reactions, which can be very hazardous.

Brown suggests the revised classification scheme diagrammed in Figure 2. The tests in Phase I should be conducted on any new material at the inventor's facility. If the material (tested only in very small quantities in Phase I) passes, it is assigned to an appropriate ICC class for shipping samples to other facilities for further testing. Larger samples are tested in Phase II tests. These tests are arranged in such a sequence that final classification, for materials which pass the confined burning test and drop weight impact test, depends on a subscale impact test such as the Susan test or a flying plate test. Brown also recommends modifications to the NOL card gap test, and substitution of the Bureau of Mines drop weight apparatus for the Bureau of Explosives apparatus.

In Reference 5, Fleischnick gives a critique of the procedures in TB 700-2, notes an earlier paper on this topic by Settles [6], and discusses at some length the determination of "TNT equivalency" for solid propellants and similar materials. Settles claims that the bulletin essentially divides materials into either a mass detonating (Class 7) hazard, or merely a fire (Class 2) hazard. He attempts to correlate violence of reaction with extent of hazard, and notes (see Fig. 3) the line of demarcation based on current classification procedures. He suggests that the division between explosion hazard and fire hazard in Figure 3 correlates poorly with accident history, and proposes instead the division in Figure 4. Neither Fleischnick nor Settles, however, discusses applications to in-process materials or tests of non-solid materials. Amster [7] has provided a careful assessment of the gap test as specified in TB 700-2, and discusses modifications to obtain additional information. He notes that the test detects only high-velocity detonation, but low-velocity detonation is

possible in some solid and liquid explosives, and such detonation can be as damaging as high-velocity detonation. Indicative of TNT equivalency tests for classification are some papers by Napadensky, Swatosh, and coworkers [8-10]. These papers show that the concept of TNT equivalency for some solid propellants is an artificial one because the blast waves generated by explosions involving these propellants exhibit properties different from TNT and because the blast strengths are usually quite dependent on degree of confinement and method of initiation. McIntyre [11] discusses problems in application of TB 700-2 tests to classifying pyrotechnic compositions. He presents a logic diagram (see Fig. 5) for classification for shipping via TB 700-2 testing which differs somewhat from that given by Brown in Figure 1. He notes the specific exclusion in the bulletin of testing related to in-process materials, and testing for electrostatic and electromagnetic stimuli. He speculates that electrostatic charges are the probable cause of many unexplainable accidents in various plants.

Some of the test methods described in References 1, 3b, 7, 9, and other sources have been evaluated for their application to hazards classification of explosives and other hazardous materials used in munitions. Amster [7], as previously noted, discusses the card gap test and suggests modifications, and Brown [4] suggests modification to and addition of several tests to improve hazards classification. King and Lasseigne provide a much more extensive evaluation of test methods for classifying explosives [12] and oxidizing materials and flammable solids [13] for transportation. Although these two studies are specifically directed toward stimuli and reactions which could occur for bulk materials and end items during transportation, some new and/or modified tests applicable to in-process situations are described and recommended. Recommended tests for explosives include [12] an electrostatic discharge test, a modified version of the No. 8 blasting cap test, and a test for pressure rise to 30 psi after ignition in a pressure vessel. A suggested revision to classification procedures for bulk explosives based on these changes is shown in Figure 6.

The work reported in Reference 13 does not refer at all to tests in TB 700-2, but instead evaluates tests for shipping classification of oxidizers and flammable solids which were developed by the Bureau of Mines. References 12 and 13 give test data for several bulk materials and some end items. Wilcox [14] reports a comprehensive review of 46 testing methods proposed for determining the hazard classification of pyrotechnic bulk materials, and munition end items containing pyrotechnics, during transportation and storage. Two pyrotechnic compounds, Green Smoke IV and Violet Smoke IV, were used to demonstrate test validity. Wilcox recommends inclusion of 15 bulk and end item test procedures in a supplement to TR 700-2 for pyrotechnics. Napadensky [15] discusses a number of impact and shock tests and their relation to sensitivity of explosives and explosive systems. Finally, Richardson, et al. [16], present one of the few papers related

to hazards during processing. They discuss what they call a Hazards Analysis Technique (HAT), shown in concept in Figure 7, and show schematically some of the initiation hazards in transport of solid materials in a processing plant. Tests related to these hazards are recommended and discussed. (Some of these tests are also covered in Ref. 3b.) They include tests to measure forces on impingement plates while also observing initiation or reaction, friction tests, and dust explosibility tests. They make no reference to TB 700-2 test procedures.

When safety procedures fail during plant operations, storage, or transportation of hazardous materials, the resulting reactions or accidents can be minor or very damaging and injurious. The quantitydistance tables in Reference 2 for various classes of materials are designed to limit the severity of explosive accidents, and several other reports and manuals are available to help one assess the severity of an accident if it occurs. Various papers in Vol. 152 of the Annals of the New York Academy of Sciences relate to damage assessment for structures and humans, Reference 3a gives similar information for solid and liquid propellants, Reference 17 gives fragmentation data for liquid propellant explosions, Reference 18 gives an overview of accidental explosions and their effects, and Reference 19 is a handbook for assessing blast and fragment hazards for liquid propellant explosions and gas vessel bursts. The total literature in effects of intentional and accidental explosions is voluminous, and we do not attempt to cover it here. Instead, we have cited only safety manuals and surveys which give broad coverage.

# WORK OF JOINT ARMY, NAVY, NASA, AND AIR FORCE (JANNAF) COMMITTEE ON HAZARDS ANALYSIS

The three-volume handbook on hazards of chemical rockets and propellants, Reference 3, was the work of a joint services and NASA committee, assisted by unpaid consultants from private firms. As noted earlier, a number of test methods other than those cited in TB 700-2 are discussed in Reference 3b, and at least some of these methods apply to hazards encountered during processing of solid propellants and explosives.

After preparing the three-volume Reference 3, the JANNAF Safety and Environmental Working Group continued, but was somewhat reorganized (in 1972). The Hazard Evaluation Committee, chaired by Mr. P. V. King, was divided into three subcommittees:

Test Evaluation - Dr. W. E. Baker, Chairman\*

<sup>\*</sup>Mr. J. Petes was chairman of this subcommittee for a short time.

Criteria Review and Evaluation - Dr. C. Da. Chairman

Incident Analysis - Mr. P. D. Wilson, Chairman

The aim of this committee is to evaluate test methods for hazardous materials, including propellants and explosive ingredients of propellants, with the purpose of recommending revisions and supplements to TB 700-2 to cover materials and situations excluded from that bulletin. The committee has tried to meet about twice a year for three-day working sessions, and individual committee members have also contributed considerable time and effort between working sessions. Because this has been a volunteer effort, progress has unfortunately been rather slow. The work is also largely unreported, other than in very general progress reports distributed by CPIA.

The Test Evaluation Subcommittee first listed materials to be considered. These were:

- (1) Military and commercial high explosives
- (2) Solid and liquid propellants
- (3) Pyrotechnics, including military pyrotechnics, fireworks, and pyrophoric materials
- (4) Fuel-oxidizer mixtures, including air as an oxidizer
- (5) Compressed gases.

They next identified what stimuli could conceivably cause release of energy contained in these materials, as shown in Table I. After these preliminary steps, the members of the subcommittee proceeded to identify various test methods associated with the stimuli of Table I, and to give their assessments of the uses or limitations of test methods related to stimuli for solid, liquid, and gaseous hazardous materials. They quickly found that they needed help in identifying tests and what they measured, and decided to ask for help from other experts. This was done by sending a letter of inquiry to over 30 individuals. Seventeen agreed to help evaluate or give information on specific hazards tests related to initiation stimuli.

From the outset, the members of the subcommittee felt that they should do more than evaluate test methods relating only to <u>stimuli</u> and <u>initiation</u> of hazardous materials and/or items. In fact, the seriousness of a hazard should truly be evaluated by the <u>outputs</u> subsequent to initiation and the <u>effects</u> on humans, buildings, vehicles, hardware, etc. <u>Outputs</u> due to energy release from hazardous materials which have been initiated were considered to be:

- (1) Blast waves and sound waves
- (2) Cratering and crater ejecta

## TABLE I. STIMULI OR MODES OF ACCIDENTAL INITIATION

#### Mechanical

Blast or hydrodynamic shock Fragment or bullet impact Drop impact Friction Adiabatic compression

#### Electrical

Electrostatic spark Lightning Contact arcing

#### Radiation

HERO and other forms of electromagnetic radiation, including light initiation, nuclear radiation, laser beams.

#### Thermal

Flame or spark
Slow cook-off (mass heating)
Hot spot initiation

Chemical changes in sensitivity

Compatibility of materials

- (3) Fragmentation
- (4) Thermal radiation and fire, including firebrands and flames
- (5) Shocks in liquids
- (6) Ground shock.

There exists a variety of test methods to measure and observe these outputs, and the subcommittee members were more or less familiar with them. So, they generated a list of these methods (see Table II).

As the work of this committee progressed, a somewhat more comprehensive plan evolved for relating various test methods to stimuli and to the effects of accidents with hazardous materials. This plan is indicated in the flow diagram of Figure 9. The list of initiating sources or stimuli changed somewhat from those of Table I, and differences caused by scaling up from laboratory tests to full-scale tests

TABLE II. TEST METHODS FOR OUTPUTS

Output	Test or Measurement Techniques
Pressure wave - (Overpressure, impulse, drag pressure, arrival	(1) Pressure transducer arrays, with electronic amplification and recording.
times, durations, etc.)	(2) Mechanical self-recording gages for pressure-time measurements.
	(3) Passive indicators such as Bikini gages, varnish cans, beer cans, bending cantilevers, etc. (Note: There are needs for standard calibration techniques and for speci-
	fications on needed accuracy.) (4) High-speed movie cameras are often used for shock velocity measurements.
Cratering and crater ejecta	(1) High-speed photography for velocities and trajectories. (2) Post-test measurements of crater size, ranges of ejecta,
	masses of ejecta. (3) Measurements of soil properties such as density, water content, seismic velocity, etc.
Fragmentation	<ol> <li>Arena tests. A MIL STD is available to describe these tests. They consist of arenas of fragment-catching material (Celotex) mounted around a munition which is statically detonated. Velocities, masses, and shapes obtained. Velocities also obtained by high-speed camera looking at impacts on metal witness plates.</li> <li>Firing of selected standard fragments with velocity screens for velocity measurement.</li> <li>TB 700-2, Chapter IV, Detonation Test A and Detonation Test B.</li> </ol>
Firebrands	High-speed photography is probably the only way to measure this effect. Trajectories, duration of burning, etc., could be obtained from such movies. As far as we are aware, no measurements have been made of firebrands.
Fireball	<ol> <li>Color photography with high-speed motion pictures are used to get size and shape of fireball with time.</li> <li>Arrays of thermocouples have been used to get temperatures as a function of location and time. This technique is limited by response time of thermocouples (at best, several milliseconds).</li> </ol>
Fire spread	Same as for fireball, except that slower response system will be adequate.
Shocks in liquids	<ol> <li>Piezoelectric pressure transducers, electronic amplifiers, tape or oscilloscope recorders.</li> <li>Photography.</li> </ol>
	(3) Passive indicators such as ball crusher gages.
Ground shock	Modified seismic equipment employed to measure ground acceler- ations and transient velocities.

are considered. The effects of possible accidents are then assessed by degree of severity ranging from no effect to "damage at a distance," which encompasses damage by blast, fragment, impact, or firebrands.

The subcommittee also evolved a set of questionnaires which were sent to the 17 experts who had agreed to evaluate tests. At present, replies to the questionnaires are being received and collated. The work of the committee will continue through 1976, and will hopefully culminate in one or more reports published through CPIA or through other government laboratories. These reports should contain rather careful evaluations of a large number of test methods (at least 80) for additions to and modification of tests in TB 700-2 to cover hazards encountered in manufacturing as well as liquid and gaseous materials.

#### CONCLUSIONS

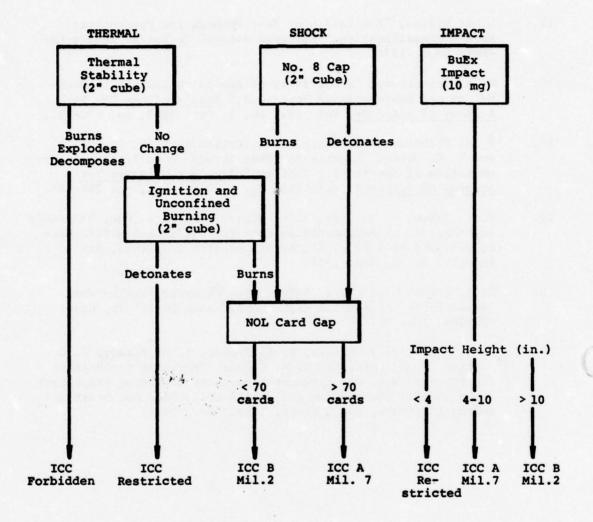
Because this is a report of a study which is still in progress, only tentative conclusions can be drawn. One such conclusion is that there is rather widespread dissatisfaction among experts with both the present requirements for testing according to TB 700-2 and the hazards classifications which are given to hazardous materials or items based on results of such tests. The experts who have been polled to date have identified and described a number of test methods and equipment which they feel to be superior to some of the methods in TB 700-2, and to supplement that bulletin for materials specifically excluded by the bulletin or inappropriate for tests required by the bulletin. In addition to the continuing work of the JANNAF committee, current but as yet unreported work at agencies such as Picatinny Arsenal and Naval Ordnance Station, Indian Head, relate to this problem. Hopefully, within the coming year, at least three three groups will report some specific recommendations for substantial improvement in hazards classification test methods for propellants in manufacture, storage, and transportation environments.

### REFERENCES

- TB 700-2, Department of the Army Technical Bulletin, <u>Explosives</u> <u>Hazard Classification Procedures</u>, 19 May 1967.
- AMCR 385-100, <u>Safety Manual</u>, Headquarters, U. S. Army Materiel Command, April 1970.
- CPIA/194, Hazards of Chemical Rockets and Propellants Handbook, May 1972.
  - Volume I, General Safety Engineering Design Criteria (AD 889-763)

- Volume II, Solid Rocket Propellant Processing, Handling, Storage and Transportation (AD 870-258)
- Volume III, Liquid Propellant Handling, Storage and Transportation (AD 870-259)
- 4. Billings Brown, "The Need for Revision of TB 700-2," Minutes of the 15th Explosives Safety Seminar, Sept. 1973, San Francisco, Calif., Vol. II, pp. 1119-1126.
- S. Fleischnick, "Some Recent Approaches in Hazards Classification," Minutes of the 15th Explosives Safety Seminar, Sept. 1973, San Francisco, Calif., Vol. II, pp. 1057-1078.
- J. E. Settles, "Deficiencies in the Testing and Classification of Dangerous Materials," <u>Annals of the New York Academy of</u> <u>Sciences</u>, Vol. 152, No. 1, Oct. 1968, pp. 199-205.
- 7. A. B. Amster, "On What We Don't Know About Shock Sensitivity or the Card Gap Test Exposed," Annals of the New York Academy of Sciences, Vol. 152, No. 1, Oct. 1968, pp. 208-219.
- 8. J. J. Swatosh, Jr., and J. Cook, "TNT Equivalency of M26E1 Propellant," IITRI Final Report J6342-1, Contract DAAA21-74-C-0521, Feb. 1975.
- H. S. Napadensky, "TNT Equivalency Investigations," Minutes of the 16th Explosives Safety Seminar, Sept. 1974, Hollywood, Fla., Vol. I, pp. 279-300.
- 10. H. S. Napadensky, J. J. Swatosh, Jr., and D. R. Morita, "TNT Equivalency Studies," Minutes of the 14th Explosives Safety Seminar, New Orleans, La., Nov. 1972, pp. 289-311.
- 11. F. L. McIntyre, "Classification and Its Pitfalls for Pyrotechnic Compositions," Minutes of the 16th Explosives Safety Seminar, Hollywood, Fla., Sept. 1974, pp. 479-486.
- 12. P. V. King, Sr., and A. H. Lasseigne, "Hazard Classification of Explosives for Transportation--Evaluation of Test Methods," Report No. TSA-20-72-5, General Electric Co., Mississippi Test Facility, Bay St. Louis, Miss., May 1972.
- 13. P. V. King, Sr., and A. H. Lasseigne, "Hazard Classification of Oxidizing Materials and Flammable Solids for Transportation--Evaluation of Test Methods," Report No. TSA-20-72-6, General Electric Co., Mississippi Test Facility, Bay St. Louis, Miss., May 1972.

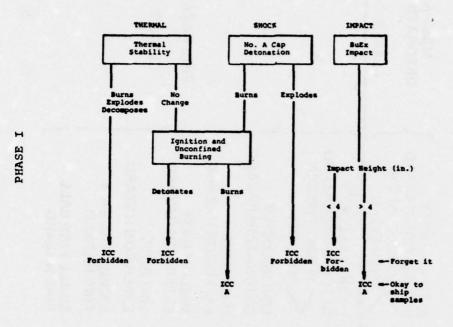
- 14. W. R. Wilcox, "Evaluation of Test Methods for Pyrotechnic Hazard Classification," Edgewood Arsenal Technical Report EA-4D01, Sept. 1974.
- 15. H. S. Napadensky, "Sensitivity of Explosive Systems to Detonation and Subdetonation Reactions," Annals of the New York Academy of Sciences, Vol. 152, No. 1, Oct. 1968, pp. 220-233.
- 16. R. H. Richardson, D. Smith, F. T. Kristoff, L. S. Treadwell, and D. K. Heere, "Hazards Analysis Through Quantitative Interpretation of Sensitivity Testing," <u>Annals of the New York Academy of Sciences</u>, Vol. 152, No. 1, Oct. 1968, pp. 269-282.
- 17. W. E. Baker, V. B. Parr, R. L. Bessey, and P. A. Cox, "Assembly and Analysis of Fragmentation Data for Liquid Propellant Vessels," NASA CR-134538, Southwest Research Institute, San Antonio, Texas, Jan. 1974.
- R. A. Strehlow and W. E. Baker, "The Characterization and Evaluation of Accidental Explosions," NASA CR-134779, Grant NSG3008, June 1975.
- W. E. Baker, J. J. Kulesz, R. E. Ricker, R. L. Bessey, P. S. Westine, V. B. Parr, and G. A. Oldham, "Workbook for Predicting Pressure Wave and Fragment Effects of Exploding Propellant Tanks and Gas Storage Vessels," NASA CR-134906, Southwest Research Institute, San Antonio, Texas, Nov. 1975.



## NOTE THAT:

- Transportation and handling (impact) safety is based on results of testing 10 mg sample only.
- . No fragment or firebrand data are obtained.

FIGURE 1. CURRENT BULK COMPOSITION TEST INTERPRETATION SCHEME UNDER TB 700-2 (1967 Revision of Procedure) (from Ref. 4)



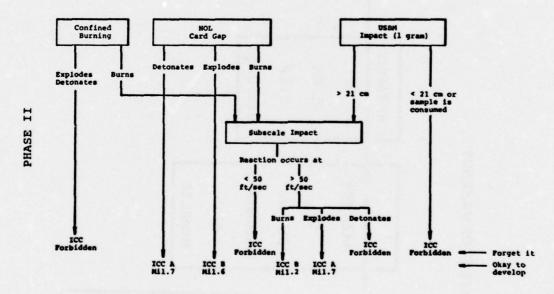


FIGURE 2. SUGGESTED REVISED CLASSIFICATION SCHEME FOR TB 700-2 (from Ref. 4)

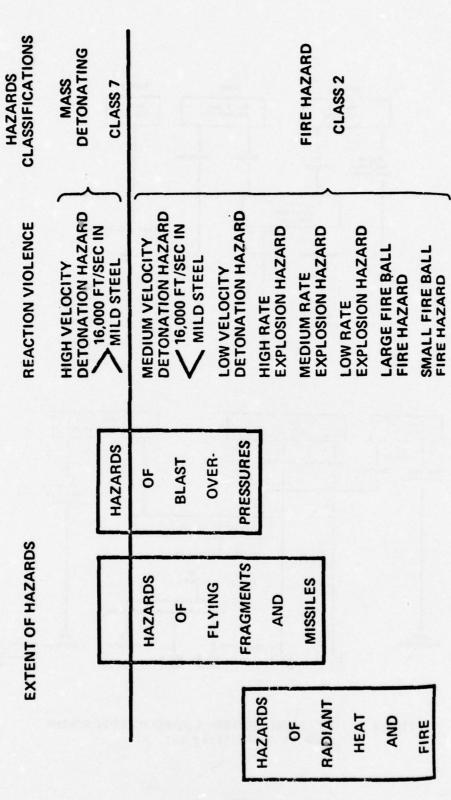


FIGURE 3. EXPLOSIVES HAZARDS SPECTRUM (Ref. 6)

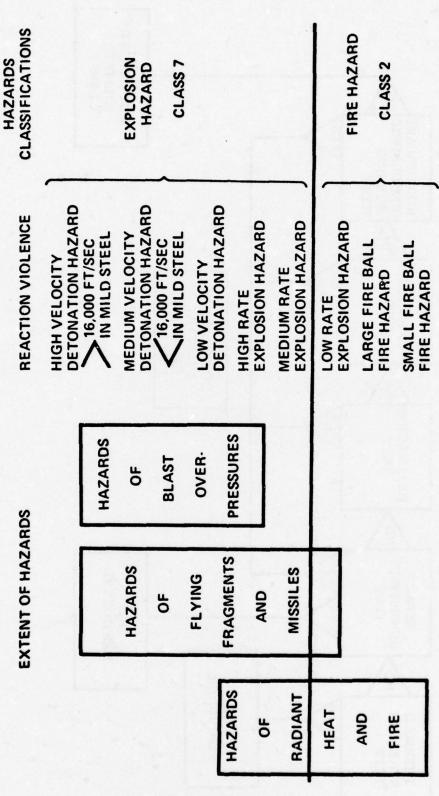


FIGURE 4. COMPLETE HAZARDS SPECTRUM (Ref. 6)

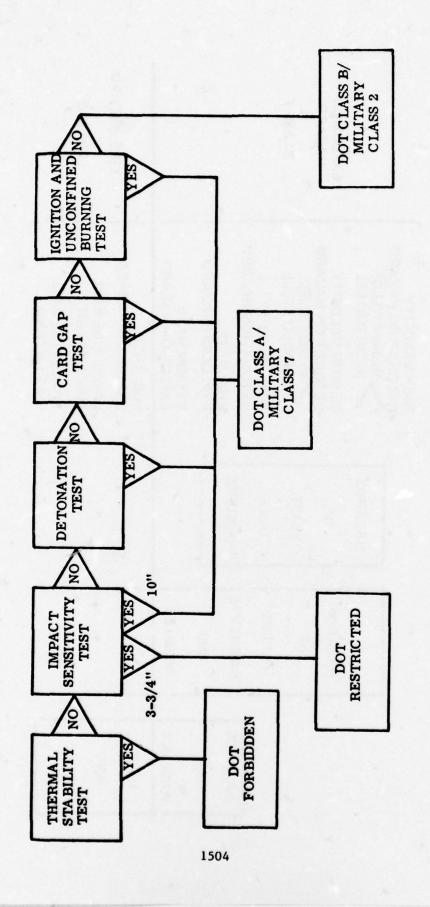


FIGURE 5. EXPLOSIVES HAZARDS CLASSIFICATION PROCEDURES PER TB 700-2 (Ref. 11)

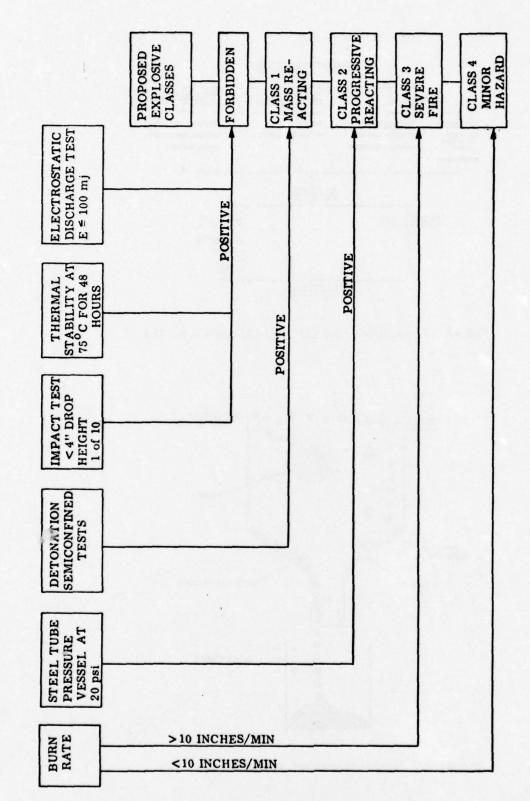


FIGURE 6. PROPOSED BULK EXPLOSIVE CLASSIFICATION SCHEME (Ref. 12)

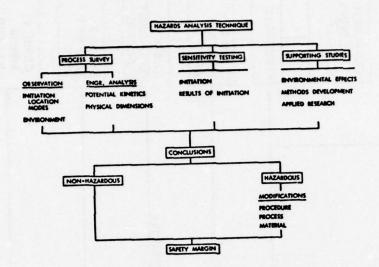


FIGURE 7. HAZARDS ANALYSIS TECHNIQUE (Ref. 16)

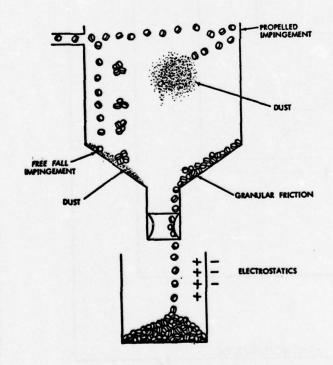


FIGURE 8. SOLID TRANSPORT HAZARDS (Ref. 16)

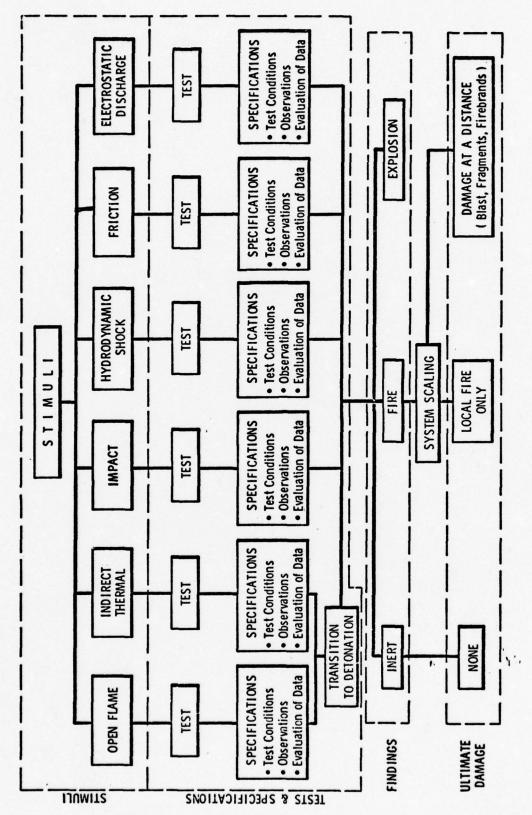


FIGURE 9. FLOW DIAGRAM

HAZARD CLASSIFICATION TESTING OF GAU-8/A 30MM AMMUNITION

Mr. F. L. West Armament Development Test Center Eglin Air Force Base, Florida

- 1. INTRODUCTION: The development of the GAU-8/A 30mm Close Air Support Gun for use in the A-10 aircraft has resulted in several new configurations of 30mm ammunition being introduced into the Air Force inventory. Preliminary tests conducted during development indicated that the aluminum cartridge cased GAU-8/A ammunition would be no more hazardous during transportation and storage than brass cased 20mm ammunition. Based on these preliminary test results, a hazard classification test program was established to compare 20mm and the GAU-8/A 30mm. The specific objective of this test program was to collect data on two types of hazard classification tests. The following tests were conducted:
  - a. Separate fast cookoff tests of 20mm TP and 30mm TP ammunition.
- b. Separate bonfire cookoff tests of 20mm High Explosive Incendiary (HEI) and 30mm HEI to investigate explosive propagation of ammunition in the packaged configuration.
- 2. AMMUNITION DESCRIPTION: Both 20mm and 30mm target practice and high explosive incendiary ammunition were used in the test program. The following is a description of the ammunition used.
- a. 20MM AMMUNITION: This test used two types of 20mm ammunition from the current inventory. All tests were conducted with the ammunition in shipping containers packed 100 rounds per can. Table 1 presents a brief description of each type; more extensive details are available in TO 11A13-4-7.
- (1) The fast cookoff test used 20mm TP, M55 ammunition. This ammunition is available in both linked and unlinked forms with unlinked considered the worse case for the purposes of this test. The linked ammunition that was provided for the test was delinked and restacked sideways in the ammunition can.
- (2) The bonfire cookoff test was conducted with 20mm HEI, M56 ammunition. This ammunition was left linked and packed as received.
- b. 30MM AMMUNITION. Both the TP and HEI 30mm ammunition used came packed 36 rounds per can as described in Table 1. Each round was individually enclosed in a cardboard tube and packed nose down. Both the top and bottom of the can were padded. The fast cookoff test utilized 30mm TP, PGU-15/B ammunition and the bonfire cookoff test utilized 30mm HEI, PGU-13/B ammunition. A sympathetic detonation test was performed with cans of 35 standard 30mm HEI, PGU-13/B cartridges and one round modified for static detonation.

Table 1. Technical description of test items

20-mm target practice ammunition	30-mm target practice ammunition
Nomenclature: M55A2, cartridge, 20-mm (target practice)	Nomenclature: PGU-15/B, cartridge, 30-mm (target practice)
Diameter: 1.165 inches	Length: 11.4 inches
Length: 6.61 inches	Weight: 1.5 pounds Cartridoe case: Aluminum
Weight: 0.56 pound	Primer: M36A-1E-1
Cartridge case: M103	Flash tube: PN 7201091-2, flash tube assembly
Primer: M52A3B1	Packaging: M548 container, 36 rounds each container, packed in cardboard tubes, nose down, padded top and bottom
Packaging: M548 container, 100 rounds each container	Propellant weight: 150 grams double base
Link: M14A2	
20-mm high explosive incendiary ammunition	30-mm high explosive incendiary ammunition
Nomenclature: M56A3, cartridge, 20-mm (high explosive incendiary)	Nomenclature: PGU-13/B, cartridge, 30-mm (high explosive incendiary)
Diameter: 1.165 inches	Length: 11.4 inches
Length: 6.61 inches	Weight: 1.5 pounds Cartridge case: Aluminum
Weight: 0.56 pound	Primer: M36A-1E-1
Cartridge case: M103	Flash tube: FN7101091-2, flash tube assembly
Primer: M52A3B1	Packaging: M548 container, 36 rounds each container, packed in cardboard tubes, nose down, padded top and bottom
Packaging: M548 container, 100 rounds each container	Propellant weight: 150 grams double base
Link: M14A1	Fuze: M505 A3 PD assembly Explosive weight: 56 grams
Fuze: M505A1	
Explosive weight: 11.8 grams	

## 3. TEST PROCEDURES AND INSTRUMENTATION.

#### a. FAST COOKOFF TESTS.

- (1) Four fast cookoff tests were conducted; two using 20mm TP and two using 30mm TP ammunition. The test setup was based on the procedures outlined in Bureau of Naval Weapons WR- $50^2$  although the fire and test item were not instrumented for temperature versus time. The test setup and scoring procedures were identical for each of the four tests.
- (2) Figure 1 shows a typical configuration for the fast cookoff test. Two setups were used for the testing to allow completion of one 20mm and one 30mm test in rapid succession on each of two test days. This procedure helped to minimize any effects of wind conditions on the temperatures experienced by the test items during the test. The test setup used and the order of testing were both alternated on the second test day to further reduce the possibility of any unforeseen effect on the data.
- (3) Each setup consisted of a 4- by 6-foot steel pan set on an asphalt surface cleared for at least 500 feet in all directions. A section of steel landing mat was placed across the pan to support the test item and approximately 60 gallons of JP-4 fuel were placed in the pan. A small bag of propellant was attached to a length of safety fuze lighter and suspended just over the surface of the fuel in each of two diagonally opposite corners of the pan. In each case, the test item consisted of one shipping container of ammunition as described in the previous paragraph.
- (4) Documentary film coverage was obtained from two angles for each shot for the entire time that smoke or flame was visible. Significant events were timed and noted by test personnel from a control tower located approximately 2,000 feet away.
- (5) After range clearance was accomplished by explosive ordnance disposal crews, the asphalt surface was carefully searched for all test item components and debris. Each item was identified, and its location with respect to the test setup was recorded.

## b. BONFIRE COOKOFF TEST.

- (1) One bonfire cookoff test was conducted on 20mm HEI and one on 30mm HEI ammunition as described in the previous paragraph. Each test used five shipping containers of ammunition for a total of 500 rounds of the 20mm HEI, and 180 rounds of the 30mm HEI.
- (2) The same two cleared, 1,000-foot-diameter, asphalt paved surfaces were used for these tests as for the fast cookoff tests. Test stands were fabricated by stacking two piles of two empty ammunition

cans each approximately 5 feet apart, and placing a section of steel landing mat across the top. This provided a platform approximately 3 feet high, under which salvage lumber was loosely stacked. Five shipping containers of the ammunition being tested were then placed side by side and banded together (Figure 2). More lumber was then piled on top of the test items to a minimum depth of 18 inches, and 15 gallons of JP-4 fuel were then added to the pile. Ignition was achieved by using fuze lighters, safety fuze, and a small bag of propellant at each of two diagonally opposite corners of the lumber pile.

- (3) Significant events were timed and recorded from the control tower located approximately 2,000 feet from the test sites. Documentary film coverage from two angles was also provided of both fires in the same manner as with the fast cookoff tests. After range clearance was accomplished by explosive ordnance disposal crews, the asphalt surface was carefully searched for all test item components and debris thrown more than 400 feet from the fire center. Each item was identified, and its location with respect to the test setup was recorded.
- (4) This test design was based on the requirements of NATO Standardization Agreement (STANAG) No. 4123 and the draft copy of "DOD Standard Hazard Classification Procedures."

## TEST RESULTS AND DISCUSSION.

## a. FAST COOKOFF TESTS.

- (1) Appendix A contains the detailed logs of significant events from each of the four fast cookoff tests. Table 2 lists the time after fire initiation to the first and last audible report as observed at the control tower. The elapsed time to the last signs of fire is also listed for comparison. The table shows no apparent differences in any of these time measurement parameters; the range of the two values for each type of ammunition overlap in all three cases.
- (2) Plots showing the locations of each unaffected round, projectile, cartridge cases, fragment, and a summation of all items recovered for each test are presented in Appendix B. The only recovered items that are not included in the plots for the sake of clarity are those items recovered from within the fuel pan or directly adjacent. Appendix C lists the location by X and Y coordinates from the fire center as well as the radius from the fire center(s). An addition has been made to each of these lists as applicable to identify the items recovered from the fire center.

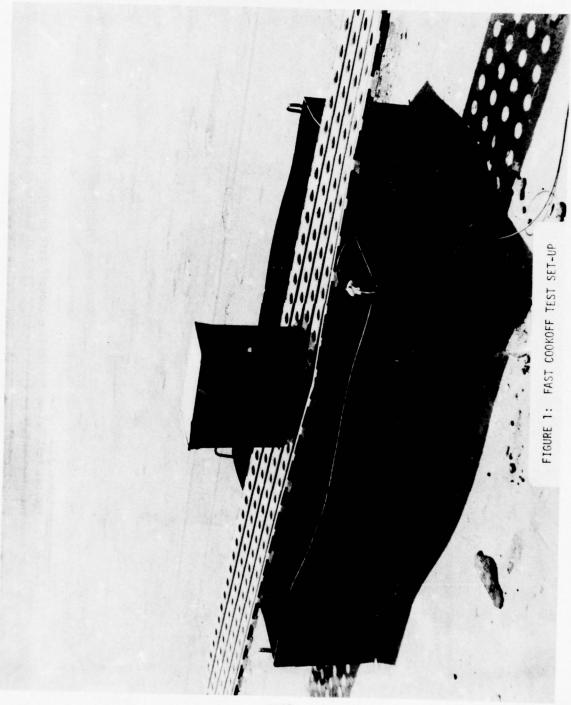




FIGURE 2: Typical test set-up for bonfire cookoff test showing: (1) ammunition shipping containers (test items), (2) steel banding, (3) empty support containers, and (4) steel landing mat.

Table 2. Fast cookoff test summary

			The second secon	
	20-mm ar	20-mm ammunition	30-mm ar	30-mm ammunition
	Test A	Test B	Test A	Test B
Number of rounds tested	•	101	36	36
Elapsed time (min:sec) from ignition to: First report Last report	3:55 17:00	3:00 10:30	2:55	3:21
Fire out	18:00	12:00	15:20	21.00
Number of unaffected rounds recovered Maximum distance from fire center (ft)	10 20.0	111	1.0	39
Number of projectiles recovered Maximum distance from fire center (ft)	85 322.5	90 296.7	35 105.3	31 16.0
Number of cartridge cases recovered Maximum distance from fire center (ft)	85 436.5	89 356.4	382.3	31
Number of fragments recovered Maximum distance from fire center (ft)	85 316.7	59 319.3	55 266.9	81 343.5
Total number of parts recovered Maximum distance from fire center (ft)	265 436.5	249 356.4	126 382.3	148 374.6
Not counted, see text for explanation.				

- (3) Logically, there were more total items recovered from the 20mm tests due to the larger number of rounds tested. The notation on the number of rounds tested is necessary due to a disparity noted between tests. It was obvious that there were 36 rounds in each can of 30mm ammunition because they are stored in cardboard tubes and any shortages would be easily noted. No so obvious is the number of rounds in a can of 20mm ammunition. Each container of 20mm ammunition was supposed to contain 100 rounds. When the results of the first test were available, they showed that all 36 projectiles and cartridge cases of 30mm ammunition were accounted for. The results showed the number of both projectiles and cartridge cases accounted for in the 20mm test to be 95. This raised the possibility of a shortage in the 20mm box which became even more suspect when the second box of 20mm ammunition was found to contain 101 rounds. The recovery of 101 projectiles and 100 cartridge cases from this second box further strengthens the likelihood of a shortage in the first box. Even if this were not the case, the accountability rates for all four tests were excellent.
- (4) Both types of ammunition had similar scatter patterns for all categories of test debris except projectiles. The 30mm projectiles were located almost entirely in the fuel pan after the fire. This can be explained by the nose-down storage configuration as opposed to the side-stacked 20mm ammunition. With the 20mm patterns, the cartridge cases and projectiles appear similar but the lighter cartridge cases were, on the average, thrown further. The maximum distances thrown in all categories (Table 2) are similar between 20mm and 30mm ammunition with the exception of projectiles.
- (5) Figures 3 and 4 show the test setups after 20mm and 30mm fast cookoff tests respectively; Figure 5 shows a closeup of the large number of 30mm projectiles still located in the ammunition container. Figures 6 and 7 show the debris collected from typical 20mm and 30mm tests respectively.

#### b. BONFIRE COOKOFF TESTS.

- (1) The only variance from the planned procedure in conducting the two bonfire cookoff tests was the addition of more JP-4 than was originally called for, due to difficulty in getting the fires to start. The wood had been stored outside and, although covered, was somewhat damp. Test personnel estimated that approximately 20 gallons of JP-4 were put on the 20mm fire while, due to several starting attempts required with the 20mm, approximately 40 gallons were put on the 30mm fire. This difference is apparent in the test logs presented in Appendix A.
- (2) Table 3 shows the total numbers and maximum distances of those items recovered at a distance greater than 400 feet from the

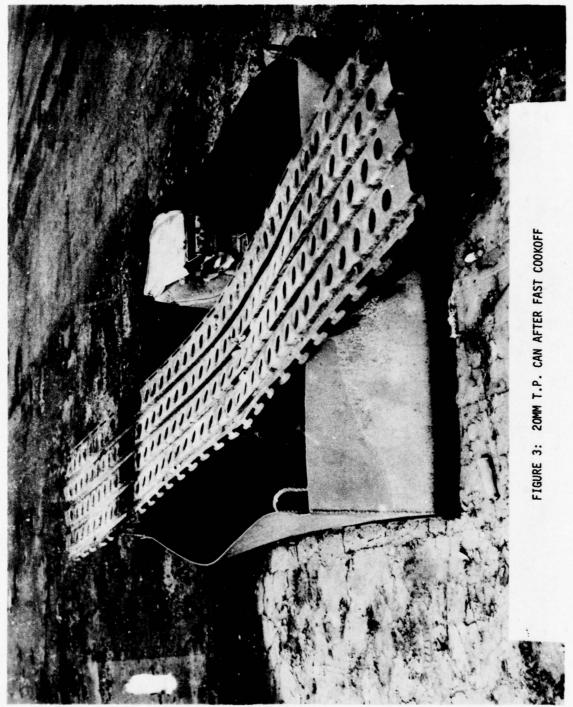




FIGURE 4: 30MM T.P. CAN AFTER FAST COOKOFF



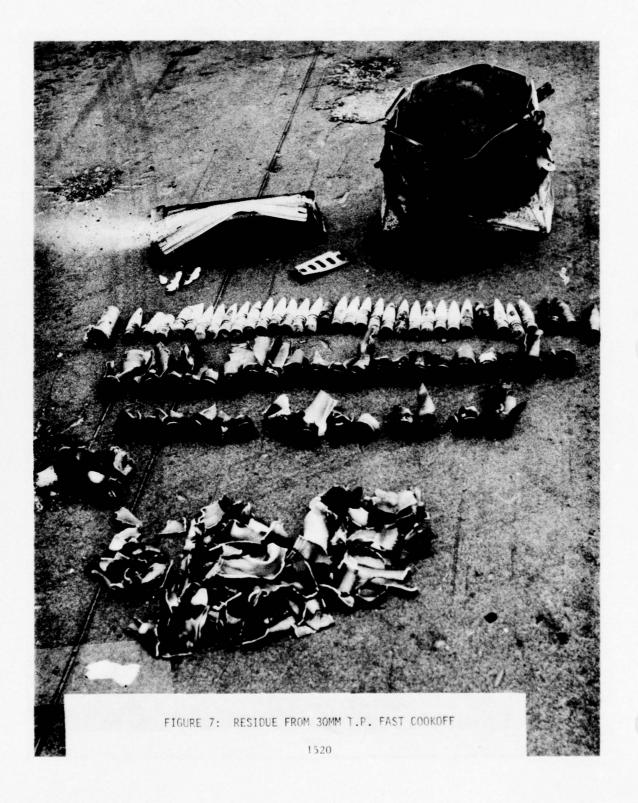




FIGURE 6: RESIDUE FROM 20MM T.P. FAST COOKOFF

Table 3. Bonfire cookoff test summary

	20-mm ammunition	30-mm ammunition
Before bonfire ignition		
Ammunition cans of HEI rounds Rounds per can Total rounds	5 100 500	5 36 180
Test debris recovered more than 400 feet from fire center		
Number of projectiles Maximum distance from fire center (ft)	5 566.9	8
Number of cartriuge cases Maximum distance from fire center (ft)	0 N/A	2 460.7
Number of fuzes Maximum distance from fire center (ft)	1 464.8	0 N/A
Number of fuze parts Maximum distance from fire center (ft)	515.6	6 543.5
Total parts number Maximum distance from fire center (ft)	13 566.9	13

fire center. The 30mm fire produced 16 total parts versus the 13 parts from the 20mm fire.

- (3) The circles drawn on the plots in Appendix B show a radius of 400 feet. Almost all of the items beyond 400 feet from the 20mm test are toward one side, suggesting the possibility that the wind or test item orientation could have played a minor part in this distribution. The somewhat more homogenous array of 30mm parts beyond 400 feet suggests that heavier weight could have reduced the wind factor in this case. Appendix C lists the exact location of each item found beyond 400 feet for both tests.
- c. DATA ANALYSIS FOR "HAZARDOUS FRAGMENTS". Since testing of both 20mm and 30mm target practice ammunition produced fragments well over 100 feet, an analysis of these fragments was performed to determine if the fragments met the "hazardous fragment" definition of DOD 5154.45. The following data are presented to show that neither the 20mm TP nor the 30mm TP produced "hazardous fragments" at distances greater than 100 feet. The data are presented in two tables.

TABLE IV

FRAGMENT TYPE	WEIGHT IN GRAINS	V <sub>H</sub> (Ft/ <sub>Sec)</sub>	D <sub>H</sub> (Ft)	E (Ft-Lbs)
20mm Projectile	1520	131	533	58
20mm Case	1800	120	447	58
*20mm Case (partial)	1100	154	736	58
30mm TP Projectile	5700	68	143	58
**30mm Case (partial)	1500	132	541	58

TAB	LE	٧
		•

FRAGMENT TYPE	WEIGHT IN GRAINS	V (Ft/Sec)	E (Ft)	E (Ft-Lbs)
20mm Projectile	1520	102	322	35
20mm Case	1800	118	436	55.6
*20mm Case (partial)	1100	118	436	34
30mm TP Projectile	5700	58	105	42
**30mm Case (partial)	1500	111	382	41

<sup>\*</sup>The partial case recovered at the maximum distance was a case base plus part of a sidewall, and was identified as a case in the test report.

<sup>\*\*</sup>Total case weight is 2300 grains. The partial case recovered at the maximum distance was a case base plus part of a sidewall, and was

identified as a case in the test report.

(NOTE: In the test report, any particle which consisted of at least a cartridge case base was identified as a "case", while pieces of sidewall were identified as a "fragment".)

The data in Table IV show the distance traveled  $(D_H)$  and the initial velocity  $(V_H)$  for the fragments type shown if they possessed 58 foot-pounds of energy at the point of origin. The fragment types are those that were recovered from the 20mm and 30mm TP cookoff tests. The fragment weight is the weight of the heaviest fragment of that type recovered from the cookoff tests. In Table V, the distance (D<sub>M</sub>) shown is the maximum measured distance a fragment of the type shown actually traveled; the velocity (V) is the initial velocity required for the fragment to travel  $D_{M}$ ; the energy (E) is the initial energy required for the fragment to travel  $D_M$  with a velocity (V). The equations used to calculate the data in Tables IV and V neglect drag. The distance traveled in both tables neglects that the fragments rolled or bounced after impact. It can be easily seen from the data in Table V that both the 20mm TP and 30mm PGU-15/B must be Quantity Distance Class 1, since the "worst case fragments" (the heaviest fragments that traveled the fartherest) never possessed 58 footpounds of energy. Therefore; neither type of ammunition produced "hazardous fragments", as defined by AFM 127-100, beyond 100 feet. Thus, hazardous fragment density is not a consideration in the assignment of Quantity Distance Classes.

An analysis of the energy of the HEI ammunition fragments beyond 400 feet was not performed because of the low fragment density. For the 30mm HEI round only 13 fragments traveled further than 400 feet, with the maximum distance traveled being 581 feet. Assuming a circle with a radius of 581 feet, the fragment density beyond 400 feet was one per 71,860 square feet. This is far below the one per 600 square foot "hazardous fragment density" of DOD 5154.45.

- 5. SUMMARY: Based on the similarity of fragment patterns for the 20mm and 30mm GAU-8/A ammunition and the "hazardous fragment" data analysis, the AFSC recommended hazard classification for the 30mm ammunition is as follows:
  - a. PGU-15/B T.P. Ammunition.

(1) Quantity Distance Class:

(2) Storage Compatibility Group: B, E, N

(3) DOT Class: Explosive C

(4) DOT Marking: "Cartridge(s), Practice Ammunition" or "Small Arms Ammunition"

(NOTE: The proposed DOT Class and Marking would require a special permit based on the requirement of Tarriff #30. This should not be a problem since a special permit was granted for 25mm "caseless" ammunition based on hazard presented rather than caliber.)

b. PGU-13/B H.E.I. Ammunition.

(1) Quantity Distance Class:

(2) Storage Compatibility Group:

(3) DOT Class:

Explosives A

(4) DOT Marking:

Ammunition for Cannon with Explosive Projectiels, Class A Explosive

The DDESB has recommended that the PGU-15/B be assigned a quantity distance class of 3 and the PGU-13/B a class of 4. These quantity distances are based on the fact that PGU-15/B fragments traveled further than 100 feet and PGU-13/B fragments traveled further than 400 feet. Guidance on these class assignments is found in paragraph 5-4, DOD 5154.45. Based on the guidance of paragraph 5-4, AFSC agrees that the DDESB quantity distance classes are correct. However, in view of this guidance, AFSC questions the need or worth, of the elaborate test instrumentation requirements of the proposed Chapter 6 of, "DOD Explosive Hazard Classification Test Procedures."

#### APPENDIX A

### TEST MISSION SIGNIFICANT EVENTS LOGS

Table A-1. Significant events log, 20-mm fast cookoff (Test A)

Time from fire initiation (min:sec)	Event
0:00	Powder detonated, fire started immediately
3:55	First report
4:00	Report
4:05	Report
4:30	Several reports
	Continuous reports for several minutes
7:05	Report
7:30	Report
7:35	Report
7:40	Report
7:55	Report
9:05	Report
12:00	Report
12:30	Report
13:00	Report
13:07	Report
13:08	Report
13:09	Report
13:45	Report
13:46	Report
15:10	Report
15:55	Report
17:00	Last report
18:00	Last flame observed

Table A-2. Significant events log, 30-mm fast cookoff (Test A)

Time from fire initiation (min:sec)	Event	
0:00	Powder detonated, fire started immediately	
2:55	First report	
4:00	Report	
4:05	Three reports	
4:25	Report	
4:30	Two reports	
4:55	Report	
5:20	Report	
5:30	Report	
5:40	Report	
6:00	Two reports	
11:40	Report	
13:01	Last report	
15:20	Last flame observed	

Table A-3. Significant events log, 20-mm fast cookoff (Test B)

Time from fire initiation (min:sec)	Event	
0:00	Powder detonated, fire started immediately	
3:00	First report	
3:10	Report	
3:20	Report	
3:30	Several reports	
3:50	Report	
4:00	Report	
4:01	Report	
4:10	Report	
4:12	Report	

CONTINUED

Table A-3. (Concluded)

Time from fire initiation (min:sec)	Event
4:15	Report
4:20	Report
4:30	Several reports
4:38	Report
4:45	Report
4:50	Report
5:00	Report
5:02	Report
5:10	Report
5:30	Report
5:50	Report
6:00	Report
7:00	Report
7:01	Report
7:10	Report
7:30	Report
9:10	Report
9:20	Report
9:22	Report
9:50	Report
10:30	Last report
12:00	Last flame observed

Table A-4. Significant events log, 30-mm fast cookoff (Test B)

Time from fire initiation (min:sec)	Event
0:00	Powder detonated, fire started immediately
3:21	First report
3:22	Report

CONTINUED

Table A-4. (Concluded)

Time from fire initiation (min:sec)	Event
3:30	Several reports
3:50	Report
4:00	Report
4:10	Report
4:30	Several reports
4:33	Report
4:40	Report
4:50	Report
5:00	Report
5:09	Report
5:28	Report
12:40	Report
13:15	Last report
21:00	Last flame observed

Table A-5. Significant events log, 20-mm bonfire cookoff test

Time from fire initiation (min:sec)	Event
0:00	Powder detonated, only slight smoke evident
18:00	Flame observed on wood
26:30	First report
27:00	Multiple reports starting
28:30	Intensity of reactions increasing
29:00	Visually apparent that HE burning
36:00	Report slowed to rate of approximately one per 15 to 30 seconds
41:30	Last report

Table A-6. Significant events log, 30-mm bonfire cookoff test

Time from fire initiation (min:sec)	Event
0:00	Powder detonated, intense fire on wood and asphalt started immediately
3:20	First report
4:00	First apparent HE reaction
6:00	Multiple high intensity reactions
10:00	HE observed burning from projectile on one side of pile
11:30	Last report

## APPENDIX B

# COOKOFF TEST SCORING PLOTS

NOTE: In the 20- and 30-mm fast cookoff Test A no unaffected rounds were located away from fire center. Ten 20-mm and one 30-mm rounds were recovered at fire center.

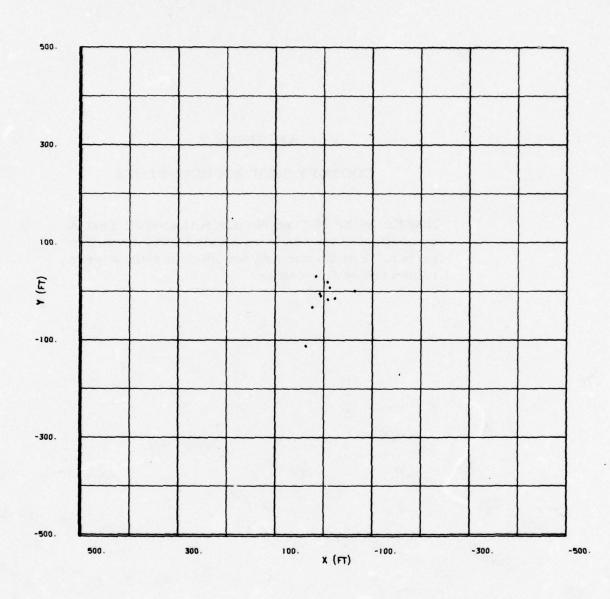


Figure B-1. Recovery plot of unaffected rounds, 20-mm fast cookoff Test B (one recovered at fire center)

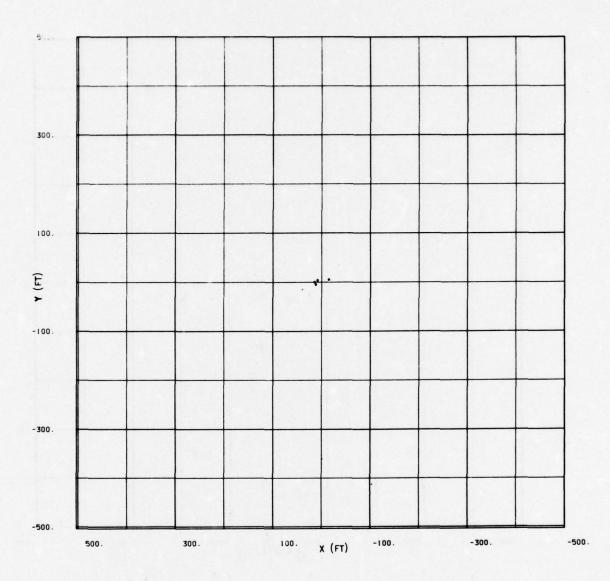


Figure B-2. Recovery plot of unaffected rounds, 30-mm fast cookoff Test B (zero recovered at fire center)

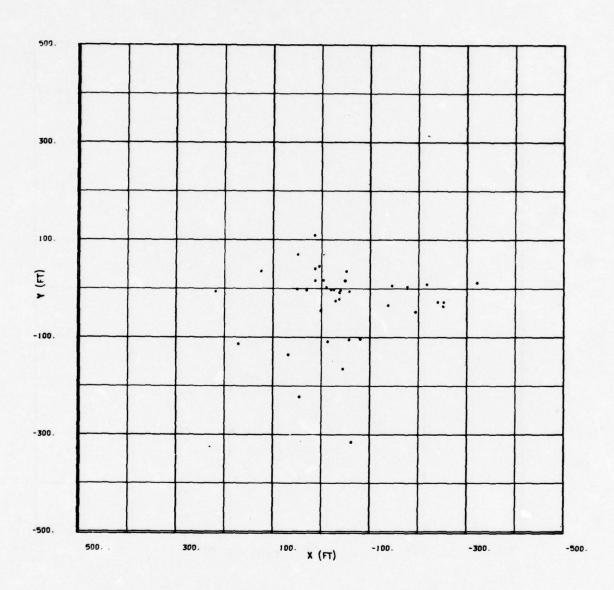


Figure B-3. Recovery plot of projectiles, 20-mm fast cookoff Test A (46 recovered at fire center)

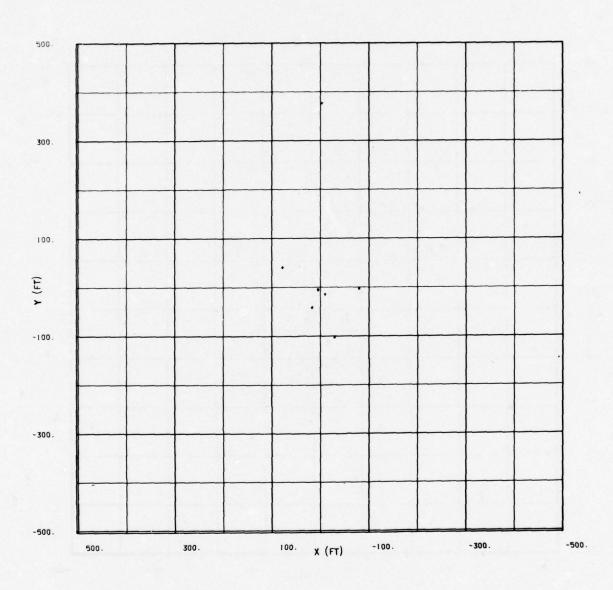


Figure B-4. Recovery plot of projectiles, 30-mm fast cookoff Test A (28 recovered at fire center)

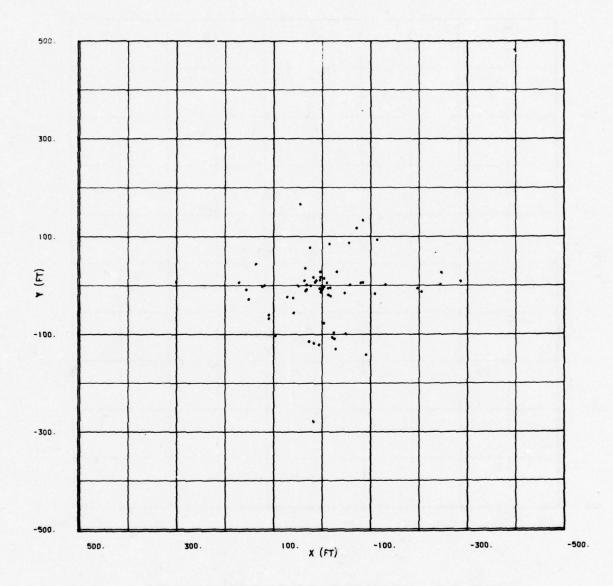


Figure B-5. Recovery plot of projectiles, 20-mm fast cookoff Test B (20 recovered at fire center)

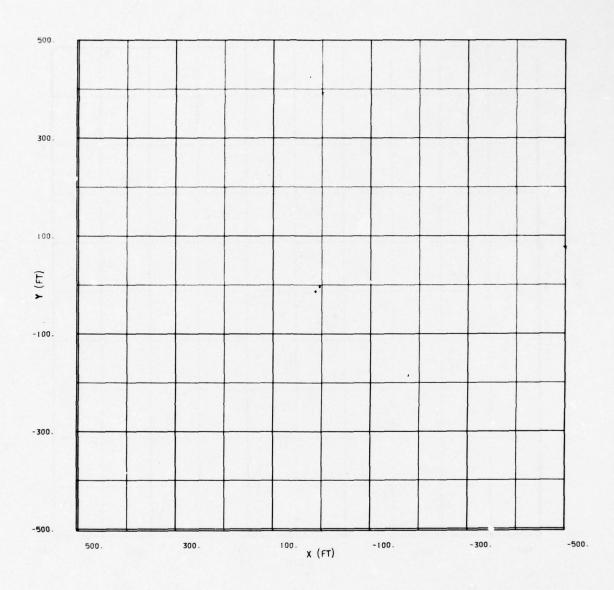


Figure B-6. Recovery plot of projectiles, 30-mm fast cookoff Test B (29 recovered at fire center)

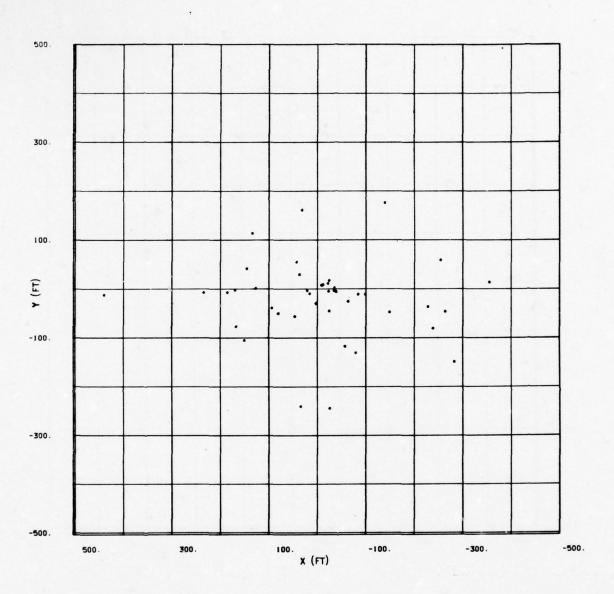


Figure B-7. Recovery plot of cartridge cases, 20-mm fast cookoff Test A (40 recovered at fire center)

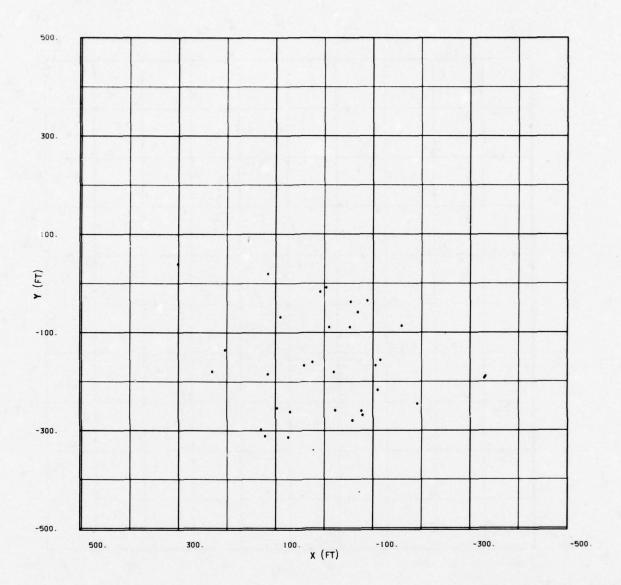


Figure B-8. Recovery plot of cartridge cases, 30-mm fast cookoff Test A (three recovered at fire center)

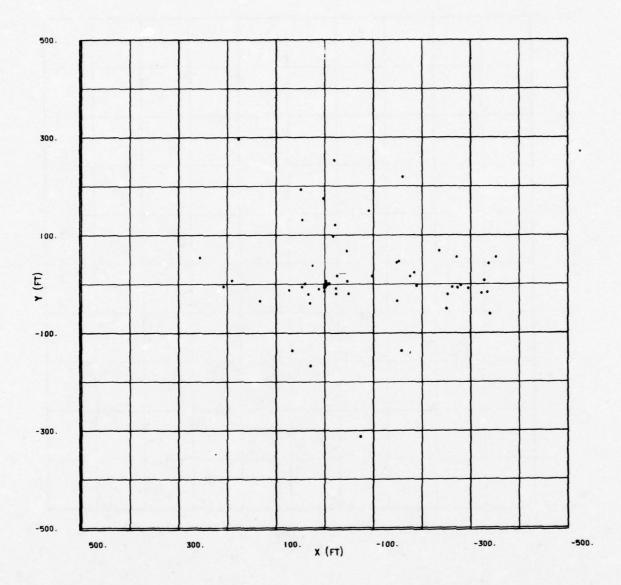


Figure B-9. Recovered plot of cartridge cases, 20-mm fast cookoff Test B (26 recovered at fire center)

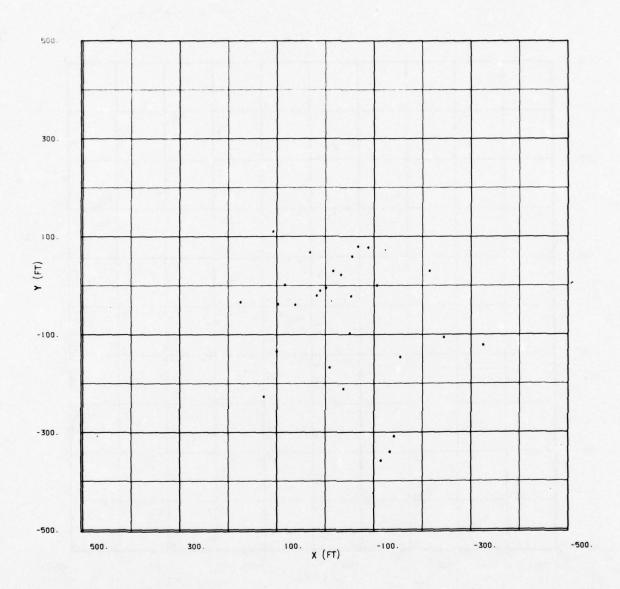


Figure B-10. Recovery plot of cartridge cases, 30-mm fast cookoff Test B (three recovered at fire center)

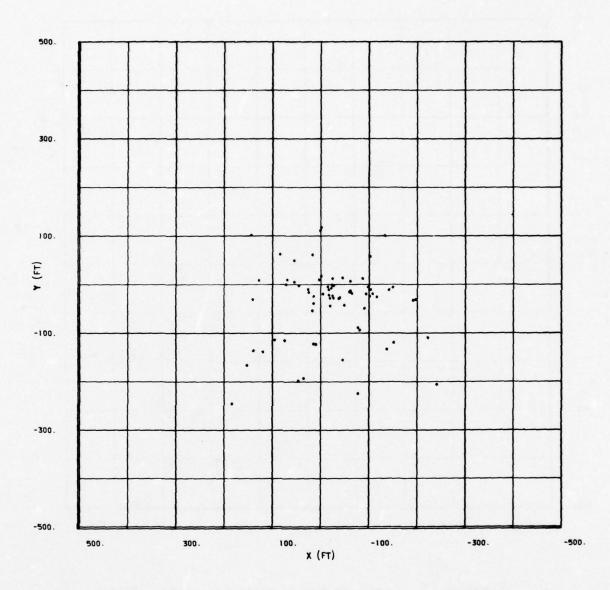


Figure B-11. Recovery plot of fragments, 20-mm fast cookoff Test A (14 recovered at fire center)

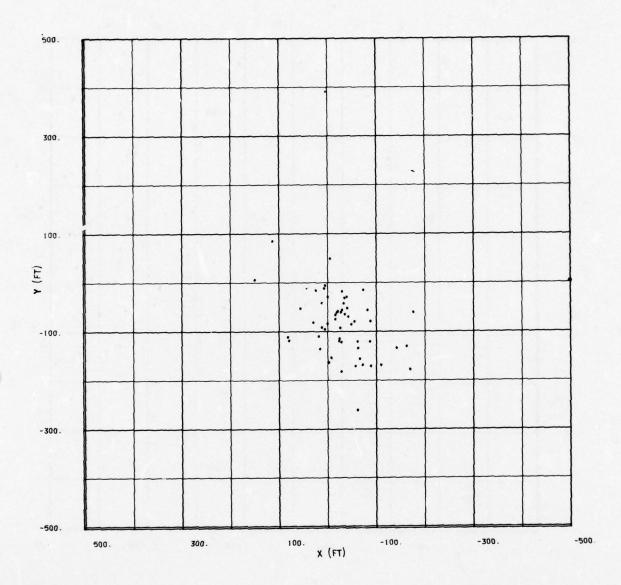


Figure B-12. Recovery plot of fragments, 30-mm fast cookoff Test A (zero recovered at fire center)

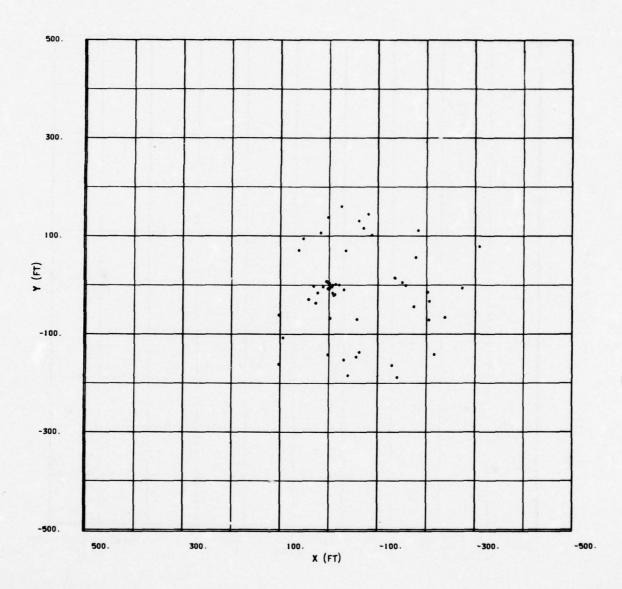


Figure B-13. Recovery plot of fragments, 20-mm fast cookoff Test B (zero recovered at fire center)

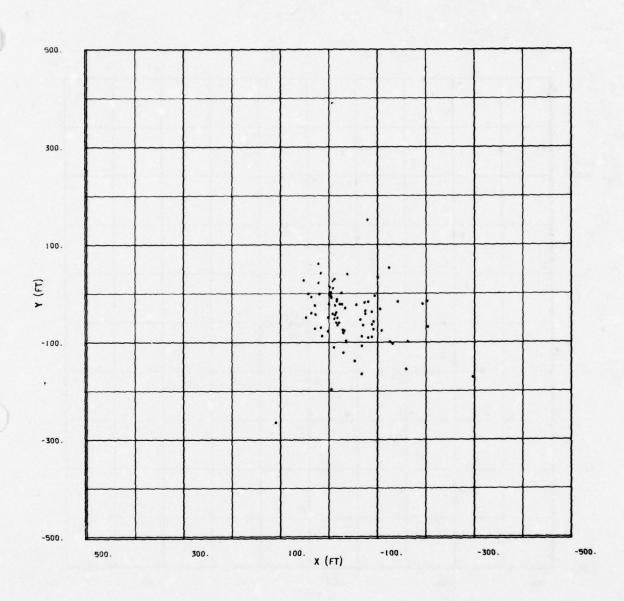


Figure B-14. Recovery plot of fragments, 30-mm fast cookoff Test B (zero recovered at fire center)

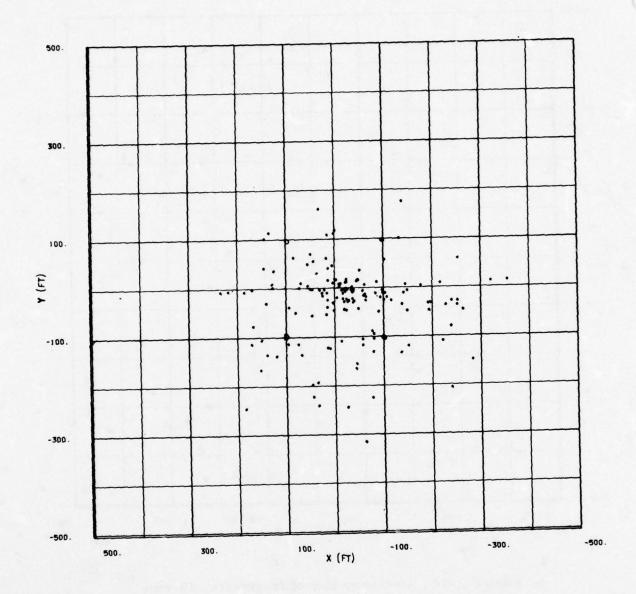


Figure B-15. Recovery plot of all parts, 20-mm fast cookoff Test A (110 recovered at fire center)

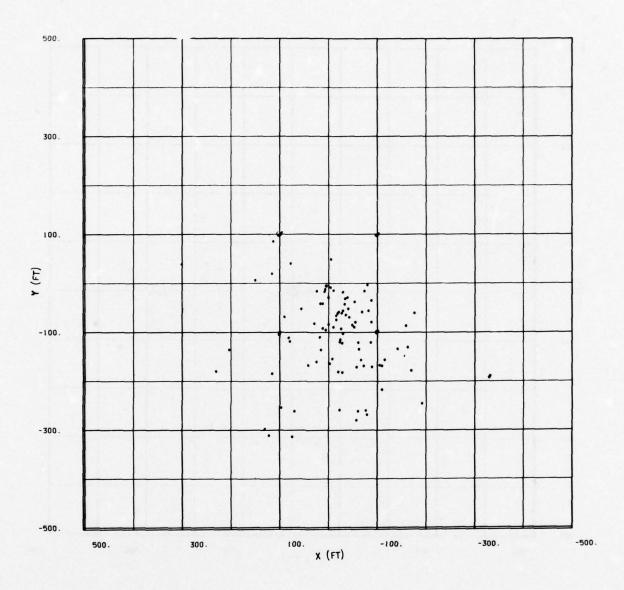


Figure B-16. Recovery plot of all parts, 30-mm fast cookoff Test A (32 recovered at fire center)

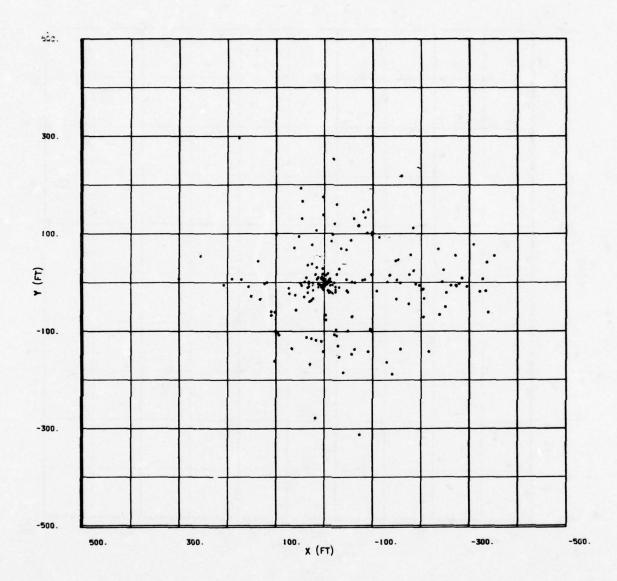


Figure B-17. Recovery plot of all parts, 20-mm fast cookoff Test B (47 recovered at fire center)

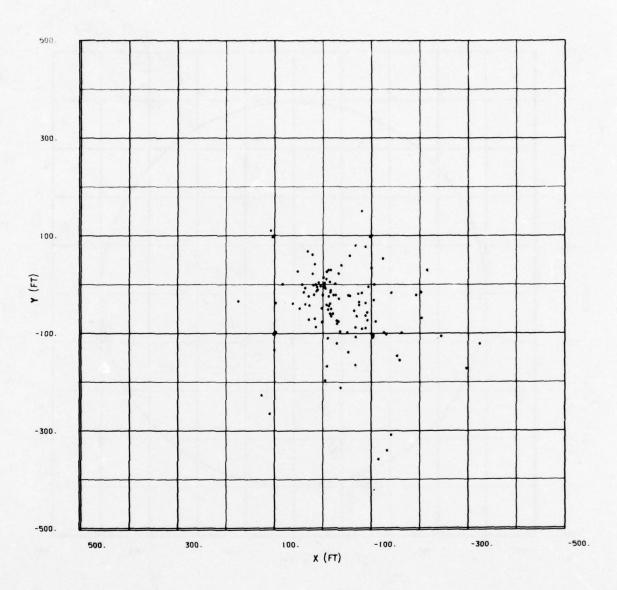


Figure B-18. Recovery plot of all parts, 30-mm fast cookoff Test B (32 recovered at fire center)

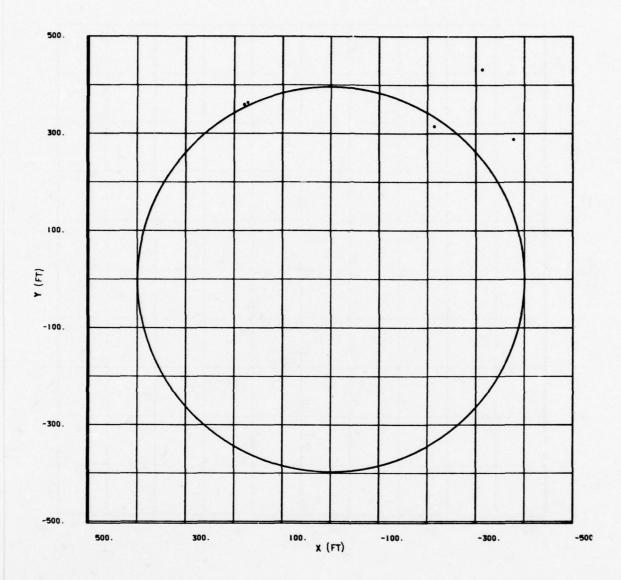


Figure B-19. Recovery plot of projectiles, 20-mm bonfire cookoff test

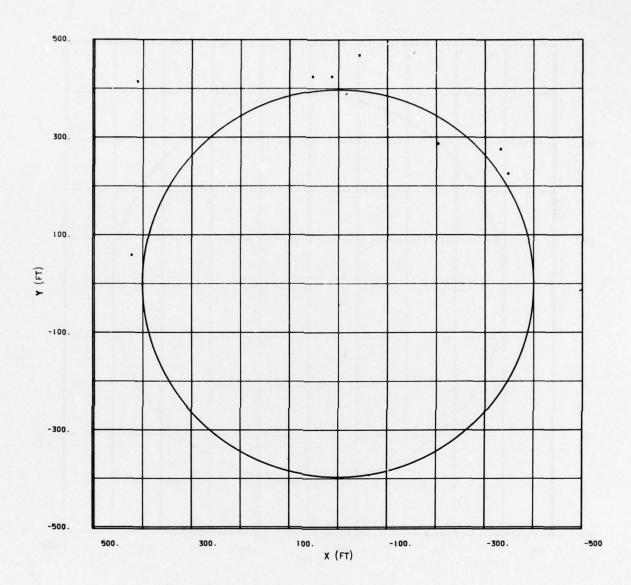


Figure B-20. Recovery plot of projectiles, 30-mm bonfire cookoff test

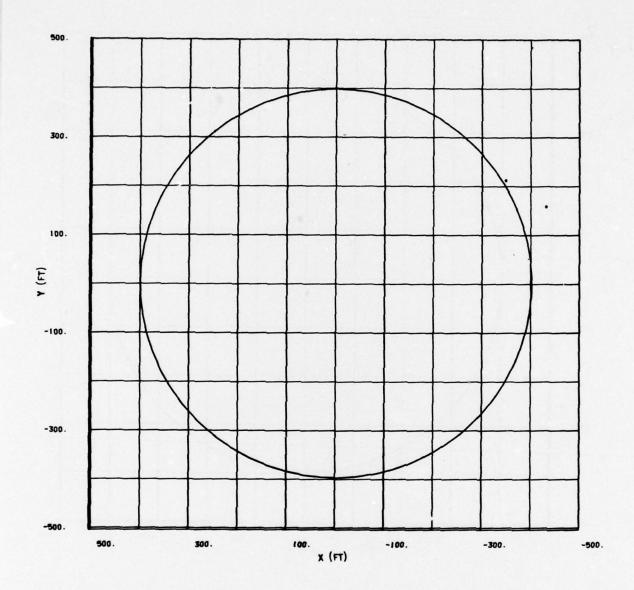


Figure B-21. Recovery plot of cartridge cases, 30-mm bonfire cookoff test

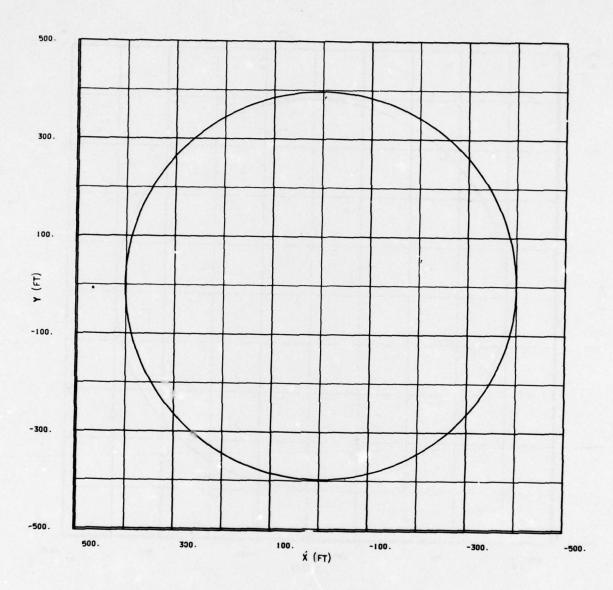


Figure B-22. Recovery plot of fuzes, 20-mm bonfire cookoff test

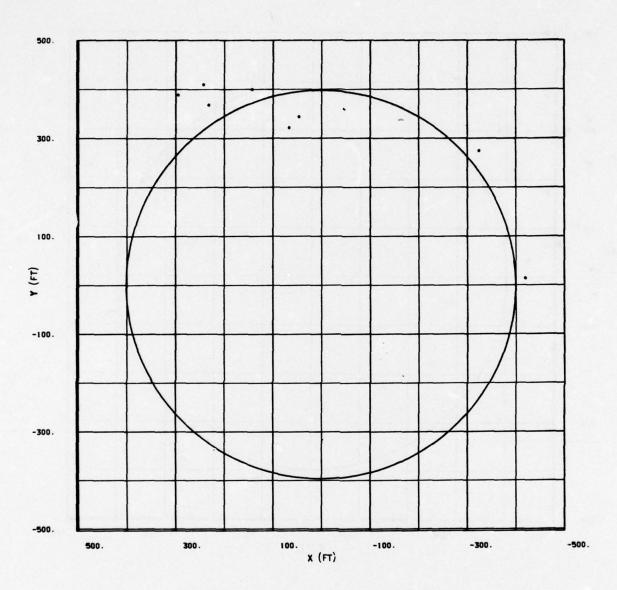


Figure B-23. Recovery plot of fuzes, 30-mm bonfire cookoff test

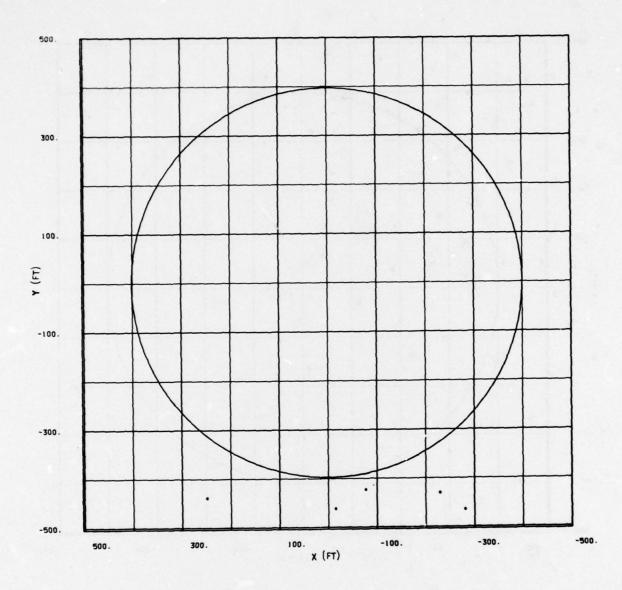


Figure B-24: Recovery plot of fuze parts, 30-mm bonfire cookoff test

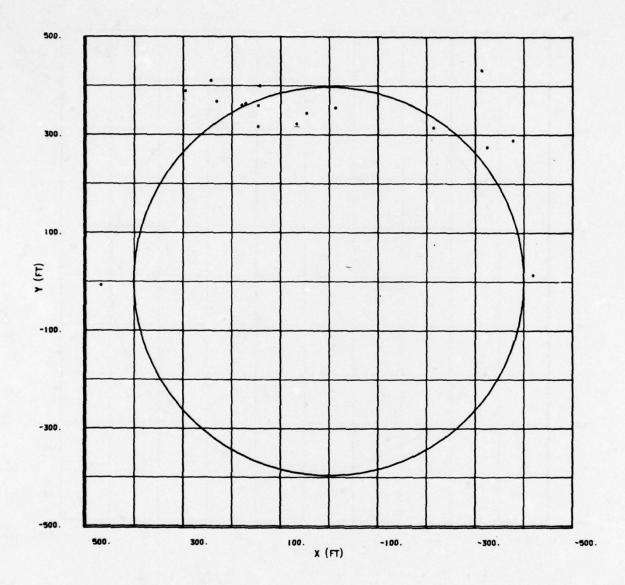


Figure B-25. Recovery plot of all parts, 20-mm bonfire cookoff test

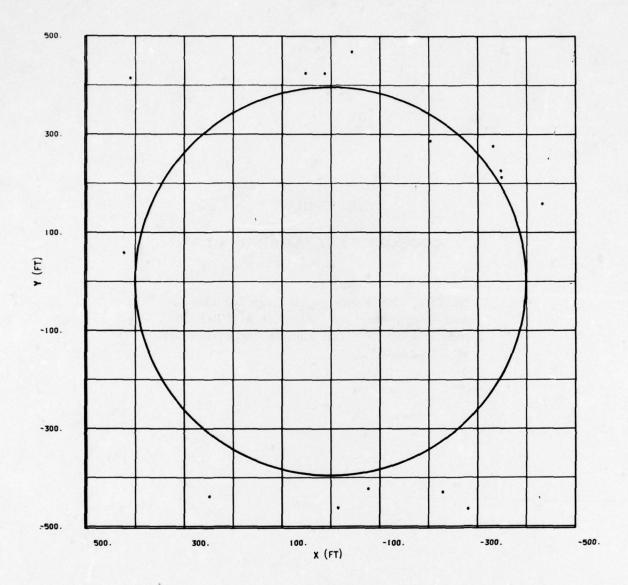


Figure B-26. Recovery plot of all parts, 30-mm bonfire cookoff test

### APPENDIX C

### COOKOFF TEST SCORING DATA

NOTE: There are no listings for the 20and 30-mm fast cookoff test A. Ten 20mm and one 30-mm rounds were recovered at fire center.

Table C-2. Unaffected rounds, 30-mm fast cookoff test B (0 recovered at fire center) Table C-1. Unaffected rounds, 20-mm fast cookoff test B Table C-5. Projectiles, 20-mm fast cookoff test B (20 recovered at fire center) Table C-3. Projectiles, 20-mm fast cookoff test A (46 recovered at fire center) Table C-4. Projectiles, 30-mm fast cookoff test A (28 recovered at fire center) (1 recovered at fire center) FEET FEET FEET.

	133 133 X 1333		######################################		FEET X FEET Z 2000 - 10		TOTAL
30-mm fast cookoff test B	FEET FEET FEET	, 20-mm fast cookoff test A	MANUAL MA	, 30-mm fast cookoff test A	1	, 20-mm fast cookoff test B	CHAPTON PROPERTY OF A CONTROL O
Table C-6. Projectiles, 30 (29 recovered at fire center)	FEET FEET FEET 16.0	Table C-7. Cartridge cases	The service of the se	able C-8. Cartri	FEET X 122 12 12 12 12 12 12 12 12 12 12 12 12	Table C.9. Cartridge cases, (26 recovered at fire center)	THE STANDARD
	FEET FEET FEET A.0		######################################	•	Manager 1 1 1 1 1 1 1 1 1 1 1 1 1 1 1 1 1 1 1		######################################

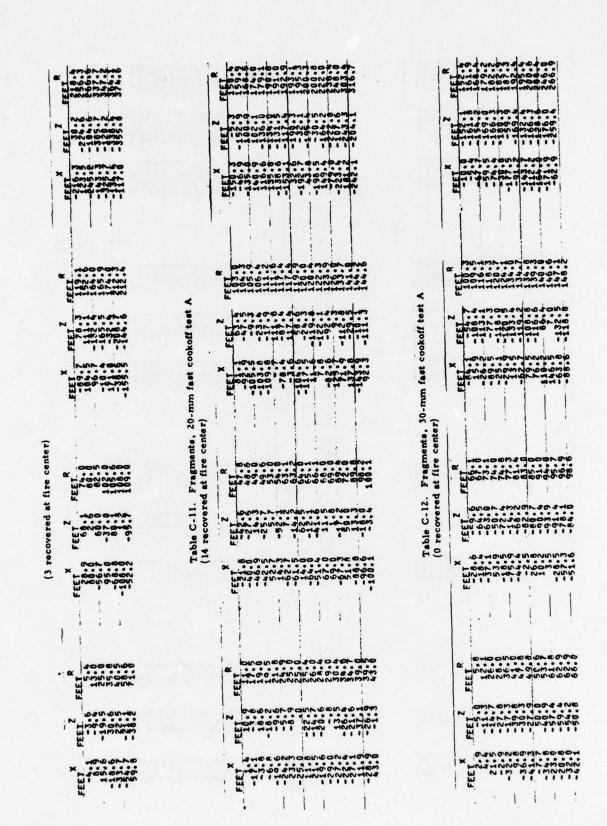


Table C-13. Fragments, 20-mm fast cookoff test B (0 recovered at fire center)

			1	1		1		-
FEET	181.2	188.6	20802	215.7	2333	258.7	319.3	
FEET	-161-8	57.6	-162.0	121	-186.1	-140.3		
FEET	-176.1	-179.8	1000	-106-7	-141.6	-217.3	309.5	
FEET	137.0	130.0	-000	145.6	151.5	155.3	200	
FEFT	1102.6	130	1000	131-1	135	-144.1	160.00	
FEET	000 000 000 000 000	-137.9	137.9	-63.4	-151-3	157.9	2000	
~	-10	900	>unc	90	nu.	-00	D+10	
FEFT	200	253	DES.	20	762	966	1100	-
FEFT	-19.7	14.4	1 11	-27.9	702.1	71.5	1001	
X YEET X	123.0	200.0	222	39.1	200	2000	100	
FFFT	5.0	200	000	2007	<b>600</b>	10.0	000	
2 233	-10	6.3	99	-6.3	3.00	-2.9	122	
×	13.1	-6.0		-1.5	-9.0	9.4	000	

Table C-14. Fragments, 30-mm fast cookoff test B (0 recovered at fire center)

	_						
*	120.9	126.6	100	166	177.	198	36255
2	-119.0	-105.6	1000	E-001	-163.0	-193.9	156.3 170.7
*	-31.6	-69.5	250	1120	-166-1	-194.2	-2004 -1600-1 -2966-9
~	76.9	801.00 64.50 1.00 1.00 1.00 1.00 1.00 1.00 1.00 1	\$000 \$10.40	\$000 400	102.1	1007	00141 00147 00150
7	-16.7	MUM MUM	200	900	-36.7	-55.5	71.7
*	-75.0	182.0	311.0	-76	-90-3	-101.9	-18680 -18680 -93.6
œ.	60.00	44. 40. 600	000	000	62.7	655.9	75.00
	-	500	r.		oon	200	77003
*	-14.8	145.6	329	000	111	-24 -24 -25 -25	2090 0090
٥	5.5	1100 1000 1000 1000	100	400	28.2	200 M	COOOO
2	 	1.7.	140	10000	25.92	203.3	022 022 022 022
×	15.0	9.4	11.	1000	120	500M	40000 40000
				-	,	,	1

FEET	179.5	180.0	1901-9	191.0	193.1	2000-3	201.4	2013	222.0	223.8	231.5	236.4	243	242	255.3	2.292	303.6	300	322.5	436.5			1	96.3	208.4	200	257.6	268.1	\$13:9	300.6	310	330.4	204.00
FEET	-136.0	-75.5	-134.0	-131.5	-190.3	-195.4	146.5	-112.2	-166.2	-219.6	94	222	-256.3	-245-1	-35.4	100	-263.3	-313	13.9	-		1	FEEL	-165.0	-120.6	-215.2	-256.	1.652	- 599:3	-1/1-5	2.2.5	-306.3	2. 17 i
FEET	116.6	164.4	135.6	-138.6	-192.7	43.0	-195.9	215.9	149.4	42.7	1000	1.62	2011.7	223	-252.8	2.552	141.2	262-	-322.2	436.3		1	- 1			1	6.29	1	1	1	1	1	١.
FEET	100	106.4	109.7	111.2	117.4	119.1	120.0	120.4	124.0	126.0	900	100	166.1	1000 1000 1000 1000 1000 1000 1000 100	140.0	150	157.9	1000	200	200			FEET		1 1 1 1 1 1 1 1 1 1 1 1 1 1 1 1 1 1 1	140.0	140	159.6	100	179.2	182.2	100	1361
	20.4	-23.	109.	-17.	117.	102.	-24	-122.	-92-	64	110	175	32		25	2	5	192	100	100	cookoff test A		- 1			1	-118.9	1	1	1	- 1	- 1	
FEET	100-	-103.8	1150	-109.8	1.00-	109	-117.5	19:61	124.0	125.	100	-12	-160	22.	11.2.	-150-	-151-1	900	-135.0		nm fast		FEET	100	79.5	110.2	100	22.	000	-59.5	-100.0	-177.5	3.16
EEEL	100		10.91	45.6 47.0	69.69	0.64	51.5	53.0	53.3	4.65	100	200	66.1	000	1000	200	92.0	00°	100	10001	All part	R R	-	- Marie 1	61.4	925	0000	300	6.96	100.5	200	110.0	114.7
~	£1.57																				9	32 recovered	FEET	125	22.0	00.0 00.0	27.5	6.00	1000	1000	000	1000	1.00
FEET		21.	30.00	67.0	-21-8	6.99	-27.2	52.7	14.3	-59.2	-61-5	Ma	-51.6	2000	-67.3	200	1.99	900	2000	-1990:		*	FEEL	200	-81.2	101	2000	25.50	1000	944	135	2000	1170.5
													- 4									*	FEET	**************************************	60	10.	300	-22	.00	7:	in	000	:
1939	64.0			10.	680	-10	-6-	**		-55-	1:	2	-20	29	13	200	-2	-3	-26.	-2-		į	FEET	100	-11	911	17.0	500	200	-56	. 554	200	
EET	444	12.4	17.	::	-3.5	-6.1	-19.6	24	25	31.6	26.1	25	19.6		27.2	35	9	2		4.4		*	1	140	6.4	ini.	200	::	:::	*	Since	101	:

Table C-17. All parts, 20-mm fast cookoff test B (47 recovered at fire center)

176.9	9.9	500	6.3	7.6	8:4	9.0	8.2	9.8	4.5	777	8.7	-		3.9	9.0	8.3	7.2	9.40	200	100		9	6.5	1.6	5.9	9.9	2.0	1	2.5	200	4.5	200
-	7	7	F		F	7	-	H	20	2	~~	2	vò	i	20	12	20	100	vi	N	V.	in.	12	~	30	~	~	7	MM	2	nm	7
1			1											1					1											1		
156.6	4	0.4	1	20		94		:	100	7	01	9	3.	:	••	30	39	2	:	**	7	*	!:	~			9	*	9-		20	
156	3	120	5	22	7	52		193	7	7	36	4	73	Ē	7	39	220	6	3	13.	Ŧ	1	75	26	19	7	7	3	40	-	97	52
-	7	•	F	1				-	•	1	77		~ '	F		1	1			7			100					7	•	ľ	~	'
me		~-	1	00	9	<b>O</b> M	-	5	~	-	~	٠,	~		0,	-	20	000	-	101	*				Im	-	ou		•	-	5.5	6
200		-	-	90	÷	69		9		3	60	4	:		40	6	200	'n.	-	*	*		'n			3	60		mo		3	6
	7	7		7	18	7	5	Ì	-2	ন	7	~	75	÷	20	30	Ņ	2	V	2	¥	5	,-	2	72	~	3	7	200	1	2	'n
	-		-									-							-		1									-		
	-											-		-																		
	3	-	Ě	5	Ŀ				8:8	3		7	5	Ŀ				6			7	9		-		Ğ	510	3	6-		9.0	
104.6	10	õ	Ξ	111	≝	37	Ē	11	125	12	127	13	13	13	13	135	NY P	13	20	3	ŀ	3	150	15	15,	151	12	15	15	100	166	160
4			ľ									-				-					1											
00	-	-14	-	•4	1	*	2	m	90	N		-	94	•	40	-	34	5	00	w.	+	4		•	200	9	-10	+		-	- ~	00
1	1	2	1	2	]	me	9	61	100	7	250	N	25	9	9:	3	V.R	2	20	2	÷	S COL	9	Ś	50	33	315	2		9	36	10
6.9	•	=1	1	17	1	Ŧ	7	-1	•	7	77	1	-	4		-		-	**	-:	7	7	ï		1	•	7	+		+	7	7
			4		1					- 1				1		1	. !		1				1									1
-56.	1	?	*	44	13	99	:	2.5		3	.5	9	50		,	12					1		.2			7	50	3	000	T	.0	
350	14	-i	2	7	12	24	7	"	10	-22	100	3	20	6	-	3	133	-2	5	133	÷	201	3	151	33	5	150		25	12	96	2
23.5	23.6	24.0	26.4	28.4	29.0	29.0	30.0	30.9	33.20	33.5	000	37.0	200	43.0	0 44	45.0	46.0	40.0	200	51.4	50.0	62.0	65.3	71.0	75.2	79.0	81.0	1119	82.5	2.70	93.0	99.1
	100	94		90	2.	U.	.5		•	-	m.	6			••	900	-10	.61	70		**	1-10	27	*		-	91.	6.		in		31
113	1	7		25	~	10	"	-18	1	9	<b>1</b>	5	75	3	10	38	7	2	20	-15	7	-2.	-65	7	75	-55	70	2	67	5	35	95
٩.,	1		-	•	1					1		1		Ī		1	1				1									1		
20	0	ma	3	•	30	0	•	-		2	ma	~	<b>T</b>			20	04	4	JU.	w.	5-	1-10	- ~		om	-	NO	0	01	m	n c	-10
12.5	1	90	3	9,0	100	5	62	2	34	32	2	=	50	2	ŗ,	300	96	39	7	6	-	2	Š	2	5.9	26	26	9	7.0	1	50	~
900	•		•	•	1			•	•	•					- (				•	•	•						•	•	11	•	•	•
1	1		1		1					1		1		1		1	1		1		1		1			1		1				
1	-		1							1		1		1		1			1				4			-		1				
-	1		-							1		1		1			-				1		!			!						
1					-					-		-		-		1					i					1						
-					-									1		-	Q:c		-										-		n -	_
00	•	311	3	5	150	•		9	•••	9	9.0	7.	:	::		96	60	6	00		3	2		3.5	,,,	3	5.0	7:1				-
4			1		1					1				1		-		•	**	1-1	-	***	1-1	-		-				171		N
					1					-						1					-					-						
34	200	~	10		90	0	200	N		5	r.r.	~		200	N	9-	00	9	-	S	-	0	00	-	200	-		0	-	,		Ne
1 -	107	+	3	*	in	9		9	HIS	9	99	4	1	9	•	-	m	00	2	N	4		S	-	~	11	S	1	12	COL	S	
	0.00			•	1	•			•	1		•	•			1					•		77	•			•		-		•	
7'7			1		1											1					1											1
11					1					4														-		-						
00		45			6	00		2		3	~	9:0	30	101	:		50	9			3				**	4.6	-10		200	m.	* -	
7'7	3	- No.	3.1		2.9	0	2.5	2:	01	-1.2	25.	2.6	200	-4.2	1:1	4.0	00	3.0	1	-11:0	120	100		9.0	111.7	4.6	16.0	-14.5	1000	100	-19.4	21.0

C-18. All parts, 30-mm fast cookoff test	30-mm fast cookoff test B
. All parts,	mm fast cod
C-18. All	
	Table C-18. All

	5.5	200	0000	~ 60	26.0	2.3	W. W. W.	24-	200	~~	· · · · · · · · · · · · · · · · · · ·
FEE						710	220	222	200	חרשרים	mm
FEET	-53:6	-135.6	132.4	1500	-163.0	-193	-200-	30.2	1224	-1705.7	-338.4
FEET	-118.7	-145-	200	173	-164-1	-194.2	155.5	-216.3	252	700	-134.4
FEET	000	63.5	40.40	9000	102.0	105.1	000 000 000	109.0	500		125.5
21333	-73.6	150	200	900	37.0	800.1	55.5	625.7	300.7	990 000	-105.0
FEET	000	190	D-10	914	900	168-0	001 001	200	900	000 000	69
!											
FEET	000 000		430	2000	200	57.4	625	65.0	7007	27.4	76.9
FEET	140	200		24	1.00	40.6	100 100 100 100 100 100 100 100 100 100	100	90M	140	16.7
FEET	MO1	200	110	000	400	200	900	200		200	-30.1
-			•								
FEET	300	9	*00	NMU	1000	2000	100	24.2	300	WAN I	300
FEET	D-11	200	יייייייייייייייייייייייייייייייייייייי	-00	112.1	200	1000	-22.6	23.3	7.95	30.6
-	000	100	-	00	NO:	-00	-me	0-	00	man	

Table C-19. Projectiles, 20-mm boufire cookoff test

FEET		FEET	500.9
FEET FEET FEET 566.4		FEET FEET FEET	414.5
FEET		FEET	407.0
FEET.	·	FEET	470.2
-314.4 430.9 -533.4	cookoff te	FEET	468.0
FEET	Table C-20. Projectiles, 30-mm bonfire cookoff test	FEET FEET FEET	-45.3
476.3	Projectiles, 3	FEET	427.3
7EET FEET 360.1 440.9	le C-20.	FEET FEET	454.4
FEET - 378.9	Tab	FEET	20.0
FEET 400.1		FEET	415.8
362.8		FEET !	225.7
FEET 168.6		FEET	-349.1

Table C-21. Cartridge cases, 30-mm bonfire cookoff test

FEET FEET FEET FEET FEET	FEET FEET FEET	FEET FEET FEET FEET FEET FEET FEET FEET	FEET FEET FEET	R FEET FEET FEET
FEET FEET FEET	FEET FEET FEET	FEET FEET FEET	α .	FEET
FEET FEET	FEET FEET FEET	FEET FEET FEET	~	FEET
FEET FEET	FEET FEET FEET	FEET FEET FEET	~	FEET
FEET	FEET FEET	FEET FEET FEET	~	FEET
	FEET	FEET FEET	~	FEET

FEET FEET Table C-22, Fures, 20-mm bonfire cookoff test FEET FEET

Table C-23. Fuze parts, 20-mm bonfire cookoff test

FEET FEET FEET	-515.2 19.4 515.6
FEET FEET FEET	238.9 409.3 473.9
EEL FEEL FEEL	.325.1 275.0 425.8
FEET FEET	3 14.4 420.5
FEET	-426.3

ole C-24. Fuze narts. 30-mm honfire cookoff tact

	FEET FEET FEET
Table C-24. Fuze parts, 30-mm bonfire cookoff test	FEET FEET FEET FEET FEET FEET FEET FEET
	FEET 428.0
	FEET -420.6
	FEET -79.6

Table C-25. All parts, 20-mm bonfire cookoff test

FEET FEET 195 533-6 -9 525-6 -9 500-9
7 7 7 7 7 7 7 7 7 7 7 7 7 7 7 7 7 7 7
7 EEE 2 3675 0 20 20 20 20 20 20 20 20 20 20 20 20 2
X 7466 4 4 4 4 4 4 4 4 4 4 4 4 4 4 4 4 4
7 + 4 + 4 + 4 + 4 + 4 + 4 + 4 + 4 + 4 +
362.8 362.8 360.1
 T44444
 munuum munuum mussana maana naana
331422 331422 331642 44661

Table C-26. All parts, 30-mm bonfire cookoff test

	FEET, F	131.2 543.5	6.4.4
	FEET	-527-4	483
	FEET 7	496.2	2000
+		1.00	
-	FEET.	-230.5	2.642
-	FEET	432.6	2000
1	FEET	275.0	1000
*	FEET 50.0	133	
!	1	1	
~	352.7	400 000	424.2
	287-1		

### THE UNITED NATIONS SYSTEM OF CLASSIFICATION OF EXPLOSIVES -- WHERE ARE WE TODAY?

Arlie E. Adams
Air Force Logistics Command
Wright-Patterson Air Force Base, Ohio

AT THE 16TH EXPLOSIVE SAFETY SEMINAR, MR. R. R. WATSON OF THE UNITED KINGDOM MINISTRY OF DEFENSE SPOKE ON THE UNITED HATIOHS SYSTEM OF CLASSIFICATION OF EXPLOSIVES. HE INCLUDED THE BACK-GROUND OF THE SYSTEM, NOW IT WAS DEVELOPED, HOW IT SHOULD WORK, AND THE BEHEFITS OF MANY COUNTRIES USING THIS SAME SYSTEM. HE CONCLUDED BY ASKING, "WHAT IS THE USA DOING ABOUT ADOPTION OF THE UN SYSTEM OF CLASSIFICATION OF EXPLOSIVES. IN A FEW YEARS MR. CHAIRMAN, YOU WILL BE OUT OF STEP WITH EVERYONE ELSE IF YOU DON'T ADOPT THE UN SYSTEM FOR EXPLOSIVES. IF YOU CAN'T BEAT US, WILL YOU NOT JOIN US?" IT IS NOW TWO YEARS LATER AND WE, IN DOD, ARE JOINING THE OTHER COUNTRIES.

THE PAPERS PRESENTED EARLIER TODAY HAVE DESCRIBED SOME OF THE PROBLEMS ASSOCIATED WITH TESTING OF PROPELLANTS, PYROTECHNICS, AND COMPLETE ROUNDS OF AMMUNITION. BASED UPON THESE TEST RESULTS, THE SPONSORING SERVICE WOULD OBTAIN TRI-SERVICE COORDINATION ON THE STORAGE AND TRANSPORTATION CRITERIA FOR THE ITEM, THAT IS, THE HAZARD CLASSIFICATION. UNTIL RECENTLY, THE HAZARD CLASSIFICATION CONSISTED OF:

- A. QUANTITY DISTANCE CLASS
- B. STORAGE COMPATIBILITY GROUP
- C. DEPARTMENT OF TRANSPORTATION (DOT) CLASS
- D. DOT MARKING

HOWEVER, IN MARCH 1976, DOD 5154.4S, "DOD AMMUNITION AND EXPLOSIVES SAFETY STANDARDS", WAS CHANGED TO REQUIRE THE USE OF A SYSTEM BASED UPON THE ONE DEVELOPED BY THE UNITED NATIONS FOR THE STORAGE OF AMMUNITION. THAT CHANGE DELETED THE QUANTITY DISTANCE CLASSES AND STORAGE COMPATIBILITY GROUPS THAT HAVE BEEN USED IN THE PAST. WE STILL RETAIN THE DOT CLASS AND THE DOT MARKING FOR TRANSPORTATION BECAUSE THE DEPARTMENT OF TRANSPORTATION STILL REQUIRES THEIR USE.

THE DOD IMPLEMENTATION OF THE UN SYSTEM WAS ACCOMPLISHED AFTER MANY HOURS OF WORK BY EACH OF THE SERVICES. AFTER EACH SERVICE CONVERTED THE INFORMATION ON ITS ITEMS TO THE UN SYSTEM AND FURNISHED THAT INFORMATION TO THE OTHER TWO SERVICES, WE FOUND THAT MANY DIFFERENCES WERE CREEPING IIITO THE SYSTEM BECAUSE OF OPINION AND LONG-STANDING OPERATING DIFFERENCES. THE DECISION WAS THEN MADE THAT EACH SERVICE WOULD MAKE A STRAIGHT LINE CONVERSION BASED ON QUANTITY DISTANCE OF ALL OF ITS ITEMS. AFTER DOING THIS, THE ARMY, MAVY, AND AIR FORCE REPRESENTATIVES MET AND COMPARED THE CONVERSIONS. BECAUSE OF THIS FACE-TO-FACE REVIEW, THE SERVICES ARE IN AGREEMENT ON THE VAST MAJORITY OF ITEMS. THE FEW PROBLEMS REMAINING CAN BEST BE RESOLVED BY ESTABLISHING A DOD MASTER LIST OR REGISTER OF HAZARD CLASSI-FICATION INFORMATION. THIS HAS BEEN SUGGESTED TO THE DDESB AND IS PRESENTLY BEING CONSIDERED.

THE UN SYSTEM OF CLASSIFICATION OF DANGEROUS GOODS CONSISTS OF NINE CLASSES OF ITEMS OR COMMODITIES. THE DOD HAS DIRECTED THE USE OF TWO OF THESE NINE, CLASS I, "EXPLOSIVES," AND CLASS VI, "POISONOUS (TOXIC) AND INFECTIOUS SUBSTANCES." EACH OF THESE CLASSES IS DIVIDED INTO SEVERAL DIVISIONS. THESE CLASS/DIVISIONS ARE DIRECTLY RELATED TO THE OLD OD CLASSES. THE VARIOUS SEPARATIONS NEEDED FOR THE QD CLASS HAVE NOT CHANGED, ONLY THE NAME ON THE HEAD OF THE TABLE WAS CHANGED. THE COMPATIBILITY GROUPS USED WITH THE NEW SYSTEM ARE DRASTICALLY DIFFERENT THAN THOSE USED IN THE PAST; HOWEVER, ITEMS THAT WERE COMPATIBLE UNDER THE OLD SYSTEM WILL, WITH SOME EXCEPTIONS, BE COMPATIBLE UNDER THE NEW SYSTEM. A WORD OF CAUTION ABOUT THESE NEW COMPATIBILITY GROUPS IS NECESSARY. THE PHRASES "WITH ITS OWN MEANS OF INITIATION" AND "WITHOUT ITS OWN MEANS OF INITIATION" MUST BE FULLY UNDERSTOOD, AS WELL AS THE DEFINITION OF GROUP S AMMUNITION, PRIOR TO DETERMINING THE PROPER COMPATIBILITY GROUP FOR AN ITEM.

AS USED IN GROUPS D, E, AND F, "WITH ITS OWN MEANS OF INITIATION" INDICATES THAT THE AMMUNITION HAS ITS NORMAL INITIATING DEVICE ASSEMBLED TO IT, AND THIS DEVICE IS CONSIDERED TO PRESENT A SIGNIFICANT RISK DURING

STORAGE. HOWEVER, THE TERM DOES NOT APPLY WHEN THE INITIATING DEVICE IS PACKAGED IN A MANNER WILLCH ELIMINATES THE RISK OF CAUSING THE DETONATION OF THE AMMUNITION IN THE EVENT OF ACCIDENTAL FUNCTIONING OF THE INITIATING DEVICE, OR WHEN FUZED EIID ITEMS ARE SO CONFIGURED AND PACKAGED TO PREVENT ARMING OF THE FUZED END ITEMS. THE INITIATING DEVICE MAY EVEN BE ASSEMBLED TO THE AMMUNITION, PROVIDED ITS SAFETY FEATURES PRECLUDE INITIATION OR DETONATION OF EXPLOSIVES FILLER OF THE END ITEM IN EVENT OF AN ACCIDENTAL FUNCTIONING OF THE INITIATING DEVICE. HAND GRENADES ARE CONSIDERED TO HAVE THEIR OWN MEANS OF INITIATION AS THE FUZE HAS NO OUT-OF-LINE COMPONENT AND WILL DETONATE THE GRENADE IF THE FUZE IS INITIATED. 20MM HEI AMMUNITION IS CONSIDERED TO BE WITHOUT ITS OWN MEANS OF INITIATION AS THE FUZE, IF INITIATED, WILL NOT DETONATE THE PROJECTILE BECAUSE OF THE OUT-OF-LINE ROTOR.

IN ADDITION TO THE CLASS AND DIVISION AND THE NEW COMPATIBILITY GROUPS, THIS SYSTEM HAS TWO UNIQUE FEATURES. IN SOME INSTANCES, CLASS/DIVISION 1.1 ITEMS, AND IN ALL INSTANCES CLASS/DIVISION 1.2 ITEMS, WILL BE PREFIXED BY A TWO-DIGIT NUMBER THAT PREPRESENTS IN HUNDREDS OF FEET THE INHABITED BUILDING DISTANCE FOR THAT ITEM. THE SECOND NEW FEATURE IS THE SERIAL NUMBER ASSIGNED TO EACH ITEM. THE ASSIGNMENT OF NEW SERIAL NUMBERS AND THE DESCRIPTION OF THE ITEMS IN THAT CATEGORY ARE CONTROLLED BY THE UNITED NATIONS ORGANIZATION.

THE SERIAL NUMBERS ARE INTENDED TO BE USED ON SHIPPING PAPERS TO PROVIDE TRANSPORTATION PERSONNEL WITH AN INDICATION OF THE ITEMS THEY ARE HANDLING. IN THIS RESPECT, THEY ARE SIMILAR TO OUR DOT MARKING OR SHIPPING NAME. THE SERIAL NUMBERS ARE DIVIDED INTO BLOCKS ACCORDING TO THE CLASS OF ITEMS, WITH SERIAL NUMBERS 0001 THROUGH 1000 RESERVED FOR CLASS I ITEMS. DON'T FORGET THAT WITHIN THE UNITED STATES, WE ARE NOT YET USING THESE SERIAL NUMBERS. THEY ARE PROVIDED ONLY FOR THOSE FORCES STATIONED IN COUNTRIES THAT ARE USING SERIAL NUMBERS.

"THIS NEW SYSTEM HAS BEEN OFFICIALLY ADOPTED BY CHANGE 1 TO THE DOD STANDARD. YOU CAN LEARN MORE ABOUT IT FROM THE PUBLICATIONS OF EACH SERVICE. THE ARMY, THROUGH THE DARCOM SAFETY OFFICE, HAS PREPARED AND STAFFED CHANGE 3 TO THEIR EXPLOSIVES SAFETY MANUAL. THAT CHANGE IS EXPECTED THIS MONTH, AND WILL EXPLAIN THE BASIC SYSTEM. THE AMMUNITION CENTER AT SAVANNA ARMY DEPOT HAS PUBLISHED AN UNOFFICIAL LISTING OF ARMY ITEMS SHOWING ALL THE INFORMATION NEEDED TO STORE THOSE ITEMS. THEY ARE DEVELOPING A COMPUTER PROGRAM SO THAT CURRENT, OFFICIAL LISTINGS CAN BE PUBLISHED ON A PERIODIC BASIS.

THE NAVY HAS MARKED UP A COPY OF THEIR OP 5 AND IS WAITING FOR FURTHER INSTRUCTIONS ON HOW AND WHEN TO PUBLISH THIS INFORMATION.

THE AIR FORCE HAS PUBLISHED TO 11-1-39 WHICH EXPLAINS THE SYSTEM AND LISTS BY NSN THE EXPLOSIVES ITEMS IN THE USAF INVENTORY. THE AIR FORCE EXPLOSIVES SAFETY MANUAL, AFM 127-100 IS PRESENTLY BEING REWRITTEN TO INCLUDE THE NEW SYSTEM AND IS TO BE PUBLISHED ABOUT THE FIRST OF NEXT YEAR.

THE DEPARTMENT OF DEFENSE IS ALSO ADOPTING A STANDARDIZED SYSTEM OF FIRE SYMBOLS AND CHEMICAL HAZARD MARKERS. THE FIRE SYMBOLS ARE DIRECTLY RELATED TO THE CLASS/DIVISION OF THE AMMUNITION. FIRE SYMBOL 1 IS USED WITH CLASS 1 DIVISION 1; FIRE SYMBOL 2 WITH CLASS 1 DIVISION 2; FIRE SYMBOL 3 WITH CLASS 1 DIVISION 3; AND FIRE SYMBOL 4 WITH CLASS 1 DIVISION 4; AND WITH CLASS 6 DIVISION 1 COMMODITIES. THE PRINCIPAL DIMENSION OF EACH OF THESE SYMBOLS IS 24 INCHES. THEY HAVE AN ORANGE BACKGROUND AND BLACK NUMBERS. THE CHEMICAL HAZARD MARKERS ARE USED TO INDICATE THE PROPER PROTECTIVE CLOTHING REQUIRED BY FIRE FIGHTING PERSONNEL, THE USEFULLNESS OF WATER AS A FIREFIGHTING AGENT, AND TO PROVIDE AN INDICATION OF THE SPECIFIC CHEMICAL AGENT PRESENT.

THE US AIR FORCE HAS BEEN REQUESTED TO MANUFACTURE THESE SYMBOLS AND MARKERS FOR DISTRIBUTION TO ALL DOD COMPONENTS. THE SACRAMENTO AIR LOGISTICS CENTER WILL PROBABLY BE

TASKED WITH THIS WORKLOAD FOR THEIR DECAL SHOP. THEY WILL USE A COMMERCIALLY AVAILABLE ADHESIVE BACKED PAPER SO THAT THE REQUESTING ORGANIZATION CAN STICK THE DECAL TO ANY LOCALLY AVAILABLE MATERIAL SUCH AS PLYWOOD, ALUMINUM, OR STEEL. SOME AIR FORCE UNITS HAVE BEEN USING THESE STICK-ON SYMBOLS FOR SEVERAL YEARS WITHOUT ANY DIFFICULTY. THE PRELIMINARY COST ESTIMATES FOR THE TWO-COLOR DECALS IS \$160.80 PER HUNDRED, AND \$691.20 PER HUNDRED FOR THE THREE-COLOR DECALS. THE AIR FORCE HAS NOT YET OFFICIALLY ACCEPTED THIS WORKLOAD, BUT WE DO NOT ANTICIPATE ANY INSURMOUNTABLE PROBLEMS.

A TARGET DATE OF 1 JANUARY 1977 FOR IMPLEMENTATION OF THE UN SYSTEM, THE FIRE SYMBOLS, AND CHEMICAL HAZARD MARKERS FOR STORAGE OF AMMUNITION HAS BEEN SUGGESTED BY THE DDESB. IT NOW APPEARS THAT AVAILABILITY OF THE MARKERS AND SYMBOLS MAY FORCE ADOPTION OF A LATER IMPLEMENTATION DATE. THE DECISION TO USE THIS SYSTEM FOR TRANSPORTATION OF AMMUNITION RESTS WITH THE DEPARTMENT OF TRANSPORTATION. WE SHOULD ENCOURAGE THEIR FAVORABLE CONSIDERATION OF THIS SYSTEM.



## **UN CLASSES**

### CLASS

1 EXPLOSIVES
2 COMPRESSED OR LIQUIFIED GASES

INFLAMMABLE LIQUIDS

INFLAMMABLE SOLIDS

OXIDIZING SUBSTANCES

POISONOUS (TOXIC) AND INFECTIOUS SUBSTANCES

7 RADIOACTIVE SUBSTANCES

CORROSIVES

MISCELLANEOUS DANGEROUS SUBSTANCES



OLD QUANTITY- DISTANCE CLASS	7	TS 3 THROUGH 6	2	Y ARD	ω	S
HAZARD	BLAST	PRAGMENTS	FIRE	RELATIVELY LITTLE HAZARD	TOXIC	INFECTIOUS
CLASS DIVISION	1.1	1.2	1.3	1.4	6.1	* 6.2

\* Included for information only, no known assets.



## **EXPLANATION**

### GROUP

- INITIATING EXPLOSIVES. BULK INITIATING EXPLOSIVES FRICTION, OR PERCUSSION TO MAKE THEM SUITABLE FOR USE AS INITIATING ELEMENTS IN AN EXPLOSIVE WHICH HAVE THE NECESSARY SENSITIVITY TO HEAT
- ITEMS CONTAINING INITIATING EXPLOSIVES THAT DETONATORS AND SIMILAR INITIATING DEVICES. ARE DESIGNED TO INITIATE OR CONTINUE THE FUNCTIONING OF AN EXPLOSIVE TRAIN. 8
- WITH OR WITHOUT THEIR MEANS OF IGNITION. ITEMS THAT UPON INITIATION WILL DEFLAGRATE, EXPLODE CHARGES, AND DEVICES CONTAINING PROPELLANT BULK PROPELLANTS, PROPELLANT PROPELLING OR DETONATE.



۵

BE EXPECTED TO EXPLODE OR DETONATE WHEN ANY CHARGE. AMMUNITION AND EXPLOSIVES THAT CAN GIVEN ITEM OR COMPONENT THEREOF IS INITIATED. AMMUNITION CONTAINING HE WITHOUT ITS OWN MEANS OF INITIATION AND WITHOUT PROPELLING BLACK POWDER, HIGH EXPLOSIVES (HE) AND

ш

AMMUNITION CONTAINING HE WITHOUT ITS OWN CHARGE. AMMUNITION OR DEVICES CONTAINING MEANS OF INITIATION AND WITH PROPELLING HE AND CONTAINING PROPELLING CHARGES.

u

PROPELLING CHARGE. HE AMMUNITION OR DEVICES (FUZED) WITH OR WITHOUT PROPELLING CHARGES. MEANS OF INITIATION AND WITH OR WITHOUT AMMUNITION CONTAINING HE WITH ITS OWN



### GROUP

- ACTIVATED OR WHICH CONTAIN WHITE PHOSPHOROUS, OR FLAMMABLE LIQUID OR GEL. AMMUNITION THAT, ILLUMINATION, LACHRYMATION, SMOKE, OR SOUND OTHER THAN THOSE MUNITIONS THAT ARE WATER JPON FUNCTIONING, RESULTS IN AN INCENDIARY, INCLUDING HC, OR TEAR PRODUCING MUNITIONS FIREWORKS, ILLUMINATING, INCENDIARY, SMOKE
- AMMUNITION CONTAINING BOTH EXPLOSIVES AND MATERIAL. AMMUNITION IN THIS GROUP CONTAINS FILLERS WHICH ARE SPONTANEOUSLY FLAMMABLE WHITE PHOSPHOROUS OR OTHER PYROPHORIC WHEN EXPOSED TO THE ATMOSPHERE. I



### GROUP

- GROUP CONTAINS FLAMMABLE LIQUIDS OR GELS OTHER THAN THOSE WHICH ARE SPONTANEOUSLY FLAMMABLE FLAMMABLE LIQUIDS OR GELS. AMMUNITION IN THIS AMMUNITION CONTAINING BOTH EXPLOSIVES AND WHEN EXPOSED TO WATER OR THE ATMOSPHERE,
  - GROUP CONTAINS CHEMICALS SPECIFICALLY DESIGNED AMMUNITION CONTAINING BOTH EXPLOSIVES AND TOXIC CHEMICAL AGENTS. AMMUNITION IN THIS FOR INCAPACITING EFFECTS MORE SEVERE THAN ACHRYMATION.
- AMMUNITION NOT INCLUDED IN OTHER COMPATIBILITY THAT DO NOT PERMIT STORAGE OF OTHER TYPES OF GROUPS. AMMUNITION HAVING CHARACTERISTICS AMMUNITION, OR KINDS OF EXPLOSIVES, OR DISSIMILAR AMMUNITION OF THIS GROUP.



EXPLOSIVE EFFECT, WHEN IN STORAGE, IS CONFINED DESTROY ALL ITEMS IN A SINGLE PACK, BUT IS NOT AMMUNITION SO DESIGNED OR PACKED THAT AN PACKAGE. THE SECOND TYPE IS AMMUNITION SO DESTROYED. FOR EITHER TYPE AN EXTERNAL FIRE WILL NOT CAUSE PRACTICALLY INSTANTANEOUS DESIGNED OR PACKED THAT AN INCIDENT MAY COMMUNICATED TO OTHER PACKS SO ALL ARE EXPLOSION OF THE TOTAL CONTENTS OF THE HAZARD. TWO TYPES OF AMMUNITION ARE AMMUNITION PRESENTING NO SIGNIFICANT AND SELF-CONTAINED WITHIN THE ITEM OR INCLUDED IN GROUP S. THE FIRST TYPE IS PACKAGE.



# SAMPLE ARMY LISTING

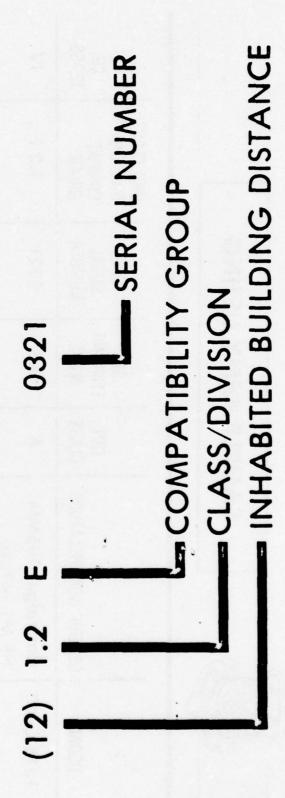
	1				
CG	≥	≥	≥	≥	₽
UNO CLASS/ DIVISION/ COMPAT GROUP	1.2 E	1.2 E	1.2 E	1.2 E	1.2 H
UNO SERIAL NUMBER	0321	0321	0321	0321	0245
DOT SHIPPING NAME	AB	AB	AB	AB	AG
DOT	<b>V</b>	∢	∢	4	∢
GENERIC NOMENCLATURE	Cartridge, 105MM HE M1 w/fuze	Cartridge, 105MM HE M1 w/fuze	Cantridge, 105MM HE M1 w/o fuze	Cartridge, 105MM HEAT M67	Cartridge, 105MM Smoke, WP M60
DODAC	1315-C443	1315-C444	1315-C445	1315-C446	1315-C447



## SAMPLE HAZARD CLASSIFICATION

ITEM: CARTRIDGE, 105MM, HE, MI, W/O FUZE

NSN: 1315-00-926-4081-C445



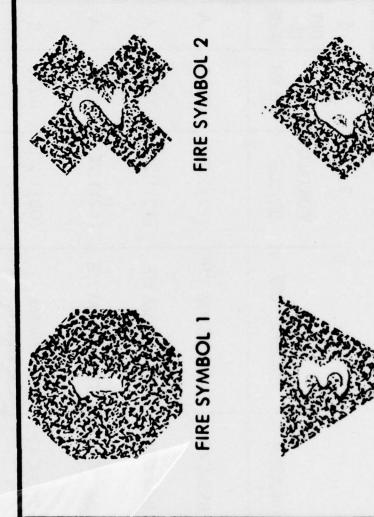


# SAMPLE USAF LISTING

			1					
	1	LAB	<	<	<	60	∢	
TION	9	MKG CODE	AG	AB	AB	ĄŁ	AB	
<b>SSIFIC</b>	S	CC. CODE	<b>4</b>	∢	∢	8	. «	
DOD HAZARD CLASSIFICATION	4	SER NO.	0245	0321	0321	0328	0015	
000	6	IBD/CLASS DIV/SCGP	(12)1.2H	(12)1.2E	(12)1.2E	(08) 1.2C	(08) 1.2G	TROUGH.
	2	NOMENCLATURE	CTG,105MM WP	CTG, 90MM HE	CTG, 105MM HE	CTG, 90MM CANISTER	CTG,81MM TP	報 第 第 第
	-	NATIONAL STOCK NUMBER	1315-00-892-4895-C454	1315-00-926-1864-C282	1315-00-926-4081-C445	1315-00-926-9243-C410	1315-00-935-1992-C227	
			1583					

## FIRE SYMBOLS



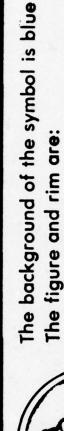


FIRE SYMBOL 4

FIRE SYMBOL 3



## CHEMICAL HAZARD MARKERS



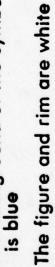
- Red for Set 1 Protective Clothing
- Yellow for Set 2 Protective Clothing
  - White for Set 3 Protective Clothing



The background of the symbol is blue



The background of the symbol is white The circle and the diagonal stripe are red The figures are black



### EXPERIMENTAL DETERMINATION OF EXPLOSIVE SENSITIVITY TO FRAGMENT IMPACT

by

R. M. Rindner
Manufacturing Technology Directorate
Picatinny Arsenal, Dover, N.J.

G. Petino, Jr. Hazards Research Corporation, Denville, N.J.

H. Napadensky IIT Research Institute, Chicago, Ill.

### Abstract

The effect of both primary and secondary fragment impact on the sensitivity of explosive end-items and in-process material has been investigated. Testing was carried out at ambient and elevated temperatures. Experimental testing conducted to date has established a fragment mass-velocity relationship below which no detonation propagation will occur for some specific realistic cases.

### Introduction

Extensive studies have been done of fragment distribution, mass and velocity, penetration and vulnerability as applied to defeat of military targets by weapons. This type of work, from another viewpoint, is of interest to the designer of the munitions manufacturing plants who must cope with the effects of an accidental explosion. Here it is important to establish the sensitivity of explosive end items and in-process materials to impact by primary (shell casing, melt kettle) fragments. Of related,

but equal importance, are the effects of secondary (concrete wall chunks and rubble) fragments.

These work areas should be intensely investigated since they would have a broad impact on the modernization of facilities and operation of existing facilities. Placement of equipment, safe separation distance of explosives, protective capacity of existing barricades, design of shielding and cubicles are but a few cases where these studies could be utilized. However, up to the present, only minimal studies involving analysis and testing have been carried out. The purpose of the tests reported here is to establish for a few specific cases a fragment mass-velocity relationship below which no detonation propagation will occur under realistic conditions.

Since the primary and secondary fragment impact studies were conducted independently\*, they will be discussed separately in this paper.

Primary Fragment Impact Tests

Be definition, primary fragments are those that result from break-up of explosive casing in the event of a detonation. Usually these fragments are characterized by having high velocity (several thousand ft/sec) and being comparatively small in size.

Analytical, and some limited experimental, work on sensitivity of explosives to primary fragment impact was performed by Picatinny Arsenal and the results of this effort were reported in Ref. 1. In this work an empirical relationship was developed which related fragment threshold detonation velocity to fragment weight and explosive casing thickness.

The work discussed in this paper is a continuation of this effort for the purpose of expanding and refining the previously developed

<sup>\*</sup> Primary - Hazards Research Corp.

<sup>\*</sup> Secondary - IITRI

relationships. The experiments were conducted using the set-up (similar to the one reported in Ref. 1) shown schematically in Fig. 1. The booster charge was composed of an E-83 cap, 50 gm Tetryl pellet and Comp B charge. The entire explosive train was placed on top of a 5 inch square Lucite buffer plate of varying thickness. Glued to the opposite side of the lucite was a square steel fragment of desired thickness and frontal area.

The entire fragment propulsion system was supported by a wooden stand that maintained a 6 ft. distance between the booster and the acceptor (target).

Two types of targets were used; namely, solid and molten Comp B.

Each type had a 3/8 in. thick square witness plate on the underside of the charge. The acceptor cover plate over the explosive was either 1/8" thick or 3/8" thick. Molten charges were contained by 6" square by 2" high steel pans.

A typical test sequence started with the selection of the fragment velocity desired, lucite thickness required to attain that velocity and cover plate thickness over the acceptor. The camera was set up 90 ft away from the detonation site. Nominal camera speed was 20,000 frames/sec. The high speed camera was the only instrumentation used to record fragment velocity. It photographed the last 24 inches of fragment travel, including fragment impact. Fragment velocity was computed by dividing the distance traversed by the time it took to travel that distance.

Prior to performing the molten Comp B tests a series of dry runs were performed to determine the cooling rate of the acceptor. It was determined that no solidification occurred within a 3 minute period.

All experiments were performed within this time frame. Fig. 2 depicts the techniques used to aim the fragment at the center of the acceptor

charge. The acceptor is placed into position at the bottom of the test stand where it is leveled in two horizontal planes. An 8 in. square steel plate is then placed on top of the plywood platform. The plate has three equi-length plumb bobs suspended from three points 60 degrees apart. The plywood platform is adjusted in two horizontal planes until the tip of each plumb bob is exactly the same distance away from the acceptor cover plate. When this is accomplished the plate is removed and the booster charge is placed into position on the plywood platform. The blasting cap is then connected to the firing circuit and the test set-up is ready to be fired by the camera.

A series of fragment calibration firings were performed to determine the variation of fragment velocity as a function of lucite spacer thickness. Fig. 3 presents the results of these firings and provides a ready reference for the various fragment velocities attainable with the Comp B booster.

#### Test Results

Impact of high velocity steel fragments on steel cased solid and molten Comp B acceptors resulted in one of the following:

- (a) no reaction (b)
- (b) deflagration and
- (c) detonation

No Reaction was characterized by a hole in the cover plate, fragmented solid Comp B or droplets of solidified explosive on the floor (molten acceptor) and a flat witness plate with a slight dent (Fig. 4).

<u>Deflagrations</u> were accompanied by clouds of smoke billowing out of the test cell and the recovery of all steel items in a fairly good condition. No physical evidence of the Comp B remained after a deflagration.

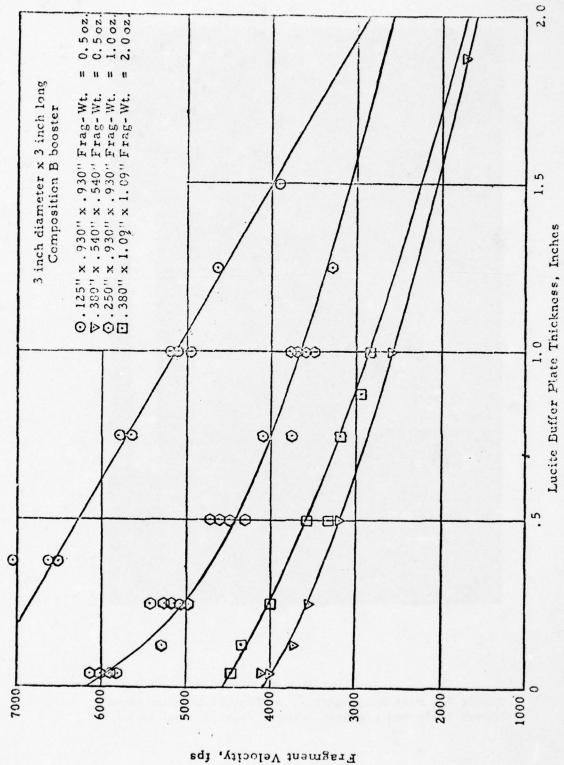


Figure 3 Fragment Velocity vs. Lucite Thickness



Figure 4 - Post Run Condition of Typical Witness Plate, Cover Plate and Fragment After a Negative Test Result

<u>Detonation</u> of both a low and high order class were considered to be positive results on this program. Detonations were characterized by either fracturing or shrapnellization of the cover plate. In addition, the witness plate was bowed several inches or driven downward into its wooden support. Fig. 5 and 6 show the low and high order detonation results respectively.

A total of 85 primary steel fragment impact tests were performed. In this series 54 tests were performed on solid Comp B while 31 tests were performed on Molten Comp B acceptors. Table I provides a summary of test results. Fig. 7, 8 and 9 graphically present the data contained in Table 1.

Fig. 9 shows that, as expected, the molten Comp B is more sensitive to fragment impact than solid Comp B. It is also noted that the difference in sensitivity is significant. Furthermore, of interest is the fact that for the range of fragment masses/unit impact area tested the relationship between sensitivity of the molten and solid states is a nearly parallel line.

The few inconsistencies in the test results could be attributed to the spacial orientation of the fragment at the moment of impact. A fragment traveling at a constant velocity is said to possess a finite quantity of kinetic energy. The distribution of this energy across the impact surface is one of the parameters that determines whether or not a detonation will occur. Therefore, in order to allow a reasonable comparison of threshold velocity data between the various fragments tested, all data were analyzed by comparing fragment mass per unit impact area to threshold velocity. One would expect that as the magnitude of the mass per unit impact area term increases, the threshold velocity level would

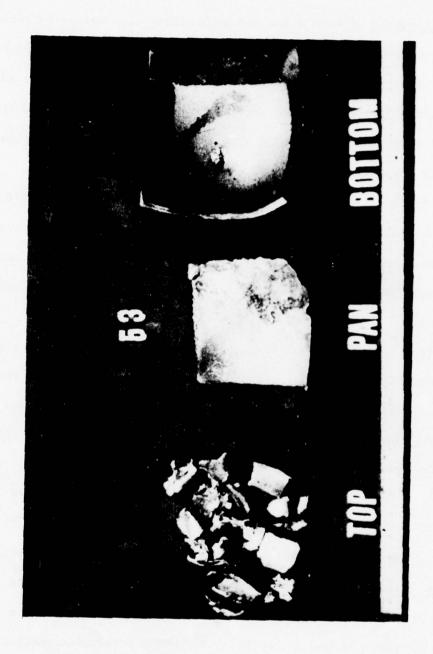


Figure 5 - Post-Run Condition of Steel Cover Plate and Witness Plate After a Low Order Detonation

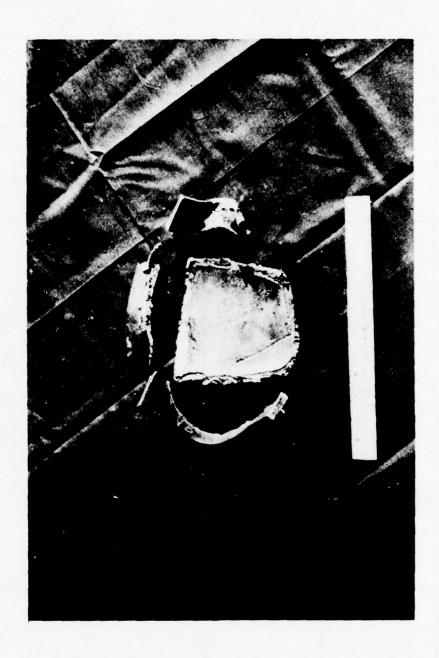
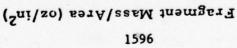
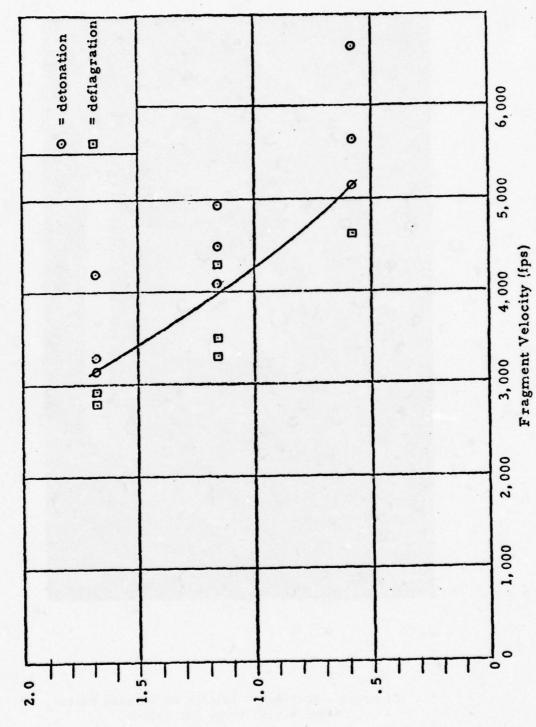
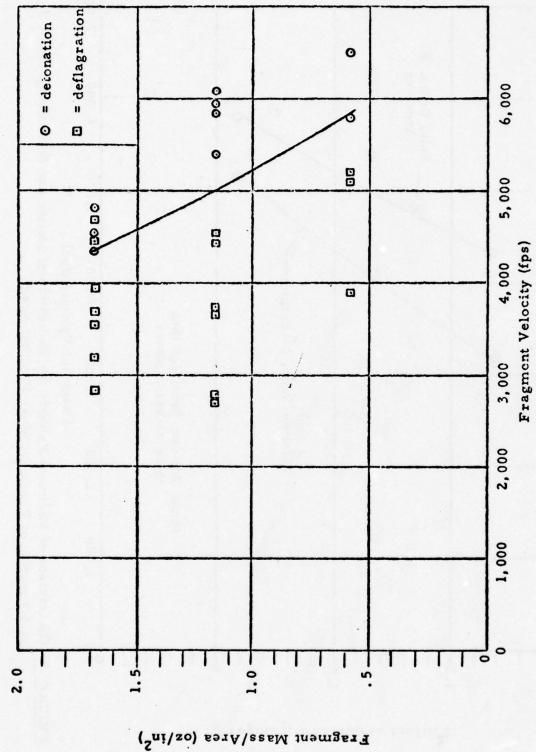


Figure 6 - Post-Run Condition of Witness Plate
After a High Order Detonation



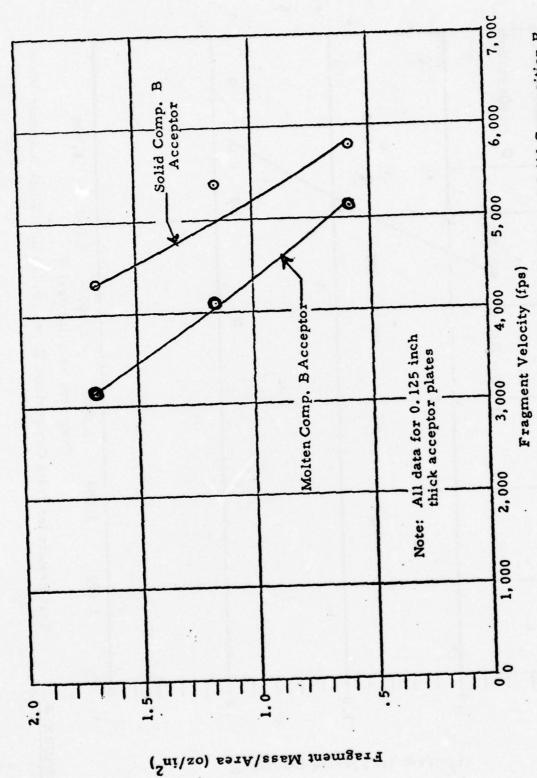


Test Results for Molten Composition B With 0.125 inch Thick Acceptor Plate



Test Results for Solid Composition B With 0. 125 inch Thick Acceptor Plate

FIGURE 8



Comparison of Minimum Velocity for Detonation of Molten and Solid Composition B as a Function of Fragment Mass Per Unit Area FIGURE 9

decrease. This phenomena does occur, as can be seen from results presented in Fig. 7, 8 and 9.

The value of using the concept of fragment mass per unit impact area instead of fragment mass can be seen if Table 1 is studied. By design, the first 0.5 oz. fragment tested had the same mass per unit area as the 2.0 oz. fragment; namely, 6.68 oz. per sq. in. Minimum velocities for detonation for these two fragments were 4,578 fps and 4,339 fps respectively, a difference of only 239 fps or less than 5%. Similarly, the second 0.5 oz. fragment with a mass per unit area of 0.58 oz. per sq. in. had a threshold velocity of 5,798 fps. If fragment mass only was plotted against fragment velocity the results would have been misleading. Two 0.5 oz. fragments would have threshold levels that differed by 1,220 fps (Table 1).

Summarizing the results obtained in this program, it was evident that the minimum fragment velocity required for detonation increases as the thickness of the acceptor cover plate increases and that the molten Comp B is significantly more sensitive to fragment impact than solid Comp B. An empirical relationship has been established between fragment mass per unit impact area and boundary velocity for most of the cases investigated. Work conducted previously by this Arsenal (Ref. 1) has been extended to allow for the effects of impact area on boundary velocity.

## Secondary Fragment Impact Tests

A series of experiments were conducted to determine explosive sensitivity to impact by concrete fragments. These tests were a continuation of the experiments, previously performed, the results of which were presented at the 16th Annual Safety Seminar (Ref. 2).

By definition, secondary fragments are those other than primary fragments that result from the detonation of explosive charges; such as wall break-up, pieces of equipment, etc. They are usually characterized by having lower velocity than primary fragments (seldom exceeding 1,000 ft/sec) and being fairly large.

The concrete fragments utilized in this program were launched from a 12 in. gun as shown in Fig. 10. This air gun is capable of launching fragments at a wide range of weights and velocities. The capabilities of the gun are shown graphically in Fig. 11. The experiments utilized two types of fragments (1) a solid concrete cylinder and (2) a cardboard container filled with pieces of concrete rubble, which was formed by packing randomly sized concrete pieces into a cardboard container.

The following configurations were tested.

- (a) The 155mm Howitzer projectile with the Comp B explosive at 150°F to simulate the facing operation.
- (b) The 155mm Howitzer projectile with the Comp B explosive at 200°F and with the loading funnel in place to simulate the just-filled condition
- (c) Melt kettle, scaled down to hold 25-40 lbs. of Comp B at 207°F.

  The projectiles were tested at elevated temperature which was achieved by use of heating tapes (Fig. 12) or a hot water bath. The temperature was monitored by chromel-alumel thermocouples. The shell was kept heated at approximately 250°F until the explosive reached the desired temperature.

The test set-up for the simulated melt kettles (Fig. 13) consisted of two concentric metal cylinders to form an annulus in which hot water was

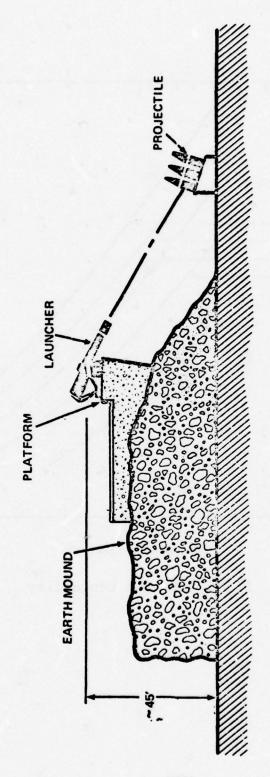


Fig 10 Secondary fragments impact test

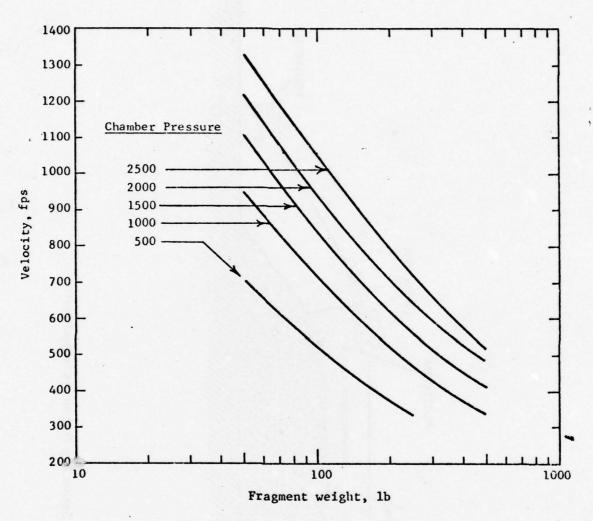


Fig 11 Air gun capability

circulated to melt the explosive in the inner cylinder. The temperature of the Comp B in the melt kettle was 207°F at the time of the test.

The initial conditions for each test and the results of each test are summarized in Tables 2 through 4. Fastax camera coverage was used for all tests. The impact velocity was measured from the film by measuring the distance the target travelled between each frame and the time between frames, as indicated on the timing marks on the film. The extent of the reaction was determined from the Fastax film and from post-test observations.

Table 2 summarizes the results of the "Just Filled" configuration. High order detonations were recorded in test JS-2 at fragment velocity of approx. 1100 ft/sec and fragment size of 50 lbs, in test JS-3 with the same fragment size and velocity, and JM-2 at 720 ft/sec and 185 lb. fragment; a low order detonation was recorded at 736 ft/sec and 185 lb. fragment in test JM-1. All other shots in this series resulted in either no reaction or deflagration.

Table 3 summarizes the results of the "facing operation" configuration. One high order detonation occurred (in the very first test) with 50 lbs. fragment impacting at approxm. 900 ft/sec. Repetition of the same test resulted in no-reaction. The remainder of the tests with fragments ranging from 50 to 375 lbs. resulted in no reaction.

Table 4 summarizes the results with the simulated melt kettle configuration. No reaction occurred during the 8 tests conducted in this series. The solid fragment impact resulted in severe crushing of the outer and inner shell. In one test the water was drained from the annulus prior to testing to see it the water attenuated the input force. The impact velocity was 1000 ft/sec. no reaction occurred in this test. The rubble concrete

Table 3
Summary of test results

Facing operation configuration

155 mm Howitzer projectile, Comp B at 150°F; impacted by 12 in. diameter concrete fragment

	Conc	rete frage	ment descr	iption		
Test no.	Туре	Length (in.)	Weight (1b)	Velocity (fps)	Kinetic <sup>a</sup> energy	Results
FS-1 FS-1R FS-2 FS-3	Solid Solid Solid Solid	6 6 6	50 50 50 50	893 884 564 370	1.0 0.98 0.40 0.17	HO No go No go
FM-1	Solid	24	185	568	1.5	No go
FM-2	Solid	24	185	504	1.2	No go
FM-3	Solid	24	185	653	2.0	No go
FL-1	Solid	48	375	400	1.5	No go
FL-2	Solid	48	375	547	2.8	No go
FL-3	Solid	48	375	470	2.1	No go
FL-4	Solid	48	375	450	1.9	No go
FR-1	Rubble	48	175	570 <sup>d</sup>	1.4	No go
FR-2	Rubble	48	175	720 <sup>d</sup>	2.3	No go
FR-3	Rubble	48	175	750 <sup>d</sup>	2.5	No go

<sup>&</sup>lt;sup>a</sup> One energy unit =  $6.2 \times 10^5$  ft lb

b No go = no reaction
HO = high order detonation

Initial flash, reaction may have immediately extinguished itself

d Average velocity of rubble

Table 4
Summary of test results

Continuous melter simulation

Water jacketed melt kettle, Comp B at 200°F; impacted by 12 in. diameter concrete fragment

	Conc	rete frag	ment descr	iption		
Test no.	Туре	Length (in.)	Weight (1b)	Velocity (fps)	Kinetic <sup>a</sup> energy	Resultsb
MCS-1 MCS-2 MCS-3	Solid Solid Solid	6 6 6	50 50 50	943 914 879	1.1 1.0 0.97	No go No go No go
MCM-1 MCM-2	Solid Solid	24 24	185 185	652 627	2.0 1.8	No go No go
MCL-1	Solid	48	375 •	510	2.5	No go
MCR-1	Rubble	48	175	720 <sup>c</sup>	2.3	No go
ETS-1	Solid	6	50	983	1.2	No go

<sup>&</sup>lt;sup>a</sup> One energy unit =  $6.2 \times 10^5$  ft lb

b No go = no reaction

c Average velocity of rubble

impact resulted in damage to the outer shell only. These tests have shown that the melt kettle does not represent a hazardous configuration when impacted by concrete fragments over the parameters tested.

Summarizing the results obtained in this test program as compared to previous tests conducted at ambient temperature (Ref. 2), it can be concluded that the 155mm Comp B filled Howitzer projectile is more sensitive to concrete fragment impact at elevated temperatures. At the highest temperature tested,  $200^{\circ}F$ , 5 out of 21 tests resulted in a reaction (HO, LO or deflagration). At  $150^{\circ}F$ , 1 out of 14 tests reacted. At ambient temperature (Ref. 2) there was no reaction in 20 tests. It can be further concluded that no detonation will occur when fragment velocity is below 500 ft/sec. The melt kettle tests showed that even at  $207^{\circ}F$  this configuration is insensitive to fragment impact.

In as much as the wall thickness of the melt kettle is much thinner than that of the 155mm projectile, one would expect that the melt kettle configuration would be more sensitive. This was not observed. We believe that the reason for this is that different initiation mechanisms are applicable to these two dissimilar configurations. In the case of the 155mm projectile it is observed after a test, when the projectile is recovered, that the projectile's case has been partially collapsed. Thus the original circular opening at the top of the projectile becomes elliptical in shape. One can readily conclude from this observation that during the collapse of the case the explosive material is extruded or squeezed out of the newly formed narrow elliptical; or slot-like opening. It is the extrusion process that is capable of converting mechanical energy of the rapidly flowing explosive into localized heating, leading to an explosion

(when the impact speeds and forces are sufficiently high).

The fact that more than 500 ft/sec is required for initiation of a detonation of the 155mm projectile is consistent with the results of other work on the sensitivity of Comp B to impact (Ref. 3) where an extrusion process rather than prompt shock initiation is the applicable initiation mechanism. The investigations cited in Ref. 3 were on large (of the order of 10 lbs) bare charges of Comp B, at ambient temperature, impacted by a 1 to 3 in.-thick steel plate. In these tests impact velocities of the order of 300 ft/sec were required for detonation. Since a large part of the energy of impact, in the 155mm projectile tests, goes into deforming the shell, a higher impact velocity is expected.

The melt kettle configuration on the other hand, because it is so frangible simply rips apart when impacted, and the molten explosive pours out. In order for initiation to occur, a minimum impact speed (or impact force) and a minimum duration of the load is required. For the melt kettle the duration of the load acting on the explosive is simply too short since the material spills before the concrete fragment has sufficient time to work on the explosive. At a much higher impact speed then tested in this area, where a shock initiation mechanism would apply, initiation would occur within microseconds after impact, (before thekettle walls would respond to discharge its contents). The required impact velocities for shock initiation are of the order of several thousand feet/sec. Velocities of this magnitude cannot be achieved as a result of concrete wall failure.

Future tests, now in progress, will investigate sensitivity of other explosive end items and in-process materials to fragment impact. It is expected that these tests will produce sufficient data to provide emperical

relationships between fragment mass/velocity, casing thickness and other physical and chemical characteristics of explosive materia. This could lead to a better understanding of the phenomena governing sensitivity and mechanismsms for detonation/propagation and thus result in more efficient design of modernized munition facilities.

#### REFERENCES

- 1. Response of Explosives to Fragment Impact by Richard M. Rindner, Annals of the New York Academy of Sciences, Vol. 152, Article 1, pp 250-268, Oct 1968.
- 2. Explosive Sensitivity of 155mm Projectile, RDX Slurry, and Black Powder to Impact by Concrete Fragments by R. Rindner, J. Swatosh, A. Humphreys, Picatinny Arsenal, TR 4594.
- 3. Sensitivity of Explosive Systems to Detonation and Subdetonation Reactions by H. Napadensky, Annals of the New York Academy of Sciences, Vol. 152, Art. 1, pp 220-233, Oct 1968.

# IMPACT INITIATION OF SLURRY (GSX) AND OTHER SMALL DIAMETER HIGH EXPLOSIVES

Lex L. Udy and Gary L. Hansen IRECO Chemicals Salt Lake City, Utah

### ABSTRACT

A number of small-diameter explosives including dynamite, IREMITE, Tovex and ammonium nitrate-fuel oil mixtures (ANFO) are tested for sensitivity to initiation by mechanical impact. These tests are an indication of the safety of these products in manufacture, storage and handling. Slurry explosives are shown to be much less sensitive to mechanical impact than commercial dynamites; they cannot be detonated by the most severe conditions of drop weight testing and are only detonable by very high velocity rifle bullets. Experimental results from these and other initiating stimuli are presented and correlated.

## 1.0 Introduction

A new generation of small diameter explosives is quickly replacing dynamites in the commercial market. The precariousness of manufacture, storage and handling of nitroglycerin (NG) containing dynamites have long been a "headache" to explosive manufacturers and miners. The nitroglycerin component of dynamite is most sensitive in its pure form and thus dynamites are most dangerous during manufacture and after adverse storage conditions where syneresis and leakage of NG might have occurred. When mixed with various types of filler materials, the NG is desensitized to the point where it can be handled relatively safely.

In contrast, gelled slurry explosives (GSX) manufactured from non-explosive ingredients are sensitive to detonation only after mixing in the proper proportions. Any improper mixing, degradation in storage, or mixing with water during use, serves only to desensitize the product. All of the individual components are less sensitive than the final product.

GSX's are also much less sensitive to accidental initiation due to impact from improper handling or from an unknown quantity of undetonated explosive being left in a muck pile. This study shows the impact sensitivities of several small diameter explosives to stimuli such as drop weight and various rifle bullets; also it includes the sensitivity to low energy blasting caps and a low voltage spark test apparatus.

# 2.0 General Description of Explosives Tested

The physical and detonation properties of the explosives tested are shown below and in Table I. A photograph of the products is shown in Figure 1.

2.1 COARSE PETN obtained from Bofors Industries, Inc., Sweden, was dried and loosely packed in 75 mm diameter polyethylene bags. Screen analysis of this material is shown below:

- 2.2 DYNAMITE, 60% GELATIN manufactured by Apache Powder Co. and labelled AMOGEL was tested in the standard paper wrapper. The sticks were 32 mm diameter x 15 cm long.
- 2.3 DYNAMITE, Hercol 2 manufactured by Hercules Powder Co. was tested as a low strength, less sensitive dynamite. It was packaged in

32 mm diameter x 50 cm long sticks with a paper wrap.

- 2.4 Pentolite is a cast explosive normally used in commercial applications as a booster material. The formulation used in this study was 50% TNT/50% PETN. This was cast into cardboard cups 75 mm diameter x 50 mm high at a weight of about 340 grams. For drop weight tests this material was ground to a fine powder.
- 2.5 Tovex 105 manufactured by DuPont was a monomethylamine nitrate sensitized slurry explosive without aluminum. It was packaged in 30 mm diameter x 40 cm long plastic sausages with a paper wrapper over the outside. It had a soft gel-like consistency.
- 2.6 IREMITE M manufactured by IRECO Chemicals was an aluminum sensitized slurry explosive. It was packaged in both 75 and 100 mm diameters for various types of tests. It had a very firm, rubbery consistency.
- 2.7 ANFO mixed in the proportions 94 ammonium nitrate/6 fuel oil was ground to the particle size shown below and packed into 100 mm diameter bags.

# 3.0 Testing Procedures and Equipment

3.1 A MINIMUM DETONATING CHARGE was determined for the explosives by using a series of hand-made blasting caps, IREDETS. A sketch of the IREDET is shown in Figure 2 and a photograph is shown in Figure 3. A small charge of granular PETN is placed in the bottom of a small aluminum shelled blasting cap and 4 grain/ft primaline (Ensign-Bickford) is used to detonate this charge. A plastic sleeve is placed between the primaline and the aluminum shell to fill the gap and allow crimping. Only hand pressure is used to compress the base charge. The PETN is weighed with a powder scale in grains, the cap number corresponding to the number of grains of PETN. The number 6 and 8 caps correspond closely with standard electric blasting caps of the same number as determined by lead block tests, initiation tests and known amounts of contained explosive.

Where a number 1/2 cap was an excessive booster, the primaline alone was used as an initiator. With PETN and both dynamites, 4-grain/ft primaline butted up against the explosive resulted in initiation. No smaller explosive initiator was tested.

- 3.2 DROP-WEIGHT TESTING was conducted using the apparatus shown in Figure 4. This apparatus is similar to that used by Picatinny Arsenal. About 0.1 gram of explosive was placed in a small steel cup with a piston disk covering the sample. When the weight was dropped the explosive was compressed at the bottom of the piston in the cup. The slurry explosives and ANFO were not sensitive to this test under the most severe conditions of elevated temperature (60°C) with the heaviest weight at the maximum height. Dropweight test data are summarized in Table IV for two different weights.
- 3.3 RIFLE BULLET TESTING was conducted using three different calibers of ammunition. A photograph of the rifle bullets used is shown in Figure 6. The small rim-fire 22-calliber bullets were used on the most sensitive explosives. The 22-250 rifle loaded to various muzzle velocities was used to determine the critical velocity of a 22-calliber 55-grain soft-point bullet. This had a maximum muzzle velocity of about 1160 meters/sec (3800 ft/sec) and was loaded down to as slow as 670 m/sec. The rifle was hand held from behind a barricade and the explosive samples were placed at a range of 25 meters. Over this range the bullet velocity decreases about 50 meters/sec as shown in Figure 5 and the velocities reported in the tables have been adjusted for range. Velocities were taken from standard reloading data hand-books.

A 30-06 rifle was also used and loaded to various velocities. A 150-grain soft-point bullet was used for determining threshold velocities with a maximum velocity of 915 m/sec at the 25 meter range. A full metal jacket military 30-06 rifle bullet was also tested to obtain data for a non-expanding projectile. This bullet weighed 150 grains and the measured velocity at impact was 850 m/sec.

A 270 Weatherby Magnum rifle was used with a single bullet weight and velocity. A 100-grain spire point bullet was loaded to a velocity of 1100 meters/sec at a 25 meter range.

3.4 EXPLOSIVELY PROPELLED PLATES. To determine the relative sensitivities of the explosives to impact by larger projectiles traveling at a lower velocity, three sizes of plates were propelled into the explosives. The propelling charges were cast 50/50 Pentolite with a 3 mm thick buffer of balsa wood placed between the explosive and the plate to reduce fragmentation. The charges were approximately the same diameter as the plate with a length to diameter ratio of about 1. The plates were hurled over a range of about one meter.

Table V shows the plate parameters and the results of tests. The kinetic energy of the large plates was high in comparison to the rifle bullets, but because of the lower velocity the slurry explosives failed. With the small plate the velocity was high

enough to detonate IREMITE but failed to detonate Tovex.

Recovered plates were fragmented to various degrees and velocities were very inconsistent indicating different velocities of fragments. Thus, these data are quite qualitative.

For the rifle bullet and plate tests the various explosives were packaged in a configuration similar to that in which they might be stored or shipped. All were shot unconfined without back-up plates. The dry PETN and ANFO were packaged in 75 mm and 100 mm diameter plastic bags respectively. These were sealed at the ends in about 15 cm lengths and the bullets and plates were shot perpendicular to the longitudinal axis.

The IREMITE was manufactured in long packages, 75 mm and 100 mm in diameter. These were then cut into 75 mm and 100 mm lengths for the tests. Bullets and plates were shot into the cut ends of the charges. It was more difficult to aim the plates, thus the IREMITE was packaged in a 100 mm diameter for these tests. The Tovex and dynamites were taped into bundles of six sticks and the bullets and plates were shot perpendicular to the longitudinal axis of the charges.

3.5 SPARK TEST APPARATUS. A spark testing apparatus was constructed using large capacitors and a low voltage supply. A voltage of 57 volts across a 0.375 Farrad Capacitance was discharged into the explosive between two electrodes similar to the extended probes of a spot welding machine. The energy of this source is calculated to be 509 Joules and the short circuit time constant was measured at 1.1 milliseconds. A photograph of the apparatus is shown in Figure 7. None of the explosives detonated from the spark.

## 4.0 Discussion of Results

The results of Tables I, IV and V show PETN and the dynamites to be extremely sensitive to all types of mechanical impact. Cast Pentolite is considerably safer and detonates with only high speed projectiles and has a relatively high minimum booster; however, when powdered it is quite sensitive to the drop weight test. Ground ANFO was insensitive to all types of mechanical impact and was not cap sensitive at the particle size used.

A summary of the Impact Sensitivities of the two slurry explosives, IREMITE and Tovex, at three different temperatures is shown in Tables II and III. The sensitivities of slurries are significantly affected by temperature--much more than dynamites or dry mixes--because of the solubilities of the oxidizer salts in the aqueous media. Growth of crystals causes greater separation of fuel and oxidizer and thus slows the reaction at the lower temperatures.

The data of Table II show IREMITE to be slightly more sensitive than

Tovex in all categories but generally in the same range. Rifle bullet data show the velocity of the projectile to be the primary parameter and bullet weight of only secondary significance. Table III shows the calculated threshold energies for both the bullets and the blasting caps for IREMITE and Tovex; there is little energy correlation. Note that the 22-250 rifle detonated Tovex at a velocity of 1110 m/sec at 5°C but the heavier 270 Magnum bullet failed at 1100 m/sec showing no improvement with bullet weight. This high dependence upon bullet velocity and apparent independence with regard to kinetic energy was observed by Watson<sup>1</sup>. Rifles used by Watson were very similar to those used in these tests and also show the 22-caliber bullets to be just as effective in initiation as the 30-caliber bullets at approximately the same speed. Since no energy correlation is apparent, it seems possible that a rate of energy delivery (power) is the parameter affecting detonation.

In order to estimate the rate of energy release into the explosive it was necessary to determine the deceleration time or distance of bullet travel through the explosive. To obtain this data some inert IREMITE was made by omitting the sensitizing aluminum from the standard IREMITE formulation. This slurry was cut to various lengths and placed against an aluminum back-up plate. The maximum thickness of slurry that each bullet would shoot through at its threshold velocity was then determined. For the 22-250 bullet at 880 m/sec this was about 12 cm and for the 30-06 bullet at 880 m/sec it was about 24 cm. Also a 30-06 full metal jacket bullet was shot into the actual IREMITE explosive packaged in a 100 mm diameter x 60 cm long tube. The bullet consistently deflected out the side of the charge at about 40 cm, thus the actual deceleration length could not be determined, but it was known to be at least the 40 cm or about twice the distance of the expanding bullet.

These deceleration distances show that the full energy of the bullet was not absorbed in the short 75 mm lengths of explosive used. Most of the energy from the 22-250 however was delivered and was delivered in a much shorter period of time than with the 30-06. The average rate of energy release from these bullets can be determined from the time of deceleration. This is determined from the average velocity and travel distance:

Time 
$$(22-250) = \frac{12 \text{ cm}}{880 \text{ m/sec/2}} = 2.7 \text{ x } 10^{-4} \text{ sec}$$

Time  $(30-06) = \frac{24 \text{ cm}}{880 \text{ m/sec/2}} = 5.4 \text{ x } 10^{-4} \text{ sec}$ 

Average Power  $(22-250) = \frac{1380 \text{ Joules}}{2.7 \text{ x } 10^{-4} \text{ sec}} = 5.1 \text{ x } 10^6 \text{ Watts}$ 

Average Power  $(30-06) = \frac{3770 \text{ Joules}}{5.4 \text{ x } 10^{-4} \text{ sec}} = 7.0 \text{ x } 10^6 \text{ Watts}$ 

To further study this concept, the energy release rate (power) as a function of distance traveled through the explosive was calculated at various points during bullet deceleration starting with the threshold impact velocity. These numbers are tabulated in Table VI and show the energy release rate during the first few centimeters of penetration to be quite close for the 22-250 and the 30-06 soft point bullets and definitely within the limits of experimental error for these measurements. Assuming a deceleration distance of 40 cm for the 30-06 full metal jacketed bullet, the average power for the first centimeter of travel is calculated to be 7.4 x  $10^6$  watts. This compares to 13.6 x  $10^6$  and 9.9 x  $10^6$  watts respectively for the 30-06 and 22-250 soft point bullets respectively. The power thus appears to be a possible parameter of correlation.

Assuming initiation occurs in the first centimeter of penetration of the IREMITE, the calculated average power for the first centimeter represents a minimum required. The power limit where initiation fails to occur can be determined for each bullet type by correlating the velocities in Table I with those in Table VI. These can be seen to overlap for the two different bullets but other parameters also must be considered such as the area of the bullets and the expansion rate of the soft lead core to a larger diameter. Perhaps a more meaningful parameter would be the power per unit area. This is also calculated in Table VI for the unexpanded bullets; however, the unknown time and area for mushrooming of the bullets makes an absolute value difficult to calculate.

The data of Table VI were calculated based on a constant rate of deceleration. This results in a constant amount of energy being lost for each centimeter of travel. The deceleration rate and energy loss during bullet expansion is probably much higher and would occur in the first few centimeters of travel. This would result in a higher power during mushrooming than calculated in Table VI. Based on these considerations and the data obtained it appears that energy must be delivered at a rate of about 10 megawatts or greater to initiate the IREMITE composition used in this study at 20°C.

Paszek<sup>2</sup> has shown that the deceleration rate is an inverse function of velocity as the threshold velocity is approached. Apparently partial reaction occurs in some explosives which aids in decelerating the fragments. This would have the effect of increasing the rate of energy delivery. In all of the tests conducted in this study, however, no partial reactions were observed; all results appeared to be either complete detonation or complete failure. Also the nonexpanding military 30-06 rifle bullet was shot into a long charge of IREMITE M for at least 40 cm at an impact velocity of 850 m/sec which indicates little or no contribution to deceleration from reacting explosive.

The power or energy release rate for the small blasting caps cannot be very well correlated to impact power data. For caps, the power is

significantly higher than for fragment impact and, in fact, is a constant for all sizes of caps assuming a constant detonation velocity in the small column of PETN. The PETN loads into the small shell at about 4 grains per centimeter. At an energy of 367 Joules per grain and a detonation velocity of 5200 m/sec, the power for the caps is  $763 \times 10^6$  watts.

However, it is expected that the energy generated by the cap must be delivered over a minimum length of time, that is, the energy must support the initiating shock wave at its threshold level until it becomes self supporting at the critical diameter. For example, if the energy would contribute to initiation for say 3 microseconds (about the time required for the shock wave to reach critical diameter) then the average power from a No. 1 cap would be 122 megawatts and from a No. 2 cap 244 megawatts, etc. The system is further complicated by realizing that caps, when embedded in a charge, initiate over a nearly spherical area, radiating the energy in all directions. Rifle bullets on the other hand, impart energy along the axis of travel in one direction only and it is distributed in more of a conical section. All of these factors serve to illustrate the complexity of the initiation processes.

Watson<sup>1,3</sup> has measured the threshold velocity for many different kinds of explosives using various rifle bullets and a non-expanding brass projectile. Data for this same projectile including shock pressure generation are shown by Weiss<sup>4</sup>. Most of these data are in relatively close agreement with the results of this study.

## 5.0 Conclusions

Gelled slurry explosives have been shown to be **v**ery safe from accidental initiation due to dropping, mistreatment, or stray fragment impact. The 22-250 and 270 magnum rifles represent two of the highest velocity firearms available, and initiation from these bullets would have to be at short range (less than 200 m) with the explosive completely unprotected by shelter walls.

In contrast to the gelled slurry explosives, the dynamites and granular PETN were highly susceptible to initiation from the various impact stimuli used in this study.

Analysis of the data has shown that power may be a possible correlation parameter between the various initiation stimuli. The sphere of influence over which the energy acts and the duration of the power application, however, are complicating factors. More study and careful experimental work are needed to arrive at an absolute parameter of correlation.

Even so, the results of these experiments do suggest that the stringent manufacturing, storage, transportation, and handling requirements established for dynamites may need to be reviewed and modified for the new GSX products now replacing these old line blasting high explosives.

# References

- 1. R. W. Watson, R. L. Brewer, R. L. McNall, On the Bullet Sensitivity of Commercial Explosives and Blasting Agents, Bureau of Mines, Pittsburgh Mining and Safety Research Center, 6 June 1975.
- 2. J. J. Paszek, J. M. Boyle, <u>Initiation of Explosives by Fragment Impact</u>, Ballistics Research Labs, Aberdeen P.G., Md.
- 3. R. W. Watson, Card Gap and Projectile Impact Sensitivity Measurements, A Compilation, Bureau of Mines Information Circular 8605, 1973.
- Milton L. Weiss, Elton L. Litchfield, <u>Projectile Initiation of Condensed Explosives</u>, Bureau of Mines Publication No. 6986, July 1967.

TABLE I Impact Sensitivities of Small-Diameter Explosives at 20°C

	Coarse PETN	Dynamite 60% Gelatin	Dynamite Hercol-2	Pentolite 50/50	Tovex 105	IREMITE M	Ground
Density (gm/cc)	0.93	1.26	1.18	1.65	1.08	1.00	0.88
Detonation Velocity (1½" dia, km/sec)	5.20	4.02	2.79	7.45	3.65	4:19	3.25 (2"
Minimum Booster (grains PETN)	*	*	•	8D/6F	3D/2F	10/1 <sub>2</sub> F	60D/16F
Rifle Bullet Tests 22 Cal Short 29 Grain Bullet 300 m/sec	<b>*</b>	****O	LL.	lu.	•	•	
22 Long Rifle 40 Grain Bullet 335 m/sec	F D W/steel [back-up plate]	•	L	L	•	*	
22-250 Rifle 55 Grain Bullet Velocity (m/sec)	620 D		620 D	1,110 F	1,020 D	880 D 850 F	1,110 F
30-06 Rifle 150 Grain Bullet Velocity (m/sec)	ı		ı	915 D 915 F	915 D 88C F	880 D 820 F	
30-06 Rifle 150 Grain Military 850 m/sec	Q	۵	۵	D/F	L	lt.	li.
270 Weatherby Rifle 100 Grain Bullet 1,100 m/sec	•		1	D/F	0	٥	•

\*4-grain Primaline butted against explosive detonated. \*\*F = failure. \*\*\*D = detonation.

TABLE II Sensitivities of Small Diameter Gelled Slurry Explosives (GSX) at Various Temperatures

		Minimum Booster (grains PETN)	22-250 Rifle 55 Grain Bullet Velocity (m/sec)	30:06 Rifle 150 Grain Bullet Velocity (m/sec)	270 Weatherby 100 Grain Bullet 1,100 m/sec
	2°C	3D/2F	1,110 D 1,020 F	915 F (max)	D/F
IREMITE M	20°C	10/½F	880 D 850 F	880 D 820 F	O
	40°C	**/*	850 D/F	880 D 820 F	
	2,0	4D/3F	1,110 D 1,020 F	915 F (max)	L.
TOVEX 105	20°€	3D/2F	1,020 D 1,000 F	915 D 880 F	Q
	40°C	3D/2F	915 D 880 F	915 D 880 F	•

\*5mm of 4-grain primaline detonated. \*\*4-grain primaline butted against explosive failed.

TABLE III Threshold Velocities and Energies for Gelled Slurry Explosives

TABLE IV Drop Weight Apparatus Test Data at 20°C

Ground		•	80F		•	28.5F
IREMITE M		•	80F		•	28.5F
Tovex 105			80F		•	28.5F
Powdered Pentolite		20/15	13/10		3.9	4.6
Hercol-2 Dynamite		36/30	25/23		7.1	8.8
60% Gelatin Dynamite		25/23	15/13		4.9	5.3
Coarse		18/14	13/10		3.5	4.6
	Drop-Weight Test Apparatus Height (cm)	2 kg wt (D/F)	3.63 kg wt (D/F)	Drop-Weight Energy for Detonation (joules)	2 kg wt	3.63 kg wt

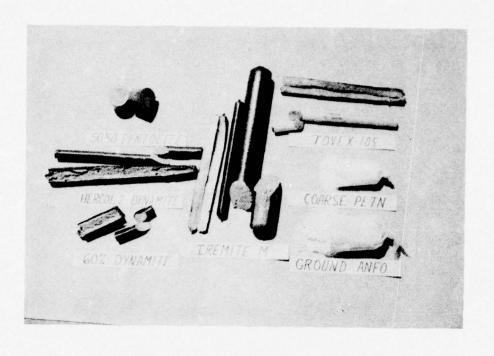
The GSX products and ground ANFO at 60°C (max. tested) showed no reaction with the 3.63 kg weight dropped from the maximum height of 80 cm. NOTE:

TABLE V Plate Impact Sensitivities of Small Diameter Explosives at 20°C

	Coarse PETN	Dynamite Dynamite Pentolite Tovex IREMITE Ground 60% Gelatin Hercol-2 50/50 105 M ANFO	Dynamite Hercol-2	Pentolite 50/50	Tovex 105	IREMITE	Ground
200 gm Plate 50 mm dia. x 13 mm 365 m/sec 13,300 Joules	•	۵	٥	6	IL.	LL ,	L
68 gm Plate 38 mm dia. x 8 mm 500 m/sec 8,500 Joules		o	a	LL.	•	μ	•
20 gm Plate 25 mm dia. x 5 mm 670 m/sec 9000 Joules	۵	۵	Q	L	LL.	۵	•

TABLE VI Bullet Parameters During Deceleration in IREMITE

22-250, 55-Grain Bullet Penetration Distance (cm)	_	-	•	~	4		=	2
	3.26	3.26	3.26	3.26	3.26		3.26	3.26
Velocity (m/sec) 8	*088	842	802	760	917	i	255	0
Time Over 1 cm (sec x 10-6)		11.6	12.2	12.8	13.6	:		78
Energy Loss Over 1 cm (Joules)		115	115	115	115	:	311	115
Average Power Over 1 cm (Watts x 106)		6.6	9.4	0.6	8.5	:	•	1.5
Average Power per m <sup>2</sup> of Bullet Area (Watts/m <sup>2</sup> x 10 <sup>12</sup> )		0.40	0.38	0.37	0.35	i	•	90.0
30-06, 150-Grain Bullet								
Penetration Distance (cm)	0	-	2	က	4	:	23	24
Rate of Deceleration (m/sec <sup>2</sup> x 10 <sup>6</sup> )	1.63	1.63	1.63	1.63	1.63	i	1.63	1.63
Velocity (m/sec)	*088	198	842	822	802	i	181	0
Time Over 1 cm (sec x 10-6)		11.5	11.7	12.0	12.3	i		110
Energy Loss Over 1 cm (Joules)		157	157	157	157	i	157	157
Average Power Over 1 cm (Watts x 106)		13.6	13.4	13.1	12.8	i		1.4
Average Power per m2 of Bullet Area (Watts/m <sup>2</sup> x 1012)		0.30	0.29	0.29	0.28	:		0.03



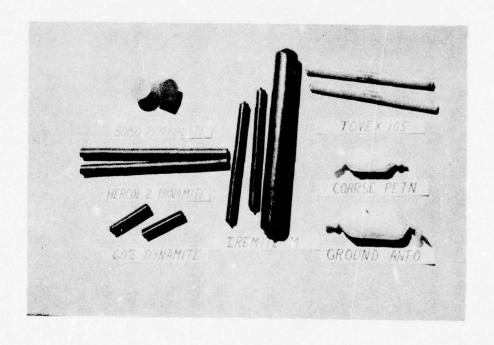


FIGURE 1. EXPLOSIVES TESTED
1626

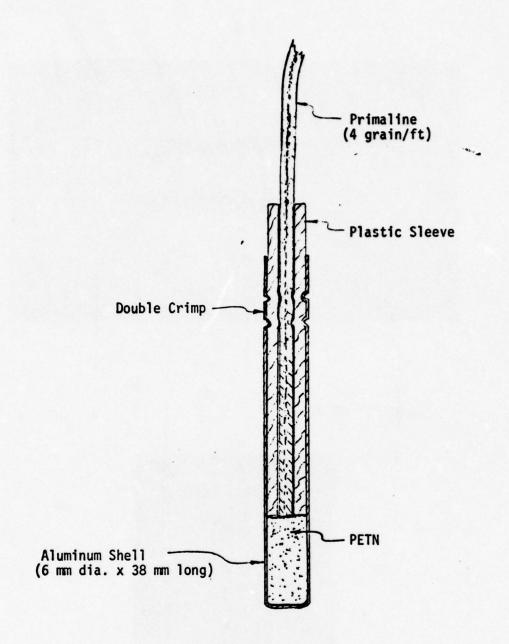


FIGURE 2. IREDET

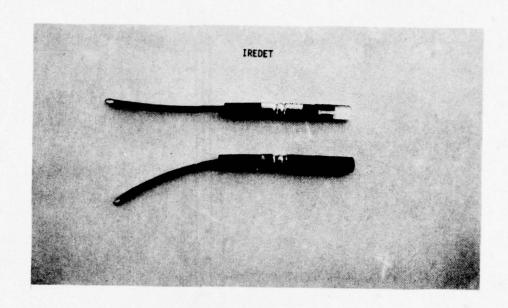


FIGURE 3. IREDET

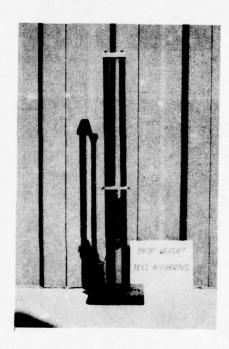
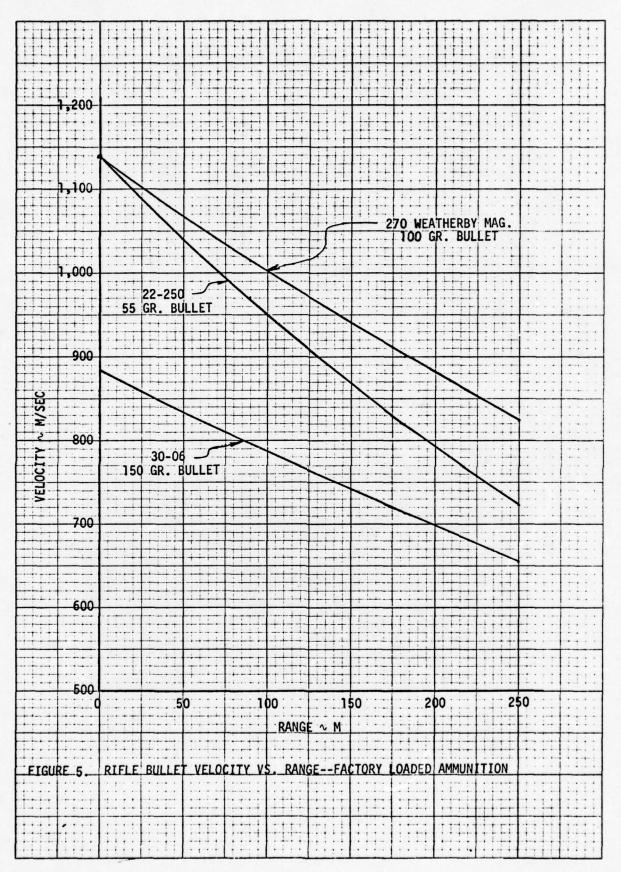


FIGURE 4. DROP-WEIGHT TESTING APPARATUS



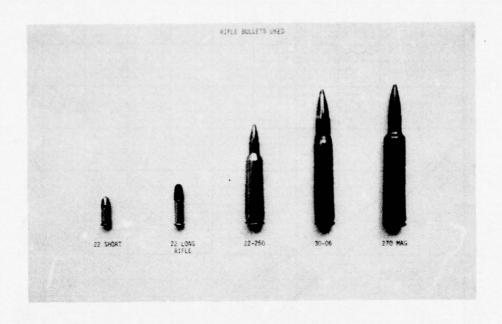


FIGURE 6. RIFLE BULLETS USED

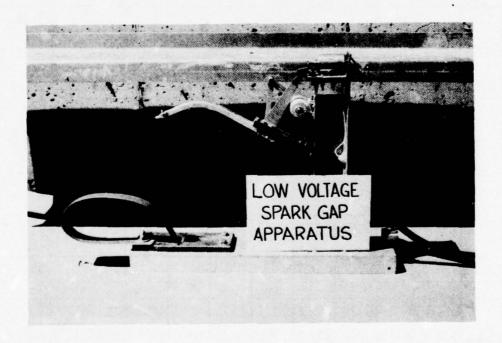


FIGURE 7. LOW-VOLTAGE SPARK TEST APPARATUS

Contribution to the Knowledge of Force-Time-Dependence on Testing the Impact Sensitivity

by

R. Wild, Bundesinstitut für chemischtechnische Untersuchungen,5357 Swisttal-Heimerzheim, West Germany

### Abstract:

With the aid of the theory of the force on collision of two masses, formulas, describing the force-time behaviour of a "fall-hammer" are deduced. These formulas could be confirmed by experiments. It could be shown, that the force transmitted to the anvil, is not only a function of the kinetic ernergy of the drop-weight, but also a function of the special drop-weight in use. The consequences of this behaviour will be discussed.

### 1. Introduction

For the purpose of transport, it is necessary to have tests for the acceptance of substances as explosives. For this classification procedure several tests, which can be quickly done, are required. By means of these tests, for example, the sensitivity to friction, the thermal sensitivity and the impact sensitivity must be evaluated. As, with the aid of such tests, it is decided, wether an explosive can be transported or not, these tests must be reliable and therefore it is of great importance to have an insight to the "physics" of these tests. This report is concerned with one of the impact sensitivity test as used in Germany.

In Germany two testers are in use, the large and the small fallhammer of the BAM. The investigations, reported here, are done with the small fallhammer, which is used to test primary and liquid explosives. With this type of machine, one can test the impact sensitivity in the range of 0.05 J - 8 J. (Figure 1 shows this fallhammer).

In the first part of the paper a brief description of the mathematical formulas, describing the force time history of the loading of the explosive, will be given. In the second part the experimental results will be reported and in the last part some conclusions will be drawn from the results obtained.

### 2. Theoretical deduction of the force time history

In order to derive the force time history during the impact of the drop-weight on the anvil, it is necessary to know the correlation between strain and force at the point of impact. Such a correlation is normally described by Hooke's law

$$K = c \cdot d \tag{1}$$

with c = force constant and d = strain.

This law, however, does not hold rigorously as already could be shown by Hertz<sup>1</sup> in 1881, in the case of two colliding balls.

Now when describing a more complex impact geometry it is obvious to assume a generalized elasticity law<sup>2</sup> of the form

$$K = c \cdot d^m \tag{2}$$

where the factor m implies the impact geometry.

With the aid of this law, the laws of conservation of momentum and energy following differential equation, describing the force time history during impact, will be derived:

$$\frac{dK}{dt} = \stackrel{+}{(-)} \sqrt{\frac{v^2}{4} - \frac{c}{M(m+1)} \cdot (\frac{K}{c})^{\frac{m+1}{m}}} \cdot m \cdot c \cdot (\frac{K}{c})^{\frac{m-1}{m}}$$
(3)

V corresponds to the velocity of impact and M to the mass of the drop-weight.

When m and c are known, this equation can be solved numerically, for example by the RUNGE-KUTTA-METHOD.

Both constants m and c can be determined by measuring the maximum force transmitted to the anvil as function of impact velocity. Setting equation (3) equal to zero following formula

for K will be obtained:

$$K_{max} = \left[\frac{(m+1) \cdot c^{\frac{1}{m}} \cdot M}{4} \cdot V^{2}\right]^{\frac{m}{m+1}} \tag{4}$$

Now, by plotting  $K_{\text{max}}$  as function of impact velocity on double logarithmic axes one should obtain a straight line of the form

$$\ln K = \ln \left[ \frac{(m+1) \cdot c^{\frac{1}{m}} \cdot M}{4} \right]^{\frac{m}{m+1}} + \frac{2 \cdot m}{m+1} \ln V$$
 (5)

and m can be calculated from the slope and c from the intercept.

### 3. Experimental investigations

As already mentioned above the experimental investigations were done with the small BAM-fallhammer (fig. 1). For measuring the maximum force a quartz was built into the fallhammer instead of the anvil. By measuring the time of fall of the drop-weights, it was possible to determine the impact velocity with an accuracy of about 3 %. Now by plotting, as already described, the variation of  $K_{\text{max}}$  with the impact velocity on double logarithmic axes the two constants m and c could be determined and the differential equation (3) could be solved.

Figure 2 shows the computed force time histories for a mass of 100 g falling from a height of 20 cm and for a mass of 500 g falling from 10 cm. In figure 3 and 4 the measured curves can be seen; one recognizes that computed and measured functions agree within normal experimental errors; especially it can be stated, that the slope is larger for smaller weights than for larger ones. Figure 5 shows the comparison between measured and calculated values of maximum force. Here, also, an agreement within experimental error limits can be seen.

When comparing measured and calculated impact times in figure 6, it seems to be, that only with small weights theory and experiment agree, whereas with large weights great differences occur. However, it must be considered, that the slope of force time dependence with large weights is very small, so

too small impact times will be found.

When considering this fact, the differences between theory and experiment will become clear.

As conclusion it can be stated, that the formulas deduced here, describe the impact behaviour of the small BAM fall-hammer.

### 4. Conclusions

The first important result is, that impact time decreases with increasing heights of fall. As can be seen from figure 6, it is not advisible to test at too small heights because impact time will be constant only at heights greater than 20 cm.

Furthermore the maximum force transmitted to the anvil does not depend only on kinetic energy but also on the design of the drop-weight in use, as can be seen from figure 5.

In addition impact times are larger for larger weights, so when using different drop-weights, the explosive will be subjected to different loading, even in the case of equal kinetic energy.

Having in mind these restrictions, the small fallhammer of BAM is a reliable instrument for testing impact sensitivity.

This paper is based on a report which will be published in "Propellant and Explosives" Vol. 1 No. 3 (1976).

### References

- 1 H. Hertz, Journal für reine und angewandte Mathematik 92, 156~181 (1881)
- 2 Berger, Das Gesetz des Kraftverlaufs beim Stoß, Braunschweig, 1924

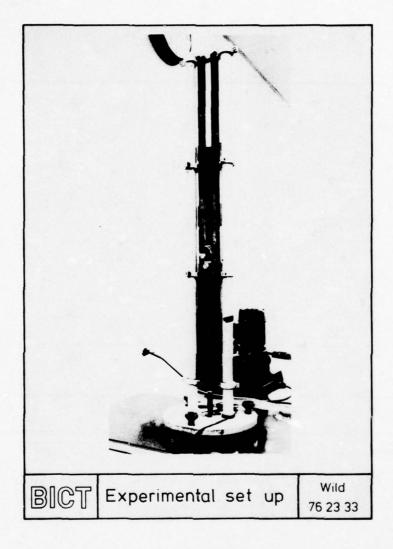


Figure 1: Small fallhammer of BAM

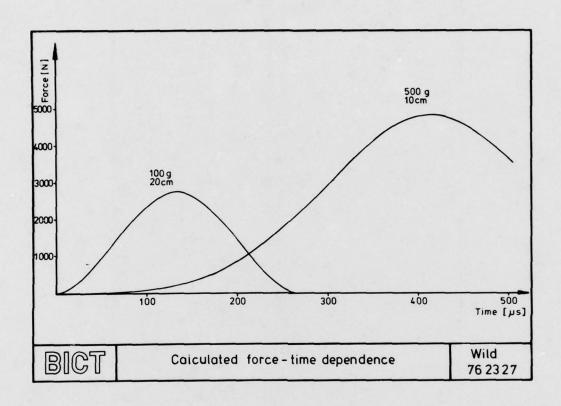


Figure 2: Calculated force time history

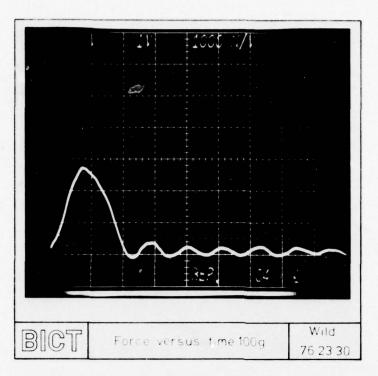


Figure 3: Measured force time history mass: 100 g height of fall: 20 cm

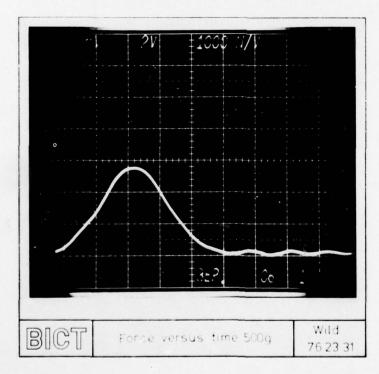


Figure 4: Measured force time history mass: 500 g height of fall: 10 cm

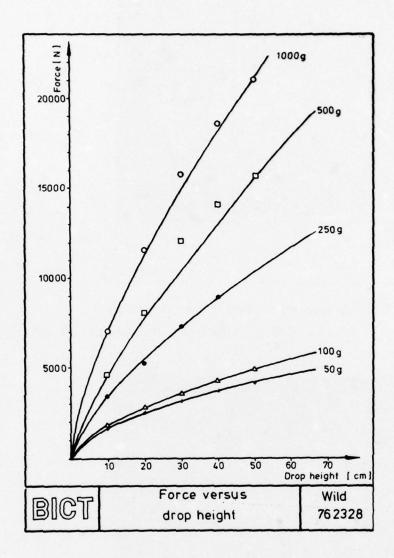


Figure 5: Maximum force as function of height of fall

The lines are the computed values,
the points are the measured values

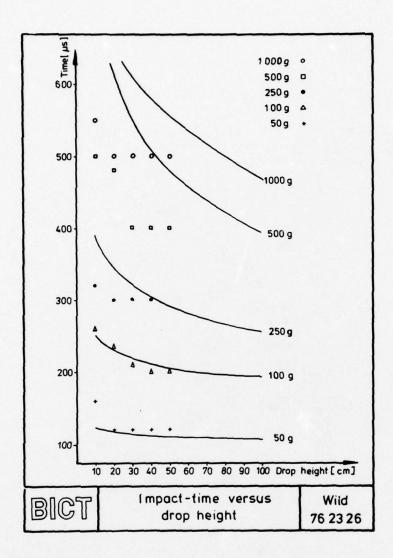


Figure 6: Impact times versus height of fall
The lines are the computed values,
the points are the measured ones.

### EN MASSE DETONATION OF EXPLOSIVE STORES PHILIP M. HOWE BALLISTIC RESEARCH LABORATORIES ABERDEEN PROVING GROUND, MARYLAND 21005

### INTRODUCTION

In the design of tanks and other armored vehicles, and in the design of fighting vessels, considerable attention has been devoted to the reduction of the probability of the occurrence of an explosives incident. The approach usually taken is to provide as much protection as possible to the ammunition, which is sequestered in localized areas.

A complementary approach which has received less attention but which, we feel, offers considerable potential is to minimize the extent of damage, given the occurrence of an incident. Thus, a significant portion of the BRL research program is directed towards the development of the technology necessary to reduce the levels of damage associated with explosive events. As we develop this technology, we are applying it to current problems. For example we have been involved in the ammunition compartmentalization studies sponsored by the Project Manager, XM-1 Tank System, we have been (and are) involved in developing concepts for container ship transportation of munitions, and hope to become involved in application of the technology to fighting vessels and to depots and storage areas. The technology is young, but we feel it is necessary to be involved in these in applications early, to insure the practicality and practicability of the technology, as it develops.

A major contribution to damage resulting from an explosives incident arises from the near-simultaneous detonation of contiguous stores. Our objectives are to define the conditions which lead to en masse detonation and to devise means of preventing en masse detonation. In these contexts,

we are concerned with interstack propagation of detonation, and interround communication. Superficially, the interstack problem might appear to be a simple extension of the interround communication problem. However, it is not. Entirely different mechanisms of propagation are involved, and entirely different solutions must be sought.

### PROPAGATION OF DETONATION BETWEEN STACKS

Under the aegis of the Department of Defense Explosive Safety
Board, a series of tests were conducted in 1973 at Tooele Army Depot,
Tooele, Utah. The purpose of these tests was to resolve questions with
respect to the fraction of munitions, packed in milvans, which would
participate in damaging blast overpressures should one or more milvans
be detonated. A description of the tests, analysis of the data, and the
test director's conclusions are presented in the final report, T-205
Milvan Container Stowage Tests (1).

In the T-205 test series at Tooele, several milvan containers were stuffed with typical types and classes of ammunitions and were emplaced below ground level in the same configuration as in the hold of a ship.

One or more of the containers were detonated to ascertain the probability of detonation transfer to contiguous containers or to containers separated by a buffer.

The acceptors and the donors were stuffed with mass detonating munitions, (Class 7 or above). The buffer containers were stuffed with non mass detonating stores, (Class 5 or below). Parameters varied in the tests included mass of the donor explosive, mass of the buffer, nature of the buffer, and mass of the acceptor. The acceptor containers

were stuffed with M-15 land mines or 500 pound bombs. The reader is referred to the original report for additional test details.

Our analysis of the T-205 test data led to the following conclusions:

- a. The buffering, as used in the T-205 tests, was inadequate.

  Whether the inadequacy was because the buffer material reacted and contributed to the donor energy, or there simply was not enough buffering to absorb the donor energy, cannot be determined from these test data.
- b. While the buffering, as used in T-205 for configurations involving one or more milvans was inadequate to prevent propagation, evidence exists which indicates that effective measures can be taken to reduce propagation if the donor mass is scaled downward. Whether the point at which effective measures can be taken is the point at which crushing ceases to be important and propagation is by means of fragment impact, remains to be shown.
- c. At the container level, using existing stuffing and packaging procedures, there appears to be no easy way of generating an acceptably safe container stacking configuration, without going to prohibitively large container separation distances. For example, if one assumes that the thickness of the buffer required between donor and acceptor must be as great as the thickness of the donor then, for a donor of one munitionsfilled container, seven buffer containers are required. This is based upon assuming a rectangular array of containers, with donors and acceptors placed together, as close as possible, and excluding side, edge, and corner contacts between donor and acceptors. This is shown in Figure 1.

In test #18 of T-205, two buffer milvans (in this case filled with 90mm cartridges) were inadequate to prevent propagation between a donor charge of one milvan of 500 1b bombs and an acceptor of 500 1b bombs. (The use of 90mm cartridges as a buffer material has been critized. The point was raised that, with a strong stimulus, such as from the 500 1b bombs, the 90mm cartridge would react, and provide a vehicle for detonation to propagate through the buffer. To check this point, we had Toole Army Depot conduct an additional tests which replicated Test #9 of the T-205, with the exception that, in place of live 90mm ammunition, inert rounds (with the same total mass and area) were used as the buffer. A milvan of 384 M15 mines served as the donor charge, and another milvan of mines served as the acceptor. Two mines were used to initiate the donor charge. One hundred eighty mines were recovered, part of which may have been from the donor. Comparative data for T-205 Test #9 and this test are shown in Table I. In this test, the fragmentation initiation mechanism

TABLE I

T-205 #9	Expl. Wt (1b)	Replica
Donor 384 ea M15 mines	8736	384 M15 Mines
Acceptor 384 ea M15 Mines	8736	384 M15 Mines
Buffer 600 ea 90mm Cartridges	5676	600 ea Inert 90mm Cartridges
Recovered 36 ea 90mm		180 ea M15 Mines
		31 ea Inert Cartridges
Crater Size 102'X96'X20'		96'X87'X17'

was precluded, both by the use of inert rounds and by staggering them in the buffer, so that fragments from the donor could not penetrate to the acceptor. Thus, the fact that fifty percent or more of the acceptor detonated clearly shows that the large scale crushing is an extremely important mechanism.

A major complication introduced by the crushing mechanisms is that crushing depends upon the total impulse delivered to the target, provided that a threshold pressure (the yield stress) is exceeded. The pressure and impulse delivered to a munition in a matrix, from a wave propagating through some sort of buffer material obeys Hopkinson-Cranz scaling. Thus, if one doubles the radius of the donor charge one can maintain the same peak pressure by doubling the separation distance of the acceptor from the donor. However, the impulse delivered to the acceptor will still be twice as great. Thus, protecting against crushing as a propagation mechanism becomes prohibitively difficult as donor charge size is increased. Furthermore, the crushing of explosives can lead to ignition and buildup to detonation at very low stress levels. A schematic showing the impact velocity required for initiation of bare explosives versus charge size is shown in Figure 2 (2). Note that, as the length of the explosive (measured along the axis of impact) approaches zero, the impact velocity required to induce reaction also diminishes. Chaudri, Fields, et al have found this effect in smaller samples, and have explained it by assuming that ignition occurs as the result of absorption of energy within the sample as it is being plastically deformed (3).

### PROPAGATION BETWEEN ROUNDS

The conclusion that the maximum acceptable donor charge is smaller than that containable in a standard container, coupled with the constraint that the smallest logistical unit be a container, requires that measures be taken to insure that detonation cannot propagate through a container. This appears to be, by a large margin, the best way to solve the overall problem. For this reason, we have been examining carefully the mechanisms of round to round propagation and techniques for reducing the probability of round to round propagation - "fratricide" reduction.

Existing data indicate that the principal means by which detonation propagates from round to round is fragment impact. For this reason, we have been carrying in rather extensive studies of the sensitivity of explosives to fragment impact. Some of this work is reported by Frey et al in the recent detonation symposium. His paper showed that (a) fragment impact initiation of bare charges occurred by a single transit shock initiation mechanism, which obeys a  $P^2t = c$  criterion, where P is shock peak pressure, t is shock duration and c is a constant; (b) in confined charges, violent reactions are observed at much lower stress levels than are required for detonation (4). Such non-detonative violent reactions are very much confinement dependent, and occur at much longer times (~ 200 µsec) than the single transit times. In order to understand how these violent reactions occur, and to define the conditions under which they transit to detonation, we are currently measuring the internal pressure histories for confined charges subjected to fragment impact and weak shock loading. A schematic of the apparatus and some preliminary data are shown in Figure 3. The pressure time history is consistent with assuming that (a) reaction is initiated by the input shock (in the

first 10 µsec); (b) a slow grain burning mechanism obtains, which continues until a pressure threshold is reached, at which time (c) the explosive breaks up, the granular surface area is greatly increased and the burning rate accelerates catastrophically. Whether or not the system detonates most strongly depends upon the confinement.

Comparison of Frey's data with Reeves' (5) data indicates that confinement has a very strong effect. Reeves' charges were heavily confined, and the V<sub>50</sub> curve lies well below Frey's. Reeves did not differentiate between violent reaction and detonation, and one would not expect a critical energy criterion to occur. However, analysis of some of his data show that, for impacts by large fragments, a critical energy criterion is obeyed (see Figure 4). We have shown the point at which the requisite energy increases is the point at which rarefactions reach the shock and begin to attenuate it prior to its reaching the explosive (see Figure 5). The theoretical implications of this are currently being explored. We are also currently looking at other mechanisms of initiation by fragment impact. For example, we are attempting to measure the temperature of fragments and casings after impact, as calculations indicate enough heat is generated to cause ignition.

Other experiments had shown that the sensitivity of an explosive charge to simultaneous multiple fragment impact was essentially the same as its sensitivity to a single impact by the largest fragment (i.e., there was no synergistic effect). This fact was used to construct a

simple model for the prediction of the 50 percent distance of separation for initiation of violent reaction or detonation in a warhead. The model, which requires the single fragment mass-velocity impact sensitivity curve for the acceptor, and the number of fragments, generated by the donor, whose mass and velocity exceed the  $P_{50}$  point for initiation, was used to predict the 50 percent separation distance for the 105mm howitzer shell. The predicted value was 12.6 cm, the measured value was 12.3. The model is currently being applied to other shell.

### FRATRICIDE REDUCTION

Anderson and Rindner, in 1973, published a report on shielding of 155 mm projectiles (6). They found that, by using steel or aluminum shielding placed between rounds, they were successful in preventing propagation of detonation at separation distances of 18 inches.

We have taken a similar approach and have been able to prevent propagation of detonation in 105 mm HE and HEP projectiles where the separation distances are as little as 5 cm. In nearly all cases, some damage occurs to the acceptor. In the case of the HEP round, which has a very thin skin, it is very difficult to prevent the acceptor from breaking open. This, of course, creates a considerable problem with fires.

We have postulated several mechanisms by which the shields worked. The ones we considered to be most important are shown in Table II.

Table II

Shadowing of Acceptor

Scattering of Fragments

Reducing Energy Delivered to Acceptor

Reducing Peak Pressure Delivered to Target

Absorption of Energy by Plastic Deformation of the Shield

Calculations showed that the energy absorption was not an important contributor. The fraction of the total kinetic energy absorbed is only a few percent. Figure 6 shows the importance of shadowing. The various frames show the fragments from a 10.5 cm diameter steel shell loaded with composition B interacting with a shield (mild steel pipe, OD 4.22 cm, ID 3.24 cm) and a 10.5 cm acceptor. The shield very effectively shadows the acceptor from fragments from the donor. In this particular case, detonation would occur. The shield itself does not have sufficient integrity to resist the fragments and deforms drastically. Fragments may perforate the shield and, subsequently, the acceptor, or the deformed shield perforates the acceptor skin. Either way, detonation of the acceptor occurs reliably with this shielding configuration. By going to a heavier gauge shield (OD 4.22 cm, ID 2.27 cm), fratricide is reliably eliminated for the HEP-HEP configuration.

By increasing the mass of the shield, one decreases the energy delivered to the acceptor, other things being equal. Thus, the ratio of the energy delivered to the acceptor with shielding and the energy

delivered without shielding is given by

$$E_s/E_o$$
 =  $\frac{M_o^2}{M_o^+ M_s}$  where  $M_o$  = mass of fragments  $M_s$  = mass of shield  $V_o$  = initial velocity of fragments.

Figure 7 shows the energy threshold for HEP warheads impacted by fragments from a HEP donor (with shielding in place), and similar results for a HE-HE configuration. While there is considerable uncertainty in the data, an energy threshold appears to apply. Thus, one would predict that, if increased effectiveness is required, one should increase the mass of the shield. This prediction is correct, but it is not a particularly desirable way to go, since, in transportation, increased weight means increased costs. Fortunately, factor 4 of Table II is very important, and allows considerable weight savings.

The strength of the shock wave transmitted to the acceptor depends strongly upon the shock impedance of the materials involved. Thus, much is to be gained if one uses shields composed of low shock impedance materials. This is born out experimentally; PVC rod was shown to be as effective a shield as any material tests. A comparison of shield materials is shown in Table III.

Most of the tests were performed with a single donor charge and one or two acceptors. In order to ascertain whether the shielding would work in larger configurations, we conducted some tests with a single donor and multiple acceptors, as shown in Figure 8. In the first such test, shielding was 3.17 cm (1 1/4") PVC pipe, with interround spacings

### TABLE III

Material	Configuration	Mass (Kg)
*Mildsteel	Tube	3.93
	OD 4.22cm	
	ID 2.27cm	
Mildsteel	Tube	2.26
	OD 4.22cm	
	ID 3.24cm	
*Mildsteel	Two ea 11/16 rod	1.9
	Presented area 3.50cm	
*PVC rod	OD 3.81 cm	0.648
*PVC rod	OD 3.81 cm	0.648

\*Effective for HEP-HEP interactions. (All were effective shields for  $105\ \text{HE-HE}$  interactions.)

of 5 cm. The witness plate and photographic coverage showed that detonation of the acceptors did not occur. However, several of the acceptors reacted violently, and all of the explosive was consumed.

### SUMMARY AND CONCLUSIONS

We feel that the results obtained to date are very promising. We have shown that, with proper shielding, we can effectively eliminate propagation of detonation between contiquous munitions.

If one is willing to pay a significant weight or volume penalty, or go to much more massive shields or larger spacings, one can reduce total damage of the munitions, to the point that no reaction is observed.

The problem of interstack propagation is not so easily solved. By analyzing existing data, we concluded that, for donor charges as large one container, buffering becomes impractical.

### **FUTURE PLANS**

We are currently investigating the mechanisms of fragment impact initiation of detonation in confined charges. We are planning to extend the data base for fragment impact of confined composition B to much larger fragments, to aid in the development of theory and for use in engineering calculations. We are currently developing scaling laws for shielding and would like very much to apply these laws to large warheads such as 500 or 750 lb bombs.

The benefits to be obtained by a combination of buffering and shielding have not been investigated. We know that by use of shielding or by increased spacing, we can reduce the probability for interround

communication. We are beginning work on an analytical model which should predict conditions required for extinction of a wave, in terms of interround probabilities. It may be quite possible to package large stores of munitions in such a way as one container full will rarely, if ever, mass detonate, even if interround communication occurs.

### REFERENCES

- 1. Parkinson, A. and Smith, K., Final Report, T-205 Milvan Container Storage Tests, Tooele Army Depot, Tooele, Utah, November 1973.
- Napadensky, H., "Initiation of Explosives by Low Velocity Impact",
   4th Symposium (International) on Detonation, ONR, (1965).
- Chaudri, Fields, et al, "Initiation of Explosives by Low Strength Shocks", 2nd Quarterly Status Report, ARO (December 1973).
- 4. Frey, R., et al, "Initiation of Violent Reaction by Projectile Impact", 6th Symposium (International) on Detonation, San Diego, (to be published).
- 5. Reeves, H., private communication.
- 6. Anderson, O., and Rindner, R., "Separation Distances of 155mm Projectiles", PATR 4425 (January 1973).

### FIGURE CAPTIONS

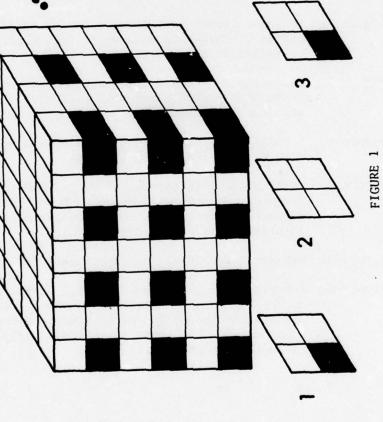
- Figure 1. A rectangular array of containers, where the black cubes represent mass detonating stores and the white cubes represent inert buffers.
- Figure 2. Threshold for initiation of bare charges (after Napadensky (2)).
- Figure 3. Schematic for the study of pressure histories of confined charges subjected to fragment impact or shock loading.
- Figure 4. Fragment impact initiation data for confined composition B charges. Threshold data don't follow critical energy criterion at high velocities.
- Figure 5. Calculated curve defining region where shock wave is attenuated prior to reaching explosive. Straight lines are data from Figure 4.
- Figure 6. X radiographs of fragments from expanding cylinder interacting with shield of mild steel tubing.
- Figure 7. Threshold for initiation of HE and HEP rounds by multiple fragments (donors were HE and HEP warheads, respectively). Parametric curves show energy delivered to acceptors for shields of different masses.
- Figure 8. Schematic for shielding experiments for 105 shell.
- Figure 9. Schematic for larger scale test. Large circles represent 105 mm HEP warheads. Small circles are 3.8 cm diameter PVC rod. Crosshatched round served as donor. Witness plate indicated round marked "D" detonated. Rounds marked "R" reacted violently enough to dent plate.

## LARGE SCALE BUFFERING

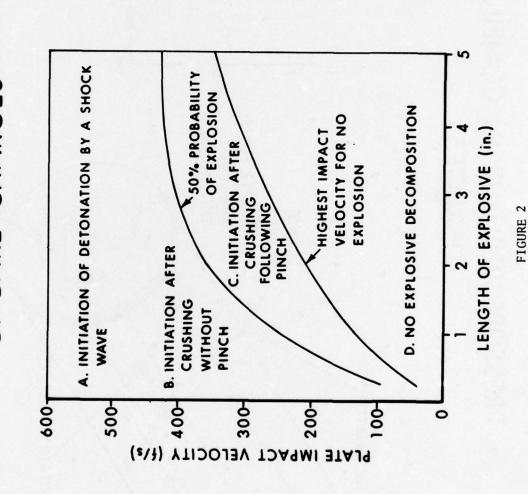
FOR BUFFERING - MUST PREVENT DONOR-ACCEPTOR CONTACTS:

NO FACES TOUCHING NO EDGES TOUCHING NO CORNERS TOUCHING

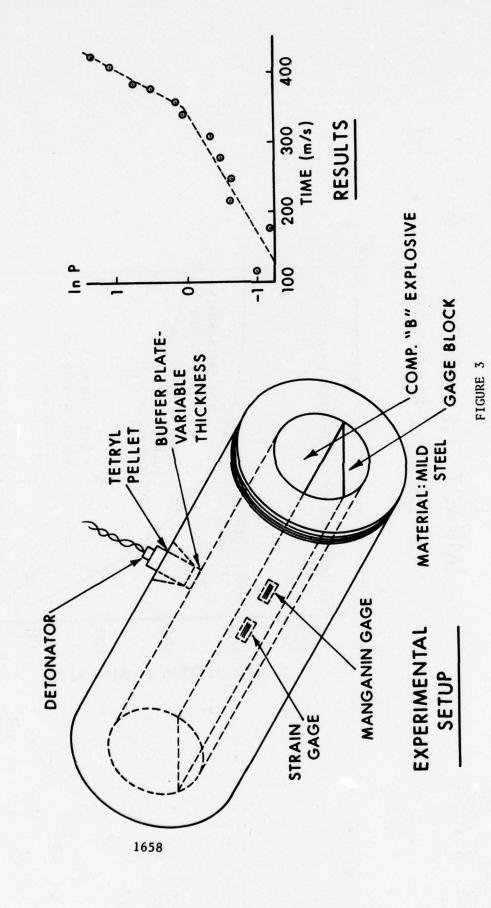
FOR EVERY DONOR . REQUIRE 7 BUFFERS



### IMPACT INITIATION OF BARE CHARGES

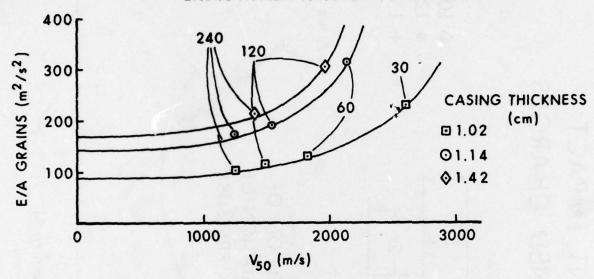


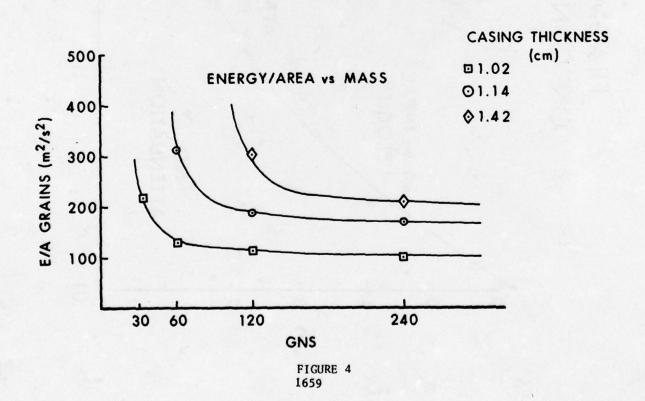
# PRESSURE BUILDUP IN CONFINED CHARGES



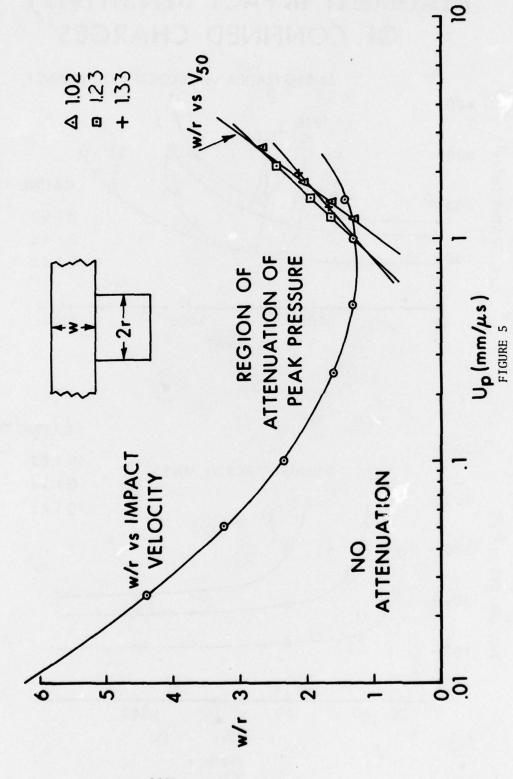
### FRAGMENT IMPACT SENSITIVITY OF CONFINED CHARGES

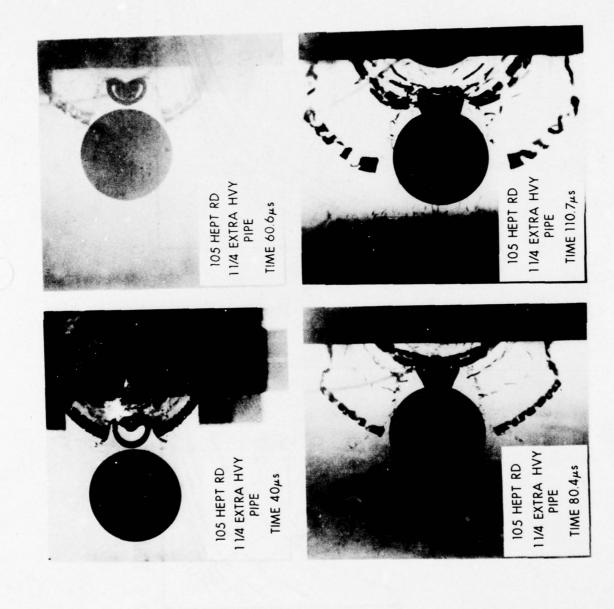
ENERGY/AREA vs VELOCITY OF IMPACT



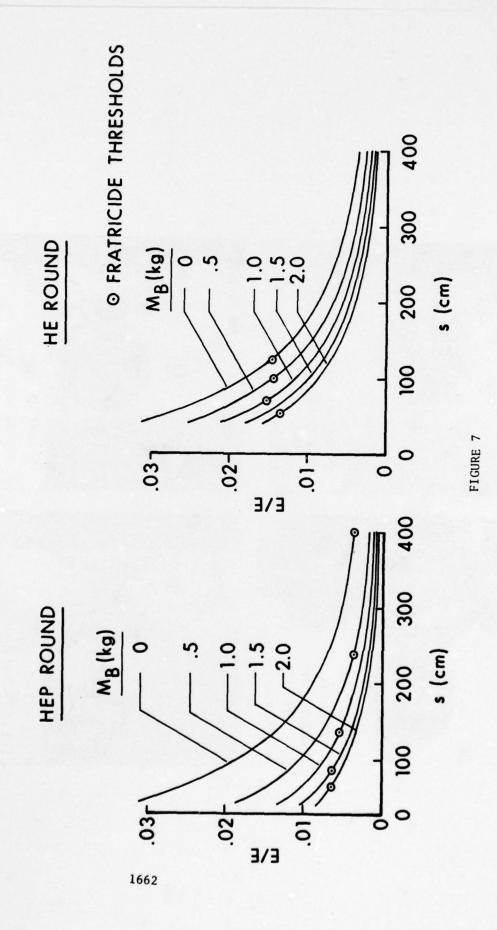


FRAGMENT IMPACT ON CONFINED CHARGES





### FRATRICIDE DATA



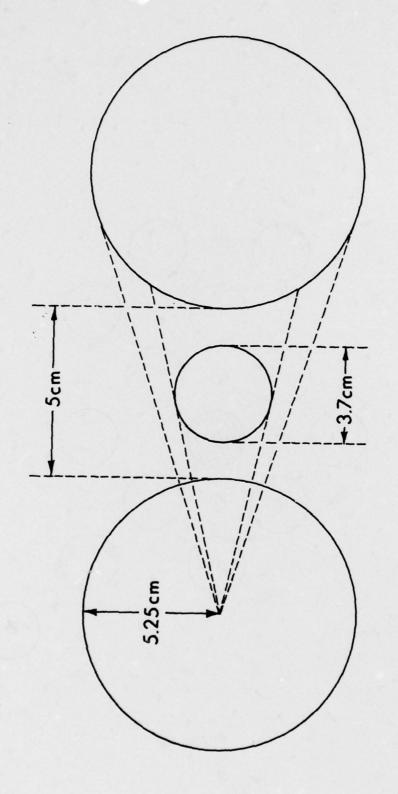


FIGURE 8

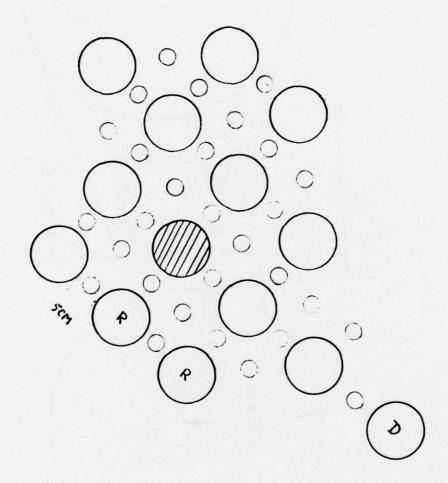


FIGURE 9

# SAFE SEPARATION DISTANCE FOR 168 POUNDS OF COMPOSITION A-7 EXPLOSIVE IN TOTE BINS

A. B. Wenzel Southwest Research Institute San Antonio, Texas

and

R. M. Rindner Picatinny Arsenal Dover, New Jersey

#### **ABSTRACT**

An interline distance of at least 100 feet between stainless steel bins containing 168 pounds of Composition A-7 is required by Army Materiel Command Regulation AMCR 385-100. Large-scale safe separation tests performed at Sierra Army Depot with unshielded tote bins indicate that detonation and/or propagation occurs at less than 130 feet. On the Composition B production line at the Holston Army Ammunition Plant, spacings greater than 130 feet are unacceptable because of production requirements and equipment constraints.

To resolve this problem, Picatinny Arsenal conducted small-scale tests designed to reduce the energy of impact of primary and secondary fragments. These tests show that an energy absorbing material, Kevlar\*\*, applied to the exterior surface of the bins appears to be the most promising solution. Full-scale confirmatory tests of this laminate have been conducted at Southwest Research Institute to determine:

- (1) the effectiveness of the Kevlar® shield,
- (2) the minimum safe separation distance in a steel-fiber glass tunnel configuration,
- (3) whether the source of detonation and/or propagation is due to primary (tote bin) or secondary (conveyor) fragments, or both,
- (4) the safe separation distance in a wooden-fiber glass tunnel, and
- (5) the effects of confinement on detonation and/or propagation of acceptors.

<sup>\*</sup> Registered trademark of E. I. Du Pont de Nemours & Co., Inc.

#### INTRODUCTION AND BACKGROUND

The tests described in this paper were performed as part of an overall safety engineering program entitled "Safety Engineering in Support of Ammunition Plants," conducted under the guidance of the Manufacturing Technology Directorate, Picatinny Arsenal, Dover, New Jersey, for the U. S. Army Armament Command (ARCOM).

The Composition B production line at Holston Army Ammunition Plant (HAAP) in Kingsport, Tennessee, requires that Composition A-7 explosive be transported slightly over 330 feet between operational buildings on a conveyor system, within a steel tunnel or on a ramp sheathed with corrugated fiber glass. This explosive, in granulated powder form, is conveyed in stainless steel tote bins which contain  $165 \pm 3$  pounds of Composition A-7 per bin. These stainless steel bins have hinged plastic lids. In the absence of empirical data concerning safe separation (non-propagative) distances for this conveying configuration, guidance was obtained from Army Materiel Command Regulation AMCR 385-100. The interline separation distance of 100 feet was adopted as a basis for design subject to experimental confirmation of non-propagation.

In 1975, a full-scale exploratory test series was undertaken by Picatinny Arsenal at Sierra Army Depot, Herlong, California, in an effort to determine a safe separation distance for the Composition B production line. There were 26 tests conducted at Sierra Army Depot. Of these tests, 5 did not utilize tunnel structures, 20 involved wood-framed, fiber glass-sheathed structures to simulate the plant tunnel or ramp, and 1 test used a steel-framed structure as a simulated tunnel. The results of these tests show that detonation and/or propagation was observed up to 90 feet without the confinement of tunnels. Detonation of an acceptor was observed at 100-foot separation with a wooden tunnel. Penetration of an acceptor without detonation occurred at 110 feet with the wooden tunnel structure. When the steel-framed tunnel structure was used, detonation of an acceptor bin was experienced at 130-foot separation.

The major conclusions derived from this program are:

- Stainless steel tote bins containing 168 pounds of Composition A-7 may not be spaced closer than 130 feet without the risk of propagation of detonation from bin to bin. (A safe spacing had not been determined.)
- Primary (tote bin) and secondary (conveyor) fragments are the most likely agents of explosive propagation.
- Since propagation by fragments is a stochastic process, definitive conclusions concerning the effect of tunnel confinement could not be drawn.

<sup>&</sup>lt;sup>1</sup>W. Seals, R. S. Kukuvka, H. Sarrett, and R. M. Rindner, "Safe Separation Tests of Composition A-7 Explosive in 165-Pound Tote Bins," Tech Memo No. 2189, Picatinny Arsenal, Dover, New Jersey, October 1975.

Because current production and equipment constraints at HAAP limit the separation to more than 130 feet, a series of small-scale tests was conducted at Picatinny Arsenal to find a means of reducing the propagation hazard, thus reducing the required safe spacing. These scaled tests considered the use of Kevlar and other hard fiber sheets attached to the tote bins, flexible stainless steel mesh suspended between tote bins, and substitution of acrylic type materials for the tote bin material. The results of this small-scale program indicated that all the above techniques appeared to reduce the required safe spacing. However, the report recommends the use of either Kevlar or NVF hard fiber shields attached to the tote bins as being the most promising solution.

Therefore, a full-scale experimental program conducted at Southwest Research Institute (SwRI) was designed to generate data to answer the following questions. This paper is a condensed version of the full report cited as Reference 2.

- (1) What is the effectiveness of the Kevlar shielding?
- (2) Can a safe separation distance of 130 feet or less be obtained in a steel tunnel configuration with shielded bins?
- (3) Is the source of detonation and/or propagation to a shielded acceptor bin due to primary (tote bin) or secondary (conveyor) fragments, or both?
- (4) Can a wooden-fiber glass tunnel structure provide safe separation distance between donor and acceptors at 130 feet?
- (5) What effect does the tunnel configuration have on detonation and/or propagation of an acceptor?

## TEST PROGRAM

The overall objective of this test program was to determine the safe separation distance between stainless steel tote bins protected with Kevlar shielding, containing 168 pounds of Composition A-7, traveling on a simulated conveyor system within a tunnel or on a ramp.

A 25-shot test program was planned and conducted. This program consisted of firing the following test shots.

 $<sup>\</sup>overline{1}_{Ibid}$ .

<sup>&</sup>lt;sup>2</sup>A. B. Wenzel, "Determination of the Effects of Shielded Tote Bins on the Safe Separation of 168 Pounds of Composition A-7 Explosive," Southwest Research Institute Report No. 02-4343, prepared for Picatinny Arsenal under Contract No. DAAA21-75-C-0324, San Antonio, Texas (to be published).

- 3 tests without a tunnel
- 4 tests with a steel-Masonite® \* tunnel
- 5 tests with a steel-fiber glass tunnel; 2 of these tests substituted the acceptors with a Celotex GT-filled box to collect the fragments arriving at the acceptor locations
- 2 tests with one-half of the tunnel made out of steel and the other half made out of wood, both covered with fiber glass
- 11 tests with a wood-fiber glass tunnel

The separation of the acceptors relative to the donor was varied from 40 to 130 feet.

The open air tests were conducted to answer question (1). The steel tunnel tests were conducted to answer questions (1), (2), (3), and (5). The Celotex<sup>®</sup> tests were conducted to answer question (3). The wooden tunnel tests were conducted to answer questions (1), (3), (4), and (5).

### EXPERIMENTAL SETUP

The experimental test layout illustrated in Figure 1 shows one donor charge in the center, with two acceptor charges on either side set at distances D<sub>1</sub> and D<sub>2</sub> from the donor. For the majority of the tests, each donor and acceptor were placed inside a tunnel structure fabricated of steel frames, wooden frames, and/or steel and wooden frames, covered with a liner material made of Masonite<sup>®</sup> and/or fiber glass to simulate a plant tunnel or ramp. Masonite<sup>®</sup> was substituted for fiber glass during the exploratory stages of this program because it was substantially cheaper than fiber glass and provided a blast reflective surface which was equal to or stiffer than the fiber glass. Each donor and acceptor consisted of 168 pounds of A-7 explosive contained in a stainless steel tote bin. The tote bins used were of the same geometry and size as the containers to be used in the conveyence system at HAAP. Figure 2 illustrates the design of these tote bins. They were fabricated of 0.072-inch-thick, welded type 304 stainless steel sheet. The hinged lids were made of Plexiglas<sup>®</sup>.

The Composition A-7 explosive used in these tests was manufactured at HAAP and was furnished in cardboard boxes, each containing 60 pounds of explosive. Each tote bin was placed on a 5-foot-long steel roller section simulating part of the conveyor system, 5 feet above the floor. The 5-foot distance

<sup>\*</sup>Registered trademark of Masonite Corporation.

Registered trademark of Celotex Corporation.

<sup>\*\*</sup> Registered trademark of Rohm & Haas Company.

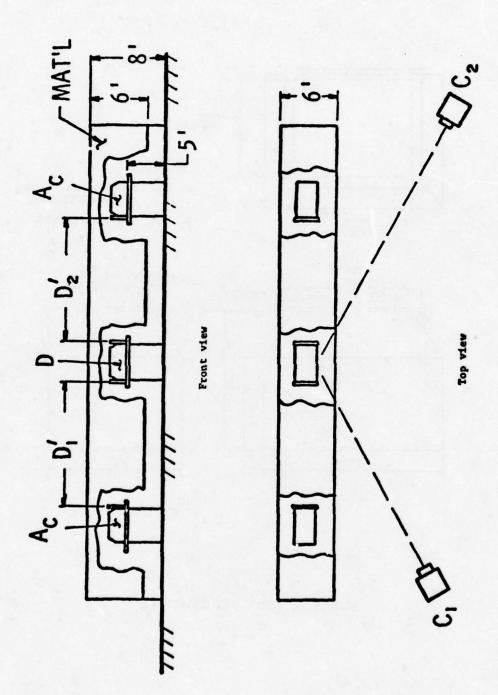


FIGURE 1. EXPERIMENTAL TEST LAYOUT

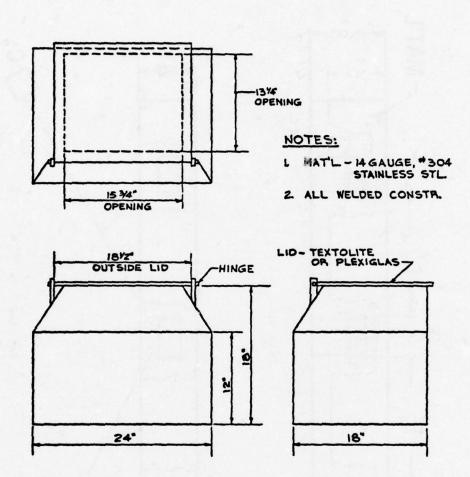


FIGURE 2. TOTE BIN GEOMETRY

to the bottom of the tote bin was accomplished by using a 24-inch-diameter Sonotube  $^{\textcircled{@}}\star$ . For all tests except one, each tote bin was protected with a sheet of 3/8-inch-thick Kevlar shielding to reduce the tote bin's vulnerability against primary and secondary fragment impact. In one test only, 3/4-inch-thick Kevlar was used.

Some tests were made in the open air, and others were made in a tunnel structure. The steel tunnels were fabricated from 1-1/2 inch by 1/8 inch angle iron. The tunnel sections measured 6 feet in width, 8 feet in height, and 8 feet long.

The wooden frame tunnel structures were constructed of 2-inch by 4-inch lumber to which the sheeting of fiber glass was attached by nailing at every 12 inches. The tunnel sections measured 6 feet in width, 8 feet in height, and 8 feet in length.

All the tests conducted using a tunnel were lined with fiber glass material with the exception of four tests for which Masonite $^{\otimes}$  was used instead. The sheathing was applied to the steel tunnel by the use of rivets, normally every 12 inches.

Figures 3 and 4 illustrate the setup of a steel tunnel and a wooden tunnel lined with fiber glass. The setup illustrated in Figure 3 shows the position of the donor relative to its two acceptors spaced at 100 and 110 feet. Figure 4 shows only one donor spaced at 130 feet from its acceptor instead of the one donor and two acceptor configurations used in all the tests except this one.

Figure 5 shows a view inside a steel tunnel lined with Masonite<sup>®</sup>, illustrating the positioning of the stainless steel tote bin, protected with the Kevlar<sup>®</sup> shield, placed on top of the steel roller system and the Sonotube<sup>®</sup>.

Initiation of the donors was accomplished by inserting a detonator equivalent to a No. 8 blasting cap into 4 ounces of Composition C-4 explosive and placing it into the Composition A-7 explosive in the tote bins. Each test was instrumented with two high-speed framing cameras (Hycams) located in positions  $C_1$  and  $C_2$ , as shown in Figure 1, and one real-time slow speed camera located in position  $C_1$ . The cameras were located approximately 350 feet from the donor and at an angle of 30° from the tunnel axis.

This level of camera coverage provided documentation of the information shown in the results of this paper. The Hycam high-speed camera settings ranged between 4000 and 5000 frames per second, and the settings for the real-time camera were 60 frames per second. Calculation of fragment velocities was made from the high-speed camera coverage when detonation of the acceptors occurred.

<sup>\*</sup>Registered trademark of Sonoco Products Co.



FIGURE 3. OVERALL VIEW OF TEST SETUP USING STEEL-MASONITE® TUNNEL

FIGURE 4. OVERALL VIEW OF TEST SETUP USING WOOD-FIBER GLASS TUNNEL

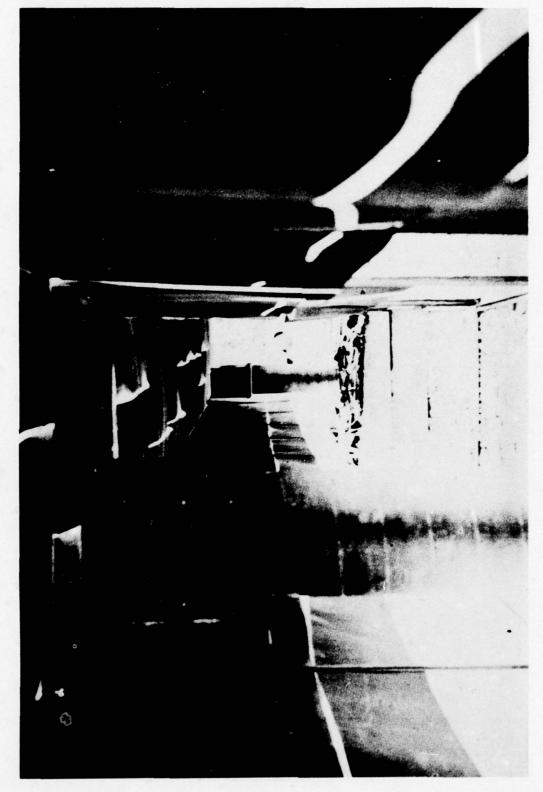


FIGURE 5. INSIDE VIEW OF STEEL-MASONITE® TUNNEL SHOWING DONOR AND ACCEPTOR

The results of these tests are summarized in Table 1 and described in more detail below. Table 1 identifies the test program by test number, test material, distance ( $D_1$ ) from donor to acceptor  $AC_1$ , distance ( $D_2$ ) from donor to acceptor  $AC_2$ , the number of impacts that the Kevlar shielding on acceptors  $AC_1$  and  $AC_2$  received, whether a detonation or burn was experienced by acceptors  $AC_1$  and  $AC_2$ , the thickness of the Kevlar shield used, and the number of penetrations experienced through the shield.

# Open Air Tests (No Tunnel)

Test Nos. 2, 3, and 4 were conducted without a tunnel configuration in an effort to determine the effectiveness of the Kevlar shielding. The separation distance of the acceptors ranged from 40 to 90 feet. A detonation was experienced at 48 feet, but none at the other distances. Note from Table 1 that the number of impacts on the Kevlar shielding ranged between 40 to 45, up to separation distances of 80 feet. The number of impacts at 90 feet ranged between 10 to 15, marking a significant decrease. All the fragments recovered from the shield were stainless steel (tote bin). No steel fragments (conveyor) were recovered from the shields. In Test No. 3, one stainless steel fragment penetrated the shield of AC<sub>1</sub> at 48 feet, denting the tote bin. In Test No. 4, AC<sub>1</sub> at 90 feet remained in an upright position. AC<sub>2</sub> at 60 feet was blown to the ground by the blast. A fragment completely penetrated the Kevlar shield of AC<sub>1</sub>, leaving an approximate 1-inch hole. A thin hole was also located approximately 2 inches above AC<sub>1</sub> tote bin.

The results of the Sierra tests reported a detonation at 100 feet from donor without a shield and a penetration of a bin above the explosive level at 110 feet. In the shielded tests, we experienced a detonation at 48 feet, with a penetration through the Kevlar<sup>®</sup> and bin at 90 feet, showing that the shield was effective in considerably reducing the separation distance in air. The fragment velocity causing the detonation of the bin in Test No. 2 was calculated from the high-speed film to be 6900 ft/sec.

It must be noted that the velocities calculated from the film were obtained by measuring the number of frames from the detonation of the donor until the acceptor detonated. By knowing the distance and the film speed, the velocity is calculated. Remember that before a detonation occurs, the fragment has to penetrate through the 3/8-inch-thick Kevlar<sup>®</sup> and 0.072 inch of stainless steel. Therefore, the velocity reported is lower than the true velocity because of the time required to penetrate the shield and the bin.

#### Steel Tunnel Tests

To determine if a safe separation distance of 130 feet or less can be obtained in a steel tunnel configuration, Tests 1, 5, 6, 7, 8, 11, 12, and 13 were conducted. Tests 1, 5, 6, and 7 were conducted using Masonite<sup>(S)</sup> as a liner material for the steel frames. Fiber glass lining was used in the other

TABLE 1. RESULTS OF TEST PROGRAM

Shot No.	Tunnel Material	<u>D</u> 1		No. of Impacts on AC <sub>1</sub>	No. of Impacts on AC <sub>1</sub>	Detonation AC <sub>1</sub>	Detonation AC <sub>2</sub>	Thickness of Kevlar	No. of Penetrations Through Kevlar <sup>®</sup>
1	S + M	80	48			DET	DET	3/8	-
2	Air	80	48	45		No	DET	3/8	
3	Air	48	40	40	40	No	No	3/8	1
4	Air	90	60	10	15	No	No	3/8	1
5	S + M	120	100	20	26	No	No	3/8	1
6	S + M	120	100	27		No	DET	3/8	2
7	S + M	110	120		30	DET	No	3/8	2
8	S + F	110	120	34	25	No	No	3/4	2
9	S + F	120	110	30	26	Celotex®	Celotex®		
10	S + F	120	110	40	15	Celotexo	Celotex®		
11	S + F	130	130	5	9	No	No	3/8	1
12	S + F	130	130		8	Burn	No	3/8	2
13	S + F W + F	130	130	-	2	Burn	No	3/8	2
14	S + F W + F	1 30	130	15	3	No	No	3/8	
15	W + F	130	130	17	7	No	No	3/8	-
16	W + F	1 30	130	18	6	No	No	3/8	1
17	W + F	1 30	1 30	3	1	No	No	3/8	•
18	W + F	130	130	9	4	No	No	3/8	-
19	W + F	130	130	1	3	No	No	3/8	-
20	W + F	130	130	5	8	No	No	3/8	
21	W + F	130	130	8	12	No	No	3/8	-
22	W + F	1 30	130	8	5	No	No	3/8	
23	W + F	130	130	6	13	No	No	3/8	-
24	W + F	130	130	4	3	No	No	3/8	
25	W + F	1 30	130	5		No		3/8	•

# NOTES:

S + M = steel-Masonite

S + F = steel-fiber glass

W + F = wood-fiber glass

Distances measured edge-to-edge of bins

tests reported in this series. The separation distance of the acceptors ranged from 48 to 130 feet. Detonations were experienced at 48, 80, 100, and 110 feet, and a complete burn at 130 feet. Note from Table 1 that no propagations were experienced at 100 and 120 feet. The reasons are twofold: (1) propagation by fragments is a stochastic process, and (2) at this stage in the program, the importance of the method of application of the shielding material to the steel framework had not been recognized. Initally, the shielding material was riveted to the steel framework at a random spacing, thereby varying the rigidity of the shielding material and the venting process. By the time Shots 12 and 13 were conducted, the importance of rigidity was recognized, and great care was taken in the application of the shielding material, ensuring that it was installed as rigidly as possible. When this was done, two consecutive burns were experienced at 130 feet.

As noted in Table 1, the total number of fragments recovered from the Kevlar® shielding ranged from 2 to 40 at separation distances up to 130 feet. In all cases, those fragments recovered from the shield material were stainless steel emanating from the donor tote bin. For the case where detonations were experienced at 48 feet and 80 feet, the velocities of the fragments as measured by the high-speed camera were 6620 ft/sec and 6670 ft/sec, respectively. Penetrations.through the Kevlar® were experienced in Tests 1, 5, 6, 7, 8, 11, 12, and 13.

Figure 6 shows the typical damage done to the steel tunnel when the acceptors detonated, as was the case in Test 1. Impact damage to the bin from a fragment impact after penetrating the shield is illustrated in Figure 7. A closeup view of the two large impacts experienced by the Kevlar<sup>®</sup> is given in Figure 8. The damage done to the tunnel structure from a detonation of a donor charge ranged only between 80 and 96 feet of total destruction, plus 40 feet which lost all the fiber glass covering. When an acceptor detonated, an additional 50 feet would be totally destroyed, plus an additional 40 feet of lost fiber glass. When a fire in the acceptor was experienced, in addition to the damage done by the donor, approximately 100 feet of the fiber glass sheathing were consumed by the fire.

From the results of this test series, the following observations can be made:

- (1) The 3/8-inch-thick Kevlar® shield did not provide sufficient protection to have a safe separation distance at 130 feet in a steel tunnel configuration.
- (2) The method of installing the fiber glass and/or Masonite® shielding to the steel frames has an effect on the results. It was observed that the more rigid the tunnel structure is made, the more vulnerable the tote bins are to fragmentation impact. A focusing effect due to the presence of the tunnel, which caused propagation of the acceptors, was observed through a comparison of the open air and steel tunnel results.



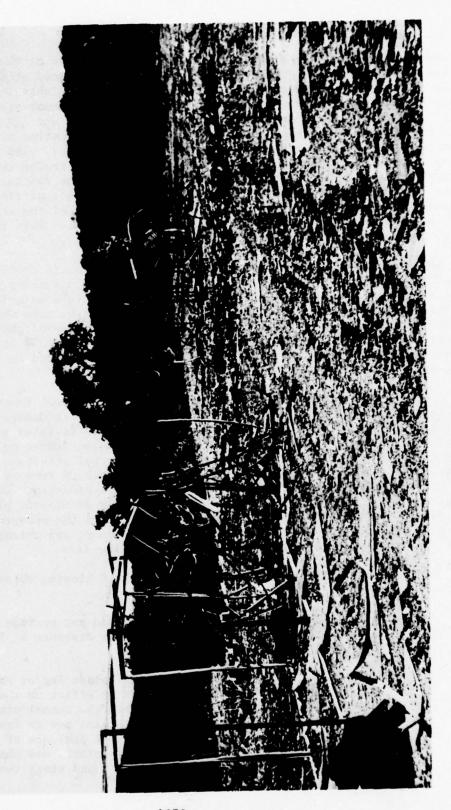




FIGURE 7. IMPACT DAMAGE TO BIN FROM FRAGMENT AFTER PENETRATING SHIELD (TEST NO. 5)



FIGURE 8. CLOSEUP VIEW OF LARGE IMPACTS INTO THE KEVLAR $^{\odot}$  SHIELD 1680

(3) All the fragments recovered from the Kevlar<sup>®</sup> shielding were of stainless steel material, indicating that the fragments arriving at the acceptor locations were from the donor tote bin.

To further substantiate these observations, two tests were conducted where the two acceptors were replaced by a box of Celotex<sup>®</sup> catcher material to capture all the fragments arriving at the acceptor locations. The results of these tests are described in the following section.

# 3. Celotex® Tests

To determine if the source of detonation and/or propagation of a shielded acceptor bin is due to primary (tote bin) and/or secondary (conveyor) fragments, two tests were conducted (Tests 9 and 10) where the acceptors were replaced by a Celotex<sup>®</sup>catcher box 4 feet wide by 4 feet high by 3 feet deep at distances from the donor of 110 and 120 feet. The catcher box was used to analyze the fragments arriving in the vicinity of the acceptors. The basic data extracted from these tests were depth of penetration into the Celotex<sup>®</sup>(P) in inches and the mass of the fragments (M) in grams. The impact velocity (V) in ft/sec was calculated by using the BRL calibration equations for velocity versus penetration into Celotex<sup>®</sup> as a function of fragment mass developed by Project THOR. The equation used for calculation impact velocity was:

$$V = \frac{872.7 P^{0.736}}{M^{0.256}}$$

The constants in this equation apply only for spall steel fragments.

The data obtained for each fragment are reported in Tables 2 and 3. Table 2 gives the fragment data for Test Nos. 9 and 10 for a catcher box location of 110 feet from the donor charge. Table 3 gives the data for Tests 9 and 10 for a catcher box location of 120 feet from the donor charge. Those fragments that have an (S) next to the value of mass denote steel fragments; all others are stainless steel.

Based on the results of Tests 9 and 10 and also from the fragments recovered from the Kevlar<sup>®</sup> panels of previous tests, indications are that the majority of the fragments and the most energetic ones arriving at the acceptor locations are of stainless steel material, originating from the tote bin of the donor. Also, fragment velocities up to 7670 ft/sec were calculated from the mass of the fragment and depth of penetration into Celotex<sup>®</sup>.

Personal communication with Mrs. Ann Hafer, U.S.A. Ballistic Research Laboratories, Aberdeen Proving Ground, MD, November 20, 1975. Evaluation quoted by Mrs. Hafer from Falcon Research and Development THOR Report No. 50, Baltimore, MD, dated February 23, 1972.

TABLE 2. FRAGMENT DATA AT 110 FT

Name	R. V. H. V.         H. V. P. H. W.         P. H. Grams         ft/sec.         grams         grams         ft/sec.         grams         grams         ft/sec.         grams         grams         ft/sec.         grams	8 grams ft/sec 791 0.20 791 0.85 546 0.86 (s) a 545 0.86 (s) a 545 0.86 (s) a 545 0.33 1560 0.33 1560 0.33 1560 0.04 5510 0.05 5210 0.05 5210 0.09 4890 0.43 3280 4.60 (s) 1790						
Richmen         ft/sec         Richmen         ft/sec         Attains         ft/sec         Attains         ft/sec         Attains         ft/sec         Attains         ft/sec         Attains         ft/sec         Attains         Attains         ft/sec         Attains         Attains         ft/sec         Attains	Richmen         ft/sec         Richmen         ft/sec         Atomatical Richmen	0.20 791 0.85 9.46 0.86(S) a 546 0.86(S) a 545		4	×	Δ	×	>
0.20 791 0.03 1280 5.5 0.62 0.85 0.85 0.85 0.89 0.062 0.85 0.89 0.00 5.5 2.31 0.89 0.86(s) a 545 0.08 1000 5.5 2.31 0.89 0.89 0.99 0.045 4000 0.62 0.89 0.30 0.37 1230 6.0 2.39 0.37 1230 6.0 2.39 0.33 1560 0.16 1880 0.02 0.29 0.25 0.00 0.03 0.180 0.02 0.02 0.03 0.180 0.05 0.02 0.04 0.05 0.16 1880 0.05 0.02 0.05 0.05 0.05 0.05 0.05 0.0	0.20 791 0.03 1280 5.5 0.65 0.85 0.85 0.85 0.85 0.85 0.85 0.85 0.8	0.20 791 0.85 \$46 0.86(s) \$545 		ᄪ	grams	ft/sec	grams	ft/sec
0.85 \$46 0.05 1130 5.5 2.31 0.86(S) \$ 545 0.08 1130 5.5 2.31 0.86(S) \$ 545 0.08 1000 5.5 2.31 0.86 0.08 1660 6.0 1.85 2790 2.30 0.33 1560 0.16 1880 6.0 2.99 0.33 1560 0.16 1880 6.5 2.99 2620 5.60 0.33 1560 0.16 1880 6.5 2.99 2620 5.60 0.34 0.05 1100 0.06 3520 8.5 2.21 3140 0.58 0.04 5510 0.05 3520 8.5 3.04 3170 0.05 1140 0.05 310	0.85 \$46 0.05 1130 5.5 2.31 0.86(S) a 545 0.08 1000 5.5 2.31 0.86(S) a 545 0.08 1000 5.5 2.31 0.86 5.008 1660 6.0 1.85 2790 2.30 0.97 1220 6.0 2.99 0.93 1560 0.16 1880 6.0 2.99 0.93 1560 0.16 1880 6.0 2.99 0.93 1560 0.16 1880 7.0 0.22 5380 2.90 0.94 5.72(S) 1100 0.06 520 8.5 33 2630 1.44 0.05 5.72(S) 1100 0.06 520 8.5 3.04 3170 0.95 1740 9.0 1.09 4390 0.09 2500 8.5 3.04 3170 0.09 2500 8.5 3.04 3170 0.09 2500 8.5 3.04 3370 0.09 2500 8.5 3.04 3370 0.09 2500 8.5 3.04 3370 0.09 2500 8.5 3.04 3370 0.09 2500 9.5 11.74 3300 0.07 2150 11.5 5.28 3440 0.09 4890 0.29 3620 11.5 6.90 3210 0.87 0.43 320 0.43 3200 0.98 2500 11.5 6.90 3210 2.39 4.60(S) 1790 2.39 250 0.43 3200 0.98 250 0.43 3200 0.98 250 0.43 3200 0.98 250 0.43 3200 0.98 250 0.43 3200 0.98 2500	0.85 546 0.86(S) a 545 	1280	5.5	0.25	0967	0.62	3460
0.86(\$)** 545 0.08 1000 5.5 2.31 0.08 1660 6.0 1.85 2790 2.30 0.18 1350 6.0 2.90 0.33 1560 0.16 1880 6.5 2.99 2620 5.60 7.80(\$) 696 0.16 1880 7.0 0.22 5380 2.90 0.47 1430 7.5 2.21 3140 0.58 0.24 2090 8.5 3.3 2630 1.44 0.24 2090 8.5 1.23 4000 0.24 2090 2.72(\$) 1100 0.06 3520 8.5 1.23 4000 0.95 1740 9.0 1.09 4300 0.90 0.05 5210 0.33 3210 11.5 5.49 3300 0.90 0.05 5210 0.39 3620 11.5 5.28 3440 0.90 0.09 4890 0.29 3620 11.5 0.23 7670 0.85 0.043 3280 0.98 2650 15.0 0.81 0.06 (\$) 1790 0.91	0.86(s) a 545 0.08 1000 5.5 2.31 0.08 1660 6.0 0.45 4000 0.62 0.08 1660 6.0 1.85 2790 2.30 0.27 1220 6.0 2.99 0.33 1560 0.16 1880 6.5 2.99 2620 5.60 7.80(s) 696 0.16 1880 7.0 0.22 5380 0.56 1360 7.0 1.54 3270 0.56 1360 7.0 1.54 3270 0.56 1360 7.0 1.54 3270 0.09 2690 8.5 1.23 4000 0.95 1740 9.0 1.09 4300 0.95 1740 9.0 1.09 4300 0.95 1740 9.0 1.09 4300 0.09 2010 0.81 2560 11.5 5.28 3.04 0.09 2010 0.81 2560 11.5 5.28 3.04 0.09 2010 0.81 2560 11.5 5.28 3.04 0.09 2010 0.81 2560 11.5 5.28 3.04 0.09 2010 0.81 2560 11.5 5.28 3.04 0.09 2010 0.81 2560 11.5 5.28 3.04 0.09 2010 0.81 2560 11.5 5.28 3.04 0.00 0.00 0.00 0.00 0.00 0.00 0.0	0.86(S) a 545	1130	5.5	1	1	0.62	3460
		0.33 1560 7.80(s) 696 	1000	5.5	1	1	2.31	2470
		0.04 \$5210 0.04 \$5210 0.05 \$2210 0.04 \$5210 0.05 \$2210 0.04 \$5210 0.05 \$2210	713	0.9	0.45	4000	0.62	3690
0.18       1350       6.0        2.60          0.27       1220       6.0        2.90         0.33       1560       0.16       1880       7.0       0.22       580         7.80(s)       696       0.16       1880       7.0       0.22       5380          0.47       1430       7.0       0.22       5380          0.65       1360       7.5       2.21       3270          0.09       2690       8.0       5.33       2630       1.44          0.09       2690       8.5       2.21       3400       1.44          0.09       2690       8.5       1.23       4000       1.44          0.09       2690       8.5       1.23       4000       1.44          0.09       2690       8.5       1.23       4000       1.44          0.09       1810       8.5       1.24       3370       1.25          0.91       1810       8.5       1.74       3970       1.25          0.04       5510       0.59 <td> 0.18 1350 6.0 2.60 0.27 1220 6.0 2.90 0.33 1560 0.16 1880 6.5 2.99 2620 5.60 7.80(s) 696 0.16 1880 7.0 0.22 5380 0.47 1430 7.0 1.54 3270 0.56 1360 7.5 2.21 3140 0.58 0.65 1360 7.6 1.23 4000 0.09 2690 8.0 5.33 2630 1.44 0.09 2690 8.0 5.33 2630 1.44 0.09 2690 8.5 1.23 4000 0.95 1700 0.08 5.72(s) 1100 0.06 3520 8.5 1.23 4000 0.95 1700 1.09 4300 0.95 1700 1.09 4300 0.95 1700 1.09 4300 0.95 1700 1.05 1.56 4400 0.070 2150 11.0 5.49 3300 0.070 2150 11.5 5.28 3440 0.09 3620 1.15 6.90 3210 0.087 0.09 4890 0.29 3620 13.5 0.0 0.87 0.43 3280 0.98 2650 15.0 0.39 4.60(s) 1790 2.39 4.60(s) 1790 2.39</td> <td>0.33 1560 7.80(s) 696 7.80(s) 696 ———————————————————————————————————</td> <td>1660</td> <td>0.9</td> <td>1.85</td> <td>2790</td> <td>2.30</td> <td>2640</td>	0.18 1350 6.0 2.60 0.27 1220 6.0 2.90 0.33 1560 0.16 1880 6.5 2.99 2620 5.60 7.80(s) 696 0.16 1880 7.0 0.22 5380 0.47 1430 7.0 1.54 3270 0.56 1360 7.5 2.21 3140 0.58 0.65 1360 7.6 1.23 4000 0.09 2690 8.0 5.33 2630 1.44 0.09 2690 8.0 5.33 2630 1.44 0.09 2690 8.5 1.23 4000 0.95 1700 0.08 5.72(s) 1100 0.06 3520 8.5 1.23 4000 0.95 1700 1.09 4300 0.95 1700 1.09 4300 0.95 1700 1.09 4300 0.95 1700 1.05 1.56 4400 0.070 2150 11.0 5.49 3300 0.070 2150 11.5 5.28 3440 0.09 3620 1.15 6.90 3210 0.087 0.09 4890 0.29 3620 13.5 0.0 0.87 0.43 3280 0.98 2650 15.0 0.39 4.60(s) 1790 2.39 4.60(s) 1790 2.39	0.33 1560 7.80(s) 696 7.80(s) 696 ———————————————————————————————————	1660	0.9	1.85	2790	2.30	2640
0.27       1220       6.0        2.90         0.33       1190       6.0         9.73         0.33       1190       6.0         9.73         7.80(s)       696       0.16       1880       7.0       0.22       5380           0.47       1430       7.0       0.22       5380         9.73          0.56       1360       7.0       0.22       5380         9.73       1.44          0.09       2690       8.0       5.33       2630       1.44          0.09       2690       8.5       2.21       3400           0.24       2090       8.5       2.26       3420           0.24       2090       8.5       2.26       3420           0.98       1740       9.0       1.09       4300           0.99       2170       11.09       4300         0.0          0.04       5510       0.31	0.27 1220 6.0 2.90 0.33 1560 0.16 1880 6.5 2.99 2620 5.60 7.80(s) 696 0.16 1880 7.0 0.22 5380  0.56 1360 7.5 2.21 3140 0.58 0.09 2690 8.5 1.23 4000  5.72(s) 1100 0.06 3520 8.5 2.26 3420  0.19 3000 9.5 1.74 3970 1.25 0.09 2150 11.5 5.28 3400  0.19 3000 9.5 1.74 3970 1.25 1.14 2340 11.5 6.90 3210  0.09 4890 0.29 3620 11.5 6.90 3210  0.09 4890 0.29 3620 13.5  0.00 0.81 13.5 0.87 0.03 3280 0.98 2650 11.5 6.90 3210  1.14 2340 11.5 6.90 3210  2.39 4.60(s) 1790 2.39	0.33 1560 7.80(s) 696 	1350	0.9	1	1	2.60	2560
0.33     1560     0.16     1880     6.5     2.99     2620     5.60       7.80(s)     696     0.16     1880     7.0     0.22     5380        7.80(s)     696     0.16     1880     7.0     0.22     5380	0.33 1560 0.16 1880 6.5 2.99 2620 5.60 7.80(S) 696 0.16 1880 6.5 2.99 2620 5.60 7.80(S) 696 0.16 1880 7.0 0.22 5380	0.33 1560 7.80(s) 696 	1220	0.9	1	1	2.90	2490
0.33     1560     0.16     1880     6.5     2.99     2620     5.60       7.80(\$\$)     696     0.16     1880     7.0     0.22     5380	0.33 1560 0.16 1880 6.5 2.99 2620 5.60 7.80(S) 696 0.16 1880 7.0 0.22 5380	0.33 1560 7.80(s) 696 	1190	0.9	1	1	9.73	1820
7.80(\$) 696 0.16 1880 7.0 0.22 5380 0.47 1430 7.0 1.54 3270 0.56 1360 7.5 2.21 3140 0.58 0.09 2690 8.0 5.33 2630 1.44 0.24 2090 8.5 1.23 4000 0.81 1810 8.5 2.26 3420 0.95 1740 9.0 1.09 4300 0.70 2150 10.5 1.56 4400 0.70 2150 11.5 5.49 3300 0.05 5210 0.33 3210 11.5 5.49 3300 0.70 2150 11.5 0.23 7670 0.85 2.09 2010 0.81 2560 11.5 6.90 3210 1.14 2340 11.5 6.90 3210 0.43 3280 0.98 2650 15.0 2.39	7.80(\$) 696 0.16 1880 7.0 0.22 5380 0.47 1430 7.0 1.54 3270 0.56 1360 7.5 2.21 3140 0.58 0.09 2690 8.0 5.33 2630 1.44 0.24 2090 8.5 1.23 4000 0.24 2090 8.5 1.23 4000 0.19 3520 8.5 2.26 3420 0.19 3000 9.5 1.74 3970 1.25 0.70 2150 10.5 1.56 4400 0.70 2150 11.0 5.49 3300 0.70 2150 11.5 0.23 7670 0.85 2.09 2010 0.81 2560 11.5 6.90 3210 1.14 2340 11.5 5.28 3440 0.09 2650 13.5 0.087 4.60(\$) 1790 2.39	7.80(\$) 696	1880	6.5	2.99	2620	2.60	2230
0.47 1430 7.0 1.54 3270 0.56 1360 7.5 2.21 3140 0.58 8.0 5.33 2630 1.44 8.5 1.23 4000 0.24 2090 8.5 1.23 4000 0.24 2090 8.5 1.23 4000 0.55 1100 0.06 3520 8.5 2.26 3420 0.95 1740 9.0 1.09 4300 0.19 3000 9.5 1.74 3970 1.25 0.70 2150 10.5 1.56 4400 0.05 5210 0.33 3210 11.0 5.49 3300 0.05 5210 0.59 2770 11.5 5.28 3440 0.09 4890 0.29 3620 11.5 6.90 3210 0.43 3280 0.29 3620 13.5 0.087 4.60(S) 1790 2.39	0.47 1430 7.0 1.54 3270 0.56 1360 7.5 2.21 3140 0.58   0.09 2690 8.0 5.33 2630 1.44   0.24 2090 8.5 1.23 4000 0.51 1100 0.06 3520 8.5 1.23 4000 0.95 1740 9.0 1.09 4300 0.95 1740 9.0 1.09 4300 0.09 1740 9.0 1.09 4300 0.09 2770 11.0 5.49 3300 0.05 5210 0.33 3210 11.5 5.28 3440 0.09 4890 0.29 3620 11.5 6.90 3210 0.08   1.14 2340 11.5 6.90 3210 0.08   1.14 2340 11.5 6.90 3210 0.08   1.14 2340 11.5 6.90 3210 0.08   1.14 2340 11.5 6.90 3210 0.08   1.14 2340 11.5 6.90 3210 0.08   1.14 2340 11.5 6.90 3210 0.08   1.14 2340 11.5 6.90 3210 0.08   1.14 2340 11.5 6.90 3210 0.08   1.14 2340 11.5 6.90 3210 0.087   1.14 2340 11.5 6.90 3210 0.087   1.14 2340 11.5 6.90 3210 0.087   1.14 2340 11.5 6.90 3210 0.087   1.14 2340 11.5 6.90 3210 0.087   1.14 2340 11.5 6.90 3210 0.087   1.14 2340 11.5 6.90 3210 0.087   0.87	5.72(s) 1100 5.72(s) 1100 6.04 6.05 6.09 6.09 6.09 6.43 6.60(s) 1790	1880	7.0	0.22	5380	1	1
0.56     1360     7.5     2.21     3140     0.58         0.09     2690     8.0     5.33     2630     1.44         0.024     2090     8.5     1.23     4000          0.06     3520     8.5     2.26     3420          0.95     1740     9.0     1.09     4300          0.19     3000     9.5     1.74     3970     1.25         0.19     3000     9.5     1.74     3970     1.25         0.70     2150     10.5     1.56     4400        0.04     5510     0.33     3210     11.0     5.49     3300          0.70     2150     11.5     0.23     7670     0.85       2.09     2010     0.81     2560     13.5       0.87       0.043     3280     0.98     2650     15.0       2.39       4.60(s)     1790 <t< td=""><td> 0.56 1360 7.5 2.21 3140 0.58 0.09 2690 8.0 5.33 2630 1.44 0.24 2090 8.5 1.23 4000 0.24 2090 8.5 1.23 4000 0.81 1810 8.5 3.04 3170 0.95 1740 9.0 1.09 4300 0.09 2770 10.5 1.56 4400 0.05 5210 0.33 3210 11.0 5.49 3300 0.05 5210 0.59 2770 11.5 0.23 7670 0.85 2.09 2010 0.81 2560 11.5 6.90 3210 1.14 2340 11.5 6.90 3210 0.09 4890 0.29 3620 13.5 1.14 2340 11.5 6.90 3210 0.043 3280 0.98 2650 15.0 2.39 4.60(S) 1790 2.39</td><td>5.72(s) 1100 5.72(s) 1100 </td><td>1430</td><td>7.0</td><td>1.54</td><td>3270</td><td>1</td><td>1</td></t<>	0.56 1360 7.5 2.21 3140 0.58 0.09 2690 8.0 5.33 2630 1.44 0.24 2090 8.5 1.23 4000 0.24 2090 8.5 1.23 4000 0.81 1810 8.5 3.04 3170 0.95 1740 9.0 1.09 4300 0.09 2770 10.5 1.56 4400 0.05 5210 0.33 3210 11.0 5.49 3300 0.05 5210 0.59 2770 11.5 0.23 7670 0.85 2.09 2010 0.81 2560 11.5 6.90 3210 1.14 2340 11.5 6.90 3210 0.09 4890 0.29 3620 13.5 1.14 2340 11.5 6.90 3210 0.043 3280 0.98 2650 15.0 2.39 4.60(S) 1790 2.39	5.72(s) 1100 5.72(s) 1100 	1430	7.0	1.54	3270	1	1
0.09       2690       8.0       5.33       2630       1.44         5.72(8)       1100       0.06       3520       8.5       1.23       4000           0.081       1810       8.5       2.26       3420           0.095       1740       9.0       1.09       4300           0.09       3000       9.5       1.74       3970       1.25          0.09       2150       10.5       1.56       4400          0.04       5510       0.33       3210       11.0       5.49       3300          2.09       2010       0.81       2560       11.5       6.90       3210          0.05       2010       0.81       2560       11.5       6.90       3210          0.09       4890       0.29       3620       13.5         0.87         0.43       3280       0.98       2650       15.0         2.39         4.60(8)       1790	5.72(S) 1100 0.06 3520 8.5 1.23 4000 5.72(S) 1100 0.06 3520 8.5 1.23 4000 6.081 1810 8.5 1.26 3420 6.095 1740 9.0 1.09 4300 6.09 2150 0.33 3210 11.0 5.49 3300 6.05 5210 0.59 2770 11.5 6.30 3210 6.09 4890 0.29 3620 13.5 6.09 4890 0.29 3620 13.5 6.09 4890 0.29 3620 13.5 7.66(S) 1790 7.74 2340 7.74 3970 1.25 7.75 1.76 1.25 7.77 1.15 6.30 7.78 1.15 6.30 3210 7.79 2010 0.81 2560 13.5 7.79 2010 0.81 2560 13.5 7.70 0.09 4890 0.29 3620 15.0 7.70 0.09 4890 0.29 3620 15.0 7.70 0.09 4890 0.29 3620 15.0 7.70 0.09 2.00 0.98 2650 15.0 7.70 0.087	5.72(s) 1100 	1360	7.5	2.21	3140	0.58	4420
5.72(S)     1100     0.24     2090     8.5     1.23     4000         0.081     1810     8.5     2.26     3420         0.081     1810     8.5     2.26     3420         0.095     1740     9.0     1.09     4300         0.09     3000     9.5     1.74     3970     1.25        0.04     5510     0.33     3210     11.09     4400        0.05     2770     11.0     5.49     3300        2.09     2010     0.81     2560     11.5     5.28     3440          1.14     2340     11.5     6.90     3210        0.09     4890     0.29     3620     13.5       0.87       4.60(S)     1790        2.39	5.72(S) 1100 0.06 3520 8.5 1.23 4000  5.72(S) 1100 0.06 3520 8.5 2.26 3420  0.81 1810 8.5 2.26 3420  0.95 1740 9.0 1.09 4300  0.04 5510 0.33 3210 11.0 5.49 3300  0.05 5210 0.59 2770 11.5 0.23 7670 0.85  2.09 2010 0.81 2560 11.5 6.90 3210  0.09 4890 0.29 3620 13.5  0.04 3280 0.98 2650 15.0  1.14 2340 15.0  1.15 0.23 3440  1.15 0.23 3440  1.16 2340 11.5 6.90 3210  2.39  4.60(S) 1790  1.10 0.00	5.72(\$) 1100 	2690	8.0	5.33	2630	1.44	3670
5.72(8)     1100     0.06     3520     8.5     2.26     3420          0.81     1810     8.5     3.04     3170          0.95     1740     9.0     1.09     4300          0.19     3000     9.5     1.74     3970     1.25         0.70     2150     10.5     1.56     4400        0.04     5510     0.33     3210     11.0     5.49     3300        2.09     2010     0.81     2560     11.5     6.90     3210        0.09     4890     0.29     3620     11.5     6.90     3210        0.43     3280     0.98     2650     15.0       2.39       4.60(S)     1790        2.39	5.72(S) 1100 0.06 3520 8.5 2.26 3420 0.81 1810 8.5 3.04 3170 0.095 1740 9.0 1.09 4300 0.19 3000 9.5 1.74 3970 1.25 0.70 2150 10.5 1.56 4400 0.05 5210 0.59 2770 11.5 0.23 7670 0.85 2.09 2010 0.81 2560 11.5 5.28 3440 1.14 2340 11.5 5.28 3440 0.09 4890 0.29 3620 13.5 1.14 2340 13.5 2.39 4.60(S) 1790 2.39	5.72(\$) 1100  0.04 5510 0.05 5210 2.09 2010  0.09 4890 0.43 3280 4.60(\$) 1790	2090	8.5	1.23	4000	1	1
0.81 1810 8.5 3.04 3170 0.95 1740 9.0 1.09 4300 0.095 1740 9.0 1.09 4300 0.019 3000 9.5 1.74 3970 1.25 0.70 2150 10.5 1.56 4400 0.05 5210 0.33 3210 11.0 5.49 3300 1.14 2560 11.5 5.28 3440 1.14 2340 11.5 6.90 3210 0.09 4890 0.29 3620 13.5 0.87 4.60(\$) 1790 2.39	0.81 1810 8.5 3.04 3170 0.95 1740 9.0 1.09 4300 0.19 3000 9.5 1.74 3970 1.25 0.19 3000 9.5 1.74 3970 1.25 0.70 2150 10.5 1.56 4400 0.05 5210 0.59 2770 11.5 5.28 3440 1.14 2340 11.5 5.28 3440 1.14 2340 11.5 6.90 3210 0.09 4890 0.29 3620 13.5 0.87 0.03 2280 0.98 2650 15.0 2.39 4.60(\$) 1790 2.39	0.04 5510 0.05 5210 2.09 2010  0.09 4890 0.43 3280 4.60(\$) 1790	3520	8.5	2.26	3420	1	1
0.95 1740 9.0 1.09 4300 0.10 3000 9.5 1.74 3970 1.25 0.19 3000 9.5 1.74 3970 1.25 0.04 5510 0.33 3210 11.0 5.49 3300 0.05 5210 0.59 2770 11.5 5.28 3440 1.14 2340 11.5 5.28 3440 1.14 2340 11.5 6.90 3210 0.04 3280 0.98 2650 15.0 2.39 4.60(\$) 1790 2.39	0.95 1740 9.0 1.09 4300 0.19 3000 9.5 1.74 3970 1.25 0.19 3000 9.5 1.74 3970 1.25 0.04 5510 0.59 2770 11.0 5.49 3300 0.05 5210 0.59 2770 11.5 5.28 3440 0.09 4890 0.29 3620 11.5 6.90 3210 0.43 3280 0.98 2650 15.0 2.39 4.60(S) 1790 2.39	0.04 5510 0.05 5210 2.09 2010  0.09 4890 0.43 3280 4.60(\$) 1790	1810	8.5	3.04	31.70	!	1
0.19 3000 9.5 1.74 3970 1.25 0.70 2150 10.5 1.56 4400 0.04 5510 0.33 3210 11.0 5.49 3300 0.05 5210 0.59 2770 11.5 0.23 7670 0.85 2.09 2010 0.81 2560 11.5 5.28 3440 0.09 4890 0.29 3620 13.5 0.87 4.60(S) 1790 2.39	0.19 3000 9.5 1.74 3970 1.25 0.70 2150 10.5 1.56 4400 0.04 5510 0.33 3210 11.0 5.49 3300 0.05 5210 0.59 2770 11.5 0.23 7670 0.85 2.09 2010 0.81 2560 11.5 5.28 3440 0.09 4890 0.29 3620 13.5 0.87 0.43 3280 0.98 2650 15.0 2.39 4.60(S) 1790 2.39	0.04 5510 0.05 5210 2.09 2010 	1740	9.0	1.09	4300	1	1
0.04 5510 0.33 3210 11.0 5.49 3300 0.05 5210 0.59 2770 11.5 0.23 7670 0.85 2.09 2010 0.81 2560 11.5 5.28 3440 0.09 4890 0.29 3620 13.5 0.43 3280 0.98 2650 15.0 4.60(S) 1790 2.39	0.70 2150 10.5 1.56 4400 0.04 5510 0.33 3210 11.0 5.49 3300 0.05 5210 0.59 2770 11.5 0.23 7670 0.85 2.09 2010 0.81 2560 11.5 5.28 3440 1.14 2340 11.5 6.90 3210 0.09 2650 13.5 0.87 4.60(S) 1790 2.39 4.60(S) 1790 2.39	0.04 5510 0.05 5210 2.09 2010 	3000	9.5	1.74	3970	1.25	4320
0.04 5510 0.33 3210 11.0 5.49 3300 — 0.05 5210 0.59 2770 11.5 0.23 7670 0.85 2.09 2010 0.81 2560 11.5 5.28 3440 — 0.09 4890 0.29 3620 11.5 6.90 3210 — 0.43 3280 0.98 2650 15.0 — 0.44 50(S) 1790 — 0.2 39	0.04 5510 0.33 3210 11.0 5.49 3300 0.05 5210 0.59 2770 11.5 0.23 7670 0.85 2.09 2010 0.81 2560 11.5 5.28 3440 0.09 4890 0.29 3620 13.5 0.43 3280 0.98 2650 15.0 4.60(S) 1790 1.14 2340 1.04ers are stainless steel.	0.04 5510 0.05 5210 2.09 2010 6.09 4890 0.43 3280 4.60(\$) 1790	2150	10.5	1.56	4400	1	!
0.05 5210 0.59 2770 11.5 0.23 7670 0.85 2.09 2010 0.81 2560 11.5 5.28 3440 0.09 4890 0.29 3620 13.5 0.43 3280 0.98 2650 15.0 4.60(S) 1790 2.39	0.05 5210 0.59 2770 11.5 0.23 7670 0.85 2.09 2010 0.81 2560 11.5 5.28 3440 1.14 2340 11.5 6.90 3210 0.09 4890 0.29 3620 13.5 0.87 0.43 3280 0.98 2650 15.0 2.39 4.60(\$) 1790 2.39 tefers to steel fragments: all others are stainless steel.	0.05 5210 2.09 2010 6.09 4890 0.43 3280 4.60(\$) 1790	3210	11.0	5.49	3300	1	1
2.09 2010 0.81 2560 11.5 5.28 3440	2.09 2010 0.81 2560 11.5 5.28 3440	2.09 2010 4890 0.43 3280 4.60(S) 1790	2770	11.5	0.23	7670	0.85	2490
0.09 4890 0.29 3620 13.5 0.87 0.43 3280 0.98 2650 15.0 2.39 4.60(S) 1790 2.39	1.14 2340 11.5 6.90 3210 0.09 4890 0.29 3620 13.5 0.87 0.43 3280 0.98 2650 15.0 2.39 4.60(S) 1790 2.39	0.09 4890 0.43 3280 4.60(\$) 1790	2560	11.5	5.28	3440	1	1
0.09 4890 0.29 3620 13.5 0.87 0.43 3280 0.98 2650 15.0 2.39 4.60(S) 1790 2.39	0.09 4890 0.29 3620 13.5 0.87 0.43 3280 0.98 2650 15.0 2.39 4.60(S) 1790 2.39	0.09 4890 0.43 3280 4.60(S) 1790	2340	11.5	06.9	3210	1	1
0.43 3280 0.98 2650 15.0 2.39 4.60(s) 1790 2.39	0.43 3280 0.98 2650 15.0 2.39 4.60(S) 1790 2.39	0.43 3280 4.60(S) 1790	3620	13.5	1	1	0.87	6140
4.60(s) 1790	4.60(S) 1790	4.60(S) 1790	2650	15.0	1	1	2.39	5130
	a (S) refers to steel fragments; all others are stainless steel.		1					
	a (S) refers to steel fragments: all others are stainless steel.							
	(S) refers to steel fragments: all others are stainless steel.							

TABLE 3. FRAGMENT DATA AT 120 FT

	Test	9	Test	10
P	M	V	M	V
in.	grams	ft/sec	grams	ft/sec
0.5	100 to		1.05	518
1.0	0.22(S) a	1290	0.03	2140
1.0	0.41(S)	1100	0.28	1210
1.0			0.38	1120
1.0			10.45	479
1.0			25.38	382
1.5	0.19(S)	1800	0.12	2020
2.0	0.29	1990	0.52	1720
2.0	0.42(S)	1810		
2.0	0.43(S)	1800		
2.0	0.50(S)	1740		
2.5	0.15(S)	2780	1.39	1570
2.5	0.52	2020	17.76	821
2.5	0.55(S)	2000		
2.5	3.34	1260		
3.0	0.95(S)	1990		
3.0	2.52(S)	1550		
3.0	2.92	1490		
3.5	1.10	2140	0.64	2460
3.5	1.15	2120		
4.0	2.43	1930	0.65	2700
4.5	1.37	2440		
4.5	1.53	2370		
5.0			2.49	2260
5.5	2.16	2510	2.32	2470
6.0	1.05	3220		
6.0	17.96	1560		
6.5			2.77	2670
7.5	1.78	3320		
8.0	1.01	4020		
8.0	1.93	3410		

<sup>&</sup>lt;sup>a</sup>(S) refers to steel fragments; all others are stainless steel.

## 4. Wooden Tunnel Tests

To answer the question of whether a wooden-fiber glass tunnel structure can provide safe separation distance between tote bins at 130 feet, a series of 13 tests was conducted where wooden frames lined with fiber glass were used. In the first two tests (Tests 13 and 14), one-half of the tunnel structure (AC1 side) was made out of steel, while the other half of the line (AC2 side) was wooden. Tests 15 through 24 consisted of firing one donor and two acceptors at 130-foot separation. Test 25 consisted of firing one donor and one acceptor at 130-foot separation. Reference is made to Table 1 for a consolidated view of the test results. No detonations or burns of the acceptors were experienced during this test series.

The total damage done to the wooden tunnel by the detonation of the donor charge ranged between 120 feet to 136 feet of total destruction, plus an additional 40 feet which lost all the fiber glass sheathing. Also, all the fragments recovered from the Kevlar shielding were stainless steel. Figure 9 illustrates the type of damage done to a wooden tunnel.

The results of these tests showed that at a distance of 130 feet, no propagation or burning of the acceptors was experienced using the wooden tunnel structure. However, comparing the effects of open air with the steel-framed and the wooden-framed tests, it is evident that the rigidity and stiffness of the tunnel have an effect on the safe separation distance. Care must be taken in interpreting the results of these tests because the rigidity and stiffness of the tunnels tested here are not typical of those present in actual production plants. The wooden tunnels existing in the production plants are more rigid than the steel frames tested in this program. Therefore, if we had tested a wooden-framed tunnel having the rigidity of those in a production plant, we suspect that, based on the results of the steel tunnel tests, separation distances greater than 130 feet would be required.

On this subject, the reader is encouraged to refer to the appendix of Reference 2 for an analytical approach to the effects of the tunnel confinement. This analysis should eventually be applied to a real-life tunnel design, but for this paper, the analysis clearly shows that a fragment can be focused into a "hit" trajectory. Depending on the number and energy of these focused fragments, the statistical probability of detonation propagation is enhanced by the tunnel confinement.

5. Effects of Tunnel Confinement Surrounding a Tote Bin Conveyor Line

Two phenomena have been demonstrated by this program:

(1) All of the fragments which struck the acceptor line were of stainless steel--therefore, they emanated from the donor tote bin and not from the tunnel support frames or wall material.

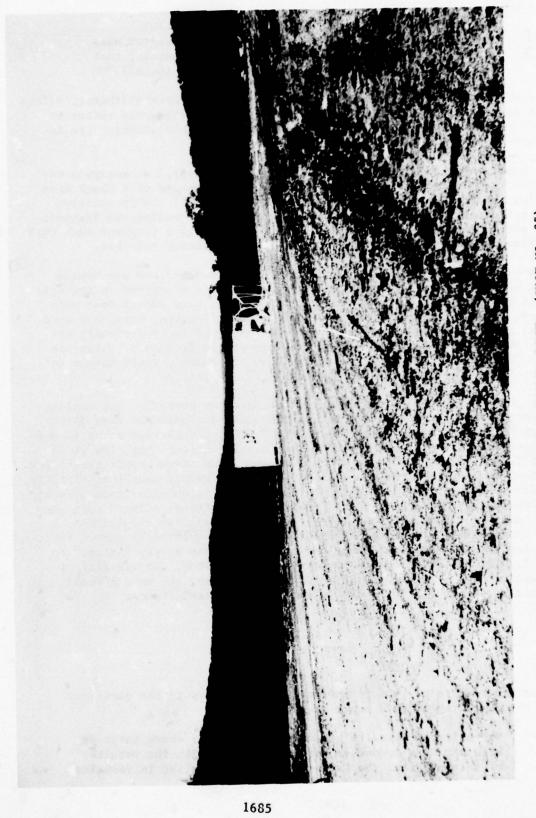


FIGURE 9. DAMAGE DONE TO A WOODEN TUNNEL (SHOT NO. 25)

(2) The minimum distances at which propagation occurred were greater for the confined tests (i.e., with tunnels) than for the unconfined tests (i.e., open air--no tunnel).

It was apparent then that the tunnel did have a significant contributory effect on the propagation, not by contributing to the fragmentation, but rather by focusing the shock wave and/or focusing more fragments into striking the acceptor tote bin.

To examine the feasibility of this "focusing concept," an analysis was carried out to calculate: (1) the peak pressure and impulse of a shock wave after being reflected off the walls of the tunnel; and (2) the interaction of those reflected waves with a fragment in terms of increasing the fragment velocity and in the possibility of redirecting (focusing) a fragment such that a "near miss" fragment would become a "hit" on the acceptor tote bin.

These calculations are shown in detail in Reference 2 and are beyond the scope of this paper. A variety of sample fragments recovered in the Celotex tests were weighed, and their presented area and drag coefficient were determined. Four random mass fragments (0.014 to 1.17 grams) were then used as typical cases, and each of these fragments was found to be seriously affected by the reflected shock. Two of the four sample fragments, which had been on a "near miss" trajectory traveling down the tunnel, would have been focused by the shock and redirected into a "hit" trajectory.

The consequences of this focusing effect are now obvious. The confinement offered by the tunnel is significant and must be considered when determining any "minimum safe separation distance." The calculations shown in Reference 2 merely verify the principle of the focusing effect, but also it is important in the future to consider the real magnitude of the confinement (i.e., steel versus wood framing and the wall material, thickness, mounting, rigidity, etc.). Although the analysis performed to date did not consider this effect, the experiments have indicated that the steel-framed tunnel offered more confinement than did the wood-framed tunnel. In retrospect, an examination of the wood-framed and steel-framed tunnels used in the experiments showed that, although the wall material was identical in both, it was simply "nailed" to the wood frames, but "riveted" to the steel frames. Thus, the rigidity of the reflecting wall surfaces was quite different. Also, the wood offered faster venting, hence falling apart faster than the steel frames.

#### SUMMARY

From the results of this test program, the answers to the questions asked at the beginning of this paper are:

(1) Comparing the results given in Reference 1, where tests in open air were conducted without shields, with the results of this program, the Kevlar shield is effective in reducing

the separation distance. However, applying 3/8-inch-thick Kevlar  $^{\textcircled{\tiny{1}}}$  for the steel tunnel case is not effective in preventing propagation at 130 feet.

- (2) As mentioned above, a safe separation distance greater than 130 feet is required in a steel tunnel configuration.
- (3) The primary source of propagation of the acceptors is fragments emanating from the donor bin.
- (4) At 130-foot separation between donor and acceptor, no propagations or detonations were experienced in the wooden tunnel configurations tested by Picatinny and SwRI. However, it was observed that the rigidity and stiffness of the tunnel have an effect on the safe separation distance. Therefore, if a tested wooden frame tunnel had the rigidity of those present in a production plant, we suspect that, based on the results of the steel tunnel tests and the analysis reported in Reference 3, separation distances greater than 130 feet are required.
- (5) The experimental results indicate that the tunnel has an effect on the safe separation distance. The analysis reported in Reference 2 demonstrates that blast focusing can affect the trajectory of the fragments, and also that it is possible to increase the fragment flight velocity when reflective surfaces are present in the vicinity of the donor.

#### ACKNOWLEDGEMENTS

The authors wish to express their sincere appreciation to test personnel at the Sierra Army Depot, Herlong, California; Picatinny Arsenal, Dover, New Jersey; Camp Bullis, a part of Ft. Sam Houston, Texas; and, in particular, Messrs. William Seals and Robert S. Kukuvka of Picatinny Arsenal for their assistance.

The work conducted at Southwest Research Institute was performed for the U. S. Army Picatinny Arsenal, Dover, New Jersey, under Contract No. DAAA21-75-C-0324.

Also, the authors wish to acknowledge the following SwRI personnel for their contributions to this program: Messrs. Luis Garza, James Kulesz, J. W. Gehring, A. C. Garcia, Robert Marin, and John F. Weschler.

## SAFE SEPARATION AND CRITICAL DEPTH TESTS FOR LONE STAR AMMUNITION PLANT

By

Robert S. Kukuvka Richard M. Rindner

Manufacturing Technology Directorate
Picatinny Arsenal
Dover, New Jersey

#### ABSTRACT

The flow of 105mm projectiles and bulk explosives on conveyors in and about the melt-pour area at the Lone Star Army Ammunition Plant was investigated with regard to safety. Testing determined the minimum non-propagative spacing between two transport carriages, each containing sixteen 105mm, HE, M-1 Projectiles loaded with Composition B explosive. Two conditions, without riser funnels (30 foot) and with riser funnels having a 3/4-inch thick steel plate shield (20 foot) were established as safe conditions. In addition, a practical method was found to prevent propagation of flake Composition B down a belt type conveyor. This was accomplished by providing  $1\frac{1}{2}$ -inch high corrugations incorporating an air space on 8-inch centers extending across the width of the belt.

#### INTRODUCTION

Presently, an Army modernization program is underway to upgrade existing and develop new explosive loading, assembly and packaging facilities (LAP). This effort will enable the Army to achieve increased production and cost effectiveness with improved safety. Although this paper deals specifically with the safety considerations relative to the flow of bulk explosives and 105mm, HE, MI projectiles in and about the melt-pour area at the Lone Star Army Ammunition Plant (LSAAP), it is also applicable to other similar loading facilities. The existing melt-pour facilities consist of the following areas as shown in Fig 1: (1) Receiving and Storage, (2) Box Opening and Inspection, (3) Melt-pour, (4) Cool, (5) Hold, (6) Funnel Pull and (7) Riser Preparation. Explosive material is transferred by automated conveyor between these work areas as also shown in Fig. 1.

Previous propagation tests have been conducted by this Arsenal to determine the safe spacing requirement for 60 lb. boxes (paper cartons) filled with Composition B explosive, the results of which were presented previously. The requirement was to establish a safe distance between

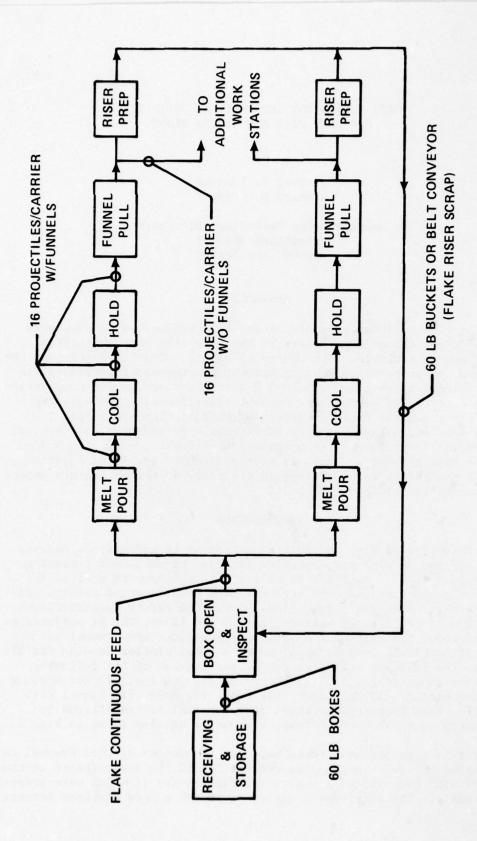


Fig 1 105MM, M1 Projectile Melt Pour Flow Diagram 1690

the boxes of explosive being transferred from the receiving and storage building to the box opening and inspection building via an interconnecting conveyance ramp. It was determined by these tests that a twelve (12) foot separation distance between the boxes will preclude a detonation from propagating. Once the boxes are received at the box opening building, they are opened and emptied directly into the receiving surge hoppers of the inspection equipment. Flaked, riser scrap explosive from the riser preparation area is also conveyed to this station to be mixed with virgin explosive. A pendent, bucket type conveyance system containing 60 lbs. per bucket is utilized in this area. Tests conducted proved that a twelve (12) foot distance between covered plastic buckets containing 60 lbs. of Comp B each, would not propagate a detonation.

The uncontaminated flake explosive is then transferred to one of the two melt buildings via a belt type conveyor on which a continuous feed system will be employed. In order to implement this feed system, safety regulations pertaining to the critical depth of the proposed explosive must be adhered to. Since no safety regulations are available, an experimental test program was initiated to alleviate the deficiency. Details of these experiments will be discussed in this paper.

Once the empty projectiles are filled with explosive under the multi-pour units in the melt-pour building, they are then transferred on a carriage and track conveyance system which incorporates sixteen (16) projectiles on each carrier. After the projectiles are filled with explosive, they are then transported to one of the cooling areas with pouring funnels still in place. Then on to a hold and funnel pull station where the funnels are removed in a continuous manner by a pneumatic mechanism. The carriages/projectiles without funnels are then transported to additional work stations. The Safety Manual AMCR 385-100 (Table 17-1) gives a safe separation distance of 109 inches between pallets containing thirty-two (32) 105mm projectiles (Comp B loaded). Since this pallet configuration differs significantly from that intended for use at LSAAP, it was necessary to experimentally establish safe separation distances for these carriages. Details of these experiments will also be discussed in this paper.

## 105 MM PROJECTILE TEST PROGRAM

## Objectives of the Test Program

The test program was developed to experimentally determine the minimum non-propagative clear spacing between two transport carriages, each containing sixteen 105mm, HE, MI projectiles loaded with Composition B under the following conditions:

- a. without riser funnels
- b. with riser funnels and various blast and/or fragment resistant shields

The program may be considered as consisting of two phases. The first phase involved exploratory testing for the purpose of establishing the required clear spacing between carriages. The second phase consisted of confirmatory testing as required to establish statistical confidence in the results.

## Criteria for the Tests

Initially, the tests were conducted in such a manner as to simulate, as closely as possible, the transfer carriage configuration to be used at LSAAP. Figure 2 shows a representative carriage assembly with blast interrupter rods attached. The transfer carriage, holding fixtures and projectile arrangements were all reproduced in the test arrangements. As the test results accumulated, it became apparent that the AMCR 385-100 specified safe distance was highly optimistic and that the explosive donor event was of such an energetic character that a great deal more testing would be required than originally anticipated. Therefore, simplifications of the test setups were introduced to substantially reduce costs.

For the exploratory phase of the program, tests were conducted with varying spacings between the donor and acceptor pallets in order to determine order of functioning and establish the required safe distance. A total of 58 tests were conducted in this phase of the program alone. Either of two results was sufficient to regard a given configuration as unsafe. The first, of course, was an observation of either a detonation or fire at the acceptor. The second was the occurrence of penetrations into the Composition B filler of the acceptor projectiles. Such penetrations were observed on several occasions without the occurrence of detonation. It was assumed, however, that communication of this kind between donor and acceptor implied a much higher risk of propagation than was acceptable even without the observance of detonation or fire. Since the loading funnels are made of substantially lighter weight metals than the

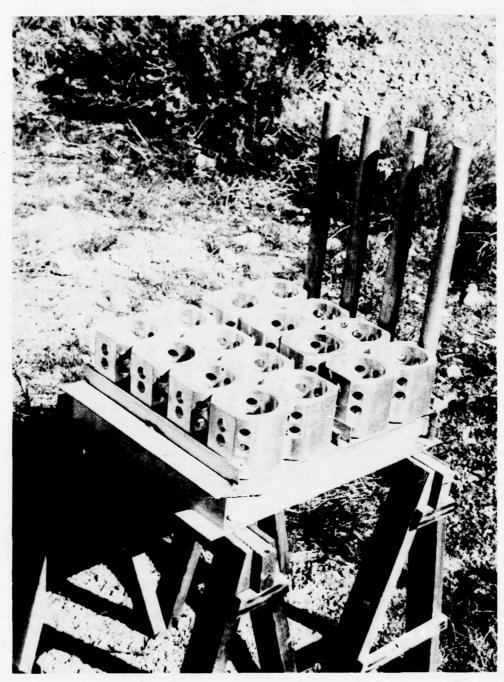


Fig 2 Plant Simulated Text Fixture with Blast Interrupter Rods

projectiles, they sustained considerable damage, including penetrations in all the tested configurations. It was felt, however, that such damage to the acceptor funnels did not constitute a significant propagation hazard. This was borne out by the confirmatory tests in which no propagation was observed despite substantial damage to the funnels.

## Test Descriptions

The exploratory phase of the program may be viewed as comprising five test sequences. The first dealt with interrupter rods mounted on the carriages as shown in Fig 3. The second examined propagation of an explosive event on a single pallet or carriage. A third series of tests was initiated to evaluate the safe spacing required without shielding (Fig 4). The use of aluminum plate blast shields mounted on the pallets was examined in the fourth test sequence (Fig. 5). Finally, a fifth series of tests explored the required spacing when steel plate blast shields were used (Fig. 5).

The confirmatory phase of the program consisted of two sequences of tests. The first attempted to establish the non-propagative spacing required with steel shields mounted on the acceptors when funnels were present. The second established the safe spacing with neither funnels nor shields.

In order to simplify the arrangements, save set-up time and thereby obtain optimum data output at the least cost, the carriages and fixtures were replaced with wooden pallets. Sixteen 105mm, HE (M1) projectiles loaded with Composition B were contained on each pallet. The projectiles were placed in the vertical position in a 4 x 4 matrix with a minimum spacing of 1 inch between projectiles. A sketch of the pallets is shown in Fig. 6. Further economics were realized by supporting the pallets approximately 30 inches above the ground on empty ammunition boxes. Three pallets were used for each test trial. The center pallet served as donor. Sections of steel roller conveyor were placed under the donor pallets to more closely simulate actual plant conditions and thereby also introduce additional shrapnel emissions. The two acceptor pallets used for each test trial were positioned on either side of the donor pallet in a manner similar to that shown in Fig. 5. The two acceptor pallets were each located at different distances from the donor pallet. Tests were conducted both with and without funnels in place. The supplementary charges and liners were removed from the projectiles in order to simulate their condition in the melt-pour area. One projectile on each donor pallet was primed with approximately 1/4 pound of Composition C4 in the fuze well cavity or in the funnel when they were used. A No. 8 blasting cap was inserted into the Comp C4 and attached to a suitable length of blasting fuze. Initiation was obtained with a manual fuze igniter.



Fig 3 Test Sequence 1 Arrangement



Fig 4 Test Arrangement without Shielding

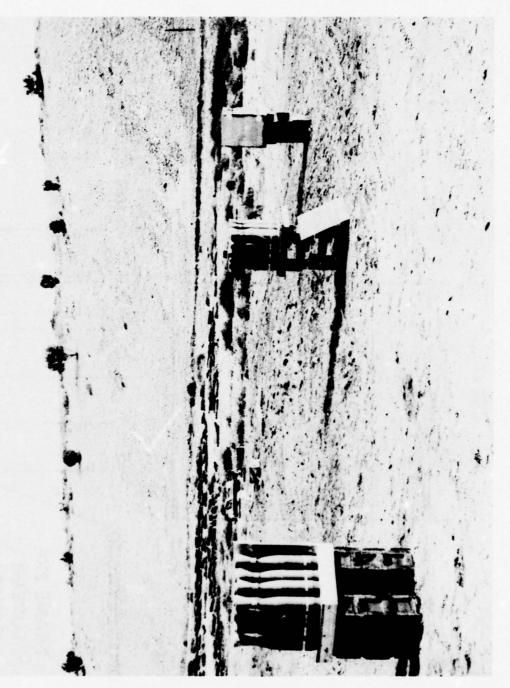


Fig 5 Test Arrangement with Funnels and Shields (Steel or Aluminum Plate)

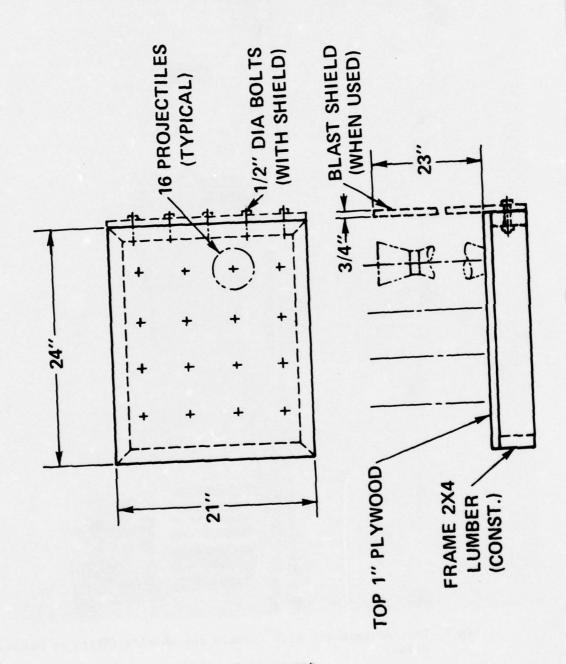


Fig 6 Simplified Pallet Arrangement

## Discussion of Results

The test program conclusively demonstrated that detonation of one projectile on a pallet results in a high order detonation of all the projectiles on the pallet. This of course yields an explosive and fragment producing event of a highly energetic character. The test results proved that the presence of the loading funnels significantly increases the potential propagation hazard and thus results in increasing the required safe spacing unless protective shields are employed. In the exploratory test series, the use of the aluminum interrupter rods (1-3/4" dia. x 23" high) proved to be relatively ineffective in preventing propagation for the distances tested, while the 3/4" thick aluminum plate shield at the 10 foot distance was totally ineffective in stopping fragments (Fig. 7). A detonation propagation occurred at the 15 foot distance with this shield. Even 3/4" thick steel plate shields mounted on acceptor pallets 20 feet from the donor were penetrated by shrapnel (Fig. 8), although this shield was effective in capturing or reducing the velocity of the donor fragments and consequently prevented propagation. A total of 49 successful (no propagation) confirmatory tests were conducted establishing a safe separation distance of 20 feet between pallets containing 16 projectiles with funnels when this shield was employed. Without the use of this shield the safe distance would be in excess of 40 feet.

The exploratory tests conducted without funnels and without shields indicated that a minimum distance of 30 feet would be required to prevent propagation. A total of 39 confirmatory tests showed neither propagation nor penetration of the acceptor projectiles with a 30 foot clear spacing between unshielded pallets without funnels. The results of all tests are summarized in Table 1.

As a result of this test program, the following techniques could be implemented into a conveyor system at a munitions facility:

- 1. Shields (3/4-inch thick steel) on potential acceptors
- 2. 30-foot spacing between carriers without funnels
- 3. Avoidance of line-of-sight between a potential donor and a candidate acceptor beyond a ramp terminus
- 4. Blast shields carried by turntables to interrupt potential propagation paths.

Any combination of these techniques may be used to insure that propagation from ramps to buildings will not occur without unduly penalizing the plant production capacity or economics. Viewed in this light, the present test results define minimum parameters to be

met in the context of protecting the 105mm production facility at LSAAP or other munitions facilities where applicable.\*

<sup>\*</sup> Reference: Picatinny Arsenal Technical Report 4869, <u>Determination</u> of <u>Minimum Nonpropagation Distance of 105mm M1 Projectile Grouped 16 on a Pallet</u>, Kukuvka, Robert S. (Picatinny Arsenal), and Sarrett, Howard (Ammann and Whitney, Consulting Engineers), September 1975.



Fig 7 Typical Fragment Damage to Aluminum Shield

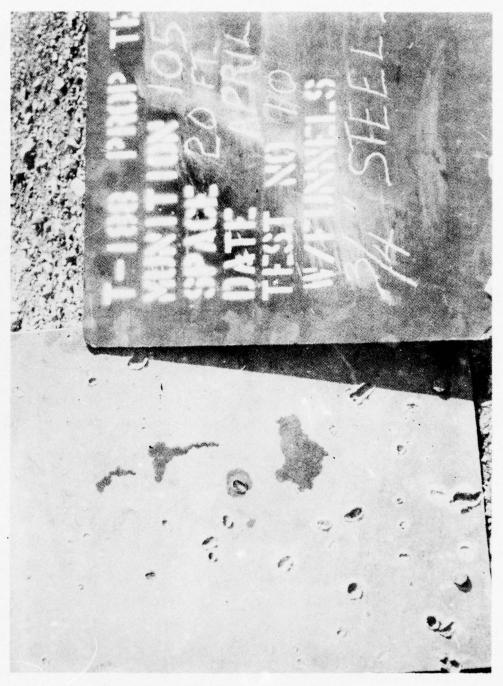


Fig 8 Typical Fragment Damage to Steel Shield

TABLE 1

# SUMMARY OF TESTS - 105MM PROJECTILE, 16/PALLET

RESULTS	D. P.	D. P.	DAMAGE TO SHIELD & FUNNELS	N. P.	PENETRATIONS IN PROJECTILES	N. P.
FUNNELS	0	YES	YES	YES	0	0
SHIELD	1-3/4" DIA ALUMINUM * RODS	3/4" THK ALUMINUM * PLATE	3/4" THK STEEL ** PLATE	3/4" THK STEEL ** PLATE	0	0
DISTANCE (FT)	9 OT 9U	UP TO 15	UP TO 15	20	UP TO 25	30
TYPE OF TESTS	EXPLORATORY	EXPLORATORY	EXPLORATORY	CONFIRMATORY	EXPLORATORY	CONFIRMATORY
NO OF TESTS	6	7	7	49	32	39

\* 6061-T6

\*\* SAE 1020

D. P. - DETONATION PROPAGATION

N. P. - NO PROPAGATION



### CRITICAL DEPTH OF COMPOSITION B TEST PROGRAM

### Objective of the Test Program

The objective of the test program was to establish a safe (non-propagative) depth of a continuous bed of flake Composition B explosive being transported on a belt type conveyor. In the event that a safe depth could not be found, a method in which batches could be separated would have to be investigated. However, to maintain a separation or air space between batches in an actual plant operation would require a precise control of the explosive feed onto the conveyor belt. Therefore, the continuous feed system would be the most practical approach from a cost and control viewpoint. In order to accomplish this goal, a test program was developed to investigate the critical depth of Composition B flake on conveyors.\*

# Criteria for the Tests

Initially the tests were conducted on simulated conveyors (troughs) of wood construction in the interest of economics, length and width flexibility and to quickly determine the reactions of the various depths or batches of the explosive. The explosive, Composition B, was bulk, flake, grade A, MIL SPEC C-401 and was supplied in 60 lb. boxes. Since the proposed LSAAP conveyance system would be enclosed in a tunnel-like structure, this was also implemented in the experiments. Earlier tests of Comp B flake by other agencies and of other items have indicated that the presence of an enclosure could enhance the possibility of propagation occurrence. Once a safe method for transferring the Comp B was established by the exploratory tests, then actual sections of the proposed conveyor would be introduced into the confirmatory series to establish reliability.

# Test Description

This program was divided into four parts (or test series). The first three series were used to determine means by which propagation could be negated whereas the fourth series was confirmatory in nature.

### Test Series No. 1

This first series consisted of sixteen individual tests. Each test was so arranged as to simulate the Composition B Flake conveyor at Lone Star AAP. The conveyor proper was simulated by mounting either rubber or wood troughs on empty ammunition boxes (Fig. 9).

\* Reference: Picatinny Arsenal Technical Report to be published shortly, Critical Depth of Composition B Flake on Conveyor



Fig 9 Simulated Conveyor Arrangement

# Discussion of Results

In summary, the overall results of this test program are considered successful in that practical means are available to prevent propagation of explosion of flake Composition B on belt type conveyors. (1) The various portions of the test program have indicated that physical means are needed to interrupt the explosion propagation of the flake and in general forming an air space of at least four inches will be sufficient. Based upon the test results, the depth of the flake should not exceed 1½ inches; however, this does not mean that greater depth of the explosive could not be used in combination with a larger air space. The possibility of using the latter arrangement would require further testing.

# **Acknowledgements**

The authors wish to express their appreciation to the personnel of Tooele Army Depot, Tooele, Utah, who conducted the testing phases of this work.

<sup>(1)</sup> The conveyors utilized in these experiments are typical commercially available types and the findings are not to be construed as an official Department of the Army position relative to the selection of one conveyor manufacturer over another.

The width of the trough was approximately 17 inches whereas the lengths varied from 5 to 16 feet. Each conveyor was covered with a 3'9'' wide x 3' 6'' high aluminum enclosure which simulated the enclosure required for the dust collection system.

In this series of tests, means for separating the explosive on the conveyor were not used; however, the depth of explosive in the troughs was varied from  $1\frac{1}{4}$  to 2 inches to determine whether this would have any effect on the propagation. Initiation of explosive was performed using 1-inch thick composition C4 booster and a No. 8 blasting cap. The height and length of each booster were the same as that of the explosive. In all sixteen tests performed, high order detonation ( $H_0O_0D_0$ ) occurred over a part or the entire length of the simulated conveyor. It was concluded from this series that some physical means would be necessary to prevent propagation.

It may be noted, that the rubber troughs used in this series were sections of a commercially available flat rubber conveyor belt having 2-3/8 inch high corrugated sides.

Summary of the test set-up and results for Series No. 1 is presented in Table 2.

# Test Series No. 2

Eighteen tests (Test Nos. 17 to 34) were conducted in connection with this test series. Except for Test No. 19, where the enclosure was omitted, the test set-up of this series was the same as in the first series. All enclosures were fabricated specially for these tests and are representative of those that will be used at LSAAP; with each having cross-sectional dimensions of 2 ft. by 3 ft. Wood troughs were used to simulate the conveyors in all tests. The booster and method of initiation were the same as that of Test Series No. 1.

Because high order propagation occurred when the explosive flake was continuous, interrupters were used in this series of tests. Empty spaces and/or cleats were investigated as interrupters. Each cleat was a 3" high by \tilde{\chi}" thick rubber pad as wide as the simulated conveyor. When used in combination with the air spaces, the cleats were found to be effective in eliminating propagation. However, when used by themselves, the cleats were ineffective. High order detonation occurred in all tests where cleats alone were used.

Based upon the results of this series it was concluded that an empty space (daylight) must be used to prevent propagation. The size of the air space may be as small as 3 inches. As will be shown, this air gap concept was developed further in the next test series.

Table 3 summarizes the test setups and results of Series No. 2.

Critical Depth Tests of Composition B (Series 1)

:	3	Conveyorb		Don'th of		Boosterf	-		
0.0	Туре	Length (ft)	Width (in.)	Explosive (in.)	Height (in.)	Thickness (in.)	Length (in.)	Weight (1bs.)	Test Results
	Rubbera	2	17.5	1.50c	1.50	1.0	17.50	1.00	H.O.D. total length9
	Rubber	2	17.5	1.50	1.50	1.0	3.50	0.50	H.O.D. total length
	Rubber	10	17.5	1.50	1.50	1.0	17.50	1.00	H.O.D. total length
	Rubber	10	17.5	1.00d	1.50	1.0	17.50	1.00	H.O.D. 6 ft. length
	Rubber	2	17.5	1.00	1.00	1.0	17.50	0.75	H.O.D. total length
	Rubber	10	17.5	1.00	1.00	1.0	17.50	0.75	H.O.D. 4 ft. length
	Rubber	80	17.5	1.25	1.25	1.0	17.50	06.0	H.O.D. 3 ft. length
	Mood	16	11.25	1.25	1.25	1.0	11.25	0.50	H.O.D. 1-1/2 ft. length
	Mood	91	11.25	1.50	1.50	1.0	11.25	0.90	H.O.D. 1-1/2 ft. length
	Mood	91	17.125	1.50	1.50	1.0	17.125	1.00	H.O.D. 10 ft. length
	Mood	91	17.125	1.50	1.50	1.0	17.125	1.30	H.O.D. 10 ft. length
	Mood	91	17.125	2.00e	5.00	1.0	17.125	2.00	H.O.D. total length
_	Mood	91	17.125	1.75	2.00	1.0	17.125	5.00	H.O.D. total length
	Mood	91	17.125	1.50	2.00	1.0	17.125	2.00	H.O.D. total length
_	Mood	91	17.125	1.25	1.75	1.0	17.125	1.50	H.O.D. 2 ft. length
	Mood	16	11.25	2.00	2.00	1.0	11.25	1.50	H.O.D. total length

Commercially available rubber belt.

Aluminum enclosure for conveyor used (3'-9" W x 3'-6" H) è.

Approximately 55 lbs. of Comp. B 9 9

Approximately 70 lbs. of Comp. B

Approximately 180 lbs. of Comp. B.

Composition C4 explosive (M112 demolition charge)

H.O.D. - High Order Detonation

Table 3

Critical Depth Tests of Composition B Flake (Series 2)

	c.	Test Results	Partial detonation. Comp. B scattered.	Partial detonation. Comp. B scattered.	H.O.D. Crater 2 ft. W x 8 ft. L x 8 in. Deep.	H.O.D. Crater 2.5 ft. W x 16 ft. L x l ft. Deep.	Partial detonation. Crater 2 ft. W x 8 ft. L x 6 in. Deep Comp. B scattered.	H.O.D. crater 2.5 ft. W x 16 ft. L x l ft. Deep.	Crater at donor side only				
		Space (S)	(c)	(e)	•	£	(6)	Œ	54	54	15	21	15
	Test Arrangement	Expl.(E) (in.)	36	<b>w</b>	95	21	<b>&amp;</b>	•	09	9	99	2	4
Unitical Depth lests of Composition B Flake (Series 2)	Test A	Configuration		3 3 5 5 5 5 5 5 5 5 5 5 5 5 5 5 5 5 5 5	Same as 17	Same as 18	Same as 18	Same as 18	E 55	Same as 23	Same as 23	E. S. E. S. E.	Same as 26
OLD L SOCIETO		Approx. Weight (1bs.)	1.0	1.0	1.0	1.33	1.0	1.0	2.0	5.0	2.0	2.0	2.0
lests of C	terb	Length (in.)	11.25	11.25	11.25	11.25	11.25	11.25	11	11	11	.71	91
cal Deptu	Boosterb	Thickness (in.)	1.0	1.0	1.0	1.0	1.0	1.0	1.0	1.0	1.0	1.0	1.0
		Height (in.)	1.50	1.50	1.50	2.00	1.50	1.50	2.00	5.00	5.00	2.00	2.00
		Depth of Explosive (in.)	1.50	1.50	1.50	2.00	1.50	1.50	2.00	2.00	2.00	2.00	2.00
	ora	Width (in.)	11.25	11.25	11.25	11.25	11.25	11.25	11	11	2	11	2
	Conveyora	Length (ft.)	8	œ	ω	92	9	92	21	21	21	8	8
		Test No.	11	82	19	2 170	23	22	23	*	52	92	22

No. (ft.) (in.) 28 12 17 29 12 17 30 12 17 31 12 17	Depth of Explosive (in.) 2.75 2.75 2.75	Height (in.) 2.75 2.75 2.75	Height Thickness (in.) 2.75 1.0 2.75 1.0	Length (in.) 17	Approx. Weight (1bs.) 2.8	Configuration			
2 2 2 2	2.75	2.75	0.1 0.1	71 11	2.8		(in.)	Expl.(E) Space (S) (in.)	Test Results
2 2 2	2.75	2.75	.0.1	11		Same as 23	09	24	Crater at donor side only N.P.
2 2	2.75	27.6	1.0		8.2	Same as 23	99	12	Crater at donor side only N.P.
2		:		11	2.8	Same as 23	9	54	Crater at donor side only N.P.
	2.75	2.75	1.0	12	8.8	Same as 23	99	12	Crater at donor side only
22 12 17	2.75	2.75	1.0	11	2.8	Same as 23	69	•	Crater at donor side only N.P.
33 12 17	2.75	2.75	1.0	11	2.8	Same as 23	2	е	Crater at donor side only N.P.
24 24 17	2.00	2.00	1.0	11	2.0	20   37   50   750 ESESESE	ខ	12	Crater at donor side only N.P.

Wooden conveyors with 2 ft. W  $\times$  3 ft. H  $\times$  8 ft. L aluminum enclosures.

Composition C4 demolition charge with J-8 blasting cap.

Explosive, Air Space, 222 Booster,
Spacer - cleats 3"H x 1/4" Thick.

N.P. - No Propagation.

Explosive bed was subdivided by 11 cleats 8 inches o.c.

Explosive bed was subdivided by 15 cleats 12 inches o.c. Explosive bed was subdivided by 23 cleats 8 inches o.c.

Explosive bed was subdivided by 31 cleats 6 inches o.c.

# Test Series No. 3

The tests (Test Nos. 35 to 55) of Series No. 3 were a continuation of the second series whereby various interrupters were investigated. In this series, square (Fig. 10) and curved (Fig. 11) rubber spacers were used. Both spacers were designed such that a flexible wiper could be used to remove all flake residues and thereby prevent propagation of explosion across the top of the spacers.

Figures 12 and 13 illustrate the test setup for both types of rubber spacers respectively.

Propagation of explosion to an acceptor portion of the simulated conveyor did not occur in any of the twenty-one tests performed in this series. This included the three tests in which Composition B dust was used to coat the tops of the rubber interrupters so as to create a more hazardous condition. The only damage sustained during the testing was the formation of craters below the donor portion of each test item. In all cases the flake from the acceptors was scattered about the site. It may be noted that in more than half of these tests, the point of initiation was located at the center of the test item. This arrangement permitted the use of two acceptor sections; one located at each end of the simulated conveyor.

Table 4 summarizes the test set up and results of Test Series No. 3.

# Test Series No. 4

The fourth and last series in the test program was the confirmatory test series. Here, a total of 20 tests were performed using the belt portion of another commercially available conveyor which had 1½" high corrugations incorporating an air space on 8 inch centers extending across the width of the belt.

Figures 14 and 15 illustrate the setup for this series of tests.

As can be seen from Table 5, a detonation propagation occurred only in Test No. 5 where the flake explosive had a 2-inch depth. This depth exceeded the  $1\frac{1}{2}$  inch depth of the conveyor corrugations (Fig. 14), and thereby provided a direct path for explosion propagation along the conveyor. In all other 19 tests the explosive depth was limited to approximately the height of the corrugations (Fig. 15) and damage was limited to the sections of the conveyors where the boosters were located.

Although damage illustrated in Figure 16 would appear to be more extensive than that mentioned above, the damage as viewed is mainly due to the collapse of the ammunition boxes as a result of the blast wave.

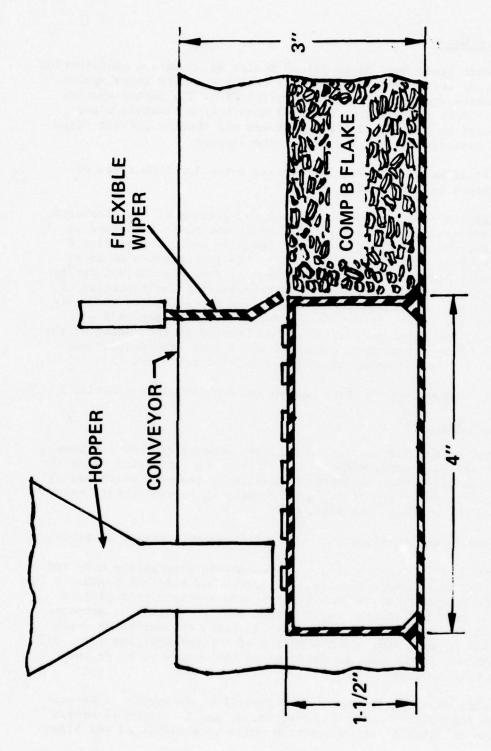


Fig 10 Schematic of Square Interrupter 1712

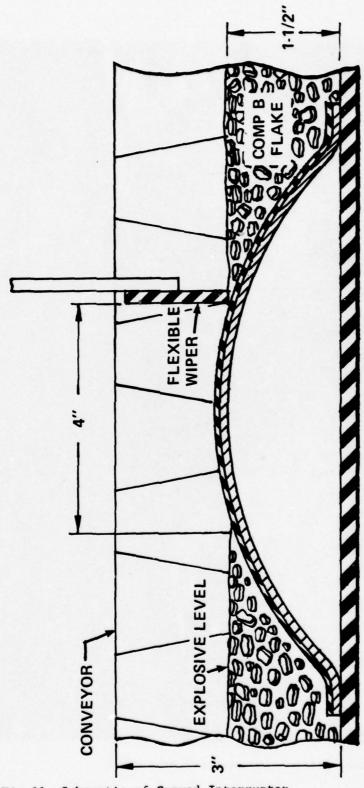


Fig 11 Schematic of Curved Interrupter 1713

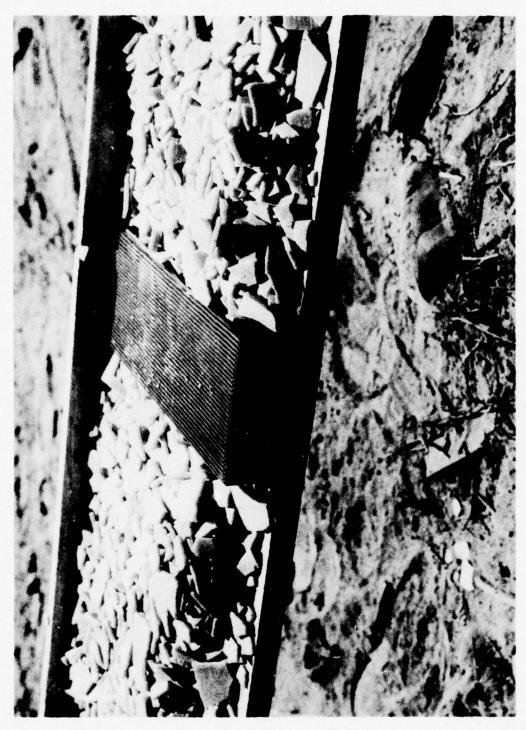


Fig 12 Test Setup Using Square Interrupter



Fig 13 Test Setup Using Curved Interrupter

1716

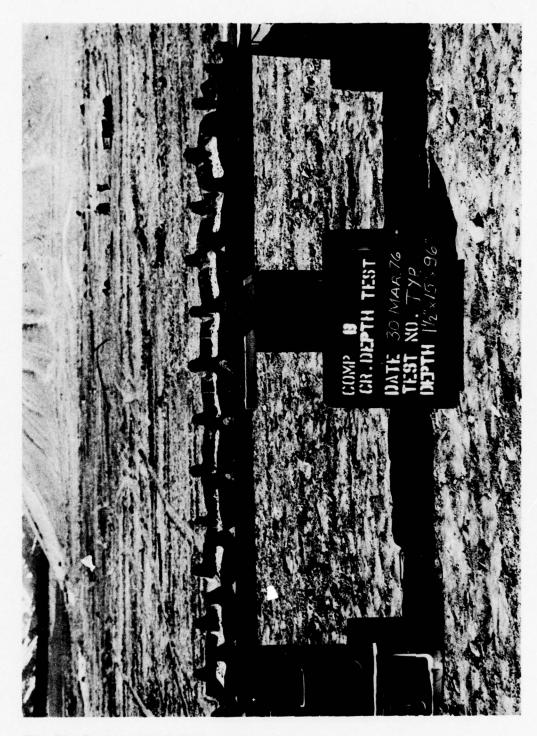


Fig 14 Longitudinal View of Conveyor

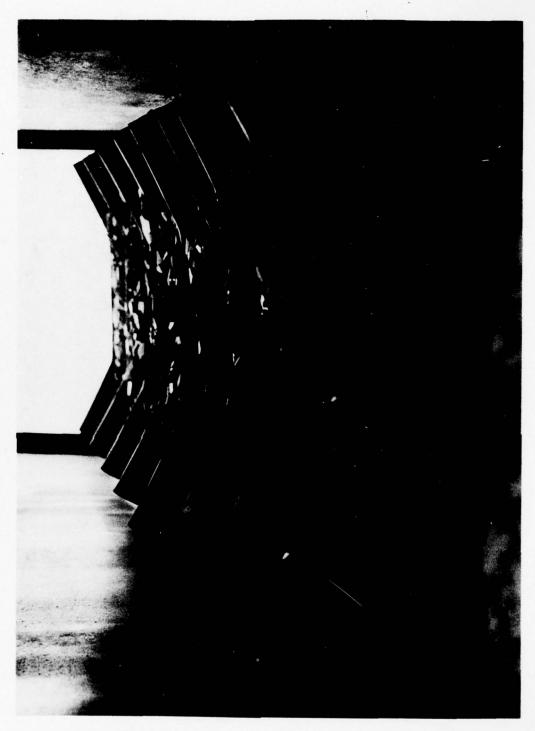


Fig 15 End View of Conveyor

CRITICAL DEPTH TESTS OF COMPOSITION B FLAKE (SERIES 4) TABLE 5

	CONVE	/OR*	EXPLOSIVE	SIVE		
NO.	LENGTH (FT)	WIDTH (IN)	DEPTH (IN)	TOT. WT. (LBS)	BOOSTER	TEST RESULTS
-	8	15	1.5	40	END	CONVEYOR DAMAGED
7	<b>∞</b>	15	1.5	40	END	AT BOOSTER –
က	<b>∞</b>	15	1.5	40	CENTER	NOTE OF STANDARD
4	8	15	1.5	40	END	NO TROPAGE ION
9	8	17	2.0	09	END	H.O.D. PROPAGATION
9	8	15	1.5	40	END	
7	<b>®</b>	15	1.5	40	END	
<b>∞</b>	<b>∞</b>	15	1.5	40	END	
6	9	15	1.5	30	CENTER	
10	80	15	1.5	40	CENTER	
11	6.5	15	1.5	33	CENTER	
12	9	15	1.5	30	CENTER	
13	9	15	1.5	30	CENTER	CONVEYOR DAMAGED
14	9	15	1.5	30	CENTER	AI BOUSIER
15	9	15	1.5	30	CENTER	NO PROPAGATION
16	9	15	1.5	30	CENTER	
17	9	15	1.5	30	CENTER	
28	9	15	1.5	30	CENTER	
19	9	15	1.5	30	CENTER	

\* COMMERCIALLY AVAILABLE RUBBER BELT WITH CORRUGATIONS

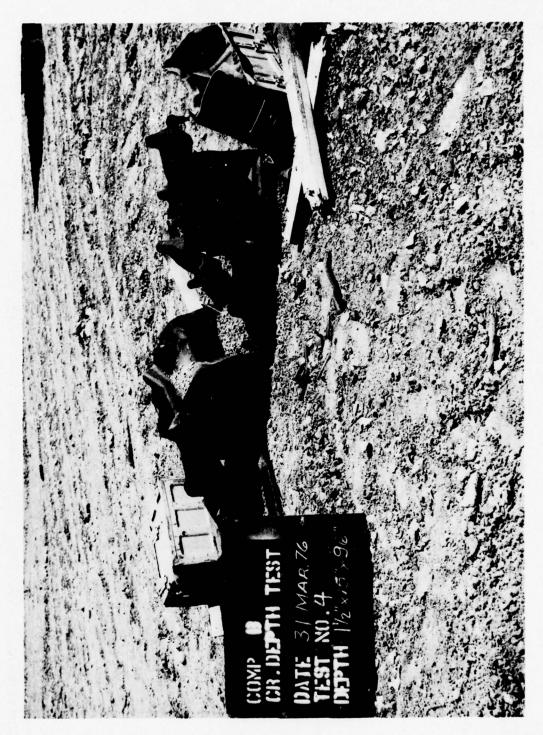


Fig 16 Post Shot View of Conveyor Tests

NON-IDEAL EXPLOSIONS
THE BLAST WAVE FROM LOW ENERGY DENSITY EXPLOSION SOURCES

Roger A. Strehlow

Department of Aeronautical and Astronautical Engineering
University of Illinois
at Urbana-Champaign

### ABSTRACT

Theoretical analyses have shown that gas phase combustion processes which yield blast waves can be adequately modeled using a heat addition - constant gamma - ideal gas working fluid model. In addition, the thermal distribution of energy between the source volume and surrounding atmosphere has been shown to be directly related to the energy density of the source.

Numerical calculations of blast wave behavior using the spherically symmetric nonsteady CLOUD program have shown that

- 1. Low energy density bursting spheres do not exhibit far field equivalency in overpressure but do exhibit this equivalency in positive impulse when Brode's formula is used for scaling.
- 2. A single graphical technique can be used to estimate the overpressure - scaled distance relationship for an idealized bursting sphere.
- 3. The time of energy addition is not too important until it becomes approximately as large as the transit time of a sound wave through the source region.
- 4. Energy density and dimensionless deposition time appear to be natural primary variables for the description of non-ideal blast wave behavior.

# NON-IDEAL EXPLOSIONS THE BLAST WAVE FROM LOW ENERGY DENSITY EXPLOSION SOURCES

by

# Roger A. Strehlow

### Introduction

The majority of accidental explosions are non-ideal in the sense that the blast wave that they produce does not conform to that produced by point source, nuclear or high explosive explosions. At the present time there are many unresolved questions as to how blast wave structure is affected by the source behavior for these explosions. (1) From a practical point of view the primary variables of importance in this respect are maximum overpressure, positive impulse and drag pressure. This is because various combinations of these have been shown to determine how physical damage is caused by different specific blast waves. From a fundamental point of view the questions of importance relate to far field equivalency, energy flows during wave propagation and the development of appropriate scaling laws.

In this presentation recent theoretical work on this problem at the University of Illinois will be summarized and current conclusions as well as future directions of the work will be described.

# Energy Density and Deposition Time

In the study of non-ideal blast waves we must concern ourselves with the way that the non-ideality of the source affects the wave. Point source, nuclear or high explosive sources have two things in common. The energy density of the source is extremely high and the deposition time is extremely rapid. It is well known that the blast wave produced by each of these sources are self similar once the shock overpressure is below about 100 atmospheres; furthermore, well tested, valid scaling laws have been developed for these "ideal" explosions. (2)

In general, non-ideal explosions are those where source energy density is low and/or energy deposition time is long. Actually there are an infinite number of non-ideal source behaviors available and these should yield blast waves with an infinite number of different structures, all of them non-ideal. For example, wave addition of energy, either as a deflagration or detonation wave frequently occurs in accidental explosions and should yield blast waves with a different structure than those produced by the relatively homogeneous addition of energy that a spark produces.

A large variety of accidental explosions of practical importance to the chemical industry involve a source fluid which behaves sufficiently like an ideal gas so that it can be modeled as one. Gaseous reactor explosions due to runaway chemical reactions, bursting vessels and vapor cloud explosions, either deflagrative or detonative, are a few that fall in this catgory. Furthermore, these can best be modeled in a self-consistent manner if one replaces the chemical processes by simple heat addition to the fluid (now an ideal gas) where the spatial and temporal functions for heat addition are chosen to closely approximate the actual deposition process that occurs in nature.

A major justification for this approach is obtained when one examines the Hugoniot curve for strictly one dimensional heat addition processes and compares it to the real Hugoniot for the complete combustion of different

fuels. (3, 4) The Hugoniots for heat addition to a constant gamma gas are rectangular hyperbolas in the (P, V) plane with asymptotes of  $P/P_1 = -(\gamma-1)/(\gamma+1)$  and  $V/V_1 = (\gamma-1)/(\gamma+1)$ . (5) Over the pressure range of  $1 < P/P_1 < 20$  one finds that the real Hugoniot for any fuel-air mixture can be fitted to such a rectangular hyperbola in the P,V plane with an accuracy of about 0.25%, yielding an effective value of q and  $\gamma$  for that particular source mixture. (4) The quantity, q, in this case is a dimensionless energy density, i.e.,  $q = Q/nC_VT_1$ , where Q is energy added per mole of mixture, n = number of moles of mixture,  $C_V = R/(\gamma-1)$  and  $T_1$  is the initial temperature of the gas at  $P_0$ ; the ambient pressure. The values of q and  $\gamma$  for six common fuels in stiochiometric mixtures with air are given in Table I. It should be mentioned that both the value of q and  $\gamma$  vary with equivalence ratio. Also, these values are rather easy to calculate for any combustible mixture, based on full chemical equilibrium in the final state.

The time over which energy is added to the source region also determines the structure of the blast wave. (4) Let us consider two idealized limit cases. In the first case, the bursting sphere may be considered to be an example of the infinitely rapid addition of energy to a source volume. Consider a sphere containing an ideal source gas at pressure P<sub>0</sub> and some fictitious low temperature T<sub>1</sub>. If one instantaneously adds energy to this volume to raise its temperature to the initial temperature of the bursting vessel and its pressure to the initial pressure of the bursting vessel the energy that one must add is

$$Q = NC_V(T_1 - T_1') = \frac{(P_1 - P_0)V}{Y - 1}$$
 (1)

where  $\gamma$  is the gamma of the gas in the sphere. In this case the energy

density is given by the equation

$$q = \frac{P_1}{P_0} - 1 = \frac{T_1}{T_1^*} - 1. \tag{2}$$

Eqn 1 is Prode's formula for the energy stored in a bursting sphere. (6)

If one calculates the fraction of this energy that is transmitted to the surroundings for the idealized process where the sphere expands slowly against a counter pressure equal to its instantaneous pressure one finds that

$$\frac{E_{s}}{Q} = \frac{1}{q} \left[ (1+q) - (1+q)^{1}/\gamma \right]$$
 (3)

This is Brinkley's (7) or Baker's (2) formula for the effective quantity of energy stored in the sphere expressed as a fraction of Brode's energy. Thus, in the limit as  $q \to \infty$  for fixed Q (point source),  $E_g/Q \to 1$  for a sphere while in the limit  $q \to 0$  for fixed Q,  $E_g/Q \to (\gamma-1)/\gamma$ .

If one now considers a second limit case where the energy is added to the source volume homogeneously, but infinitely slowly, the pressure of the source region would remain at  $P_0$  and the energy transmitted to the surroundings would be given by the equation

$$E_{A}/Q = (\gamma - 1)/\gamma \tag{4}$$

irrespective of the source volume. This is exactly the limit for the infinitely rapid addition of energy to a very large volume, even though the two processes are quite different. Notice that in both of these limit cases, i.e.,  $q \to 0$  for the bursting sphere or time of addition infinitely slow, there would be no blast wave.

Specific Cases that have been Considered

For all the cases discussed in this section, the time-dependent blast wave structure was calculated using the CLOUD program, modified to allow heat addition along particle paths.\* This program is a Lagrangian, artificial viscosity numerical program which calculates the flow structure along constant time lines. In all cases calculated thus far, we have started the calculation with an arbitrary initial pressure distribution, but with the flow velocity, u = 0 over all space. With these initial conditions we have not observed any instabilities in the output. In all cases the surrounding gas was assumed to be an ideal gas with a gamma of 1.4.

### Case I: The Bursting Sphere

Eleven cases have been calculated over the range 5 < q < 100 with a number of different  $T_1/T_0$ 's and  $\gamma = 1.2$ , 1.4, and 1.667.(8) The numerical results agreed well with the assumption that the initial pressure at the contact surface that separated the source region from the surroundings could be calculated by invoking the one dimensional shock tube formula.

The curves for overpressure always start at pressures lower than point source pressures and remain below the point source curve for some distance. Furthermore, they tend to parallel each other. This allowed us to develop a general graphical method of predicting overpressure versus scaled radius for all ideal sphere bursts. A dimensional analysis\*\* showed that the important correlating variables are  $P_1/P_0$ ,  $\gamma/\gamma_0$  and  $a_1/a_0$ , where the subscript

The CLOUD program was obtained from Professor Oppenheim, University of California at Berkeley and was modified to allow arbitrary heat addition along particle paths in the source region with the help of Professor L. D. Savage of the Mechanical Engineering Department, UIUC.

Performed by Dr. W. E. Baker, SwRI, San Antonio, Texas.

o means atmospheric conditions.

Figure 1 contains a set of curves which were constructed from the calculations by smoothing. Overlaying these curves are three straight lines of slope (-3) and a number of dashed lines representing two examples of how one would determine the proper overpressure - scaled distance curve for a specific gas and pressure in the sphere. The straight lines of slope (-3) were constructed as follows. Eqn 1 may be written

$$1 \log_{10} \overline{R}_{SP} = \frac{1}{3} \log_{10} \overline{P}_{SP} + \frac{1}{3} \log_{10} \frac{4\pi}{3(\gamma_1 - 1)}$$
 (5)

where  $\overline{R}_{SP} = r_0/R_0$  and  $\overline{P}_{SP} = (P_1 - P_0)/P_0$ . The three lines are plots of Eqn 5 for  $\gamma = 1.2$ , 1.4 and 1.667. Points A and C on Figure 1 represent the dimensionless sphere radii and pressure level,  $\overline{R}_{SP}$  and  $\overline{P}_{SP}$ , for a sphere filled with Helium at  $T_2 = T_0$  and  $P_2/P_0 = 50$  and one filled with air at  $T_2 = T_0$  and  $T_2/P_0 = 20$  respectively.

After one finds  $\overline{P}_{SP}$  and  $\overline{R}_{SP}$ , one must determine the contact surface pressure for the particular sphere gas/surround gas combination which is under consideration, in order to calculate the starting location for a graphical determination of  $\overline{P}_{S}$  vs  $\overline{R}_{S}$ . The equation for this pressure ratio is given in Liepman and Roshko (9) and is repeated here as Eqn 6. Using our notation their equation becomes

$$\frac{P_1}{P_0} = \frac{P_S}{P_0} \left[ 1 - \frac{(\gamma - 1)(a_0/a_1)(P_S/P_0 - 1)}{\{2\gamma_0[2\gamma_0 + (\gamma_0 + 1)(P_S/P_0 - 1)]\}^{1/2}} \right]^{\frac{-2\gamma}{(\gamma - 1)}}$$
(6)

Since Eqn 6 contains the desired unknown, the initial shock pressure,  $P_1/P_0$ , implicitly, it must be solved by an iterative technique. Also, since in Figure 1,  $\log_{10} \left[ (P_2 - P_0)/(P_8 - P_0) \right] = \xi$ , a relative pressure

drop due to contact surface requirements, and  $\xi$  represents a vertical distance irrespective of pressure level, it is appropriate to determine  $\xi$  as a function of  $(P/P_0)$ ,  $(a/a_0)$ ,  $\gamma$  and  $\gamma_0$ . Note here that since  $\gamma$  and  $\gamma_0$  do not appear as simple ratios in Eqn 6 they must be uniquely specified to perform a calculation. However, since  $P/P_0$  and  $a/a_0$  appear only as ratios initial values need not be specified. We chose  $\gamma_0$  = 1.4 and thus limit ourselves to an external atmosphere with this value of gamma. There is no limitation on either  $P_0$  or  $a_0$  for this calculation.

Figure 2 is a plot of  $\xi$  for  $\gamma_0$  = 1.4 over a large range of  $a/a_0$  and  $\gamma$  values and over a sphere pressure range,  $\overline{P}_{SP}$ , of from 4 to 124. Figure 3 contains the results of the same calculation for seven different common gases in the sphere.

Either Figure 2 or Figure 3 may be used to determine an appropriate value of  $\xi$  for any set of initial conditions. Using Figure 3 to continue working our example we find values of  $\xi$  = 0.68 for He and 0.83 for Air. When we plot these vertical distances on Figure 1 we obtain points B and D respectively. Points B and D represent the starting points for determining the  $\overline{P}_{\xi}$  versus  $\overline{R}_{\xi}$  relationship for these two cases.

Note from Figure 1 that for high sphere pressures, Brode's formula for calculating the energy yields the correct far field values. That is, far field equivalency is obtained for these cases. Also note that for low sphere pressures (i.e., for low energy densities) the overpressure curves systematically remain below that for a point source wave. Thus it appears that far field equivalency is lost when the initial sphere pressure is low, if the sphere energy is calculated using Brode's formula.

It is interesting to note, Figure 4, that this is not true for

positive impulse. Our results indicate that far field positive impulse is correctly scaled, even for relatively low energy density bursts, if Brode's formula is used for scaling.

Case II: Slow, Homogeneous Addition of Energy

We have performed a number of calculations of the flow field which results from the exponential homogeneous addition of energy to a source volume. (4) In this study, both the energy density and time of deposition were varied by two orders of magnitude. Energy density values were 4, 40 and 400; times of deposition, nondimensionlized to the initial transit time of a sound wave in the source ball, were  $^{T}_{f}$  = 2.0, 0.2 and 0.02 where

$$\tau_{f} = \frac{t_{d}}{t} = \frac{t_{d}^{a_{0}}}{\sqrt{\gamma} r_{0}}$$

The pressure fields that result are illustrated in Figure 5 for the 9 cases considered. Note that the near field shock overpressure is a strong function of the energy density and that for the two most rapid rates of energy deposition it is relatively independent of the rate of deposition. However, where the energy is added with  $\tau_f$  = 2.0 the maximum overpressure is considerably less than for the more rapid addition of energy. The oscillation in the source region for the case q = 400  $\tau_f$  = 2.0 are real and are due to the reflection of waves in the source region during the energy deposition process. Figure 6 is a plot of the dimensionless shock overpressure versus scaled radius for the nine cases illustrated in Figure 5.

Figure 7 is a plot of the dimensionless positive impulses for the 9 cases of Figure 5 plotted versus  $\overline{R}$ . Note that even though near field overpressure is markedly diminished by slow energy deposition, impulse is not.

This result is in agreement with the bursting sphere results discussed earlier.

Figure 8 is a matrix of the 9 cases illustrated in Figure 5. Each dot of the 3 x 3 matrix represents a calculation in energy density-deposition time space. The heavy lines and arrows on this diagram illustrate limit behaviors that we infer as a result of these calculations.

### Current and Future Work

We are currently calculating cases involving wave propagation in the source region. We also plan to calculate sphere bursts followed by subsequent combustion and other possible combination cases as appropriate. We are also attempting to attack the problem of far field equivalency in a general manner.

### Tentative Conclusions

For that class of explosions where the source behavior can be modeled as energy addition to an ideal gas we have learned that

- 1. Not all the energy goes to the surroundings.
- Low energy density bursting spheres do not exhibit far field equivalency in overpressure but do exhibit this equivalency in positive impulse, when Brode's formula is used for scaling.
- A simple graphical technique can be used to estimate the overpressure-scaled distance relationship for an idealized bursting sphere.
- 4. The time over which the energy is added to a source region

is not too important until it becomes approximately equal to or greater than the transit time of a sound wave in the source region.

 Energy density and dimensionless deposition time appear to be natural primary variables for the description of non-ideal blast wave behavior.

# Acknowlegment

The work reported here was supported by NASA Grant NSG 3008, Technical Monitor, Dr. Robert Siewert, Aerospace Safety Research and Data Institute, NASA, and by AFOSR Grant 73-2524, Dr. B. T. Wolfson, Technical Monitor.

### Literature cited

- Strehlow, R. A., and Baker, W. E., "The Characterization and Evaluation of Accidental Explosions," NASA CR 134779, AAE 75-3, (June 1975).
- Baker, W. E., "Explosions in Air," University of Texas Press, Austin, Texas (1973).
- Zajac, L. J., and Oppenheim, A. K., "Thermodynamic Computations for the Gas Dynamic Analysis of Explosion Phenomena," <u>Comb. and Flame</u>, 13 537-550 (1969).
- 4. Adamczyk, A. A., "An Investigation of Blast Waves Generated by Non-Ideal Energy Sources," Ph.D. Thesis, Department of Aeronautical and Astronautical Engineering, University of Illinois, Urbana, IL 61801 (September 1975), 147 pp.
- Strehlow, R. A., "Fundamentals of Combustion." International Textbook
   Co., Scranton, PA (1968), pp. 149-155.
- 6. Brode, H. L., "Numerical Solutions of Spherical Blast Waves," <u>J. Appl.</u>

  Physics 26 766-775, (1955).
- 7. Brinkley, S. R., "Determination of Explosive Yields," AICHE Loss Prevention 3 79-82 (1969).
- 8. Strehlow, R. A., and Ricker, R. E., "The Blast Wave from a Bursting Sphere," Loss Prevention, Vol. 10 (in press).
- 9. Liepman, H. W., and Roshko, A., "Elements of Gas Dynamics." Wiley & Sons, New York (1957), p. 81.
- Zajac, L. J., and Oppenheim, A. K., "The Dynamics of an Explosive Reaction Center. <u>AIAA Journal 9 545-553 (1971).</u>

TABLE I HUGONIOT CURVE FIT DATA

				•	φ = 1.0		
Fuel	AHC Low Value MJ/Kg moles Fuel	ΔH <sub>C</sub> Low Value MJ/Kg Fuel	Q MJ/Kg Fuel	Q MJ/Kg M1x	ъ	Å	Q VH C
H <sub>2</sub>	241.8	120.00	140.80	3.989	5.864	1.173	1.174
*	802.3	50.01	63.98	3.508	7.934	1.202	1.271
C2H2	1256.	48.22	55.21	3.867	8.734	1.195	1.145
C2H4	1323.	47.16	58.49	3.705	8.615	1.199	1.240
C2H40	1264.	28.69	34.41	3.89	9.593	1.203	1.159
C3H8	2044.	46.35	61.60	3.695	9.169	1.208	1.329
					·		

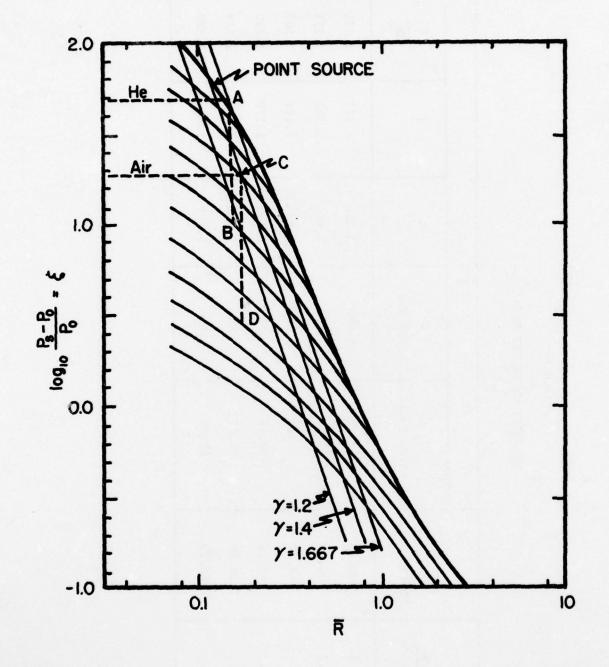


Figure 1. Scaled overpressure versus energy scaled distance for an idealized pressurized sphere burst.

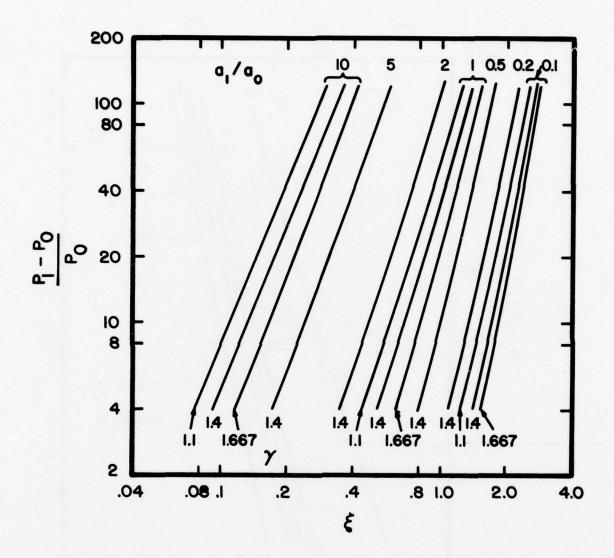


Figure 2. Shock-rarefaction fan contact surface pressure drop for an ideal gas in the sphere.

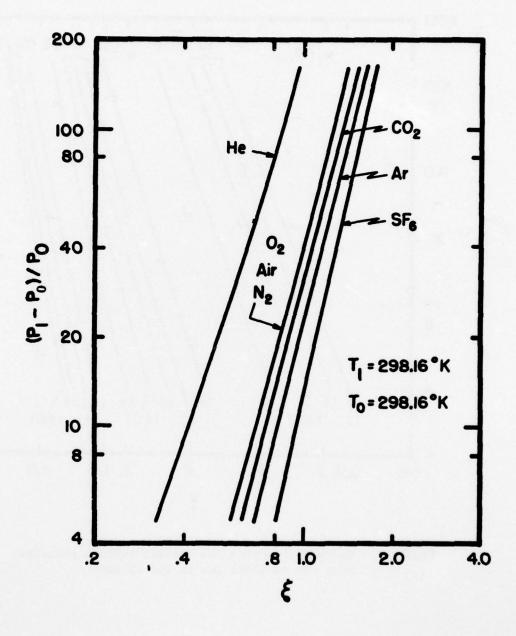


Figure 3. Shock-rarefaction fan contact surface pressure drop for seven different sphere gases.

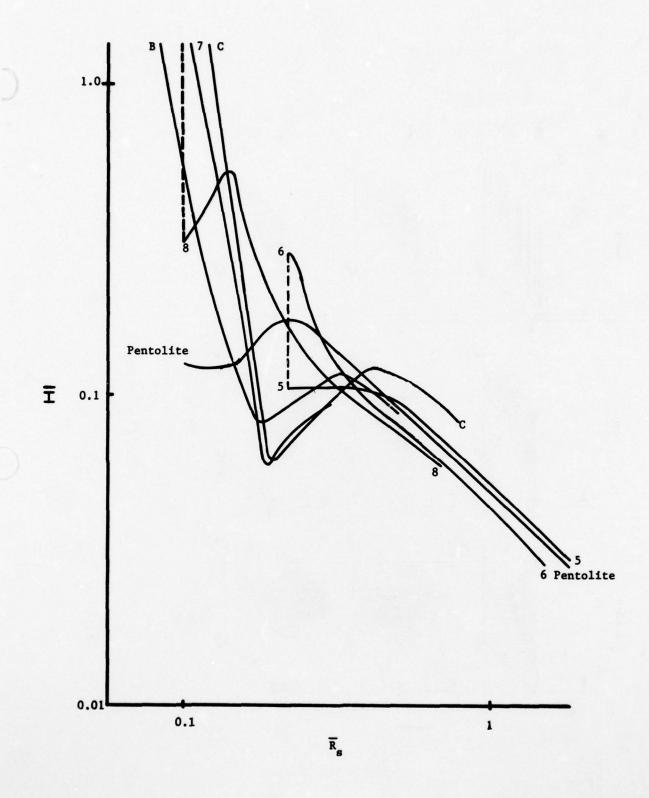


Figure 4. Scaled impulse (Sach's scaling) versus energy scaled distance for an idealized pressurized sphere burst.

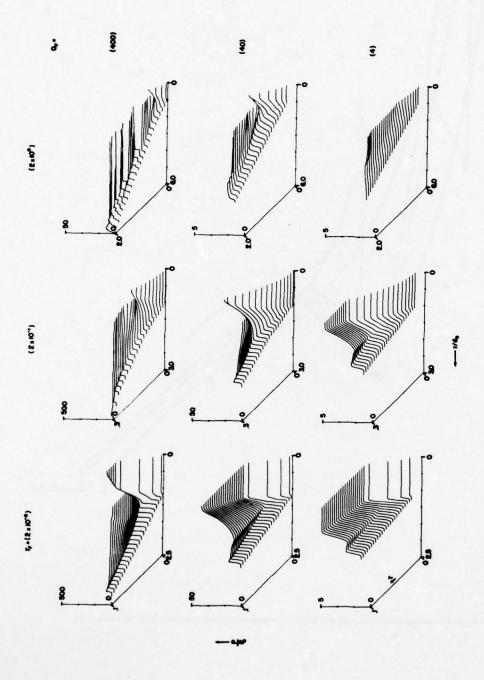


Figure 5. Initial pressure field for nine cases with energy densities of 4, 40 and 400 and deposition times of 0.02, 0.2, and 2.0.

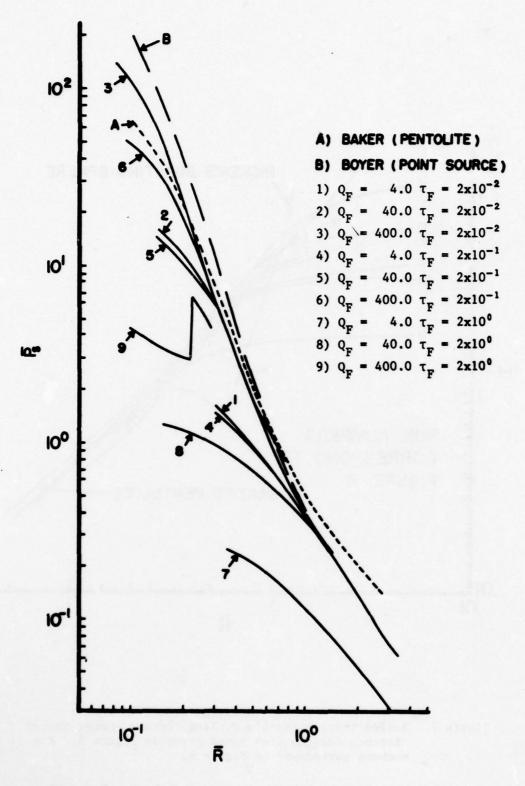


Figure 6. Scaled overpressure versus energy scaled distance for the nine cases given in Figure 5.

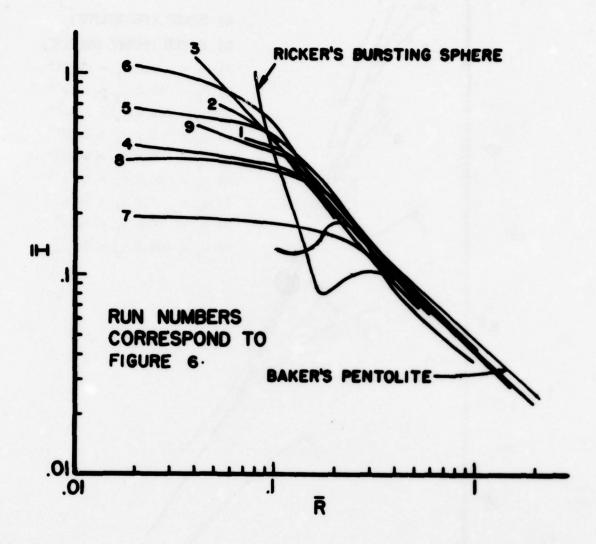


Figure 7. Scaled impulse (Sach's scaling) versus energy scaled distance for the nine cases given in Figure 5. Run numbers correspond to Figure 6.

# BLAST WAVE PROPERTIES - FIXED Q

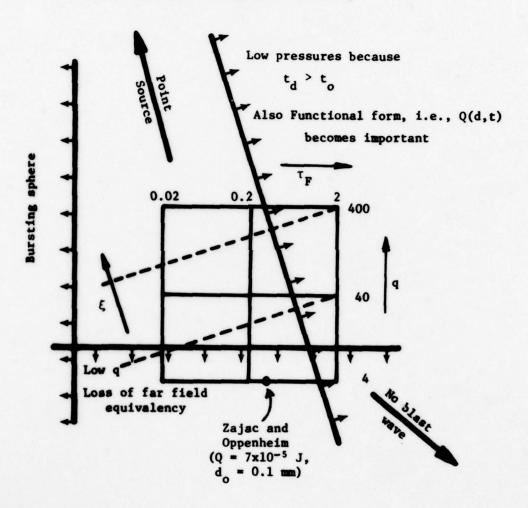


Figure 8. The matrix of points in Figure 5 illustrating the effect of deposition time and energy density of the source on blast wave behavior. The Zajac and Oppenheim point represents the location in this field of one calculation in ref 10 which agrees quite well with our results.

# AIR-TO-WATER BLAST WAVE TRANSFER

# by P. J. Peckham

Naval Surface Weapons Center

# 1. Introduction

Data on the underwater blast waves transmitted across an air-water interface from an explosion in air are limited. Some inconclusive data were generated at the NSWC/WOL in 1962 (References 1 and 2). In addition, data are available from a program in which 12-kg TNT spheres were fired above a water surface and underwater pressures were measured (reference 3). To add to this paucity of data, the NSWC/WOL is conducting a program to study the effects of airblast induced underwater shocks from both cylindrical and spherical charges.

The data discussed here came from pentolite spheres and cylinders weighing either 0.454 or 3.63 kg. The spherical charge data are from centrally initiated spheres fired at scaled burst heights of 0.4 and 1.6 m/kg<sup>1</sup>/3. The cylindrical charge data are from cylinders with a length to diameter ratio of 3.68:1. All cylinders were fired with their major axis normal to the water surface. The point of detonation was on the major axis either at the center of the charge or one quarter of the charge length from the end of the charge toward the water. Scaled burst heights for the cylinders were either 0.4, 1.0, or 1.6 m/kg<sup>1</sup>/3. Data from this investigation will be available in an NSWC/WOL technical report now in the process of publication. Only the data from the cylindrical charges that were centrally detonated are discussed here.

The program was fired in an artificial pond at the NSWC/WOL test facility at Stump Neck, MD. The underwater gage array is shown in Figure 1.1. Airblast gages were flush mounted at the water surface. Seven gage positions were used extending from a point almost directly under the charge out to about 3 meters. Gages were approximately 0.4 m/kg<sup>1/3</sup> apart.

# 2. Comparison of the Airblast Observations

Figure 2.1 shows the airblast overpressures from pentolite spheres plotted as a function of distance along the water surface from a point beneath the charge. Curves for two scaled burst heights are shown; one at 0.4  $m/kg^{1/3}$  and the other at 1.6  $m/kg^{1/3}$ . Note that for either burst height the pressures decay smoothly from a maximum at the point most nearly beneath the charge out to the maximum measured range. Beyond a range of 1.5  $m/kg^{1/3}$ , the data converge into a single curve.

- (1) Swift, E., "Underwater Shockwaves from Explosions in Air," private communication, 4 April 1962.
- (2) Conway, M., "Investigation of the Characteristics of Air-to Water Shocks," private communication, 11 June 1962.
- (3) Sakurai, A., and Pinkston, J., "Water Shockwaves Resulting from Explosions Above and Air-Water Interface," Waterways Experiments Station Report No. 1-771, April 1967.

The airblast overpressures from centrally detonated pentolite cylinders are shown in Figure 2.2. These are also plotted as a function of distance along the water surface from a point directly beneath the charge. Recall, the cylinders were oriented with their axis perpendicular to the water surface. Note that the airblast pressures for the two larger burst heights show a marked decrease at a range of about 0.7 m/kg<sup>1/3</sup>. The pressures from the lowest burst height show no such decrease; nor does the spherical charge data in Figure 2.1.

The dips in the pressure-horizontal range curves for the two higher bursts in Figure 2.2 result from the non-spherical airblast wave front produced by a cylindrical charge explosion. Figure 2.3 shows the fireball silhouette from cylinders at the time that the fireball end lobe has just contacted the water surface. Also shown is the airblast wave front for the lower portion of the cylinder at this time. The fireball outline is traced from a high speed camera frame exposed at the time shown. The airblast wave-form is based on shadowgraph photos of the shock from a 13-gram cylinder fired under similar scaled conditions. These pictures lead to the following description of the airblast shockwave formation by a cylindrical explosion. The explosion products show strong outward motion from the ends of the cylinder along the major or long axis. In addition, outward radial motion off the sides of the cylinder takes the form of a toroid. The explosion product motion along the axis of the cylinder (or end lobe fireball growth) push a bow shock that pictures show to be attached to the explosion products at the bottom. At the same time, the radial expansion of the explosion products generate an airblast shockfront with the general toroidal shape of the explosion products. Where these two shocks would intersect a bridge wave is formed.

Airblast pressures along the water surface show the effects of the above phenomena. The reflected airblast pressures are very intense beneath the charge where the end lobe bow shock undergoes nearly normal reflection. However, as the shock propagates outward, the pressure decreases rapidly because the motion is now parallel to the water surface. (The bow shock shows no evidence of the mach stem formation associated with spherical blast wave reflection.) This rapid decay obtains until the bridge wave and the toroidal shock arrive at the water surface. Their arrival briefly increases the airblast pressures at the water surface, after which, normal pressure-distance decay begins.

The airblast pressures at the water surface from the charge fired at an HOB of 0.61 meters shows no such behavior. The bow shock arrival at the water surface is followed almost immediately by the arrival of the bridge wave and toroidal shock. Their shape in the early phase of development is almost spherical as may be seen in Figure 2.3

# 3. Underwater Blast Field

Underwater blast gages were positioned as shown in Figure 1.1. Note that the gages are positioned in 5 columns. Each column contains three gages, one gage each at scaled depths of 0.4, 0.8, and 1.6 m/kg<sup>1/3</sup> below the water surface. The horizontal separation between the columns was 0.8 m/kg<sup>1/3</sup>. Underwater blast pressure-time histories were recorded from each gage using cathode ray oscilloscopes. These records were digitized and processed on a computer to give pressure, impulse, and energy flux density in the shockwave as a function of time. In this paper, only the shockwave pressure data will be discussed.

The underwater blast field is generated by the reflection of the airblast wave front at the air-water interface. At the lower burst heights the explosion products probably contribute energy to the underwater blast. The surface area over which the airburst makes its contributions to the underwater blast field is generally very small for a spherical explosion and even smaller for a cylindrical explosion. For the spherical burst, the above area is that where regular reflection occurs. For a cylindrical explosion, the area is limited to that where the end lobe shockwave and explosion products strike the water, although the toroidal shock (Figure 2.1) makes a small contribution at positions well away from Surface Zero.

The underwater shock wave pressure-time histories induced by an airburst are similar to those from a shallow underwater explosion with two exceptions. First, they are made up of multiple pressure pulses. (See Figure 3.1) These multiple pulses result in part from the perturbations on the airblast shockfront and the explosion products front. These perturbations reflecting off the interface act as separate sources for the underwater shockwave. Thus, the underwater pressure-time history shows a number of pressure peaks corresponding to the arrival of the shock generated by each perturbation. However, the above explanation may not account for all the spikes on the pressure-time histories. Hydrocode calculations show the possibility of a reverberation of the airshock between the product front and the water surface.

Underwater pressure-time histories recorded from a cylindrical air burst are shown in Figure 3.2. The pulse from the toroidal shock is seen in the pressure trace taken farthest from Surface Zero for the burst height of 1.6 m/kg $^{1/3}$ .

Figures 3.3 through 3.7 compare the airblast pressures measured at the air-water interface with those measured underwater at a depth of 0.4 m/kg $^{1/3}$ . Figures 3.3 and 3.4 are for spherical charges fired at burst heights of 0.4 and 1.6 m/kg $^{1/3}$ , respectively. The underwater pressures directly below the charge are down by a factor of two from the airblast pressure measured at the surface. However, as horizontal range increases, the underwater pressures rise

above the measured airblast pressures for the 0.4 m/kg $^{1/3}$  burst height (Figure 3.3). The underwater pressures for the burst height of 1.6 m/kg $^{1/3}$  in Figure 3.4, remain below the measured airblast pressures.

Figure 3.5 compares the airblast measured at the surface with the pressures measured underwater from a cylindrical charge burst at a height of 0.4 m/kg $^{1/3}$ . Here, the underwater pressures follow somewhat closely, the measured airblast. Figure 3.6 compares airblast and underwater pressures from a cylinder burst at a height of  $1.0 \, \text{m/kg}^{1/3}$ . In this case, there is reasonable agreement between the underwater and airblast pressures for a cylindrical burst at a height of 1.6 m/kg $^{1/3}$  (Figure 3.7).

The above behavior fits no simple model for underwater shockwave generation by an airburst. However, computer models are being developed and a model will be reported at a later date.

Finally, all the underwater blast pressure data obtained to date are summarized in Figures 3.8 through 3.11. These data are plotted as isopressure contours.

# 4. Summary

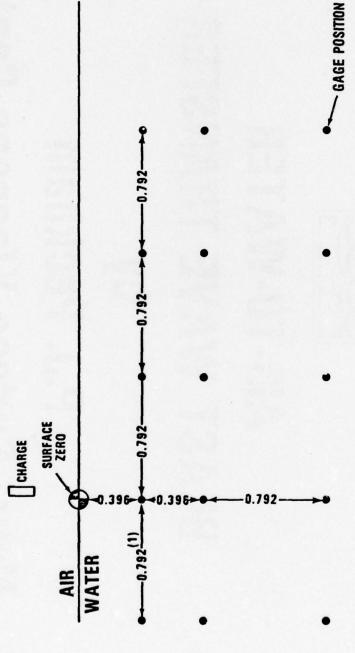
Some preliminary results from a program to measure the underwater blast field produced by an explosion in air have been presented. There are differences between the blast field from cylinders and spheres but they cannot be generalized. For a burst height of 0.4 m/kg<sup>1/3</sup>, the underwater blast fields are similar for cylinders and spheres. For the higher burst heights, the cylinders seem to generate a blast field giving the appearance of having come from a smaller more intense source than does the field from a spherical explosion.



# Naval Surface Weapons Center BLAST WAVE TRANSFER AIR-TO-WATER J. Peckham



# UNDERWATER GAGE ARRAY FOR POND PROGRAM

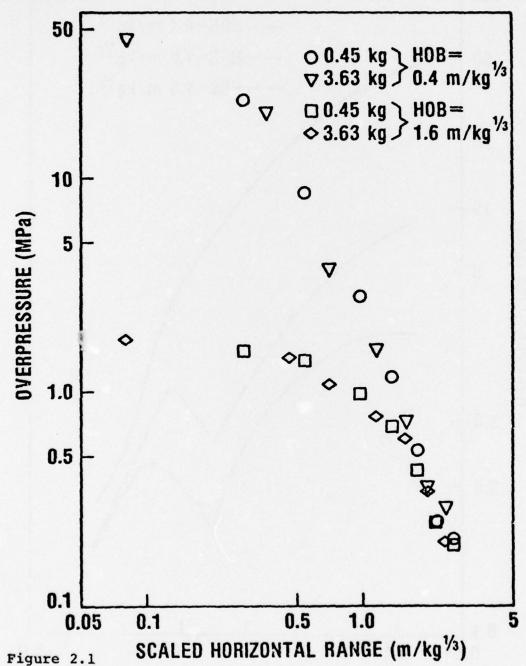


# POND BOTTOM (2)

- (1) DISTANCES ARE IN METERS/KILOGRAMS 1/3
- (2) POND BOTTOM 0.46 METERS FROM LOWEST GAGE ON 3.63-KG CHARGE ARRAY POND BOTTOM 1.68 METERS FROM LOWEST GAGE ON 0.45-KG CHARGE ARRAY

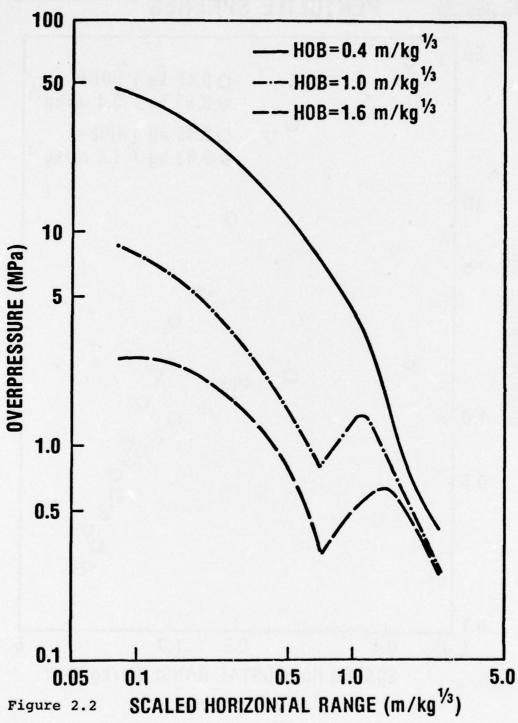


# AIRBLAST PRESSURE FROM PENTOLITE SPHERES



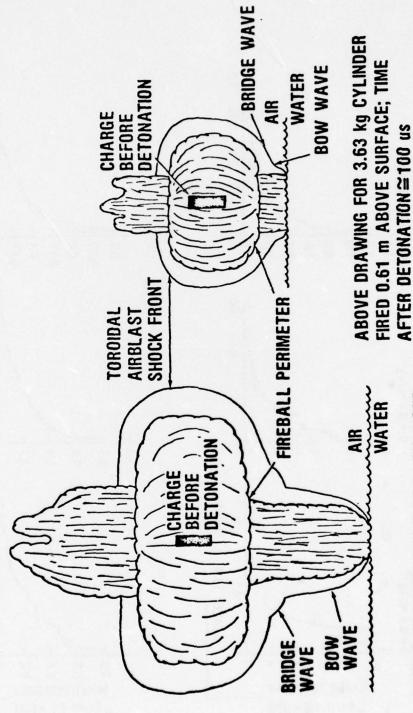


# AIRBLAST PRESSURES FROM PENTOLITE CYLINDERS





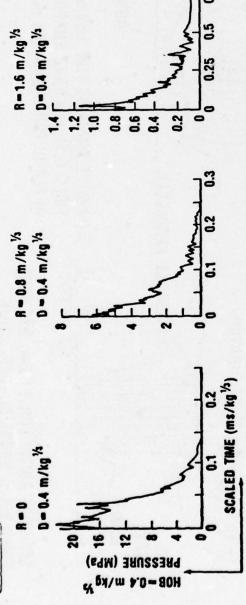
# CYLINDRICAL CHARGE FIRED IN AIR NEAR A WATER SURFACE FIREBALL-SHOCKWAVE RELATION FOR

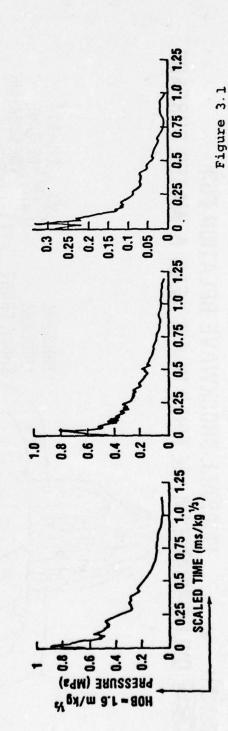


ABOVE DRAWING FOR 3.63 kg CYLINDER FIRED 1.5 m ABOVE SURFACE; TIME AFTER DETONATION≅360 us

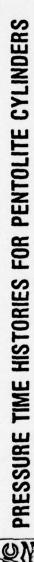
Figure 2.3

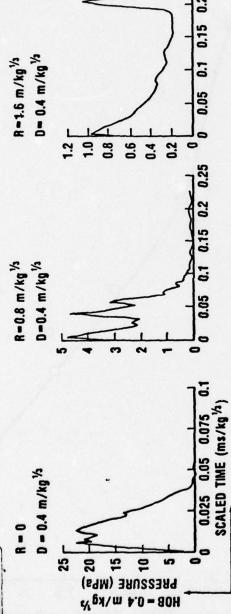
PRESSURE TIME HISTORIES FOR PENTOLITE SPHERES

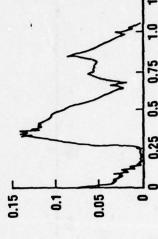












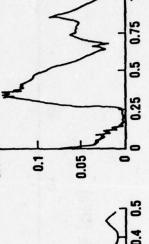
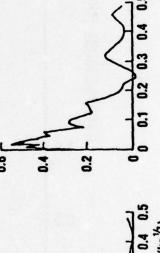
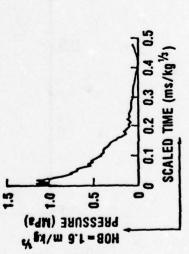


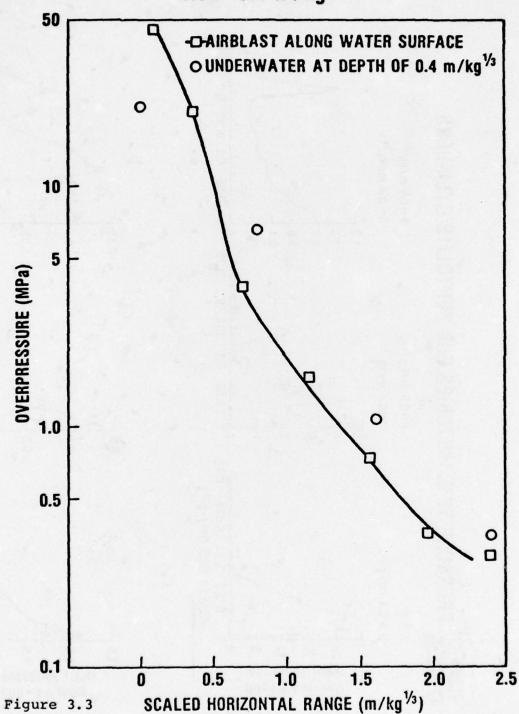
Figure 3.2





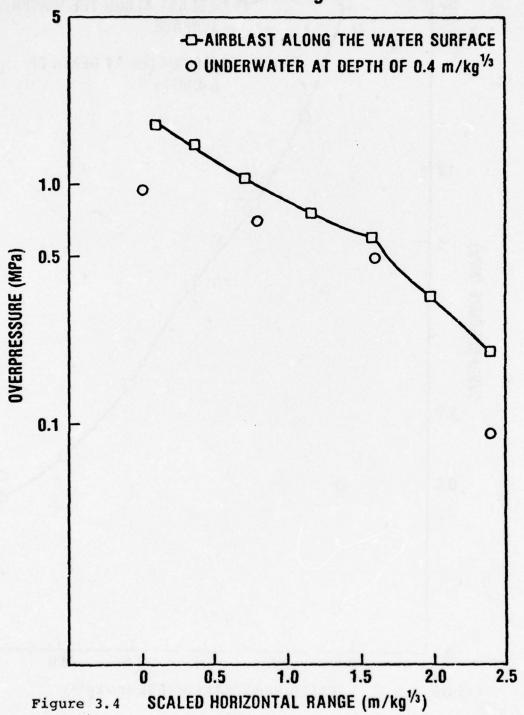


# COMPARISON OF AIRBLAST AND UNDERWATER PRESSURES; PENTOLITE SPHERES FIRED AT $HOB\!=\!0.4~m/kg^{1/3}$



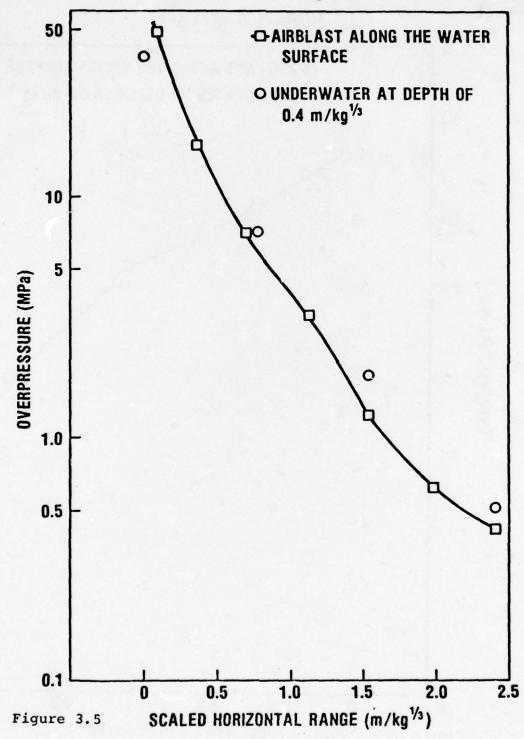


# COMPARISON OF AIRBLAST AND UNDERWATER PRESSURES; PENTOLITE SPHERES FIRED AT $HOB=1.6~m/kg^{1/3}$



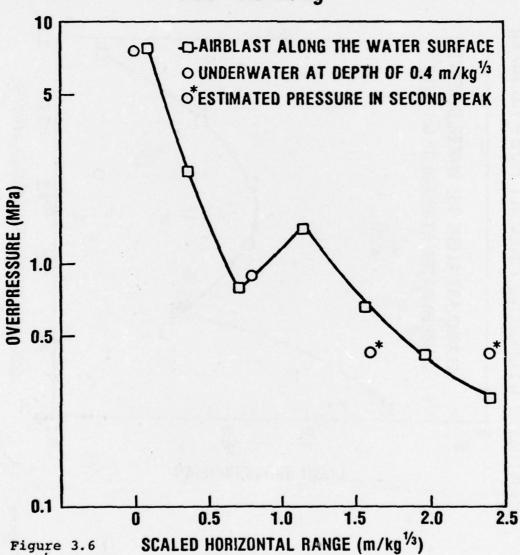


# COMPARISON OF AIRBLAST AND UNDERWATER PRESSURES; PENTOLITE CYLINDERS FIRED AT HOB=0.4 m/kg<sup>1/3</sup>



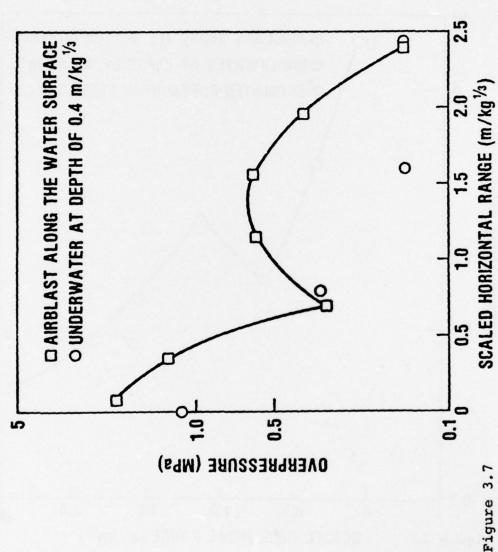


# COMPARISON OF AIRBLAST AND UNDERWATER PRESSURES; PENTOLITE CYLINDERS FIRED AT $HOB=1.0~m/kg^{1/3}$



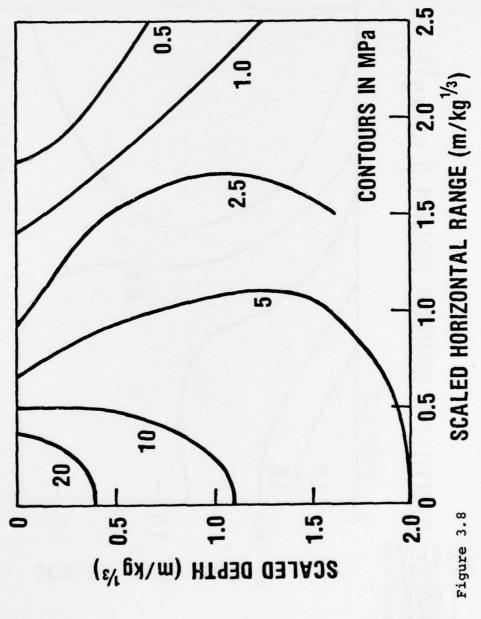


# COMPARISON OF AIRBLAST AND UNDERWATER PRESSURES; PENTOLITE CYLINDERS FIRED AT HOB=1.6 m/kg<sup>1/3</sup>

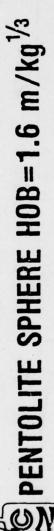


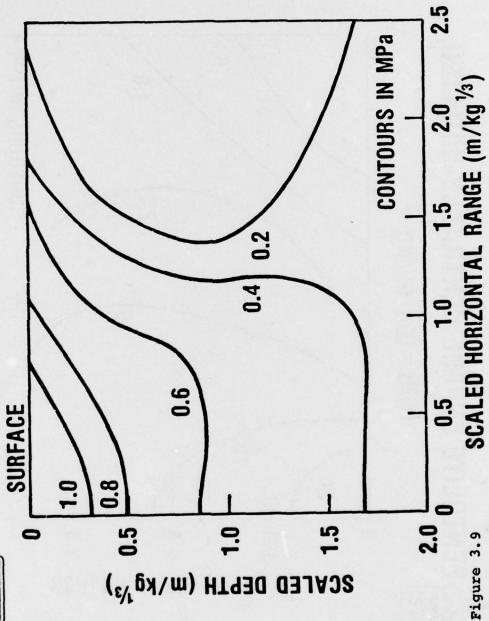


# PENTOLITE SPHERE CENTRALLY INITIATED, $H0B = 0.4 \text{ m/kg}^{1/3}$



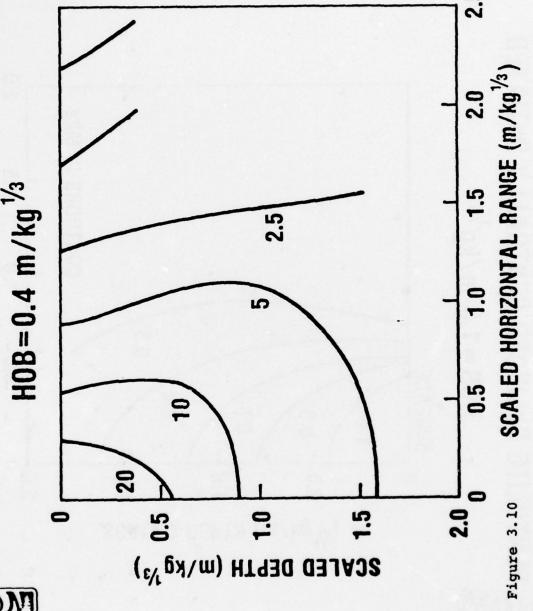














# PENTOLITE CYLINDER CENTRALLY INITIATED

 $H0B = 1.6 \text{ m/kg}^{1/3}$ 

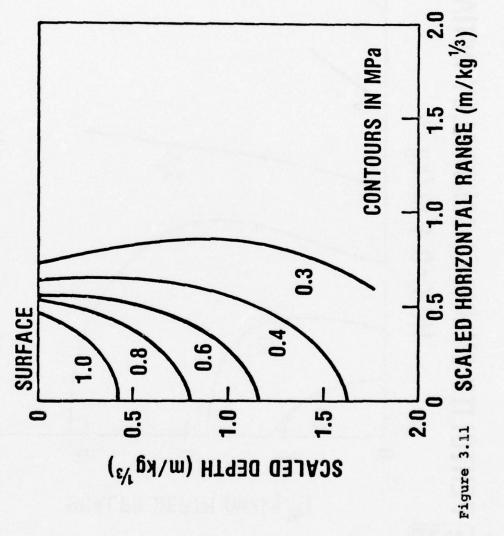


Figure 3.11

### BLAST PARAMETERS FROM EXPLOSIONS IN MODEL EARTH COVERED MAGAZINES

by

Charles N. Kingery George A. Coulter

### **ABSTRACT**

This report contains the results obtained from a series of high explosive tests designed to determine the blast parameters around a 1/50 scale model of an earth covered munition storage magazine. The tests were conducted using hemi-cylindrical pentolite charges of scaled weights to simulate the effects of an accidental explosion occurring in standard munition magazines when filled with 100,000, 300,000, and 500,000 pounds of explosives. The thickness of the earth cover was varied to determine the blast attenuation associated with double the standard earth cover thickness, the standard earth cover and one-half the standard earth cover thickness relative to no earth cover. Excellent correlation was obtained with limited data from one full-size storage magazine test.

USA BALLISTIC RESEARCH LABORATORY
ABERDEEN PROVING GROUND, MARYLAND 21005

### I. INTRODUCTION

### A. Background

This report covers a general study sponsored by the Department of Defense Explosive Safety Board (DDESB) to establish the effect of earth cover on the blast parameters generated from accidental explosions in munition storage magazines. This kind of study would be prohibitively expensive to do with full-size magazines and large amounts of explosive, but in theory, the relative effects could be documented using scaled models and high explosive charges.

The Ballistic Research Laboratory (BRL) proposed to conduct a series of model tests and relate the results to effects that might be expected from full-size magazines. This proposal was accepted and funded by DDESB.

# B. Objectives

The primary objectives of the proposed tests were as follows:

- 1. Determine the blast parameters propagating along blast lines extending to the front, side, and rear of a 1/50 scale model magazine with a standard earth cover.
- 2. Determine the effect on blast parameters when the earth cover was varied from no cover, to one-half the standard cover, and to double the standard cover.
- 3. Determine the effect on blast parameters when the amount of explosive stored in the magazine was varied.

### II. TEST PROCEDURE

The procedures used to meet the objectives were to, first design the model magazine, second design the high explosive charge weight and configuration, and third establish the instrumentation and blast lines.

### A. Model Magazine Design

The standard munition storage magazine being modeled for this series tests is shown in Figure 1. The overall width is 90 feet (27.43 metres) with a length of 95 feet (28.96 metres). The total volume of the earth cover for this size magazine is 58812 feet  $^3$  (1665 m $^3$ ), while the interior volume is approximately 17,500 feet  $^3$  (496 m $^3$ ). The 1/50 scaled model designed for this project is presented in Figure 2. All linear dimensions have been scaled by a factor of 50. This makes the volume of the earth cover for the model 0.47 feet  $^3$  (.0133 m $^3$ ) and the internal volume of the model is 0.14 feet  $^3$  (.00396 m $^3$ ). A photograph of the interior portion of the model without the earth cover is shown in Figure 3. The model

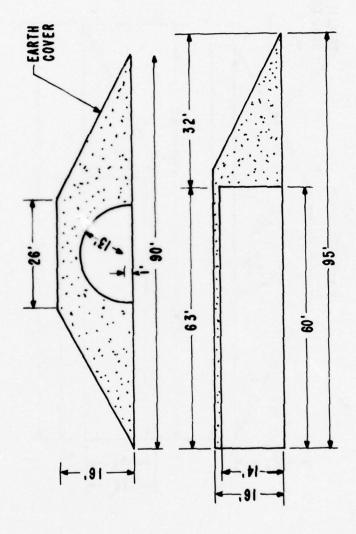


Figure 1. Standard Munition Storage Magazine

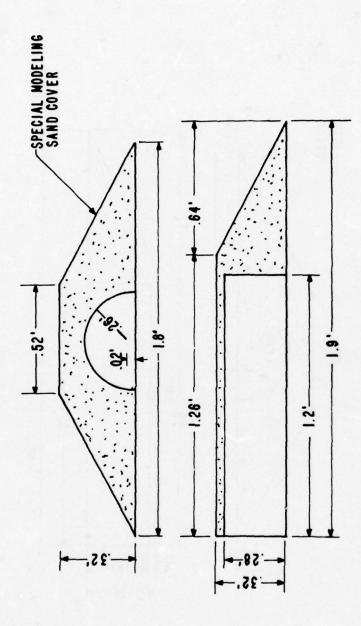
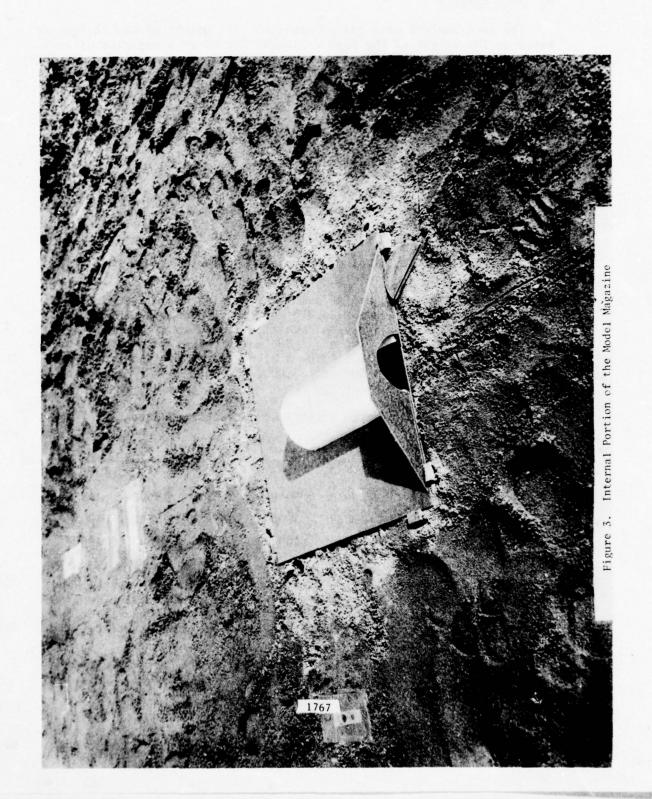


Figure 2. 1/50 Scaled Model Munition Storage Magazine



magazine with earth cover is shown with the first two gage stations for each line in Figure 4.

# B. Test Charges

The test charges were cast pentolite. The weight of the charges was based on the weight of the high explosive stored in a magazine of specified volume. The ratio of the charge weight to storage volume should be the same when scaling from the full size structure to a model structure.

$$\frac{W}{V} = \frac{W_{M}}{V_{M}} , \qquad (1)$$

where

W = Weight of munition explosive,

V = Volume of Standard Magazine

 $W_{M}$  = Weight of model charge, and

 $V_{M}$  = Volume of Model Magazine.

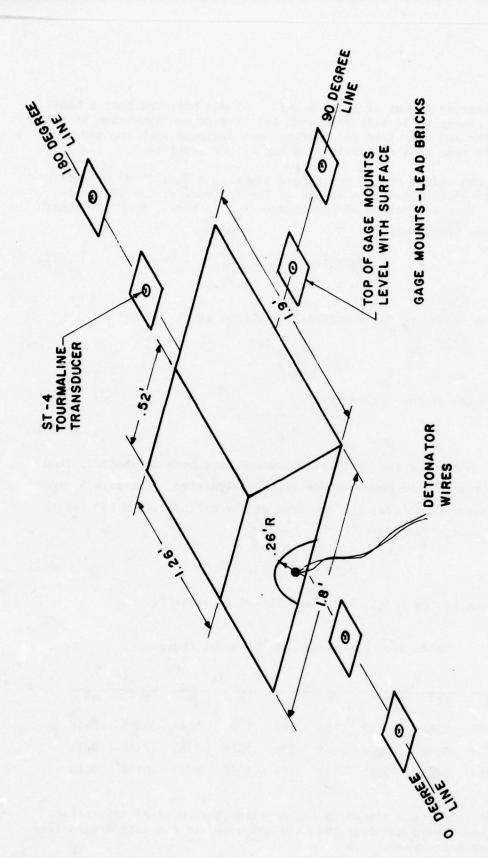
The program was designed to simulate the blast from the accidental explosion of 500,000 pounds (226,800 kg), 300,000 pounds (136,080 kg), and 100,000 pounds (45,360 kg) of munition stored in a magazine having a volume of 17,500 feet<sup>3</sup> (496 m<sup>3</sup>). The model charge weights were determined as presented in Table I. The scaling factor for the model volume and the charge weights is  $50^3$  or 125,000.

Table I. Charge Weights and Structure Volumes

W <sub>M</sub>		V <sub>M</sub>		1	W	V	
1b	kg	ft <sup>3</sup>	m <sup>3</sup>	1b	kg	ft <sup>3</sup>	m <sup>3</sup>
4.0	1.814	0.14	.00396	500000	226800	17500	496
2.4	1.088	0.14	.00396	300000	136080	17500	496
0.8	.363	0.14	.00396	100000	45360	17500	496

After the volume of the 1/50 scale model magazine was established, then the charge weights were determined and the configuration designed. There are data available on the airblast propagation from cylindrical charges (Reference 1) resting horizontally on the ground surface, with

R. Reisler, L. Giglio-Tos, and G. Teel, "Air Blast Parameters from Pentolite Cylinders Detonated on the Ground," BRL MR-2471, April 1975. AD #B003883L.



MODEL MAGAZINE TO TH SCALE

Figure 4. Model Magazine 1/50th Scale

length to diameter ratios of 3, 6, and 12. It was believed that a hemicylindrical charge would best represent the storage configuration in a model magazine and therefore the charges were designed with the end surface area the same as a cylindrical charge of L/D equal to 3.

Knowing the weight of the charge and assuming a density of pentolite of 103 lb/ft $^3$  (1.65 g/cm $^3$ ) the volume of the cylindrical charge can be calculated. When the volume of the charge ( $V_c$ ) is known, then the other dimensions can be calculated.

$$V_c = \pi r_c^2 L \text{ for } L/D = 3$$
 $L = 6r_c$ 
(2)

Therefore the radius r for a cylindrical charge is

$$r_c = \left(\frac{V_c}{6\pi}\right)^{1/3}$$

and the end area of the cylindrical is

$$A_{c} = \pi r_{c}^{2}. \tag{3}$$

When  $A_c$ ,  $r_c$ , and L for the cylindrical charge have been determined, then the radius,  $r_h$ , for the hemicylinder can be calculated. The area  $A_h$  for the hemicylinder must equal  $A_c$ , the area of the cylinder, for the length L to be the same. Therefore,

$$r_{h} = \left(\frac{2A_{c}}{\pi}\right)^{1/2} \tag{4}$$

The dimensions of the model charge are listed in Table II.

Table II. Dimensions of the Model Charges

W <sub>h</sub>		$v_h$		L <sub>h</sub>		$r_h$		A <sub>h</sub>	
1b	kg	ft <sup>3</sup>	m <sup>3</sup>	ft	m	ft	m	ft <sup>2</sup>	m <sup>2</sup>
4.0	1.814	.0388	.00110	.763	.229	.1798	.0548	.0508	.0046
2.4	1.088	.0233	.00066	.644	.196	.1518	.0463	.0362	.0034
0.8	0.363	.0078	.00022	.447	.136	.1052	.0321	.0174	.0016

When the charge was placed in the magazine the point of initiation was on the end toward the door and this was noted as the zero degree line for the blast measurements.

# C. Test Instrumentation

The details of the complete instrumentation systems will be presented in this section. The system includes 1) the pressure transducer, 2) the amplifier, and 3) the recorder. Because of the small charges used and the requirement for close-in documentation; i.e., high overpressures, two instrumentation systems were utilized.

- 1. Oscilloscope Recorder System Three Tektronix 565 dual beam oscilloscopes were used to record the pressure versus time from six stations. Susquehanna Instruments Model ST-4 piezo gages with tourmaline sensors were the primary transducers used throughout the series of tests. The signal from the gage and source follower was fed directly into the oscilloscope where it was displayed on a video tube and photographed on a high contrast poloroid film. The analog display on the film was converted into a digital format using a film reader and punching IBM cards which were then processed through a computer. The digitized data was then tabulated and plotted. A block diagram of the oscilloscope recorder system is presented in Figure 5.
- 2. Tape Recorder System The tape recorder consisted of four basic units. The gages which have already been described, the power supply and voltage calibrator, the amplifier, and the FM recorder. The FM tape recorder used was a Honeywell 7600 having a frequency response of 80 kHz. Once the signal was recorded on the magnetic tape it was played back and recorded on a CEC-5-124 oscillograph for a quick look at the records. The analog signal on the magnetic tape was processed for an automatic digital conversion and was then programmed through the computer for a digital output which was tabulated and plotted. The tape recorder system and other field instruments are shown in Figure 5.

# D. Test Layout

A requirement to meet the stated objectives is to measure the blast parameters at the current safe separation distances between storage magazines. Therefore, the blast lines, see Figure 6, were installed to measure overpressure and impulse in three principal directions in the near field. Stations to the front (0 degree line) should start at a scaled separation distance of 2 ft/lb $^{1/3}$  (.8 m/kg $^{1/3}$ ) and extend out to about 10 ft/lb $^{1/3}$  (4 m/kg $^{1/3}$ ). Stations to the rear (180 degree line) should start at and end at the same distances. The gage line extending from the side of the structure (90 degree line) should start at a scaled distance of 1.25 ft/lb $^{1/3}$  (.5 m/kg $^{1/3}$ ), and extend out to 50 ft/lb $^{1/3}$  (20 m/kg $^{1/3}$ ). The separation distance is measured from the internal wall of the steel arch for side to side separation distances and from the end walls for front and back separations rather than the center of the storage area. The gage station distances were measured from the geometric center of the flat side of the charge and therefore an adjusted distance of .26 feet (.079 m) was added to the separation distance on the 90 degree line

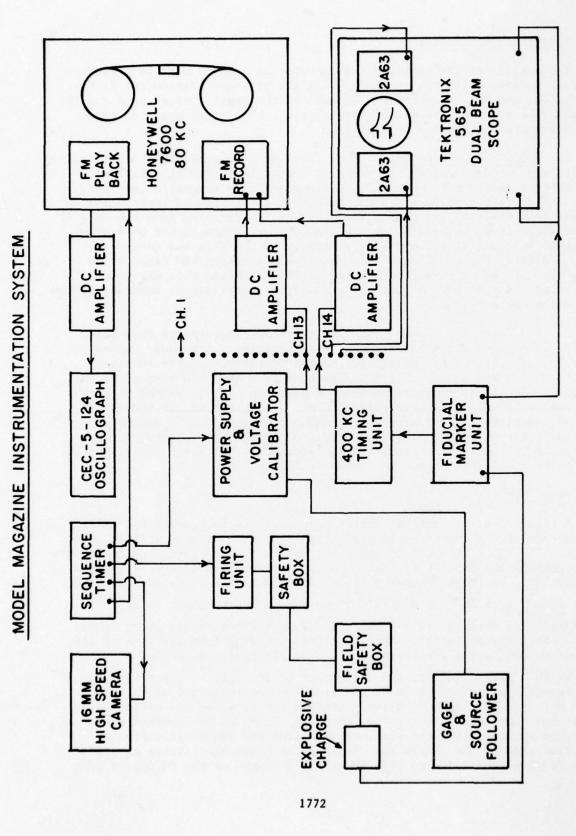
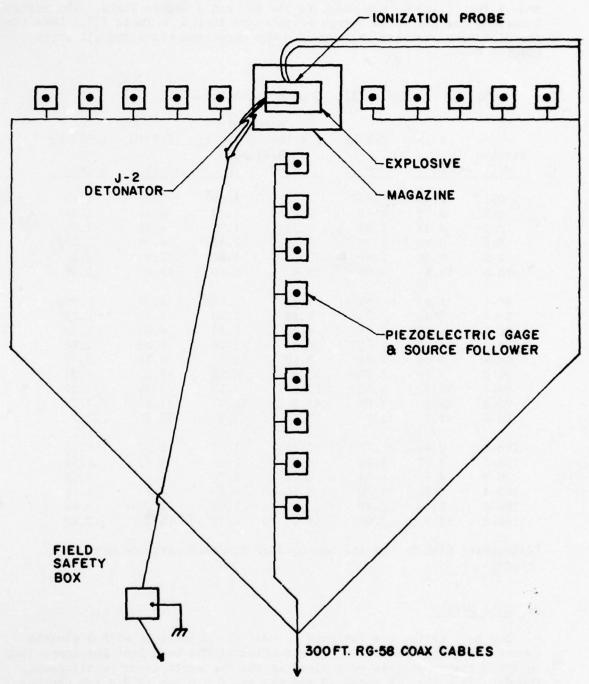


Figure 5. Model Magazine Instrumentation System

### MODEL MAGAZINE FIELD LAYOUT



# TO INSTRUMENTION

Figure 6. Model Magazine Field Layout

and .6 feet (.183 m) was added to the 180 and 0 degree lines. The station locations for the three charge weights are listed in Table III. Note that the distances remained the same for the uncovered tests and all earth covered tests.

Table III. Gage Station Locations

			CHAI	RGE WT.		
	.8 1b	.363 kg	2.4 lb	1.088 kg	4.0 lb	1.814 kg
Station			DIS	STANCE		
No.	ft	m	ft	m	ft	m
0-1	2.46	.750	3.28	1.00	3.77	1.15
0-2	3.77	1.15	4.41	1.34	4.41	1.34
0-3	4.41	1.34	5.88	1.79	5.88	1.79
0-4	5.88	1.79	8.16	2.49	8.16	2.49
0-5	8.16	2.49	12.0	3.66	12.0	3.66
*0-6	12.0	3.66	18.0	5.49	18.0	5.49
90-1	1.42	.433	1.93	.588	2.24	.683
90-2	2.46	.750	3.28	1.00	3.77	1.15
90-3	3.77	1.15	4.67	1.42	4.67	1.42
90-4	4.67	1.42	6.68	2.04	6.68	2.04
90-5	6.68	2.04	9.10	2.77	9.10	2.77
90-6	9.10	2.77	13.3	4.05	13.3	4.05
90-7	13.3	4.05	23.2	7.07	23.2	7.07
90-8	23.2	7.07	41.7	12.7	41.7	12.7
90-9	41.7	12.7	73.5	22.4	73.5	22.4
180-1	2.46	.750	3.28	1.00	3.77	1.15
180-2	3.77	1.15	4.41	1.34	4.41	1.34
180-3	4.41	1.34	5.88	1.79	5.88	1.79
180-4	5.88	1.79	8.16	2.49	8.16	2.49
180-5	8.16	2.49	12.0	3.66	21.0	3.66
*180-6	12.0	3.66	18.0	5.49	18.0	5.49

<sup>\*</sup>Additional Station for the one-half of standard earth covered model tests.

#### E. Test Matrix

The test series was designed to meet the objectives with a minimum number of shots. Therefore, in establishing the base line for comparison only two charge weights were fired in the "no earth cover" environment. The data from the 0.8 pound (0.363 kg) and 4.0 pound (1.814 kg) charges were used to predict the blast parameters for the 2.4 pound (1.088 kg) charge. The study of the blast attenuation from the one-half covered model was added to the series after the completion of the standard and

double cover. The use of the dual-beam oscilliscopes was dropped in favor of a second magnetic tape recorder. Therefore, a test shot was fired to repeat one of the conditions of the first series to check the change in instrumentation as well as a new lot of modeling sand used for simulating the earth cover. The repeat shot was with a standard earth cover model containing a 0.8 pound (0.363 kg) explosive charge. The number of shots fired, the charge weights, and the test conditions are listed in Table IV.

Table IV. Test Matrix

	arge ight	M <sub>N</sub> No Cover	M <sub>S</sub> Standard Cover	M <sub>D</sub> Double Cover	M <sub>H</sub> One-Half Cover
1b	kg				
0.8	0.363	3	4	3	3
2.4	1.088		3		3
4.0	1.814	3	3	3	3

 ${\rm M}_{\rm N}$  - will be used to denote the test firings with a bare charge - no cover

 $\rm ^{M}S$  - will denote a model test with the standard earth cover - 0.04 feet (0.012 m) covering the apex of the arch

 ${
m M}_{
m D}$  - will denote a model test with double the standard earth cover, 0.08 feet (0.024 m) covering the apex of the arch

 $_{
m H}^{
m M}$  - will denote a model test with one-half the standard earth cover 0.02 feet (0.006 m) covering the apex of the arch.

#### III. RESULTS

The results will be presented for the individual charge weights because each one represents a specific amount of explosive stored in a full size magazine. The volume of the model remains constant and therefore direct scaling from one charge weight to another should not be expected.

The complete overpressure versus time was recorded at each gage station. The data presented in this report will include the peak overpressure and impulse in tabular and graphic form. With the exception of the standard cover and smallest charge, three shots were fired for each configuration but average or mean values will be tabulated and plotted.

# A. The 0.8 Pound (0.363 kg) Charge

This charge was modeled to represent 100,000 pounds (45,360 kg) of high explosive munition stored in a standard 60 foot magazine. The first series of shots was fired with the bare hemicylindrical charge placed with the flat side resting on the surface and the detonator end of the charge near the 0 degree blast line. The peak overpressure and impulse measured along the three blast lines are listed in Tables V and VI for the four conditions; i.e., uncovered, standard cover, double cover, and one-half cover.

Blast Parameters Along O Degree Line The average peak overpressure values versus distance measured along the 0 degree blast line for the four conditions are listed in Table V and plotted in Figure 7. The peak overpressure along the zero degree blast line was expected to be higher when the charge was covered because the mass of earth around the other three sides of the structure tend to focus more of the blast energy out the front of the structure. The pressure value at the second station for the double cover test is based on only one datum point which is probably lower than it should be. There appears to be little difference in the magnitude of the blast pressures along the 0 degree gage line between the standard and double covered magazine for this charge weight. The peak overpressures versus distance recorded for the half-covered model follow the same trend as the uncovered charge but with pressure enhancement of approximately 40 percent. There is a pressure enhancement of approximately 100 percent for the standard and double covered model over the uncovered charge.

The positive pressure impulse measured under the same conditions as described in the preceeding paragraph are listed in Table VI. The values listed are average values from three data points. The average values listed in the table are plotted in Figure 8. The same trend established for the peak overpressure is again shown in the impulse, in that the impulse is higher when the earth cover is over the charge. The accuracy of impulse measured at the first station is very questionable for the uncovered condition and the datum point has not been plotted in Figure 8. A dashed line indicates the possible trend. There is an enhancement of impulse recorded when the one-half standard earth cover model is placed over the charge. There is an increased impulse enhancement when the standard earth covered model is used. But when the double earth covered model configuration was used there appeared to be no further increase in the recorded impulse along the 0 degree line. The data from the standard and double models are represented with one curve in Figure 8. They show approximately the same enhancement (100 percent) as noted for the peak overpressure at the first three stations but the enhancement only about 30 percent at the last two stations. The one-half cover model data show approximately 40 percent enhancement at the first three stations and less than 10 percent at the last two stations.

Table V. Peak Overpressure from a 0.8 Pound (0.363 kg) Charge

	Diet	900	Incovered	parad	P+5	Cover	Double Cover	Cover	One Hal	f Cover
from	9 8	9	Pe	Peak	oru.	Peak	Peak	cover	Olle-nair Peak	Peak
Ground	اح	ind Zero	Overpr	Overpressure	Overpr	Overpressure	Overpressure	ssure	Overp	Overpressure
feet	-	metres	psi	bar	psi	bar	psi	bar	psi	bar
.46		.750	83.7	5.84	179.	12.3	181.	12.5	150.	10.3
		1.15	74.9	3.30	84.4	5.82	60.5	4.17	64.4	4.44
.41		1.34	29.3	2.02	59.0	4.07	49.8	3.43	42.3	2.92
.88		1.79	20.4	1,41	34.5	2.38	37.2	2.56	24.8	1.71
.16		2.49	9.88	.681	18.5	1.28	20.6	1.42	13.0	968.
0.		3.66			5.70	.393			7.34	.506
1.42		.433	832.	57.4	45.2	3.12	31.5	2.17	53.9	3.72
		.750	334.	23.0	29.6	2.04	20.6	1.42	40.3	2.78
.77		1.15	101.	96.9	17.6	1.21	12.8	.882	24.6	1.70
.67		1.42	47.4	3.27	14.0	.965	8.34	.575	18.9	1.30
.68		2.04			10.4	.717	7.50	.517	12.2	.841
.10		2.77	10.6	.731	7.01	.483	5.52	.381	7.30	.503
.3		4.05	5.16	.356	4.23	.292	3.76	.259	4.58	.316
.2		7.07	1.94	.134	1.73	.119	1.53	.105	1.88	.130
.7		12.7	0.79	.054	0.78	.054	0.74	.051	0.76	.052
.45		.750	639.	44.1	22.2	1.53	17.6	1.21	38.0	2.62
.77		1.15	312.	21.5	13.6	.938	12.3	.848	18.2	1.25
.41		1.34	158.	10.9	12.0	.827	10.1	969.	14.8	1.02
88.		1.79	38.4	2.65	8.72	.601	8.61	.594	10.6	.731
.16		2.49	10.0	689.	5.93	.409	5.27	.363	6.46	.445
0.		3.66	•		3.24	.223		•	3.62	. 249

Table VI. Impulse from the 0.8 Pound (0.363 kg) Charge

Peet         psi-         bar-         psi-         psi- <th< th=""><th>Station</th><th>Dista</th><th>Distance from Ground Zero</th><th>Unco</th><th>Uncovered Impulse</th><th>Std.</th><th>Std. Cover Impulse</th><th>Doub1</th><th>Double Cover Impulse</th><th>One-H</th><th>One-Half Cover Impulse</th></th<>	Station	Dista	Distance from Ground Zero	Unco	Uncovered Impulse	Std.	Std. Cover Impulse	Doub1	Double Cover Impulse	One-H	One-Half Cover Impulse
2.46       .750       25.8       1.78       23.6       1.63       24.7       1.70       19.9       1         3.77       1.15       10.5       .724       19.8       1.36       19.1       1.32       15.5       1         4.41       1.34       8.2       .565       15.1       1.04       13.0       .896       11.9       11.9       15.0       19.9       11.9       15.0       15.0       15.0       11.9       15.0       11.9       15.0       15.0       15.0       11.9       15.0		feet	metres	psi- msec	bar- msec	psi- msec	bar- msec	psi- msec	bar- msec	psi- msec	bar- msec
3.77       1.15       10.5       .724       19.8       1.36       19.1       1.32       15.5         4.41       1.34       8.2       .565       15.1       1.04       13.0       .896       11.9         5.88       1.79       8.9       .614       10.8       .745       11.8       .814       9.66         12.0       3.66       -       -       5.2       .358       -       4.31         1.42       .433       34.2       2.36       10.4       .717       8.5       .586       12.0         2.46       .750       13.5       .930       8.1       .578       7.4       .510       10.1         3.77       1.15       11.1       .765       .76       .524       6.9       .476       8.63         4.67       1.42       8.9       .614       6.0       .414       5.2       .386       7.74         6.68       2.04       -       -       6.1       .421       5.9       .407       6.50         9.10       2.77       6.2       .427       4.9       .338       4.9       .338       5.01         13.3       4.05       4.3       .296       <	0-1	2.46	.750	25.8	1.78	23.6	1.63	24.7	1.70	19.9	1.37
4.41       1.34       8.2       .565       15.1       1.04       13.0       .896       11.9         5.88       1.79       8.9       .614       10.8       .745       11.8       .814       9.66         8.16       2.49       6.9       .476       7.4       .510       8.1       .558       7.40         12.0       3.66       -       -       -       5.2       .358       -       -       4.31         1.42       .453       34.2       2.36       10.4       .717       8.5       .586       12.0         2.46       .750       13.5       .930       8.1       .58       .74       .510       10.1         3.77       1.15       11.1       .765       7.6       .524       6.9       .476       8.63         4.67       1.42       8.9       .614       6.0       .414       5.2       .358       7.74         6.68       2.04       -       -       6.1       .421       5.9       .476       8.63         9.10       2.77       6.2       .427       4.9       .338       4.9       .338       5.01         13.3       4.05       4.3 <td>0-2</td> <td>3.77</td> <td>1.15</td> <td>10.5</td> <td>.724</td> <td>19.8</td> <td>1.36</td> <td>19.1</td> <td>1.32</td> <td>15.5</td> <td>1.07</td>	0-2	3.77	1.15	10.5	.724	19.8	1.36	19.1	1.32	15.5	1.07
5.88       1.79       8.9       .614       10.8       .745       11.8       .814       9.66         8.16       2.49       6.9       .476       7.4       .510       8.1       .558       7.40         12.0       3.66       -       -       -       5.2       .358       -       -       4.31         12.0       3.66       -       -       -       5.2       .586       12.0         2.46       .750       13.5       .930       8.1       .558       7.4       .510       10.1         3.77       1.15       11.1       .765       7.6       .524       6.9       .476       8.63         4.67       1.42       8.9       .614       6.0       .414       5.2       .358       7.74         6.68       2.04       -       -       6.1       .421       5.9       .407       6.5         9.10       2.77       6.2       .427       4.9       .338       5.0       .348       5.73         41.7       12.7       1.6       .110       1.4       .096       1.2       .083       1.33         23.2       7.07       2.6       .179 <t< td=""><td>0-3</td><td>4.41</td><td>1.34</td><td>8.2</td><td>.565</td><td>15.1</td><td>1.04</td><td>13.0</td><td>968.</td><td>11.9</td><td>.820</td></t<>	0-3	4.41	1.34	8.2	.565	15.1	1.04	13.0	968.	11.9	.820
8.16       2.49       6.9       .476       7.4       .510       8.1       .558       7.40         12.0       3.66       -       -       5.2       .358       -       -       4.31         1.42       .433       34.2       2.36       10.4       .717       8.5       .586       12.0         2.46       .750       13.5       .930       8.1       .558       7.4       .510       10.1         3.77       1.15       11.1       .765       7.6       .524       6.9       .476       8.63         4.67       1.42       8.9       .614       6.0       .414       5.2       .358       7.74         6.68       2.04       -       -       6.1       .427       4.9       .338       7.74         6.68       2.04       -       -       6.1       .427       4.9       .338       7.74         6.68       2.04       -       -       6.1       .427       4.9       .338       7.74         9.10       2.77       6.2       .248       3.5       .241       3.73         41.7       12.7       1.6       .110       1.4       .096       <	0-4	5.88	1.79	8.9	.614	10.8	.745	11.8	.814	99.6	999.
12.0       3.66       -       -       5.2       .358       -       -       4.31         1.42       .433       34.2       2.36       10.4       .717       8.5       .586       12.0         2.46       .750       13.5       .930       8.1       .558       7.4       .510       10.1         3.77       1.15       11.11       .765       7.6       .524       6.9       .476       8.63         4.67       1.42       8.9       .614       6.0       .414       5.2       .358       7.74         6.68       2.04       -       -       6.1       .421       5.9       .407       6.50         9.10       2.77       6.2       .427       4.9       .338       4.9       .338       5.01         13.3       4.05       4.3       .296       3.6       .248       3.5       .241       3.73         23.2       7.07       2.6       .179       2.3       .159       2.1       .145       2.27         41.7       12.7       1.6       .110       1.4       .096       1.2       .083       1.35         2.46       .750       27.1       1.87<	0-5	8.16	2.49	6.9	.476	7.4	.510	8.1	.558	7.40	.510
1.42       .433       34.2       2.36       10.4       .717       8.5       .586         2.46       .750       13.5       .930       8.1       .558       7.4       .510         3.77       1.15       11.1       .765       7.6       .524       6.9       .476         4.67       1.42       8.9       .614       6.0       .414       5.2       .358         6.68       2.04       -       -       6.1       .421       5.9       .407         9.10       2.77       6.2       .427       4.9       .338       4.9       .338         13.3       4.05       4.3       .296       3.6       .248       3.5       .241         23.2       7.07       2.6       .179       2.3       .159       2.1       .145         41.7       12.7       1.6       .110       1.4       .096       1.2       .083         2.46       .750       27.1       1.87       5.4       .372       5.4       .372         3.77       1.15       -       -       -       -       -       .083         4.41       1.34       20.5       1.41       3.5	9-0	12.0	3.66			5.2	.358	•		4.31	.297
2.46       .750       13.5       .930       8.1       .558       7.4       .510         3.77       1.15       11.1       .765       7.6       .524       6.9       .476         4.67       1.42       8.9       .614       6.0       .414       5.2       .476         6.68       2.04       -       -       -       6.1       .421       5.9       .407         9.10       2.77       6.2       .427       4.9       .338       4.9       .338         13.3       4.05       4.3       .296       3.6       .248       3.5       .241         23.2       7.07       2.6       .179       2.3       .159       2.1       .145         41.7       12.7       1.6       .110       1.4       .096       1.2       .083         2.46       .750       27.1       1.87       5.4       .372       5.4       .372         3.77       1.15       -       -       -       5.3       3.65       5.0       .345         4.41       1.34       20.5       1.41       3.5       2.41       3.6       .248         5.88       1.79       10.1	90-1	1.42	.433	34.2	2.36	10.4	.717	8.5	.586	12.0	.827
3.77       1.15       11.1       .765       7.6       .524       6.9       .476         4.67       1.42       8.9       .614       6.0       .414       5.2       .358         6.68       2.04       -       -       6.1       .421       5.9       .407         9.10       2.77       6.2       .427       4.9       .338       4.9       .338         13.3       4.05       4.3       .296       3.6       .248       3.5       .241         23.2       7.07       2.6       .179       2.3       .159       2.1       .145         41.7       12.7       1.6       .110       1.4       .096       1.2       .083         2.46       .750       27.1       1.87       5.4       .372       5.4       .372         3.77       1.15       -       -       -       5.3       3.65       5.0       .345         4.41       1.34       20.5       1.41       4.9       .338       5.0       .345         5.88       1.79       10.1       .697       4.3       2.96       4.4       .303         8.16       2.49       -       -	90-2	2.46	.750	13.5	.930	8.1	.558	7.4	.510	10.1	969.
4.67       1.42       8.9       .614       6.0       .414       5.2       .358         6.68       2.04       -       -       6.1       .421       5.9       .407         9.10       2.77       6.2       .427       4.9       .338       4.9       .338         13.3       4.05       4.3       .296       3.6       .248       3.5       .241         23.2       7.07       2.6       .179       2.3       .159       2.1       .145         41.7       12.7       1.6       .110       1.4       .096       1.2       .083         2.46       .750       27.1       1.87       5.4       .372       5.4       .372         3.77       1.15       -       -       -       5.3       .365       5.0       .345         4.41       1.34       20.5       1.41       4.9       .338       5.0       .345         5.88       1.79       10.1       .697       4.3       2.96       4.4       .303         8.16       2.49       6.0       .414       3.5       .241       3.6       -         -       -       -       -       - <td>90-3</td> <td>3.77</td> <td>1.15</td> <td>11.1</td> <td>.765</td> <td>7.6</td> <td>.524</td> <td>6.9</td> <td>.476</td> <td>8.63</td> <td>.595</td>	90-3	3.77	1.15	11.1	.765	7.6	.524	6.9	.476	8.63	.595
6.68       2.04       -       -       6.1       .421       5.9       .407         9.10       2.77       6.2       .427       4.9       .338       4.9       .338         13.3       4.05       4.3       .296       3.6       .248       3.5       .241         23.2       7.07       2.6       .179       2.3       .159       2.1       .145         41.7       12.7       1.6       .110       1.4       .096       1.2       .083         2.46       .750       27.1       1.87       5.4       .372       5.4       .372         3.77       1.15       -       -       5.3       .365       5.0       .345         4.41       1.34       20.5       1.41       4.9       .338       5.0       .345         5.88       1.79       10.1       .697       4.3       2.96       4.4       .303         8.16       2.49       6.0       .414       3.5       .241       3.6       -         -       -       -       2.7       .186       -       -	90-4	4.67	1.42	8.9	.614	6.0	.414	5.2	.358	7.74	.534
9.10       2.77       6.2       .427       4.9       .338       4.9       .338         13.3       4.05       4.3       .296       3.6       .248       3.5       .241         23.2       7.07       2.6       .179       2.3       .159       2.1       .145         41.7       12.7       1.6       .110       1.4       .096       1.2       .083         2.46       .750       27.1       1.87       5.4       .372       5.4       .372         3.77       1.15       -       -       5.3       .365       5.0       .345         4.41       1.34       20.5       1.41       4.9       .338       5.0       .345         5.88       1.79       10.1       .697       4.3       2.96       4.4       .303         8.16       2.49       6.0       .414       3.5       .241       3.6       -       -         12.0       3.66       -       -       2.7       .186       -       -	90-5	89.9	2.04		1	6.1	.421	5.9	.407	6.50	.448
13.3       4.05       4.3       .296       3.6       .248       3.5       .241         23.2       7.07       2.6       .179       2.3       .159       2.1       .145         41.7       12.7       1.6       .110       1.4       .096       1.2       .083         2.46       .750       27.1       1.87       5.4       .372       5.4       .372         3.77       1.15       -       -       5.3       .365       5.0       .345         4.41       1.34       20.5       1.41       4.9       .338       5.0       .345         5.88       1.79       10.1       .697       4.3       2.96       4.4       .303         8.16       2.49       6.0       .414       3.5       .241       3.6       -       -         12.0       3.66       -       -       2.7       .186       -       -	9-06	9.10	2.77	6.2	.427	4.9	.338	4.9	.338	5.01	.345
23.2       7.07       2.6       .179       2.3       .159       2.1       .145         41.7       12.7       1.6       .110       1.4       .096       1.2       .083         2.46       .750       27.1       1.87       5.4       .372       5.4       .372         3.77       1.15       -       -       5.3       .365       5.0       .345         4.41       1.34       20.5       1.41       4.9       .338       5.0       .345         5.88       1.79       10.1       .697       4.3       2.96       4.4       .303         8.16       2.49       6.0       .414       3.5       .241       3.6       -         12.0       3.66       -       -       2.7       .186       -       -	2-06	13.3	4.05	4.3	.296	3.6	.248	3.5	.241	3.73	.257
2.46       .750       27.1       1.87       5.4       .372       5.4       .372         3.77       1.15       -       -       5.3       .365       5.0       .345         4.41       1.34       20.5       1.41       4.9       .338       5.0       .345         5.88       1.79       10.1       .697       4.3       2.96       4.4       .303         8.16       2.49       6.0       .414       3.5       .241       3.6       -       -         12.0       3.66       -       -       2.7       .186       -       -	8-06	23.2	7.07	5.6	.179	2.3	.159	2.1	.145	2.27	.156
2.46       .750       27.1       1.87       5.4       .372       5.4       .372         3.77       1.15       -       -       5.3       .365       5.0       .345         4.41       1.34       20.5       1.41       4.9       .338       5.0       .345         5.88       1.79       10.1       .697       4.3       2.96       4.4       .303         8.16       2.49       6.0       .414       3.5       .241       3.6       -       -         12.0       3.66       -       -       2.7       .186       -       -	6-06	41.7	12.7	1.6	.110	1.4	960.	1.2	.083	1.32	.091
3.77       1.15       -       -       5.3       .365       5.0       .345         4.41       1.34       20.5       1.41       4.9       .338       5.0       .345         5.88       1.79       10.1       .697       4.3       2.96       4.4       .303         8.16       2.49       6.0       .414       3.5       .241       3.6       -       -         12.0       3.66       -       -       2.7       .186       -       -       -	180-1	2.46	.750	27.1	1.87	5.4	.372	5.4	.372	6.04	.416
4.41     1.34     20.5     1.41     4.9     .338     5.0     .345       5.88     1.79     10.1     .697     4.3     2.96     4.4     .303       8.16     2.49     6.0     .414     3.5     .241     3.6     .248       12.0     3.66     -     -     2.7     .186     -     -	180-2	3.77	1.15			5.3	.365	5.0	.345	5.75	.396
5.88       1.79       10.1       .697       4.3       2.96       4.4       .303         8.16       2.49       6.0       .414       3.5       .241       3.6       .248         12.0       3.66       -       -       2.7       .186       -       -	180-3	4.41	1.34	20.5	1.41	4.9	.338	5.0	.345	5.41	.373
8.16 2.49 6.0 .414 3.5 .241 3.6 .248 12.0 3.66 2.7 .186	180-4	5.88	1.79	10.1	769.	4.3	2.96	4.4	.303	4.46	.307
12.0 3.66 2.7 .186	180-5	8.16	2.49	0.9	.414	3.5	.241	3.6	.248	3.77	.260
	180-6	12.0	3.66			2.7	.186	•	1	2.81	.194

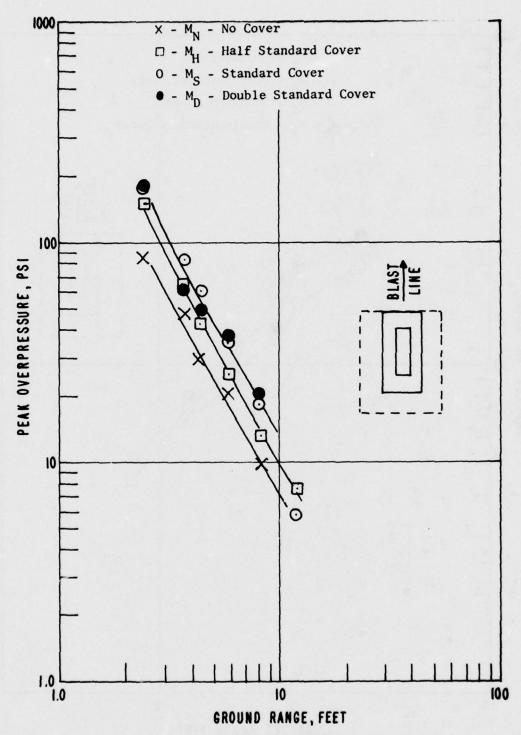


Figure 7. Pressure versus Distance Along the 0 Degree Line as a Function of Earth Cover for a 0.8 Pound (0.363 kg) Charge

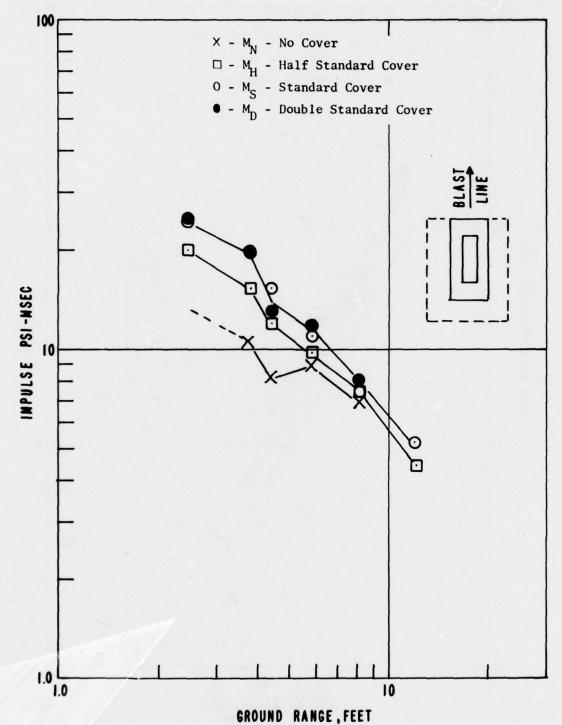


Figure 8. Impulse versus Distance Along the 0 Degree
Line as a Function of Earth Cover for a
0.8 Pound (0.363 kg) Charge

2. Blast Parameters Along the 90 Degree Line Measured peak overpressure and impulse along the 90 degree blast line for the four test conditions are listed in Tables V and VI. A total of nine stations were instrumented starting at a scaled separation distance of 1.25 ft/lb  $^{1/3}$  (.5 m/kg $^{1/3}$ ). The peak overpressure results listed in Table V for the 90 degree blast line are presented graphically in Figure 9. As the earth cover is increased, the blast attenuation is increased. It should also be noted that as the distance increases the peak overpressure attenuation decreases. The difference in the four average values of pressure measured at the last station is  $\pm 3$  percent.

The impulse versus distance measured along the 90 degree line for the four test configurations are listed in Table VI and plotted in Figure 10. Here the impulse measurements show a trend similar to the one established for the peak overpressure with the exception of the decrease in attenuation with distance. From the fifth station to the last station the percentage of attenuation remains approximately constant. The half-cover and standard covered models show approximately a 15 percent attenuation while the double earth covered model gives a 20 percent attenuation.

3. Blast Parameters Along the 180 Degree Line The 180 degree line was established to the rear of the structure. The peak overpressure measured along this line is listed in Table V. The values from Table V are plotted in Figure 11. There is a dramatic drop in the peak overpressure at the close-in positions when one-half standard earth cover model was tested and the results compared with an uncovered charge. The peak overpressures measured from the standard cover and double cover models show further reductions. Approximately a 10 percent pressure reduction is noted when going from the standard to the double cover magazine.

The impulse measurements along the 180 degree line are listed in Table VI and plotted in Figure 12. There is no measurable difference in the recorded impulse from the 0.8 pound (0.363 kg) charge detonated in the standard and double earth covered models. There is only a 10 percent greater value noted at the first three stations from the same charge weight detonated in a one-half standard earth cover model.

# B. The 2.4 Pound (1.088 kg) Charge

There were six 2.4 pound (1.088 kg) charges fired. Three were detonated in the standard earth covered model magazine and three were detonated with one half of the standard earth cover in place. To establish a basis for comparing the effect of the earth covers versus no cover the results from the 0.8 pound (0.363 kg) and 4 pound (1.814 kg) charges fired without cover were scaled to a 2.4 pound (1.088 kg) equivalent. There were no tests conducted for the 2.4 pound (1.088 kg) charge detonated in a model magazine with double the standard earth cover. It was assumed that results from the 0.8 pound (0.363 kg) and 4 pound (1.814 kg) charges could be used to interpolate effects for the mid-range

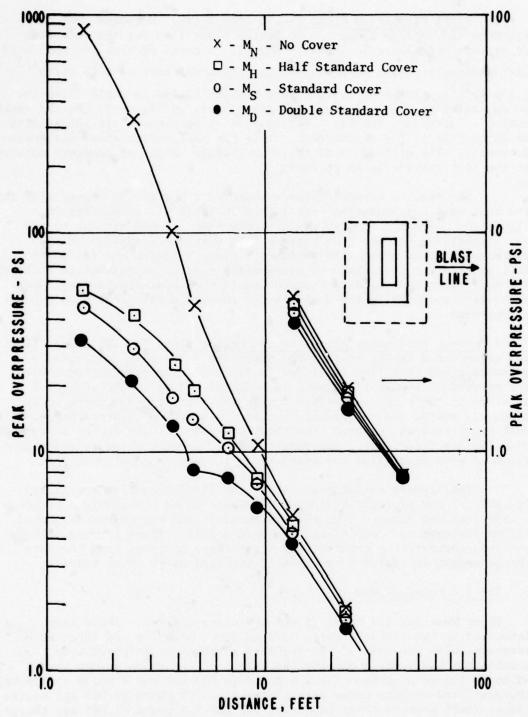


Figure 9. Pressure versus Distance Along the 90 Degree Line as a Function of Earth Cover for a 0.8 Pound (0.363 kg) Charge

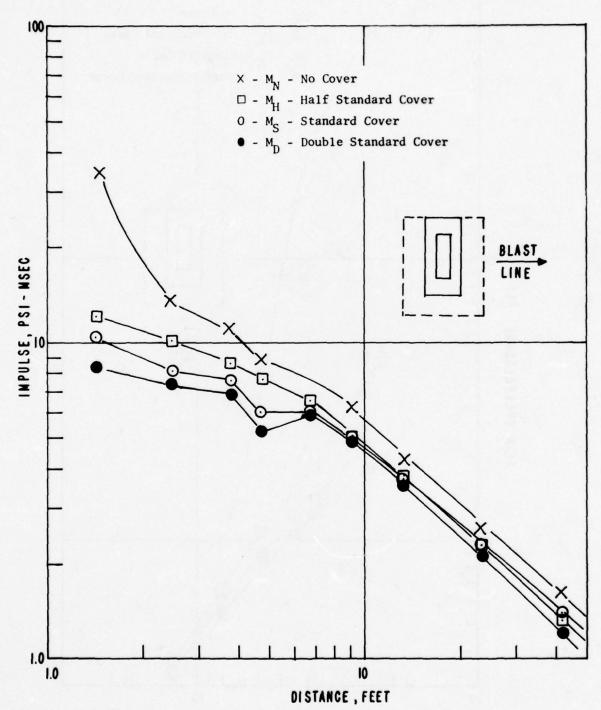


Figure 10. Impulse versus Distance Along the 90 Degree Line as a Function of Earth Cover for a 0.8 Pound (0.363 kg) Charge

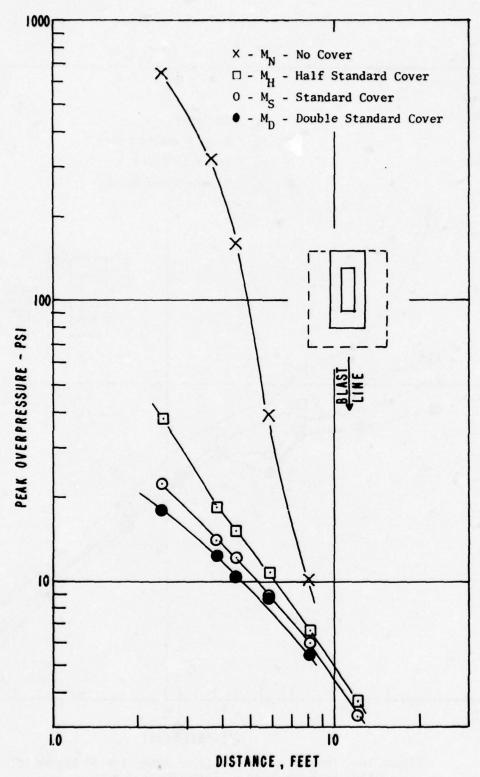


Figure 11. Pressure versus Distance Along the 180 Degree Line as a Function of Earth Cover for a 0.8 Pound (0.363 kg) Charge

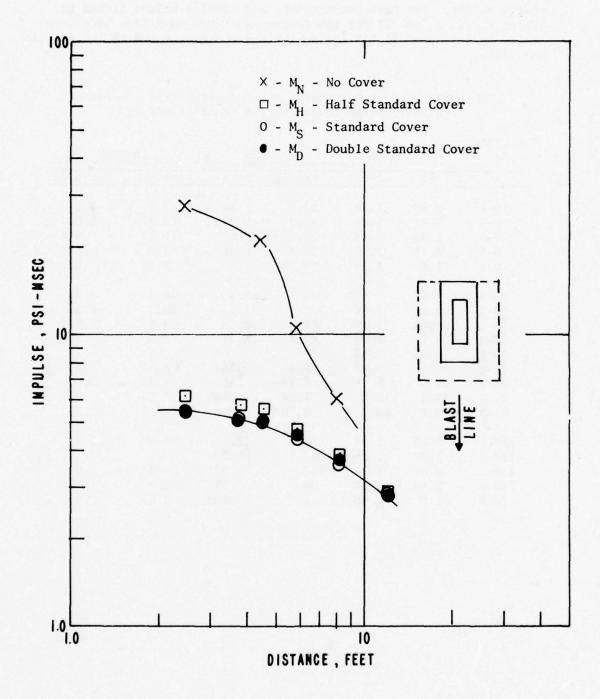


Figure 12. Impulse versus Distance Along the 180 Degree Line as a Function of Earth Cover for a 0.8 Pound (0.363 kg) Charge

charge weight. The peak overpressure and impulse values listed in Tables V, VI, X, and XI for the uncovered charge condition have been scaled to 2.4 pound (1.088 kg) equivalent and are listed in Tables VIIa and VIIb.

Table VIIa. Peak Overpressure and Impulse from 0.8 Pound (0.363) Charge Scaled to 2.4 Pound (1.088 kg)

Dis	tance	Pres	sure	Impi	ulse
feet	metres	psi	bars	psi-msec	bar-msec
3.55	1.08	84.7	5.84	37.2	2.56
5.44	1.66	47.9	3.28	15.1	1.04
6.36	1.94	29.3	2.02	11.8	.814
8.48	2.58	20.4	1.41	12.8	.882
11.8	3.60	9.88	.681	9.96	.687
2.05	.625	832.	57.4	49.4	3.41
3.55	1.08	334.	23.0	19.5	1.34
5.44	1.66	101.	6.96	16.0	1.10
6.74	2.05	47.4	3.27	12.8	.882
9.36	2.85			-	-
13.1	3.99	10.6	.731	8.94	.616
19.2	5.85	5.16	.356	6.20	.427
33.5	10.2	1.94	.134	3.75	.259
60.1	18.3	0.79	.054	2.31	.159
3.55	1.08	639.	44.1	39.0	2.69
5.44	1.66	312.	21.5	_ ?	-
6.36	1.94	158.	10.9	29.6	2.04
8.48	2.58	38.4	2.65	15.7	1.08
11.8	3.60	10.0	.689	8.65	.596
	3.55 5.44 6.36 8.48 11.8 2.05 3.55 5.44 6.74 9.36 13.1 19.2 33.5 60.1 3.55 5.44 6.36 8.48	3.55 1.08 5.44 1.66 6.36 1.94 8.48 2.58 11.8 3.60 2.05 .625 3.55 1.08 5.44 1.66 6.74 2.05 9.36 2.85 13.1 3.99 19.2 5.85 33.5 10.2 60.1 18.3 3.55 1.08 5.44 1.66 6.36 1.94 8.48 2.58	feet         metres         psi           3.55         1.08         84.7           5.44         1.66         47.9           6.36         1.94         29.3           8.48         2.58         20.4           11.8         3.60         9.88           2.05         .625         832.           3.55         1.08         334.           5.44         1.66         101.           6.74         2.05         47.4           9.36         2.85         -           13.1         3.99         10.6           19.2         5.85         5.16           33.5         10.2         1.94           60.1         18.3         0.79           3.55         1.08         639.           5.44         1.66         312.           6.36         1.94         158.           8.48         2.58         38.4	feet         metres         psi         bars           3.55         1.08         84.7         5.84           5.44         1.66         47.9         3.28           6.36         1.94         29.3         2.02           8.48         2.58         20.4         1.41           11.8         3.60         9.88         .681           2.05         .625         832.         57.4           3.55         1.08         334.         23.0           5.44         1.66         101.         6.96           6.74         2.05         47.4         3.27           9.36         2.85         -         -           13.1         3.99         10.6         .731           19.2         5.85         5.16         .356           33.5         10.2         1.94         .134           60.1         18.3         0.79         .054           3.55         1.08         639.         44.1           5.44         1.66         312.         21.5           6.36         1.94         158.         10.9           8.48         2.58         38.4         2.65	feet         metres         psi         bars         psi-msec           3.55         1.08         84.7         5.84         37.2           5.44         1.66         47.9         3.28         15.1           6.36         1.94         29.3         2.02         11.8           8.48         2.58         20.4         1.41         12.8           11.8         3.60         9.88         .681         9.96           2.05         .625         832.         57.4         49.4           3.55         1.08         334.         23.0         19.5           5.44         1.66         101.         6.96         16.0           6.74         2.05         47.4         3.27         12.8           9.36         2.85         -         -         -           13.1         3.99         10.6         .731         8.94           19.2         5.85         5.16         .356         6.20           33.5         10.2         1.94         .134         3.75           60.1         18.3         0.79         .054         2.31           3.55         1.08         639.         44.1         39.0

Table VIIb. Peak Overpressure and Impulse from a 4.0 Pound (1.814 kg) Charge Scaled to 2.4 Pound (1.088 kg)

Dis	tance	Pres	sure	Imp	ulse
feet	metres	psi	bars	psi-msec	bar-msec
3.18	.969	175.	12.1	23.0	1.59
3.72	1.13	133.	9.17	30.4	2.10
4.96	1.51	72.6	5.01	21.4	1.47
6.88	2.10	28.6	1.97	13.8	.951
10.1	3.08	12.1	.834	11.2	.772
1.89	.576	900.	62.1	37.8	2.61
3.18	.969	483.	33.3	60.2	4.15
3.94	1.20	229.	15.8	25.2	1.74
5.63	1.72	67.5	4.65	18.8	1.30
7.68	2.34	37.6	2.59	13.1	.903
11.2	3.41	15.2	1.05	10.8	.745
19.6	5.97	4.40	.303	6.41	.442
35.2	10.7	1.91	.132	3.88	.265
62.0	18.9	0.52	.036	1.60	.110
3.18	.969	659.	42.1	62.2	4.29
3.72	1.13	635.	43.8	39.1	2.70
4.96	1.51	467.	32.2	35.1	2.42
6.88	2.10	138.	9.51	24.6	1.70
10.1	3.08	21.8	1.50	10.1	.696
	3.18 3.72 4.96 6.88 10.1 1.89 3.18 3.94 5.63 7.68 11.2 19.6 35.2 62.0 3.18 3.72 4.96 6.88	3.18 .969 3.72 1.13 4.96 1.51 6.88 2.10 10.1 3.08  1.89 .576 3.18 .969 3.94 1.20 5.63 1.72 7.68 2.34 11.2 3.41 19.6 5.97 35.2 10.7 62.0 18.9  3.18 .969 3.72 1.13 4.96 1.51 6.88 2.10	feet         metres         psi           3.18         .969         175.           3.72         1.13         133.           4.96         1.51         72.6           6.88         2.10         28.6           10.1         3.08         12.1           1.89         .576         900.           3.18         .969         483.           3.94         1.20         229.           5.63         1.72         67.5           7.68         2.34         37.6           11.2         3.41         15.2           19.6         5.97         4.40           35.2         10.7         1.91           62.0         18.9         0.52           3.18         .969         659.           3.72         1.13         635.           4.96         1.51         467.           6.88         2.10         138.	feet         metres         psi         bars           3.18         .969         175.         12.1           3.72         1.13         133.         9.17           4.96         1.51         72.6         5.01           6.88         2.10         28.6         1.97           10.1         3.08         12.1         .834           1.89         .576         900.         62.1           3.18         .969         483.         33.3           3.94         1.20         229.         15.8           5.63         1.72         67.5         4.65           7.68         2.34         37.6         2.59           11.2         3.41         15.2         1.05           19.6         5.97         4.40         .303           35.2         10.7         1.91         .132           62.0         18.9         0.52         .036           3.18         .969         659.         42.1           3.72         1.13         635.         43.8           4.96         1.51         467.         32.2           6.88         2.10         138.         9.51	feet         metres         psi         bars         psi-msec           3.18         .969         175.         12.1         23.0           3.72         1.13         133.         9.17         30.4           4.96         1.51         72.6         5.01         21.4           6.88         2.10         28.6         1.97         13.8           10.1         3.08         12.1         .834         11.2           1.89         .576         900.         62.1         37.8           3.18         .969         483.         33.3         60.2           3.94         1.20         229.         15.8         25.2           5.63         1.72         67.5         4.65         18.8           7.68         2.34         37.6         2.59         13.1           11.2         3.41         15.2         1.05         10.8           19.6         5.97         4.40         .303         6.41           35.2         10.7         1.91         .132         3.88           62.0         18.9         0.52         .036         1.60           3.18         .969         659.         42.1

1. Blast Parameters Along the 0 Degree Line The peak overpressures and impulses measured along the 0 degree instrumentation line from the detonation of a 2.4 pound (1.088 kg) charge for the model magazine with a standard earth cover and with a one-half standard earth cover are listed in Tables VIII and IX. The peak overpressure values listed are plotted in Figure 13 with peak overpressure as a function of distance for the three conditions. There was no significant difference in pressure measured between the standard earth cover model and the one-half standard earth cover along the 0 degree line. The peak overpressures were approximately 30 percent higher than those measured for the uncovered condition.

The positive impulse values listed in Table VIIb for the uncovered condition and in Table IX for the standard and one-half earth cover model are presented in Figure 14. The positive impulse is plotted as a function of distance for the three conditions. There was no significant difference measured in the standard and one-half earth cover models. A comparison of the covered and uncovered condition indicate similar values close-in and beyond 8 feet (2.44 metres), but the values of impulse for the uncovered condition are lower than the covered condition over the mid-range distance.

Table VIII. Peak Overpressure from a 2.4 Pound (1.088 kg) Charge

Station	f	tance rom nd Zero	Std. (Pea Overpre	ak	One-Hall Cover Overpre	Peak
	feet	metres	psi	bar	psi	bar
0-1 0-2	3.28 4.41	1.00	178. 121.	12.3	198. 123.	13.7 8.40
0-3	5.88	1.79	72.0	4.96	58.0	4.00
0-4	8.16	2.49	28.5	1.96	28.9	1.99
0-5	12.0	3.66	13.3	.917	10.1	.696
0-6	18.0				4.83	.333
90-1	1.43	.588	63.4	4.37	79.0	5.45
90-2	3.28	1.00	39.8	2.74	43.6	3.01
90-3	4.67	1.42	25.8	1.78	28.8	1.99
90-4	6.68	2.04	15.1	1.04	20.9	1.44
90-5	9.10	2.77	12.3	.848	16.0	1.10
90-6	13.3	4.05	8.04	.554	8.46	.583
90-7	23.2	7.07	3.85	.265	4.26	.294
90-8	41.7	12.7	1.81	.125	1.85	.128
90-9	73.5	22.4	0.76	.052	0.78	.054
180-1	3.28	1.00	31.9	2.20	40.1	2.76
180-2	4.41	1.34	19.3	1.33	26.7	1.84
180-3	5.88	1.79	12.4	.855	16.7	1.15
180-4	8.16	2.49	9.40	.648	11.3	.779
180-5	12.0	3.66	5.63	.388	6.58	.454
180-6	18.0				3.76	.259

Table IX. Impulse from a 2.4 Pound (1.088 kg) Charge

Station	f	tance rom nd Zero	Std.	Cover ulse	One-l Std. ( Imp	
	feet	metres	psi-msec	bar-msec	psi-ms	bar-ms
0-1	3.28	1.00	25.8	1.78	22.3	1.54
0-2	4.41	1.34	31.9	2.20	30.5	2.10
0-3	5.88	1.79	21.5	1.48	21.9	1.51
0-4	8.16	2.49	14.9	1.03	13.7	.945
0-5	12.0	3.66	9.13	.629	8.93	.616
0-6	18.0	5.49			3.83	. 264
90-1	1.93	.588	16.4	.841	19.5	1.24
90-2	3.28	1.00	14.5	1.00	16.4	1.13
90-3	4.67	1.42	13.2	.910	14.7	1.01
90-4	6.68	2.04	10.1	.696	12.9	.889
90-5	9.10	2.77	11.3	.779	12.2	.841
90-6	13.3	4.05	9.0	.620	8.79	.600
90-7	23.2	7.07	5.29	.365	6.19	.427
90-8	41.7	12.7	3.42	.236	3.68	. 254
90-9	73.5	22.4	1.93	.133	2.05	.141
180-1	3.28	1.00	10.6	.731	9.86	.680
180-2	4.41	1.34	8.4	.579	9.77	.674
180-3	5.88	1.79	8.26	.570	8.50	.586
180-4	8.16	2.49	7.69	.530	7.58	.523
180-5	12.0	3.66	6.80	.469	6.34	.437
180-6	18.0	5.49			5.26	.363

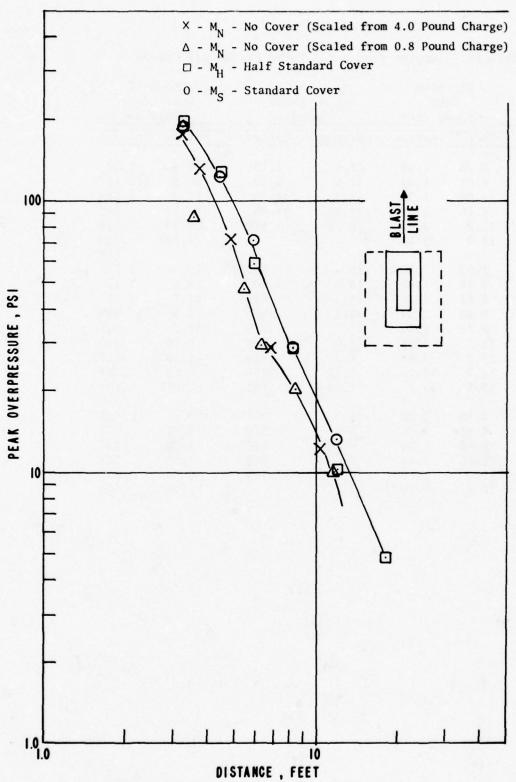


Figure 13. Pressure versus Distance Along the O Degree Line as a Function of Earth Cover for a 2.4 Pound (1.088 kg) Charge

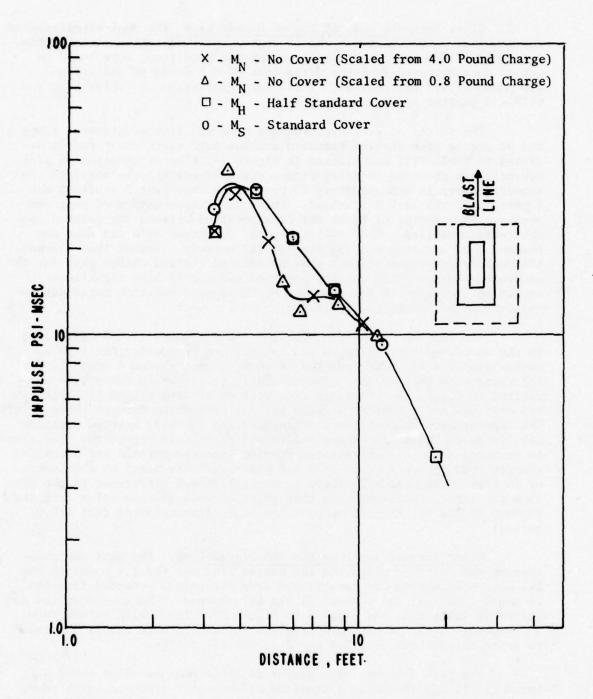


Figure 14. Impulse versus Distance Along the O Degree Line as a Function of Earth Cover for a 2.4 Pound (1.088 kg) Charge

2. Blast Parameters Along the 90 Degree Line The peak overpressures and impulses predicted along the 90 degree instrumentation line for the 2.4 pound (1.088 kg) charge in the uncovered condition, were based on scaled data measured from the detonation of 0.8 pound (0.363 kg) and 4.0 pound (1.814 kg) charges. These data are listed in Tables VIIa and VIIb and plotted in Figures 15 and 16.

The values of peak overpressure as a function of distance along the 90 degree line for the standard and one-half earth cover models are listed in Table VIII and plotted in Figure 15. The attenuation of peak overpressure measured in going from a one-half earth cover model to the standard cover is approximately 20 percent at the first 5 stations and 5 percent at the last 4 stations. There is an attenuation of peak overpressure by a factor of 10 at the first station between the covered and uncovered condition. This factor rapidly decreases with distance and becomes 1 at a distance of 17 feet (5.182 metres). Beyond that distance the peak overpressure becomes greater for the covered charge than for the uncovered charge. This was not expected and should have significant impact on the relative locations of earth covered munition magazines and residential or inhabited structures.

The impulse versus distance for the 2.4 pound (1.088 kg) charge in the uncovered configuration was established by scaling the impulse versus distance measured from the .8 pound (.363 kg) and 4 pound (1.814 kg) charges to that weight. These values are listed in Table VIIb and plotted in Figure 16. There is wide scatter of data points at the first two stations and therefore a curve has not been drawn through those points. The impulse measurements for the standard and one-half covered magazine are listed in Table XI. These values are plotted in Figure 16. The trend to be noted here is that measured impulse from the covered and uncovered charges converge at a value of 9 psi-msec (.621 bar-msec) at a distance of 13 feet (3.96 metres). There is no significant difference in the data from the three conditions from that point on with the one value from the 4 pound (1.814 kg) charges appears low at a distance of 62 feet (18.9 metres).

3. Blast Parameters Along the 180 Degree Line. The peak overpressure versus distance along the 180 degree line for the 2.4 pound (1.088 kg) charge uncovered was established from the values recorded from the .8 pound (.363 kg) and 4 pound (1.814 kg) charges. The scaled values are listed in Table VIIa and plotted in Figure 17. The scaled values show a reasonable decay of peak overpressure versus distance and is concluded to be representative of a 2.4 pound (1.088 kg) charge.

The peak overpressures versus distance measured from the 2.4 pound (1.088 kg) charge in a standard and one-half standard earth cover magazine are listed in Table VIII. These values are plotted in Figure 17. There is a significant attenuation in peak overpressure to the rear of the structure when the charge is fired in the covered magazine models. The attenuation becomes less with increasing distance and it appears that

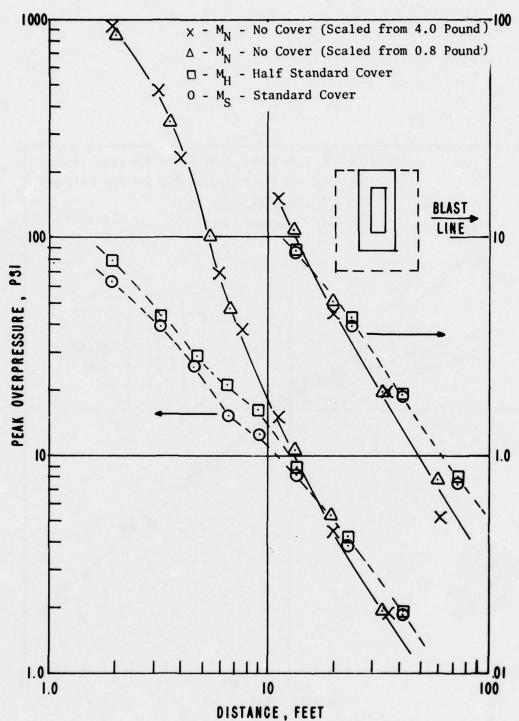


Figure 15. Pressure versus Distance Along the 90 Degree
Line as a Function of Earth Cover for a
2.4 Pound (1.088 kg) Charge

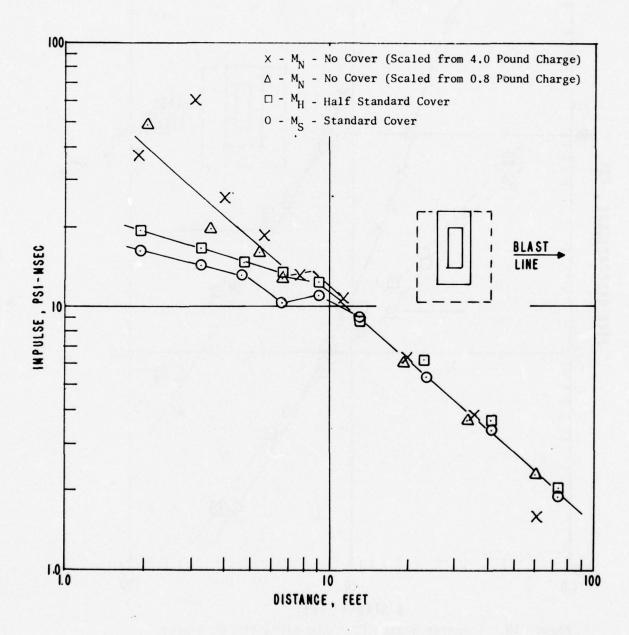


Figure 16. Impulse versus Distance Along the 90 Degree Line as a Function of Earth Cover for a 2.4 Pound (1.088 kg) Charge

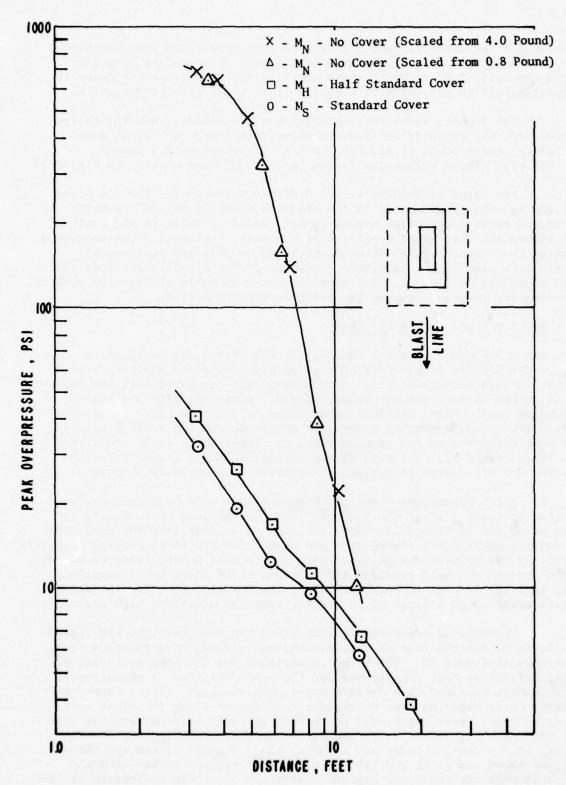


Figure 17. Pressure versus Distance Along the 180 Degree Line as a Function of Earth Cover for a 2.4 Pound (1.088 kg) Charge

curves for the uncovered and one-half covered conditions will converge at greater distances. The attenuation of peak overpressure in going from one-half standard earth cover model to the standard earth cover is approximately 20 percent with slightly less at the greater distances.

The impulse versus distance for the 2.4 pound (1.088 kg) charge uncovered, was established from the measurements made on the .8 pound (.363 kg) and 4 pound (1.814 kg) charges and scaled to 2.4 pounds (1.058 kg). These values are listed in Table VIIb and plotted in Figure 18.

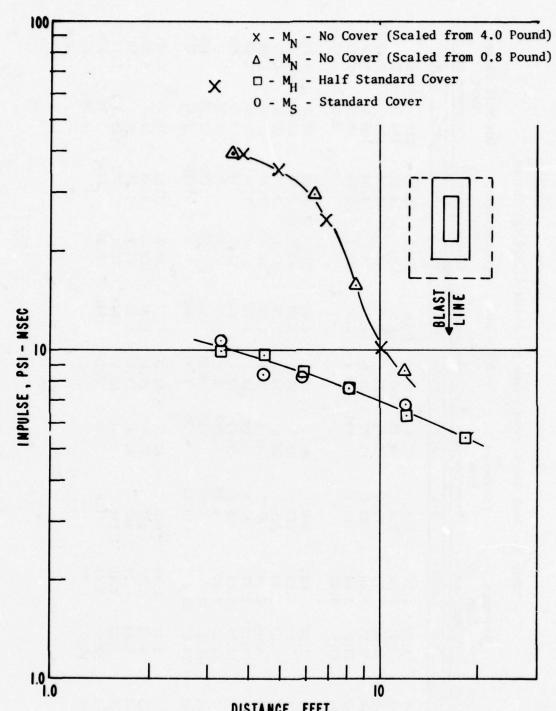
The value of impulse versus distance measured for the 2.4 pound (1.088 kg) charge detonated in the standard earth cover and one-half standard earth cover model magazines are listed in Table IX and plotted in Figure 18. The impulse plotted at the first station for the uncovered charge is a questionable datum point based on only one measurement. There is a significant impulse attenuation at the close-in stations when the explosive is covered. But there was no measurable attenuation between the impulse recorded for the two earth covered conditions.

# C. The 4.0 Pound (1.814 kg) Charge

The 4.0 pound (1.814 kg) hemicylindrical charge was designed to represent 500,000 pounds (226,800 kg) of high explosive munition stored in a standard storage magazine. The charge was detonated with the flat side on the surface without cover, in model magazines with one-half standard earth cover, standard earth cover, and double earth cover. Three tests were conducted under each condition and the average values of peak overpressure and impulse along the three blast lines are listed in Tables X and XI. The mean values listed in Tables X and XI for the 0, 90, and 180 degree directions are plotted in Figures 19 through 24.

1. Blast Parameters Along the 0 Degree Line The peak overpressures listed in Table X along the 0 degree line for the four test conditions are presented in Figure 19. Here it is quite evident that the peak overpressures along the 0 degree line are higher for the three covered magazines than for the uncovered magazine. This increase is in the order of 50 percent for the one-half standard and standard earth cover model magazines. The increase in peak overpressure along the 0 degree line for the double earth cover is an average of 80 percent over the uncovered high explosive.

The impulse measurements made along the 0 degree line are listed in Table XI for the four test conditions and plotted as a function of distance in Figure 20. The trend established for the impulse is not as well defined as that established for the peak overpressure measurements. The impulse measured from detonations in the one-half, single cover, and double cover magazine show only minor differences along the blast line. Similar values were documented at the two close-in stations and the last station with significant differences measured at the third and fourth stations. A similar trend was noted on the 2.4 pound (1.088 kg) charge weight where the first and last stations have similar values with the covered magazine recording higher impulse values at the in-between stations.



DISTANCE, FEET
Figure 18. Impulse versus Distance Along the 180 Degree
Line as a Function of Earth Cover for a
2.4 Pound (1.088 kg) Charge

Table X. Peak Overpressure from a 4 Pound (1.814 kg) Charge

•	Dis	istance	Uncovered Peak	covered	Std. Cover Peak	Cover	Double Cover Peak	Cover	One-Half Cover Peak	f Cover
Station	Grou	nd Zero	Overpr	Overpressure	Overpressure	essure	Overpressure	essure	Overpressure	ssure
	feet	metres	psi	bar	psi	bar	psi	bar	psi	bar
0-1	3.77	1.15	175.	12.1	218.	15.0	221.	15.2	219.	15.1
0-2	4.41	1.34	133.	9.17	187.	12.9	204.	14.1	174.	12.0
0-3	5.88	1.79	72.6	5.01	122.	8.41	118.	8.14	104.	7.17
0-4	8.16	2.49	28.6	1.97	0.69	4.76	71.7	4.94	9.09	4.18
0-5	12.0	3.66	12.1	.834	19.0	1.31	26.2	1.81	18.5	1.28
9-0	18.0	5.49		,	•			,	6.14	.423
90-1	2.24		006	62 1	0 00	28 9	74.6	5 14	2 00	6 23
2-06	3 77		483	33.3	51.0	2 5 5	41.5	2 86	55.3	2 80
200	4 67		220	25.50	32.8	20.0	21.1	2.30	40.6	2 80
000	6 4 8		67.5	7 65	0.01	2.1	1001	1 24	27.0	1 06
90-4	0.00		.07.3	4.03	10.0	1.50	10.0	1.24	0.72	1.00
90-5	9.10		37.6	2:59	18.1	1.25	17.0	1.17	20.8	1.43
9-06	13.3		15.2	1.05	12.9	688.	11.5	.793	12.6	869
2-06	23.2		4.40	.303	5.90	.407	00.9	.414	5.99	.413
8-06	41.7		1.87	.131	2.53	.172	2.53	.172	2.55	.176
6-06	73.5	22.4	0.52	.036	1.00	690.	08.0	.055	1.00	690.
180-1	3.77	1.15	610.	42.1	32.2	2.22	22.0	1.52	38.0	2.62
180-2	4.41	1.34	. 209	41.9	28.6	1.97	19.4	1.34	32.4	2.23
180-3	5.88	1.79	467.	32.2	18.5	1.28	15.9	1.10	23.1	1.59
180-4	8.16	2.49	138.	9.51	12.3	.848	11.5	.793	16.3	1.12
180-5	12.0	3.66	21.8	1.50	8.50	.586	7.27	.503	9.79	.675
180-6	18.0	5.49			1	•	1	•	5.90	.407

Table XI. Impulse from a 4 Pound (1,814 kg) Charge

Cover	1	1																						
	bar-	msec	1.90	2.12	2.24	1.34	.951	.511		1.55	1.38	1.30	1.11	1.14	.751	.601	.364	.203	.848	968.	.807	.765	.653	.545
One-Half Impuls	-isd	msec	27.5	30.8	32.5	19.5	13.8	7.41		22.5	20.0	18.8	16.1	16.5	10.9	8.72	5.28	2.95	12.3	13.0	11.7	11.1	9.47	7.91
Double Cover Impulse	bar-	msec	2.06	2.35	2.46	1.66	.910	•		1.40	1.29	1.06	.841	1.05	968.	.554	.310	.147	.723	.586	.738	.752	.625	•
Doubl Im	psi-	msec	30.1	34.1	35.7	24.1	13.2	•		20.3	18.7	15.4	12.2	15.3	13.0	8.03	4.50	2.13	10.5	8.5	10.7	10.9	9.07	
Std. Cover Impulse	bar-	msec	2.76	2.26	2.25	1.67	.855		*	1.61	1.34	1.12	.882	1.10	.931	.598	.356	.207	.786	.807	.800	.862	.703	•
Std.	psi-	msec	40.0	32.8	32.6	24.2	12.4	•		23.3	19.5	16.3	12.8	16.0	13.5	8.67	5.17	3.00	11.4	11.7	11.6	12.5	10.2	<b>'1</b>
Uncovered Impulse	bar-	msec	1.89	2.48	1.75	1.13	.917	•		3.96	4.92	2.06	1.54	1.21	.882	.524	.317	.129	4.51	3.27	2.87	2.01	.827	•
Unco	-isd	msec	27.4	36.0	25.4	16.4	13.3	,		57.2	71.4	29.9	22.3	17.5	12.8	7.60	4.60	1.87	65.4	47.5	41.6	29.2	12.0	1
istance from Ground Zero		metres	1.15	1.34	1.79	2.49	3.66	5.49		.683	1.15	1.42	2.04	2.77	4.05	7.07	12.7	22.1	1.15	1.34	1.79	2.49	3.66	5.49
Distance Ground 2		feet	3.77	4.41	5.88	8.16	12.0	18.0		2.24	3.77	4.67	89.9	9.10	13.3	23.2	41.7	72.5	3.77	4.41	5.88	8.16	12.0	18.0
Station			0-1	0-2	0-3	0-4	0-5	9-0		90-1	90-2	90-3	90-4	90-5	9-06	2-06	8-06	6-06	180-1	180-2	180-3	180-4	180-5	180-6

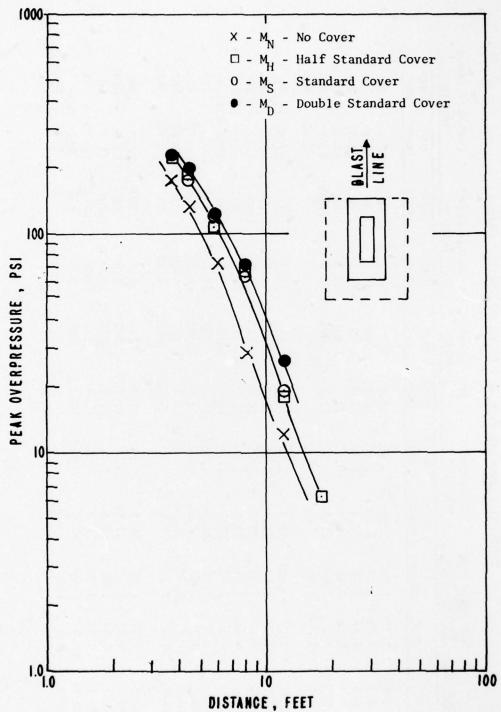


Figure 19. Pressure versus Distance Along the O Degree Line as a Function of Earth Cover for a 4.0 Pound (1.814 kg) Charge

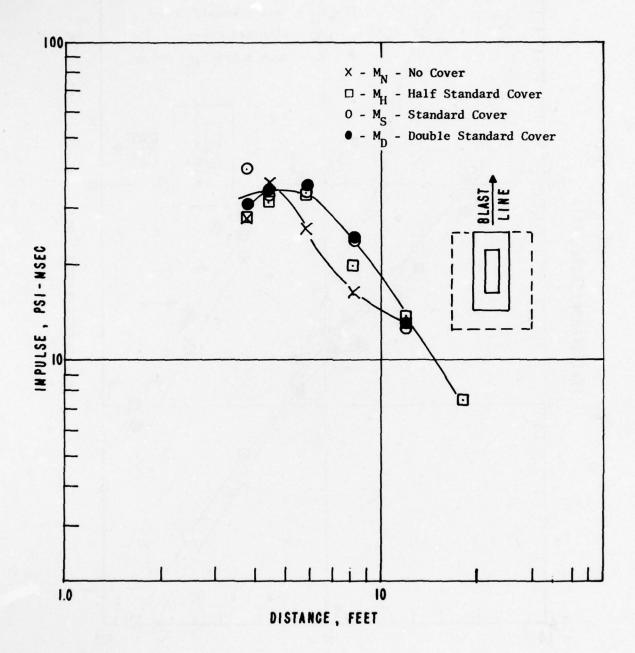


Figure 20. Impulse versus Distance Along the O Degree Line as a Function of Earth Cover for a 4.0 Pound (1.814 kg) Charge

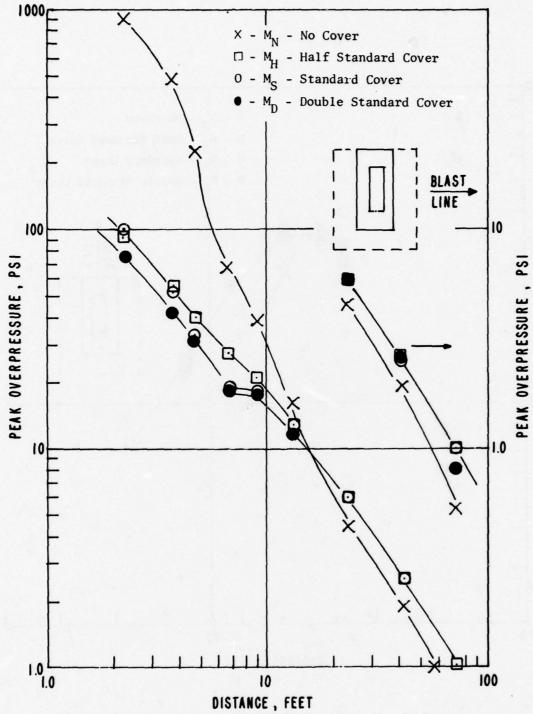


Figure 21. Pressure versus Distance Along the 90 Degree Line as a Function of Earth Cover for a 4.0 Pound (1.814 kg) Charge

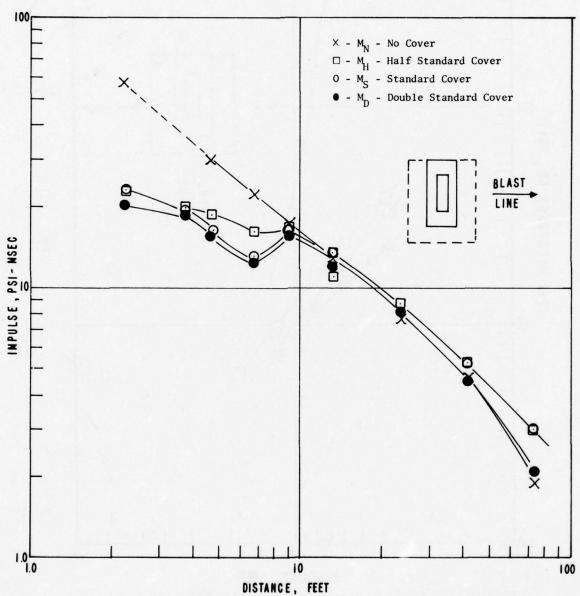


Figure 22. Impulse versus Distance Along the 90 Degree Line as a Function of Earth Cover for a 4.0 Pound (1.814 kg) Charge

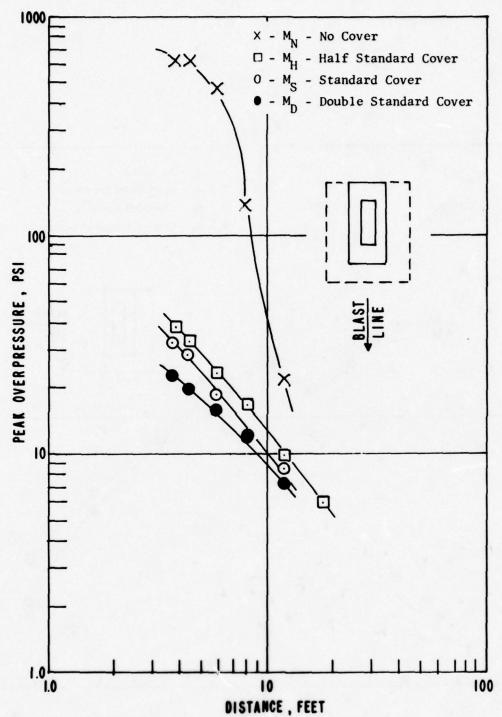


Figure 23. Pressure versus Distance Along the 180 Degree Line as a Function of Earth Cover for a 4.0 Pound (1.814 kg) Charge

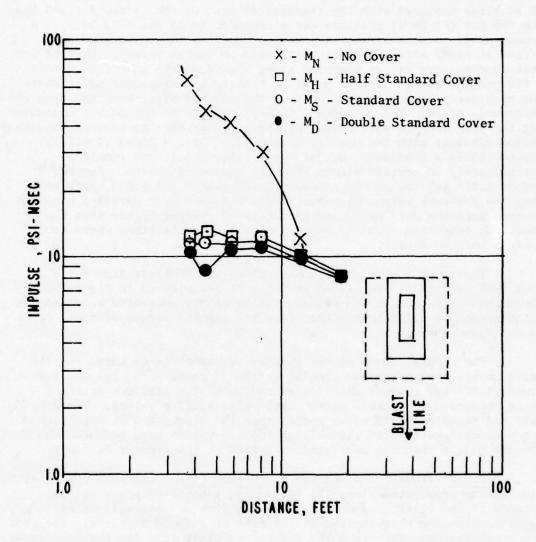


Figure 24. Impulse versus Distance Along the 180 Degree Line as a Function of Earth Cover for a 4.0 Pound (1.814 kg) Charge

2. Blast Parameters Along the 90 Degree Line The peak overpressures measured along the 90 degree line are listed in Table X for the four test conditions and plotted as peak overpressure versus distance in Figure 21. There are three things to note in Figure 21. First, the charge is larger and therefore the earth cover will have less effect in attenuating the peak overpressure. This can be seen at the first station where 900 psi (62) bars) measured on the uncovered condition has been reduced to 100 psi (6.89 bars) measured with the standard cover. On the .8 pound (.363 kg) the 900 psi (62 bars) pressure was attenuated to 48 psi (3.3 bars). A second point to note in that the change in cover thickness has less effect in blast attenuation with increase in charge weight. Most of the peak overpressure values measured along the 90 degree line fall within a ±10 percent band. A third point to note is the crossover point where the peak overpressure is greater from the covered magazines than from the. uncovered charge. The .8 pound (.363 kg) charge did not show a crossover but the peak-overpressure versus distance curves for the covered magazines became parallel with the one for uncovered. The 2.4 pound (1.088 kg) charge showed a crossover, but at 5 psi (.345 bars), and remained approximately 30 percent higher than the uncovered charge. For the 4 pound (1.814 kg) charge the crossover occurs at 9 psi (.620 bars) and then the pressure versus distance curves become almost parallel with the covered magazine data being approximately 40 percent higher than the uncovered condition with the exception of the last station where it is greater than 40 percent.

The impulse measurements made along the 90 blast line for the four test conditions are listed in Table XI and plotted in Figure 22. The impulse measured at the second station on the uncovered condition is of questionable validity and therefore the impulse versus distance curve is not drawn through it.

The general shape of the impulse versus distance curve for the earth covered magazines are similar to the .8 pound (.363 kg) and 2.4 pound (1.088 kg) charges with the exception of the last two stations where uncovered and double earth models give similar values. The one-half and standard earth cover models show the same trend as established for peak overpressure in that higher impulse values were measured on covered models than the uncovered condition at the greater distance.

3. Blast Parameters Along the 180 Degree Line The peak overpressure and impulse propagated along the 180 degree line is of prime interest because of the blast load developed on the door and headwall of an acceptor magazine when located at the rear of a donor magazine. The peak overpressures measured along the 180 degree blast line for the four conditions tested with a 4 pound (1.814 kg) charge are listed in Table X and plotted in Figure 23. All three covered magazines cause significant pressure attenuation at the close-in stations. The double earth cover model attenuates the peak overpressure from 40 to 10 percent more than the standard earth cover model. The larger attenuation occurs at the first station. The standard earth cover model attenuates an average of 20 percent more than the one-half earth cover model.

The impulse values recorded to the rear of the structure (180 degree line) for the four test conditions are listed in Table XI and plotted in Figure 24 as function of distance for each test condition. It is of interest to note that although the peak overpressure along the 180 degree line decreased with distance the impulse remains almost constant over the first four stations, with a small decay occuring at the last two stations. There is less than a  $\pm 10$  percent spread in the data points plotted for the three earth cover conditions with the exception of the second station with a double earth cover model.

#### D. Comparison of Model and Full-Scale Magazine Results

When this experimental program was first proposed and designed it was the opinion of the authors that relative differences in the effects of earth cover on blast parameters could be obtained from the 1/50 scaled models if the charge weights to interior structure volume ratios were maintained. It was also the opinion of the authors that these relative differences could be applied to full-size munition magazines. It was hoped, but not as strongly anticipated, that direct correlation of results from the model tests and full-scale tests could be achieved.

Results from a series of full-scale tests conducted during 1962 - 1963 are reported in Reference 2. In test six of the series, a donor charge of 100,000 pounds (45,360 kg) in a standard 60 foot (18.29 m) storage magazine was detonated and the blast parameters to the front, side, and rear were measured. This charge weight to structure volume ratio matches the 0.8 pound (0.363 kg) charge detonated in the 1/50th scale model magazine. Both the full scale and the 1/50th scale conditions have been scaled to a 1.0 pound (0.454 kg) charge at sea level and comparisons of blast parameters are made in the following sections.

1. Blast Parameters Along the 0 Degree Line The peak overpressure and impulse measured along the 0 degree line from the 0.8 pound (0.363 kg) charge have been scaled to 1.0 pound (0.454 kg) and listed in Table XII. The same blast parameters measured on the full-scale test 100,000 pounds (45,360 kg) have also been scaled to 1.0 pound (0.454 kg) and listed in Table XIII. The results of measured peak overpressure recorded from both scaled and full-size are plotted in Figure 25 as a function of scaled distance  $(R/W^{1/3})$  where R is the distance in feet from the charge that the measurement was made and W is the weight of the explosive in pounds.

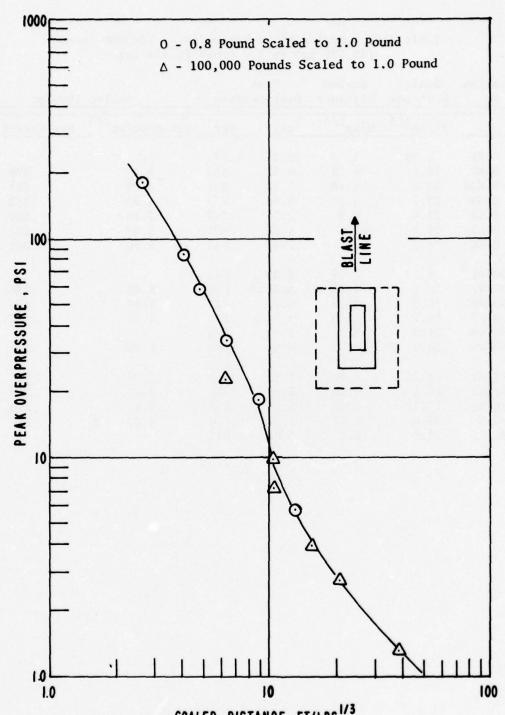
In Figure 25 it can be seen that excellent correlation was obtained between the model and full-scale results. The obvious low value of the full-scale test (Reference 2) at a scaled distance of 6.29 is a questionable datum point since the self-recording gage pre-initiated and recorded only a peak value.

Table XII. Scaled Blast Parameters - 0.8 Pound (0.363 kg) to 1.0 Pound (0.454 kg) - Standard Earth Cover

Station	Scaled	Scaled	Pea			
No.	Distance	Distance	Overpre	essure	Scaled	Impulse
	ft/1b <sup>1/3</sup>	m/kg <sup>1/3</sup>	psi	bar	psi-msec/1b <sup>1/3</sup>	bar-msec/kg <sup>1/3</sup>
0-1	2.65	1.05	179.	12.3	25.4	2.12
0-2	4.06	1.61	84.4	5.82	21.3	1.77
0-3	4.75	1.88	59.0	4.07	16.3	1.35
0-4	6.33	2.51	34.5	2.38	11.6	.970
0-5	8.79	3.49	18.5	1.28	7.97	.664
0-6	12.9	5.13	5.70	. 393	5.60	.466
90-1	1.53	.607	45.2	3.12	11.2	.933
90-2	2.65	1.05	29.6	2.04	8.72	.726
90-3	4.06	1.61	17.6	1.21	8.19	.682
90-4	5.03	1.99	14.0	.965	6.46	.539
90-5	7.20	2.86	10.4	.717	6.57	.548
90-6	9.80	3.88	7.0	.483	5.28	.440
90-7	14.3	5.68	4.23	.292	3.88	.323
90-8	25.0	9.91	1.73	.119	2.48	.207
90-9	44.9	17.8	0.78	.054	1.51	.125
180-1	2.65	1.05	22.2	1.53	5.82	.484
180-2	4.06	1.61	13.6	.938	5.71	.475
180-3	4.75	1.88	12.0	.827	5.28	.440
180-4	6.33	2.51	8.73	.601	4.63	.385
180-5	8.79	3.49	5.93	.409	3.77	.314
180-6	12.9	5.13	3.24	.223	2.91	.242

Table XIII. Scaled Blast Parameters - 100,000 Pounds (45,359 kg) to 1.0 Pound (0.454 kg)

Station No.	Scaled Distance	Scaled Distance	Peal Overpr		Scaled	Impulse
	ft/1b <sup>1/3</sup>	m/kg <sup>1/3</sup>	psi	bar	psi-msec/lb <sup>1/3</sup>	bar-msec/kg <sup>1/3</sup>
0-N1	6.29	2.49	22.8	1.57	_	
0-N2	10.5	4.18	9.62	.663	6.45	.578
0-N2A	10.5	4.18	7.12	.491	4.29	.384
0-N3	15.7	6.26	3.98	.274	3.93	.352
0-N4	21.0	8.37	2.71	.187	3.45	.309
0-N5	38.9	15.5	1.32	.091	2.09	.187
0-N6	76.1	30.3	0.43	.030	0.90	.081
90-W1	6.29	2.49	8.39	.578	_	_
90-W2	10.5	4.18	5.95	.410	5.45	.488
90-W2A	10.5	4.18	6.12	.422	5.54	.496
90-W3	15.7	6.26	4.04	.279	3.15	.282
90-W4	21.0	8.37	2.43	.168	-	
90-W5	38.9	15.5	0.99	.068	1.59	.142
180-S1	6.29	2.49	11.1	.765	4.99	.447
180-S2	10.5	4.18	5.09	.351	3.11	.279
180-S3	15.7	6.26	2.69	.185	2.41	.216
180-S4	21.0	8.37	1.94	.134	2.07	.185
180-S5	38.9	15.5	0.60	.041		



SCALED DISTANCE, FT/LBS 1/3
Figure 25. Pressure versus Scaled Distance Along the 0 Degree Line from a Full-Size Magazine and a 1/50 Scaled Model

The scaled impulse values  $I/W^{1/3}$  where I is measured impulse from a charge weight of W pounds listed in Table XII and XIII are plotted in Figure 26 as a function of scaled distance. Here again the correlation of impulse measured to the front of the structures is excellent.

2. Blast Parameters Along the 90 Degree Blast Line The peak overpressures, scaled distances and scaled impulses recorded along the 90 degree blast line for both the model and full-size structure are listed in Tables XII and XIII.

The peak overpressures are plotted as a function of scaled distance in Figure 27. The peak overpressure measured at a scaled distance of 6.29 on the full scale test (Reference 2) is low but here again only a peak value was obtained because the gage failed to run. There was also an acceptor magazine in place along side of the donor magazine which could have caused a decrease in the peak overpressure at that distance. The solid curve was developed from the results of the scaled model tests but it fits the scaled results from the full size tests quite well.

The scaled impulse and scaled distance along the 90 degree line for both model and full-size tests are listed in Tables XII and XIII and plotted in Figure 28. Here again it can be seen that using simple cube root scaling gives good correlation of impulse as well'as peak overpressure.

3. Blast Parameters Along the 180 Degree Blast Line The blast parameters recorded to the rear (180 degrees) of the full size and model structure have been scaled to a 1 pound (.454 kg) charge equivalent and listed in Tables XII and XIII.

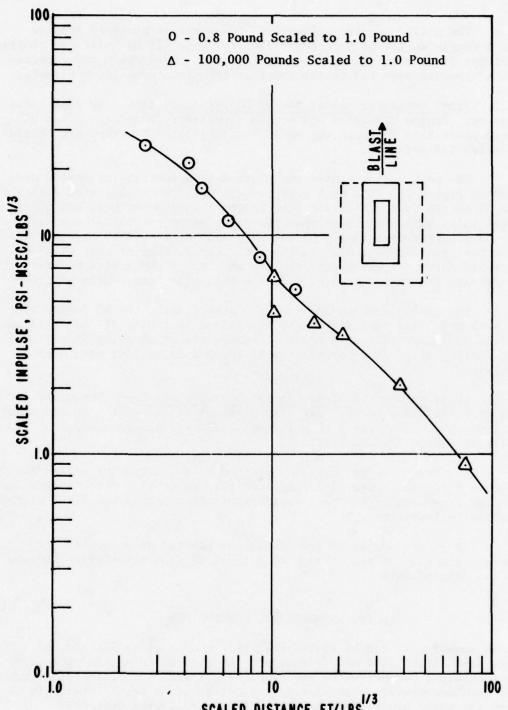
The peak overpressures are plotted as a function of scaled distance in Figure 29. The correlation of the two sets of data is excellent with the exception of the peak overpressure measured at the first station from the full-size test.

In Figure 30 the scaled impulse is plotted as a function of scaled distance. It can be seen that there is good correlation between the two sets of data.

## IV. SUMMARY AND CONCLUSIONS

In summary, it can be stated that the results of this series of tests have established many trends and the effects of varying the earth cover on blast parameters to the front, side, and rear of the structure have been documented. Some specific conclusions on earth cover effects along the three blast lines are given in the following sections.

<sup>&</sup>lt;sup>2</sup>A. R. Sound, "Summary Report of Earth-Covered Steel-Arch Magazine Tests," NOTS TP 3843, July 1965.



SCALED DISTANCE, FT/LBS

Figure 26. Scaled Impulse versus Scaled Distance Along the 0 Degree Time from a Full-Scale Magazine and a 1/50 Scaled Model

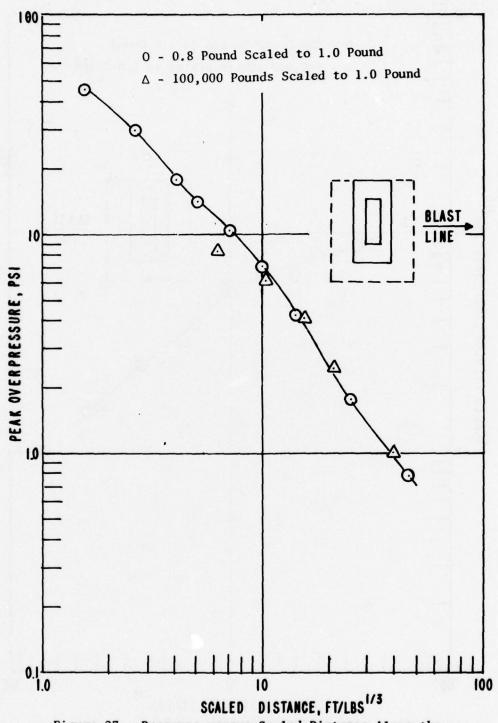


Figure 27. Pressure versus Scaled Distance Along the 90 Degree Line from a Full-Size Magazine and a 1/50 Scaled Model

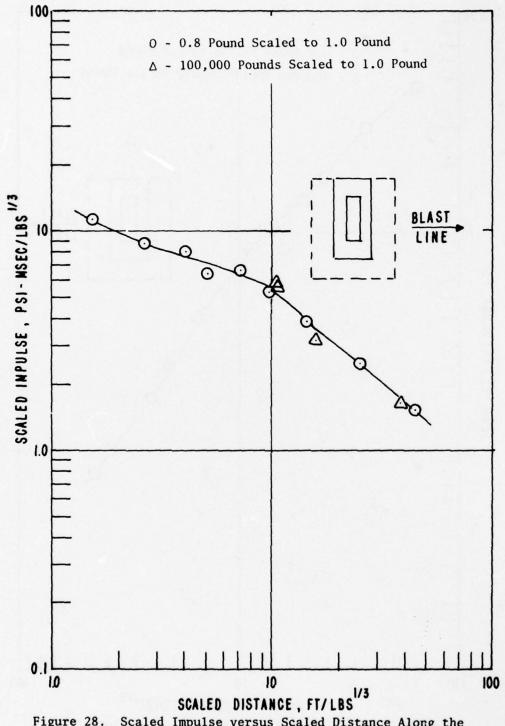
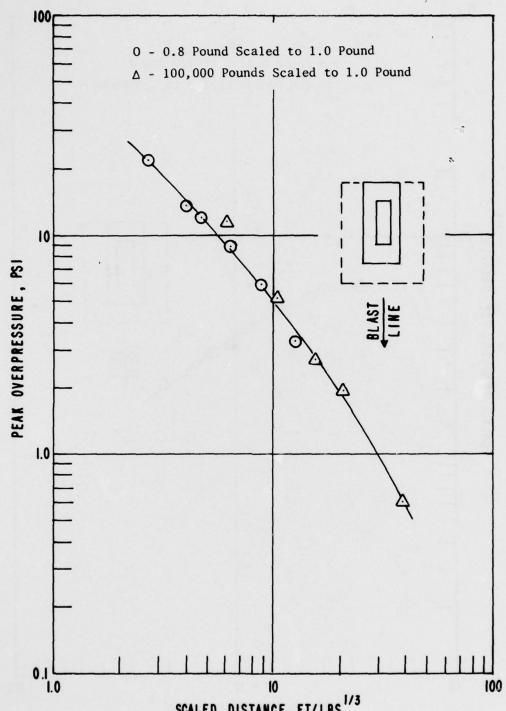


Figure 28. Scaled Impulse versus Scaled Distance Along the 90 Degree Line from a Full-Size Magazine and a 1/50 Scaled Model



SCALED DISTANCE, FT/LBS

Figure 29. Pressure versus Scaled Distance Along the 180 Degree Line from a Full-Size Magazine and a 1/50 Scaled Model

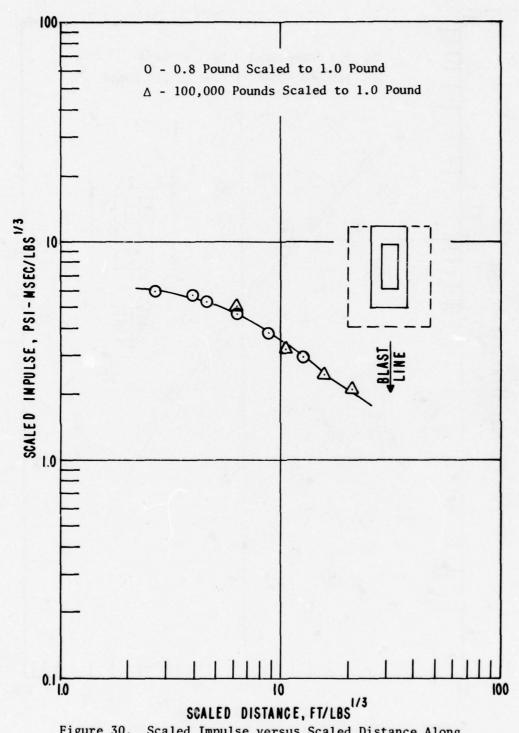


Figure 30. Scaled Impulse versus Scaled Distance Along the 180 Degree Line from a Full-Size Magazine and a 1/50 Scaled Model

## A. The O Degree Blast Line

The peak overpressure and impulse recorded at the first five stations along the blast line to the front of the structure were always greater when the earth cover was placed over the charge than when it was uncovered. This is apparently due to earth walls focussing the blast energy from the three sides to the front headwall where there is no earth cover. The one-half earth cover model produced an increase in peak overpressure and impulse over the uncovered charge while the standard earth cover model produced an increase in values over the one-half earth cover model. The double earth cover model did not produce an increase in values over the standard cover model. This leads to the conclusion that the addition of earth cover greater than the standard thickness does not increase the pressure and impulse to the front of the structure.

## B. The 90 Degree Blast Line

The peak overpressures and impulses measured from the side of the structure will be discussed separately because different trends were established as a function of charge weight and earth cover.

1. Peak Overpressure The peak overpressure recorded from the 0.8 pound (0.363 kg) charge as a function of distance for the three earth covers followed the expected trend. That is the more earth cover the more blast attenuation. The attenuation became less as the distance increased. At the last station the pressure values were 0.054, 0.052, 0.054, and 0.051 pounds per square inch going from the uncovered charge to the half, standard, and double cover model.

The peak overpressure recorded on the 2.4 pound (1.088 kg) tests as a function of distance produced an unexpected trend. The half earth cover model tests produced slightly less blast attenuation than the standard earth cover. At the first six stations the peak overpressures from both model tests were lower than the uncovered charge but beyond station 6 the trend reversed and the values recorded for the covered models were greater than the uncovered charge. This same trend was noted on the results from the 4 pound (1.814 kg) charge (see Figures 15 and 21).

2. Overpressure Impulse The impulses measured along the 90 degree line from the detonation of the 0.8 pound (.363 kg) charge showed the same trend as established for peak overpressure in that the three earth covered models recorded impulses less than the uncovered charge.

The impulse recorded along the 90 degree line from the 2.4 pound (1.088 kg) charge followed the same trend as the peak overpressure over the first five stations. At the greater distances the uncovered charge, the one-half earth cover model, and the standard earth cover model record similar impulses as a function of distance (see Figure 16).

The impulses recorded along the 90 degree line for the 4.0 pound (1.814 kg) charge as a function of distance and earth cover did not establish a trend similar to the peak overpressure. At station six and beyond the uncovered charge and the double standard earth cover model produced similar values while the other two models produced higher impulse values. The reason for this trend has not been established.

There is an anomaly in the impulse recorded at the fourth and fifth stations along the 90 degree line for the three charge weights. At the fourth station there is an apparent decrease in the impulse recorded for the double and standard earth cover followed by an increase of the impulse recorded at the fifth station. There is no explanation offered for this behavior at this time.

## C. The 180 Degree Line

Blast measurements made along the 180 degree line were to the rear of the structure.

- 1. Peak Overpressure The peak overpressure followed the same trend for all three charge weights. There was a very large attenuation observed at the close-in station, becoming less as the distance from the charge increased (see Figures 11, 17, and 23). The attenuation of peak overpressure became greater as the earth cover was increased.
- 2. Overpressure Impulse The overpressure impulse recorded along the 180 degree line was greatly attenuated at the close-in stations when the charges were covered with the models. As noted with the peak overpressure, this attenuation became less with increasing distance. The difference to be noted here is that the impulse is not very sensitive to the change in earth cover. It does not decay as rapidly with distance when covered as compared to uncovered models (see Figures 12, 18, and 24).

## REFERENCES

- R. Reisler, L. Giglio-Tos, and G. Teel, "Air Blast Parameters from Pentolite Cylinders Detonated on the Ground," BRL MR-2471, April 1975. AD #B003883L.
- A. R. Sound, "Summary Report of Earth-Covered Steel-Arch Magazine Tests," NOTS TP 3843, July 1965.

## ANALYSIS OF AN EXPLOSION BY G.S.Biasutti

Dr. Ing. Mario BIAZZI Soc. An. Vevey, Switzerland

In the realm of explosives manufacture, nitroglycerine explosions are the most devastating.

In the past, due to the total destruction of the equipment and the death of the eye-witnesses, very little remained which could help determine the causes of the accident.

Today, thanks to automation and remote control, much information can be gathered after an explosion.

The following is the story of a particularly interesting and instructive case. I wish and hope that my comments will help to prevent similar occurrences in the future.

It was a typical case of a combination of several unusual conditions, each one of which would not have been sufficient to lead to an explosion.

The accident occurred in a continuous and automatic nitroglycerine manufacturing plant, the location of which cannot be disclosed for security reasons. The amount of nitroglycerine involved in the explosion was about 900 lbs. There were no casualties but the destruction was total inside the building mounds.

It was one of twin units; the first had been commissioned a few months before the accident. The second one was due to be started-up by a qualified commissioning team.

Unfortunately the decision was taken not to wait for the experts and to start-up the plant on the basis of the know-ledge and experience gathered from the first unit.

The adjustment of the automatic controls and safety protection systems was done by insufficiently experienced people in an approximate manner and several mistakes were made.

Among these, the interface control instrument in the spent acid separator, which automatically maintains the nitrogly-cerine-spent acid interface at a constant level, was inoperative. Another instrument, which, on the basis of the specific gravity, detects in time any nitroglycerine which might escape with the spent acid, was not set properly.

Finally, the automatic control for the water flow to the spent acid leaving the separator was maladjusted.

This water, added in small amounts to the spent acid in cold weather, increases its solubility for nitroglycerine, preventing its separation at a lower temperature.

Water addition has a negative effect on the spent acid stability, therefore it must be used with caution.

In this particular case, due to the warm climatic conditions, no water addition was necessary. But, as a consequence of the wrong setting of the water flow control, water could flow to the spent acid at its maximum rate.

Three runs were made on the second unit under these unstable and unsafe conditions. They were uneventful but they produced a great quantity of highly diluted and hence unstable spent acid.

On the day of the accident the unit was started-up as usual by remote control. After a few hours, however, during a checkup visit to the unit, the personnel ascertained that the interface in the separator was quite low and a large amount of nitroglycerine had accumulated in it.

After having vainly tried to raise the interface, the foreman decided to shut-down.

The shut-down operation of a continuous nitration unit is done by letting spent acid enter the nitrator and slowly displacing all the nitroglycerine from the nitrator and separator towards the washers. The spent acid used for this purpose can be the same which has been produced in the plant.

This spent acid, stored in an outside storage tank, consisted of some old acid produced months before in the first unit and the new acid obtained from the second unit, which contained a high amount of water.

The analysis of this acid, made on the day of the explosion, showed a very high content of nitrous acid. This nitrous acid is slowly formed by hydrolysis and oxidation of the dissolved nitroglycerine upon standing. The velocity of this reaction is increased by the temperature.

Nitrous acid has the property of catalizing the oxidation reaction, which thus becomes self-accelerated.

The products of the hydrolysis of nitroglycerine are of various nature.

The first stage is the formation of glycerol dinitrate.  $C_3H_5 \ (NO_2)_2 \ OH.$ 

The oxidation of glycerol trinitrate molecules with nitric acid takes place very slowly; however, the presence of hydroxyl groups favours the oxidation reaction, which very rapidly increases with the increase of the amount of hydroxyls.

It has been demonstrated (Oehman, Explosivstoffe, 6-7, 1960, p.10) that practically no oxidation of nitroglycerine dissolved in spent acid occurs in a hydroxyl free system.

The old spent acid of the storage tank used for the displacement on the day of the accident contained a large amount of nitrous acid and, on account of the unnecessary water addition to the newly produced acid, a large amount of glycerol dinitrate. Its stability was very low. (Fig. 1)

Due to the previously mentioned unfortunate situation of the low nitroglycerine level in the separator, the very unstable displacement acid droplets had to travel through the nitroglycerine layer during the separation phase in order to reach the bottom of the separator. This does not happen when the displacement acid enters the separator at interface level.

Under these conditions, the glycerol dinitrate and the nitrous acid contained in the spent acid were transferred to the organic phase. The stable nitroglycerine produced on that day became unstable.

On account of the large amount of nitroglycerine in the separator, the displacement process lasted much longer than usual. The displacement acid became progressively more unstable and warmer.

Slowly but surely, the decomposition reaction began in the spent acid layer, with development of heat and nitrous oxides.

Both were soon transferred to the emulsion layer where the unstable nitroglycerine began to decompose. When its explosion temperature was reached, the whole mass detonated.

To conclude, the direct cause of the explosion was the use of very unstable spent acid for displacement.

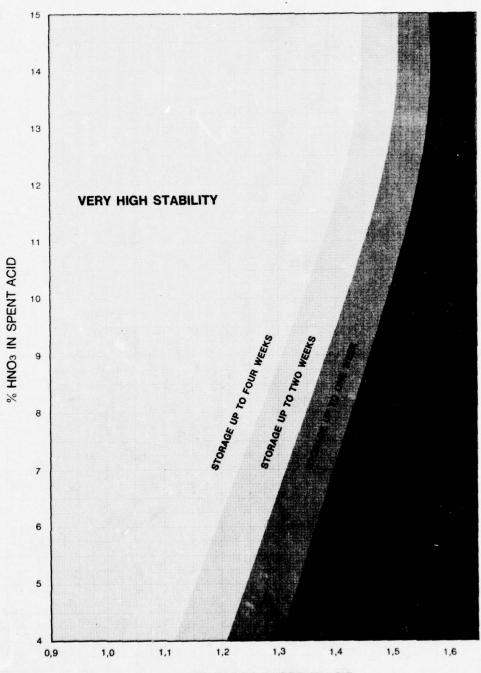
## The primary causes were :

- Loss of control of the water flow system to the spent acid which caused excessive dilution.
- 2) Failure of the separator interface control, allowing the nitroglycerine to reach the bottom of the separator and the unstable displacement acid to seep through the nitroglycerine.

A consequence of this low interface level was that the sensor of the thermostatic control which causes the drowning of the charge if the temperature reaches 90°F was in the nitroglycerine instead of in the emulsion layer. Due to the bad conductivity of the nitroglycerine, the heat generated by the starting decomposition in the emulsion zone could not be transmitted in time to the transducer.

Dr. Ing. Mario Biazzi Soc. An.

## STABILITY OF THE NG SPENT ACID AT 35°C



[H2O]: [H2SO4] IN SPENT ACID

## APPLICATION OF SUPPRESSIVE SHIELDING IN LAP PLANTS

David J. Katsanis
Edgewood Arsenal
Aberdeen Proving Ground, MD 21010

## ABSTRACT

Five groups of suppressive shields have been approved by Safety Offices for protection of hazardous munition production operations in US Army ammunition plants. These steel composite structures are designed to contain all fragments from an accidental explosion and to suppress any hazardous blast or flame effect to a safe level. Safety approved shields range in size from a 2-foot diameter steel shell to a 10-foot diameter steel cylinder.

The design of the safety approved shields will be discussed and several unique functional characteristics will be highlighted. Considerations pertaining to operational applications in US Army production plants responsible for load, assembly, and packaging of munitions will be presented together with some comments on potential for future applications.

## APPLICATION OF SUPPRESSIVE SHIELDING IN LAP PLANTS

## I. INTRODUCTION

## VG #1 - Title

Gentlemen, I'm Dr. David J. Katsanis from Edgewood Arsenal and today I will discuss the Application of Suppressive Shields to munitions plants responsible for load, assemble and pack (LAP) of explosive munitions. The development of suppressive shields has been performed for the Project Manager for the Army Production Base Modernization and Expansion (PBM&E) Program. This program is nearing completion and as a result numerous applications for suppressive shields are indicated.

## VG #2 - Fireball from 50 Pounds of Illuminate Mix

Suppressive Shields have been developed to provide a protective capability currently not available in the safety inventory. The fireball illustrated in this viewgraph results from the burning of 50 pounds of pyrotechnic illuminant mix (55% Sodium Nitrate and 45% Granulated Magnesium). Without protection an entire production line could be lost as a result of the fire caused by this type of reaction.

VG #3 - Suppression of Fireball with Group 5 Shield

Group 5 shield is shown in this viewgraph attenuating the fireball such that no flames exit the shield. Thus, the suppressive shield reduces a catastrophic Category IV hazard to Category I.

Suppressive shields have been developed by Edgewood Arsenal and safety approved by the DOD Explosive Safety Board. I will review the safety approved shields; describe their use, functional characteristics, current applications and highlight some of the design details developed for application to LAP plants.

## II. SAFETY APPROVED SHIELDS

## VG #4 - Safety Approved Suppressive Shields

We have designed, fabricated, proof tested and obtained safety approval for five specific suppressive shields. Originally, seven categories (now termed shield groups) of suppressive shields were defined to cover the numerous applications of these structures to hazardous operations in Army ammunition plants. Due to changes in the Army's Production Base Modernization and Expansion program shield groups 1, 2 and 7 were eliminated. These safety approved shields can be used for hazardous operations involving 37 pounds of explosive material or 30 pounds of pyrotechnic material. Included are cylindrical, rectangular box and spherical shaped structures which provide protection to hazardous operations ranging from cavity facing and fuze torquing of HE munitions to the transport of highly sensitive material such as lead ozide.

In the following series of viewgraphs, each approved shield will be illustrated and briefly discussed.

## VG #5 - Group 3 Shield

The group 3 shield is shown in this viewgraph. This structure consists of a cylindrical cage made up of a series of interlocking I-beams, reinforced with steel bands around the cylinder to withstand the hoop stresses developed. Three successful proof tests with 45 pounds of 50/50 pentolite has been conducted in the shield.

## VG #6 - I-beam Configuration

The interlocking I-beam design is shown in this viewgraph with closure strips and a corrugated steel liner to minimize the venting. This configuration has achieved an 84 percent reduction in pressure at the interline distance.

## VG #7 - Group 4 Shield

Group 4 shield testing was conducted at Dugway Proving Ground. This shield is safety approved for use in hazardous operations involved two 105 mm HE projectiles or an equivalent explosive yield (i.e., 9 pounds of 50/50 pentolite). A rotating product door which allows munitions to pass throught he shield on a conveyor was also successful tested in this shield.

## VG #8 - Rotary Product Door

This viewgraph illustrates the product door, which mounts in the shield wall. The door is designed to achieve greater pressure attenuation than the shield panel and prevent fragment escape.

## VG #9 - Group 5 Shield

Group 5 shield has been successfully designed and tested for application to non-explosive, deflagration, type material such as pyrotechnic compositions and propellants. Thirty pounds of illuminant mix was ignited in this shield and the hazardous fireball resulting was attenuated to a safe level several feet from the exterior of the shield.

## VG #10 - Group 6 Shield

The group 6 shield is a unique spherical design. The requirement for this shield is that an operator be capable of transporting on a push type cart small quantities of extremely hazardous primary explosive material. Due to the close proximity of the operator to the shield and the hazardous materials involved it was not feasible to allow any gas pressure to vent the shield. Use of this shield will result in a \$2.8 million savings at the IOWA AAP by eliminating a costly, automated conveyor system.

## VG #11 - 81 mm Shield

The 81 mm shield is currently safety approved for two 81 mm M347 mortar projectiles, however, this shield has been successfully proof tested with six 81 mm projectiles. Safety approval is being requested to uprate this shield accordingly.

A major benefit obtained by using suppressive shields in LAP plants is the reduction in quantity distance due to the pressure attenuation and fragment containment achieved. Therefore, the real estate required to provide adequate safety in ammunition plants is reduced.

## VG #12 - Manufacturing Area with Concrete Blast Wall

The "protective space" required for 500 pounds of high explosive is illustrated in this viewgraph for four munition loading lines. Suppressive shielding will allow a 10-fold reduction in real estate required to provide sufficient distance to meet existing army safety standards.

## VG #13 - Typical Manufacturing Area with Suppressive Shielding

This unique feature of suppressive shielding also allows the distance between operating lines and buildings to be reduced. In many plants being modernized automated conveyor systems to transport munitions between buildings cost \$1000 per foot of conveyor. Since safety demands large distances to prevent the propagation of an explosion, the cost of these conveyor systems is extremely high. Suppressive shielding can minimize these costs.

## VG #14 - Suppressive Shield Functional Characteristics

To be cost competitive with existing protective techniques, suppressive shields contain several unique functional characteristics. I will highlight the limit design and ease of assembly characteristics in the next series of viewgraphs. Structures are designed for a one accident life and must be replaced after an accidental detonation. This is necessary to allow the use of the "limit design" technique in suppressive shielding.

## VG #15 - Plastic Deformation in 81 mm Shield

"Limit design" means that the structure is designed to plastically deform as illustrated by the deformation of this suppressive shield build and tested for application to 81 mm mortar round production operations.

## VG #16 - Original Condition of 81 mm Shield

The shield prior to testing is shown in this viewgraph for comparison purposes.

All shield designs to date have relied on available off-the-shelf structural steel components. Most suppressive structures consist of three basic components: (1) A structural frame, (2) Panel members which mount to the frame, and (3) A foundation to prevent cratering when an explosion occurs.

## VG #17 - Modular Panels of Group 5 Shield

Typical modular panel members are illustrated in the viewgraph, ready for mounting to the foundation.

## VG #18 - Erection of Modular Panels of Group 5 Shield

On this particular design you will notice the frame is an integral part of the panel allowing rapid assembly.

## VG #19 - Assembled Group 5 Shield

This is the completed assembly.

Suppressive structures can be designed and configured to meet the specific requirements of any given application and still provide the desired protection. The modular characteristic allows greater flexibility in plant line layouts. In munition plants where pilot lines are investigated these shields can be moved to meet the requirements of the specific operations.

## $\frac{\text{VG } \#20}{\text{Modernization}}$ - Suppressive Shield Applications to Army Production Base Modernization and Expansion Program

Applications of suppressive shield to the Army's Modernization Program are indicated in this viewgraph. Engineers at Edgewood Arsenal are actively working with plant personnel to coordinate the application of shields at Milan, Lake City, and Iowa ammunition Plants. The proposed uses of shields on 55 separate modernization project results in over 300 individual shields.

## VG #21

The first shield to be installed in an LAP plant is the 81 mm shield. This shield will be used to protect the fuze cavity facing operation on Line C at Milan AAP. The prototype 81 mm shield size has been reduced by one panel length to reduce the shield cost.

Illustrated in the viewgraph are numerous penetrations required to make the shield operational.

## VG #22 - Utility Penetration Concent

A typical shield penetration is illustrated in this viewgraph. One concept being investigated for the penetration of utility lines through the shield is a junction box mounted on the inside wall of the shield. The cover plate is design to stop any hazardous fragments from penetrating a utility line.

## VG #23 - Lake City LAP Suppressive Shield

Another application for the 81 mm shield is the hazardous pressing operation for 20/30 mm HEI projectiles. For this application, the shield length was doubled. This illustrates the modularity of suppressive shields. This shield will be part of the SCAMP Mod B line at Lake City AAP. User requirements may require the use of the group 3 shield in this application if the quantity of hazardous material used in each press is increased.

## VG #24 - General Applications of Suppressive Shields

There are many other applications for suppressive shielding which have not been investigated in detail at this time and future development programs will evaluate the applicability of suppressive shields to these areas.

## VG #25 - Summary Suppressive Shielding

In the early conceptual design phases of a munition LAP production line when problems are encountered such as excessive quantity distance, tight space requirements for spacing ammunition on the line, in-plant transport and storage which places restriction on the operation, the application of suppressive shielding should be considered as a solution.

We at Edgewood Arsenal are confident that suppressive shielding will have a major impact throughout the Government and offers promise of major applications to the industrial community as well. Edgewood Arsenal has functioned in the past as consultants to review, evaluate and recommend suppressive shield designs and will continue to do so.

However, total development of suppressive shields for your specific applications is the preferred procedure. Gentlemen, its been my pleasure to brief you today and look forward to future discussions concerning suppressive shielding.

# DEPARTMENT OF DEFENSE EXPLOSIVES SAFETY SEMINAR

**SEPT 1976** 

APPLICATION OF SUPPRESSIVE SHIELDING TO LAP PLANTS

by

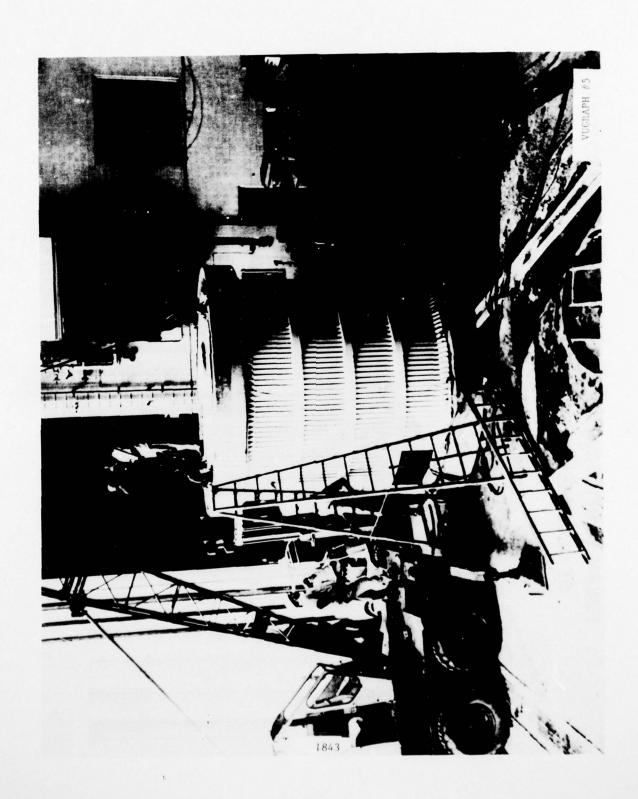
DR. DAVID J. KATSANIS Manufacturing Technology Directorate Edgewood Arsenal SEPT 76

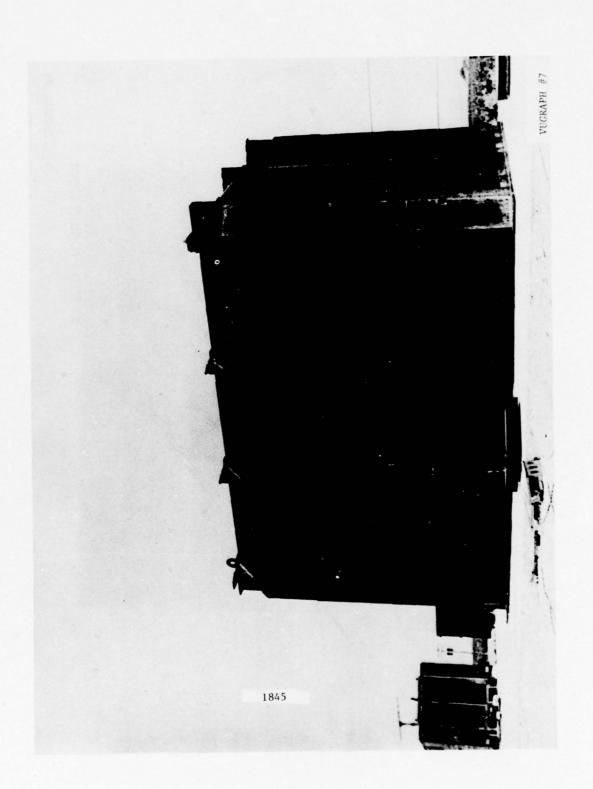


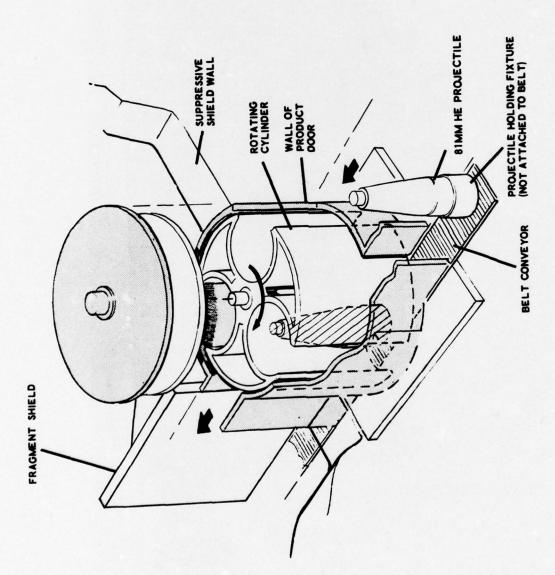


## SAFETY APPROVED SUPPRESSIVE SHIELDS

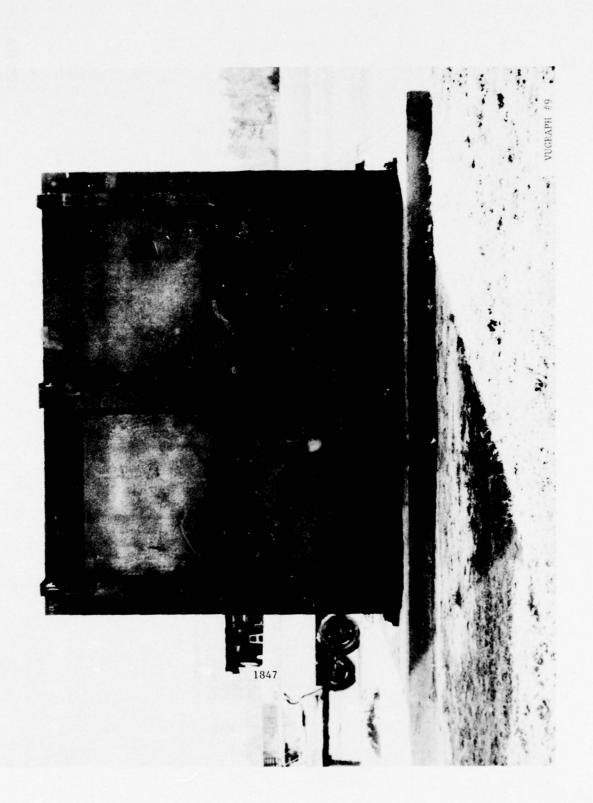
SHIELD TYPE	MATERIAL LIMIT	OPERATOR SAFE DISTANCE (feet)	SIZE (feet)
GROUP 3	37 LB. PENTOLITE	6.2	11.25 DIA. X 10h
GROUP 4	9 LB. PENTOLITE	19	9.2 X 13.1 X 9.3h
3 di l'UB5	1.84 LB. C-4	3.7	45 0 4 01 0 4 01
	30 LB. ILLUMINANT MIX	₽	10.0 × +.01 × +.01
GROUP 6	13.6-0Z. PENTOLITE	\ \	2 DIA.
81MM	2 - 81MM RDS 2.8 LB. C-4	3	14 X 18.7 X 12.4h



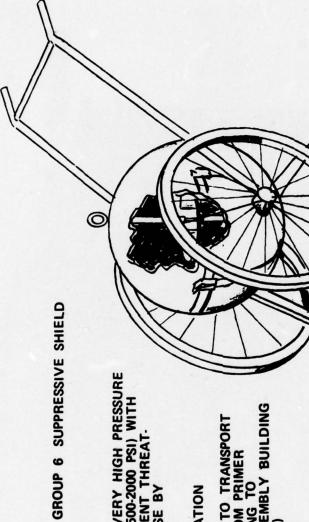




## 81 mm Product Door



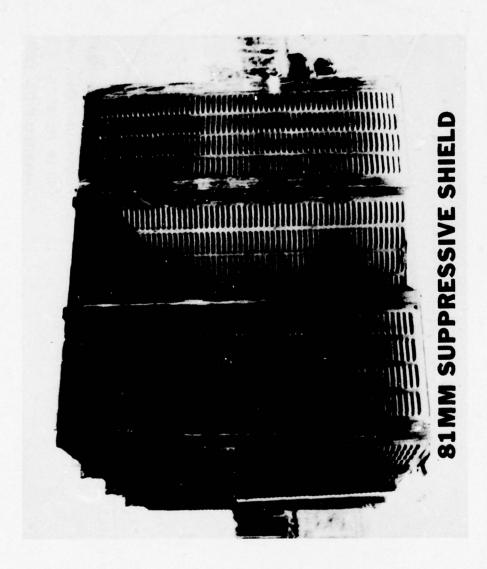
SEP 76



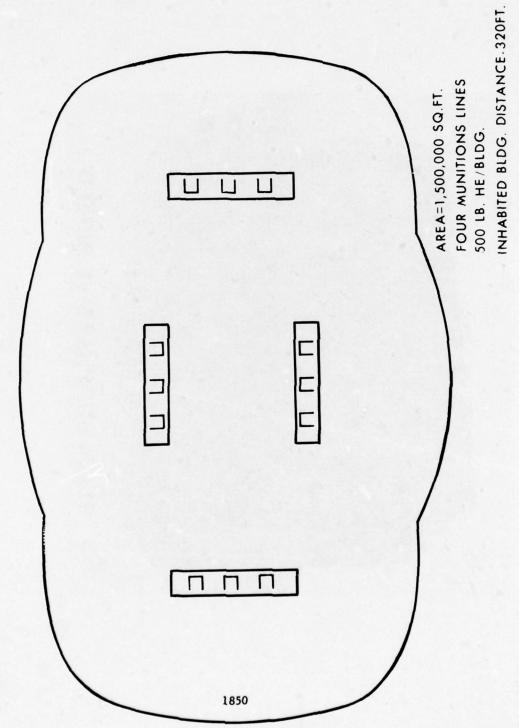
DESIGNED FOR VERY HIGH PRESSURE APPLICATIONS—(500-2000 PSI) WITH MINIMAL FRAGMENT THREAT-PERSONNEL CLOSE BY

TYPICAL APPLICATION

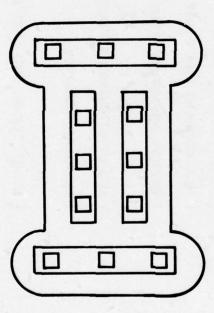
USE AS A CART TO TRANSPORT PRIMER MIX FROM PRIMER PROCESS BUILDING TO DETONATOR ASSEMBLY BUILDING (IOWA BACKLINE)



## MANUFACTURING AREA WITH CONCRETE BLAST WALL



VUGRAPH #12



AREA-132,000SO. FT. 500 LB. HE/BLDG. FOUR MUNITIONS LINES BLDG. SEPARATION DISTANCE 61 FT.

3C 035

VUGRAPH #13

## SUPPRESSIVE SHIELD FUNCTIONAL CHARACTERISTICS

LIMIT DESIGN

ONE ACCIDENT LIFE CYCLE

ENERGY ABSORBING STRUCTURE

EASE OF ASSEMBLY

USE OF STANDARD STRUCTURAL STEEL MEMBERS

MODULAR ASSEMBLY

BLAST, FLAME, AND CHEMICAL AEROSOL ATTENUATION

MAXIMUM PROTECTION

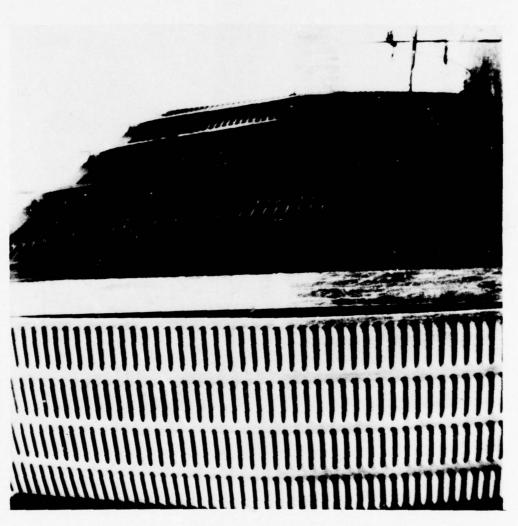
COMPLETE FRAGMENT CONTAINMENT

SEP 76

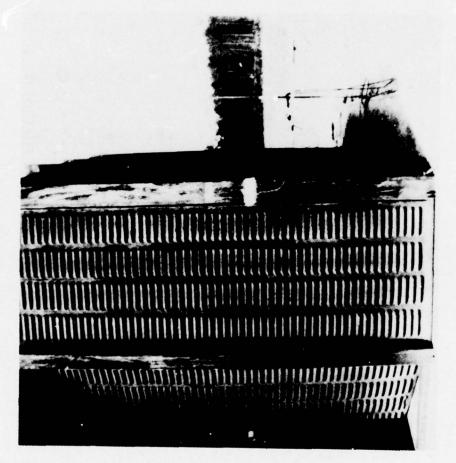
WGRAPH #14

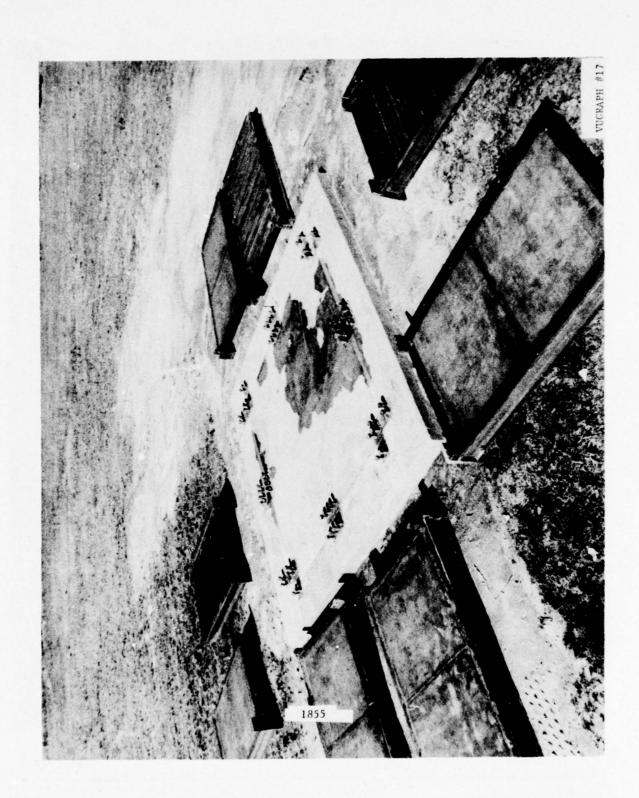
VUGRAPH #15

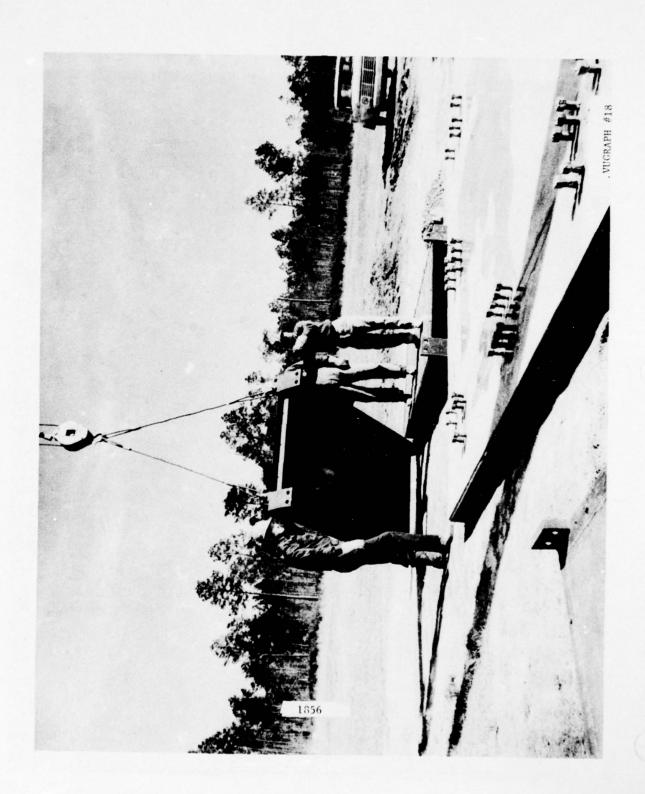
DAMAGE TO 81mm SUPPRESSIVE SHIELD IN 6 ROUND TEST (RIGHT FRONT)

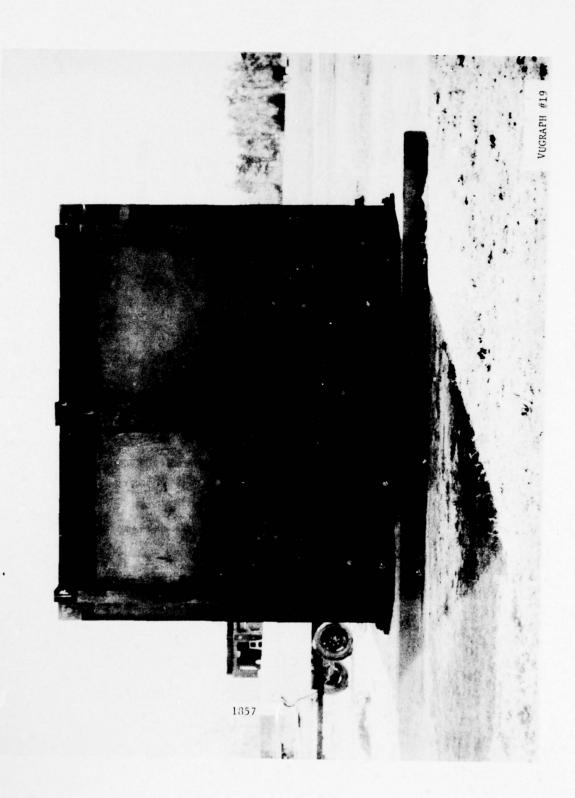


**SEP 76** 









# SUPPRESSIVE SHIELD APPLICATIONS TO PBM & E PROGRAM

1	ļ	ı	
i	ł		
		ı	
,		ı	
•		ı	
•	١	ı	
P	١	ı	
1	1	ı	
ı	I	ı	
	i	ı	

IOWA AAP - - TRANSPORTATION OF LEAD AZIDE ON DETONATOR LAKE CITY AAP - - 20/30MM HEI PRESS LOADING OPERATION MILAN APP - - 81MM DRILL AND FACE OPERATION

PROPOSED

1358

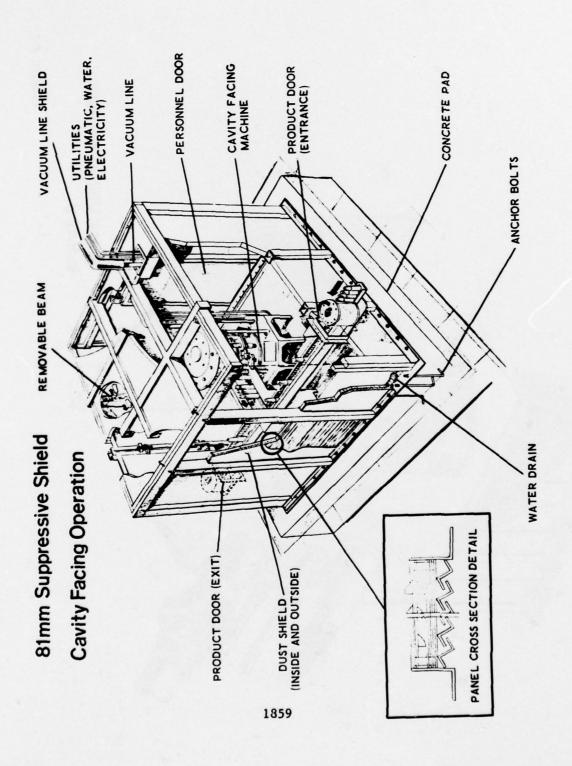
MELT – POUR PROJECTS 17
ICM PROJECTS 10
DETONATOR PROJECTS 3
OTHER LAP PROJECTS 25

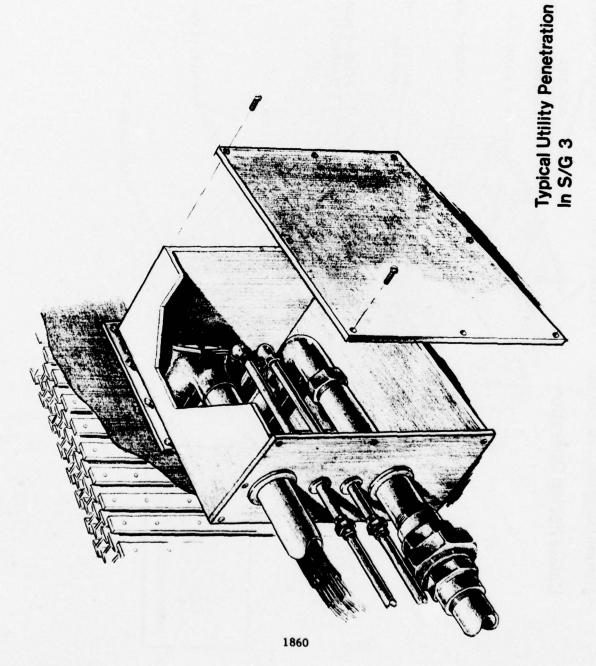
**SEPT 1976** 

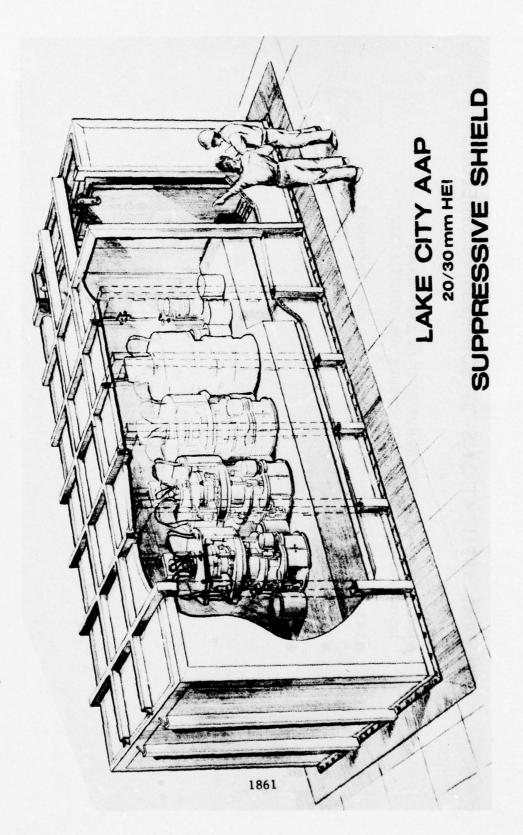
55

TOTAL

VUGRAPH #20







## GENERAL APPLICATIONS OF SUPPRESSIVE SHIELDS

● HAZARDOUS MUNITIONS MANUFACTURING OPERATIONS INVOLVING EXPLOSIVES, PYROTECHNICS, AND PROPELLANTS

TRANSPORTATION AND STORAGE OF HAZARDOUS MATERIALS

**EXPLOSIVES FORMING** 

STATIC FIRING RANGES

SEP 76

### SEPT 76

### SUMMARY SUPPRESSIVE SHIELDING

BETTER PROTECTION

■ COST EFFECTIVE CONSTRUCTION

• USEFUL IN AMMUNITION ACTIVITIES

EXPANDING ARMY USE

PROMOTING WORLD-WIDE APPLICATION

DEDGEWOOD ARSENAL PROGRAM LEADER

### SUPPRESSIVE SHIELDING TECHNOLOGY PROGRAM

Bruce Jezek Edgewood Arsenal, MD

Engineers and scientists at Edgewood Arsenal have conducted a series of in-depth studies to develop methods and procedures for the accurate prediction of shield design parameters. It was found early in the program that inadequate information was available for accurately predicting the effects of blast, fire, and fragmentation that would occur during the accidental detonation of an explosive in a munition operation. The purpose of these studies was to develop a design engineering handbook suitable for use by plant engineers so that they could adequately design their own shields in the future. phenomena studies were conducted in an effort to define and quantify the pressures and forces that are created in a shield during an explosion. This test data was then checked against known analytical codes to determine the adequacy of these design equations. Design loads and stress analysis methods were also developed to aid the designers with the capability of predicting the loads in a given structure. Fragmentation characteristics were also analyzed both for the primary and the secondary fragments resulting from the explosion. It was found early in the program that all too often the fragments threat dictated the size and material thickness required to suppress the effects of a given detonation. Structural response studies were also conducted to determine the effect in the structure of the impulsive dynamic quasi-static loads.

This paper will review these studies to present some of the results that were obtained by Edgewood Arsenal. Results of these studies will be incorporated in the engineering design handbook by June 1977, and should be available to design engineers by the end of calendar year 1977.

### SUPPRESSIVE SHIELDING TECHNOLOGY PROGRAM

### I. INTRODUCTION

### VG #1

Gentlemen, I'm Bruce Jezek of Edgewood Arsenal and my paper today covers the technology development phase of suppressive shielding. Dr. Katsanis has discussed the hardware development of suppressive shielding and the applications of shields which have been proven through explosive testing. I will present the software developed in the past several years which provides the analytical tools to design future suppressive shields.

### VG #2

Technology development of suppressive shields has proceeded along the lines illustrated in this chart. In the event of an accidental detonation, blast, fragment and fireball hazards result. Definition of these hazards is essential to the design of a shield. Each of these hazards poses a special problem to the designer and requires consideration, not only singularly but synergetically. Procedures to predict the suppression of the blast, fragment, and fireball hazard is the next step in the technology development. Consideration of the loading imposed on the structure and the associated structural response is necessary to provide a safe shield. The hazard suppression requirements must be satisfied as well as the structural requirements and trade-offs made in the design to obtain the best shield.

### VG #3

Edgewood Arsenal has been the lead agency for suppressive shielding technology development and has obtained support from the performers shown on this viewgraph. Ballistics Research Laboratories (BRL) located at Aberdeen Proving Ground has been tasked with major efforts in the areas of blast and fragment definition, blast and fragment suppression, fireball definition, and structural analysis. The NASA National Space Technology Laboratories (NSTL) located in Bay St. Louis, MS has been used to perform testing in suppressive shields fabricated as part of the hardware development program. Extensive instrumentation was used to record blast pressure data and structural response data for verification of predictive analytical techniques. The Naval Surface Weapons Center (NSWC), formerly Naval Ordnance Laboratory (NOL), at White Oak, MD provided blast codes for defining gas pressures inside suppressive shields. Southwest Research Institute (SwRI) has provided contractural support in all analytical development areas and has developed scale model laws for defining the blast pressure attenuation outside of suppressive shields.

### II. SCENARIO DEFINITION

### VG #4

Prior to design of a suppressive shield, the scenario for the specific application of the shield must be defined. This could be simply a matter of describing the characteristics of the explosive, i.e. yield, type, and shape, for application of suppressive shields to explosive storage, or, very complex, where hazardous operations involving equipment support the manufacture of a munition.

Basically, this task requires describing "what is happening". This view-graph illustrates the machinery and associated support items involved in the cavity facing operation of an HE projectile. The location of the munition, its orientation, and the position of conveyors and other equipment surrounding the operation must be defined to allow prediction of the blast, fragment, and fireball threats that the shield will encounter. Due to the limited time of this presentation, only the blast and fragment aspects associated with suppressive shields will be discussed.

### III. BLAST ENVIRONMENT

### VG #5 - Free-Air Reflected Pressure Comparison

This VG (#5) illustrates the predictive capability available for defining the reflected pressure as a function of time for an explosive detonation in free air. As illustrated by the excellent correlation between the theory and the experimental data, this technology is known and available for use. However, by surrounding the explosive with a suppressive shield causes a more complex blast profile inside the shield. The shock waves resulting from the detonation are reflected off the shield walls and re-reflected many times inside the shields causing a non-uniform pressure loading on the shield.

### VG #6 - Blast Environment

The blast environment task is to define the blast field associated with suppressive structures. This requires the definition of the internal pressures - reflected and quasi-static and the external incident pressure as a function of such parameters as charge size, shape and geometry; shield venting characteristics; and the shield configuration.

### VG #7 - Reflected Impulse for One Pound Pentolite Charge

This viewgraph depicts one wall of a suppressive shield with the reflected impulse in various positions indicated. The reflected impulse is appreciably higher in the corner locations of the shield. This loading profile must be addressed in the design of a suppressive shield. (The reflected impulse values shown are in psi - ms and are for the detonation of one pound of 50/50 pentolite in a 3 foot cubical shield attached to a concrete foundation.)

VG #8 - Three Dimensional Plot of Blast Pressure in 1/4 Scale Group 1 Shield

Another example of the pressure loading inside a shield is shown in this viewgraph. This three dimensional plot of the blast pressure was obtained from the WUNDY/DORF computer code prepared by Ballistics Research Lab.

Pressure is represented by the vertical axis with the X-axis being the distance from the center of the charge to the shield roof and the Y-axis being the distance from the charge to the shield wall. The reflected pressure for 45.7 pounds of 50/50 pentolite in the 1/4 scale group 1 shield is illustrated just after the initial shock wave has been reflected from the roof.

VG #9

The second internal pressure of concern in the design of suppressive shields is the quasi-static pressure. When a explosion is confined in a fixed volume as in a suppressive shield, a long-term gas pressure results from the oxidation of the explosion products. This gas pressure build-up is termed the quasi-static pressure and is illustrated in this viewgraph.

The peak quasi-static pressure is normally much lower (162 vs 4000 psi) than the reflected pressure, however the duration is much longer (0.32 vs 50 milliseconds). Therefore, the quasi-static must be considered in the structural loading. Prediction of this pressure is extremely difficult even though numerous methods exist for computing the quasi-static pressure. Attempts to accurately measure the quasi-static pressure proved difficult, since the pressure gauge is first exposed to the high blast pressure. The gauge must be capable of withstanding this blast pressure, and yet accurately record the much lower quasi-static pressure.

### VG #10 - Quasi-Static Pressure Inside Shield

One method to predict the quasi-static pressure was to use the NOL INBLAS computer code to match the experimental results. By doing this the peak quasi-static pressure would be approximately 200 psi for the data plotted in this viewgraph. This value results for the 45.7 pound 50/50 pentolite charge used in the 1/4 scale group 1 shield.

### IV. BLAST ATTENUATION

### VG #11 - Blast Attenuation

Blast attenuation in a suppressive shield is achieved by a controlled venting of the pressure through various combinations of nested structural members. Definition of these venting characteristics was achieved by conducting shock tube tests using scale model suppressive panels and conducting explosive tests in scale model suppressive shields.

VG #12 - Percent Attenuation in Pressure vs Percent Venting (From Shock Tube)

The 10 cm shock tube at Ballistic Research Labs was used to investigate the effects of venting on pressure attenuation. By varying the venting conditions such as the hole diameter, number and vent area for perforated plates, the effects of each parameter on the pressure attenuation was determined. This viewgraph illustrates the effect of one design parameter, the hole size in a perforated plate, on the pressure attenuation. For the conditions tested (in this case constant vent area), pressure attenuation was independent of hole size. Ballistic Research Labs has published several reports summarizing these tests.

VG #13 - Curve Fit to Blast Pressure Outside Suppressive Structures

Using model analysis techniques and experimental data from numerous scale model and prototype tests, an equation for predicting the blast pressure outside a suppressive shield was developed by Southwest Research Institute. The equation shown on this viewgraph is dependent on the explosive yield (W) vent ratio (0), standoff distance from the charge (R), and width of the shield (X). Use of this equation allows the prediction of external pressure based on any given set of shield design parameters. It should be noted that suppressive structures are designed to meet the user's requirement, and in Army ammunition plants, safety requires that pressures at operator locations not exceed 2.3 psi (peak side-on or incident pressure). Knowing the pressure level (P<sub>S</sub>), the standoff distance (R), and the shield size (X), allows the vent ratio (0) to be determined and incorporated in the shield design.

### V. FRAGMENT ENVIRONMENT

### VG #14 - Fragment Hazards

The second major element to be considered in the design of a suppressive structure is the fragmentation threat. When a detonation occurs, the blast pressure accelerates the munition components and items surrounding the munition to high velocities, posing a severe hazard to operating equipment and personnel. Fragment hazards are classified as (1) Primary: those fragments in direct contact with the explosive such as the shell casing of an HE projectile, and (2) Secondary: those fragments not in immediate contact with the explosive material.

### VG #15

For example, parts of the equipment shown in this viewgraph are defined as secondary fragments, and require special consideration. Items such as rollers for rotating the munition during fuze assembly operations, the roller shaft, and the like, all are classified as secondary fragments. Though more massive than the small high velocity primary fragments of an HE projectile, in some instances, these secondary fragments pose a more severe threat.

### VG #16

Data exists in the Joint Munitions Effectiveness Manual for defining the mass and velocity of primary fragments from various munitions. These data were obtained by exploding a munition in a circular arena and catching the fragments in a soft media (wall board). This allowed determination of individual fragment mass and velocity which are essential parameters for predicting the fragment hazard.

### VG #17

To establish methodology to predict the secondary fragment characteristics, an experimental model test program was developed. This viewgraph illustrates the explosive charges, explosive type, and secondary fragments used in the conduct of these tests. These parameter values were selected to cover the range of values anticipated from an accidental detonation in an Army Ammunition Plant.

### VG #18

The secondary fragment test set-up is illustrated in this viewgraph.

The secondary fragment was located at a given stand-off distance from the explosive and the explosive was detonated propelling the fragment past an orthogonal bank of X-ray tubes. Analysis of the X-rays allows measurement of the fragment velocity. Both constrained and un-constrained fragments are being considered nstrained fragments require additional energy to break the fragment from its constraints. These explosive tests are nearing completion at Ballistic Research Labs on this technology phase.

### VI. FRAGMENT CONTAINMENT

### VG #19 - Fragment Containment

Suppressive shields are designed to contain all fragments resulting from an accidental detonation. Fragment containment technology development is described in this viewgraph. A complementary test program and model analysis has been conducted to establish methodology to predict the fragment-stopping capability of suppressive structures. Panel parameters such as spacing, thickness, and configuration and fragment parameters such as mass, velocity, geometry, and area have been incorporated in this investigation.

### VG #20 - Large Bore Gun For Fragment Tests

The test program was conducted using a large bore gun to ballistic launch controlled fragment shapes at various suppressive panels.

### VG #21 - Typical Suppressive Panel Target

This viewgraph illustrates a small section of a suppressive panel which the gun launched fragment impacted. These target panels were used to evaluate the effects of spacing on the fragment-stopping capability of suppressive panels. The striking velocity of the fragment was measured and orthogonal X-rays were used to determine the "behind-the-plate" mass and velocity after fragment penetration of the panel members.

### VG #22

This viewgraph shows a typical series of X-rays illustrating a cylindrical fragment simulator penetrating a segment of the 81mm suppressive shield panel. The fragment break-up (if any occurs) can be observed along with the orientation. Data from these X-rays provide residual velocity data necessary to predict the fragment stopping capability of a suppressive panel.

VG #23 - Behind The Target Model for a Fragment Attacking a Spaced Target

To develop an analytical model for predicting the fragment-stopping

capability of a given panel design, the parameters illustrated in this viewgraph must be described. These include striking velocity  $(V_1)$ , striking mass  $(\theta_1)$  fragment presented area (AP), panel thickness  $(T_1)$ , panel angle of obliquity  $(M_1)$  and the fragment orientation or impact angle  $(\mu_1)$ . After penetration the exit (subscript 2) parameters must also be defined. These exist parameters are used as the input or striking parameters for the next layer in the suppressive panel.

VG #24 - Predictive Equation for Fragment Ballistic Limit Velocity

Ballistic Research Labs has used the experimental test data to develop empirical models to predict fragment penetrations. This viewgraph illustrates a typical fragment velocity equations. Note that numerous empirical constants are required.

VG #25 - 273 Gram Aluminum (2024-T3) Cylinder Attacking Spacing Target

The common practice for assessing the fragment-stopping capability of the target is to determine the V vs V or residual velocity vs striking R S velocity curve for a given target/fragment configuration. The residual velocity is defined as the fragment velocity after penetration. The data on this viewgraph are for two spacing distances between two structural elements (in this case a Z bar and a perforated plate) and indicates that the results are insensitive to the spacing parameter. The analytical model developed during the suppressive shielding technology program predicts the results shown by the dashed curve (use overlay, in red, during talk) plotted on the V vs V graph. Excellent agreement between the theory and the experimental R S data is indicated.

### VG #26 - Unique Fragment Simulators

Future tests in the fragment area will be conducted with more massive plates and pipes to simulate secondary fragments. Analytical models will be developed to predict the penetration effects of these fragments.

### VG #27 - Secondary Fragment Limit Speeds

To illustrate the progress made during the past year, the limit velocity predictions for small secondary fragments emanating from the fuze torque operation on a 105mm projectile are compared. The FY75 predictions were best estimates prior to the technology development on the suppressive shielding program. Accurate determination of the material thickness necessary for containment of fragment hazards is essential for the design of cost effective protective shields and the reductions illustrated in this viewgraph will significantly effect the shield design and final cost.

### VII. ENGINEERING DESIGN HANDBOOK

### VG #28 - Suppressive Shielding Engineering Design Handbook

Our technology development program will culminate with the preparation of an engineering design handbook for suppressive structures. It is envisioned that this handbook will complement the existing design manual for laced reinforced concrete (TM 5-1300) and incorporate chapters show in this viewgraph,

### VIII. SUMMARY

### VG #29 - Summary

In summary, technology has been developed to predict the hazards posed to suppressive structures and methodology developed to predict the procedures to suppress or attenuate these hazards. I have not discussed the structural response aspects of this technology development, however, standard structural analysis procedures are available and are being used in the design of suppressive structures.

### DEPARTMENT OF DEFENSE EXPLOSIVE SAFETY SEMINAR

**SEPT 1976** 

### SUPPRESSIVE SHIELDING TECHNOLOGY PROGRAM

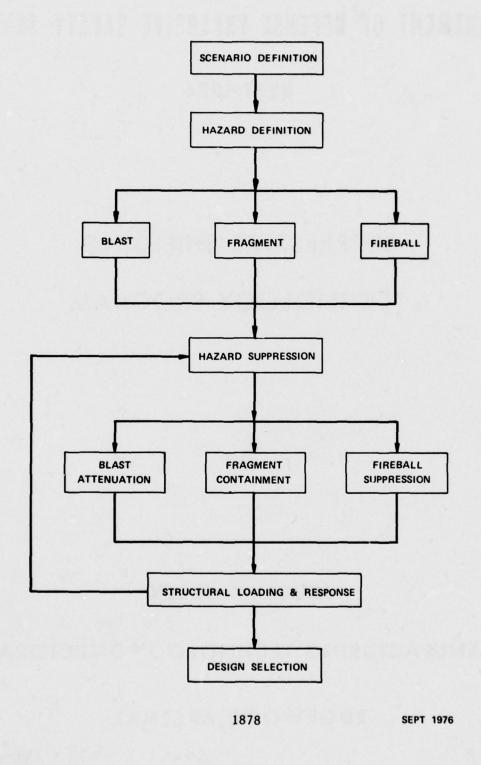
by

BRUCE W. JEZEK

MANUFACTURING TECHNOLOGY DIRECTORATE

EDGEWOOD ARSENAL

### TECHNOLOGY FLOW CHART



### VUGRAPH #3

## APPLIED TECHNOLOGY PARTICIPANTS

### BALLISTIC RESEARCH LAB (BRL)

- 1) MAJOR CONTRIBUTOR
- 2) DEVELOP TECHNOLOGY IN AREAS OF:
  BLAST
  FRAGMENTATION
  THERMAL

## NASA NATIONAL SPACE TECHNOLOGY LAB (NASA-NSTL)

STRUCTURAL

- TEST/FABRICATION SUPPORT
- 2) OBTAIN APPLIED DATA FROM GROUP SHIELDS

## NAVAL SURFACE WEAPONS CENTER (NSWC) (FORMERLY NAVAL ORDNANCE LAB-NOL)

1) TECHNICAL SUPPORT IN: BLAST CODES STRUCTURAL ANALYSIS

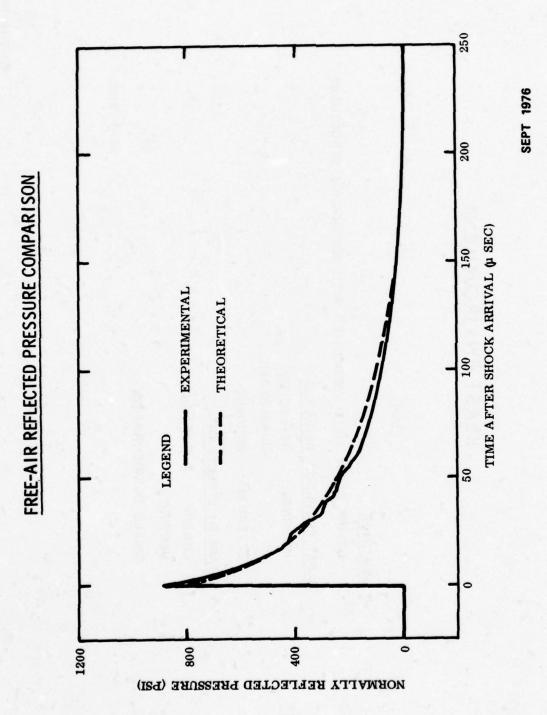
### SOUTHWEST RESEARCH INSTITUTE (SWRI)

(CONTRACTOR)

- 1) CONSULTANT SERVICES
- ) DATA ANALYSIS
- 3) MODEL/SCALING LAW DEVELOPMENT

VUGRAPH #4





### VUGRAPH #6

### **BLAST ENVIRONMENT**

OBJECTIVE

DEFINE BLAST FIELD ASSOCIATED WITH SUPPRESSIVE STRUCTURES

BLAST PRESSURES REQUIRED

INTERNAL - REFLECTED

QUASI-STATIC

EXTERNAL - INCIDENT

ESTABLISH EFFECTS OF

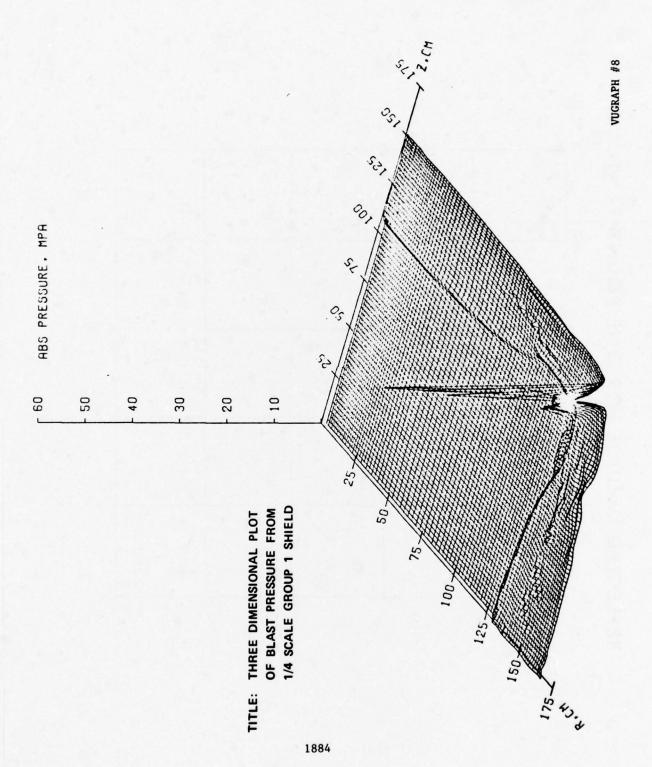
CHARGE - SIZE, SHAPE, GEOMETRY

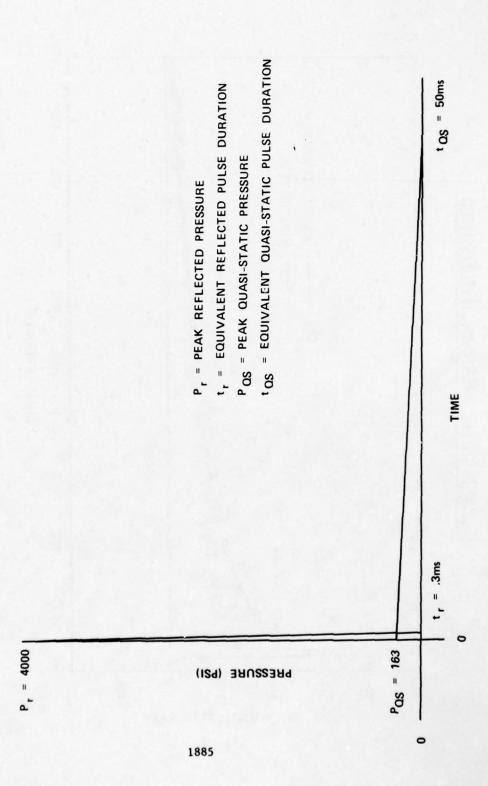
VENTING

SHIELD CONFIGURATION

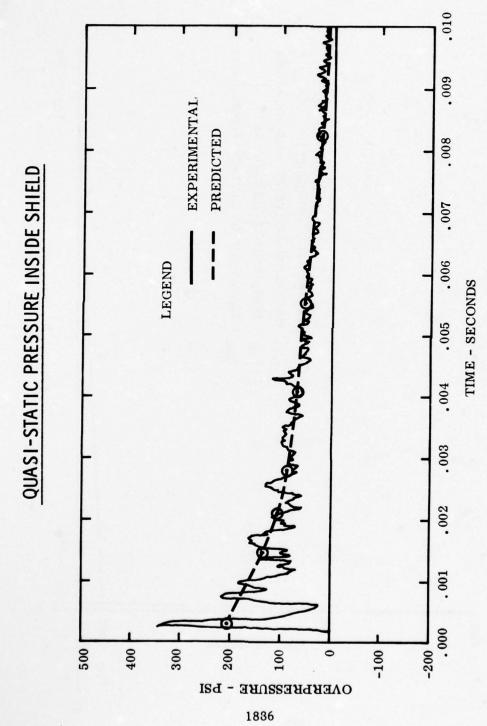
## REFLECTED IMPULSE FOR ONE POUND PENTOLITE

661	464	464	464	661
464	403	385	403	464
464	385	363	385	464
464	403	385	403	464
661	464	464	464	661





SEPT 1976



### BLAST SUPPRESSION

SHOCK TUBE TESTS

HOLE SIZE SINGLE PLATES -

REFLECTED PRESSURE

OTHER CONFIGURATIONS MULTI-PLATES

SCALE PANEL TESTS

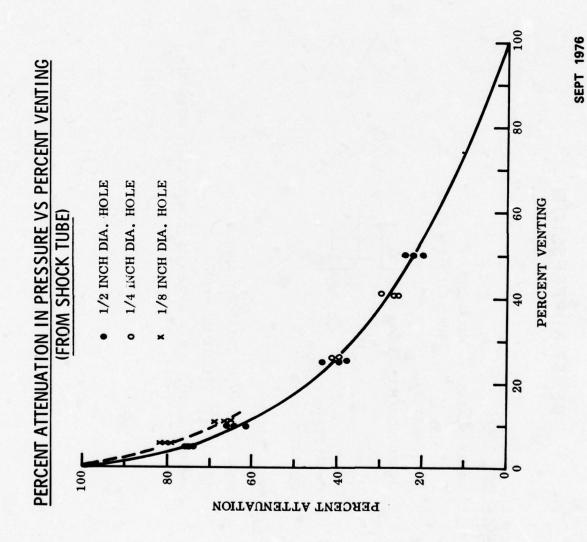
DURATION OF P - T

QUASI-STATIC

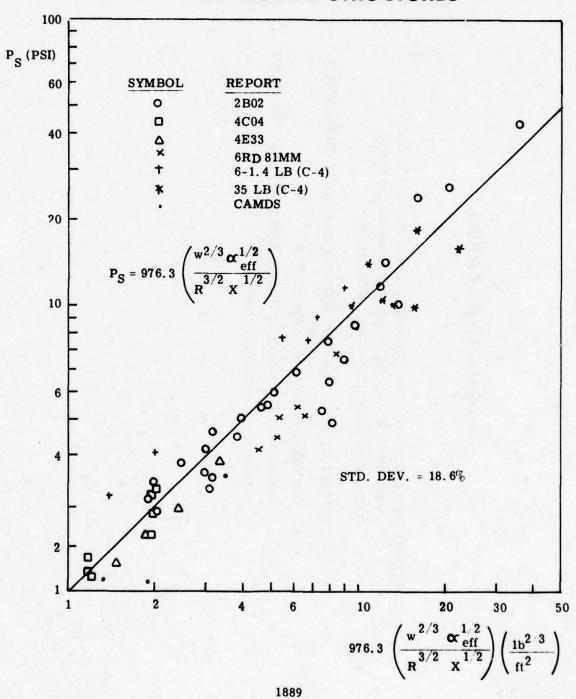
SIMULATE C/V OF CATEGORY SHIELD

INVESTIGATE EFFECT OF HEIGHT

FABRICATE NEW BOX - EVALUATE CONTROLLED VENTING



### CURVE FIT TO BLAST PRESSURES OUTSIDE SUPPRESSIVE STRUCTURES

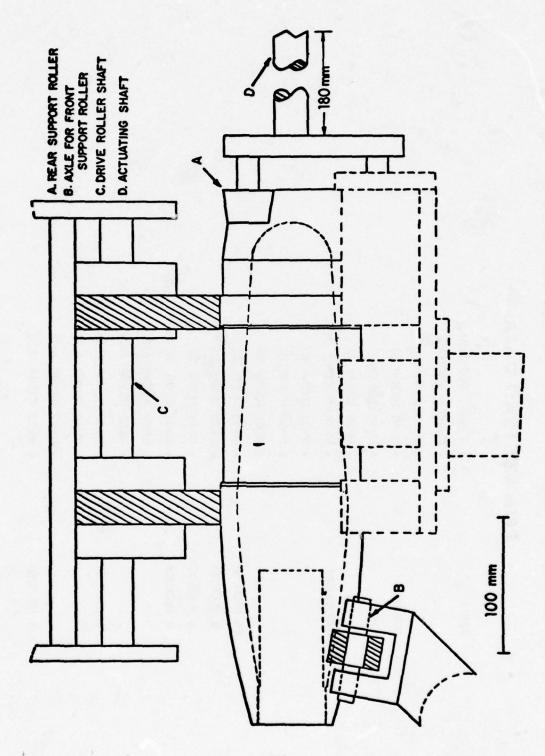


### FRAGMENT HAZARDS

OBJECTIVE: DEVELOP ANALYTIC TECHNIQUES FOR PREDICTING WORST CASE PRIMARY AND SECONDARY FRAGMENT HAZARDS ASSOCIATED WITH EXPLOSIVE OPERATIONS.

EFFECTS OF FOLLOWING PARAMETERS SHOULD BE DETERMINED:

HE WEIGHT, TYPE CONFINEMENT SEPARATION DISTANCE BETWEEN EXPLOSIVE AND EQUIPMENT EQUIPMENT CONFIGURATION



## JOINT MUNITIONS EFFECTIVENESS MANUAL

### PRIMARY FRAG DATA

• M-56E2 (RDX/AL)

M-56A1 (MOX/2B)

**20MM** 

M-56E5 (RDX/AL)

• M-16 (COMP B)

MINES

• M-18A1 (COMP C-4)

• M-26 (COMP B)

M-26A1 (COMP B)

GRENADES

M-32 (COMP B)

• M-40 (COMP B)

• M-67 (COMP B)

• Mk13 (EXPL D)

16 INCH/50 8 INCH/55 6 INCH/47

Mk25 (EXPL D)

Mk34 (EXPL D)

MK41 (EXPL D, COMP A-3)

5 INCH/54

• MK55 (COMP A-3)

• MK58 (COMP A-3)

• Mk49 (COMP A-3) Mk56 (COMP A-3)

5 INCH/38

• MK57 (COMP A-3)

Mk33 (COMP A-3)

3 INCH/50

**SEPT 1976** 

# EXPERIMENTAL AND ANALYTIC PROGRAM

20.8 kg 79 9 2.8 kg 28.1 g COMPOSITION B, PENOLITE, H - 6 19.7 g 2.8 kg 2.2 kg 1.2 g 1.3 kg 1.1 9 (3) SECONDARY FRAGMENTS: E EXPLOSIVES: **EXPLOSIVE** CHARGES:

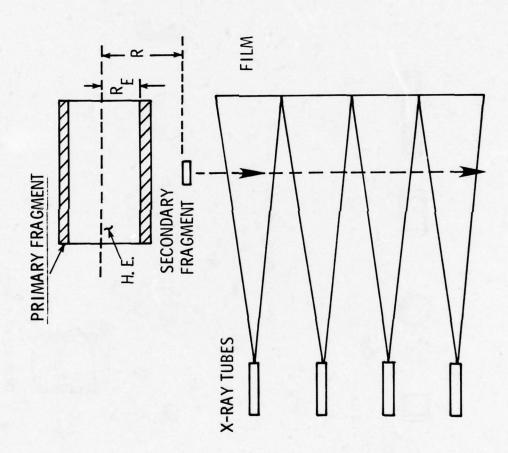
VUGRAPH #17

SEPT 76

301 9

13000 g (not to scale)

SECONDARY FRAGMENT TEST SET-UP



## FRAGMENT CONTAINMENT

OBJECTIVE: PROVIDE THE SCALING LAWS AND PENETRATION EQUATIONS NECESSARY TO DESIGN PANELS TO CONTAIN PRIMARY AND SECONDARY FRAGMENTS.

PARAMETERS INCLUDED IN INVESTIGATION:

PANEL

SPACING

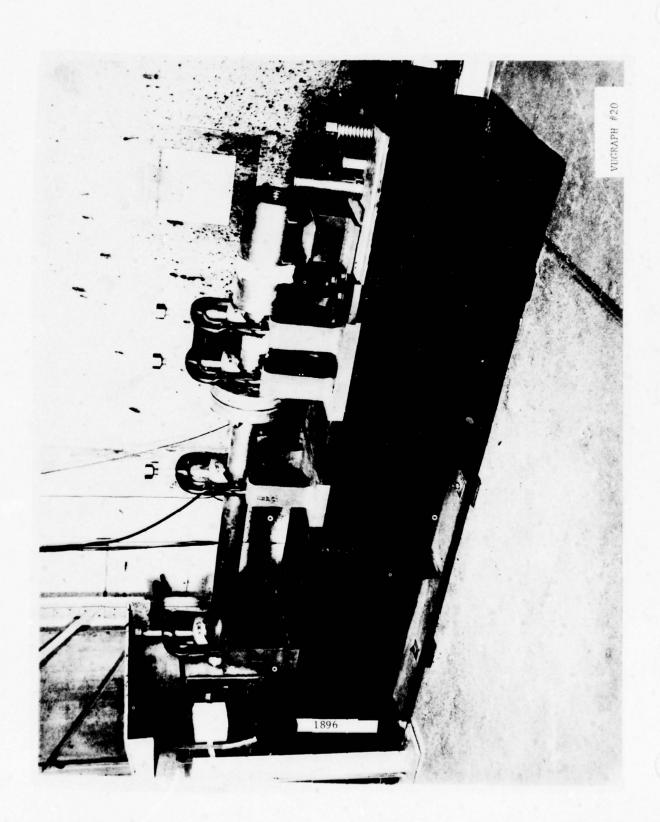
THICKNESS
CONFIGURATION

FRAGMENT

MASS

GEOMETRY

AREA



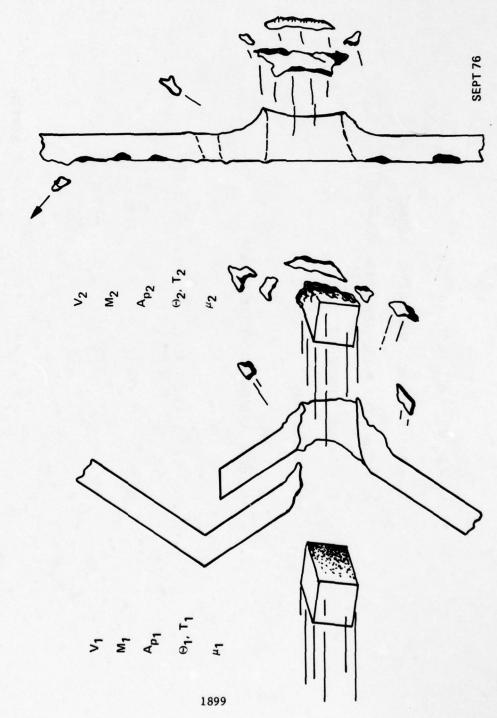


## ALUMINUM CYLINDER ATTACKING 81 MM SUPPRESSIVE STRUCTURE



1898

BEHIND-THE- TARGET MODEL FOR A FRAGMENT ATTACKING A SPACED TARGET



# PREDICTIVE EQUATION OF FRAGMENT BALLISTIC LIMIT VELOCITY

$$V_L = A_o M^{-1/2} A_p^m (T SEC \Theta)^n$$

VL = BALLISTIC LIMIT VELOCITY M/S

Ap = FRAGMENT PRESENTED AREA mm2

T = TARGET THICKNESS

mm

() = OBLIQUITY

Ao, m, n ARE EMPIRICAL CONSTANTS

LIGHT STEEL HE < 26 GR.

HEAVIER STEEL

71.69

0.295

0.291

0.92

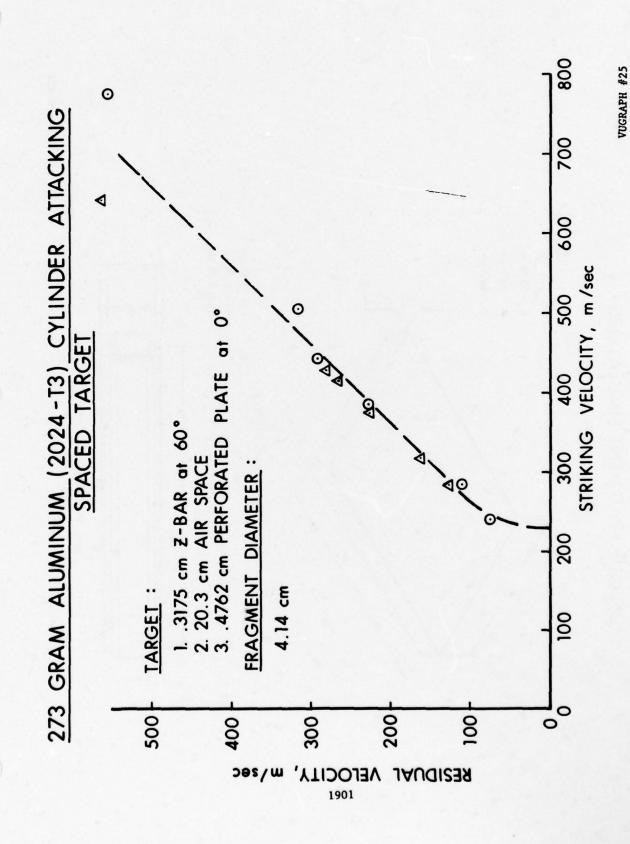
94.17

**P** 

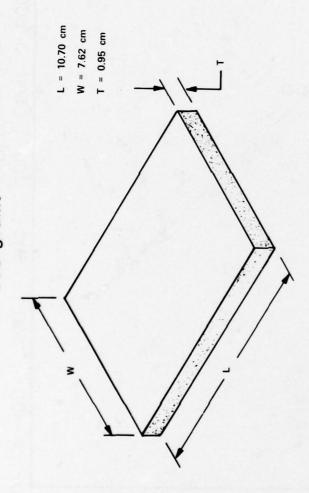
Ε

0.91

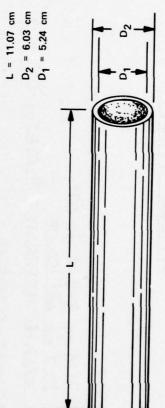
SEPT 76



### UNIQUE FRAGMENT SIMULATORS 608 grams



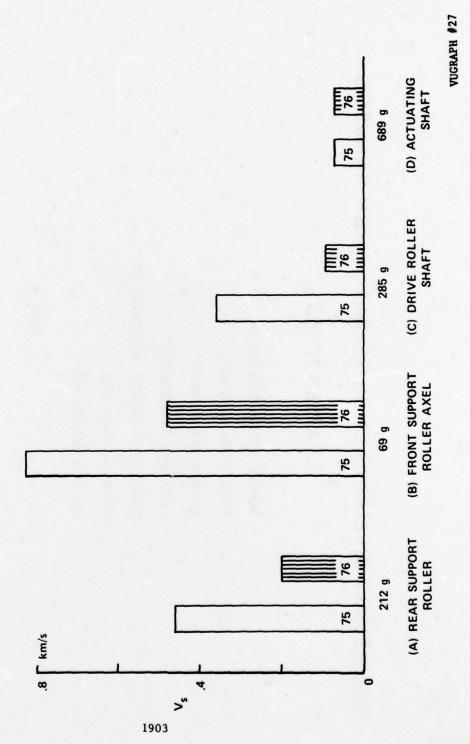
304L STAINLESS STEEL PLATE



304L STAINLESS STEEL PIPE

SEPT 76

SECONDARY FRAGMENT LIMIT SPEEDS 1975 (BRL IMR 332) vs 1976 105 mm M1 FUZE TORQUE OPERATION



### VUGRAPH #28

# SUPPRESSIVE SHIELDING ENGINEERING DESIGN HANDBOOK

### CHAPTER TITLES

SAFETY APPROVED SHIELDS

STRUCTURAL DETAILS

STRUCTURAL DAMAGE

**EXPLOSIVE ENVIRONMENT** 

STRUCTURAL DESIGN AND ANALYSIS

**ECONOMIC ANALYSIS** 

QUALITY ASSURANCE

### SUPPRESSIVE SHIELD TECHNOLOGY SUMMARY

● NO TECHNOLOGY BARRIERS

PREDÍCTIVE CAPABILITY AVAILABLE

● SCALING LAWS APPEAR VALID FOR SMALL EXPLOSIVE CHARGES

### LIST OF ATTENDEES

AMLIE, Dr. June T.
ADAMS, A. E.
ADAMS, R. T.
AGUILAR, Francisco
AINSWORTH, D. E.
ALEXANDER, A. A., MAJ (Land)
ANDERSON, C. M.
ANDREW, E. A.
ANSALVISH, F. B.
ATKINS, J. R.
ASHCRAFT, Dr. F. M.

BACHMAN, Georgia C. BAILETS, R. J. BAILEY, J. K. BAILEY, M. R. BAKER, C. F. BAKER, G. A. BAKER, Dr. W. E. BARAN, Chester BARB, J. C. BARKER, J. P. BARRETTE, P. S. BEECH, G. G., MAJ (Air) BEITER, R. H., CPT, USA BENT, R. L. BETZ, R. J. BIASUTTI, S. G. BINCKLEY, E. T. BLANKENSHIP, C. W. BODISCO, M. A. BOGGS, W. H. BOSWELL, S.L., JR., MAJ, USAF BOUDREAU, A. E. BOX, J. R. BOYLE, Dr. R. E. BRENT, E. H. BRINKMAN, E. J. BROCK, N. H. BRODELL, R. L. BROOKS, I. G. BROWN, H. O. BROWN, S. L.

BROWN, W. D.

David W. Taylor NavShip R&D Ctr, Bethesda, MD AFLC, Wright-Patterson AFB, OH NavFacEngCom, Alexandria, VA Explosivos Rio Tinto, Madrid, Spain NavSeaSupCtr Pacific, San Diego, CA Natl Defense Hq, Ottawa, Ontario, Canada NWC China Lake, CA Olin Corp., E. Alton, IL Aberdeen Proving Ground, MD JFK Space Center, FL MAC, Scott AFB, IL

DDESB, Washington, D. C. AFFTC, Edwards AFB, CA Union Carbide Nuc Div, Oak Ridge, TN DARCOM Fld Safety Acty, Charlestown, IN UnivCal, Lawrence Livermore Lab, CA NAD Hawthorne, NV Southwest Research Inst, San Antonio, TX 21AF, MAC, McGuire AFB, NJ BRL, Aberdeen Proving Ground, MD NAPEC, NWSC Crane, IN DARCOM, Alexandria, VA Natl Defense Hq, Ottawa, Ontario, Canada DNA, Washington, D. C. Thiokol Corp., Louisiana AAP, Shreveport, LA Dept of Labor, OSHA, Denver, CO Dr. Ing. Mario BIAZZI Soc. An., Vevey, Switzerland Flight Systems Inc., Newport Beach, CA Martin Marietta Alum Sales, Milan AAP, TN BuAlcohol, Tobacco&Firearms, San Francisco, CA NASA, JFK Space Center, FL 1 Strat Aerosp Div, Vandenberg AFB, CA DCASR, Boston, MA Robins AFB. GA Rocky Mountain Arsenal, Denver, CO Embassy of Australia, Washington, D. C. Olin Corp., East Alton, IL Air Products & Cmls Inc., Allentown, PA NSWC White Oak, Silver Spring, MD AFWL, Kirtland AFB, NM 4900ABW, Kirtland AFB, NM DCASR, Philadelphia, PA Iowa AAP, Middletown, IA

BRYAN, K. M.
BUCHANAN, H. G.
BUCKNER, A. K.
BUNCH, S. E., CPT, USAF
BURKE, R. H.
BUSSE, R. F.

BYRD, J. L., Jr. CADOW, W. S., CDR, USN CAIN, W. M. CALLAHAN, H. L. CAMERA, Ettore CAMPBELL, C. J. CANTOR, Issie CAREW, D. L. CARLSON, R. D., CPT, USAF CARRINGTON, C. C. CARROLL, D. E. CASEY, R. E., Sr. CASIMO, S. P. CAVIN, D. L. CECH, Ed CHANG, Wei Shing CHAR, W. T. CHARTIER, H. A. CHIANG, G. D. C. CHISLAGHI, D. R. CHRISTNER, R. K. CHRISTY, V. W. CLEAVELAND, Leroy CLINTON, W. S. CLOUSER, B. A. COAKLEY, J. V. COFFIN, J. P. COLEMAN, J. M., CPT, USA CONLEY, J. H. CONN, Dr. A. F. CONNELLY, J. M. CORAK, G. J., COL, USAF CORNEY, J. K., CPT, USAF CRAWFORD, J. L. CRIST, F. H. CROSLEY, W. A. CROSS, J. F. CRUYSBERG, E. E. A. CRUZ, I. T. CUMNOCK, F. L.

CUSTARD, G. H.

CUTSHALL, J. S.

UNC/USF Korea
BRL, Aberdeen Proving Ground, MD
Kansas AAP, Parsons, KS
Hq Alaskan Air Command
NavSeaSupCtr, Pacific, San Diego, CA
Chamberlain Mfg Corp, Waterloo, IA
DARCOM Ammunition Ctr, Savanna, IL

Naval EOD Facy, Indian Head, MD Hq 32d AADCOM, APO New York Black & Veatch, Kansas City, MO Dr.Ing. Mario BIAZZI Soc.An., Vevey, Switzerland Rock Island Arsenal, IL Ogden ALC, Hill AFB, UT ADCOM, Ent AFB, CO ADTC, Eglin AFB, FL NavFac, Atlantic Div, Norfolk, VA AFLC, Wright-Patterson AFB, OH NavSeaSupCtr, Pac, San Diego, CA Aberdeen Proving Ground, MD NAD Hawthorne, NV Lester B. Knight & Assoc. Inc., Chicago, IL Bureau of Explosives, Edison, NJ USA Engineer Div, Huntsville, AL Commissariat A L'Energie Atomique, France DARCOM Intern Tr Ctr, Red River AD, TX ASD, Wright-Patterson AFB, OH AFLC, Oklahoma City, OK Sandia Laboratories, Albuquerque, NM Day & Zimmermann, Inc., Kansas AAP, KS Arnold AFS, TN Lexington-Blue Grass AD, KY HQDA (DAIG-SD), Washington, D. C. Thiokol Corp., Newtown, PA 66 Ord Det (EOD), Homestead AFB, FL Aberdeen Proving Ground, MD Hydronautics, Inc., Laurel, MD Atlas Powder Co., Dallas, TX AFISC, Norton AFB, CA (AF Member, DDESB) AFAL, Eglin AFB, FL DARCOM, Alexandria, VA Tooele Army Depot, UT DETRONICS, Minneapolis, MN Hercules Inc., Magna, UT Technological Lab TNO, The Netherlands NWS Yorktown, VA Pine Bluff Arsenal, AR Falcon R&D Co., Denver, CO Sacramento ALC, McClellan AFB, CA

DALE, Dr. C. B. DAVIDSON, T. W. DEANS, H. L. DEGIOVANNI, Joseph DELLAMONICA, Louis DEL REGNO, Lawrence DEMPSEY, R. D. DeSHA, E. L., LCDR, USN DICKERSON, C. L. DITTMAN, H. A. DITTMANN, D. J. DIXON, L. C. DOBBS, Norval DODGEN, J. E. DONALDSON, L. O. DONEGAN, D. P. DONLEY, W. J. DOW, G. S. DRAKE, J. T. DRAKE, R. W. DRAUT, Charles DREYER, O. F.

EDWARDS, C. R. ELKINS, L. O. ELSASSER, F. M. ENGLISH, D. M. EVERETT, L. A.

DUNN, M. L.

FALCK, D. A.
FERRARO, Carlo, Jr.
FERRITTO, J. M.
FLIAKAS, Perry J.
FLYNN, W. F.
FONTAINE, P. H.
FORBUS, K. V.
FORSYTHE, F. J.
FOWLER, W. T.
FREEMAN, R. B.
FREIMANIS, Alvis

GALLES, F. P.
GERRON, R. A.
GIBBLE, J. W.
GILMORE, A. E.
GLASSMAN, I. M.
GLENN, R. E., CPT, USA

NOS Indian Head, MD USA Missile Command, Redstone Arsenal, AL DDESB, Washington, D. C. Hercules Inc., ABL, Cumberland, MD NAD Hawthorne, NV DCASR, Dallas, TX USA Engineer Div, Huntsville, AL Pac Missile Test Ctr, Point Mugu, CA NavSeaSupCtr, Atlantic, Portsmouth, VA DCASR, Cleveland, OH Hercules Inc., Port Ewen, NY NSWC White Oak Lab, Silver Spring, MD Ammann & Whitney, New York, NY Dodgen Engr Co., Colorado Springs, CO HQ 22AF, Travis AFB, CA Royal Ordnance Factory, England Naval EOD Facy, Indian Head, MD DSA (DCAS-QS), Alexandria, VA DDESB, Washington, D. C. Los Alamos Scientific Lab, Los Alamos, NM Monsanto Research Corp, Miamisburg, OH Lockheed Missiles & Space Co., Sunnyvale, CA DDESB, Washington, D. C.

Hercules Inc., Radford AAP, VA
AFATL, AFSC, Eglin AFB, FL
60 MAW, Travis AFB, CA
Edgewood Arsenal, Aberdeen Proving Ground, MD
DSA (DCAS-QS), Alexandria, VA

Edgewood Arsenal, Aberdeen Proving Ground, MD ERDA, Washington, D. C.
Civil Engr Lab, Port Hueneme CA
DepAsstSecDef(I&H), Washington, D. C.
USAMMCS, Redstone Arsenal, AL
S.N.P.E., Paris, France
Anniston Army Depot, AL
Joliet AAP, IL
Radford AAP, VA
ICI United States Inc., Volunteer AAP, TN
Lester B. Knight & Assoc, Chicago, IL

NTS Keyport, WA
JFK Space Center, NASA, FL
NavAirSysCom, Washington, D. C.
NAPEC, NWSC, Crane, IN
Rocky Mountain Arsenal, Denver, CO
USA Env Hygiene Agency, Aberdeen PG, MD

GLENNON, J. P., CPT, USA
GOLIGER, J. G.
GORDON, R. B.
GREEN, R. C.
GREGORY, F. H.
GREY, Lloyd
GROSCOST, K. R.
GUERKE, G. H.

HAHN, J. C. HALL, Clyde HALL, P. H. HALTER, D. I. HALTOM, P. T. HANKS, C. M. HANNA, R. J. HANNAH, M. M. HANSEN, G. L. HANSEN, S. G. HARPER, J. D. HARTON, E. E., Jr. HARVEY, T. K. HATHAWAY, J. A., LTC, USA HAWES, J. M. HAWS, L. D. HEDGELAND, P.M.S., Air Vice Marshal, RAF HEESEMAN, A1 HELLE, C. J. HENRY, R. E. HERCHBERGER, C. K. HERMAN, R. C. HILL, W. V. HILLMAN, R. H. HOARD, J. W. HOFERER, F. M. HOLLANDER, W. V. HOLLOWAY, B. G. HOPKINS, Don HORNE, K. E. HORNIG, H. C. HOUSTON, W. F. HOWE, Dr. P. M. HOWELL, E. D. HUANG, C. C. HUDSON, M. C.

HUHN, Wilfried, MAJ, Army

USA Med Bioeng R&D Lab, Fort Detrick, MD Societe Nat des Poudres et Expl, France Aeronutronic Ford, Newport Beach, CA Aerojet Nuclear Co., Idaho Falls, ID BRL, Aberdeen Proving Ground, MD Vandenberg AFB, CA DARCOM Ammunition Center, Savanna, IL Ernst - Mach Institut, Fed Repub. of Germany

Martin Marietta Aerospace, Orlando, FL Austin Powder Co., McArthur, OH 437MAWG (MAC), Charleston AFB, SC Red River Army Depot, Texarkana, TX DARCOM Intern Tr Ctr, Red River AD, TX Leonard Bros Trucking, Houston, TX Boeing Aerospace Co., Seattle, WA 63MAW, Norton AFB, CA IRECO Chemicals Inc., Salt Lake City, UT Pacific Missile Test Ctr, Point Mugu, CA Los Alamos Scientific Lab, Los Alamos, NM DOT, Washington, D. C. Polaris Msl Facy Atlantic, Charleston, SC USAEHA, Aberdeen Proving Ground, MD DDESB, Washington, D. C. Monsanto Research Corp, Miamisburg, OH UK Ordnance Board, London, England

Wyle Laboratories, Norco, CA Cia. Brasileira de Cartuchos, Sao Paulo, Brazil Lawrence Livermore Lab, Livermore, CA NWS Seal Beach, CA DDESB, Washington, D. C. Black & Veatch, Kansas City, MO Martin Marietta Aerospace, Denver, CO Holston Defense Corp., Kingsport, TN OEA, Inc., Denver, CO Olin Corp., New Haven, CT Volunteer AAP, Chattanooga, TN Leonard Bros Trucking, Oakland, CA Jet Research Ctr, Inc., Arlington, TX Lawrence Livermore Lab, Univ of Cal, CA HQ 172D INF BDE (AK), APO Seattle BRL, Aberdeen Proving Ground, MD DDESB, Washington, D. C. USA Engineer Div, Huntsville, AL NOS Indian Head, MD Wehrbereichskommando V (GE), Stuttgart, FRG

INGMAN, J. F., LTC, USA INGRAM, L. F.

JAMISON, J. E.
JENKINS, J. L.
JENKS, Dr. G. J.
JEZEK, B. W.
JOACHIM, C. E.
JOHNSON, M. C.
JOHNSON, R. E.
JOHNSON, R. E.
JONES, C. P.
JONES, C. F.
JONES, F. M.

KAHLER, R. J. KAPLAN, Kenneth KATSANIS, Dr. D. J. KATTMANN, R. H., CAPT, USN KEEFE, R. L. KEENAN, W. A. KELLEY, P. G., Jr., COL, USA KENDRICK, H. E. KERNS, A. J. KHWAJA, A. A. KINEKE, John KINGERY, C. N. KIRTLEY, Donallan KNASEL, B. L. KNOTT, E. F. KNUTSON, D. W., CAPT, USN KOEGEL, C. F. KOWAL, W. T. KRISTOFF, F. T. KRONENBERGER, J. A. KUSHNER, A. S.

LAIBSON, L. R.
LAMB, H. C.
LANG, R. A.
LANTZ, J. D., CPT, USA
LARSEN, J. L.
LARSEN, T. E.
LAWRENCE-ARCHER, J. H.,
Brigadier, RA

LACOPO, T. L.

KYRKJEBØ, Gunnar, LTC Army

MTMC, Washington, D. C. USA Eng Waterways Exp Stn, Vicksburg, MS

Mason & Hanger-Silas Mason, Iowa AAP, IA
NAD Hawthorne, NV
Materials Res Labs, Victoria, Australia
Edgewood Arsenal, MD
USA Eng Waterways Exp Stn, Vicksburg, MS
USA Armament Com, Rock Island, IL
Olin Corp., Badger AAP, Baraboo, WI
SWFPAC, Silverdale, WA
NavSeaSysCom, Washington, D. C.
Dugway Proving Ground, UT
Aerojet Solid Propulsion Co., Sacramento, CA

Mason & Hanger-Silas Mason, Amarillo, TX Scientific Service Inc, Redwood City, CA Edgewood Arsenal, Aberdeen Proving Ground, MD DDESB, Washington, D. C. Hercules Inc., Magna, UT Civil Engr Lab, Port Hueneme, CA Chairman, DDESB, Washington, D. C. ERDA, Las Vegas, NV Newton, NJ USA Armament Com, Rock Island, IL BRL, Aberdeen Proving Ground, MD BRL, Aberdeen Proving Ground, MD Hercules Inc, Wilmington, DE DDESB, Washington, D. C. NOTU, Patrick AFB, FI. OCNO, Washington, D. C. (Navy Member, DDESB) DCASR, New York, NY Boeing Co., Hill AFB, UT Hercules Inc, Radford AAP, VA Monsanto Research Corp, Miamisburg, OH NSWC White Oak, Silver Spring, MD Ministry of Defence Ammo Saf Cte; Raufoss, Norway

Uniroyal, Inc, Newport AAP, IN
PMOBME, Picatinny Arsenal, NJ
NavFacEngCom, Alexandria, VA
DCASR, Chicago, IL
HQ US Army Japan/IX Corps
Letterkenny Army Depot, Chambersburg, PA
DETRONICS, Minneapolis, MN
Chief Inspector Land Service Ammunition, UK

LEANDER, R. C.
LEE, Dr. P. R.
LEVEY, D. V.
LEWIS, H. L.
LEWIS, W. R.
LOMINICK, R. T.
LONGINOW, Anatole
LONGO, Vito, COL, USAF
LOVING, F. A.
LOWE, W. F.
LYMAN, O. R.
LYNCH, Dr. R. H.

McCAY, W. C.
McCLAIN, Dr. W. H.
McCLOSKEY, E. J.
McDEVITT, Joyce A.
McDONALD, J. B.
McDOWELL, R. C.
McGEHEE, D. C.
McLAIN, J. P.
McQUAIDE, P. B.

MANGINO, J. M. MARKINE, G. E. MARTIN, D. A. MARTIN, Glynn MASON, A. R., CPT, USA MAST, Beverly J. MEAD, J. M. MELLEN, H. J. METCALF, H. L. MICKLE, A. A. MITCHELL, W. D. MOORE, C. J. MOORE, W. J. MORRISON, D. W. MUELLER, D. R. MULLINS, R. K. MUMMA, G. B. MUNCH, C. R. MYERS, R. L.

NAPADENSKY, Hyla S.
NEMETH, G. R.
NEWBERN, R. G., Jr.
NICHOLSON, H. X., LT, USN
NOGLE, K. E.
NORBERG, D. W.

Thiokol Corp, Longhorn Div, Marshall, TX
Royal Armament R&D Estab, Kent, England
GOEX Inc, Cleburne, TX
Naval Sea Sup Ctr Pacific, San Diego, CA
Red River Army Depot, Texarkana, TX
Boeing Aerospace Co, Seattle, WA
IIT Research Institute, Chicago, IL
AFISC/SEW, Norton AFB, CA (Alt AF Mbr, DDESB)
E I duPont de Nemours, Martinsburg, WV
AFAL, Eglin AFB, FL
BRL, Aberdeen Proving Ground, MD
British Embassy, Washington, D. C.

Longhorn AAP, Marshall, TX
Southwest Research Inst, San Antonio, TX
Monsanto Research Corp, Miamisburg, OH
HQ AFSC, Andrews AFB, MD
Brunswick Corp, Skokie, IL
19th Sup Bde, APO San Francisco
Aerojet Solid Propulsion Co., Sacramento, CA
New Mexico Inst of Min & Tech, Socorro, NM
PMTC Point Mugu, CA

SAMTEC, Vandenberg AFB, CA Dugway Proving Ground, UT Edgewood Arsenal Res Lab, Bay St Louis, MS NSWC Dahlgren Lab, Dahlgren, VA Fort Douglas, UT DDESB, Washington, D. C. Uniroyal Inc, Joliet AAP, IL USA Engineer Div, Huntsville, AL OASD(I&L), Washington, D. C. 3460TCHTG, Lowry AFB, CO Redstone Arsenal, Huntsville, AL Lackland AFB, TX Western Div NavFac, San Bruno, CA Fed Highway Admin, Washington, D. C. USA Test & Evaluation Com, Aberdeen PG, MD Lawrence Livermore Lab, UnivCal, CA Martin Marietta Aerospace, Denver, CO NavSea Safety School, NWSC Crane, IN DARCOM Fld Safety Acty, Charlestown, IN

IIT Research Institute, Chicago, IL OPMCD&IR, Aberdeen Proving Ground, MD AFSC, Andrews AFB, MD Strat SysProjOfc, Sunnyvale, CA AFSC, Andrews AFB, MD Stearns-Roger Inc, Denver, CO ODELLO, R. J.
O'KONSKI, A. R.
OLSEN, F. N.
OLSON, S. R., LTC, USA
OPEL, M. C.
ORNELLAS, G. S.
OROZCO, Josefina L.
OYLER, G. W.
OZBURN, J. E.
OZENGHAR, H. H.

PAGE, D. O. PAKULAK, J. M., Jr. PALFREEMAN, B. D. PARKS, D. K. PATALIVE, J. A. PATER, L. L. PAYNE, L. H. PECKHAM, P. J. PEI, R. S. K. PELLOW, R. D. PERKINS, R. G. PERRY, C. W. PERRY, R. B. PETERSEN, A. H. PETES, Joseph PETINO, George, Jr. PICKLER, W. C. PILLERSDORF, Arthur PITTMAN, J. F. PLATE, S. W. PLOETZ, C. F., CPT, USAF POLLOCK, D. J. PORZEL, F. B. PRICE, Dr. G. V. PRICE, P. D. PRIOR, L. C. PRITCHARD, G. C.

QUEEN, W. J.

RANDALL, H. J.
RANGER, P. T.
RAUSIN, G. D., COL, USAF
REDDY, P. D.
REED, J. W.
REEVES, H. J.
REIDER, Roy

Civil Engr Lab, NCBC Port Hueneme, CA
OPMMPBM&E, Dover, NJ
Boeing Co., Seattle, WA
Louisiana AAP, Shreveport, LA
ICI United States Inc, Indiana AAP, IN
CDT 14th Naval Dist Staff, FPO San Francisco
OEA Inc, Denver, CO
ASD, Wright-Patterson AFB, OH
Leonard Bros Trucking Co, Pensacola, FL
DSA, DCRL, Inglewood, CA

Monsanto Research Corp, Miamisburg, OH NWC China Lake, CA Canadian Industries, Ltd, Quebec, Canada Falcon R&D Co., Denver, CO McDonnell Douglas Astro Co, Huntington Beach, CA NSWC Dahlgren Lab, Dahlgren, VA NWS Charleston, SC NSWC White Oak, Silver Spring, MD DARCOM Fld Safety Agency, Charlestown, IN 62MAW/SEV, McChord AFB, WA DDESB, Washington, D. C. Stearns-Roger Inc., Denver, CO OPMCD&IR, Aberdeen PG, MD Detector Electronics Corp, Minneapolis, MN NSWC White Oak, Silver Spring, MD Hazards Research Corp, Denville, NJ NSWC White Oak, Silver Spring, MD Edgewood Arsenal, Aberdeen Proving Ground, MD NSWC White Oak, Silver Spring, MD Tri-State Motor Transit Co, Arlington, VA 6515 Test (Sup) Sqdn, Edwards AFB, CA Hill AFB, UT NSWC White Oak, Silver Spring, MD Defence Res Estab, Suffield, Alberta, Canada Picatinny Arsenal, Dover, NJ Cal Inst of Tech, JPL, Pasadena, CA NWC China Lake, CA

DARCOM, Alexandria, VA (Alt Army Mbr, DDESB)

DCASR, Los Angeles, CA
Red River Army Depot, Texarkana, TX
DDESB, Washington, D. C.
Agbabian Assoc., El Segundo, CA
Sandia Laboratories, Albuquerque, NM
BRL, Aberdeen Proving Ground, MD
Los Alamos Scientific Lab, Los Alamos, NM

RHINEBECK, G. C., CDR, USN RHODES, D. B. RILEY, W. E. RITTMAN, H. T., Jr. ROBINSON, P. E. ROBINSON, R. L. RODGER, Robert ROGERS, John ROGERS, R. N. ROOKE, A. D., Jr. ROSENVINGE, R. C. ROTHERY, C. M. ROTHERY, K. M. ROURE, J. J., Ingenieur General de l'Armement ROWLEY, T. W., CPT, USAF ROYLANCE, H. M.

RUDIN, A. G.
RUNKEN, R. G., LTC, ARNG
RUSSELL, J. W., CAPT (Navy)

SAFFIAN, L. W. SAINDON, B. W. SANCHEZ, F. B. SANDS, C. A., COL, USA SAVAIKO, B. M. SCHAFFER, M. B. SCHAICH, E. E. S., CPT, AF SCHNEIDER, L. J., Jr., LT, USN SCHNEIDER, Thomas SCHUETT, K. A. SCHULTZ, L. F. SCHUMACHER, R. N. SCHWARTZ, R. M. SCOGGIN, G. L. SCOTT, Dr. R. A., JR SCOTT, R. W., CDR, USN SEARD, E. H. SEAVERS, R. H. SHALABI, G. K. SHANKS, E. R. SHAW, R. F., Jr. SILER, A. K. SIMPSON, J. L. SIMON, R. J.

SIRIANNE, R. A. SKINNER, C. S.

SMEBY, O. N.

NWS Concord, CA
Lone Star AAP, Texarkana, TX
SMTC, Vandenberg AFB, CA
E I duPont de Nemours, Wilmington, DE
Edgewood Arsenal, Aberdeen Proving Ground, MD
NL Baroid Petroleum Svcs, Houston, TX
Rocky Mountain Arsenal, Denver, CO
Sandia Laboratories, Livermore, CA
UCal, Los Alamos Scientific Lab, NM
USA Engr Waterways Exp Stn, Vicksburg, MS
Union Carbide, Oak Ridge, TN
DCASR, St. Louis, MO
DCASR, Los Angeles, CA

Ministere de la Defense, France 3460 TCHTG, Lowry AFB, CO Vitro Laboratories, Arlington, VA NatInspecExplosiv&Flammables, Solna, Sweden NGB, Aberdeen Proving Ground, MD Dir General Ammo, Ottawa, Ontario, Canada

Picatinny Arsenal, Dover, NJ Rocky Mountain Arsenal, Denver, CO NSWC Dahlgren Lab, Dahlgren, VA DDESB, Washington, D. C. USA Electronics Com, Fort Monmouth, NJ Science Applications Inc, La Jolla, CA Ministry of Defense, Bonn, Germany NPB Rep Ofc, Magna, UT Basler & Hofmann Cons Engr, Zurich, Switzerland USA Aviation SysCom, St. Louis, MO NPB Rep Ofc, SSPO, Lockheed, Sunnyvale, CA BRL, Aberdeen Proving Ground, MD Day & Zimmermann, Inc., Philadelphia, PA Chamberlain Mfg Co, Waterloo, IA DDESB, Washington, D. C. NSC, NAS Norfolk, VA DARCOM Ammunition Ctr, Savanna, IL Redstone Arsenal, Huntsville, AL Badger AAP, Baraboo, WI Rocketdyne, Canoga Park, CA Honeywell Inc, Twin Cities AAP, New Brighton, MN DCASR, Marietta, GA Martin Marietta Aerospace, Denver, CO AMSAA, Aberdeen Proving Ground, MD TRADOC, Fort Monroe, VA Booz Allen & Hamilton Inc, Cleveland, OH Raufoss Ammunisjonsfabrikker, Raufoss, Norway

SMITH, J. R. SMITH, L. E. SMITH, North SMITH, R. J. SMITH, R. L. SMITH, W. A. SMITH, W. J. SOULE, K. O. SPENCER, J. R. STAMPS, R. U. STANDLEY, R. S. STEVENS, C. J. STOCK, J. A. STOFFERS, F. W. STREHLOW, R. A. SULLIVAN, E. P. SWISDAK, M. M., Jr. SWITLIK, C. T.

TAKAHASHI, T. H.
TAYLOR, Dr. W. J., Jr.
TEICHMANN, E. C.
TEREO, Michael
TETRICK, C. J.
THOMAS, C. A.
THOMAS, R. K.
THOMAS, W. C.
TOWNSEND, J. E.
TROTT, B. D.
TULL, J. D.

VALANT, K. E.
VAN ERP, Dirk
VETTER, R. F.
VINSON, J. L.
VOINOVICH, Nick
VORECK, W. E.
VOSE, W. F.

WALDMAN, Benjamin WALSH, J. J. WALTERS, J. O. WARNE, D. E. WATSON, R. R.

WAWRZASZEK, S. F. WEALS, F. H.

Aerospace Corp, Los Angeles, CA PMCD&IR, Aberdeen Proving Ground, MD USA Cold Region R&E Lab, Hanover, NH Natl Security Agency, Fort Meade, MD Hercules Inc, Sunflower AAP, Lawrence, KS Battelle Columbus Labs, OH McDonnell Douglas Astro. Co., St. Louis, MO Rockwell Int Corp, Canoga Park, CA Lake City AAP, MO USAIC, Fort Benning, GA ARMCO Steel Corp, Middletown, OH NavFacEngCom, Alexandria, VA NavFacEngCom Atlantic Div, Norfolk, VA Jet Propulsion Lab, Pasadena, CA Aero & Astro Engr Dept, Univ IL, Urbana, IL Atlantic Research Corp, Gainesville, VA NSWC White Oak, Silver Spring, MD NWS Concord, CA

Sandia Laboratories, Livermore, CA
Atlas Powder Co., Dallas, TX
6th Ord Group, APO New York
NWS Earle, Colts Neck, NJ
NAD Hawthorne, NV
Hughes Aircraft Co., Tucson, AZ
Rocky Mountain Arsenal, Denver, CO
NUC San Diego, CA
NSWC Dahlgren, VA
Battelle Columbus Labs, Columbus, OH
Lockheed Missiles & Space Co, Santa Cruz, CA

DARCOM Ammunition Ctr, Savanna, IL
Keller & Gannon, San Francisco, CA
NWC China Lake, CA
Remington Arms Co Inc, Lake City AAP, Indep., MO
BuAlcohol, Tobacco, Firearms, Washington, D. C.
Picatinny Arsenal, Dover, NJ
NSC, NAS Norfolk, VA

Picatinny Arsenal, Dover, NJ
NSWC Dahlgren, VA
DARCOM, Alexandria, VA
Science Applications, Inc., La Jolla, CA
UK Explosives, Storage & Transport Committee,
London, England
DPCA, Fort Belvoir, VA
NWC China Lake, CA

WEEDING, G. S.
WEISSMAN, Samuel
WELLER, J. F.
WELLMAN, G. D., MSGT, USA
WENZEL, A. B.
WEST, F. L.
WEST, L. D.
WESTINE, P. S.
WIGHT, R. L.
WILD, Roland

WILKAITIS, N. J.
WILLIAMS, P. C., LTC, USAF
WILLIS, D. I.
WILLIS, V. G., Sr.
WILSON, D. E.
WISS, J. F.
WORKUM, A. D.
WRAY, G. H.

YAGER, M. L.
YOUNG, G. L., CDR, USN
YOUNG, R. E.

ZAKER, Dr. T. A.
ZAGZEBSKI, K. P.
ZALMANEK, J. A.
ZAUGG, M. M.
ZEIDMAN, G. G.
ZOLLICKER, S. H.
ZUKE, W. G.

Falcon R&D Co., Denver, CO Ammann & Whitney Cons. Engrs., New York, NY NAPEC, NWSC Crane, IN 130rdDet (EOD), Fort Gillem, GA Southwest Research Inst, San Antonio, TX ADTC/SES, Eglin AFB, FL Hercules Inc., Wilmington, DE Southwest Research Inst, San Antonio, TX Ofc Chief of Engineers, DA, Washington, D. C. Bundesinstitut fur chem. tech. Untersuchungen, W. Germany Olin Corp., Marion, IL DirNuclear Safety, AFISC, Kirtland AFB, NM DARCOM Ammo Ctr, Savanna, IL NSWC Crane, IN NOS Indian Head, MD Wiss Janney Elstner & Assoc., Northbrook, IL McDonnell Douglas Astro., Titusville, FL Day & Zimmermann, Inc., Texarkana, TX

Aerojet Ord & Mfg Co, Downey, CA CINCPACFLT, FPO San Francisco USA Armaments Com, Rock Island Arsenal, IL

DDESB, Washington, D. C.
Ralph M. Parsons Co., Pasadena, CA
AFPRO/Martin Marietta, Denver, CO
Tooele Army Depot, UT
Battelle Columbus Labs, Columbus, OH
Hercules Inc, Sunflower AAP, KS
NavAirSysCom, Washington, D. C.